INTERNATIONAL COUNCIL FOR RESEARCH AND INNOVATION
IN BUILDING AND CONSTRUCTION

WORKING COMMISSION W18 - TIMBER STRUCTURES

CIB - W18

MEETING FORTY

BLED

SOLVENIA

AUGUST 2007

Lehrstuhl für Ingenieurholzbau und Baukonstruktionen
Universität Karlsruhe
Germany
Compiled by Rainer Görlacher
2007

ISSN 1864-1784

CONTENTS

0 List of Participants

INTERNATIONAL COUNCIL FOR RESEARCH AND INNOVATION IN BUILDING AND CONSTRUCTION
WORKING COMMISSION W18 - TIMBER STRUCTURES

MEETING FOURTY
Bled, Slovenia, 28 - 31 August 2007

LIST OF PARTICIPANTS

AUSTRALIA	
K Crews	University of Technology Sydney UTS
P Paevere	CISRO
AUSTRIA	
T Bogensperger	TU Graz
R Brandner	Kompetenzzentum holz.bau.forschungs.gmbh
A Jöbstl	TU Graz
G Schickhofer	TU Graz
CANADA	
Chun Ni	Forintek, Vancouver
E Karacabeyli	Forintek, Vancouver
F Lam	UBC, Vancouver
G Lehoux	Royal Military College of Canada, Kingston
M Popovski	Forintek, Vancouver
A Salenikovich	Universite Laval, Quebec
I Smith	University of New Brunswick, Fredericton
CROATIA	
V Rajcic	University of Zagreb
DENMARK	
H J Larsen	Copenhagen
FINLAND	
A Hanhijärvi	VTT Technical Research Centre of Finland, Espoo
A Ranta-Maunus	VTT Technical Research Centre of Finland, Espoo
FRANCE	
L Blaskovic	INSA de Lyon
C Faye	FCBA-CTBA, Bordeaux
F Rouger	FCB-CTBA, Paris
GERMANY	
H J Blaß	Universität Karlsruhe
J Denzler	Technical University of Munich
M Frese	Universität Karlsruhe
R Görlacher	Universität Karlsruhe
A Heiduschke	TU Dresden
U Kuhlmann	Universität Stuttgart
P Linsenmann	Technical University of Munich
K Rautenstrauch	Bauhaus University, Weimar

J Schänzlin	Universität Stuttgart
T Uibel	Universität Karlsruhe
IRELAND	
A Harte	National University of Ireland, Galway
ITALY	
M Ballerini	University of Trento
A Ceccotti	IVALSA-CNR
M Fragiacomo	University of Sassari, Alghero
JAPAN	
K Komatsu	Kyoto University
M Yasumura	Shizuoka University
NEW ZEALAND	
P Quenneville	Auckland University
SLOVENIA	
B Dujic	University of Ljubljana
J Srpcic	Slovenian National Building and Civil Engineering Institute
R Zarnic	University of Ljubljana
SWEDEN	
C Bengtsson	SP, Boras
U A Girhammar	Umea University
J König	SP Trätek, Stockholm
S Thelandersson	Lund University
SWITZERLAND	
E Gehri	ETH Zürich
A Frangi	ETH Zürich
M Deublein	ETH Zürich
J Köhler	ETH Zürich
R Steiger	EMPA Wood Laboratory, Dübendorf
THE NETHERLANDS	
A Jorissen	SHR Timber Research, Doetinchem
A J M Leijten	TU Eindhoven
J W van de Kuilen	Delft University of Technology
P de Vries	Delft University of Technology
UK	
A Kermani	CTE, Napier University
USA	
T Williamson	American Plywood Association, Tacoma
B Yeh	American Plywood Association, Tacoma

1. Chairman's Introduction
2. General Topics
3. Stress Grading
4. Stresses for Solid Timber
5. Timber Joints and Fasteners
6. Timber Beams
7. Laminated Members
8. Trussed Rafters
9. Structural Stability
10. Fire
11. Test Methods
12. Any Other Business
13. Venue and Program for Next Meeting
14. Close

INTERNATIONAL COUNCIL FOR RESEARCH AND INNOVATION
IN BUILDING AND CONSTRUCTION

WORKING COMMISSION W18 - TIMBER STRUCTURES

MEETING FORTY

BLED, SLOVENIA 28 TO 31 AUGUST 2007

M I N U T E S
(F Lam)

1 CHAIRMAN'S INTRODUCTION

Prof. Hans Blass welcomed the delegates to the 40th CIB-W18 Meeting in Bled, Slovenia. Thirty three papers will be presented this year. This is the highest number of papers ever in CIB-W18 meeting. The presentations are limited to 20 minutes each, allowing time for meaningful discussions after each paper. The Chair asked the presenters to conclude the presentation with a general proposal or statements concerning impact of the research results on existing or future potential application and development in codes and standards. R. Görlacher will deal with questions regarding the meeting proceedings. The participants were asked to check the participant address list under circulation for accuracy.

Papers brought directly to the meeting would not be accepted for presentation, discussions, or publication. Papers presented by non-authors or non-coauthors are not recommended except in exceptional situations because the discussion process might be compromised.

There are 9 topics covered in this meeting: stress grading (2 papers), stresses for solid timber (3 papers), timber joints and fasteners (8 papers), timber beams (1 paper), laminated members (7 papers), trussed rafters (1 paper), structural stability (7 papers), fire (2 papers), and test methods (2 papers).

B. Dujic discussed organizational matters for the meeting. R. Zarnic on behalf of the host organization University of Ljubljana welcomed the delegates and thanked the sponsors for their support of the meeting.

2 GENERAL TOPICS

M. Yasumura invited the delegates to participate in the upcoming WCTE 2008 conference in Miyazaki Japan during June 2 to 5, 2008. Approximately 480 abstracts have been received. Further information can be obtained from the conference website www.wcte2008.com.

A. Ceccotti informed the delegates that unfortunately in Italy a conservative safety factor of 1.5 rather than 1.3 was adopted for Eurocode 5. He also informed about the Italian project on the largest timber building to be tested on a shake table in Japan (cost ~ 0.9 million euros). The 7 story structure is 23 m tall. The testing will take pace on October 23, 2007. The delegates were invited to view the test.

J. Köhler informed the delegates about COST action E55 on "Modelling the performance of Structures".

3 STRESS GRADING

40 - 5 - 1 Development of Grading Rules for Re-Cycled Timber Used in Structural Applications - **K Crews**

Presented by K. Crews

H. Blass commented that in Europe material after 500 years of service did not show duration of load effect. He received clarification that the moisture content of the material was at least 30%; therefore, considered as unseasoned. Also new timber was available for comparisons. H. Blass asked whether the wood was treated. K. Crews replied that the wood was untreated because the hardwood would have low preservative penetration. If the material was the softwood radiate pine then it would have been treated.

A. Ceccotti commented that he was surprised by the results with reference to duration of load effects and cited J. Kuipers work from previous CIB meeting as example.

J.W. Van de Kuilen questioned the ratio between the stresses experienced by members from loading and their strength. K. Crews replied that with wharfs and bridge timber, high loads for short period and also high dead load from the concrete would be expected. Roof timbers seemed to have little or no effect from duration of loads.

F. Rouger asked whether new duration of load factors are needed for this material. K. Crews replied that they may be needed but currently did not have firm answer.

I. Smith commented that the influence of moisture history might be an explanation rather than duration of load and suggested not to refer the observed strength lost as duration of load effect. I. Smith further commented that re-sawing the checked material and the influence of checking on smaller material need to be considered. K. Crews agreed especially when the material was applied in nail plate structures.

E. Karacabeyli asked why minimal difference in MOE but large difference in MOR. K. Crews said that may be some creep recovery related issue in involved.

40 - 5 - 2 The Efficient Control of Grading Machine Settings - **M Sandomeer (neé Deublein), J Köhler, P Linsenmann**

Presented by M. Deublein

J. W.G. van de Kuilen asked if machine settings were adjustable what sawmills would do? M. Deublein responded that sawmills should adjust the setting to ensure quality of the product.

P. Quenneville asked if the purpose of the work is intended to ensure reliability of design and would lower quality material be put in lower grade. M. Deublein responded that the work is intended to ensure quality and reliability of grade.

F. Lam commented that the work tested the robustness of the CUSUM process but comparison with the proposed Bayesian process was not done. M. Deublein responded that the process continuously detected shift in properties of the predictor which differed from the CUSUM approach.

F. Rouger commented that machine control system avoids "tricky" behaviour and it is supposed to be safe. If you have a low quality material, machine control system should be able to detect this without the aim of optimization. Bayesian approach depends on the regression approach. This is an interesting concept to fill the gap between machine and output control. M. Deublein said that flexibility to make adjustment is important.

J Köhler commented that this method would have the possibility to change and make adjustments.

4 STRESSES FOR SOLID TIMBER

40 - 6 - 1 Bearing Strength Perpendicular to the Grain of Locally Loaded Timber Blocks - **A J M. Leijten, J C M Schoenmakers**

Presented by A. Leijten

H. Blass commented that the Van de Put model relies on slip lines and is more appropriate for granular material. In timber the failure mode would be very different from the assumed failure mode in the model. A. Leijten discussed equilibrium and redistribution of stresses phenomena that lead to plasticity. He said that failure modes do not need to be exact. H. Blass commented that B. Madsen's results and model were not included in the paper for comparison which is the basis for the EC5 A1 model. The results related to EC5 A1 reported in the paper are not correct and there is a need to discuss this more in detail.

I. Smith commented that Forintek did tests on the two loaded surface case. Although there are lots of theories that are totally wrong but can be applied, he issue is how can one extrapolate the wrong theory to other cases.

H. Larsen commented that Van de Put's work is difficult to understand and one needs to check assumptions. Old EC5 method is 100% empirical. One has to find better ways to predict perpendicular to grain capacity even though there are not too many cases of failure. Also tension perpendicular to grain always takes place which is not accounted for in Van der Put's model.

40 - 6 - 2 Experimental Study of Compression and Shear Strength of Spruce Timber - **M Poussa, P Tukiainen, A Ranta-Maunus**

Presented by A. Ranta-Maunus

H.J. Larsen questioned whether there is an explanation why the shear strength measured by the I-beams and other methods are so different. He does not agree with the suggestion of adopting a constant value of 3.8 MPa for shear stress. He will discuss more independently on the subject with A. Ranta-Maunus. A. Ranta-Maunus responded that there is stress interaction between compression perpendicular to grain and shear in the I-beam tests.

B.J. Yeh commented that in ASTM standard the compression perpendicular to grain strength is determined using 1.0 mm as the limit state. As this paper considers 2.5 mm as the limit state, the values may be quite comparable if 1.0 mm was used as the limit state in this paper.

H.J. Larsen commented that the discussion of shear strength is interesting. True material properties should be considered rather than using experimental method with more complicated stress state. For example in this case the failure always takes place between web and flange which is not realistic. A. Ranta-Maunus responded that there is more motivation to do these types of experiments. In Europe, the tendency is to reduce shear strength because we have seen some related failures. The test materials do not have cracks and cracks due to moisture influence must be determined independently.

S. Thelandersson commented that compression perpendicular to grain strengths have much impact on design. One needs to distinguish serviceability from strength as serviceability governs designs in most cases.

40 - 6 - 3 Analysis of Tension and Bending strength of Graded Spruce Timber - **A Hanhijärvi, A Ranta-Maunus, H Sarkama, M Kohsaku, M Poussa, J Puttonen**

Presented b A. Ranta-Maunus

R. Steiger commented that the fb/ft relationship is similar to the results presented by Steiger in the Florence CIBW18 meeting last year.

A. Jorissen asked why 50 specimens were used to establish the 5th percentile values. A. Ranta-Maunus replied that 100 was also used but showed the results were not sensitive and he clarified coefficients used in equation for size effect.

J. Köhler and A. Ranta-Maunus discussed the point that one could use grading machines values to conduct similar studies.

I. Smith wondered about using the laboratory based test values to establish the floating fb/ft values in relation to the issue of actual structural system. As members may be subjected to combined stresses, one should exercise caution. A. Ranta-Maunus commented in Europe we use 0.6 which is lower than other countries. This seems to be too conservative.

E. Gehri agreed with I. Smith and commented that C40 did not achieve the values based on his test results.

5 TIMBER JOINTS AND FASTENERS

40 - 7 - 1 *Predicting the Strength of Bolted Timber Connections Subjected to Fire* - **M Fragiacomo, A Buchanan, D Carshalton, P Moss, C Austruy**

Presented by M. Fragiacomo

A. Frangi commented that heated tests are completely different from fire test as there are strong temperature and moisture gradients in fire tests. One cannot use material properties to predict fire test results. M. Fragiacomo disagrees as this work is a strong starting point.

S. Thelandersson commented that this work is interesting as it shows it is most critical to keep down the temperature rise in the bolt; therefore, protecting the steel is most important.

J. König commented this presentation deals with 12 mm bolts. This is okay to restrict to this diameter. Steel-Wood-Steel failure in 8 minutes is okay. Temperature of the bolt is 350° C at 8 minutes and the temperature of the interface and wood is the same; therefore, temperature of the bolt is constant. The influence of moisture content is not important here. If there is temperature gradient along the bolt or material then this work does not apply.

H. Blass commented that if charring were observed between the steel plate and wood then Johansen formula in the code would not be valid.

G. Schickhofer received confirmation that the yield moment was measured according to the principles of EN40 (3 versus 4 point in EN 409).

40 - 7 - 2 *Edge Joints with Dowel Type Fasteners in Cross Laminated Timber* - **H J Blaß, T Uibel**

Presented by T. Uibel

I. Smith questioned how to calculate the forces these types of connectors see. T. Uibel said the walls are considered as rigid body and forces are equally distributed to the fasteners and there are no data on creep tests yet. I. Smith asked about why the pull-out tests are conducted at lower load level. T. Uibel answered that the screws loaded parallel to grain of solid timber has low capacity. Capacity under permanent load for these screws would be low, therefore, the chosen low load level.

A. Jorissen received clarification of the density values used in the model.

B.J. Yeh asked if the dowel located at a gap would get lower results. H. Blass answered yes but one would not be sure how large is the difference. Therefore, it was decided not to consider this as individual case but combined the various modes together.

40 - 7 - 3 Design Method against Timber Failure Mechanisms of Dowelled Steel-to-Timber Connections - **A Hanhijärvi, A Kevarinmäki**

Presented by A. Hanhijärvi

H. Blass asked in the new model which conditions would lead to the governing Johansen formula (embedment failure). A. Hanhijärvi said that it only add complication. Embedment failures could be included for the sake of completeness. He also stated that row shear failure was not considered in Annex A of Eurocode 5; therefore, this study is important. H. Blass questioned the factor of two associated with tensile strength and the splitting effects in other rows of dowel. A. Hanhijärvi suggested there is small volume in joint area; therefore, increased factor for tension strength also failure would occur at centre line. P. Quenneville commented that the glulam specimens are all brittle failures. A. Hanhijärvi said that there are no embedment failures even though experiment had different end distances and spacing.

A. Jorissen received confirmation about spacing and end distances per explained in paper. A. Jorissen also commented that the work by H. Johnsson on block shear should have been considered. A. Jorissen and A. Hanhijärvi discussed the differences between this approach and the current Eurocode 5 Annex A approach. A. Hanhijärvi further clarified that the interaction between shear and tension comes from A. Ranta-Maunus presented work of tension and tension failure length,

I. Smith mentioned that UNB students did work with lower quality wood and engineered wood products. He commented this work is good but may not be universal. He wondered how much better the proposed procedure is in terms of a regression relationship. A. Hanhijärvi commented that row shear is considered beyond the current Eurocode.

40 - 7 - 4 A EYM Based Simplified Design Formula for the Load-carrying Capacity of Dowel-type Connections - **M Ballerini**

Presented by M. Ballerini

H. Larsen commented that the exact formulae are easier to use than the proposed simplified ones. M. Ballerini suggested the reliance on computers to use the exact formulae may lead to human errors.

I. Smith asked in terms of rope effect and what type of deformation levels is assumed and suggested that in Canadian approach rope effects were ignored as large deformation are needed to develop it. M. Ballerini said that it depends on different cases. H. Blass stated that rope effect does not require large deformation. H. Larsen added that rope and friction effects are provided by the tension action of the fastener. H. Blass clarified the number 4 in the denominator comes from the friction. H. Larsen concluded that the deformation is there anyway why doesn't one take into account the added capacity due to the deformation regardless one likes the deformation or not.

40 - 7 - 5 Evaluation of the Slip Modulus for Ultimate Limit State Verifications of Timber-Concrete Composite Structures - **E Lukaszewska, M Fragiacomo,A Frangi**

Presented by M. Fragiacomo

H. Blass pointed out that the term non-conservative for the slip modulus is incorrect because non-conservative could mean either too high or too low. M. Fragiacomo agreed and will revise Table 5.

S. Thelandersson questioned how slip modulus compared to stress level between experiment and FEM at ultimate and serviceability limit state. M. Fragiacomo responded that failure loads were not compared which may not be that sensitive.

H. Larsen commented that these stiffness values are confusing and questioned why one doesn't just use the theory of plasticity for the composite beam. M. Fragiacomo responded that the brittleness of some cases show the proposed equations are important.

40 - 7 - 6 Models for the Predictions of the Ductile and Brittle Failure Modes (Parallel-to-Grain) of Timber Rivet Connections - **M Marjerrison, P Quenneville**

Presented by P. Quenneville

E. Gehri questioned about the stiffness of timber rivet connection as the member width is wide and would have considerable moment. He questioned the ductility of the connection in relation to its low moment capacity as the uni-tension capacity is rather large. P. Quenneville said that the moment capacity of these connections is not considered in design.

H. Blass discussed the ductile failure mode. In the timber to timber failure implied limited embedment strength for the steel is considered whereas in Eurocode 5 the embedment strength of steel plate is considered as infinite. H. Blass commented that both loads parallel and perpendicular to grain need to be considered. P. Quenneville agreed.

I. Smith commented that in Saskatchewan one building had connections where over 1000 rivets were used and it carried moment successfully. P. Quenneville discussed that they might have behaved like a punch metal plate.

A. Jorissen received clarification that the Canadian code is on the unsafe side.

V. Rajcic received clarification about current Canadian design procedures with timber rivets.

40 - 7 - 7 Creep of Timber and Timber-Concrete Joints. - **J W G van de Kuilen, A M P G Dias**

Presented by J. W. G. van de Kuilen

V. Rajcic commented that on the concrete timber structure testing and suggested that may be one should consider cyclic loading. J.W. van de Kuilen replied that it would complicate matters.

S. Thelandersson commented about designing for permanent loads and the concept of time averaging of load to predict creep behaviour.

I. Smith asked where are these creep factors used. J.W. van de Kuilen responded that the factors can be used with MOE for both concrete connections and timber.

40 - 7 - 8 Lag Screwed Timber Joints with Timber Side Members- **K Komatsu, S Takino, H Tateishi**

Presented by K. Komatsu

F. Lam asked whether the difference detected between sawn timber and glulam is species effect as connection in glulam is shown to be weaker than the connection in sawn timber. K. Komatsu said that the members are intended for girders. In Japan both types of wood (Douglas fir and Redwood glulam) are recognized and therefore tested. For the Douglas fir

if MOE is high then strength would be high but some low MOE Douglas fir would exhibit low strength. F. Lam commented that the grade of the material would be important and asked if these members were intended for girders why cyclic testing was conducted. K. Komatsu stated that Japan is earthquake important. This may apply to connections in girders.

H. Larsen received confirmation that lags screws were not allowed in Japan but small diameter screw were okay. He received further clarification about allowable strength proposal in AIJ and shank versus screw diameter.

H. Blass commented that the group action factor of 2 to 10 screws shown in diagram should be 1 to 5 screws. K. Komatsu agreed.

6 TIMBER BEAMS

40 - 10 - 1 Extension of EC5 Annex B Formulas for the Design of Timber-concrete Composite Structures - **J Schänzlin, M Fragiacomo**

Presented by J. Schänzlin

A. Ceccotti asked which problems are anticipated with shrinkage of concrete. J. Schänzlin said that bending failure of the timber may be possible. This will depend on span where over 5 m serviceability governs and less than 5 m ultimate limit state governs. A. Ceccotti suggested that one should survey existing concrete timber systems of over 10 years old to see if there are indeed issues as he has not heard of any problem. M. Fragiacomo replies that University of Colorado has experience with a case of 3.5 m span where excessive deformation was encountered.

40 - 10 - 2 Simplified Design Method for Mechanically Jointed Beams - **U A Girhammar**

Presented by U.A. Girhammar

H. Blass commented on the choice of buckling length to come close to exact solution.

A. Frangi questioned the influence of variability of the material properties which is more important than the calculation work. U.A. Girhammar agreed but stated why not use a better method.

7 LAMINATED MEMBERS

40 - 12 - 1 Development of New Constructions of Glulam Beams in Canada - **F Lam, N Mohadevan**

Presented by F. Lam

H. Blass asked how the laminating factors were developed. F. Lam replied that they were obtained via a model calibration procedure where the smaller (0.3 m) beams were used in the calibration and the deeper (0.6 m) confirmed the factors. Also this type of factor was reported by Falk.

J. Köhler asked about the correlation between the tension strength of the laminae and the finger joints considered. F. Lam replied that it was not considered; even though there might be some correlations, the program still gives good results when it was ignored.

40 - 12 - 2 Determination of Modulus of Shear and Elasticity of Glued Laminated Timber and Related Examination - **R Brandner, E Gehri, T Bogensperger, G Schickhofer**

Presented by R. Brandner

H. Blass commented that the factor for one lamination has no meaning and this is only important for beams greater than 600 mm. He asked whether it would be possible to use the mean rather than the 5th percentile. R. Brandner agreed in general but replied that for other markets where thin beams are considered this is also important. This factor is also important for buckling not just lateral torsional buckling.

I. Smith commented that vibration data from UNB can be made available.

40 - 12 - 3 Comparative Examination of Creep of GTL and CLT-Slabs in Bending - **R A Jöbstl, G Schickhofer**

Presented by R. A. Jöbstl

J.W. van de Kuilen asked how constant was the constant climate and what would happen if variable climate was used? R. A. Jöbstl replied that the condition was mostly constant except in one case where the specimen was near the door and there may be some issue. R. A. Jöbstl said that for non-constant climate there is no information about the shear behaviour. There are examples of 19 laminate CLT used in bridge plate behaving well.

40 - 12 - 4 Standard Practice for the Derivation of Design Properties of Structural Glued Laminated Timber in the United States - **T G Williamson, B Yeh**

Presented by T. Williamson

H. Larsen mentioned he was confused by the paper and asked if the test results for thousands of beams tested are available. T. Williamson replied that the results are available in reports.

A. Ranta-Maunus commented that this type of information is needed.

40 - 12 - 5 Creep and Creep-Rupture Behaviour of Structural Composite Lumber Evaluated in Accordance with ASTM D 6815 - **B J Yeh, T G Williamson**

Presented by B.J. Yeh

A. Salenikovich asked whether the LVL were tested on edge or on flat. B.J. Yeh replied that edgewise loading was considered.

H. Blass questioned whether testing at laboratory condition where climate is not controlled would be an issue. B.J. Yeh replied that the moisture content of the specimen after testing was checked to be always less than 16%.

F. Lam commented that the Madison Curve represented clear wood behaviour not lumber. Also 3 months test may not be sufficient to develop full understanding of the material behaviour especially when dealing with a very uniform product such as OSL. Different from lumber, this type of product may pass the 90 days test but it is possible that many can still break suddenly soon after 90 days.

E. Karacabeyli agreed with F. Lam that 90 days may not be enough. Products that nearly pass the test should not be used. He said that loading at 55% of the 5th percentile stress level should not fail any specimen in 30 year. May be one should not expect failure.

B.J. Yeh replied Forintek data was used and the chosen stress level should see failure. The

aim is to protect against the minimal performance.

E. Karacabeyli said that the 2.0 factor comes from lumber with average at approximately 1.6. Creep recovery should be considered in future changes.

A. Hanhijärvi stated that it has been shown that inside the wood moisture gradient can affect the strength. He asked about the type of conditioning with respect to short term and longer term test. These may have influence on composites. Also this can influence creep.

B.J. Yeh replied that the specimens were preconditioned at least 30 days prior to testing. After the 90 days test the product cannot deviate from short term moisture content by more than 2%. Products will be used in unconditioned indoors condition so we are trying to simulate this. Moisture cycle is difficult to perform.

A. Hanhijärvi stated that during erection the material may get wet.

B.J. Yeh replied that in Canada there is a requirement of 3 week soaking and then re-drying to address this issue but it may be too severe and not used in the U.S.

40 - 12 - 6 Bending Strength of Combined Beech-Spruce Glulam - **M Frese, H J Blaß**

Presented by M. Frese

R. Brandner received clarification about the finger joint and the characteristic of the spruce beam as the outer laminations are the most important for bending strength.

A. Frangi asked whether it is possible to substitute with low quality material such as wind damaged wood. M. Frese stated that since the tensile strength of the low quality material is unknown may be it can be used in the middle 20% and check their shear strength. R. Steiger stated that testing of the wind damage material showed that the MOE was not affected but the strength goes down. This work was presented last year in Florence (CIB38-5-1 by Arnold and Steiger). For example for C20 and C40 bending strength is okay but tension strength drops down significantly. One should be careful with structural use of this material.

40 - 12 - 7 Quality Control of Glulam: Shear Tests of Glue Lines - **R Steiger, E Gehri**

Presented by R. Steiger

H. Larsen commented it is interesting that the method is based on certain agreement. Part of the proposed work is based on equilibrium and part based on failure criterion. Interaction between combined stresses can influence failure load. R. Steiger stated that the equilibrium condition is valid also for orthotropic material and there are additional test results from 1930's that the failure criterion is okay. The paper will be updated. H. Larsen commented that this might be academic as the device finds higher stresses or strengths then requirement must be increased accordingly. R. Steiger agreed.

8 TRUSSED RAFTERS

40 - 14 - 1 Timber Trusses with Punched Metal Plate Fasteners - Design for Transport and Erection - **H J Blaß**

Presented by H. Blass

R. Zarnic commented that this work may be applicable to consider out of plane loading of trusses due to earthquakes.

P. Paevere received clarification about controlling factors for long span and for splice joint.

H. Larsen and H. Blass discussed about the applicability of rope model. H. Blass stated

that profiled teeth may perform better and the request for this type of work came from the industry. He has experienced with strong-tie product when the rope factor works well. Here continual movement due to dynamic load was not considered and the work is a rough proposal.

P. Paevere stated he has developed withdrawal test for different reasons.

T. Williamson stated that in U.S. builder tips as guidelines are available although they did not work for all cases.

There were further discussions on consequences of failure caused by damage during transport and erection. H. Blass agreed that sometimes damage cannot be easily detected.

9 STRUCTURAL STABILITY

40 - 15 - 1 Design of Safe Timber Structures – How Can we Learn from Structural Failures? - **S Thelandersson, E Frühwald**

Presented by S. Thelandersson

R. Zarnic supposed suggestion about count of consequence as a requirement and the probability that something will be done should be higher.

U. Kuhlmann stated that Cost action started on this issue of robustness and invite interested to participate. Example includes joint ductility and redistribution of load to account for robustness. S. Thelandersson stated that he is fully aware of the Cost action.

T. Williamson stated that in US the number of statistics will be different. Largest errors are construction. Since the Northridge earthquake, the seismic part of the code has been upgraded. Wind loads have also been upgraded.

I. Smith stated that robustness consideration began in the 60's and 70's. Insurance companies do not differentiate between materials. Design code considers single member rather than system behaviour.

P. Quenneville mentioned that newspaper article on railing failures indicated not due to faulty material.

H. Gehri stated that it is good to hear no failure due to code as the code is for verification of design. There is a need to define robustness, redundancy, and ductility in code. S. Thelandersson agreed.

P. Paevere questioned whether the loads are biased which may give designers a bad name. S. Thelandersson stated one example is failure in Denmark was due to the structure's dead weight. P. Paevere said that earthquakes have not been considered. S. Thelandersson stated that they are not important for N. Europe.

40 - 15 - 2 Effect of Transverse Walls on Capacity of Wood-Framed Wall Diaphragms - Part 2 - **U A Girhammar, B Källsner**

Presented by U.A. Girhammar

F. Lam commented that one should also consider the deformation aspect as it is important in terms of damage and drift demand in earthquake. In particular the claim that one can rely on the transverse walls to replace hold-downs needs to be refined for earthquake applications. U.A. Girhammar replied that this is intended only for monotonic loads and not for earthquakes.

I. Smith stated that test of actual building shows the importance of rigidity of upper and lower floors. He aggress with F. Lam's comment that tie down situation will need to

consider both elastic end as well as plastic end. U.A. Girhammar agreed.

E. Karacabeyli received explanation from U.A. Girhammar of example of when to use fix end and when to use free end. H. Blass commented it would be safe to assume free end in design.

R. Zarnic received explanation from U.A. Girhammar about the test set up boundary condition and the real situation is a combination of both free and fix ends.

N. Chun commented that f1 does not reach fp. Panel closest to one end may fail before the end panel reaches fp. U.A. Girhammar replied that the model already considered this issue.

40 - 15 - 3 Midply Wood Shear Wall System: Concept, Performance and Code Implementation - **Chun Ni, M Popovski, E Karacabeyli, E Varoglu, S Stiemer**

Presented by C. Ni

B. Dujic asked about the end stud detail with respect to the gap. C. Ni replied that the end stud will also need the 3 mm gap.

I. Smith commented that the same increase for both wind and seismic design was suggested. He asked whether one should use the same capacity for both situations. C. Ni replied in Canadian code one does not distinguish these cases in terms of base shear capacities. I. Smith stated that even though this is done in codes, it may not be acceptable and one can't just increase capacity for all situations especially when larger displacements are involved in one case.

A. Ceccotti asked if these walls were anticipated to be used with other walls. C. Ni replied that this could be done if different R factors were used. F. Lam stated that one should be careful when one combines midply with other systems as different systems have different stiffness which can influence the distribution of loads through diaphragm action.

M. Yasumura asked about the hold-downs for standard and midply walls. C. Ni replied that higher capacity hold-downs would be needed.

40 - 15 - 4 Seismic Behaviour of Tall Wood-Frame Walls - **M Popovski, A Peterson, E Karacabeyli**

Presented by M. Popovski

B.J Yeh asked about the 1:1 aspect ratio of the walls as "tall" walls are mostly more slender. M. Popovski clarified that the actual application will involve cases when the walls will be longer so the aspect ratio of "tall" walls will not be an issue. He also explained that the application of the vertical load was applied to the bottom plate rather than the top plate.

A. Salenikovich received clarification of spiral nails versus ring shank nails. M. Popovski stated that spiral nail and common nails were used and there is significant difference between the behaviour of both connections. He also explained 1.7E LSL was used as plates for all walls and different type of studs were considered.

F. Lam asked about the possible influence of wetting and re-drying during construction if LSL was used as stud. M. Popovski said that they do not have information but walls are built with LSL in practice. Expect industry would have data on the subject and perhaps factory manufacturing can avoid the wetting and re-drying issues. F. Lam suggested one to conduct connection tests to check whether this is an issue.

40 - 15 - 5 International Standard Development of Lateral Load Test Method for Shear Walls - **M Yasumura, E Karacabeyli**

Presented by M. Yasumura

B. Dujic asked about the recommendation for the next approach and how many specimens would be needed. I. Smith questioned what would be the implication with respect to design as different test methods lead to different results; i.e., how to interpret the results as designers should not be put in a situation to do the interpretation. M. Yasumura replied that the ISO standards should not be involved in the interpretation of results as this is the responsibility of individual nations. E. Karacabeyli explained that method A is more or less the approach used in most design codes and method B is used in the U.K. as the lower bound.

A. Ceccotti received clarification on Figure 5.

A. Salenikovich commented that this work should be coordinated with ASTM initiatives. He asked about perforated walls. M. Yasumura replied that the perforated walls were not considered but they can be tested in method two where length of specimen becomes an issue and in method 1 where standard length can be used. Method 2 has no limitation on length. A. Salenikovich commented that loading beam stiffness needs consideration. M. Yasumura agreed.

B.J. Yeh commented the ASTM initiative is considering the number of specimens and will share the information. The influence of loading beam is important based on APA experience. The reason why this research did not show a difference may be because vertical load was already applied and the aspect ratio of the walls.

40 - 15 - 6 Influence of Openings on Shear Capacity of Wooden Walls - **B Dujič, S Klobcar, R Žarnić**

Presented by B. Dujič

H. Blass comment that some systems behaved more like frames than shear walls.

G. Schickhofer received clarification on small specimen shear test configuration with respect to Figure 13 as an approach common in masonry structure research. He commented that may be other methods for shear modulus evaluation is more appropriate.

He asked whether the results can be extended to 5 layer plates. B. Dujic replied yes if anchor failures also governs but can't confirm.

B.J. Yeh questioned whether energy dissipation were compared and commented on the issue of end of wall buckling failure under compression. B. Dujic replied that hysteresis loops seemed to indicate narrower loops compared to conventional walls. B.J. Yeh commented that this is more similar to moment frame compared to conventional wall; therefore, different R factors may be warranted.

F. Lam commented that the presence of transverse wall should prevent buckling from happening and therefore would not be an issue. He mentioned that the 1/200 drift limit seems severe as a serviceability requirement compared to N. America. B. Dujic agreed with the transverse wall comment and explained the range of drift limit states considered in Europe.

A. Ceccotti commented R is a little lower than for wood frame.

R. Steiger commented for assessment of stiffness properties modal analysis and NDT methods can be used.

10 FIRE

40 - 16 - 1 Bonded Timber Deck Plates in Fire - **J König, J Schmid**

Presented by J. König

H. Blass asked whether the results are applicable to beams. J. König replied that the results are not applicable to beams therefore beams are okay.

A. Frangi asked if the possibility of char layer falling off was considered in the study. J. König replied that the assumption is that the char layer remains intact. The possibility of char layer falling off would represent complication as temperature increases as char protection level increases provided the char layer stays intact. Char layer falling would mean a bond line issue.

40 - 16 - 2 Design of Timber Frame Floor Assemblies in Fire - **A Frangi, C Erchinger**

Presented by A. Frangi

J. König commented that at the time of drafting of Eurocode 5 narrow cross section was assumed. He discussed the issue of zero strength layer. If one increases the charring model, it would be easier to model the influence of temperature on cross section. He would like to see an expansion of the model to consider 4 sides. A. Frangi agreed that expansion to column where the 4 side issue might be important. He agreed that the zero strength layer not to be fixed but a function of properties.

I. Smith commented that in the structural design side mechanistic calculations are considered too complicated for structural engineers. He wondered whether the same reactions are faced with the fire side. A. Frangi replied one needs only two extra minutes for this type of calculations and it should not be a problem for the design engineers. H. Blass commented the engineers tend to avoid anything new in code until the old version is deemed obsolete.

11 TEST METHODS

40 - 21 - 1 ASTM D198 - Interlaboratory Study for Modulus of Elasticity of Lumber in Bending - **A Salenikovich**

Presented by A. Salenikovich

E. Gehri commented that this shows limitations of our measurements. Even with simple tests 1st two figures may be correct but other figures are not accurate.

I. Smith wondered whether actual MOE are less variable than measured ones and commented that two sided MOE measurement be done.

40 - 21 - 2 New Test Configuration for CLT-Wall-Elements under Shear Load - **T Bogensperger, T Moosbrugger, G Schickhofer**

Presented by T. Bogensperger

H. Blass and T. Bogensperger discussed issues relating the shear strength of glue line versus the shear strength of the material.

R. Zarnic asked about the efficiency of simple model versus the more complicated test method. T. Bogensperger and G. Schickhofer responded the simple one is not wrong with respect to stiffness but there are some issues with respect to strength as shown in the paper; therefore, comparison is not appropriate. R. Zarnic commented that the simple method is

cheaper and would like to see some harmonization of available methods. G. Schickhofer agreed that the more complicated method is expensive and maybe the less expensive method that can yield accurate results is also needed.

There were further discussions and clarifications that the shear strength is in the plane parallel to the element. Rolling shear can occur but not the main mode. The shear locking effect was discussed and geometry of the board with respect to the glue area will have an influence.

B.J. Yeh commented that the overhang can increase shear strength significantly. G. Schickhofer replied that the overhang did not affect the shear strength as the failure mode in bending is in the cross ply.

12 ANY OTHER BUSINESS

A. Frangi suggested the order of presentation be reversed in every two years so that the papers about fire do not need to be presented always on the last day. It was agreed.

R. Zarnic presented information on the possibility of influencing research funding opportunities under the EU COST program for research. He encouraged participants to supply research ideas to ECTP under the strategic research agenda. Information can be obtained from www.ectp.org

13 VENUE AND PROGRAMME FOR NEXT MEETING

The possible meeting venues for next five years are: Canada (2008), Switzerland (2009), New Zealand (2010), Italy (2011), the Netherlands (2012).

I. Smith invites CIB W18 delegate to participate in next year's CIB W18 meeting Aug 25 – 28, 2008 in Canada and provided information about the venue.

P. Quenneville made a presentation on behalf of A. Buchanan to invite the CIB W18 meeting to come to Christchurch New Zealand in 2010.

M. Fragiacomo made a presentation to invite the CIB W18 meeting to come to Sardinia Italy in 2011.

Master copy of the paper with any corrections should be send to R Görlacher at the end of September 2007. Some of the papers will be renumbered. Changes to papers only needed if errors were identified.

Photographs and participant list for 40th CIB W18 and their contact information will be available from the password protected area of the CIB W18 website.

14 CLOSE

The chair thanked the speakers for their presentations and the delegates for their participation. Also thanks were extended to B. Dujic and the host team for their efforts to organize the meeting.

15. List of CIB-W18 Papers, Bled, Slovenia 2007

List of CIB-W18 Papers, Bled, Slovenia 2007

40 - 5 - 1	Development of Grading Rules for Re-Cycled Timber Used in Structural Applications - **K Crews**
40 - 5 - 2	The Efficient Control of Grading Machine Settings - **M Sandomeer, J Köhler, P Linsenmann**
40 - 6 - 1	Bearing Strength Perpendicular to the Grain of Locally Loaded Timber Blocks - **A J M. Leijten, J C M Schoenmakers**
40 - 6 - 2	Experimental Study of Compression and Shear Strength of Spruce Timber - **M Poussa, P Tukiainen, A Ranta-Maunus**
40 - 6 - 3	Analysis of Tension and Bending strength of Graded Spruce Timber - **A Hanhijärvi, A Ranta-Maunus, H Sarkama, M Kohsaku, M Poussa, J Puttonen**
40 - 7 - 1	Predicting the Strength of Bolted Timber Connections Subjected to Fire - **M Fragiacomo, A Buchanan, D Carshalton, P Moss, C Austruy**
40 - 7 - 2	Edge Joints with Dowel Type Fasteners in Cross Laminated Timber - **H J Blaß, T Uibel**
40 - 7 - 3	Design Method against Timber Failure Mechanisms of Dowelled Steel-to-Timber Connections - **A Hanhijärvi, A Kevarinmäki**
40 - 7 - 4	A EYM Based Simplified Design Formula for the Load-carrying Capacity of Dowel-type Connections - **M Ballerini**
40 - 7 - 5	Evaluation of the Slip Modulus for Ultimate Limit State Verifications of Timber-Concrete Composite Structures - **E Lukaszewska, M Fragiacomo, A Frangi**
40 - 7 - 6	Model for the Predictions of the Ductile and Brittle Failure Modes (Parallel-to-Grain) of Timber Rivet Connections - **M Marjerrison, P Quenneville**
40 - 7 - 7	Creep of Timber and Timber-Concrete Joints. - **J W G van de Kuilen, A M P G Dias**
40 - 7 - 8	Lag Screwed Timber Joints with Timber Side Members- **K Komatsu, S Takino, H Tateishi**
40 - 10 - 1	Extension of EC5 Annex B Formulas for the Design of Timber-concrete Composite Structures - **J Schänzlin, M Fragiacomo**
40 - 10 - 2	Simplified Design Method for Mechanically Jointed Beams - **U A Girhammar**
40 - 12 - 1	Development of New Constructions of Glulam Beams in Canada - **F Lam, N Mohadevan**
40 - 12 - 2	Determination of Modulus of Shear and Elasticity of Glued Laminated Timber and Related Examination - **R Brandner, E Gehri, T Bogensperger, G Schickhofer**

16. Current List of CIB-W18(A) Papers

CURRENT LIST OF CIB-W18(A) PAPERS

Technical papers presented to CIB-W18(A) are identified by a code CIB-W18(A)/a-b-c, where:

a denotes the meeting at which the paper was presented. Meetings are classified in chronological order:

1 Princes Risborough, England; March 1973
2 Copenhagen, Denmark; October 1973
3 Delft, Netherlands; June 1974
4 Paris, France; February 1975
5 Karlsruhe, Federal Republic of Germany; October 1975
6 Aalborg, Denmark; June 1976
7 Stockholm, Sweden; February/March 1977
8 Brussels, Belgium; October 1977
9 Perth, Scotland; June 1978
10 Vancouver, Canada; August 1978
11 Vienna, Austria; March 1979
12 Bordeaux, France; October 1979
13 Otaniemi, Finland; June 1980
14 Warsaw, Poland; May 1981
15 Karlsruhe, Federal Republic of Germany; June 1982
16 Lillehammer, Norway; May/June 1983
17 Rapperswil, Switzerland; May 1984
18 Beit Oren, Israel; June 1985
19 Florence, Italy; September 1986
20 Dublin, Ireland; September 1987
21 Parksville, Canada; September 1988
22 Berlin, German Democratic Republic; September 1989
23 Lisbon, Portugal; September 1990
24 Oxford, United Kingdom; September 1991
25 Åhus, Sweden; August 1992
26 Athens, USA; August 1993
27 Sydney, Australia; July 1994
28 Copenhagen, Denmark; April 1995
29 Bordeaux, France; August 1996
30 Vancouver, Canada; August 1997
31 Savonlinna, Finland; August 1998
32 Graz, Austria, August 1999
33 Delft, The Netherlands; August 2000
34 Venice, Italy; August 2001
35 Kyoto, Japan; September 2002
36 Colorado, USA; August 2003
37 Edinburgh, Scotland, August 2004
38 Karlsruhe, Germany, August 2005
39 Florence, Italy, August 2006
40 Bled, Slovenia, August 2007

b denotes the subject:

1 Limit State Design
2 Timber Columns
3 Symbols
4 Plywood
5 Stress Grading
6 Stresses for Solid Timber
7 Timber Joints and Fasteners
8 Load Sharing
9 Duration of Load
10 Timber Beams
11 Environmental Conditions
12 Laminated Members
13 Particle and Fibre Building Boards
14 Trussed Rafters
15 Structural Stability
16 Fire
17 Statistics and Data Analysis
18 Glued Joints
19 Fracture Mechanics
20 Serviceability
21 Test Methods
100 CIB Timber Code
101 Loading Codes
102 Structural Design Codes
103 International Standards Organisation
104 Joint Committee on Structural Safety
105 CIB Programme, Policy and Meetings
106 International Union of Forestry Research Organisations

c is simply a number given to the papers in the order in which they appear:

Example: CIB-W18/4-102-5 refers to paper 5 on subject 102 presented at the fourth meeting of W18.

Listed below, by subjects, are all papers that have to date been presented to W18. When appropriate some papers are listed under more than one subject heading.

LIMIT STATE DESIGN

1-1-1	Limit State Design - H J Larsen
1-1-2	The Use of Partial Safety Factors in the New Norwegian Design Code for Timber Structures - O Brynildsen
1-1-3	Swedish Code Revision Concerning Timber Structures - B Noren
1-1-4	Working Stresses Report to British Standards Institution Committee BLCP/17/2
6-1-1	On the Application of the Uncertainty Theoretical Methods for the Definition of the Fundamental Concepts of Structural Safety - K Skov and O Ditlevsen
11-1-1	Safety Design of Timber Structures - H J Larsen
18-1-1	Notes on the Development of a UK Limit States Design Code for Timber - A R Fewell and C B Pierce
18-1-2	Eurocode 5, Timber Structures - H J Larsen
19-1-1	Duration of Load Effects and Reliability Based Design (Single Member) - R O Foschi and Z C Yao
21-102-1	Research Activities Towards a New GDR Timber Design Code Based on Limit States Design - W Rug and M Badstube
22-1-1	Reliability-Theoretical Investigation into Timber Components Proposal for a Supplement of the Design Concept - M Badstube, W Rug and R Plessow
23-1-1	Some Remarks about the Safety of Timber Structures - J Kuipers
23-1-2	Reliability of Wood Structural Elements: A Probabilistic Method to Eurocode 5 Calibration - F Rouger, N Lheritier, P Racher and M Fogli
31-1-1	A Limit States Design Approach to Timber Framed Walls - C J Mettem, R Bainbridge and J A Gordon
32 -1-1	Determination of Partial Coefficients and Modification Factors- H J Larsen, S Svensson and S Thelandersson
32 -1-2	Design by Testing of Structural Timber Components - V Enjily and L Whale
33-1-1	Aspects on Reliability Calibration of Safety Factors for Timber Structures – S Svensson and S Thelandersson
33-1-2	Sensitivity studies on the reliability of timber structures – A Ranta-Maunus, M Fonselius, J Kurkela and T Toratti

TIMBER COLUMNS

2-2-1	The Design of Solid Timber Columns - H J Larsen
3-2-1	The Design of Built-Up Timber Columns - H J Larsen
4-2-1	Tests with Centrally Loaded Timber Columns - H J Larsen and S S Pedersen
4-2-2	Lateral-Torsional Buckling of Eccentrically Loaded Timber Columns- B Johansson
5-9-1	Strength of a Wood Column in Combined Compression and Bending with Respect to Creep - B Källsner and B Norén
5-100-1	Design of Solid Timber Columns (First Draft) - H J Larsen
6-100-1	Comments on Document 5-100-1, Design of Solid Timber Columns - H J Larsen and E Theilgaard
6-2-1	Lattice Columns - H J Larsen
6-2-2	A Mathematical Basis for Design Aids for Timber Columns - H J Burgess
6-2-3	Comparison of Larsen and Perry Formulas for Solid Timber Columns- H J Burgess

7-2-1	Lateral Bracing of Timber Struts - J A Simon
8-15-1	Laterally Loaded Timber Columns: Tests and Theory - H J Larsen
17-2-1	Model for Timber Strength under Axial Load and Moment - T Poutanen
18-2-1	Column Design Methods for Timber Engineering - A H Buchanan, K C Johns, B Madsen
19-2-1	Creep Buckling Strength of Timber Beams and Columns - R H Leicester
19-12-2	Strength Model for Glulam Columns - H J Blaß
20-2-1	Lateral Buckling Theory for Rectangular Section Deep Beam-Columns- H J Burgess
20-2-2	Design of Timber Columns - H J Blaß
21-2-1	Format for Buckling Strength - R H Leicester
21-2-2	Beam-Column Formulae for Design Codes - R H Leicester
21-15-1	Rectangular Section Deep Beam - Columns with Continuous Lateral Restraint - H J Burgess
21-15-2	Buckling Modes and Permissible Axial Loads for Continuously Braced Columns - H J Burgess
21-15-3	Simple Approaches for Column Bracing Calculations - H J Burgess
21-15-4	Calculations for Discrete Column Restraints - H J Burgess
22-2-1	Buckling and Reliability Checking of Timber Columns - S Huang, P M Yu and J Y Hong
22-2-2	Proposal for the Design of Compressed Timber Members by Adopting the Second-Order Stress Theory - P Kaiser
30-2-1	Beam-Column Formula for Specific Truss Applications - W Lau, F Lam and J D Barrett
31-2-1	Deformation and Stability of Columns of Viscoelastic Material Wood - P Becker and K Rautenstrauch
34-2-1	Long-Term Experiments with Columns: Results and Possible Consequences on Column Design – W Moorkamp, W Schelling, P Becker, K Rautenstrauch
34-2-2	Proposal for Compressive Member Design Based on Long-Term Simulation Studies – P Becker, K Rautenstrauch
35-2-1	Computer Simulations on the Reliability of Timber Columns Regarding Hygrothermal Effects- R Hartnack, K-U Schober, K Rautenstrauch
36-2-1	The Reliability of Timber Columns Based on Stochastical Principles - K Rautenstrauch, R Hartnack
38-2-1	Long-term Load Bearing of Wooden Columns Influenced by Climate – View on Code - R Hartnack, K Rautenstrauch

SYMBOLS

3-3-1	Symbols for Structural Timber Design - J Kuipers and B Norén
4-3-1	Symbols for Timber Structure Design - J Kuipers and B Norén
28-3-1	Symbols for Timber and Wood-Based Materials - J Kuipers and B Noren
1	Symbols for Use in Structural Timber Design

PLYWOOD

2-4-1	The Presentation of Structural Design Data for Plywood - L G Booth

3-4-1	Standard Methods of Testing for the Determination of Mechanical Properties of Plywood - J Kuipers
3-4-2	Bending Strength and Stiffness of Multiple Species Plywood - C K A Stieda
4-4-4	Standard Methods of Testing for the Determination of Mechanical Properties of Plywood - Council of Forest Industries, B.C.
5-4-1	The Determination of Design Stresses for Plywood in the Revision of CP 112 - L G Booth
5-4-2	Veneer Plywood for Construction - Quality Specifications - ISO/TC 139. Plywood, Working Group 6
6-4-1	The Determination of the Mechanical Properties of Plywood Containing Defects - L G Booth
6-4-2	Comparsion of the Size and Type of Specimen and Type of Test on Plywood Bending Strength and Stiffness - C R Wilson and P Eng
6-4-3	Buckling Strength of Plywood: Results of Tests and Recommendations for Calculations - J Kuipers and H Ploos van Amstel
7-4-1	Methods of Test for the Determination of Mechanical Properties of Plywood - L G Booth, J Kuipers, B Norén, C R Wilson
7-4-2	Comments Received on Paper 7-4-1
7-4-3	The Effect of Rate of Testing Speed on the Ultimate Tensile Stress of Plywood - C R Wilson and A V Parasin
7-4-4	Comparison of the Effect of Specimen Size on the Flexural Properties of Plywood Using the Pure Moment Test - C R Wilson and A V Parasin
8-4-1	Sampling Plywood and the Evaluation of Test Results - B Norén
9-4-1	Shear and Torsional Rigidity of Plywood - H J Larsen
9-4-2	The Evaluation of Test Data on the Strength Properties of Plywood - L G Booth
9-4-3	The Sampling of Plywood and the Derivation of Strength Values (Second Draft) - B Norén
9-4-4	On the Use of the CIB/RILEM Plywood Plate Twisting Test: a progress report - L G Booth
10-4-1	Buckling Strength of Plywood - J Dekker, J Kuipers and H Ploos van Amstel
11-4-1	Analysis of Plywood Stressed Skin Panels with Rigid or Semi-Rigid Connections- I Smith
11-4-2	A Comparison of Plywood Modulus of Rigidity Determined by the ASTM and RILEM CIB/3-TT Test Methods - C R Wilson and A V Parasin
11-4-3	Sampling of Plywood for Testing Strength - B Norén
12-4-1	Procedures for Analysis of Plywood Test Data and Determination of Characteristic Values Suitable for Code Presentation - C R Wilson
14-4-1	An Introduction to Performance Standards for Wood-base Panel Products - D H Brown
14-4-2	Proposal for Presenting Data on the Properties of Structural Panels - T Schmidt
16-4-1	Planar Shear Capacity of Plywood in Bending - C K A Stieda
17-4-1	Determination of Panel Shear Strength and Panel Shear Modulus of Beech-Plywood in Structural Sizes - J Ehlbeck and F Colling
17-4-2	Ultimate Strength of Plywood Webs - R H Leicester and L Pham
20-4-1	Considerations of Reliability - Based Design for Structural Composite Products - M R O'Halloran, J A Johnson, E G Elias and T P Cunningham

21-4-1 Modelling for Prediction of Strength of Veneer Having Knots - Y Hirashima

22-4-1 Scientific Research into Plywood and Plywood Building Constructions the Results and Findings of which are Incorporated into Construction Standard Specifications of the USSR - I M Guskov

22-4-2 Evaluation of Characteristic values for Wood-Based Sheet Materials - E G Elias

24-4-1 APA Structural-Use Design Values: An Update to Panel Design Capacities - A L Kuchar, E G Elias, B Yeh and M R O'Halloran

STRESS GRADING

1-5-1 Quality Specifications for Sawn Timber and Precision Timber - Norwegian Standard NS 3080

1-5-2 Specification for Timber Grades for Structural Use - British Standard BS 4978

4-5-1 Draft Proposal for an International Standard for Stress Grading Coniferous Sawn Softwood - ECE Timber Committee

16-5-1 Grading Errors in Practice - B Thunell

16-5-2 On the Effect of Measurement Errors when Grading Structural Timber- L Nordberg and B Thunell

19-5-1 Stress-Grading by ECE Standards of Italian-Grown Douglas-Fir Dimension Lumber from Young Thinnings - L Uzielli

19-5-2 Structural Softwood from Afforestation Regions in Western Norway - R Lackner

21-5-1 Non-Destructive Test by Frequency of Full Size Timber for Grading - T Nakai

22-5-1 Fundamental Vibration Frequency as a Parameter for Grading Sawn Timber - T Nakai, T Tanaka and H Nagao

24-5-1 Influence of Stress Grading System on Length Effect Factors for Lumber Loaded in Compression - A Campos and I Smith

26-5-1 Structural Properties of French Grown Timber According to Various Grading Methods - F Rouger, C De Lafond and A El Quadrani

28-5-1 Grading Methods for Structural Timber - Principles for Approval - S Ohlsson

28-5-2 Relationship of Moduli of Elasticity in Tension and in Bending of Solid Timber - N Burger and P Glos

29-5-1 The Effect of Edge Knots on the Strength of SPF MSR Lumber - T Courchene, F Lam and J D Barrett

29-5-2 Determination of Moment Configuration Factors using Grading Machine Readings - T D G Canisius and T Isaksson

31-5-1 Influence of Varying Growth Characteristics on Stiffness Grading of Structural Timber - S Ormarsson, H Petersson, O Dahlblom and K Persson

31-5-2 A Comparison of In-Grade Test Procedures - R H Leicester, H Breitinger and H Fordham

32-5-1 Actual Possibilities of the Machine Grading of Timber - K Frühwald and A Bernasconi

32-5-2 Detection of Severe Timber Defects by Machine Grading - A Bernasconi, L Boström and B Schacht

34-5-1 Influence of Proof Loading on the Reliability of Members – F Lam, S Abayakoon, S Svensson, C Gyamfi

36-5-1 Settings for Strength Grading Machines – Evaluation of the Procedure according to prEN 14081, part 2 - C Bengtsson, M Fonselius

36-5-2 A Probabilistic Approach to Cost Optimal Timber Grading - J Köhler, M H Faber

36-7-11 Reliability of Timber Structures, Theory and Dowel-Type Connection Failures - A Ranta-Maunus, A Kevarinmäki

38-5-1 Are Wind-Induced Compression Failures Grading Relevant - M Arnold, R Steiger

39-5-1 A Discussion on the Control of Grading Machine Settings – Current Approach, Potential and Outlook - J Köhler, R Steiger

39-5-2 Tensile Proof Loading to Assure Quality of Finger-Jointed Structural timber - R Katzengruber, G Jeitler, G Schickhofer

40-5-1 Development of Grading Rules for Re-Cycled Timber Used in Structural Applications - K Crews

40-5-2 The Efficient Control of Grading Machine Settings - M Sandomeer, J Köhler, P Linsenmann

STRESSES FOR SOLID TIMBER

4-6-1 Derivation of Grade Stresses for Timber in the UK - W T Curry

5-6-1 Standard Methods of Test for Determining some Physical and Mechanical Properties of Timber in Structural Sizes - W T Curry

5-6-2 The Description of Timber Strength Data - J R Tory

5-6-3 Stresses for EC1 and EC2 Stress Grades - J R Tory

6-6-1 Standard Methods of Test for the Determination of some Physical and Mechanical Properties of Timber in Structural Sizes (third draft) - W T Curry

7-6-1 Strength and Long-term Behaviour of Lumber and Glued Laminated Timber under Torsion Loads - K Möhler

9-6-1 Classification of Structural Timber - H J Larsen

9-6-2 Code Rules for Tension Perpendicular to Grain - H J Larsen

9-6-3 Tension at an Angle to the Grain - K Möhler

9-6-4 Consideration of Combined Stresses for Lumber and Glued Laminated Timber - K Möhler

11-6-1 Evaluation of Lumber Properties in the United States - W L Galligan and J H Haskell

11-6-2 Stresses Perpendicular to Grain - K Möhler

11-6-3 Consideration of Combined Stresses for Lumber and Glued Laminated Timber (addition to Paper CIB-W18/9-6-4) - K Möhler

12-6-1 Strength Classifications for Timber Engineering Codes - R H Leicester and W G Keating

12-6-2 Strength Classes for British Standard BS 5268 - J R Tory

13-6-1 Strength Classes for the CIB Code - J R Tory

13-6-2 Consideration of Size Effects and Longitudinal Shear Strength for Uncracked Beams - R O Foschi and J D Barrett

13-6-3 Consideration of Shear Strength on End-Cracked Beams - J D Barrett and R O Foschi

15-6-1 Characteristic Strength Values for the ECE Standard for Timber - J G Sunley

16-6-1 Size Factors for Timber Bending and Tension Stresses - A R Fewell

16-6-2 Strength Classes for International Codes - A R Fewell and J G Sunley

17-6-1 The Determination of Grade Stresses from Characteristic Stresses for BS 5268: Part 2 - A R Fewell

17-6-2	The Determination of Softwood Strength Properties for Grades, Strength Classes and Laminated Timber for BS 5268: Part 2 - A R Fewell
18-6-1	Comment on Papers: 18-6-2 and 18-6-3 - R H Leicester
18-6-2	Configuration Factors for the Bending Strength of Timber - R H Leicester
18-6-3	Notes on Sampling Factors for Characteristic Values - R H Leicester
18-6-4	Size Effects in Timber Explained by a Modified Weakest Link Theory- B Madsen and A H Buchanan
18-6-5	Placement and Selection of Growth Defects in Test Specimens - H Riberholt
18-6-6	Partial Safety-Coefficients for the Load-Carrying Capacity of Timber Structures - B Norén and J-0 Nylander
19-6-1	Effect of Age and/or Load on Timber Strength - J Kuipers
19-6-2	Confidence in Estimates of Characteristic Values - R H Leicester
19-6-3	Fracture Toughness of Wood - Mode I - K Wright and M Fonselius
19-6-4	Fracture Toughness of Pine - Mode II - K Wright
19-6-5	Drying Stresses in Round Timber - A Ranta-Maunus
19-6-6	A Dynamic Method for Determining Elastic Properties of Wood - R Görlacher
20-6-1	A Comparative Investigation of the Engineering Properties of "Whitewoods" Imported to Israel from Various Origins - U Korin
20-6-2	Effects of Yield Class, Tree Section, Forest and Size on Strength of Home Grown Sitka Spruce - V Picardo
20-6-3	Determination of Shear Strength and Strength Perpendicular to Grain - H J Larsen
21-6-1	Draft Australian Standard: Methods for Evaluation of Strength and Stiffness of Graded Timber - R H Leicester
21-6-2	The Determination of Characteristic Strength Values for Stress Grades of Structural Timber. Part 1 - A R Fewell and P Glos
21-6-3	Shear Strength in Bending of Timber - U Korin
22-6-1	Size Effects and Property Relationships for Canadian 2-inch Dimension Lumber - J D Barrett and H Griffin
22-6-2	Moisture Content Adjustements for In-Grade Data - J D Barrett and W Lau
22-6-3	A Discussion of Lumber Property Relationships in Eurocode 5 - D W Green and D E Kretschmann
22-6-4	Effect of Wood Preservatives on the Strength Properties of Wood - F Ronai
23-6-1	Timber in Compression Perpendicular to Grain - U Korin
24-6-1	Discussion of the Failure Criterion for Combined Bending and Compression - T A C M van der Put
24-6-3	Effect of Within Member Variability on Bending Strength of Structural Timber - I Czmoch, S Thelandersson and H J Larsen
24-6-4	Protection of Structural Timber Against Fungal Attack Requirements and Testing- K Jaworska, M Rylko and W Nozynski
24-6-5	Derivation of the Characteristic Bending Strength of Solid Timber According to CEN-Document prEN 384 - A J M Leijten
25-6-1	Moment Configuration Factors for Simple Beams- T D G Canisius
25-6-3	Bearing Capacity of Timber - U Korin
25-6-4	On Design Criteria for Tension Perpendicular to Grain - H Petersson

25-6-5	Size Effects in Visually Graded Softwood Structural Lumber - J D Barrett, F Lam and W Lau
26-6-1	Discussion and Proposal of a General Failure Criterion for Wood - T A C M van der Put
27-6-1	Development of the "Critical Bearing": Design Clause in CSA-086.1 - C Lum and E Karacabeyli
27-6-2	Size Effects in Timber: Novelty Never Ends - F Rouger and T Fewell
27-6-3	Comparison of Full-Size Sugi (Cryptomeria japonica D.Don) Structural Performance in Bending of Round Timber, Two Surfaces Sawn Timber and Square Sawn Timber - T Nakai, H Nagao and T Tanaka
28-6-1	Shear Strength of Canadian Softwood Structural Lumber - F Lam, H Yee and J D Barrett
28-6-2	Shear Strength of Douglas Fir Timbers - B Madsen
28-6-3	On the Influence of the Loading Head Profiles on Determined Bending Strength - L Muszyñsky and R Szukala
28-6-4	Effect of Test Standard, Length and Load Configuration on Bending Strength of Structural Timber- T Isaksson and S Thelandersson
28-6-5	Grading Machine Readings and their Use in the Calculation of Moment Configuration Factors - T Canisius, T Isaksson and S Thelandersson
28-6-6	End Conditions for Tension Testing of Solid Timber Perpendicular to Grain - T Canisius
29-6-1	Effect of Size on Tensile Strength of Timber - N Burger and P Glos
29-6-2	Equivalence of In-Grade Testing Standards - R H Leicester, H O Breitinger and H F Fordham
30-6-1	Strength Relationships in Structural Timber Subjected to Bending and Tension - N Burger and P Glos
30-6-2	Characteristic Design Stresses in Tension for Radiata Pine Grown in Canterbury - A Tsehaye, J C F Walker and A H Buchanan
30-6-3	Timber as a Natural Composite: Explanation of Some Peculiarities in the Mechanical Behaviour - E Gehri
31-6-1	Length and Moment Configuration Factors - T Isaksson
31-6-2	Tensile Strength Perpendicular to Grain According to EN 1193 - H J Blaß and M Schmid
31-6-3	Strength of Small Diameter Round Timber - A Ranta-Maunus, U Saarelainen and H Boren
31-6-4	Compression Strength Perpendicular to Grain of Structural Timber and Glulam - L Damkilde, P Hoffmeyer and T N Pedersen
31-6-5	Bearing Strength of Timber Beams - R H Leicester, H Fordham and H Breitinger
32-6-1	Development of High-Resistance Glued Robinia Products and an Attempt to Assign Such Products to the European System of Strength Classes - G Schickhofer and B Obermayr
32-6-2	Length and Load Configuration Effects in the Code Format - T Isaksson
32-6-3	Length Effect on the Tensile Strength of Truss Chord Members - F Lam
32-6-4	Tensile Strength Perpendicular to Grain of Glued Laminated Timber - H J Blaß and M Schmid
32-6-5	On the Reliability-based Strength Adjustment Factors for Timber Design - T D G Canisius

34-6-1 Material Strength Properties for Canadian Species Used in Japanese Post and Beam Construction - J D Barrett, F Lam, S Nakajima

35-6-1 Evaluation of Different Size Effect Models for Tension Perpendicular to Grain Design - S Aicher, G Dill-Langer

35-6-2 Tensile Strength of Glulam Perpendicular to Grain - Effects of Moisture Gradients - J Jönsson, S Thelandersson

36-6-1 Characteristic Shear Strength Values Based on Tests According to EN 1193 - P Glos, J Denzler

37-6-1 Tensile Strength of Nordic Birch - K H Solli

37-6-2 Effect of Test Piece Orientation on Characteristic Bending Strength of Structural Timber - P Glos, J K Denzler

37-6-3 Strength and Stiffness Behaviour of Beech Laminations for High Strength Glulam - P Glos, J K Denzler, P W Linsenmann

37-6-4 A Review of Existing Standards Related to Calculation of Characteristic Values of Timber - F Rouger

37-6-5 Influence of the Rolling-Shear Modulus on the Strength and Stiffness of Structural Bonded Timber Elements - P Fellmoser, H J Blass

38-6-1 Design Specifications for Notched Beams in AS:1720 - R H Leicester

38-6-2 Characteristic Bending Strength of Beech Glulam - H J Blaß, M Frese

38-6-3 Shear Strength of Glued Laminated Timber - H Klapp, H Brüninghoff

39-6-1 Allocation of Central European hardwoods into EN 1912 - P Glos, J K Denzler

39-6-2 Revisiting EN 338 and EN 384 Basics and Procedures - R Steiger, M Arnold, M Fontana

40-6-1 Bearing Strength Perpendicular to the Grain of Locally Loaded Timber Blocks - A J M Leijten, J C M Schoenmakers

40-6-2 Experimental Study of Compression and Shear Strength of Spruce Timber - M Poussa, P Tukiainen, A Ranta-Maunus

40-6-3 Analysis of Tension and Bending strength of Graded Spruce Timber - A Hanhijärvi, A Ranta-Maunus, H Sarkama, M Kohsaku, M Poussa, J Puttonen

TIMBER JOINTS AND FASTENERS

1-7-1 Mechanical Fasteners and Fastenings in Timber Structures - E G Stern

4-7-1 Proposal for a Basic Test Method for the Evaluation of Structural Timber Joints with Mechanical Fasteners and Connectors - RILEM 3TT Committee

4-7-2 Test Methods for Wood Fasteners - K Möhler

5-7-1 Influence of Loading Procedure on Strength and Slip-Behaviour in Testing Timber Joints - K Möhler

5-7-2 Recommendations for Testing Methods for Joints with Mechanical Fasteners and Connectors in Load-Bearing Timber Structures - RILEM 3 TT Committee

5-7-3 CIB-Recommendations for the Evaluation of Results of Tests on Joints with Mechanical Fasteners and Connectors used in Load-Bearing Timber Structures - J Kuipers

6-7-1 Recommendations for Testing Methods for Joints with Mechanical Fasteners and Connectors in Load-Bearing Timber Structures (seventh draft) - RILEM 3 TT Committee

6-7-2 Proposal for Testing Integral Nail Plates as Timber Joints - K Möhler

6-7-3 Rules for Evaluation of Values of Strength and Deformation from Test Results - Mechanical Timber Joints - M Johansen, J Kuipers, B Norén

6-7-4	Comments to Rules for Testing Timber Joints and Derivation of Characteristic Values for Rigidity and Strength - B Norén
7-7-1	Testing of Integral Nail Plates as Timber Joints - K Möhler
7-7-2	Long Duration Tests on Timber Joints - J Kuipers
7-7-3	Tests with Mechanically Jointed Beams with a Varying Spacing of Fasteners - K Möhler
7-100-1	CIB-Timber Code Chapter 5.3 Mechanical Fasteners;CIB-Timber Standard 06 and 07 - H J Larsen
9-7-1	Design of Truss Plate Joints - F J Keenan
9-7-2	Staples - K Möhler
11-7-1	A Draft Proposal for International Standard: ISO Document ISO/TC 165N 38E
12-7-1	Load-Carrying Capacity and Deformation Characteristics of Nailed Joints - J Ehlbeck
12-7-2	Design of Bolted Joints - H J Larsen
12-7-3	Design of Joints with Nail Plates - B Norén
13-7-1	Polish Standard BN-80/7159-04: Parts 00-01-02-03-04-05. "Structures from Wood and Wood-based Materials. Methods of Test and Strength Criteria for Joints with Mechanical Fasteners"
13-7-2	Investigation of the Effect of Number of Nails in a Joint on its Load Carrying Ability - W Nozynski
13-7-3	International Acceptance of Manufacture, Marking and Control of Finger-jointed Structural Timber - B Norén
13-7-4	Design of Joints with Nail Plates - Calculation of Slip - B Norén
13-7-5	Design of Joints with Nail Plates - The Heel Joint - B Källsner
13-7-6	Nail Deflection Data for Design - H J Burgess
13-7-7	Test on Bolted Joints - P Vermeyden
13-7-8	Comments to paper CIB-W18/12-7-3 "Design of Joints with Nail Plates"- B Norén
13-7-9	Strength of Finger Joints - H J Larsen
13-100-4	CIB Structural Timber Design Code. Proposal for Section 6.1.5 Nail Plates - N I Bovim
14-7-1	Design of Joints with Nail Plates (second edition) - B Norén
14-7-2	Method of Testing Nails in Wood (second draft, August 1980) - B Norén
14-7-3	Load-Slip Relationship of Nailed Joints - J Ehlbeck and H J Larsen
14-7-4	Wood Failure in Joints with Nail Plates - B Norén
14-7-5	The Effect of Support Eccentricity on the Design of W- and WW-Trussed with Nail Plate Connectors - B Källsner
14-7-6	Derivation of the Allowable Load in Case of Nail Plate Joints Perpendicular to Grain - K Möhler
14-7-7	Comments on CIB-W18/14-7-1 - T A C M van der Put
15-7-1	Final Recommendation TT-1A: Testing Methods for Joints with Mechanical Fasteners in Load-Bearing Timber Structures. Annex A Punched Metal Plate Fasteners - Joint Committee RILEM/CIB-3TT
16-7-1	Load Carrying Capacity of Dowels - E Gehri
16-7-2	Bolted Timber Joints: A Literature Survey - N Harding

16-7-3 Bolted Timber Joints: Practical Aspects of Construction and Design; a Survey - N Harding

16-7-4 Bolted Timber Joints: Draft Experimental Work Plan - Building Research Association of New Zealand

17-7-1 Mechanical Properties of Nails and their Influence on Mechanical Properties of Nailed Timber Joints Subjected to Lateral Loads - I Smith, L R J Whale, C Anderson and L Held

17-7-2 Notes on the Effective Number of Dowels and Nails in Timber Joints - G Steck

18-7-1 Model Specification for Driven Fasteners for Assembly of Pallets and Related Structures - E G Stern and W B Wallin

18-7-2 The Influence of the Orientation of Mechanical Joints on their Mechanical Properties - I Smith and L R J Whale

18-7-3 Influence of Number of Rows of Fasteners or Connectors upon the Ultimate Capacity of Axially Loaded Timber Joints - I Smith and G Steck

18-7-4 A Detailed Testing Method for Nailplate Joints - J Kangas

18-7-5 Principles for Design Values of Nailplates in Finland - J Kangas

18-7-6 The Strength of Nailplates - N I Bovim and E Aasheim

19-7-1 Behaviour of Nailed and Bolted Joints under Short-Term Lateral Load - Conclusions from Some Recent Research - L R J Whale, I Smith and B O Hilson

19-7-2 Glued Bolts in Glulam - H Riberholt

19-7-3 Effectiveness of Multiple Fastener Joints According to National Codes and Eurocode 5 (Draft) - G Steck

19-7-4 The Prediction of the Long-Term Load Carrying Capacity of Joints in Wood Structures - Y M Ivanov and Y Y Slavic

19-7-5 Slip in Joints under Long-Term Loading - T Feldborg and M Johansen

19-7-6 The Derivation of Design Clauses for Nailed and Bolted Joints in Eurocode 5 - L R J Whale and I Smith

19-7-7 Design of Joints with Nail Plates - Principles - B Norén

19-7-8 Shear Tests for Nail Plates - B Norén

19-7-9 Advances in Technology of Joints for Laminated Timber - Analyses of the Structural Behaviour - M Piazza and G Turrini

19-15-1 Connections Deformability in Timber Structures: A Theoretical Evaluation of its Influence on Seismic Effects - A Ceccotti and A Vignoli

20-7-1 Design of Nailed and Bolted Joints-Proposals for the Revision of Existing Formulae in Draft Eurocode 5 and the CIB Code - L R J Whale, I Smith and H J Larsen

20-7-2 Slip in Joints under Long Term Loading - T Feldborg and M Johansen

20-7-3 Ultimate Properties of Bolted Joints in Glued-Laminated Timber - M Yasumura, T Murota and H Sakai

20-7-4 Modelling the Load-Deformation Behaviour of Connections with Pin-Type Fasteners under Combined Moment, Thrust and Shear Forces - I Smith

21-7-1 Nails under Long-Term Withdrawal Loading - T Feldborg and M Johansen

21-7-2 Glued Bolts in Glulam-Proposals for CIB Code - H Riberholt

21-7-3 Nail Plate Joint Behaviour under Shear Loading - T Poutanen

21-7-4 Design of Joints with Laterally Loaded Dowels. Proposals for Improving the Design Rules in the CIB Code and the Draft Eurocode 5 - J Ehlbeck and H Werner

21-7-5	Axially Loaded Nails: Proposals for a Supplement to the CIB Code - J Ehlbeck and W Siebert
22-7-1	End Grain Connections with Laterally Loaded Steel Bolts A draft proposal for design rules in the CIB Code - J Ehlbeck and M Gerold
22-7-2	Determination of Perpendicular-to-Grain Tensile Stresses in Joints with Dowel-Type Fasteners - A draft proposal for design rules - J Ehlbeck, R Görlacher and H Werner
22-7-3	Design of Double-Shear Joints with Non-Metallic Dowels A proposal for a supplement of the design concept - J Ehlbeck and O Eberhart
22-7-4	The Effect of Load on Strength of Timber Joints at high Working Load Level - A J M Leijten
22-7-5	Plasticity Requirements for Portal Frame Corners - R Gunnewijk and A J M Leijten
22-7-6	Background Information on Design of Glulam Rivet Connections in CSA/CAN3-086.1-M89 - A proposal for a supplement of the design concept - E Karacabeyli and D P Janssens
22-7-7	Mechanical Properties of Joints in Glued-Laminated Beams under Reversed Cyclic Loading - M Yasumura
22-7-8	Strength of Glued Lap Timber Joints - P Glos and H Horstmann
22-7-9	Toothed Rings Type Bistyp 075 at the Joints of Fir Wood - J Kerste
22-7-10	Calculation of Joints and Fastenings as Compared with the International State - K Zimmer and K Lissner
22-7-11	Joints on Glued-in Steel Bars Present Relatively New and Progressive Solution in Terms of Timber Structure Design - G N Zubarev, F A Boitemirov and V M Golovina
22-7-12	The Development of Design Codes for Timber Structures made of Compositive Bars with Plate Joints based on Cyclindrical Nails - Y V Piskunov
22-7-13	Designing of Glued Wood Structures Joints on Glued-in Bars - S B Turkovsky
23-7-1	Proposal for a Design Code for Nail Plates - E Aasheim and K H Solli
23-7-2	Load Distribution in Nailed Joints - H J Blass
24-7-1	Theoretical and Experimental Tension and Shear Capacity of Nail Plate Connections - B Källsner and J Kangas
24-7-2	Testing Method and Determination of Basic Working Loads for Timber Joints with Mechanical Fasteners - Y Hirashima and F Kamiya
24-7-3	Anchorage Capacity of Nail Plate - J Kangas
25-7-2	Softwood and Hardwood Embedding Strength for Dowel type Fasteners - J Ehlbeck and H Werner
25-7-4	A Guide for Application of Quality Indexes for Driven Fasteners Used in Connections in Wood Structures - E G Stern
25-7-5	35 Years of Experience with Certain Types of Connectors and Connector Plates Used for the Assembly of Wood Structures and their Components- E G Stern
25-7-6	Characteristic Strength of Split-ring and Shear-plate Connections - H J Blass, J Ehlbeck and M Schlager
25-7-7	Characteristic Strength of Tooth-plate Connector Joints - H J Blass, J Ehlbeck and M Schlager
25-7-8	Extending Yield Theory to Screw Connections - T E McLain
25-7-9	Determination of k_{def} for Nailed Joints - J W G van de Kuilen

25-7-10	Characteristic Strength of UK Timber Connectors - A V Page and C J Mettem
25-7-11	Multiple-fastener Dowel-type Joints, a Selected Review of Research and Codes - C J Mettem and A V Page
25-7-12	Load Distributions in Multiple-fastener Bolted Joints in European Whitewood Glulam, with Steel Side Plates - C J Mettem and A V Page
26-7-1	Proposed Test Method for Dynamic Properties of Connections Assembled with Mechanical Fasteners - J D Dolan
26-7-2	Validatory Tests and Proposed Design Formulae for the Load-Carrying Capacity of Toothed-Plate Connectored Joints - C J Mettem, A V Page and G Davis
26-7-3	Definitions of Terms and Multi-Language Terminology Pertaining to Metal Connector Plates - E G Stern
26-7-4	Design of Joints Based on in V-Shape Glued-in Rods - J Kangas
26-7-5	Tests on Timber Concrete Composite Structural Elements (TCCs) - A U Meierhofer
27-7-1	Glulam Arch Bridge and Design of it's Moment-Resisting Joints - K Komatsu and S Usuku
27-7-2	Characteristic Load - Carrying Capacity of Joints with Dowel - type Fasteners in Regard to the System Properties - H Werner
27-7-3	Steel Failure Design in Truss Plate Joints - T Poutanen
28-7-1	Expanded Tube Joint in Locally DP Reinforced Timber - A J M Leijten, P Ragupathy and K S Virdi
28-7-2	A Strength and Stiffness Model for the Expanded Tube Joint - A J M Leijten
28-7-3	Load-carrying Capacity of Steel-to Timber Joints with Annular Ring Shanked Nails. A Comparison with the EC5 Design Method - R Görlacher
28-7-4	Dynamic Effects on Metal-Plate Connected Wood Truss Joints - S Kent, R Gupta and T Miller
28-7-5	Failure of the Timber Bolted Joints Subjected to Lateral Load Perpendicular to Grain - M Yasumura and L Daudeville
28-7-6	Design Procedure for Locally Reinforced Joints with Dowel-type Fasteners - H Werner
28-7-7	Variability and Effects of Moisture Content on the Withdrawal Characteristics for Lumber as Opposed to Clear Wood - J D Dolan and J W Stelmokas
28-7-8	Nail Plate Capacity in Joint Line - A Kevarinmäki and J Kangas
28-7-9	Axial Strength of Glued-In Bolts - Calculation Model Based on Non-Linear Fracture Mechanics - A Preliminary Study - C J Johansson, E Serrano, P J Gustafsson and B Enquist
28-7-10	Cyclic Lateral Dowel Connection Tests for seismic and Wind Evaluation - J D Dolan
29-7-1	A Simple Method for Lateral Load-Carrying Capacity of Dowel-Type Fasteners - J Kangas and J Kurkela
29-7-2	Nail Plate Joint Behaviour at Low Versus High Load Level - T Poutanen
29-7-3	The Moment Resistance of Tee and Butt - Joint Nail Plate Test Specimens - A Comparison with Current Design Methods - A Reffold, L R J Whale and B S Choo
29-7-4	A Critical Review of the Moment Rotation Test Method Proposed in prEN 1075 - M Bettison, B S Choo and L R J Whale
29-7-5	Explanation of the Translation and Rotation Behaviour of Prestressed Moment Timber Joints - A J M Leijten

29-7-6	Design of Joints and Frame Corners using Dowel-Type Fasteners - E Gehri
29-7-7	Quasi-Static Reversed-Cyclic Testing of Nailed Joints - E Karacabeyli and A Ceccotti
29-7-8	Failure of Bolted Joints Loaded Parallel to the Grain: Experiment and Simulation - L Davenne, L Daudeville and M Yasumura
30-7-1	Flexural Behaviour of GLT Beams End-Jointed by Glued-in Hardwood Dowels - K Komatsu, A Koizumi, J Jensen, T Sasaki and Y Iijima
30-7-2	Modelling of the Block Tearing Failure in Nailed Steel-to-Timber Joints - J Kangas, K Aalto and A Kevarinmäki
30-7-3	Cyclic Testing of Joints with Dowels and Slotted-in Steel Plates - E Aasheim
30-7-4	A Steel-to-Timber Dowelled Joint of High Performance in Combination with a High Strength Wood Composite (Parallam) - E Gehri
30-7-5	Multiple Fastener Timber Connections with Dowel Type Fasteners - A Jorissen
30-7-6	Influence of Ductility on Load-Carrying Capacity of Joints with Dowel-Type Fasteners - A Mischler
31-7-1	Mechanical Properties of Dowel Type Joints under Reversed Cyclic Lateral Loading - M Yasumura
31-7-2	Design of Joints with Laterally Loaded Dowels - A Mischler
31-7-3	Flexural Behaviour of Glulam Beams Edge-Jointed by Lagscrews with Steel Splice Plates - K Komatsu
31-7-4	Design on Timber Capacity in Nailed Steel-to-Timber Joints - J Kangas and J Vesa
31-7-5	Timber Contact in Chord Splices of Nail Plate Structures - A Kevarinmäki
31-7-6	The Fastener Yield Strength in Bending - A Jorissen and H J Blaß
31-7-7	A Proposal for Simplification of Johansen`s Formulae, Dealing With the Design of Dowelled-Type Fasteners - F Rouger
31-7-8	Simplified Design of Connections with Dowel-type fasteners - H J Blaß and J Ehlbeck
32-7-1	Behaviour of Wood-Steel-Wood Bolted Glulam Connections - M Mohammad and J H P Quenneville
32-7-2	A new set of experimental tests on beams loaded perpendicular-to-grain by dowel-type joints- M Ballerini
32-7-3	Design and Analysis of Bolted Timber Joints under Lateral Force Perpendicular to Grain - M Yasumura and L Daudeville
32-7-4	Predicting Capacities of Joints with Laterally Loaded Nails - I Smith and P Quenneville
32-7-5	Strength Reduction Rules for Multiple Fastener Joints - A Mischler and E Gehri
32-7-6	The Stiffness of Multiple Bolted Connections - A Jorissen
32-7-7	Concentric Loading Tests on Girder Truss Components - T N Reynolds, A Reffold, V Enjily and L Whale
32-7-8	Dowel Type Connections with Slotted-In Steel Plates - M U Pedersen, C O Clorius, L Damkilde, P Hoffmeyer and L Esklidsen
32-7-9	Creep of Nail Plate Reinforced Bolt Joints - J Vesa and A Kevarinmäki
32-7-10	The Behaviour of Timber Joints with Ring Connectors - E Gehri and A Mischler
32-7-11	Non-Metallic, Adhesiveless Joints for Timber Structures - R D Drake, M P Ansell, C J Mettem and R Bainbridge

32-7-12	Effect of Spacing and Edge Distance on the Axial Strength of Glued-in Rods - H J Blaß and B Laskewitz
32-7-13	Evaluation of Material Combinations for Bonded in Rods to Achieve Improved Timber Connections - C J Mettem, R J Bainbridge, K Harvey, M P Ansell, J G Broughton and A R Hutchinson
33-7-1	Determination of Yield Strength and Ultimate Strength of Dowel-Type Timber Joints – M Yasumura and K Sawata
33-7-2	Lateral Shear Capacity of Nailed Joints – U Korin
33-7-3	Height-Adjustable Connector for Composite Beams – Y V Piskunov and E G Stern
33-7-4	Engineering Ductility Assessment for a Nailed Slotted-In Steel Connection in Glulam– L Stehn and H Johansson
33-7-5	Effective Bending Capacity of Dowel-Type Fasteners - H J Blaß, A Bienhaus and V Krämer
33-7-6	Load-Carrying Capacity of Joints with Dowel-Type Fasteners and Interlayers - H J Blaß and B Laskewitz
33-7-7	Evaluation of Perpendicular to Grain Failure of Beams caused by Concentrated Loads of Joints – A J M Leijten and T A C M van der Put
33-7-8	Test Methods for Glued-In Rods for Timber Structures – C Bengtsson and C J Johansson
33-7-9	Stiffness Analysis of Nail Plates – P Ellegaard
33-7-10	Capacity, Fire Resistance and Gluing Pattern of the Rods in V-Connections – J Kangas
33-7-11	Bonded-In Pultrusions for Moment-Resisting Timber Connections – K Harvey, M P Ansell, C J Mettem, R J Bainbridge and N Alexandre
33-7-12	Fatigue Performance of Bonded-In Rods in Glulam, Using Three Adhesive Types - R J Bainbridge, K Harvey, C J Mettem and M P Ansell
34-7-1	Splitting Strength of Beams Loaded by Connections Perpendicular to Grain, Model Validation – A J M Leijten, A Jorissen
34-7-2	Numerical LEFM analyses for the evaluation of failure loads of beams loaded perpendicular-to-grain by single-dowel connections – M Ballerini, R Bezzi
34-7-3	Dowel joints loaded perpendicular to grain - H J Larsen, P J Gustafsson
34-7-4	Quality Control of Connections based on in V-shape glued-in Steel Rods – J Kangas, A Kevarinmäki
34-7-5	Testing Connector Types for Laminated-Timber-Concrete Composite Elements – M Grosse, S Lehmann, K Rautenstrauch
34-7-6	Behaviour of Axially Loaded Glued-in Rods - Requirements and Resistance, Especially for Spruce Timber Perpendicular to the Grain Direction – A Bernasconi
34-7-7	Embedding characteristics on fibre reinforcement and densified timber joints - P Haller, J Wehsener, T Birk
34-7-8	GIROD – Glued-in Rods for Timber Structures – C Bengtsson, C-J Johansson
34-7-9	Criteria for Damage and Failure of Dowel-Type Joints Subjected to Force Perpendicular to the Grain – M Yasumura
34-7-10	Interaction Between Splitting and Block Shear Failure of Joints – A J M Leijten, A Jorissen, J Kuipers
34-7-11	Limit states design of dowel-fastener joints – Placement of modification factors and partial factors, and calculation of variability in resistance – I Smith, G Foliente
34-7-12	Design and Modelling of Knee Joints - J Nielsen, P Ellegaard
34-7-13	Timber-Steel Shot Fired Nail Connections at Ultimate Limit States - R J Bainbridge, P Larsen, C J Mettem, P Alam, M P Ansell

35-7-1 New Estimating Method of Bolted Cross-lapped Joints with Timber Side Members - M Noguchi, K Komatsu

35-7-2 Analysis on Multiple Lag Screwed Timber Joints with Timber Side Members - K Komatsu, S Takino, M Nakatani, H Tateishi

35-7-3 Joints with Inclined Screws - A Kevarinmäki

35-7-4 Joints with Inclined Screws - I Bejtka, H J Blaß

35-7-5 Effect of distances, Spacing and Number of Dowels in a Row an the Load Carrying Capacity of Connections with Dowels failing by Splitting - M Schmid, R Frasson, H J Blaß

35-7 6 Effect of Row Spacing on the Capacity of Bolted Timber Connections Loaded Perpendicular-to-grain - P Quenneville, M Kasim

35-7-7 Splitting Strength of Beams Loaded by Connections, Model Comparison - A J M Leijten

35-7-8 Load-Carrying Capacity of Perpendicular to the Grain Loaded Timber Joints with Multiple Fasteners - O Borth, K U Schober, K Rautenstrauch

35-7-9 Determination of fracture parameter for dowel-type joints loaded perpendicular to wooden grain and its application - M Yasumura

35-7-10 Analysis and Design of Modified Attic Trusses with Punched Metal Plate Fasteners - P Ellegaard

35-7-11 Joint Properties of Plybamboo Sheets in Prefabricated Housing - G E Gonzalez

35-7-12 Fiber-Reinforced Beam-to-Column Connections for Seismic Applications - B Kasal, A Heiduschke, P Haller

36-7-1 Shear Tests in Timber-LWAC with Screw-Type Connections - L Jorge, H Cruz, S Lopes

36-7-2 Plug Shear Failure in Nailed Timber Connections: Experimental Studies - H Johnsson

36-7-3 Nail-Laminated Timber Elements in Natural Surface-Composite with Mineral Bound Layer - S Lehmann, K Rautenstrauch

36-7-4 Mechanical Properties of Timber-Concrete Joints Made With Steel Dowels - A Dias, J W G van de Kuilen, H Cruz

36-7-5 Comparison of Hysteresis Responses of Different Sheating to Framing Joints - B Dujič, R Zarnić

36-7- 6 Evaluation and Estimation of the Performance of the Nail Joints and Shear Walls under Dry/Humid Cyclic Climate - S Nakajima

36-7-7 Beams Transversally Loaded by Dowel-Type Joints: Influence on Splitting Strength of Beam Thickness and Dowel Size - M Ballerini, A Giovanella

36-7-8 Splitting Strength of Beams Loaded by Connections - J L Jensen

36-7-9 A Tensile Fracture Model for Joints with Rods or Dowels loaded Perpendicular-to-Grain - J L Jensen, P J Gustafsson, H J Larsen

36-7-10 A Numerical Model to Simulate the Load-Displacement Time-History of Mutiple-Bolt Connections Subjected to Various Loadings - C P Heine, J D Dolan

36-7-11 Reliability of Timber Structures, Theory and Dowel-Type Connection Failures - A Ranta-Maunus, A Kevarinmäki

37-7-1 Development of the "Displaced Volume Model" to Predict Failure for Multiple-Bolt Timber Joints - D M Carradine, J D Dolan, C P Heine

37-7-2 Mechanical Models of the Knee Joints with Cross-Lapped Glued Joints and Glued in Steel Rods - M Noguchi, K Komatsu

37-7-3 Simplification of the Neural Network Model for Predicting the Load-Carrying Capacity of Dowel-Type Connections - A Cointe, F Rouger

37-7-4	Bolted Wood Connections Loaded Perpendicular-to-Grain- A Proposed Design Approach - M C G Lehoux, J H P Quenneville
37-7-5	A New Prediction Formula for the Splitting Strength of Beams Loaded by Dowel Type Connections - M Ballerini
37-7-6	Plug Shear Failure: The Tensile Failure Mode and the Effect of Spacing - H Johnsson
37-7-7	Block Shear Failure Test with Dowel-Type Connection in Diagonal LVL Structure - M Kairi
37-7-8	Glued-in Steel Rods: A Design Approach for Axially Loaded Single Rods Set Parallel to the Grain - R Steiger, E Gehri, R Widmann
37-7-9	Glued in Rods in Load Bearing Timber Structures - Status regarding European Standards for Test Procedures - B Källander
37-7-10	French Data Concerning Glued-in Rods - C Faye, L Le Magorou, P Morlier, J Surleau
37-7-11	Enhancement of Dowel-Type Fasteners by Glued Connectors - C O Clorius, A Højman
37-7-12	Review of Probability Data for Timber Connections with Dowel-Type Fasteners - A J M Leijten, J Köhler, A Jorissen
37-7-13	Behaviour of Fasteners and Glued-in Rods Produced From Stainless Steel - A Kevarinmäki
37-7-14	Dowel joints in Engineered Wood Products: Assessment of Simple Fracture Mechanics Models - M Snow, I Smith, A Asiz
37-7-15	Numerical Modelling of Timber and Connection Elements Used in Timber-Concrete-Composite Constructions - M Grosse, K Rautenstrauch
38-7-1	A Numerical Investigation on the Splitting Strength of Beams Loaded Perpendicular-to-grain by Multiple-dowel Connections – M Ballerini, M Rizzi
38-7-2	A Probabilistic Framework for the Reliability Assessment of Connections with Dowel Type Fasteners - J Köhler
38-7-3	Load Carrying Capacity of Curved Glulam Beams Reinforced with self-tapping Screws - J Jönsson, S Thelandersson
38-7-4	Self-tapping Screws as Reinforcements in Connections with Dowel-Type Fasteners- I Bejtka, H J Blaß
38-7-5	The Yield Capacity of Dowel Type Fasteners - A Jorissen, A Leijten
38-7-6	Nails in Spruce - Splitting Sensitivity, End Grain Joints and Withdrawal Strength - A Kevarinmäki
38-7-7	Design of Timber Connections with Slotted-in Steel Plates and Small Diameter Steel Tube Fasteners - B Murty, I Smith, A Asiz
39-7-1	Effective in-row Capacity of Multiple-Fastener Connections - P Quenneville, M Bickerdike
39-7-2	Self-tapping Screws as Reinforcements in Beam Supports - I Bejtka, H J Blaß
39-7-3	Connectors for Timber-concrete Composite-Bridges - A Döhrer, K Rautenstrauch
39-7-4	Block Shear Failure at Dowelled Double Shear Steel-to-timber Connections - A Hanhijärvi, A Kevarinmäki, R Yli-Koski
39-7-5	Load Carrying Capacity of Joints with Dowel Type Fasteners in Solid Wood Panels - T Uibel, H J Blaß
39-7-6	Generalised Canadian Approach for Design of Connections with Dowel Fasteners - P Quenneville, I Smith, A Asiz, M Snow, Y H Chui
40-7-1	Predicting the Strength of Bolted Timber Connections Subjected to Fire - M Fragiacomo, A Buchanan, D Carshalton, P Moss, C Austruy
40-7-2	Edge Joints with Dowel Type Fasteners in Cross Laminated Timber - H J Blaß, T Uibel

40-7-3 Design Method against Timber Failure Mechanisms of Dowelled Steel-to-Timber Connections - A Hanhijärvi, A Kevarinmäki

40-7-4 A EYM Based Simplified Design Formula for the Load-carrying Capacity of Dowel-type Connections - M Ballerini

40-7-5 Evaluation of the Slip Modulus for Ultimate Limit State Verifications of Timber-Concrete Composite Structures - E Lukaszewska, M Fragiacomo, A Frangi

40-7-6 Models for the Predictions of the Ductile and Brittle Failure Modes (Parallel-to-Grain) of Timber Rivet Connections - M Marjerrison, P Quenneville

40-7-7 Creep of Timber and Timber-Concrete Joints. - J W G van de Kuilen, A M P G Dias

40-7-8 Lag Screwed Timber Joints with Timber Side Members- K Komatsu, S Takino, H Tateishi

LOAD SHARING

3-8-1 Load Sharing - An Investigation on the State of Research and Development of Design Criteria - E Levin

4-8-1 A Review of Load-Sharing in Theory and Practice - E Levin

4-8-2 Load Sharing - B Norén

19-8-1 Predicting the Natural Frequencies of Light-Weight Wooden Floors - I Smith and Y H Chui

20-8-1 Proposed Code Requirements for Vibrational Serviceability of Timber Floors - Y H Chui and I Smith

21-8-1 An Addendum to Paper 20-8-1 - Proposed Code Requirements for Vibrational Serviceability of Timber Floors - Y H Chui and I Smith

21-8-2 Floor Vibrational Serviceability and the CIB Model Code - S Ohlsson

22-8-1 Reliability Analysis of Viscoelastic Floors - F Rouger, J D Barrett and R O Foschi

24-8-1 On the Possibility of Applying Neutral Vibrational Serviceability Criteria to Joisted Wood Floors - I Smith and Y H Chui

25-8-1 Analysis of Glulam Semi-rigid Portal Frames under Long-term Load - K Komatsu and N Kawamoto

34-8-1 System Effect in Sheathed Parallel Timber Beam Structures – M Hansson, T Isaksson

35-8-1 System Effects in Sheathed Parallel Timber Beam Structures part II. - M Hansson, T Isaksson

39-8-1 Overview of a new Canadian Approach to Handling System Effects in Timber Structures - I Smith, Y H Chui, P Quenneville

DURATION OF LOAD

3-9-1 Definitions of Long Term Loading for the Code of Practice - B Norén

4-9-1 Long Term Loading of Trussed Rafters with Different Connection Systems - T Feldborg and M Johansen

5-9-1 Strength of a Wood Column in Combined Compression and Bending with Respect to Creep - B Källsner and B Norén

6-9-1 Long Term Loading for the Code of Practice (Part 2) - B Norén

6-9-2 Long Term Loading - K Möhler

6-9-3 Deflection of Trussed Rafters under Alternating Loading during a Year - T Feldborg and M Johansen

7-6-1	Strength and Long Term Behaviour of Lumber and Glued-Laminated Timber under Torsion Loads - K Möhler
7-9-1	Code Rules Concerning Strength and Loading Time - H J Larsen and E Theilgaard
17-9-1	On the Long-Term Carrying Capacity of Wood Structures - Y M Ivanov and Y Y Slavic
18-9-1	Prediction of Creep Deformations of Joints - J Kuipers
19-9-1	Another Look at Three Duration of Load Models - R O Foschi and Z C Yao
19-9-2	Duration of Load Effects for Spruce Timber with Special Reference to Moisture Influence - A Status Report - P Hoffmeyer
19-9-3	A Model of Deformation and Damage Processes Based on the Reaction Kinetics of Bond Exchange - T A C M van der Put
19-9-4	Non-Linear Creep Superposition - U Korin
19-9-5	Determination of Creep Data for the Component Parts of Stressed-Skin Panels - R Kliger
19-9-6	Creep an Lifetime of Timber Loaded in Tension and Compression - P Glos
19-1-1	Duration of Load Effects and Reliability Based Design (Single Member) - R O Foschi and Z C Yao
19-6-1	Effect of Age and/or Load on Timber Strength - J Kuipers
19-7-4	The Prediction of the Long-Term Load Carrying Capacity of Joints in Wood Structures - Y M Ivanov and Y Y Slavic
19-7-5	Slip in Joints under Long-Term Loading - T Feldborg and M Johansen
20-7-2	Slip in Joints under Long-Term Loading - T Feldborg and M Johansen
22-9-1	Long-Term Tests with Glued Laminated Timber Girders - M Badstube, W Rug and W Schöne
22-9-2	Strength of One-Layer solid and Lengthways Glued Elements of Wood Structures and its Alteration from Sustained Load - L M Kovaltchuk, I N Boitemirova and G B Uspenskaya
24-9-1	Long Term Bending Creep of Wood - T Toratti
24-9-2	Collection of Creep Data of Timber - A Ranta-Maunus
24-9-3	Deformation Modification Factors for Calculating Built-up Wood-Based Structures - I R Kliger
25-9-2	DVM Analysis of Wood. Lifetime, Residual Strength and Quality - L F Nielsen
26-9-1	Long Term Deformations in Wood Based Panels under Natural Climate Conditions. A Comparative Study - S Thelandersson, J Nordh, T Nordh and S Sandahl
28-9-1	Evaluation of Creep Behavior of Structural Lumber in Natural Environment - R Gupta and R Shen
30-9-1	DOL Effect in Tension Perpendicular to the Grain of Glulam Depending on Service Classes and Volume - S Aicher and G Dill-Langer
30-9-2	Damage Modelling of Glulam in Tension Perpendicular to Grain in Variable Climate - G Dill-Langer and S Aicher
31-9-1	Duration of Load Effect in Tension Perpendicular to Grain in Curved Glulam - A Ranta-Maunus
32-9-1	Bending-Stress-Redistribution Caused by Different Creep in Tension and Compression and Resulting DOL-Effect - P Becker and K Rautenstrauch
32-9-2	The Long Term Performance of Ply-Web Beams - R Grantham and V Enjily

36-9-1 Load Duration Factors for Instantaneous Loads - A J M Leijten, B Jansson

39-9-1 Simplified Approach for the Long-Term Behaviour of Timber-Concrete Composite Beams According to the Eurocode 5 Provisions - M Fragiacomo, A Ceccotti

TIMBER BEAMS

4-10-1 The Design of Simple Beams - H J Burgess

4-10-2 Calculation of Timber Beams Subjected to Bending and Normal Force - H J Larsen

5-10-1 The Design of Timber Beams - H J Larsen

9-10-1 The Distribution of Shear Stresses in Timber Beams - F J Keenan

9-10-2 Beams Notched at the Ends - K Möhler

11-10-1 Tapered Timber Beams - H Riberholt

13-6-2 Consideration of Size Effects in Longitudinal Shear Strength for Uncracked Beams - R O Foschi and J D Barrett

13-6-3 Consideration of Shear Strength on End-Cracked Beams - J D Barrett and R O Foschi

18-10-1 Submission to the CIB-W18 Committee on the Design of Ply Web Beams by Consideration of the Type of Stress in the Flanges - J A Baird

18-10-2 Longitudinal Shear Design of Glued Laminated Beams - R O Foschi

19-10-1 Possible Code Approaches to Lateral Buckling in Beams - H J Burgess

19-2-1 Creep Buckling Strength of Timber Beams and Columns - R H Leicester

20-2-1 Lateral Buckling Theory for Rectangular Section Deep Beam-Columns - H J Burgess

20-10-1 Draft Clause for CIB Code for Beams with Initial Imperfections - H J Burgess

20-10-2 Space Joists in Irish Timber - W J Robinson

20-10-3 Composite Structure of Timber Joists and Concrete Slab - T Poutanen

21-10-1 A Study of Strength of Notched Beams - P J Gustafsson

22-10-1 Design of Endnotched Beams - H J Larsen and P J Gustafsson

22-10-2 Dimensions of Wooden Flexural Members under Constant Loads - A Pozgai

22-10-3 Thin-Walled Wood-Based Flanges in Composite Beams - J König

22-10-4 The Calculation of Wooden Bars with flexible Joints in Accordance with the Polish Standart Code and Strict Theoretical Methods - Z Mielczarek

23-10-1 Tension Perpendicular to the Grain at Notches and Joints - T A C M van der Put

23-10-2 Dimensioning of Beams with Cracks, Notches and Holes. An Application of Fracture Mechanics - K Riipola

23-10-3 Size Factors for the Bending and Tension Strength of Structural Timber - J D Barret and A R Fewell

23-12-1 Bending Strength of Glulam Beams, a Design Proposal - J Ehlbeck and F Colling

23-12-3 Glulam Beams, Bending Strength in Relation to the Bending Strength of the Finger Joints - H Riberholt

24-10-1 Shear Strength of Continuous Beams - R H Leicester and F G Young

25-10-1 The Strength of Norwegian Glued Laminated Beams - K Solli, E Aasheim and R H Falk

25-10-2 The Influence of the Elastic Modulus on the Simulated Bending Strength of Hyperstatic Timber Beams - T D G Canisius

27-10-1 Determination of Shear Modulus - R Görlacher and J Kürth

29-10-1 Time Dependent Lateral Buckling of Timber Beams - F Rouger

29-10-2 Determination of Modulus of Elasticity in Bending According to EN 408 - K H Solli

29-10-3 On Determination of Modulus of Elasticity in Bending - L Boström, S Ormarsson and O Dahlblom

29-10-4 Relation of Moduli of Elasticity in Flatwise and Edgewise Bending of Solid Timber - C J Johansson, A Steffen and E W Wormuth

30-10-1 Nondestructive Evaluation of Wood-based Members and Structures with the Help of Modal Analysis - P Kuklik

30-10-2 Measurement of Modulus of Elasticity in Bending - L Boström

30-10-3 A Weak Zone Model for Timber in Bending - B Källsner, K Salmela and O Ditlevsen

30-10-4 Load Carrying Capacity of Timber Beams with Narrow Moment Peaks - T Isaksson and J Freysoldt

37-10-1 Design of Rim Boards for Use with I-Joists Framing Systems - B Yeh, T G Williamson

40-10- 1 Extension of EC5 Annex B Formulas for the Design of Timber-concrete Composite Structures - J Schänzlin, M Fragiacomo

40-10-2 Simplified Design Method for Mechanically Jointed Beams - U A Girhammar

ENVIRONMENTAL CONDITIONS

5-11-1 Climate Grading for the Code of Practice - B Norén

6-11-1 Climate Grading (2) - B Norén

9-11-1 Climate Classes for Timber Design - F J Keenan

19-11-1 Experimental Analysis on Ancient Downgraded Timber Structures - B Leggeri and L Paolini

19-6-5 Drying Stresses in Round Timber - A Ranta-Maunus

22-11-1 Corrosion and Adaptation Factors for Chemically Aggressive Media with Timber Structures - K Erler

29-11-1 Load Duration Effect on Structural Beams under Varying Climate Influence of Size and Shape - P Galimard and P Morlier

30-11-1 Probabilistic Design Models for the Durability of Timber Constructions - R H Leicester

36-11-1 Structural Durability of Timber in Ground Contact – R H Leicester, C H Wang, M N Nguyen, G C Foliente, C McKenzie

38-11-1 Design Specifications for the Durability of Timber – R H Leicester, C-H Wang, M Nguyen, G C Foliente

38-11-2 Consideration of Moisture Exposure of Timber Structures as an Action - M Häglund, S Thelandersson

LAMINATED MEMBERS

6-12-1 Directives for the Fabrication of Load-Bearing Structures of Glued Timber - A van der Velden and J Kuipers

8-12-1 Testing of Big Glulam Timber Beams - H Kolb and P Frech

8-12-2	Instruction for the Reinforcement of Apertures in Glulam Beams - H Kolb and P Frech
8-12-3	Glulam Standard Part 1: Glued Timber Structures; Requirements for Timber (Second Draft)
9-12-1	Experiments to Provide for Elevated Forces at the Supports of Wooden Beams with Particular Regard to Shearing Stresses and Long-Term Loadings - F Wassipaul and R Lackner
9-12-2	Two Laminated Timber Arch Railway Bridges Built in Perth in 1849 - L G Booth
9-6-4	Consideration of Combined Stresses for Lumber and Glued Laminated Timber - K Möhler
11-6-3	Consideration of Combined Stresses for Lumber and Glued Laminated Timber (addition to Paper CIB-W18/9-6-4) - K Möhler
12-12-1	Glulam Standard Part 2: Glued Timber Structures; Rating (3rd draft)
12-12-2	Glulam Standard Part 3: Glued Timber Structures; Performance (3 rd draft)
13-12-1	Glulam Standard Part 3: Glued Timber Structures; Performance (4th draft)
14-12-1	Proposals for CEI-Bois/CIB-W18 Glulam Standards - H J Larsen
14-12-2	Guidelines for the Manufacturing of Glued Load-Bearing Timber Structures - Stevin Laboratory
14-12-3	Double Tapered Curved Glulam Beams - H Riberholt
14-12-4	Comment on CIB-W18/14-12-3 - E Gehri
18-12-1	Report on European Glulam Control and Production Standard - H Riberholt
18-10-2	Longitudinal Shear Design of Glued Laminated Beams - R O Foschi
19-12-1	Strength of Glued Laminated Timber - J Ehlbeck and F Colling
19-12-2	Strength Model for Glulam Columns - H J Blaß
19-12-3	Influence of Volume and Stress Distribution on the Shear Strength and Tensile Strength Perpendicular to Grain - F Colling
19-12-4	Time-Dependent Behaviour of Glued-Laminated Beams - F Zaupa
21-12-1	Modulus of Rupture of Glulam Beam Composed of Arbitrary Laminae - K Komatsu and N Kawamoto
21-12-2	An Appraisal of the Young's Modulus Values Specified for Glulam in Eurocode 5- L R J Whale, B O Hilson and P D Rodd
21-12-3	The Strength of Glued Laminated Timber (Glulam): Influence of Lamination Qualities and Strength of Finger Joints - J Ehlbeck and F Colling
21-12-4	Comparison of a Shear Strength Design Method in Eurocode 5 and a More Traditional One - H Riberholt
22-12-1	The Dependence of the Bending Strength on the Glued Laminated Timber Girder Depth - M Badstube, W Rug and W Schöne
22-12-2	Acid Deterioration of Glulam Beams in Buildings from the Early Half of the 1960s - Prelimination summary of the research project; Overhead pictures - B A Hedlund
22-12-3	Experimental Investigation of normal Stress Distribution in Glue Laminated Wooden Arches - Z Mielczarek and W Chanaj
22-12-4	Ultimate Strength of Wooden Beams with Tension Reinforcement as a Function of Random Material Properties - R Candowicz and T Dziuba
23-12-1	Bending Strength of Glulam Beams, a Design Proposal - J Ehlbeck and F Colling
23-12-2	Probability Based Design Method for Glued Laminated Timber - M F Stone

23-12-3 Glulam Beams, Bending Strength in Relation to the Bending Strength of the Finger Joints - H Riberholt

23-12-4 Glued Laminated Timber - Strength Classes and Determination of Characteristic Properties - H Riberholt, J Ehlbeck and A Fewell

24-12-1 Contribution to the Determination of the Bending Strength of Glulam Beams - F Colling, J Ehlbeck and R Görlacher

24-12-2 Influence of Perpendicular-to-Grain Stressed Volume on the Load-Carrying Capacity of Curved and Tapered Glulam Beams - J Ehlbeck and J Kürth

25-12-1 Determination of Characteristic Bending Values of Glued Laminated Timber. EN-Approach and Reality - E Gehri

26-12-1 Norwegian Bending Tests with Glued Laminated Beams-Comparative Calculations with the "Karlsruhe Calculation Model" - E Aasheim, K Solli, F Colling, R H Falk, J Ehlbeck and R Görlacher

26-12-2 Simulation Analysis of Norwegian Spruce Glued-Laminated Timber - R Hernandez and R H Falk

26-12-3 Investigation of Laminating Effects in Glued-Laminated Timber - F Colling and R H Falk

26-12-4 Comparing Design Results for Glulam Beams According to Eurocode 5 and to the French Working Stress Design Code (CB71) - F Rouger

27-12-1 State of the Art Report: Glulam Timber Bridge Design in the U.S. - M A Ritter and T G Williamson

27-12-2 Common Design Practice for Timber Bridges in the United Kingdom - C J Mettem, J P Marcroft and G Davis

27-12-3 Influence of Weak Zones on Stress Distribution in Glulam Beams - E Serrano and H J Larsen

28-12-1 Determination of Characteristic Bending Strength of Glued Laminated Timber - E Gehri

28-12-2 Size Factor of Norwegian Glued Laminated Beams - E Aasheim and K H Solli

28-12-3 Design of Glulam Beams with Holes - K Riipola

28-12-4 Compression Resistance of Glued Laminated Timber Short Columns- U Korin

29-12-1 Development of Efficient Glued Laminated Timber - G Schickhofer

30-12-1 Experimental Investigation and Analysis of Reinforced Glulam Beams - K Oiger

31-12-1 Depth Factor for Glued Laminated Timber-Discussion of the Eurocode 5 Approach - B Källsner, O Carling and C J Johansson

32-12-1 The bending stiffness of nail-laminated timber elements in transverse direction- T Wolf and O Schäfer

Internal Stresses in the Cross-Grain Direction of Wood Induced by Climate Variation – J Jönsson and S Svensson

34-12-1 High-Strength I-Joist Compatible Glulam Manufactured with LVL Tension Laminations – B Yeh, T G Williamson

34-12-2 Evaluation of Glulam Shear Strength Using A Full-Size Four-Point Test Method – B Yeh, T G Williamson

34-12-3 Design Model for FRP Reinforced Glulam Beams – M Romani, H J Blaß

34-12-4 Moisture induced stresses in glulam cross sections – J Jönsson

34-12-5 Load Carrying Capacity of Nail-Laminated Timber under Concentrated Loads – V Krämer, H J Blaß

34-12-6	Determination of Shear Strength Values for GLT Using Visual and Machine Graded Spruce Laminations – G Schickhofer
34-12-7	Mechanically Jointed Beams: Possibilities of Analysis and some special Problems – H Kreuzinger
35-12-1	Glulam Beams with Round Holes – a Comparison of Different Design Approaches vs. Test Data - S Aicher L Höfflin
36-12-1	Problems with Shear and Bearing Strength of LVL in Highly Loaded Structures - H Bier
36-12-2	Weibull Based Design of Round Holes in Glulam - L Höfflin, S Aicher
37-12-1	Development of Structural LVL from Tropical Wood and Evaluation of Their Performance for the Structural Components of Wooden Houses. Part-1. Application of Tropical LVL to a Roof Truss - K Komatsu, Y Idris, S Yuwasdiki, B Subiyakto, A Firmanti
37-12-2	Reinforcement of LVL Beams With Bonded-in Plates and Rods - Effect of Placement of Steel and FRP Reinforcements on Beam Strength and Stiffness - P Alam, M P Ansell, D Smedley
39-12-1	Recommended Procedures for Determination of Distribution Widths in the Design of Stress Laminated Timber Plate Decks - K Crews
39-12-2	In-situ Strengthening of Timber Structures with CFRP - K U Schober, S Franke, K Rautenstrauch
39-12-3	Effect of Checking and Non-Glued Edge Joints on the Shear Strength of Structural Glued Laminated Timber Beams - B Yeh, T G Williamson, Z A Martin
39-12-4	A Contribution to the Design and System Effect of Cross Laminated Timber (CLT) - R Jöbstl, T Moosbrugger, T Bogensperger, G Schickhofer
39-12-5	Behaviour of Glulam in Compression Perpendicular to Grain in Different Strength Grades and Load Configurations - M Augustin, A Ruli, R Brandner, G Schickhofer
40-12-1	Development of New Constructions of Glulam Beams in Canada - F Lam, N Mohadevan
40-12-2	Determination of Modulus of Shear and Elasticity of Glued Laminated Timber and Related Examination - R Brandner, E Gehri, T Bogensperger, G Schickhofer
40-12-3	Comparative Examination of Creep of GTL and CLT-Slabs in Bending - R A Jöbstl, G Schickhofer,
40-12-4	Standard Practice for the Derivation of Design Properties of Structural Glued Laminated Timber in the United States - T G Williamson, B Yeh
40-12-5	Creep and Creep-Rupture Behaviour of Structural Composite Lumber Evaluated in Accordance with ASTM D 6815 - B Yeh, T G Williamson.
40-12-6	Bending Strength of Combined Beech-Spruce Glulam - M Frese, H J Blaß
40-12-7	Quality Control of Glulam: Shear Tests of Glue Lines - R Steiger, E Gehri

PARTICLE AND FIBRE BUILDING BOARDS

7-13-1	Fibre Building Boards for CIB Timber Code (First Draft)- O Brynildsen
9-13-1	Determination of the Bearing Strength and the Load-Deformation Characteristics of Particleboard - K Möhler, T Budianto and J Ehlbeck
9-13-2	The Structural Use of Tempered Hardboard - W W L Chan
11-13-1	Tests on Laminated Beams from Hardboard under Short- and Longterm Load - W Nozynski
11-13-2	Determination of Deformation of Special Densified Hardboard under Long-term Load and Varying Temperature and Humidity Conditions - W Halfar

11-13-3 Determination of Deformation of Hardboard under Long-term Load in Changing Climate - W Halfar

14-4-1 An Introduction to Performance Standards for Wood-Base Panel Products - D H Brown

14-4-2 Proposal for Presenting Data on the Properties of Structural Panels - T Schmidt

16-13-1 Effect of Test Piece Size on Panel Bending Properties - P W Post

20-4-1 Considerations of Reliability - Based Design for Structural Composite Products - M R O'Halloran, J A Johnson, E G Elias and T P Cunningham

20-13-1 Classification Systems for Structural Wood-Based Sheet Materials - V C Kearley and A R Abbott

21-13-1 Design Values for Nailed Chipboard - Timber Joints - A R Abbott

25-13-1 Bending Strength and Stiffness of Izopanel Plates - Z Mielczarek

28-13-1 Background Information for "Design Rated Oriented Strand Board (OSB)" in CSA Standards - Summary of Short-term Test Results - E Karacabeyli, P Lau, C R Henderson, F V Meakes and W Deacon

28-13-2 Torsional Stiffness of Wood-Hardboard Composed I-Beam - P Olejniczak

TRUSSED RAFTERS

4-9-1 Long-term Loading of Trussed Rafters with Different Connection Systems - T Feldborg and M Johansen

6-9-3 Deflection of Trussed Rafters under Alternating Loading During a Year - T Feldborg and M Johansen

7-2-1 Lateral Bracing of Timber Struts - J A Simon

9-14-1 Timber Trusses - Code Related Problems - T F Williams

9-7-1 Design of Truss Plate Joints - F J Keenan

10-14-1 Design of Roof Bracing - The State of the Art in South Africa - P A V Bryant and J A Simon

11-14-1 Design of Metal Plate Connected Wood Trusses - A R Egerup

12-14-1 A Simple Design Method for Standard Trusses - A R Egerup

13-14-1 Truss Design Method for CIB Timber Code - A R Egerup

13-14-2 Trussed Rafters, Static Models - H Riberholt

13-14-3 Comparison of 3 Truss Models Designed by Different Assumptions for Slip and E-Modulus - K Möhler

14-14-1 Wood Trussed Rafter Design - T Feldborg and M Johansen

14-14-2 Truss-Plate Modelling in the Analysis of Trusses - R O Foschi

14-14-3 Cantilevered Timber Trusses - A R Egerup

14-7-5 The Effect of Support Eccentricity on the Design of W- and WW-Trusses with Nail Plate Connectors - B Källsner

15-14-1 Guidelines for Static Models of Trussed Rafters - H Riberholt

15-14-2 The Influence of Various Factors on the Accuracy of the Structural Analysis of Timber Roof Trusses - F R P Pienaar

15-14-3 Bracing Calculations for Trussed Rafter Roofs - H J Burgess

15-14-4 The Design of Continuous Members in Timber Trussed Rafters with Punched Metal Connector Plates - P O Reece

15-14-5	A Rafter Design Method Matching U.K. Test Results for Trussed Rafters - H J Burgess
16-14-1	Full-Scale Tests on Timber Fink Trusses Made from Irish Grown Sitka Spruce - V Picardo
17-14-1	Data from Full Scale Tests on Prefabricated Trussed Rafters - V Picardo
17-14-2	Simplified Static Analysis and Dimensioning of Trussed Rafters - H Riberholt
17-14-3	Simplified Calculation Method for W-Trusses - B Källsner
18-14-1	Simplified Calculation Method for W-Trusses (Part 2) - B Källsner
18-14-2	Model for Trussed Rafter Design - T Poutanen
19-14-1	Annex on Simplified Design of W-Trusses - H J Larsen
19-14-2	Simplified Static Analysis and Dimensioning of Trussed Rafters - Part 2 - H Riberholt
19-14-3	Joint Eccentricity in Trussed Rafters - T Poutanen
20-14-1	Some Notes about Testing Nail Plates Subjected to Moment Load - T Poutanen
20-14-2	Moment Distribution in Trussed Rafters - T Poutanen
20-14-3	Practical Design Methods for Trussed Rafters - A R Egerup
22-14-1	Guidelines for Design of Timber Trussed Rafters - H Riberholt
23-14-1	Analyses of Timber Trussed Rafters of the W-Type - H Riberholt
23-14-2	Proposal for Eurocode 5 Text on Timber Trussed Rafters - H Riberholt
24-14-1	Capacity of Support Areas Reinforced with Nail Plates in Trussed Rafters - A Kevarinmäki
25-14-1	Moment Anchorage Capacity of Nail Plates in Shear Tests - A Kevarinmaki and J. Kangas
25-14-2	Design Values of Anchorage Strength of Nail Plate Joints by 2-curve Method and Interpolation - J Kangas and A Kevarinmaki
26-14-1	Test of Nail Plates Subjected to Moment - E Aasheim
26-14-2	Moment Anchorage Capacity of Nail Plates - A Kevarinmäki and J Kangas
26-14-3	Rotational Stiffness of Nail Plates in Moment Anchorage - A Kevarinmäki and J Kangas
26-14-4	Solution of Plastic Moment Anchorage Stress in Nail Plates - A Kevarinmäki
26-14-5	Testing of Metal-Plate-Connected Wood-Truss Joints - R Gupta
26-14-6	Simulated Accidental Events on a Trussed Rafter Roofed Building - C J Mettem and J P Marcroft
30-14-1	The Stability Behaviour of Timber Trussed Rafter Roofs - Studies Based on Eurocode 5 and Full Scale Testing - R J Bainbridge, C J Mettern, A Reffold and T Studer
32-14-1	Analysis of Timber Reinforced with Punched Metal Plate Fasteners- J Nielsen
33-14-1	Moment Capacity of Timber Beams Loaded in Four-Point Bending and Reinforced with Punched Metal Plate Fasteners – J Nielsen
36-14-1	Effect of Chord Splice Joints on Force Distribution in Trusses with Punched Metal Plate Fasteners - P Ellegaard
36-14-2	Monte Carlo Simulation and Reliability Analysis of Roof Trusses with Punched Metal Plate Fasteners - M Hansson, P Ellegaard
36-14-3	Truss Trouble – R H Leicester, J Goldfinch, P Paevere, G C Foliente

40-14-1 Timber Trusses with Punched Metal Plate Fasteners - Design for Transport and Erection - H J Blaß

STRUCTURAL STABILITY

8-15-1 Laterally Loaded Timber Columns: Tests and Theory - H J Larsen

13-15-1 Timber and Wood-Based Products Structures. Panels for Roof Coverings. Methods of Testing and Strength Assessment Criteria. Polish Standard BN-78/7159-03

16-15-1 Determination of Bracing Structures for Compression Members and Beams - H Brüninghoff

17-15-1 Proposal for Chapter 7.4 Bracing - H Brüninghoff

17-15-2 Seismic Design of Small Wood Framed Houses - K F Hansen

18-15-1 Full-Scale Structures in Glued Laminated Timber, Dynamic Tests: Theoretical and Experimental Studies - A Ceccotti and A Vignoli

18-15-2 Stabilizing Bracings - H Brüninghoff

19-15-1 Connections Deformability in Timber Structures: a Theoretical Evaluation of its Influence on Seismic Effects - A Ceccotti and A Vignoli

19-15-2 The Bracing of Trussed Beams - M H Kessel and J Natterer

19-15-3 Racking Resistance of Wooden Frame Walls with Various Openings - M Yasumura

19-15-4 Some Experiences of Restoration of Timber Structures for Country Buildings - G Cardinale and P Spinelli

19-15-5 Non-Destructive Vibration Tests on Existing Wooden Dwellings - Y Hirashima

20-15-1 Behaviour Factor of Timber Structures in Seismic Zones. - A Ceccotti and A Vignoli

21-15-1 Rectangular Section Deep Beam - Columns with Continuous Lateral Restraint - H J Burgess

21-15-2 Buckling Modes and Permissible Axial Loads for Continuously Braced Columns- H J Burgess

21-15-3 Simple Approaches for Column Bracing Calculations - H J Burgess

21-15-4 Calculations for Discrete Column Restraints - H J Burgess

21-15-5 Behaviour Factor of Timber Structures in Seismic Zones (Part Two) - A Ceccotti and A Vignoli

22-15-1 Suggested Changes in Code Bracing Recommendations for Beams and Columns - H J Burgess

22-15-2 Research and Development of Timber Frame Structures for Agriculture in Poland- S Kus and J Kerste

22-15-3 Ensuring of Three-Dimensional Stiffness of Buildings with Wood Structures - A K Shenghelia

22-15-5 Seismic Behavior of Arched Frames in Timber Construction - M Yasumura

22-15-6 The Robustness of Timber Structures - C J Mettem and J P Marcroft

22-15-7 Influence of Geometrical and Structural Imperfections on the Limit Load of Wood Columns - P Dutko

23-15-1 Calculation of a Wind Girder Loaded also by Discretely Spaced Braces for Roof Members - H J Burgess

23-15-2	Stability Design and Code Rules for Straight Timber Beams - T A C M van der Put
23-15-3	A Brief Description of Formula of Beam-Columns in China Code - S Y Huang
23-15-4	Seismic Behavior of Braced Frames in Timber Construction - M Yasumara
23-15-5	On a Better Evaluation of the Seismic Behavior Factor of Low-Dissipative Timber Structures - A Ceccotti and A Vignoli
23-15-6	Disproportionate Collapse of Timber Structures - C J Mettem and J P Marcroft
23-15-7	Performance of Timber Frame Structures During the Loma Prieta California Earthquake - M R O'Halloran and E G Elias
24-15-2	Discussion About the Description of Timber Beam-Column Formula - S Y Huang
24-15-3	Seismic Behavior of Wood-Framed Shear Walls - M Yasumura
25-15-1	Structural Assessment of Timber Framed Building Systems - U Korin
25-15-3	Mechanical Properties of Wood-framed Shear Walls Subjected to Reversed Cyclic Lateral Loading - M Yasumura
26-15-1	Bracing Requirements to Prevent Lateral Buckling in Trussed Rafters - C J Mettem and P J Moss
26-15-2	Eurocode 8 - Part 1.3 - Chapter 5 - Specific Rules for Timber Buildings in Seismic Regions - K Becker, A Ceccotti, H Charlier, E Katsaragakis, H J Larsen and H Zeitter
26-15-3	Hurricane Andrew - Structural Performance of Buildings in South Florida - M R O'Halloran, E L Keith, J D Rose and T P Cunningham
29-15-1	Lateral Resistance of Wood Based Shear Walls with Oversized Sheathing Panels - F Lam, H G L Prion and M He
29-15-2	Damage of Wooden Buildings Caused by the 1995 Hyogo-Ken Nanbu Earthquake - M Yasumura, N Kawai, N Yamaguchi and S Nakajima
29-15-3	The Racking Resistance of Timber Frame Walls: Design by Test and Calculation - D R Griffiths, C J Mettem, V Enjily, P J Steer
29-15-4	Current Developments in Medium-Rise Timber Frame Buildings in the UK - C J Mettem, G C Pitts, P J Steer, V Enjily
29-15-5	Natural Frequency Prediction for Timber Floors - R J Bainbridge, and C J Mettem
30-15-1	Cyclic Performance of Perforated Wood Shear Walls with Oversize Oriented Strand Board Panels - Ming He, H Magnusson, F Lam, and H G L Prion
30-15-2	A Numerical Analysis of Shear Walls Structural Performances - L Davenne, L Daudeville, N Kawai and M Yasumura
30-15-3	Seismic Force Modification Factors for the Design of Multi-Storey Wood-Frame Platform Construction - E Karacabeyli and A Ceccotti
30-15-4	Evaluation of Wood Framed Shear Walls Subjected to Lateral Load - M Yasumura and N Kawai
31-15-1	Seismic Performance Testing On Wood-Framed Shear Wall - N Kawai
31-15-2	Robustness Principles in the Design of Medium-Rise Timber-Framed Buildings - C J Mettem, M W Milner, R J Bainbridge and V. Enjily
31-15-3	Numerical Simulation of Pseudo-Dynamic Tests Performed to Shear Walls - L Daudeville, L Davenne, N Richard, N Kawai and M Yasumura
31-15-4	Force Modification Factors for Braced Timber Frames - H G L Prion, M Popovski and E Karacabeyli
32-15-1	Three-Dimensional Interaction in Stabilisation of Multi-Storey Timber Frame Buildings - S Andreasson

32-15-2 Application of Capacity Spectrum Method to Timber Houses - N Kawai

32-15-3 Design Methods for Shear Walls with Openings - C Ni, E Karacabeyli and A Ceccotti

32-15-4 Static Cyclic Lateral Loading Tests on Nailed Plywood Shear Walls - K Komatsu, K H Hwang and Y Itou

33-15-1 Lateral Load Capacities of Horizontally Sheathed Unblocked Shear Walls – C Ni, E Karacabeyli and A Ceccotti

33-15-2 Prediction of Earthquake Response of Timber Houses Considering Shear Deformation of Horizontal Frames – N Kawai

33-15-3 Eurocode 5 Rules for Bracing – H J Larsen

34-15-1 A simplified plastic model for design of partially anchored wood-framed shear walls – B Källsner, U A Girhammar, Liping Wu

34-15-2 The Effect of the Moisture Content on the Performance of the Shear Walls – S Nakajima

34-15-3 Evaluation of Damping Capacity of Timber Structures for Seismic Design – M Yasumura

35-15-1 On test methods for determining racking strength and stiffness of wood-framed shear walls - B Källsner, U A Girhammar, L Wu

35-15-2 A Plastic Design Model for Partially Anchored Wood-framed Shear Walls with Openings - U A Girhammar, L Wu, B Källsner

35-15-3 Evaluation and Estimation of the Performance of the Shear Walls in Humid Climate - S Nakajima

35-15-4 Influence of Vertical Load on Lateral Resistance of Timber Frame Walls - B Dujič, R Žarnić

35-15-5 Cyclic and Seismic Performances of a Timber-Concrete System - Local and Full Scale Experimental Results - E Fournely, P Racher

35-15-6 Design of timber-concrete composite structures according to EC5 - 2002 version - A Ceccotti, M Fragiacomo, R M Gutkowski

35-15-7 Design of timber structures in seismic zones according to EC8- 2002 version - A Ceccotti, T Toratti, B Dujič

35-15-8 Design Methods to Prevent Premature Failure of Joints at Shear Wall Corners - N Kawai, H Okiura

36-15-1 Monitoring Light-Frame Timber Buildings: Environmental Loads and Load Paths – I Smith et al.

36-15-2 Applicability of Design Methods to Prevent Premature Failure of Joints at Shear Wall Corners in Case of Post and Beam Construction - N Kawai, H Isoda

36-15-3 Effects of Screw Spacing and Edge Boards on the Cyclic Performance of Timber Frame and Structural Insulated Panel Roof Systems - D M Carradine, J D Dolan, F E Woeste

36-15-4 Pseudo-Dynamic Tests on Conventional Timber Structures with Shear Walls - M Yasumura

36-15-5 Experimental Investigation of Laminated Timber Frames with Fiber-reinforced Connections under Earthquake Loads - B Kasal, P Haller, S Pospisil, I Jirovsky, A Heiduschke, M Drdacky

36-15-6 Effect of Test Configurations and Protocols on the Performance of Shear Walls - F Lam, D Jossen, J Gu, N Yamaguchi, H G L Prion

36-15-7 Comparison of Monotonic and Cyclic Performance of Light-Frame Shear Walls - J D Dolan, A J Toothman

37-15-1 Estimating 3D Behavior of Conventional Timber Structures with Shear Walls by Pseudodynamic Tests - M Yasumura, M Uesugi, L Davenne

37-15-2	Testing of Racking Behavior of Massive Wooden Wall Panels - B Dujič, J Pucelj, R Žarnić
37-15-3	Influence of Framing Joints on Plastic Capacity of Partially Anchored Wood-Framed Shear Walls - B Källsner, U A Girhammar
37-15-4	Bracing of Timber Members in Compression - J Munch-Andersen
37-15-5	Acceptance Criteria for the Use of Structural Insulated Panels in High Risk Seismic Areas - B Yeh, T D Skaggs, T G Williamson Z A Martin
37-15-6	Predicting Load Paths in Shearwalls - Hongyong Mi, Ying-Hei Chui, I Smith, M Mohammad
38-15-1	Background Information on ISO STANDARD 16670 for Cyclic Testing of Connections - E Karacabeyli, M Yasumura, G C Foliente, A Ceccotti
38-15-2	Testing & Product Standards – a Comparison of EN to ASTM, AS/NZ and ISO Standards – A Ranta-Maunus, V Enjily
38-15-3	Framework for Lateral Load Design Provisions for Engineered Wood Structures in Canada - M Popovski, E Karacabeyli
38-15-4	Design of Shear Walls without Hold-Downs - Chun Ni, E Karacabeyli
38-15-5	Plastic design of partially anchored wood-framed wall diaphragms with and without openings - B Källsner, U A Girhammar
38-15-6	Racking of Wooden Walls Exposed to Different Boundary Conditions - B Dujič, S Aicher, R Žarnić
38-15-7	A Portal Frame Design for Raised Wood Floor Applications - T G Williamson, Z A Martin, B Yeh
38-15-8	Linear Elastic Design Method for Timber Framed Ceiling, Floor and Wall Diaphragms - Jarmo Leskelä
38-15-9	A Unified Design Method for the Racking Resistance of Timber Framed Walls for Inclusion in EUROCODE 5 - R Griffiths, B Källsner, H J Blass, V Enjily
39-15-1	Effect of Transverse Walls on Capacity of Wood-Framed Wall Diaphragms - U A Girhammar, B Källsner
39-15-2	Which Seismic Behaviour Factor for Multi-Storey Buildings made of Cross-Laminated Wooden Panels? - M Follesa, M P Lauriola, C Minowa, N Kawai, C Sandhaas, M Yasumura, A Ceccotti
39-15-3	Laminated Timber Frames under dynamic Loadings - A Heiduschke, B Kasal, P Haller
39-15-4	Code Provisions for Seismic Design of Multi-storey Post-tensioned Timber Buildings - S Pampanin, A Palermo, A Buchanan, M Fragiacomo, B Deam
40-15-1	Design of Safe Timber Structures – How Can we Learn from Structural Failures? - S Thelandersson, E Frühwald
40-15-2	Effect of Transverse Walls on Capacity of Wood-Framed Wall Diaphragms—Part 2 - U A Girhammar, B Källsner
40-15-3	Midply Wood Shear Wall System: Concept, Performance and Code Implementation - Chun Ni, M Popovski, E Karacabeyli, E Varoglu, S Stiemer
40-15-4	Seismic Behaviour of Tall Wood-Frame Walls - M Popovski, A Peterson, E Karacabeyli
40-15-5	International Standard Development of Lateral Load Test Method for Shear Walls - M Yasumura, E Karacabeyli
40-15-6	Influence of Openings on Shear Capacity of Wooden Walls - B Dujič, S Klobcar, R Žarnić

FIRE

12-16-1 British Standard BS 5268 the Structural Use of Timber: Part 4 Fire Resistance of Timber Structures

13-100-2 CIB Structural Timber Design Code. Chapter 9. Performance in Fire

19-16-1 Simulation of Fire in Tests of Axially Loaded Wood Wall Studs - J König

24-16-1 Modelling the Effective Cross Section of Timber Frame Members Exposed to Fire - J König

25-16-1 The Effect of Density on Charring and Loss of Bending Strength in Fire - J König

25-16-2 Tests on Glued-Laminated Beams in Bending Exposed to Natural Fires - F Bolonius Olesen and J König

26-16-1 Structural Fire Design According to Eurocode 5, Part 1.2 - J König

31-16-1 Revision of ENV 1995-1-2: Charring and Degradation of Strength and Stiffness - J König

33-16-1 A Design Model for Load-carrying Timber Frame Members in Walls and Floors Exposed to Fire - J König

33-16-2 A Review of Component Additive Methods Used for the Determination of Fire Resistance of Separating Light Timber Frame Construction - J König, T Oksanen and K Towler

33-16-3 Thermal and Mechanical Properties of Timber and Some Other Materials Used in Light Timber Frame Construction - B Källsner and J König

34-16-1 Influence of the Strength Determining Factors on the Fire Resistance Capability of Timber Structural Members – I Totev, D Dakov

34-16-2 Cross section properties of fire exposed rectangular timber members - J König, B Källsner

34-16-3 Pull-Out Tests on Glued-in Rods at High Temperatures – A Mischler, A Frangi

35-16-1 Basic and Notional Charring Rates - J König

37 - 16 - 1 Effective Values of Thermal Properties of Timber and Thermal Actions During the Decay Phase of Natural Fires - J König

37 - 16 - 2 Fire Tests on Timber Connections with Dowel-type Fasteners - A Frangi, A Mischler

38-16-1 Fire Behaviour of Multiple Shear Steel-to-Timber Connections with Dowels - C Erchinger, A Frangi, A Mischler

38-16-2 Fire Tests on Light Timber Frame Wall Assemblies - V Schleifer, A Frangi

39-16-1 Fire Performance of FRP Reinforced Glulam - T G Williamson, B Yeh

39-16-2 An Easy-to-use Model for the Design of Wooden I-joists in Fire - J König, B Källsner

39-16-3 A Design Model for Timber Slabs Made of Hollow Core Elements in Fire - A Frangi, M Fontana

40-16-1 Bonded Timber Deck Plates in Fire - J König, J Schmid

40-16-2 Design of Timber Frame Floor Assemblies in Fire - A Frangi, C Erchinger

STATISTICS AND DATA ANALYSIS

13-17-1 On Testing Whether a Prescribed Exclusion Limit is Attained - W G Warren

16-17-1 Notes on Sampling and Strength Prediction of Stress Graded Structural Timber - P Glos

16-17-2 Sampling to Predict by Testing the Capacity of Joints, Components and Structures - B Norén

16-17-3 Discussion of Sampling and Analysis Procedures - P W Post

17-17-1 Sampling of Wood for Joint Tests on the Basis of Density - I Smith, L R J Whale

17-17-2 Sampling Strategy for Physical and Mechanical Properties of Irish Grown Sitka Spruce - V Picardo

18-17-1 Sampling of Timber in Structural Sizes - P Glos

18-6-3 Notes on Sampling Factors for Characteristic Values - R H Leicester

19-17-1 Load Factors for Proof and Prototype Testing - R H Leicester

19-6-2 Confidence in Estimates of Characteristic Values - R H Leicester

21-6-1 Draft Australian Standard: Methods for Evaluation of Strength and Stiffness of Graded Timber - R H Leicester

21-6-2 The Determination of Characteristic Strength Values for Stress Grades of Structural Timber. Part 1 - A R Fewell and P Glos

22-17-1 Comment on the Strength Classes in Eurocode 5 by an Analysis of a Stochastic Model of Grading - A proposal for a supplement of the design concept - M Kiesel

24-17-1 Use of Small Samples for In-Service Strength Measurement - R H Leicester and F G Young

24-17-2 Equivalence of Characteristic Values - R H Leicester and F G Young

24-17-3 Effect of Sampling Size on Accuracy of Characteristic Values of Machine Grades - Y H Chui, R Turner and I Smith

24-17-4 Harmonisation of LSD Codes - R H Leicester

25-17-2 A Body for Confirming the Declaration of Characteristic Values - J Sunley

25-17-3 Moisture Content Adjustment Procedures for Engineering Standards - D W Green and J W Evans

27-17-1 Statistical Control of Timber Strength - R H Leicester and H O Breitinger

30-17-1 A New Statistical Method for the Establishment of Machine Settings - F Rouger

35-17-1 Probabilistic Modelling of Duration of Load Effects in Timber Structures - J Köhler, S Svenson

38-17-1 Analysis of Censored Data - Examples in Timber Engineering Research - R Steiger, J Köhler

39-17-1 Possible Canadian / ISO Approach to Deriving Design Values from Test Data - I Smith, A Asiz, M Snow, Y H Chui

GLUED JOINTS

20-18-1 Wood Materials under Combined Mechanical and Hygral Loading - A Martensson and S Thelandersson

20-18-2 Analysis of Generalized Volkersen - Joints in Terms of Linear Fracture Mechanics - P J Gustafsson

20-18-3 The Complete Stress-Slip Curve of Wood-Adhesives in Pure Shear - H Wernersson and P J Gustafsson

22-18-1 Perspective Adhesives and Protective Coatings for Wood Structures - A S Freidin

34-18-1 Performance Based Classification of Adhesives for Structural Timber Applications - R J Bainbridge, C J Mettem, J G Broughton, A R Hutchinson

35-18-1 Creep Testing Wood Adhesives for Structural Use - C Bengtsson, B Källander

38-18-1 Adhesive Performance at Elevated Temperatures for Engineered Wood Products - B Yeh, B Herzog, T G Williamson

39-18-1 Comparison of the Pull–out Strength of Steel Bars Glued in Glulam Elements Obtained Experimentally and Numerically - V Rajčić, A Bjelanović, M Rak

39-18-2 The Influence of the Grading Method on the Finger Joint Bending Strength of Beech - M Frese, H J Blaß

FRACTURE MECHANICS

21-10-1 A Study of Strength of Notched Beams - P J Gustafsson

22-10-1 Design of Endnotched Beams - H J Larsen and P J Gustafsson

23-10-1 Tension Perpendicular to the Grain at Notches and Joints - T A C M van der Put

23-10-2 Dimensioning of Beams with Cracks, Notches and Holes. An Application of Fracture Mechanics - K Riipola

23-19-1 Determination of the Fracture Energie of Wood for Tension Perpendicular to the Grain - W Rug, M Badstube and W Schöne

23-19-2 The Fracture Energy of Wood in Tension Perpendicular to the Grain. Results from a Joint Testing Project - H J Larsen and P J Gustafsson

23-19-3 Application of Fracture Mechanics to Timber Structures - A Ranta-Maunus

24-19-1 The Fracture Energy of Wood in Tension Perpendicular to the Grain - H J Larsen and P J Gustafsson

28-19-1 Fracture of Wood in Tension Perpendicular to the Grain: Experiment and Numerical Simulation by Damage Mechanics - L Daudeville, M Yasumura and J D Lanvin

28-19-2 A New Method of Determining Fracture Energy in Forward Shear along the Grain - H D Mansfield-Williams

28-19-3 Fracture Design Analysis of Wooden Beams with Holes and Notches. Finite Element Analysis based on Energy Release Rate Approach - H Petersson

28-19-4 Design of Timber Beams with Holes by Means of Fracture Mechanics - S Aicher, J Schmidt and S Brunold

30-19-1 Failure Analysis of Single-Bolt Joints - L Daudeville, L Davenne and M Yasumura

37 - 19 - 1 Determination of Fracture Mechanics Parameters for Wood with the Help of Close Range Photogrammetry - S Franke, B Franke, K Rautenstrauch

39-19-1 First Evaluation Steps of Design Rules in the European and German codes of Transverse Tension Areas - S Franke, B Franke, K Rautenstrauch

SERVICEABILITY

27-20-1 Codification of Serviceability Criteria - R H Leicester

27-20-2 On the Experimental Determination of Factor k_{def} and Slip Modulus k_{ser} from Short- and Long-Term Tests on a Timber-Concrete Composite (TCC) Beam - S Capretti and A Ceccotti

27-20-3 Serviceability Limit States: A Proposal for Updating Eurocode 5 with Respect to Eurocode 1 - P Racher and F Rouger

27-20-4 Creep Behavior of Timber under External Conditions - C Le Govic, F Rouger, T Toratti and P Morlier

30-20-1 Design Principles for Timber in Compression Perpendicular to Grain - S Thelandersson and A Mårtensson

30-20-2 Serviceability Performance of Timber Floors - Eurocode 5 and Full Scale Testing - R J Bainbridge and C J Mettem

32-20-1 Floor Vibrations - B Mohr

37 - 20 - 1 A New Design Method to Control Vibrations Induced by Foot Steps in Timber Floors - Lin J Hu, Y H Chui

37 - 20 - 2 Serviceability Limit States of Wooden Footbridges. Vibrations Caused by Pedestrians - P Hamm

TEST METHODS

31-21-1 Development of an Optimised Test Configuration to Determine Shear Strength of Glued Laminated Timber - G Schickhofer and B Obermayr

31-21-2 An Impact Strength Test Method for Structural Timber. The Theory and a Preliminary Study - T D G Canisius

35-21-1 Full-Scale Edgewise Shear Tests for Laminated Veneer Lumber- B Yeh, T G Williamson

39-21-1 Timber Density Restrictions for Timber Connection Tests According to EN28970/ISO8970 - A Leijten, J Köhler, A Jorissen

39-21-2 The Mechanical Inconsistence in the Evaluation of the Modulus of Elasticity According to EN384 - T Bogensperger, H Unterwieser, G Schickhofer

40 - 21 - 1 ASTM D198 - Interlaboratory Study for Modulus of Elasticity of Lumber in Bending - A Salenikovich

40 - 21 - 2 New Test Configuration for CLT-Wall-Elements under Shear Load - T Bogensperger, T Moosbrugger, G Schickhofer

CIB TIMBER CODE

2-100-1 A Framework for the Production of an International Code of Practice for the Structural Use of Timber - W T Curry

5-100-1 Design of Solid Timber Columns (First Draft) - H J Larsen

5-100-2 A Draft Outline of a Code for Timber Structures - L G Booth

6-100-1 Comments on Document 5-100-1; Design of Solid Timber Columns - H J Larsen and E Theilgaard

6-100-2 CIB Timber Code: CIB Timber Standards - H J Larsen and E Theilgaard

7-100-1 CIB Timber Code Chapter 5.3 Mechanical Fasteners; CIB Timber Standard 06 and 07 - H J Larsen

8-100-1 CIB Timber Code - List of Contents (Second Draft) - H J Larsen

9-100-1 The CIB Timber Code (Second Draft)

11-100-1 CIB Structural Timber Design Code (Third Draft)

11-100-2 Comments Received on the CIB Code
U Saarelainen; Y M Ivanov, R H Leicester, W Nozynski, W R A Meyer, P Beckmann; R Marsh

11-100-3 CIB Structural Timber Design Code; Chapter 3 - H J Larsen

12-100-1 Comment on the CIB Code - Sous-Commission Glulam

12-100-2 Comment on the CIB Code - R H Leicester

12-100-3 CIB Structural Timber Design Code (Fourth Draft)

13-100-1 Agreed Changes to CIB Structural Timber Design Code

13-100-2 CIB Structural Timber Design Code. Chapter 9: Performance in Fire

13-100-3a Comments on CIB Structural Timber Design Code

13-100-3b Comments on CIB Structural Timber Design Code - W R A Meyer

13-100-3c Comments on CIB Structural Timber Design Code - British Standards Institution

13-100-4 CIB Structural Timber Design Code. Proposal for Section 6.1.5 Nail Plates - N I Bovim

14-103-2 Comments on the CIB Structural Timber Design Code - R H Leicester

15-103-1 Resolutions of TC 165-meeting in Athens 1981-10-12/13

21-100-1 CIB Structural Timber Design Code. Proposed Changes of Sections on Lateral Instability, Columns and Nails - H J Larsen

22-100-1 Proposal for Including an Updated Design Method for Bearing Stresses in CIB W18 - Structural Timber Design Code - B Madsen

22-100-2 Proposal for Including Size Effects in CIB W18A Timber Design Code - B Madsen

22-100-3 CIB Structural Timber Design Code - Proposed Changes of Section on Thin-Flanged Beams - J König

22-100-4 Modification Factor for "Aggressive Media" - a Proposal for a Supplement to the CIB Model Code - K Erler and W Rug

22-100-5 Timber Design Code in Czechoslovakia and Comparison with CIB Model Code - P Dutko and B Kozelouh

LOADING CODES

4-101-1 Loading Regulations - Nordic Committee for Building Regulations

4-101-2 Comments on the Loading Regulations - Nordic Committee for Building Regulations

37-101-1 Action Combination Processing for the Eurocodes Basis of Software to Assist the Engineer - Y Robert, A V Page, R Thépaut, C J Mettem

STRUCTURAL DESIGN CODES

1-102-1 Survey of Status of Building Codes, Specifications etc., in USA - E G Stern

1-102-2 Australian Codes for Use of Timber in Structures - R H Leicester

1-102-3 Contemporary Concepts for Structural Timber Codes - R H Leicester

1-102-4 Revision of CP 112 - First Draft, July 1972 - British Standards Institution

4-102-1 Comparsion of Codes and Safety Requirements for Timber Structures in EEC Countries - Timber Research and Development Association

4-102-2 Nordic Proposals for Safety Code for Structures and Loading Code for Design of Structures - O A Brynildsen

4-102-3 Proposal for Safety Codes for Load-Carrying Structures - Nordic Committee for Building Regulations

4-102-4 Comments to Proposal for Safety Codes for Load-Carrying Structures - Nordic Committee for Building Regulations

4-102-5 Extract from Norwegian Standard NS 3470 "Timber Structures"

4-102-6 Draft for Revision of CP 112 "The Structural Use of Timber" - W T Curry

8-102-1 Polish Standard PN-73/B-03150: Timber Structures; Statistical Calculations and Designing

8-102-2 The Russian Timber Code: Summary of Contents

9-102-1 Svensk Byggnorm 1975 (2nd Edition); Chapter 27: Timber Construction

11-102-1 Eurocodes - H J Larsen

13-102-1 Program of Standardisation Work Involving Timber Structures and Wood-Based Products in Poland

17-102-1	Safety Principles - H J Larsen and H Riberholt
17-102-2	Partial Coefficients Limit States Design Codes for Structural Timberwork - I Smith
18-102-1	Antiseismic Rules for Timber Structures: an Italian Proposal - G Augusti and A Ceccotti
18-1-2	Eurocode 5, Timber Structures - H J Larsen
19-102-1	Eurocode 5 - Requirements to Timber - Drafting Panel Eurocode 5
19-102-2	Eurocode 5 and CIB Structural Timber Design Code - H J Larsen
19-102-3	Comments on the Format of Eurocode 5 - A R Fewell
19-102-4	New Developments of Limit States Design for the New GDR Timber Design Code - W Rug and M Badstube
19-7-3	Effectiveness of Multiple Fastener Joints According to National Codes and Eurocode 5 (Draft) - G Steck
19-7-6	The Derivation of Design Clauses for Nailed and Bolted Joints in Eurocode5 - L R J Whale and I Smith
19-14-1	Annex on Simplified Design of W-Trusses - H J Larsen
20-102-1	Development of a GDR Limit States Design Code for Timber Structures - W Rug and M Badstube
21-102-1	Research Activities Towards a New GDR Timber Design Code Based on Limit States Design - W Rug and M Badstube
22-102-1	New GDR Timber Design Code, State and Development - W Rug, M Badstube and W Kofent
22-102-2	Timber Strength Parameters for the New USSR Design Code and its Comparison with International Code - Y Y Slavik, N D Denesh and E B Ryumina
22-102-3	Norwegian Timber Design Code - Extract from a New Version - E Aasheim and K H Solli
23-7-1	Proposal for a Design Code for Nail Plates - E Aasheim and K H Solli
24-102-2	Timber Footbridges: A Comparison Between Static and Dynamic Design Criteria - A Ceccotti and N de Robertis
25-102-1	Latest Development of Eurocode 5 - H J Larsen
25-102-1A	Annex to Paper CIB-W18/25-102-1. Eurocode 5 - Design of Notched Beams - H J Larsen, H Riberholt and P J Gustafsson
25-102-2	Control of Deflections in Timber Structures with Reference to Eurocode 5 - A Martensson and S Thelandersson
28-102-1	Eurocode 5 - Design of Timber Structures - Part 2: Bridges - D Bajolet, E Gehri, J König, H Kreuzinger, H J Larsen, R Mäkipuro and C Mettem
28-102-2	Racking Strength of Wall Diaphragms - Discussion of the Eurocode 5 Approach - B Källsner
29-102-1	Model Code for the Probabilistic Design of Timber Structures - H J Larsen, T Isaksson and S Thelandersson
30-102-1	Concepts for Drafting International Codes and Standards for Timber Constructions - R H Leicester
33-102-1	International Standards for Bamboo – J J A Janssen
35-102-1	Design Characteristics and Results According to EUROCODE 5 and SNiP Procedures - L Ozola, T Keskküla
35-102-2	Model Code for the Reliability-Based Design of Timber Structures - H J Larsen

36-102-1 Predicted Reliability of Elements and Classification of Timber Structures - L Ozola, T Keskküla

36-102-2 Calibration of Reliability-Based Timber Design Codes: Choosing a Fatigue Model - I Smith

38-102-1 A New Generation of Timber Design Practices and Code Provisions Linking System and Connection Design - A Asiz, I Smith

38-102-2 Uncertainties Involved in Structural Timber Design by Different Code Formats - L Ozola, T Keskküla

38-102-3 Comparison of the Eurocode 5 and Actual Croatian Codes for Wood Classification and Design With the Proposal for More Objective Way of Classification - V Rajcic A Bjelanovic

39-102-1 Calibration of Partial Factors in the Danish Timber Code - H Riberholt

INTERNATIONAL STANDARDS ORGANISATION

3-103-1 Method for the Preparation of Standards Concerning the Safety of Structures (ISO/DIS 3250) - International Standards Organisation ISO/TC98

4-103-1 A Proposal for Undertaking the Preparation of an International Standard on Timber Structures - International Standards Organisation

5-103-1 Comments on the Report of the Consultion with Member Bodies Concerning ISO/TC/P129 - Timber Structures - Dansk Ingeniorforening

7-103-1 ISO Technical Committees and Membership of ISO/TC 165

8-103-1 Draft Resolutions of ISO/TC 165

12-103-1 ISO/TC 165 Ottawa, September 1979

13-103-1 Report from ISO/TC 165 - A Sorensen

14-103-1 Comments on ISO/TC 165 N52 "Timber Structures; Solid Timber in Structural Sizes; Determination of Some Physical and Mechanical Properties"

14-103-2 Comments on the CIB Structural Timber Design Code - R H Leicester

21-103-1 Concept of a Complete Set of Standards - R H Leicester

JOINT COMMITTEE ON STRUCTURAL SAFETY

3-104-1 International System on Unified Standard Codes of Practice for Structures - Comité Européen du Béton (CEB)

7-104-1 Volume 1: Common Unified Rules for Different Types of Construction and Material – CEB

37-104-1 Proposal for a Probabilistic Model Code for Design of Timber Structures - J Köhler, H Faber

CIB PROGRAMME, POLICY AND MEETINGS

1-105-1 A Note on International Organisations Active in the Field of Utilisation of Timber - P Sonnemans

5-105-1 The Work and Objectives of CIB-W18-Timber Structures - J G Sunley

10-105-1 The Work of CIB-W18 Timber Structures - J G Sunley

15-105-1 Terms of Reference for Timber - Framed Housing Sub-Group of CIB-W18

19-105-1 Tropical and Hardwood Timbers Structures - R H Leicester

21-105-1 First Conference of CIB-W18B, Tropical and Hardwood Timber Structures Singapore, 26 - 28 October 1987 - R H Leicester

INTERNATIONAL UNION OF FORESTRY RESEARCH ORGANISATIONS

7-106-1 Time and Moisture Effects - CIB W18/IUFRO 55.02-03 Working Party

INTERNATIONAL COUNCIL FOR RESEARCH AND INNOVATION
IN BUILDING AND CONSTRUCTION

WORKING COMMISSION W18 - TIMBER STRUCTURES

DEVELOPMENT OF GRADING RULES FOR RE-CYCLED TIMBER USED IN STRUCTURAL APPLICATIONS

K Crews

Centre for Built Infrastructure Research
University of Technology, Sydney

AUSTRALIA

MEETING FORTY

BLED

SLOVENIA

AUGUST 2007

Presented by K. Crews

H. Blass commented that in Europe material after 500 years of service did not show duration of load effect. He received clarification that the moisture content of the material was at least 30%; therefore, considered as unseasoned. Also new timber was available for comparisons.

H. Blass asked whether the wood was treated. K. Crews replied that the wood was untreated because the hardwood would have low preservative penetration. If the material was the softwood radiate pine then it would have been treated.

A. Ceccotti commented that he was surprised by the results with reference to duration of load effects and cited J. Kuipers work from previous CIB meeting as example.

J.W. Van de Kuilen questioned the ratio between the stresses experienced by members from loading and their strength. K. Crews replied that with wharfs and bridge timber, high loads for short period and also high dead load from the concrete would be expected. Roof timbers seemed to have little or no effect from duration of loads.

F. Rouger asked whether new duration of load factors are needed for this material. K. Crews replied that they may be needed but currently did not have firm answer.

I. Smith commented that the influence of moisture history might be an explanation rather than duration of load and suggested not to refer the observed strength lost as duration of load effect. I. Smith further commented that re-sawing the checked material and the influence of checking on smaller material need to be considered. K. Crews agreed especially when the material was applied in nail plate structures.

E. Karacabeyli asked why minimal difference in MOE but large difference in MOR. K. Crews said that may be some creep recovery related issue in involved.

DEVELOPMENT OF GRADING RULES FOR RE-CYCLED TIMBER USED IN STRUCTURAL APPLICATIONS

Professor Keith Crews
Deputy Director, Centre for Built Infrastructure Research
University of Technology, Sydney, Australia

SYNOPSIS

1 INTRODUCTION

Until recently, the usual method of disposal of timber used in structures has been demolition and disposal. For example, at the time of writing, Australians are placing approximately 1 million tonnes of wood waste into landfill sites. However, reduced availability of native hardwoods has created a situation where use of recycled timber has significant environmental and economic potential, particularly where recycled products can be incorporated into new construction or in some cases retro-fitting of existing buildings and structures.

Currently, there are no standards or recommendations for assigning design properties for structural reuse of wood and the use of recycled timber in decorative products tends to rely on subjective application of visual grading rules developed for new timber. In order to address this problem and utilise the recycled timber resource effectively and reliably, the author has undertaken a research project in conjunction with Timber Queensland (funded by the Forest and Wood Products Research and Development Corporation).

The aim of this project is to develop appropriate (visual) grading systems that take into account the properties of recycled timber; in particular, how the history and previous use of the timber has effected its properties in terms of being fit for purpose in a re-use application. The paper will present the findings of this project to date involving research to quantify the mechanical properties and develop appropriate (visual) grading systems that take into account the properties of recycled timber; for use in both structural and aesthetic applications.

2 BACKGROUND

In many parts of the world including Australia, the traditional "end of life" scenario for structural timbers has been disposal – either by burning or dumping as land fill.

However, in recent times it has been recognised that the use of recycled timber has significant economic potential, particularly where recycled products can be incorporated into new construction or in some cases retro-fitting of existing buildings and structures. Thus the economics of recycled timber products is dependent no only on the "practicality of recovery versus disposal but also on the acceptance of used products in new construction" (Falk, 1994).

Currently, there are no standards or recommendations for assigning design properties for structural reuse of wood and the use of recycled timber in decorative products tends to rely on subjective application of visual grading rules developed for new timber. Recycled or reused timbers potentially include defects which have resulted from the in situ conditions and application of the timber prior to being decommissioned and recycled. For example, "cracks, splits, and checks may be developed from moisture cycling, drying stresses, and/or overstress. Additionally, fastener holes originating from initial construction techniques are commonly present in timbers that may be selected for reuse" (Fridley, Williams & Cofer, 2001).

Thus, in order to utilise the recycled timber resource effectively and reliably we need to have appropriate (visual) grading systems in place that take into account the properties of recycled timber, in particular, how the history and previous use of the timber has effected its properties in terms of being fit for purpose in a re-use application. The development of grading rules for recycled timber need to take into account such issues – particularly for re-use in structural applications where the

presence of defects and the type of loading history can have a significant effect on mechanical properties, resulting in reduced strength when compared with new timber of the same species or strength group.

A significant amount of research has been undertaken in North America (notably by the Forest Products Laboratory in Madison, Wisconsin) that seeks to address some of these challenges to the use of recycled timber and attempt to quantify these effects and how the properties of timber have changed after such timber has been "in-service" for a considerable period of time (Rammer, 1999).

The same issues are apparent in Australia, where there are no specific grading rules that apply to recycled timber used as either Decorative or Structural Products. At present, producers of recycled timber products use the existing visual grading standards AS 2796 and AS 2082 to "grade" material to be "fit for purpose". Whilst these hardwood grading rules can be applied (at least to some extent) to recycled timber, the use of these grading rules which were developed for "new" timbers will have a level of uncertainty associated with them – which can be significant for structural applications.

The main area of uncertainty associated with recycled timber is the fact that in most cases the history of the timber is unknown and as noted by Falk, "From a structural use standpoint, the most distinguishing feature of recycled wood (compared with freshly sawn timber) is the presence of damage. This damage may be a result of the original construction process, building use and/or the deconstruction process" (Falk et al., 1999).

3 DETAILS OF THE R&D PROJECT

At the outset of the project, a number of specific considerations in relation to recycled timber which the project would need to address were identified, including the following:

- The need for development of Stress Grades that are based on the species, size and distribution of characteristics. Such Grades would be preferably compatible with existing visual stress grades;
- The need for development of Appearance Grades that account for expected 'characteristics' common to recycled timber products;
- Recognition of the variations in moisture content of recycled timber – noting that some pieces would be classed as seasoned, whilst others would be regarded as unseasoned timber grades. Most members would have originally been installed unseasoned and would now be in a seasoned or semi-seasoned condition – at least on the surface;
- The moisture content in the core of large end-section members may exceed AS 2082 requirements and, therefore, unseasoned stress grades would apply. The outer case of the member may, however, be in a seasoned condition which would take most of the loading;
- The need to define appropriate limits for sizing tolerances, squareness and straightness – noting that there is likely to be a need for specific requirements for recycled timber;
- Recycled large end sections develop large checks, splits and loose gum veins during its time in service – all of which potentially reduce the mechanical properties of timber members;
- Recycled wood may be unsound, particularly with large end sections which develop large checks, splits and loose gum veins during their service life;
- Decay and wood surrounding nail and bolt holes may have decay but in areas that are difficult to inspect and it is necessary to quantifying the effects of mechanical damage;
- Acknowledgement that characteristics of recycled timber may alter with time – particularly duration of load effects on timber which would affect the strength of the timber section;
- Requirements to develop specifications regarding preservative treatments pursuant to current Australian preservative treatment standards;
- The development of a comparable and reliable marking system or grading stamp.

Whilst all of these issues need to be addressed for recycled timber used in structural applications, it was recognised that many of them are not particularly relevant to appearance products such as wall panels and flooring – although minimum standards of performance would need to be defined for the later concerning definition of "fit for purpose" criteria.

4 GRADING OF APPEARANCE (OR DECORATIVE) PRODUCTS

The grading of appearance products presents grading agencies with some inherent difficulties. The term "appearance', as defined for traditional timber products, defines timber without or with very limited natural blemishes. Design specifications requiring the use of recycled timber is undoubtedly for aesthetic reasons. The 'character' of recycled timber allows it to provide a warmth and desirable appearance in structural applications. The appeal of recycled timber is that it will have features and characteristics as a result of its previous use. This in turn, effectively limits its appearance grade when current standards of visual assessment are carried out.

Australian Standard 2082 – Timber – Hardwood – Visually Stress-Graded for Structural Purposes provides a greater restraint on the number and size of features present within a section of timber, than can be met by many recycled products. Also with appearance products, such as flooring and other decorative products, the surface finish of recycled products can vary considerably. It must, therefore, be recognised that product performance and appearance can differ in the marketplace with recycled products when compared to products produced to Australian Standard 2796 – Timber – Hardwood – Sawn and Milled Products.

The current Standard (AS 2796) specifies three appearance grades. The grading system categorises timber with respect to the number and size of features present in the selected piece. The grades range from those with small features (referred to as Select Grade) to large features (referred to as High Feature Grade). In all other respects, that is moisture content, tolerances and machining imperfections, there is no difference between the grades

Characteristics of recycled timber; in particular, holes; checks; stains; and discolouration are contrary to the features specified in visual grading of new timbers. The High Feature Grade requirements in the Standard specify tolerances that would be exceeded by much of the recycled timbers under assessment, for example, the existence of bolt and nail holes.

"It is in these aspects that the grading rules are contrary to the nature of recycled timber. As well as features such as bolt and nail holes, staining is often evident and there are other aspects of past use which can also influence the appearance. Surface checking for example can be more prevalent and influence the appearance of the finished product, with staining more likely within the checks. Similarly, water marks and other contact with steel can result in discolouration." (Timber Queensland, 2006).

The 'characteristics' that enhance the appeal of recycled timbers are considered not to have such a detrimental effect on its performance as current grading standards perceive; such characteristics merely modify its performance. As such, it is considered that the incompatible sections regarding appearance grades create a catalyst for developing grading standards that do not limit the value and possible reuse option for recycled timber.

It is important to note that AS 2796 is focused on decorative as opposed to structural applications. In using AS 2796 to grade recycled timber the terms "character" or "feature" may be better words to replace "appearance", which implies minimal feature.

From work undertaken to date, a three tier grading system for character is considered appropriate:

- 'Clean' 'Rustic' 'Rustic Overlay' could be the grade names
- Rustic overlay grade should not be used in any "structural" applications (such as flooring, and as such might only be used in flooring as an overlay
- Nail holes, Borer and Marine borer activity needs to be included as a feature
- Specialist sizes may be considered appropriate – for example testing to confirm use of thinner flooring or panelling may be used to demonstrate "equivalency" with new material
- Specification of "random" sizes may also be considered acceptable provided the product is installed as "fit for purpose" (which may need to be noted as a design / construction issue beyond the scope of the Standard)
- The "old board" market (reused but not re-machined) could be permitted under the above provisions for recycled timbers
- There may be a need to prohibit certain species on the basis of previous use / history. For example, Turpentine sourced from a wet environment tends to opens up when re-used in dry environment.

5 GRADING OF STRUCTURAL PRODUCTS

It was decided that quantification of the strength reducing effects of characteristics would be addressed in part, during the testing stages of this project. Initially, the following recommendations were made to link the current visual grading Standard (AS 2082) with the additional "characteristics' inherent in recycled timber members.

a) Bolt holes (including any localised soft rot) would to be treated as knots extending through the full cross section of the timber.

b) Effects of variable moisture content must be considered – for large section members, recycled timber should be considered as unseasoned.

c) Where the extent of any piping has been quantified, this material should be deducted from the gross cross section of the timber for design purposes.

d) Notches and some natural defects may also reduce the effective cross section and where this is the case, the design cross section should be defined as the gross section less the effected area.

e) Flexibility in tolerances is necessary and specific size availability (based on the minimum effective cross section) may need to be the basis of supply

f) As a general rule, timber that has come from internal environments and not subjected to heavy, long term loads should be considered to be at least 1 stress grade lower than that indicated for new timbers graded using AS 2082. For heavily loaded timbers, or where the previous loading history is unknown, the recycled timber should be considered to be at least 2 stress grades lower than that indicated for new timbers graded using AS 2082 (Fuller, 1999).

g) AS 3818 Timber – Heavy structural products – visually graded which permits off-centre heart in large end sections. This standard has been recently published and specifies select and standard grade for timber with a cross section of 0.016 m2 or greater (e.g. 225 x 75 mm minimum size). It permits off centre heart and requirements differ between beams and columns.

5.1 GRADE LIMITATIONS AND GRADING FOR STRUCTURAL APPLICATIONS

AS 2082 provides limitations on the amount characteristics or combination of characteristics in the wood. Specifically, section 1.9.4 refers to mechanical damage inflicted on the timber. This would be a common feature of timber recycled via a deconstruction process. Checks and bolt holes are common features of recycled timber and would often exceed tolerances outlined in section 1.9, without additional fabrication. New provisions will be required to cover characteristics of recycled timbers used in structural applications, in order to permit better resource utilisation.

To some extent, this is offset by the fact that timber that was original sourced from old growth forests is generally clear and denser than faster growing species manufactured today – noting that knots are often less common in older dense wood.

It must be remembered that customers often seek recycled timber for its aesthetic appeal. 'Characteristics' limited by AS 2082 are a common selling tool for the recycled timber products, where appearance is an essential design criterion, in addition to providing adequate strength.

Recycled timbers may be retrieved in parcels containing various species and grades. The species with the lowest mechanical properties will dictate the assigned grade for the parcel of timber (Clause 1.10.3) and therefore regrading of the whole parcel would be necessary.

Specific tolerances addressed by Clause 1.10.5 include seasoning checks, splits, end splits, shakes and the development of loose gum veins. These are all considered common characteristics of recycled timber and require specific tolerances for recycled timber products. If recycled wood has a significant amount of treatment or is painted, this layer may need to be removed for the ease of identification and visual grading / assessment of the likely properties of the timber.

6 TESTING PROGRAM

In order to quantify mechanical properties for specific types of recycled timber, a testing program was designed with the aim of trying to identify the extent to which aging and duration of load effects from previous load histories have effected the bending properties of members fabricated from large end section previously used timbers. The test program is summarised in Table 1 below.

TABLE 1: Proposed Testing Program – Recycled Hardwood Timbers

Timber description	Cross section	Length required	Number Required	Proposed testing	Comments	Sketch
(1) Sawn timber beams	150 x 50 or 125 x 50	3.0m	30	MOE, MOR, density check and mc's	Cut from large timbers previously subjected to high loads (wharf structures). Cut from compression side of girders Same strength group (SG1 or 2) if possible – species ID if possible	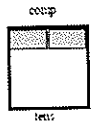
(2) Sawn timber beams	150 x 50 or 125 x 50	3.0m	30	MOE, MOR, density check and mc's	Cut from large timbers previously subjected to high loads (wharf structures). Cut from tension side of girders Same strength group (SG1 or 2) if possible – species ID if possible	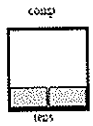
(3) Sawn timber beams	150 x 50 or 125 x 50	3.0m	30	MOE, MOR, density check and mc's	Cut from large timbers previously subjected to low to moderate loads (bridge girders, metal roof structures or domestic history). Identify location in original girder. Same strength group (SG1 or 2) if possible	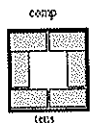
(4) Sawn timber columns (HI)	150 x 150	0.6m	30	Compression strength and stiffness, density check and mc's	Heart in columns – determine compression capacity; heart "boxed" – nominally in middle half, but possibly on edges	
(5) 15mm end butt flooring	15 x ??? (whatever is preferred width)	1.8m	30	MOE, MOR, density check and mc's – identify effects of visual characteristics	Check "equivalency" of boards cut from old rectangular timbers with other flooring products	
(6) Girders / large sawn sections	350 x 350 or similar	6.0 to 7.5m	10	MOE, MOR, density check and mc's.	Optional – full scale tests; ideally girders with some possible degrade that might be considered "borderline" in terms of re-use as solid sections. Develop "pre-selection" grading rules for either structural or aesthetic re-use	
(7) Sawn timber beams – notched on edge	150 x 50 or 125 x 50	3.0m	30	MOE, MOR, density check and mc's	Rectangular sections with notches or holes on tension side – nominally 20% loss of section Same strength group (SG1 or 2) if possible	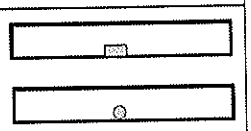
(8) Sawn timber beams – rot pockets or notched away from edge	150 x 50 or 125 x 50	3.0m	30	MOE, MOR, density check and mc's	Rectangular sections with notches or holes in middle 50% zone, – nominally 30 – 40% loss of section Same strength group (SG1 or 2) if possible	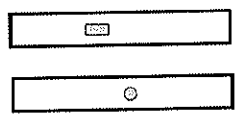

GENERAL NOTES:

- Test series 1 and 2 are required to attempt to quantify suspected differences in strength between the tension and compression sides of beams exposed to long term bending under large loads.
- Test series 3 will quantify long term strength reductions for timber previously used in low load level applications.
- Test series 4 will hopefully validate the use of heart material that is the left over after cutting off edge beams / boards from large end section timbers
- Test series 5, should ideally have species ID so that comparison can be made with "new" timber floor boards of greater thickness
- Test series 6 is aimed at identifying the "limits" of visible defects (particularly on edges) to quantify effects on strength and develop some simple pre-selection grading rules for large timbers
- Test series 7 & 8 should ideally be sourced from the same type of material used in Test series 3, so that a comparison can be made between defect effected and non defect timbers, with the aim of quantifying the strength reduction effects of notches and holes.

To date, 90 pieces of timber (each 125 x 50 mm) have been assessed, from items 1 to 3 of Table 1 - focusing on material that has been cut from girders where the variations in the structural capacity of timber in the compression side of a girder can be compared to the tension side. The members were cut from large section material nominally at least 300mm x 300mm from either structural grade 1 or 2 timbers. This is illustrated in Figure 1.

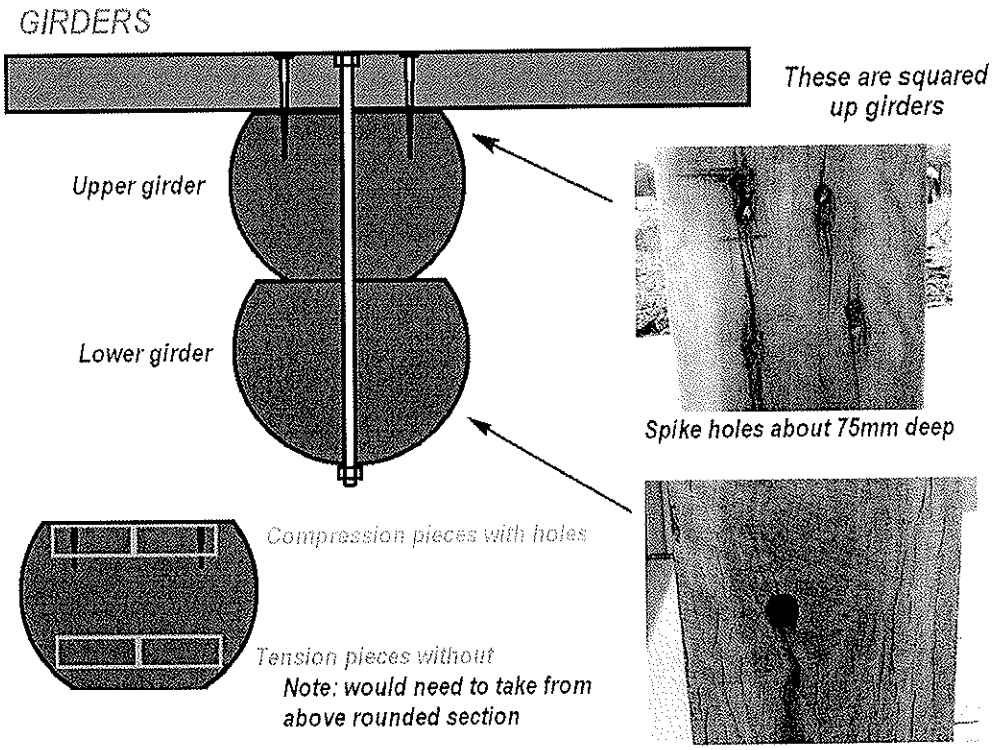

Figure 1 – Typical large end section timbers used in Bridge Girders

Following the initial breakdown the 50 mm thick flitches from the tension and compression sides of the girders were re-sawn into two pieces with nominal dimensions of 125 x 50 mm. The final test material therefore contained a mix of characteristics including spike holes and bolt holes as well as checking and natural features. However, from a visual assessment, the timber material was considered to be relatively clean of defects resulting from the recycling process.

In addition to MOE and MOR testing undertaken on these test pieces each stick of timber was also allocated a 'grade' based on an ultra sonic hand held grader. Due to the nature of recycled timber, containing nail holes, bolt holes and possibly decay around such characteristics, it was of interest to determine how such a device would perform. This work was undertaken through and additional in-kind contribution to the project by Mr Bill Kranenburg of KITT.

7 PRELIMINARY ANALYSIS AND RESULTS

Trial 1 consisted of 60 pieces of timber, extracted from large structural members that had been previously subjected to high loads. 30 pieces were cut fro the tension edge and 30 from the compression edge of the larger members, as noted in Items 1 & 2 in Table 1. Trial 2 consisted of 30 pieces of timber cut from large timbers previously subjected to low to moderate loading. The cutting patterns were in accordance with Item 3 in Table 1. Provisional analysis of the results from this testing indicates the following trends:

Stiffness:
1a) The modulus of elasticity (MoE) of all specimens was consistent with that expected for new timber with a grade of F27, which is the grade that would have been expected if the timber had been visually graded in accordance with AS2082. The average MoE for all 90 specimens was 18618 MPa with a COV of 14%.

1b) In terms of MoE, there was no significant difference between the specimens in trial one and trial 2. In other words, previous loading history had no significant effect on MoE.

1c) There was also no significant effect on MoE as a result of where the specimens were cut from the larger members. In other words the location of the specimens in the original larger members (whether on the tension or compression edges or on the sides) had no effect on the MoE.

2) Whilst there are some marked discrepancies between individual results for specific pieces of timber, the correlation between the MTG method for predicting MoE and the actual test results, indicated that the MTG method over estimates MoE by approximately 27%, with an average MoE of 23626 MPa and a COV of 13%. This is illustrated graphically in Figure 2 below.

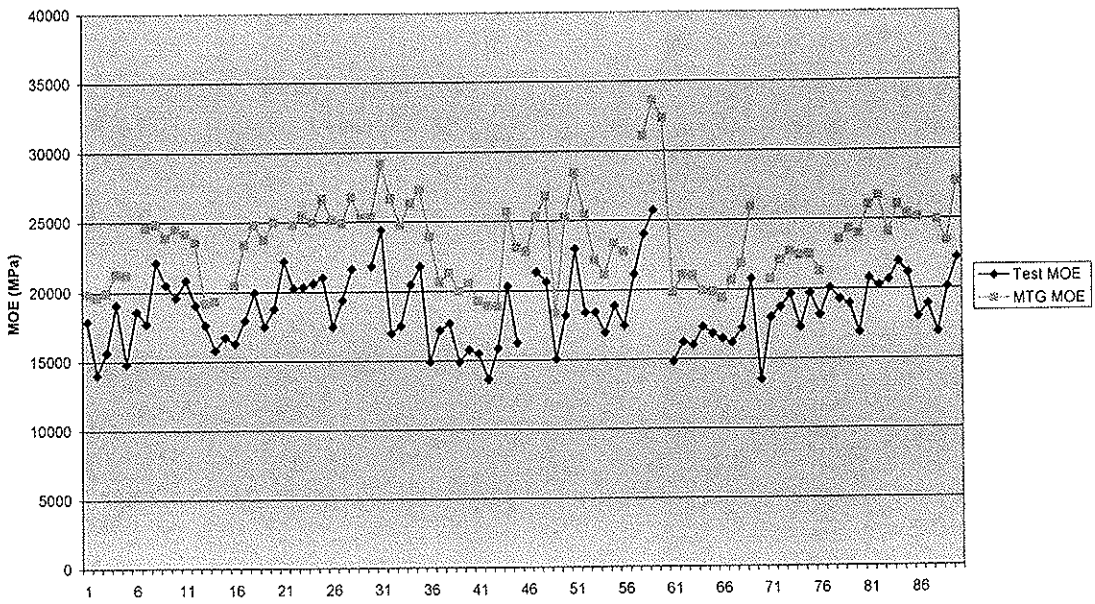

Figure 2: Comparison of MoE values obtained from testing, with those predicted using the MTG grader.

Strength:

3a) The modulus of rupture (MoR) for bending for specimens from both trials, indicates that there is an observable difference between the average strength (and variability) of specimens obtained for the compression edge, when compared to those obtained from the tension edge. This can be observed in figure 3 for trial 1.

For trial 1, the compression average = 76 MPa, whilst the tension average = 87 MPa. The effect of the difference in 5th percentile estimates of bending strength between compression and tension specimens from trial 1 is seen markedly in figure 4, using a Weibull distribution.

3b) Initial analysis of the compression specimens in trial 1, indicates a 5th percentile MoR of 43.6 MPa with a COV of 22%, compared to a predicted 5th percentile value of 47.2MPa with a COV of 27% for the tension specimens, based on a non parametric analysis. These values represent 55% and 59% respectively of the expected characteristic strength for new timber visually graded as F27.

3c) However, analysis assuming a cumulative distribution (AS/NZS 4063) of the tension and compression specimens indicates that the 5th percentile values are essentially identical, with an estimated value of 42.1 MPa, which is approximately 53% of the expected value for F27 timber.

3d) The difference in the two methods for predicting 5th percentile values is probably not significant for the number of specimens and the important thing to note is that these values are essentially consistent with the duration of load factor of 0.57 used in AS 1720.1, for long term permanent loads.

3e) Based on these preliminary analyses, the recommendation for design purposes would be to consider timber extracted from large structural members that had been previously subjected to high loads, as having the same stiffness as that predicted using the current visual grading rules (AS2082), but a characteristic bending strength 50% of that predicted from visual grading.

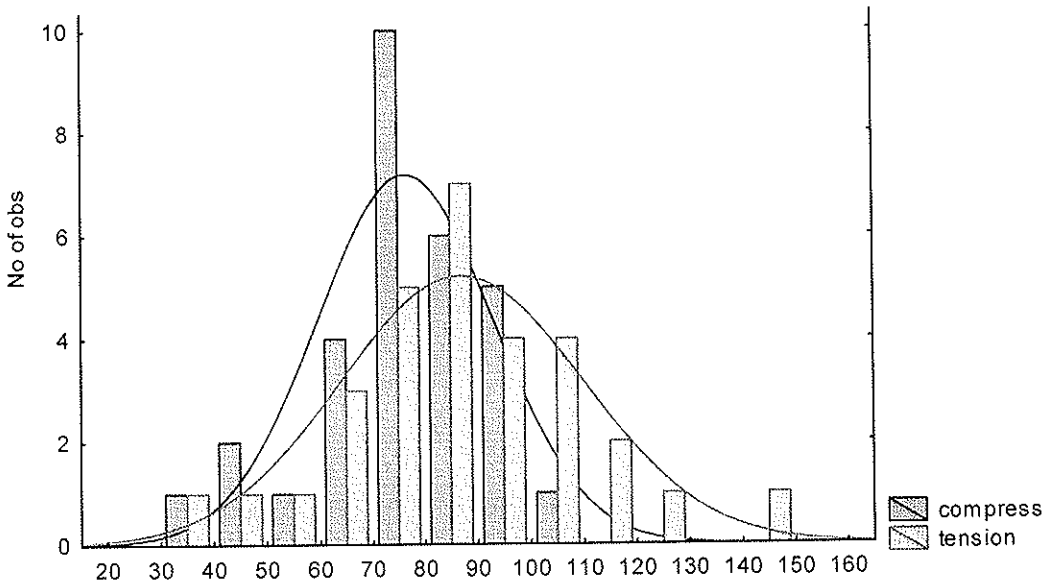

Figure 3 – Comparison of compression and tension bending strengths, Trial 1

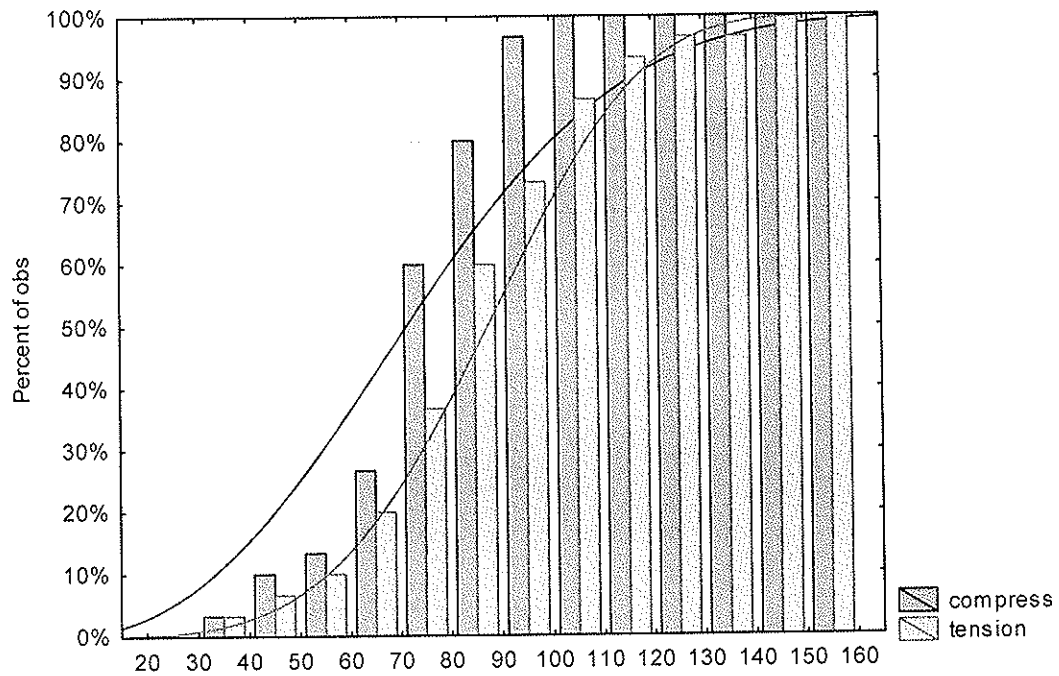

Figure 4 – Cumulative analysis of compression and tension bending strengths, Trial 1 using Weibull distribution.

4a) The same difference in bending strengths for compression and tension specimens, was observed in trial 2 (refer figure 5). The respective average values for compression, tension and side specimens, were 78.2 MPa, 76.4 MPa and 88.6 MPa.

4b) Analysis assuming a cumulative distribution (AS/NZS 4063) of the compression and tension specimens in trial 2 indicates that the 5^{th} percentile values of 49.9 MPa and 58.5 MPa, respectively.

The 5th percentile values for the specimens obtained from the sides of the larger members, was estimated at 52.4 MPa. The cumulative distribution is illustrated in figure 6.

These respectively represent 62%, 73% and 66% of the characteristic bending strength for new F27 timber, graded using AS 2082. If all the data is pooled, the 5th percentile estimation would be 52.1 MPa (65%), with a COV of approximately 25%.

4c) The results indicate that the characteristic strength of material subjected to lower levels of load, have not suffered as much fibre damage, and hence have higher strengths than those subjected to higher levels of load, for longer durations.

4d) Based on these preliminary analyses, timber extracted from larger members with a known loading history of low level / shorter term loads, could be assumed to have the same stiffness as that predicted using the current visual grading rules (AS2082), but a characteristic bending strength 65% of that predicted from visual grading.

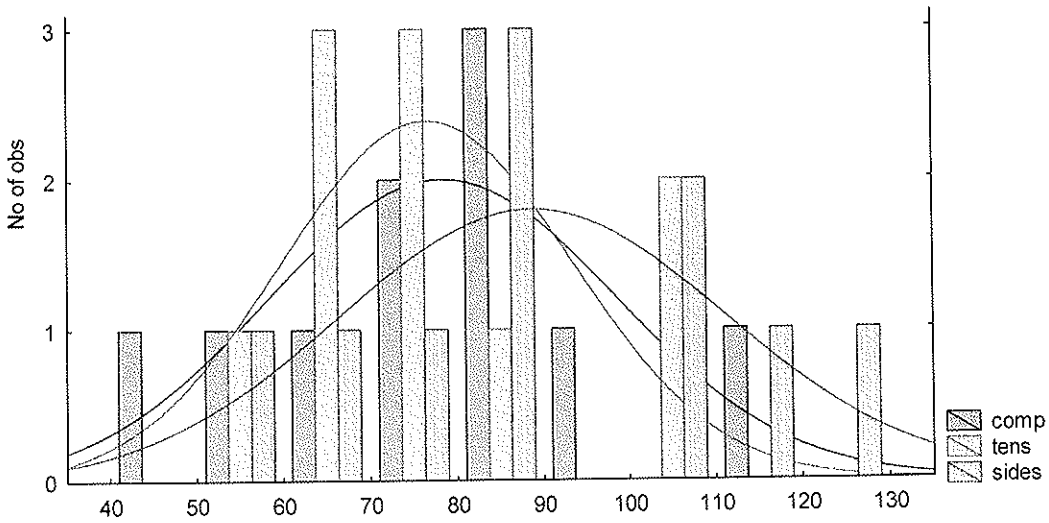

Figure 5 – Normal Distribution for trial 2 specimens

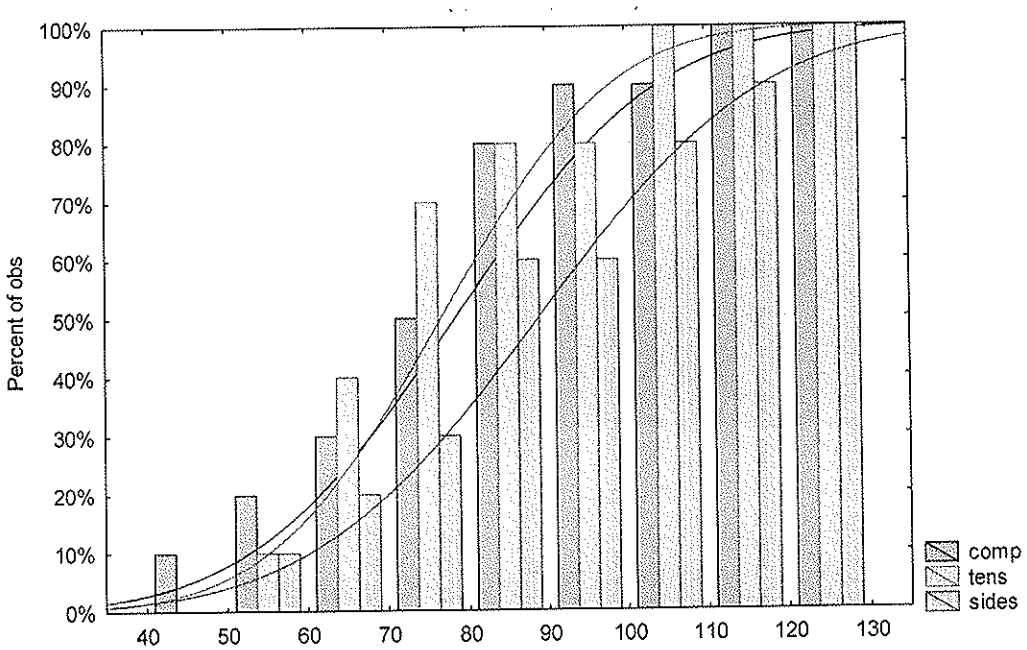

Figure 6 – Cumulative Normal distribution of specimens for trial 2.

8 CONCLUSIONS AND RECOMMENDATIONS

Only 90 specimens have been tested to date and additional testing is currently being undertaken to gain more data and hopefully improve confidence in the results. However, from analysis of these preliminary results some trends are apparent.

Based on the initial test results, it can be concluded that application of existing visual grading rules (AS 2082) can be used to assign properties for timber cut from larger members (and not containing defects such as degrade and bolt holes) on the following provisios:

1) MoE values are valid and can be assumed to be similar to those of new material.

2) MoR values must be reduced when compared to new material to take into account duration of load effects. These reductions are estimated to be between 35% for material with a load history of short term / low magnitude loading (such as roof structures with light weight cladding), and 50% for material with a load history of longer term / high magnitude loading (such as warehouse / wharf storage floors).

Two interim grading documents are currently being prepared. Both drafts have been developed in consultation with relevant industry groups.

The first deals with Appearance Grade products and is based on AS 2796, but incorporates specific clauses for classification of recycling characteristics and their "impact" on appearance – such as holes from fasteners and surface "imperfections" resulting from previous usage.

The second draft details structural grading rules for recycled hardwood timber and has been prepared as a blend of both AS 2082 and AS 3818 to cover both smaller end-section material and larger end-section material included in AS 3818. The draft will be a stand alone document specific to recycled timber and considers separately smaller end-section timber where there is closer alliance to AS 2082 and larger end-section timber that is more closely aligned to AS 3818.

Due to the inherent differences between recycled and "new" timber, traditional "strength groups" have not been used in the draft, however a similar concept referred to as "Species Group" has been included, so that species of recycled timber displaying similar properties and characteristics affecting the stress grade can be grouped together. This has been done to facilitate an efficient means of applying the stress grades, whilst at the same time keeping the number of rules to a workable minimum.

It should also be noted that the draft documents are being developed as interim "Industry Standards" to provide an orderly introduction into the marketplace, within a shorter time frame than would be possible implementing using the "Standards" development process. Whilst the documents are specific to recycled timber, they have also been developed to be very much in line with current applicable Australian Standards, with the intention that after "evolution", the documents will achieve full "Standards" status.

It is anticipated that the outcomes of this project will enhance the use of recycled timber products in the market place, whilst at the same time providing appropriate standards for defining "fit for use applications" and ensuring safe characteristic properties are used by designers when using recycled timber members in structural applications.

9 ACKNOWLEDGEMENTS

The author wishes to acknowledge the following persons for their assistance and input in undertaking the project to date:

- Colin MacKenzie and Dave Hayward – Timber Queensland
- Michael Kennedy – Kennedy's Classic Aged Timbers
- Dr Glen Kile and Dr Chris Lafferty – Forest & Wood Products Research and Development Association (Australia)
- Damon McGrath, Stephen Flynn and Matthew Thomason – Final year students at UTS
- Staff in the UTS structures and material testing laboratory

10 REFERENCES

Australian Standard, 1604.1-2005: Specification of Preservative Treatment. Part 1: Sawn and Round Timber

Australian Standard, 2796.1-1999: Timber – Hardwood – Sawn and Milled Products. Part 1: Product Specification

Australian Standard, 2082-2000: Timber – Hardwood – Visually Stress-Graded for Structural Purposes

Australian Standard, 2858-2004: Timber – Softwood – Visually Graded for Structural Purposes

Australian Standard, 3818.1-2003: Timber – Heavy Structural Products – Visually Graded. Part 1: General Requirements

Australian Standard, 3818.7-2006: Timber – Heavy Structural Products – Visually Graded. Part 7: Large Cross-Section Sawn Hardwood Engineering Timbers

Australian Standard, 4361.2-1998: Guide to Lead Paint Management. Part 2: Residential and Commercial Buildings

Falk, R., 1994, "Building Products from Recycled Wood Waste", *Proceedings of the Energy Efficient Building Association Conference,* February, Dallas, Texas

Falk, R.H., DeVisser, D., Cook, S. & Stansbury, D. 1999, "Effect of damage on the grade yield of recycled lumber", *Forest Products Journal*, vol. 49, no. 7/8, pp. 71-79.

Fridley, K.J, Williams, J.M. & Cofer, W.F. 2001, "Reliability of reused sawn lumber: effect of fastener holes", *Journal of Structural Engineering*, April, pp.412-417.

Fuller, P.J. 1999 "Engineering Properties of Australian Timbers Recovered from Demolition Sites" *Undergraduate Project Thesis*, Civil & Environmental Engineering, University of Technology, Sydney

Rammer, D.R. 1999, "Evaluation of recycled timber members", *Proceedings of the Fifth ASCE Materials Engineering Congress*, Cincinnati, Ohio, pp. 46-51.

Timber Queensland, 2006, "Timber Queensland Policy Statement: Making Sustainability Our Competitive Advantage", *Timber Queensland, Fortitude Valley, Queensland*

INTERNATIONAL COUNCIL FOR RESEARCH AND INNOVATION
IN BUILDING AND CONSTRUCTION

WORKING COMMISSION W18 - TIMBER STRUCTURES

THE EFFICIENT CONTROL OF GRADING MACHINE SETTINGS

M Sandomeer (née Deublein)

J Köhler

Swiss Federal Institute of Technology, Zürich

SWITZERLAND

P Linsenmann

Technical University of Munich

GERMANY

MEETING FORTY

BLED

SLOVENIA

AUGUST 2007

Presented by M. Sandomeer (née Deublein)

J. W.G. van de Kuilen asked if machine settings were adjustable what sawmills would do? M. Deublein responded that sawmills should adjust the setting to ensure quality of the product.

P. Quenneville asked if the purpose of the work is intended to ensure reliability of design and would lower quality material be put in lower grade. M. Deublein responded that the work is intended to ensure quality and reliability of grade.

F. Lam commented that the work tested the robustness of the CUSUM process but comparison with the proposed Bayesian process was not done. M. Deublein responded that the process continuously detected shift in properties of the predictor which differed from the CUSUM approach.

F. Rouger commented that machine control system avoids "tricky" behaviour and it is supposed to be safe. If you have a low quality material, machine control system should be able to detect this without the aim of optimization. Bayesian approach depends on the regression approach. This is an interesting concept to fill the gap between machine and output control. M. Deublein said that flexibility to make adjustment is important.

J Köhler commented that this method would have the possibility to change and make adjustments.

The efficient control of grading machine settings

Markus K. Sandomeer (née Deublein) & Jochen Köhler
Swiss Federal Institute of Technology, Zurich, Switzerland

Peter Linsenmann
Technical University of Munich, Germany

Abstract

Machine grading systems operate according to similar principles; one or more indicative properties of the timber to be graded are measured by the machine and based on these measurements a sample of ungraded timber is subdivided into subsamples of graded timber. The grading acceptance criteria are formulated in form of boundary values for indicative properties that have to be matched to qualify a piece of timber to a certain grade. These boundaries are termed grading machine settings. The grading performance, i.e. the statistical characteristics of the output of grading machines strongly depends on these settings, and in general very much attention is given on how to control them.
Currently applied procedures to control the grading machine settings are either machine controlled or output controlled, however, both procedures do not facilitate the efficient use of information which is gathered prior and during the runtime of the grading machine. The utilization of the entire available information is required for the accurate representation of uncertainty in modeling the material properties of graded timber.
In this paper the efficiency of existing control procedures for timber grading machines is discussed with regard to the capability of the procedures to assess systematic changes in the quality of the timber supply. Experience gained during the application of these methods is presented. An alternative approach for the control of grading machine settings is introduced which can be seen as a combination of the machine and output control procedure. It facilitates the consistent consideration of new information gained prior and during the grading process. The approach is summarized in a coherent and implementable format and possible benefits of its application in practice are discussed.

1 The Variability of Timber Material Properties

The safe and efficient use of materials in construction necessitates that the life-cycle performance of structures can be predicted and reassessed with sufficient accuracy. Beside the formulation of physical models for the prediction of structural performance it is required that uncertainties are consistently taken into account, i.e. uncertainties related to:

- inherent natural variability, or randomness
- model uncertainty, i.e. uncertainty associated with the idealised mathematical description of the real world, and
- statistical uncertainty, i.e. uncertainty arising from incomplete statistical information.

For the modelling of the performance of timber structures the probabilistic representation of the variability of timber material properties is an issue of special interest. Timber is a complex building material and its properties are in general highly sensitive to scale, climate and loading variations. Material properties can be represented by random variables and the statistical characteristics of these variables can be described by distribution models together with the corresponding parameters which are calibrated based on data taken from standard

test samples. Statistical uncertainties and model uncertainties can be taken into account by describing the variable with its predictive distribution function. The variation of timber material properties on this level may be described by the term *meso level variability*.

In practical design situations uncertainties as arising from the variability of timber material properties have to be taken into account. This is in general done implicitly by choosing certain classes of timber material for the construction and by deriving certain design values for the timber material properties correspondingly. These design values for timber material characteristics are combined with design values for the considered load scenarios and a safe and efficient design solution may be identified. The timber (strength) class system, the procedure how design values for loads and material resistance have to be derived and the formulation of design equations is prescribed by codes and standards.

While the explicit consideration of uncertainties is not of particular interest for the engineer when designing a timber structure, it is of utmost importance that uncertainties are considered properly when the system of regulations for the design of timber structures is derived. It is important to note that e.g. the variability of timber material properties which has to be taken into account is not of the above introduced meso type, i.e. is not simply the variation within one sample of timber specimen. The variation between different samples has to be additionally taken into account. In design it is only known that timber of a certain strength class is used. However, no information is given with regard to the different grading schemes, the origins of the raw timber material, the species, etc. Variability in timber material properties modelled on this level might be termed *macro variability*. The difference between meso and macro variability is illustrated in *Figure 1*.

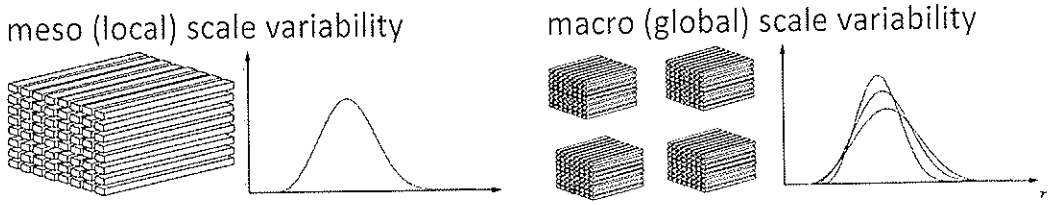

Figure 1: *Macro and meso scale spatial variability of timber material properties.*

It is important to note, that the above described types of variability relate only to spatial variability. Variability due to different climate conditions and load conditions are not considered in this scheme.

2 Machine Grading of Structural Timber

Grading machines operate according to similar principles; one or more indicating properties of the timber to be graded are measured by the machine and based on these measurements a sample of ungraded timber is subdivided into subsamples of graded timber. However, the capability of indirect measurements for predicting the strength can never be perfect and therefore, uncertainties are always present which have to be considered in the underlying grading model.

In general grading acceptance criteria are formulated for the indicating property in form of boundary values *(grading machine settings)* which have to be matched to qualify a piece of timber as belonging to a certain grade. The performance, i.e. the statistical characteristics of the output of grading machines strongly depends on these settings, and in general very much attention is kept on how to control them. In *Figure 2* observations on the indicating property and the property of interest are illustrated. Boundary values of the indicating property (IP1 and IP2) subdivide the sample into subsamples assigned to grade 1, grade 2 and reject.

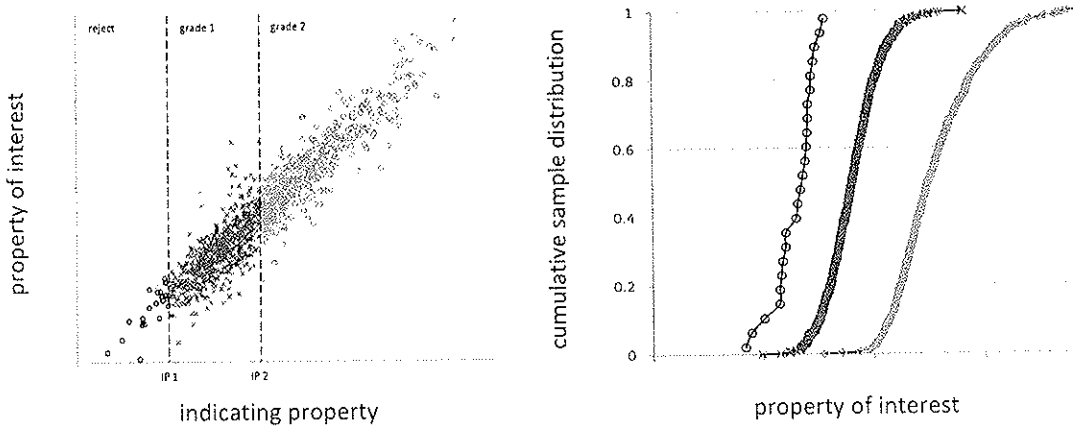

Figure 2: *left: Observations on the indicating property and the property of interest. The grading machine settings (IP1 and IP2) subdivide a sample into subsamples assigned to 'grade 1', 'grade 2' and 'reject'.*
right: *Cumulative sample distribution of the property of interest of the graded subsamples.*

When considering the control of grading machine settings it is in general distinguished between two procedures, the so-called *machine controlled* system and the so-called *output controlled* system.
To get an idea of the different approaches and underlying requirements of different countries or continents an overview of the existing standards for the control of grading machine settings is given in the following paragraphs.

International standards:
In the international standard ISO 13912 methods for machine strength grading are represented. To ensure the repeatability, calibration and the consistency of the grading machines, evaluation checks based on the *output control* scheme are prescribed. This includes a detailed description of daily or periodic output control checks. The required characteristic values for subdividing the timber samples into strength classes are given in the corresponding standard ISO 13910. The goal of these standards is to specify the essential features common to all machine strength grading operations and for worldwide applications.

Europe:
In Europe the relevant standard is EN 14081 comprising four parts regarding general requirements for visual and machine strength grading, additional requirements for initial type testing as well as factory production control for machine strength grading and a list of utilized grading machine settings. According to this standard, either *machine control* or *output control* systems can be implemented. A detailed statement on the procedure of the machine controlled system is given in Chapter 3.2 of this paper. The output controlled system according to EN 14081, part 2 is described in 3.3. Both methods require a visual override inspection to ensure the detection of strength-reducing characteristics that are not automatically sensed by the machine.

Australia:
In the Australian standards it is distinguished between *mechanically graded timber* which has to conform to the requirements of AS/NZS 1748 and *proof graded timber* fulfilling the regulations given in AS 3519. The Australian standard AS 3519 has been developed for a stress-grading system that incorporates the use of continuous proof testing machines which is comparable to the European output control system. Methods and tables allowing the estimation of the required proof-stress are included.
In AS/NZS 1748 the most important structural properties of the mechanically stress graded

timber are evaluated both during an initial testing program and at regular intervals thereafter. The procedure for monitoring structural properties of machine graded timber is described in the AS/NZS 4490. This standard sets out procedures for the initial evaluation process using in-grade testing and subsequent periodic monitoring, also with proof testing procedures.
To confirm the structural properties of a consignment of mechanically stress-graded timber sampling an initial testing shall be undertaken in accordance with the AS/NZS 4063.

North-America:
Under the American Lumber Standard Committee (ALSC) the grading procedures of the US evolved to an output-based system for both, qualification/certification and quality control *(Galligan & Devisser, 2004)*. In the "Machine Graded Lumber Policy" of the ALSC *(ALSC, 1998)* minimum criteria for the machine grades being qualified by output control are listed. Following the ALSC PS20-05 grading agencies are responsible for qualification of mills to produce machine graded timber. In the ASTM D6570 a periodic evaluation of at least one assigned property of a grade is required.
The quality control procedures given in the Canadian standard of the National Lumber Grades Authority NLGA SPS2, part B are based on the cumulative sum (*CUSUM*) method of the output control system which is described in Chapter 3.3 of this paper. Other unspecified methods for quality control are allowed as long as they meet the general requirements for machine stress-rated or machine evaluated lumber given in part A of the NLGA SPS2.

The different control procedures mentioned in the particular international standards are applicable for various types of grading devices. To get a general idea of existing strength grading machines for structural timber and their operating principles reference is given to *(Boström et al., 2000)* and *(Denzler et al., 2005)*.

In the following, three methods for the control of grading machine settings are considered in more detail. The so-called CUSUM (cumulative sum) method is a method to perform *output control*, the method prescribed in EN 14081, part 2 is denoted as the "cost matrix method" and applied to perform *machine control*. Furthermore, a new method is presented where an attempt is made to combine both, machine and output control. This method is based on Bayesian regression analysis.

3 Illustration of different schemes for the control of grading machine settings

3.1 Data

The goal of the experimental investigations is to simulate situations where a clear quality shift between initial tested timber material and subsequent applied input material is observable. Aim of this investigation is not to derive optimal settings for the considered grading machine and strength class combination, but to apply existing machine settings given in EN 14081, part 4 and to observe the capability of the three methods to react on quality caused distribution shifts of the input material.

A dataset of 650 specimens of Norway spruce (Picea abies) from the Central European countries Germany, Austria and Czech Republic is machine graded and tested in tension load. According to the different origins and dimensions the total sample can be subdivided into the subsamples given in *Figure 3*.
Comparing the cumulative sample distributions in *Figure 3* it becomes apparent that the subsample H representing one origin has an observable higher mean value (about 25%) of the tension strength than the remaining subsamples from other origins. Therefore subsample

H is compared to the remaining subsamples to simulate the timber material supply of two different origins with dissimilar material property values.

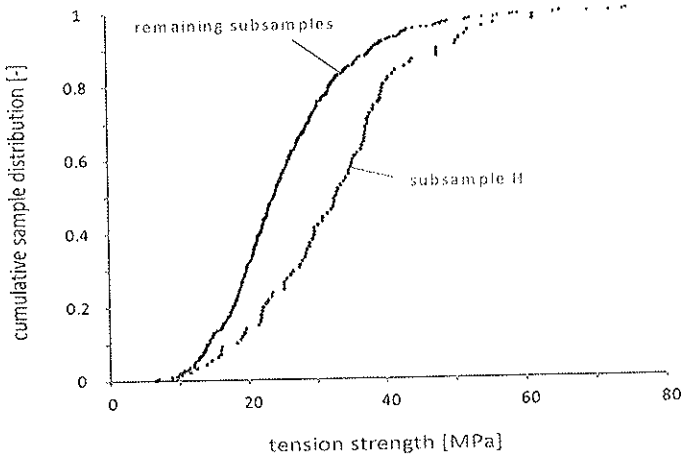

Figure 3: Cumulative sample distribution of the strength property of subsample H and the remaining subsamples.

Machine strength grading is conducted by applying the GoldenEye 706 multi-sensor grading machine. The GoldenEye 706 is a combination of an optical vibration measurement device for quantifying the dynamic modulus of elasticity and an X-ray scanning device for measurement of dimension, density and knot values of the boards. These observed predicting properties of the machine were combined by regression analysis to calculate one indicating property (IP) *(Glos et al., 2006)*.

After machine grading the pieces are tested in tension according to EN 408. The characteristic properties for each piece are determined in accordance with EN 384. The values of tension strength are adjusted to 150 mm width (k_h factor), the values of modulus of elasticity to a moisture content of 12 % according to EN 384.

3.2 Cost Matrix Method

The control of grading machine settings based on the *machine control* system was developed in Europe almost 40 years ago and different methods have been used. A new approach was introduced by Rouger (1996, 1997) in which the performance of the machine is compared with that of a 'perfect' machine capable of grading each specimen to its optimum grade. In the comparison of the *assigned grade* and the *optimum grade* a cost analysis is used where weighting factors are applied to pieces that are wrongly upgraded or downgraded. This method for machine control found its way into the actual European standard EN 14081, part 2 and is denoted as the *"cost matrix method"*. Today, all grading machines in Europe producing timber for the European market are operating with machine control systems *(Boström et al., 2000)*. Elaborate descriptions of the single steps of the machine control procedure have been carried out earlier and can be found e.g. in EN 14081, part 2, Rouger (1997), Bengtsson & Fonselius (2003), Köhler (2006) and Köhler & Steiger (2006).

Example

All grading machines together with their grade determining settings for the indicating properties are enlisted in the European standard EN 14081, part 4, subject to the condition that they are approved in accordance with the requirements given in the same standard. This list is updated approximately every half a year, each time shortly after the Technical

Committee CEN/TC124 has adjudicated upon the approval of new grading machines or new application ranges of existing grading machines.

Lamellas for GLULAM manufacturing processes can be assigned to the following L-classes with the corresponding required characteristic values as specified in *Table 1*.

Table 1: *Requirements for the characteristic values of strength class L25 (Glos et al., 2006):*

	tension strength (5^{th}-percentile value) [MPa]	tension MOE ($0.95 * \overline{x}$) [MPa]	density (mean – $1.65 * \sigma$) [kg/m³]
L 25	14.5	10450	350

The settings for grading the samples with the GoldenEye 706 into the strength class combination L25/reject to be utilized e.g. for GLULAM production are taken from the tables given in EN 14081, part 4. These settings are applied for grading at first subsample H and subsequently the remaining subsamples (*Figure 3*) into strength class L25.

The characteristic values (underlined) and the yields of the particular grades are given in *Table 2* and *Table 3*.

Table 2: *Subsample H (n=103): Characteristic values and yield of the strength class combination L25/reject.*

L25	tension strength [MPa]	tension MOE [MPa]	density [kg/m³]	yield [-] / [%]
mean value	33.7	12041 (10450)	446.5	98 / 95.1
standard deviation	10.9	1960	37.1	
coefficient of variation [%]	32.4	16.3	8.3	
5th-percentile	16.0 (14.5)	9162	386.7	
5th-percentile (normal distributed)	--	--	385.5 (350.0)	
REJECT				5 / 4.9

The characteristic values gained by grading subsample H into the strength class L25 lie remarkably above the required characteristic values in brackets and in *Table 1*. The yield of 95.1% in L25 also confirms the high quality level of the timber material in this subsample.

Table 3: *Remaining subsamples (n=547): Characteristic values and yield of the strength class combination L25/reject.*

L25	tension strength [MPa]	tension MOE [MPa]	density [kg/m³]	yield [-] / [%]
mean value	28.6	10656 (10450)	418.4	397 / 72.6
standard deviation	10.2	1899	50.3	
coefficient of variation [%]	35.6	16.3	12.0	
5th-percentile	16.2 (14.5)	8152	350.9	
5th-percentile (normal distributed)	--	--	335.6 (350.0)	
REJECT				150 / 27.4

Comparing the results of grading the remaining subsamples into L25 with the requirements given in the brackets and in *Table 1* it can be seen that the characteristic values for tension strength and stiffness reach the required level. The characteristic value for density is too low. The mean value of the modulus of elasticity signalizes the quality shift within the input material slightly however, considering only the 5^{th}-percentile value of the tension strength no quality shift would be observable.

Summarizing the results of the machine control procedure to detect variability in the timber material input it has to be stated that the quality shift is identified only faintly. In practice

situations quality variability is difficult to be detected at all, because regular checks of the output of a machine controlled grading system are not mandatory. However, even when a quality shift is detected a substantial sampling procedure would be required to gather new data for the assignment of adjusted grading machine settings. Settings derived once, are fixed by recording them in EN14081, part 4. Information gathered during and after the grading process cannot be utilized and incorporated into the grading model afterwards.

3.3 Cumulative Sum Method - CUSUM

Considering the control procedures of the *CUSUM* method a limited number of specimens of each grade and dimension has to be selected a certain number of times per working shift. The selected specimens have to be proof-loaded to check that the quality of the timber is within desirable limits. If the timber survives the proof loading, it is deemed to have acceptable strength properties. Successive values of a variable are compared with a defined target or reference value, and the cumulative sum of deviations from this value is recorded in tabulation and plotted on charts. If the accumulation reaches or exceeds a pre-determined decision interval, this is taken to indicate that a change has occurred in the mean level of the variable and the process runs *out of control*. The *CUSUM* approach assumes that the process is initially *in control*. This can be ensured by some initial qualification or certification test which has to be passed prior to the establishment of the continuous control program.
CUSUM operates with two separate types of charts, an *attributes chart* and a *variables chart*. In the attributes chart the number of pieces that fails when proof loaded is recorded, while in the variables chart the actual values of the modulus of elasticity are used and their mean value is calculated for the assessment of the cumulative sum. If the process runs out of control a different set of charts has to be applied until the process returns to in control.
When the process switches to out of control, in general, some check of the stress grading process must be performed. If the process does not return to in control after a defined series of test samples the production has to be stopped and investigation of the process and corrective action may be undertaken before several nonconforming units are manufactured.

Example

The investigation of the effectiveness of the output control system is performed by applying subsample H *(n=103)* for the initial evaluation procedure given in EN 14081, part 2. For this purpose existing grading machine settings for strength class L25 listed in part 4 of the standard are used to grade the subsample and the graded sample belonging to L25 is checked to fulfill the requirements for initial testing of output control according to EN 14081, part 2. The subsequent control procedures following the *CUSUM* method given in EN 14081, part 3 are undertaken by applying the dataset of the remaining subsamples *(n=547)*.
The goal is to observe the run-length of the different control charts until the variation within the timber input resource qualities of the subsamples as shown in *Figure 3* is detected.

In order to simulate the method of *CUSUM* charts given in EN 14081, part 3 the following assumptions have to be made:

1. Since only the proof loading with regard to bending strength and bending stiffness is described in EN 14081 it is assumed that the equation for the assessment of the critical proof stress is also valid for tension strength and is calculated with the equation given in EN 14081, part 2

$$f_{t,proof} = 0.96 \cdot f_{t,k} . \qquad (1)$$

Therefore, the proof stress for strength class L25 is 0.96·14.5 [MPa] and equal to 13.92 [MPa].

2. Since the required characteristic MOE value according to the L-classes is already reduced to the 0.95%-mean value the measured mean MOE is compared to the required characteristic value given in *Table 1*.
3. The tension strength values of the applied dataset are adjusted to 150 mm width. Therefore the different dimensions within the subsamples of the dataset are under no further consideration.

The test pieces to be used in the subsequent *CUSUM* charts have to belong to the strength class L25 (cp. *Table 1*) and are chosen from this graded sample randomly. In accordance to EN 14081, part 3 each test sample for proof loading contains 5 or 10 specimens for normal daily control or the control of new settings, respectively.

Proof loading is simulated by comparing the values of the tension strength with the critical proof stress of 13.92 [MPa] and the numbers of failures are tabulated in the attributes chart to assess the cumulative sum. In order to calculate the *CUSUM* of the modulus of elasticity the mean value of each test sample is recorded in the variables charts. Detailed descriptions of the charting procedures based on three parameters denoted by *K, Y* and *Z* are given in previous publications (Köhler & Steiger, 2006; Köhler, 2006; Boström et al., 2000) and in the European Standard EN14081, part 3. The results of the experiments are illustrated in the *CUSUM* variables and attributes charts as shown in *Figure 4*:

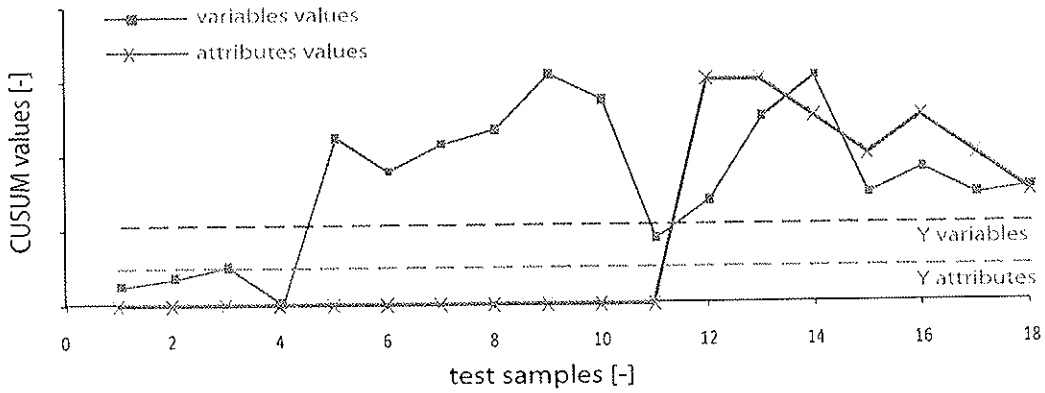

Figure 4: *Variables and attributes charts of proof loaded test samples.*

It can be observed that the variables chart indicates an out of control condition the first time after 5 test samples have been proof loaded. The run length of the attributes chart lasted to the 11th test sample of the proof loading procedure. The obvious delay in the attributes chart to detect a quality shift in the timber supply verifies previous results of simulations of the output-control described in *(Leicester & Breitinger, 1994)* and *(Boström et al., 2000)*.

The *CUSUM* charts are capable of recognizing quality shifts in the input material properties in dependency of the applied grading settings gained during the initial evaluation testing of subsample H. In comparison to the characteristic values of the machine controlled grading of the remaining subsamples into strength class L25 (*Table 3*) where 5th-percentile value of tension strength doesn't indicate the quality shift the proof loading of the output material and especially the variables chart seems to be sensitive to the macro variability.
The considered method offers the possibility to respond to detected quality shifts spontaneously by adjusting the grading machine settings. However, statistical uncertainties are incorporated into the grading process insufficiently, because the complete evaluation procedure of the output of the grading machine is carried out only within the gathered sample data.

3.4 Probabilistic Method

An alternative method for the control of grading machine settings was already proposed in Köhler (2003), Pöhlmann & Rackwitz (1981) and Faber et al. (2004). This method facilitates the consideration of uncertainties throughout the modeling of the grading process and probabilistic models of the material properties of graded timber material can be derived. Furthermore the proposed model framework enables the (statistically) efficient utilization of information gathered during the approval phase as well as during the running phase of the grading machine; that is, the statistical characteristics of graded timber material properties can be expressed and communicated by means of probability distribution functions, up to date in regard to the currently available information. However, the method appeared rather theoretical for practical application. Furthermore it is not clear how the statistical information about the graded timber material properties should be communicated, since the derived probability distributions are not part of a standard distribution family.

The new method which is outlined in the following attempts to overcome these shortcomings by simplifying the statistical methodology. The basis of the presented method is a statistical representation of the relation of the material properties of interest and the measurements of the grading machine by simple linear regression analysis. A Bayesian framework is presented since it consistently facilitates the integration of new knowledge, which might be obtained during the running phase of the grading machine.

Bayesian linear regression with non-informative prior

The aim of linear regression analysis is to relate observations of a set of explanatory variables to one response variable. The general model can be written as

$$y_i = \sum_{j=1}^{r} x_{ij}\beta_j + \varepsilon_i \qquad (2)$$

where the βs are the regression parameters, the x_is are observations of j different properties, and y_i is the corresponding observation of the response variable. The ε_i is the independent realisation of the error of the regression model. In general, the errors are assumed to follow a normal distribution. Usually, but not necessarily, $x_{i1} = 1$ for every i. For instance when $r = 2$ and $x_{i1} = 1$, the model above becomes

$$y_i = \beta_1 + \beta_2 x_{i2} + \varepsilon_i \qquad (3)$$

If the above model is expressed algebraically it can be written as

$$\mathbf{y} = \mathbf{X}\boldsymbol{\beta} + \boldsymbol{\varepsilon} \qquad (4)$$

The vector $\mathbf{y}$ has n elements, corresponding to n observations. The matrix $\mathbf{X}$ has n rows, corresponding to the observations, and r columns corresponding to the number of predictors. If the regression includes an intercept, one of the columns of $\mathbf{X}$ is a column of ones. The parameters are the regression coefficients $\boldsymbol{\beta}$ and the variance of the fitted model, i.e. the variance in ε is σ^2. The model that relates observations and parameters is written:

$$\left(\mathbf{y}\,|\boldsymbol{\beta}, h, \mathbf{X}\right) \sim \text{Normal}\left(\mathbf{X}\boldsymbol{\beta}, \mathbf{I}\sigma^2\right) \qquad (5)$$

In words, this model states that the distribution of $\mathbf{y}$ given parameters $\boldsymbol{\beta}$ and σ^2 and predictors $\mathbf{X}$ is a normal distribution with mean $\mathbf{X}\boldsymbol{\beta}$ and variance σ^2. $\mathbf{I}$ is the identity matrix with rank r.

The regression parameters may be estimated as normal distributed random variables, as

$$\left(\boldsymbol{\beta}\,|h, \mathbf{X}, \mathbf{y}\right) \sim \text{Normal}\left(\mathbf{E}_\beta, \mathbf{V}_\beta\sigma^2\right) \qquad (6)$$

Equation (10) states that the probability distribution of $\boldsymbol{\beta}$ is normal with mean $\mathbf{E}_\beta$ and variance $\mathbf{V}_\beta\sigma^2$. The parameters can be estimated with

$$\mathbf{E}_\beta = \mathbf{b} \qquad (7) \qquad\qquad \mathbf{V}_\beta = \mathbf{n}^{-1} \qquad (8)$$

where $\mathbf{n} = \mathbf{X}^T\mathbf{X}$ and $\mathbf{b} = \mathbf{n}^{-1}\mathbf{X}^T\mathbf{y}$. The variance σ^2 can be estimated on basis of the 'conventional' least squares estimate.

Predictive distribution of $\mathbf{y}$ *by given set of observations of* $\mathbf{X}$

The probability distribution of $\mathbf{y}$ by given set of $\tilde{\mathbf{X}} = (\tilde{x}_1,...,\tilde{x}_r)$ can be formulated as the predictive distribution of $\mathbf{y}$, i.e. a normal distribution containing all involved uncertainties, with mean and variance:

$$\mathbf{E}_{y|\tilde{\mathbf{X}}} = \tilde{\mathbf{X}}\mathbf{E}_\beta \qquad (9) \qquad\qquad \mathbf{V}_{y|\tilde{\mathbf{X}}} = \left(\mathbf{I} + \tilde{\mathbf{X}}\mathbf{V}_\beta\tilde{\mathbf{X}}^T\right)\sigma^2 \qquad (10)$$

Given a sample of n new observations on $\tilde{\mathbf{X}}_1,...,\tilde{\mathbf{X}}_n$, the probability density function of the corresponding sample of predictions of $\mathbf{y}$ may be obtained by coupling the predictive density functions as

$$f\left(y\middle|\tilde{\mathbf{X}}, \mathbf{E}_{y|\tilde{\mathbf{X}}}, \mathbf{V}_{y|\tilde{\mathbf{X}}}\right) = \frac{1}{n}\sum_{i=1}^{n} f\left(y\middle|\tilde{X}_i, E_{y|\tilde{X}_i}, V_{y|\tilde{X}_i}\right) \qquad (11)$$

The density function given by Equation (11) can be well approximated by a normal distribution.

Updating the regression parameters

Given a sample of n new observations on $\tilde{\mathbf{X}}_1,...,\tilde{\mathbf{X}}_n$ and on $\tilde{y}_1,...,\tilde{y}_n$, the probability density function of the regression parameters may be updated taking into account the new information, with:

$$\mathbf{E}_{\beta,u} = \mathbf{n}''^{-1}\left(\mathbf{n}'\mathbf{b}' + \tilde{\mathbf{X}}^T\tilde{\mathbf{y}}\right) \qquad (12)$$

$$\mathbf{V}_{\beta,u} = \mathbf{n}''^{-1} \qquad (13)$$

with $\mathbf{n}'$ and $\mathbf{b}'$ are taken from the prior regression analysis, $\mathbf{n}'' = \mathbf{n}' + \tilde{\mathbf{n}}$ with $\tilde{\mathbf{n}}$ derived based on the new observations $\tilde{\mathbf{X}}_1,...,\tilde{\mathbf{X}}_n$ as $\tilde{\mathbf{n}} = \tilde{\mathbf{X}}^T\tilde{\mathbf{X}}$.

Example

The approval of a grading machine is generally based on test samples which are tested first nondestructively by the grading machine, then strength and stiffness properties are measured in destructive tests and the timber density is measured. As a result data is available which facilitates that the samples are virtually graded and the effect of the grading process on strength and stiffness properties and the density is assessed.
In the case of the Golden Eye grading machine and the GLULAM lamellas data of the IP_MOR, IP_MOE, IP_density and laboratory measurements of MOR, MOE and density are available. The relation of the IP measurements of the grading machine and the corresponding material properties of interest is illustrated in *Figure 5*.

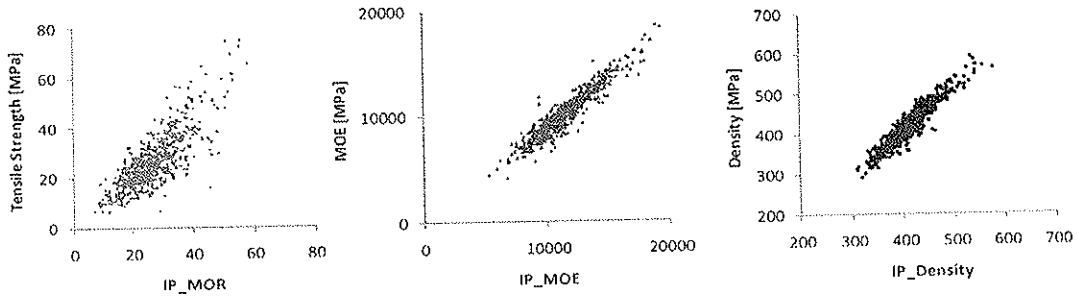

Figure 5: *Illustration of the relationship between grading machine indicative properties and material properties of interest.*

With a linear regression model the material property of interest can be estimated based on observations on a measurement of the grading machine. The uncertainty of the estimation can be consistently considered by the fact that the prediction of the material property of interest is a normal distributed random variable. The main model assumption is hereby that the prediction error is an independent random variable. In *Figure 5* it can be observed that this assumption seems to be reasonable for the MOE and the density relations but not for the tension strength relation. The error seems to depend on the value of IP_MOR. Furthermore, it is generally accepted that the statistical properties of the tension strength and the MOE are best represented by a log-normal distribution; the prediction of tension strength and MOE based on grading machine measurements should be also log-normal distributed. This problem might be overcome by proper transformation of the data. After a logarithmic transformation of the tension strength, the MOE and the IP_MOE the relationships seem to be linear and the error is uniformly distributed over the IP values.

The described approach is illustrated by a short example. The data set described above is utilized to demonstrate how material properties of interest can be predicted based on information about the grading machine IPs and the corresponding regression parameters.

Regression analysis

Following the approach outlined above regression parameters are estimated for simultaneous observations on the timber density, the MOE, the tension strength and their corresponding machine IPs as present for sample H.

Prediction of strength values of sample H

The GoldenEye706 machine setting suggested in EN 14081, part 4 for 'L25 – reject' is applied to the data of grading machine IP measurements of sample H. The material properties of interest are predicted with application of Equations (5 – 8). The results are compared with the corresponding characteristics of sample H, *Table 4*.

Table 4: *Model predictions of the limiting strength characteristics, compared with characteristics of subsample H.*

	L25 - requirements	Predicted characteristics	Sample characteristics
$f_{t,k}$ [MPa]	14.5	17.48	16.0
$MOE_{t,mean}$ [MPa]	10 450	11 810	12 041
$\rho_{12,k}$ [kg/m^3]	350	383	385

In *Table 4* it can be observed that the requirements for strength class L25 are met for all relevant properties. The 5th-percentile value of the tension strength predicted by the probabilistic model might appear quite conservatively however, it should be noted that the

model prediction represents the predictive value of the 5% fractile value containing all uncertainties due to model assumptions and due to lack of data.

In *Figure 6* the cumulative distribution of the observed sample data compared with the predictive cumulative distribution function is illustrated. It can be observed that the 5^{th}-percentile is representing the characteristic of the individual sample to a large extend. It should be noted that variations in the timber material supply can cause considerable fluctuations and uncertainties regarding the characteristic values estimated on the basis of sample statistics.

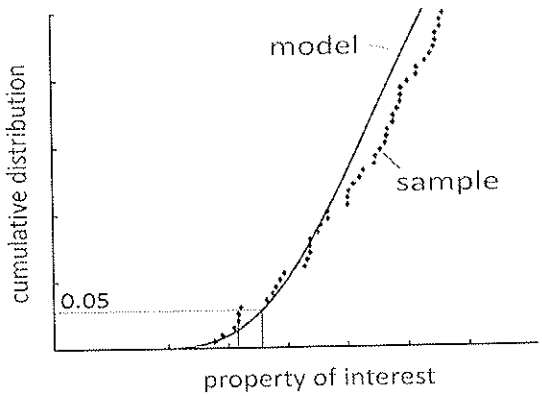

Figure 6: *Comparison of the cumulative distribution of the sample data and the probabilistic model. The difference of the 5^{th}-percentile value can be observed.*

With the same regression models, the remaining samples are virtually graded and the model predictions for the material properties of interest are compared with the corresponding sample characteristics.

Table 5: *Model predictions of the limiting strength characteristics, compared with characteristics of other samples.*

	L25 - requirements	Predicted characteristics	Sample characteristics
$f_{t,k}$ [MPa]	14.5	14.7	16.2
$MOE_{t,mean}$ [MPa]	10 450	10 505	10 656
$\rho_{12,k}$ [kg/m^3]	350	347	335

By grading the remaining subsamples with the regression models based on subsample H it can be observed that the strength class L25 cannot be obtained. Since the required characteristic values of the tension strength and modulus of elasticity are achieved, neither the evaluation of the characteristic values based on ordered sample statistics nor the probabilistic approach on the basis of regression analysis meet the required characteristic values of the density.

As a consequence the grading procedure might be changed by modifying the machine settings or by updating the regression parameters. Note that the above check with the model can be continuously made during the operation phase of the grading machine, since the information required is obtained during the grading process anyway.

4 Conclusions

The goal of the present paper is to simulate situations where a noticeable quality shift between initial tested timber material and subsequent applied input material is observable. A method for the machine control (*cost matrix method*), the output control (*CUSUM*) and the

combination of both (*probability based approach*) is used to assess the macro and meso variability of the material supply and the results are compared. The capability of the methods to incorporate statistical uncertainties as well as model related uncertainties into the grading process is of special interest.

The results show that the macro variability between different subsamples of the timber material supply is detected by the cost matrix method only faintly. In the case that quality shifts are identified a substantial reassessment of adjusted grading machine settings is required. The incorporation of uncertainties is done implicitly; i.e. by sampling different subsamples of different origins and by comparing assigned strength grades with the optimum grades. However, as long as the characteristic values of the derived strength classes are assessed by means of sample statistics considering solely the underlying set of data it is not possible to represent all uncertainties in a consistent matter.

The application of the output control by means of *CUSUM* control charts is observed to be capable to detect the aberrations in the quality of the material supply. However, compared with the results of the variables chart the average run length of the attributes chart indicates a remarkable delay in identifying the quality shift of the material input resource. Though very much attention is given on how to sample the test specimens randomly in order to manage the underlying statistical uncertainties, the method is still based on sample statistics and therefore only capable to qualify shifts of quality of the timber supply but not to quantify them.

The probabilistic approach shows to be a consistent combination of both methods described above. There is a crucial difference in the basic statistical concept of the models. The presented approach is based on a regression model which represents the interrelation of properties of interest and indicating properties. Based on this information, predictive distributions for the material properties of interest can be quantified taking into account a certain set of grading machine settings. This probabilistic approach offers also the chance to assess shifts in the material quality by controlling the values of the indicating properties for the material properties of interest continuously. Note, that this information is always available without additional costs. Assessed aberrations of quality may be counteracted by means of updating the regression parameters of the probabilistic grading model. In consequence of updating the regression model it is a straightforward task to assign adjusted grading machine settings without additional substantial test procedures.

The statistical assessment of timber material properties has been considered with special emphasis on the modeling of the effect of macro and meso variability within the timber material supply. The suggested probabilistic approach not only forms a very strong tool for the statistical quantification of the material characteristics of timber but furthermore provides a consistent basis for quantifying the efficiency of different quality control and grading procedures.

Acknowledgements

Contributions by *MiCROTEC Brixen (Italy)* are acknowledged with gratitude for allowing us to publish the results of machine grading by the grading device *GoldenEye 706* and laboratory experiments performed by *Holzforschung München*.

References

ALSC (1998). Machine Graded Lumber Policy. Notification of the American Lumber Standard Committee, Incorporated. November 6,1998.

Bengtsson C. & Fonselius M. (2003). Settings for strength grading machines – evaluation of the procedure according to prEN 14081, part 2. Proceedings of the 36th Meeting, International Council for Research and Innovation in Building and Construction, Working Commission W18 – Timber Structures, CIB-W18, Paper No. 36-5-1, Colorado, USA, 2003.

Boström L., Enjily V., Gaede G., Glos P., Holland C., Holmqvist C., Joyet P. (2000). Control of Timber Strength Grading Machines. SP REPORT 2000:11.

Denzler J., Diebold R., Glos P. (2005). Machine strength grading – Commercially used grading machines – current developments. Symposium on Nondestructive Testing of Wood, Hannover, 2005.

Faber M. H., Köhler J. and Sørensen, J. D. (2004). Probabilistic modelling of graded timber material properties. Journal of Structural Safety, 26(3), pp. 295-309.

Galligan W.& Devisser D. (2004).Machine Grading under the American Lumber Standard. Information of the West Coast Lumber Inspection Bureau. 2004.

Glos P., Linsenmann P., Denzler J. K. (2006). Grading Machine Settings for GoldenEye 706 for Norway spruce using the Method proposed in prEN 14081. Holzforschung München, report no. 05518.

Köhler J. & Faber M. H. (2003). A probabilistic approach to cost optimal timber grading. Proceedings of the 36th Meeting, International Council for Research and Innovation in Building and Construction, Working Commission W18 – Timber Structures, CIB-W18, Paper No. 36-5-2, Colorado, USA, 2003.

Köhler J. (2006). Reliability of Timber Structures. Dissertation ETH no. 16378. Swiss Federal Institute of Technology, Zurich, Switzerland.

Köhler J. & Steiger R. (2006). A discussion on the control of grading machine settings – Current Approach, Potential and Outlook. Proceedings of the 36th Meeting, International Council for Research and Innovation in Building and Construction, Working Commission W18 – Timber Structures, CIB-W18, Paper No.39-5-1, Florence, Italy, 2006.

Leicester R. H. & Breitinger H. O. (1994). Statistical control of timber strength. Proceedings of the 27th Meeting, International Council for Research and Innovation in Building and Construction, Working Commission W18 – Timber Structures, CIB-W18, Paper No. 27-17-1, Sydney, Australia, 1994.

Leicester R. H. (2004). Grading for structural timber. Prog. Struct. Engng Mater, 6, pp. 69-78.

Pöhlmann, S. and Rackwitz, R. (1981). Zur Verteilungsfunktion der Festigkeitseigenschaften bei kontinuierlich durchgeführter Sortierung. Materialprüfung 23, Munich, Germany, Hanser.

Rackwitz R. & Müller K. F. (1977). Zum Qualitätsangebot von Beton, II. Beton, 27(10), pp. 391-393.

Rouger F. (1996). Application of a modified statistical segmentation method to timber machine strength grading. Wood and Fibre Science. 28(4).

Rouger F. (1997). A new statistical method for the establishment of machine settings. Proceedings of the 30th Meeting, International Council for Research and Innovation in Building and Construction, Working Commission W18 – Timber Structures, CIB-W18, Paper No. 30-17-1, Vancouver, Canada, 1997.

ALSC PS 20-05: Voluntary Product Standard: American Softwood Lumber Standard. NIST National Institute of Standards and Technology. Washington, USA, 2005.

AS 3519: Australian Standard: Timber - Machine proof grading. Sydney, Australia, 2005.

AS/NZS 1748: Australian/New Zealand Standard: Timber – Stress graded – Product requirements for mechanically stress-graded timber. Sydney, Australia, 1992.

AS/NZS 4063: Australian/New Zealand Standard: Timber – Stress graded – In-grade strength and stiffness evaluation. Sydney, Australia, 1992.

AS/NZS 4490: Australian/New Zealand Standard: Timber – Stress graded – Procedures for monitoring structural properties. Sydney, Australia, 1997.

ASTM D 6570-04: Standard Practice for Assigning Allowable Properties for Mechanically-Graded Lumber. ASTM Book of Standards. West Conshohocken, USA, 2004.

EN 14081 parts 1-4: Timber Structures – Strength Graded Timber with rectangular Cross Section. Comité Européen de Normalisation, Brussels, Belgium, 2005.

EN 338: Structural Timber – Strength Classes. Comité Européen de Normalisation, Brussels, Belgium, 2003.

EN 384: Structural timber - Determination of characteristic values of mechanical properties and density. Comité Européen de Normalisation, Brussels, Belgium, 2004.

EN 408: European Standard: Timber structures - Structural Timber - Determination of some physical and mechanical properties. Comité Européen de Normalisation, Brussels, Belgium, 2004.

ISO 13910: Structural timber – Characteristic values of strength-graded timber – Sampling, full-size testing and evaluation. International Organisation for Standardisation, 2005.

ISO 13912: Structural timber – Machine strength grading – Basic priciples. International Organisation for Standardisation, 2005.

NLGA SPS2: Special Product Standard for Machine Graded Lumber. NLGA National Lumber Grading Agency. Canada, 2003, Revision 2006.

INTERNATIONAL COUNCIL FOR RESEARCH AND INNOVATION
IN BUILDING AND CONSTRUCTION

WORKING COMMISSION W18 - TIMBER STRUCTURES

BEARING STRENGTH PERPENDICULAR TO THE GRAIN OF LOCALLY LOADED TIMBER BLOCKS

A J M Leijten
J C M Schoenmakers

Eindhoven University of Technology

THE NETHERLANDS

MEETING FORTY

BLED

SLOVENIA

AUGUST 2007

Presented by A. Leijten

H. Blass commented that the Van de Put model relies on slip lines and is more appropriate for granular material. In timber the failure mode would be very different from the assumed failure mode in the model. A. Leijten discussed equilibrium and redistribution of stresses phenomena that lead to plasticity. He said that failure modes do not need to be exact. H. Blass commented that B. Madsen's results and model were not included in the paper for comparison which is the basis for the EC5 A1 model. The results related to EC5 A1 reported in the paper are not correct and there is a need to discuss this more in detail.

I. Smith commented that Forintek did tests on the two loaded surface case. Although there are lots of theories that are totally wrong but can be applied, he issue is how can one extrapolate the wrong theory to other cases.

H. Larsen commented that Van de Put's work is difficult to understand and one needs to check assumptions. Old EC5 method is 100% empirical. One has to find better ways to predict perpendicular to grain capacity even though there are not too many cases of failure. Also tension perpendicular to grain always takes place which is not accounted for in Van der Put's model.

Bearing strength perpendicular to the grain of locally loaded timber blocks

A.J.M. Leijten and J.C.M. Schoenmakers
Eindhoven University of Technology, Eindhoven, The Netherlands

Abstract
The compressive strength perpendicular to the grain is one of those wood properties that are important for structural design but are difficult to tackle due to its semi-plastic behaviour. It depends on deformation, the specimen type and loading condition. For long no common definition for the standard compressive strength was agreed. A comprehensive survey of research work is given by Augustin and Schickhofer [1], Kollmann [4], Gehri [3], Madsen [6] and Blass and Görlacher [2]. Some empirical models were proposed by Madsen [6] and Riberholt [7]. Van der Put [10] presented a physical model as early as 1988, based on plasticity theory. He showed the ability and accuracy of his model with test data from literature. Despite of his effort the absence of any reference to his model in later publications indicate the model is not well understood. To convince those who are still in doubt a comparison follows between the Van der Put model and the empirical model of Eurocode 5. It is concluded that Eurocode 5 is unsafe while Van der Put's model is by far superior.

1 Introduction

In Figure 1 a number of load cases relevant for building practise are illustrated. The attention will be focussed on load cases 1, 2 and 3 where in case 3 the beam is fully supported while loaded area is close or adjacent to the end grain face.

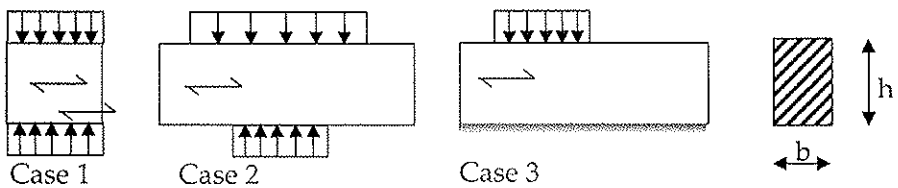

Figure 1: Load cases; case 1 standard test piece, 2) opposite loads, 3) fully supported

A problem in comparing compressive strength data perpendicular to grain from various sources is the lack of an agreed definition. As shown in Figure 2 the load displacement curves are very different depending on the type of specimen and loading area. The test piece loaded over the full area will exhibit almost perfect yielding while the window-sill type test piece shows considerable hardening. In EN 408 a clear definition is given for the compressive strength being the stress attained at the intersection with a $0{,}01h$ off-set line parallel to the linear part of the stress-strain curve, where h is the specimen depth, Figure 2. This standard or reference strength is determined using prismatic cross-section specimens.

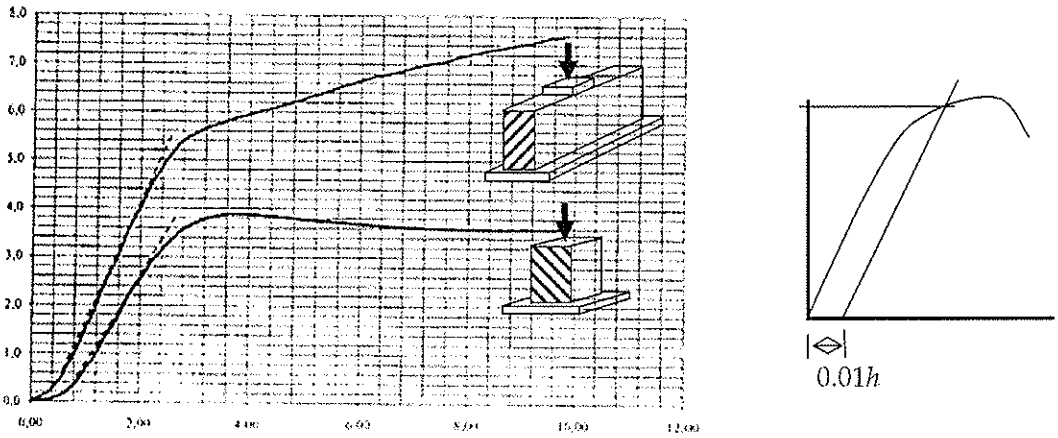

Figure 2: Compressive stress-strain curves from [7] and definition of compressive strength according to EN408.

1 Van der Put model

Van der Put [10] applied the theory of plasticity, an equilibrium method well known as the slip-line field theory for solids, right part of Figure 3, to explain the bearing strength of perpendicular to grain locally loaded blocks. The conditions for application of this theory are; 1) plane strain deformation 2) quasi static loading 3) rigid perfect plastic Mises solid. Although one might question the validity of this theory for timber loaded perpendicular, as shown later it matches too many data sets in too many loading cases to ignore.
Test data shows that the bearing strength, f_s, just under the upper loading plate is dependent of the size and geometry of the supporting area. This effect is explained by Van der Put [10][7] who shows the strength to be proportional with the ratio between the loading area; dimensions l, and the support area given by l_{eff}, Figure 3.

$$f_s = c\, f_{c;90} \sqrt{\frac{l_{ef}}{l}} = 1.08\, f_{c;90} \sqrt{\frac{l_{ef}}{l}} = \mu\, f_{c;90} k_c \qquad [\mathrm{N/mm^2}] \qquad (1)$$

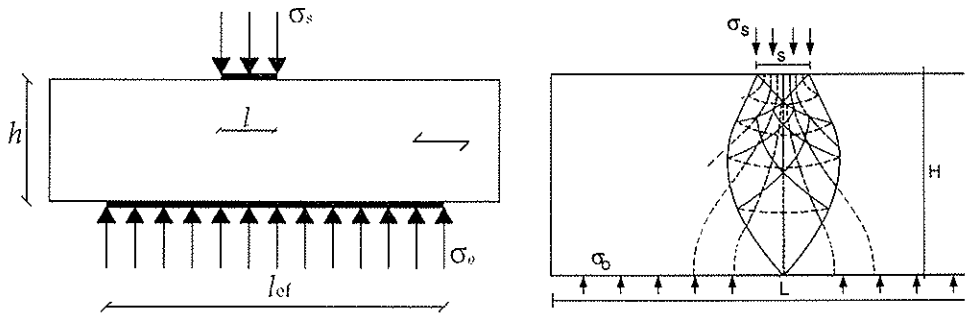

Figure 3: Stress distribution according to Van der Put model [10]

The bearing strength f_s increases thus with a factor $\mu\, k_c = 1.08\ \sqrt{(l_{ef}/l)}$. The factor μ=1,08 is an empirical factor related to the type of specimen used for the "reference" or standard compressive strength, which either is a prismatic specimen as defined by EN408 or a cubic specimen. In the evaluation of this model a μ = 1,0 is taken as a lower bound approach. However, sometimes a better fit with experimental data is found using μ = 1,1.

Van der Put shows by using the theory of slip-lines the local stressed area to be limited to about 45^0 (1:1) for small deformations up to 34^0 (1:1,5) for large 10% deformation as illustrated in Figure 4.

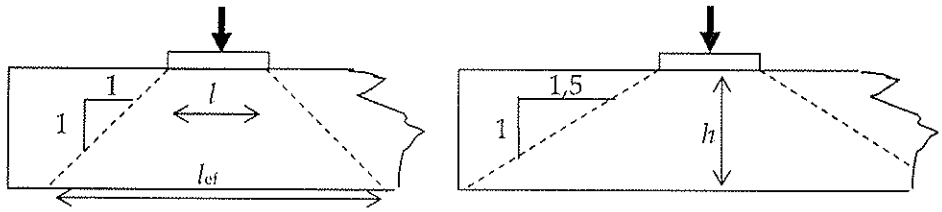

Figure 4: The slope of bearing stresses for small (left) and large deformations (right).

The maximum distribution length, l_{eff}, theoretically derived by Van der Put in 1988 was confirmed many years later by Riberholt [7] who states that FEM analyses showed the stress field to be contained within the length of l_{eff}=l+3h. This means end distances, a, Figure 6, greater than 1,5h do not influence the compressive strength. This conclusion was leading for the size of his test specimens.
Regarding the third dimension b (thickness) of the specimens Figure 5, it was already mentioned by Van der Put and Leijten [11] in appendix 2 p.5 that for slender specimens other slip-line failure mechanisms may occur like rolling shear deformation. Depending of the friction between the load introducing plate and the test piece the timber fails side ways and the theory might overestimate the strength. Only the test series by Riberholt [7] contains some slender test pieces where $h > 2.5b$.

Figure 5: Rolling shear

2 Eurocode 5

The bases for the design guidelines provided by Eurocode 5 are given in Riberholt [7], Figure 2. For a beam a continuously supported the following Eurocode 5 design rules apply:

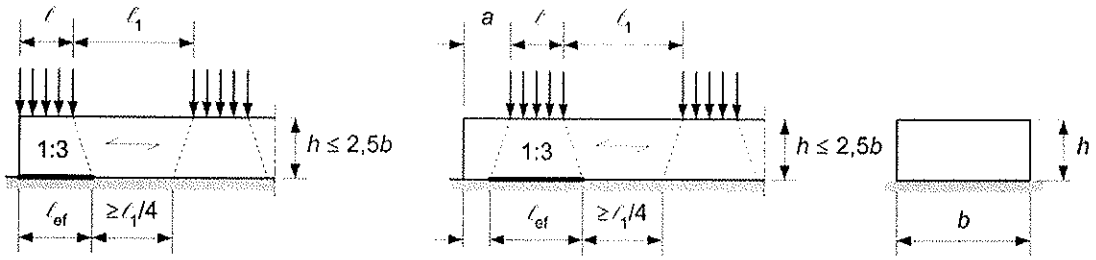

Figure 6: The distribution of the stresses according to Eurocode 5 for $h \le 2{,}5\ b$.

The compressive strength of a fully supported beam is:

$$f_s = k_c f_{c,90} \tag{2}$$

and

$$1 \le k_c \le 4$$

were:

f_s is the compressive strength in the contact area perpendicular to the grain;
$f_{c,90}$ is the reference compressive strength according to EN 408;
k_c is a factor taking into account the load configuration, possibility of splitting and degree of compressive deformation.

- For $h \le 2{,}5b$ the factor k_c is given by:

$$k_c = \left(2{,}38 - \frac{l}{250}\right)\sqrt{\frac{l_{eff}}{l}} \le 4 \tag{3}$$

Where the l_{ef} is the effective length of bearing stresses and l is the contact length, Figure 6.

- For $h > 2{,}5b$ the factor $k_{c,90}$ should be calculated according to expression (4), were the contact length ℓ is less than the greater of h or 100 mm:

$$k_c = \frac{l_{eff}}{l} \tag{4}$$

The effective length of distribution should not extend by more than ℓ beyond either edge of the contact length.

Note that in Eq. (3) $k_c = 1{,}0$ only for $l_{ef} = 345$ mm whatever the size of the reference compressive specimen. This clearly indicates the formula to be empirical.

3 Evaluation of Van de Put model and Eurocode 5

**Tests by Suenson [8]*

The compressive strength values f_s are taken as the maximum values of Figure 1 curves. The reference specimen "a" with a full loaded prismatic cross-section shows a maximum compressive stress, f_s, of approximately 3.6 N/mm ^{2} at 15% strain. This is taken as the reference compressive strength for both models. It is typically for the Eurocode 5 that equation (3) leads to large deviations compared to Van der Put's model, Table 1.

Table 1: Model comparison with data by Suenson [8]

Curve	loaded length / mm	Test data N/mm2	model Put	model EC5	Ratio Put/data	Ratio EC5/data	strain %
a	150	**3,63***	**3,63**	**3,63**	1,00	1,00	15
b	150	5,5	5,5	9,14	1,00	1,66	5,5
c	150	6,95	6,95	11,19	1,00	1,31	13
d	150	8	8	12,92	1,00	1,40	15
e	150	8,3	8,3	14,45	1,00	1,56	10

*) reference compressive strength

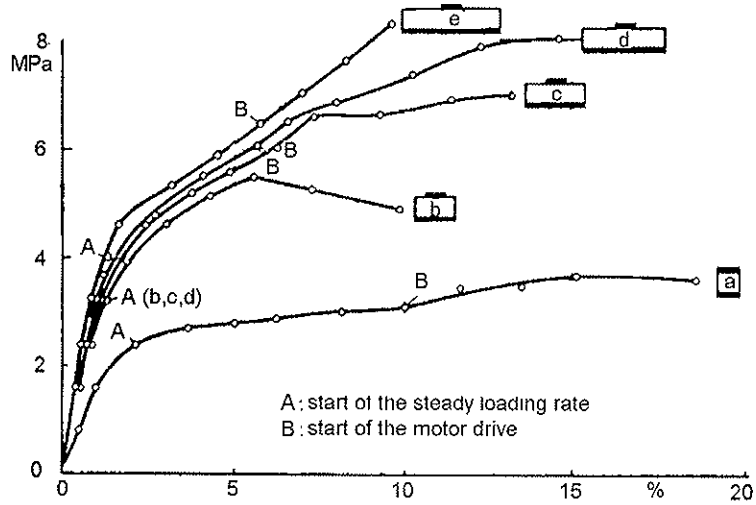

Fig. 7 - Compressive strength f_s perpendicular to the grain by Suenson [8].
Specimen size 150 x 150 mm, effective bearing lengths: l_{eff} = 150, 300, 450, 600, 750 mm, of curve "a" to "e" respectively,

**Test by Korin [5]*
Korin [5] published two sets of data, one series of central loaded specimens and one series with end loaded specimens, Figure 8. The specimen size was constant (b x h x l) 40 x 90 x 180mm (h < 2,5b). The ultimate strain was in the range of 2,5% and for Van der Put's model the slope in distribution of the bearing stresses is assumed to be 45^0. The specimen depth h was such that specimen length < $2h + l$ and therefore the effective bearing l_{eff} = 180mm for all central loaded specimens. Korin increased the length of the loaded surface in steps (n=3 for each step) until the specimen upper surface was totally uniformly loaded (n=9). The compressive strength from this case was taken as the reference strength, $f_{c,90}$. Using the Eurocode 5 equation (3), which is valid since the specimen depth h < 2,5b, the k_c values lead to values that deviate considerably from the test data, Table 2.
When the reference compressive strength of the end loaded series is compared with the central loaded series one notice almost the same mean value, 2,62N/mm^2 and 2, 54 N/mm^2. For the end loaded series Eurocode 5 results deviate considerably from the experimental data, Table 3.

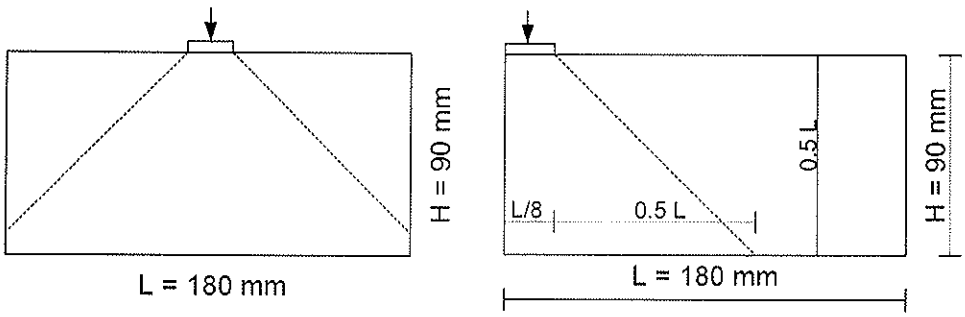

Figure 8: Dimensions of the test specimens by Korin [5]; thickness b = 40mm.

Table 2: Model comparison of centre loaded series Korin [5].

Korin	40*90*180mm	mean			Ratio		
Centre loadedl	loaded length	test data	model Put	model EC5	Put/data	EC5/data	strain %
1	22,50	7,05	7,34	11,50	1,04	1,63	2,5
2	45,00	5,47	5,24	8,81	0,96	1,61	2,5
3	67,50	4,72	4,27	7,60	0,90	1,61	2,5
4	90,00	4,63	3,70	6,84	0,80	1,48	2,5
5	112,50	4,10	3,33	6,27	0,81	1,53	2,5
6	135,00	3,00	3,04	5,57	1,01	1,86	2,5
7	157,50	3,13	2,81	4,91	0,90	1,57	2,5
8	180,00	**2,62***	**2,62**	**2,62**	1,00	1,00	2,5

*) reference compressive strength

Table 3: Model comparison of end loaded Series Korin [5].

Korin	40*90*180mm	mean			Ratio		
End loaded	loaded length	test data	model Put	model EC5	Put/data	EC5/data	strain %
1	22,50	6,37	5,58	8,87	0,88	1,39	2,5
2	45,00	4,50	4,39	7,20	0,98	1,60	2,5
3	67,50	3,67	3,88	6,44	1,06	1,76	2,5
4	90,00	4,40	3,58	5,92	0,81	1,35	2,5
5	112,50	3,80	3,22	5,51	0,85	1,45	2,5
6	135,00	3,17	2,94	5,16	0,93	1,63	2,5
7	157,50	3,10	2,71	4,75	0,88	1,53	2,5
8	180,00	**2,54***	**2,54**	**2.54**	1,00	1,00	2,5

*) reference compressive strength

** Tests by Graf reported by Kollmann [4]*

In Figure 9 compressive test curves by Graf are reported by Kollmann [4]. The tests were performed on locally loaded long blocks at opposite sides. Some of the curves show a cut off, curves 2, 5 and 6, which suggests a constant loading rate with a sudden instability at the end of the test.

To determine the effective bearing length, l_{ef}, Eurocode 5 has adopted the approach of Van der Put although the slope of the compressive stresses is different. When assuming a slope of 1:1,5 (Figure 4) both stress fields of upper and bottom loaded surface meet at αh, Figure 9 and thus the effective bearing length can be determined as follows:

$l + 3\,\alpha h = l_s + 3.(1 - \alpha)\,h$

$\alpha = 0{,}5 + \dfrac{l_s - l}{6h}$ and with $l_{eff} = l + 3\alpha h$ substituted in (1)

$$k_c = \sqrt{\frac{l_{eff}}{l}} = \sqrt{\frac{l + 3\alpha h}{l}} = \sqrt{0{,}5 + \frac{3h + l_s}{2l}} \qquad (5)$$

To have an equal deformation for all test pieces the compressive strength values are taken at 5 mm deformation resulting about 3% strain (5/178). To keep in line with the previous analyses of tests where for 3% strain a slope of 45^0 is taken (5) changes to:

$$k_c = \sqrt{\frac{l_{eff}}{l}} = \sqrt{\frac{l + 2\alpha h}{l}} = \sqrt{0{,}5 + \frac{2h + l_s}{2l}} \qquad (6)$$

With h= 179mm; l = 350mm and b = 181mm in (6) it follows:

$$k_c = \sqrt{0{,}5 + \frac{2x178 + 350}{2l}} = \sqrt{0{,}5 + \frac{353}{l}} \tag{7}$$

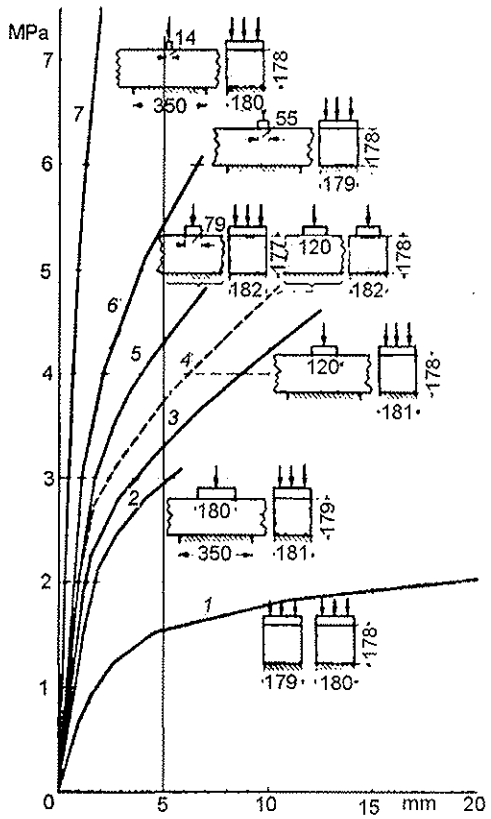

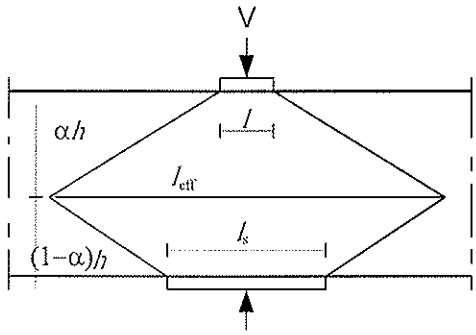

Possible distributions of compressive stresses were l is the top loaded length and l_s is the bottom loaded length.

Figure 9- Opposite loading cases by Graf reported by Kollmann [4].

In Table 4 the results are presented. A better fit would have been achieved with μ =1,1 in Van der Put's model.

Table 4: Model comparison of opposite sides loaded specimens by Graf

Graf	180*180mm	mean			Ratio		
Two sides	loaded length	test data	model Put	model EC5	Put/data	EC5/data	strain %
1	180	**1,6***	**1,6**	**1,6**	1,00	1,00	3
2	180	3	2,51	3,56	0,84	1,19	3
3	120	3,3	2,97	4,76	0,90	1,44	3
4	79	4,3	3,57	4,99	0,83	1,16	3
5	55	5,4	4,21	7,54	0,78	1,40	3
6	14	>7,5	8,11	15,43			3

*) reference compressive strength

* *Tests reported by Riberholt [7]*
Tests were conducted by J. J. Petersen of the TU- Denmark supervised by P. Hoffmeyer. Three replicates per test series were used but six specimens to determine the reference compressive strength with prismatic test pieces. The specimens were of constant 40mm thickness while the test piece length was always equal to the loaded surface plus 3 times the depth ($l_{eff} = 3h+l$). Argument being that FEM-element analyses showed the compressive stress field contained within this length. Longer specimens were not needed. This confirms Van der Put's conclusion many years earlier.

As in the past a number of researchers checked the compressive strength dependent of the annual ring orientation a number of test pieces were loaded in radial and tangential direction. This however was found of no significant influence. For this reason these data are combined. The loaded length l varied from 5, 15, 40, 80 up to 145mm. As a loaded length of 5mm will cause cracks of the top surface fibres with increasing deformation Van der Put argues that a volume affect should be introduced to explain these test values. However, this issue is closely connected with the embedment strength of timber perpendicular to grain and has been dealt with by Van der Put and Leijten [11]. For this reason this small loaded length is being omitted from the evaluation.

Riberholt [7] reports data related to deformations of 1% according to EN 408 and 10%. In Tables 5 to 7 the mean of the reference compressive strength test is presented as well as the data for 1% deformation. Table 5, 6 and 7 deals with specimens of 40, 80 and 145mm depth, respectively.

Table 5: Compressive test results Riberholt [7] and model prediction
Specimens depth h = 40mm; b = 40mm; $l_{eff} = 120+l$

depth h = 40mm					
loaded length l	Compr strength	model Put	model EC5	Ratio Put/data	Ratio EC5/data
40	**3,20***	**3,2**	**3,2**	1.0	1.0
15	7,36	8,1	12,0	1,09	1,63
40	4,74	5,5	8,9	1,17	1,87
80	4,20	4,5	7,4	1,08	1,76
145	4,11	4,0	6,1	0,97	1,48

*) reference compressive strength

Table 6: Compressive test results Riberholt [7] and model prediction.
Specimens depth h = 80mm; b = 40mm; $l_{eff} = 240+l$

depth h= 80					
loaded length l	Compr strength	model Put	model EC5	Ratio Put/data	Ratio EC5/data
80	**3,50***	**3,50**	**3,50**	1.0	1.0
40	5,5	7,8	10,5	1,43	1,92
145	4,1	6,8	6,5	1,66	1,59

*) reference compressive strength

Table 7: Compressive test results Riberholt [7] and model prediction
Specimens depth h = 145mm; b = 40mm; $l_{eff} = 435+l$

depth h=145>2,5b					
loaded length l	Compr strength	model Put	model EC5	Ratio Put/data	Ratio EC5/data
145	**2,70***	**2,70**	**2,70**		
15	10,5	12,2	13,1	1,16	1,25
40	5,3	7,8	6,8	1,46	1,29
80	4,9	5,8	5,0	1,18	1,01
145	3,5	4,7	4,1	1,34	1,18

*) reference compressive strength

As all specimens are only 40 mm thick the slenderness of some of the test pieces with depth 145mm is rather high. This may lead to different failure mechanisms than pure compression perpendicular to grain like side way shear deformation (rolling shear), which leads to lower values than the yield theory of Van der Put predicts. Among others, it also depends on the friction between the timber and loaded surface. For this reason the data in the column with depth 145mm actually requires a different model by which yield lines follow the side way deformation (Van der Put and Leijten [11] appendix 2 p.5). However, no attempt was yet made to formulate such approach. For this particular case Eurocode 5 prescribes Eq(4) with more success..

**Test reported by Augustin and Schickhofer [1]*
A comprehensive research programme with glued laminated timber blocks was conducted to show the compressive strength perpendicular to the grain to be grade independent. The standard test method of EN 408 was applied for all tests, resulting in a well defined value for the reference compressive strength and other data. The reference compressive test pieces were 160x160mm with a depth h of 200 (n=122) and 480 mm (n=8), respectively. Additional sill-type specimens were tested as shown in Figure 10, which were loaded at three different locations, called case 1, 2 and 3. The compressive strength appeared independent of the timber grade. Table 8 shows the data and prediction by both models. Because the 1% permanent strain (≈ 3% total strain) is chosen as ultimate strain, a slope for the compressive stresses is assumed to be 45°, Figure 4. The mean test results are presented in Figure 11 and Table 8.

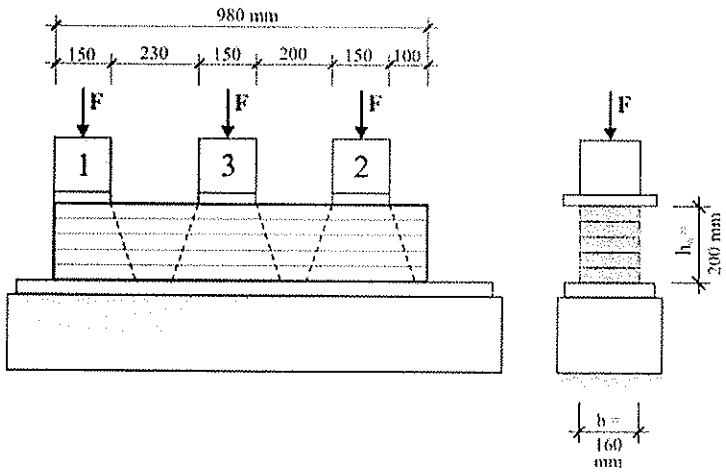

Figure 10: Sill-type type II test specimens by Augustin and Schickhofer [1].

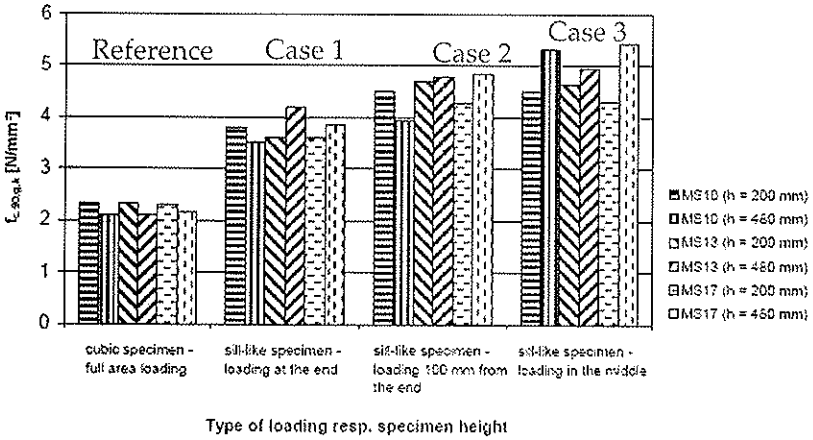

Figure 11: Compressive strength of all grade and test cases.

Table 8 – Model verification with data by Augustin and Schickhofer [1].

Augustin et al.	Compr. strength	≈ 3% strain		Compr strength	≈ 3% strain	
Standard compressive strength test						
160x160x**200**	EN 408	n	160x160x**480**	EN 408	n	
case 1	3,35	41	case 1	2,89	6	
case 2	3,43	40	case 2	2,87	6	
case 3	3,16	41	case 3	2,84	6	
mean	**3,31***	122	mean	**2,87***	18	
Test data			**Model prediction**			
h = **200** mm	EN408	n	V.d.Put	EC5	Ratio	
case 1	4,42	54	5,07	7,09	1,15	1,60
case 2	5,7	54	5,73	8,11	1,01	1,42
case 3	6,03	54	6,33	8,11	1,05	1,34
h = **400** mm						
case 1	4,66	54	5,88	7,34	1,26	1,57
case 2	5,76	54	6,34	8,44	1,10	1,46
case 3	6,35	54	7,34	9,03	1,16	1,42

*) reference compressive strength

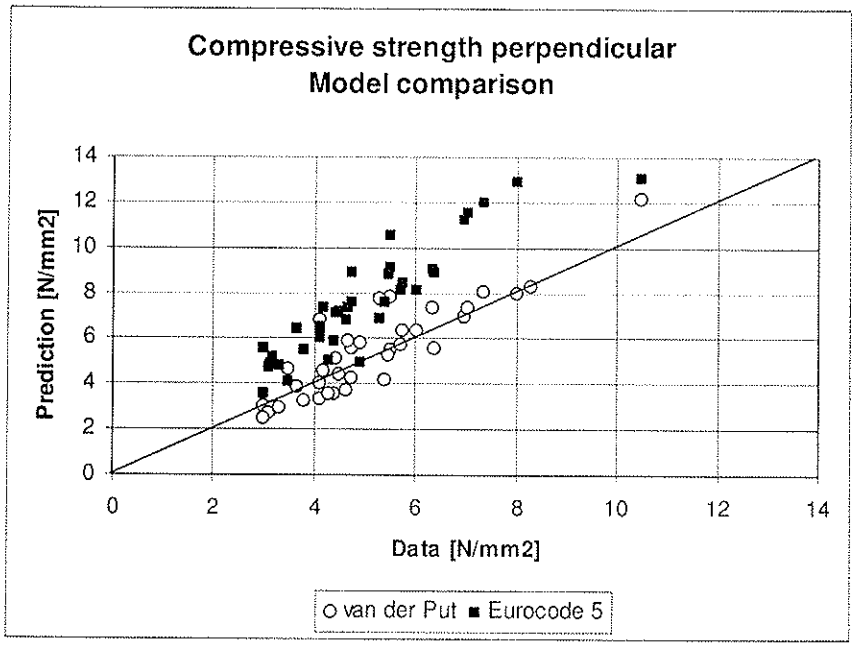

Figure 12: Review of all mean model predictions versus mean test results

4 Conclusions

In Figure 12 all the values of Tables 1 to 8, with mean test data versus the model predictions are presented excluding the reference strength values. From this graph it can be concluded that the theory of Van der Put results in much better prediction of the compressive strength perpendicular to grain than the Eurocde 5 model. The evaluation was limited to data by Suenson, Graf, Korin, Riberholt and Augustin et al. Although more data sets can be used for evaluation the sources from which they are taken are independent so that strong deviating future results are not foreseen.

This paper is concluded with some proposals by Van der Put for future change of the Eurocode 5 of fully supported beams:

$\sigma_{c,90,d} \leq k_{c,90} \cdot f_{c,90,d}$, where: $k_{c,90} = \sqrt{\frac{l_{ef}}{l}}$

(slope 1 :1,5)

with: $l_{eff} = min\begin{cases} a + l + l_1/2 \\ 3h + l \end{cases}$

For safe rules (when friction is only in the width direction), the conditions are:
(slope 1:1)

$$l_{eff} = min\begin{cases} 2a + l \\ l + l_1 \\ 2h + l \end{cases}$$

For the bearing strength of a middle section of a beam loaded on two opposite sides;

$$k_{c,90} = \sqrt{0{,}5 + \frac{3h + l_s}{2l}} \leq 5$$

These rules for bearing blocks **don't** apply for stresses at supports of beams. Where combined stresses parallel and perpendicular to grain occur the failure criterion of Van der Put [9] has to be applied. When this exact approach is not followed, the compressive strength perpendicular to the grain of a continuous beam over a support should safely be limited to $f_{c,90}/2$ in order to maintain the ultimate compressive bending strength.

5 Acknowledgement

T.A.C.M. (Tom) van der Put is acknowledged for his cooperation and advice in using some of his earlier evaluation studies and willingness to correspond about the details of his model.

6 References

[1] Augustin, M. and Schickhofer, G.: *Behavior of glulam in compression perpendicular to grain in different strength grades and load configurations.* Proceedings of CIB-W18 / paper 39-12-6, 2006, Florence, Italy.

[2] Blass, H.J. and Görlacher, R.: *Compression perpendicular to the grain.* WCTE - Finland, 2, 2004,

[3] Gehri, E.: Timber in compression perpendicular to the grain. IUFRO S 5.02 Timber Engineering, 16-6-1997, Copenhagen.

[4] Kollmann, F.: *Technologie des Holzes der Holzwerkstoffe.* Zweiter Band, 1955, Munich, Germany,

[5] Korin, U.: *Timber in compression perpendicular to the grain.* CIB-W18/ 23-6-1, 1990,

[6] Madsen, B., Leijten, A.J.M., Gehri, E., Mischler, A., and Jorissen, A.J.M.: *Behaviour of Timber Connections.* first, 2000, Timber Engineering Ltd, Vancouver. 1-55056-738-1.

[7] Ribberholt, H.: *Compression perpendicular to the grain of wood.* COWI-report P-42239-1, 3-8-2000,

[8] Suenson, E.: *Zulässiger Druk auf Querholz.* 1938, xxxx.

[9] Van der Put, T.A.C.M.: *A general failure criterion for wood.* Proceedings of IUFRO S5.02, 1982, Boras, Sweden.

[10] Van der Put, T.A.C.M.: *Derivation of the bearing strength perpendicular to the grain of locally loaded timber blocks.* Publication of Delft Wood Science Foundation, 2006, www.DWSF.nl.

[11] Van der Put, T.A.C.M. and Leijten, A.J.M.: *Evaluation of perpendicular to grain failure of beams caused by concentrated loads of joints.* Proceedings of CIB-W18 / paper 33-7-7, 2000, Delft, The Netherlands.

INTERNATIONAL COUNCIL FOR RESEARCH AND INNOVATION
IN BUILDING AND CONSTRUCTION

WORKING COMMISSION W18 - TIMBER STRUCTURES

EXPERIMENTAL STUDY OF COMPRESSION AND SHEAR STRENGTH OF SPRUCE TIMBER

M Poussa
P Tukiainen
TKK, Helsinki University of Technology

A Ranta-Maunus
VTT, Technical Research Centre of Finland

FINLAND

MEETING FORTY
BLED
SLOVENIA
AUGUST 2007

Presented by A. Ranta-Maunus

H.J. Larsen questioned whether there is an explanation why the shear strength measured by the I-beams and other methods are so different. He does not agree with the suggestion of adopting a constant value of 3.8 MPa for shear stress. He will discuss more independently on the subject with A. Ranta-Maunus. A. Ranta-Maunus responded that there is stress interaction between compression perpendicular to grain and shear in the I-beam tests.

B.J. Yeh commented that in ASTM standard the compression perpendicular to grain strength is determined using 1.0 mm as the limit state. As this paper considers 2.5 mm as the limit state, the values may be quite comparable if 1.0 mm was used as the limit state in this paper.

H.J. Larsen commented that the discussion of shear strength is interesting. True material properties should be considered rather than using experimental method with more complicated stress state. For example in this case the failure always takes place between web and flange which is not realistic. A. Ranta-Maunus responded that there is more motivation to do these types of experiments. In Europe, the tendency is to reduce shear strength because we have seen some related failures. The test materials do not have cracks and cracks due to moisture influence must be determined independently.

S. Thelandersson commented that compression perpendicular to grain strengths have much impact on design. One needs to distinguish serviceability from strength as serviceability governs designs in most cases.

Experimental study of compression and shear strength of spruce timber

Matti Poussa, Pekka Tukiainen
TKK, Helsinki University of Technology, Finland

Alpo Ranta-Maunus
VTT, Technical Research Centre of Finland

1 Introduction

The European standards EN 338 and EN 384 provide a strength class system for structural timber and strength profiles (characteristic strength values for bending, tension, compression and shear stresses) for each strength class. Basis of the system when placing a piece of timber to a strength class is bending strength supported by modulus of elasticity and density which are also grade determining properties. All other characteristic values are determined by calculation from bending strength or density.

Characteristic shear strength values of EN 338 are based on relation

$$f_{v,k} = 0{,}2 f_{m,k}^{0.8}, \text{ max } 3{,}8 \text{ MPa} \quad (1)$$

which indicates that shear strength increases with increasing bending strength until $f_{m,k}$ =40 MPa. Only few test results based on test method of EN408 are published. German experiments give characteristic shear strength value of 3,8 MPa and COV = 0,20 for spruce from C18 to C30, on average [4]. There are also other test results which suggest that shear strength of timber is practically independent of grade or is even higher for lower grades. In this paper new results are published on shear strength of timber when tested by the use of different test methods.

Characteristic compression strength perpendicular to grain values of EN 338 are based on density of wood:

$$f_{c.90,k} = 0{,}007\ \rho_k \quad (2)$$

and characteristic compression strength in grain direction is given as function of bending strength

$$f_{c,0,k} = 5\ f_{m,k}^{0.45} \quad (3)$$

In this paper new tested compression strength values are published and different testing standards compared. Results are obtained in "Combigrade" project which was intended mainly for development of strength grading, but produced also other strength data.

2 Materials and methods

Sampling of test material was made from five regions of which three were in Finland and two in North-Western Russia. Test material and non-destructive testing performed for logs and sawn timber is described in detail by Hanhijärvi and Ranta-Maunus [3], and by Hanhijärvi et al [1]. Species is Norway spruce (*Picea abies*).

All destructive tests are made according to standard EN408, unless otherwise reported. Test material was conditioned to 12% MC. Test methods and results are reported in detail by Poussa et al [4].

3 Compression strength results

3.1 Compression parallel to grain

Three dimensions were tested in compression parallel to grain. Length of test specimen was six times smaller dimension, about 300 mm. Statistical summary of the results is given in Table 1. In total 403 specimens were tested. Compression strength shows fairly good correlation to density (R^2=0,5...0,6), see Figure 1. 282 specimens were visually strength graded according to the Nordic INSTA rules, and most specimens qualified to T3. Reason for high quality is that bending specimens had first been taken from the same planks with intention to include the weakest material in bending specimen, and compression specimen is taken from the remaining part. Results for visually graded material are shown in Table 2. Characteristic values are 30% higher than those given in EN338 for an equivalent grade.

Table 1. Summary of results in compression parallel to grain.

Test		50x100 2 ex log	50x150 2 ex log	44x200 4 ex log	All
N		120	144	139	403
minimum (MPa)	$f_{c,0,min}$	24,3	23,9	21,1	21,1
mean (MPa)	f_{mean}	36,5	38,0	36,2	36,9
maximum(MPa)	$f_{c,0,max}$	47,2	53,5	51,0	53,5
coeff. of variation		0,14	0,15	0,16	0,15
5 percentile (MPa)	$f_{c,0,k}$	27,9	29,2	26,3	27,9
density (kg/m^3)	ρ_{mean}	445,4	438,2	426,1	436,1
coeff. of variation		0,10	0,10	0,10	0,10

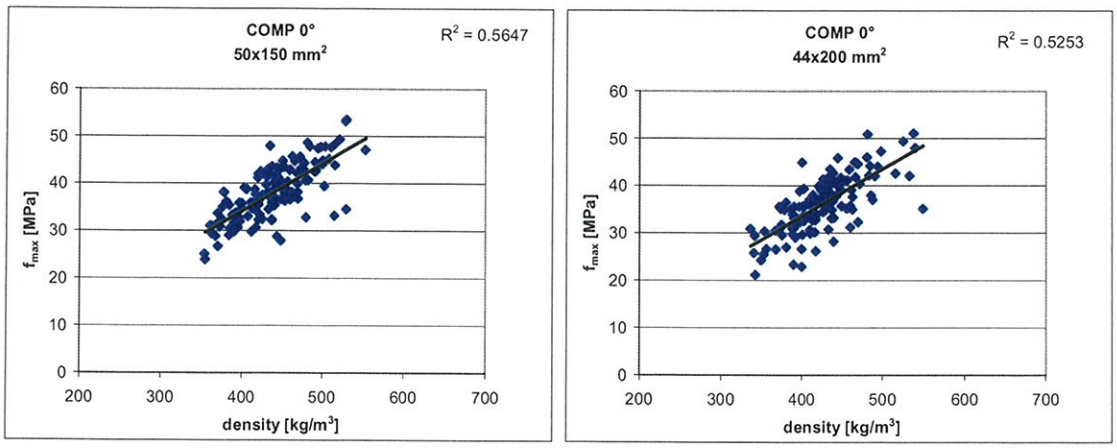

Figure 1. Compression strength parallel to grain vs. density for spruce.

Table 2. Compression strength of visually INSTA T-graded spruce compared to EN338 strength values. Characteristic values are calculated also with prEN14358 -method.

	T1/C18	T2/C24	T3/C30
N	13	58	211
average [MPa]	30,2	34,0	38,6
standard dev. [MPa]	4,2	4,7	5,1
$f_{c,0,k}$ nonparametric	24,2	26,2	29,8
$f_{c,0,k}$ acc. to EN14358	22,5	26,4	29,4
$f_{c,0,k}$ in EN338	18	21	23

Compression strength was modelled as function of density and KAR by using the same type of equation as Glos in [6]. We obtained

$$\ln f_c = 2.701029 + 0.002222 \cdot \rho - 0{,}62042 \cdot KAR \qquad (4)$$

Observed compression strength vs. modelled strength is shown in Figure 2 and has r^2 = 0,64. Same picture shows also prediction of characteristic value based on sliding 5 percentiles.

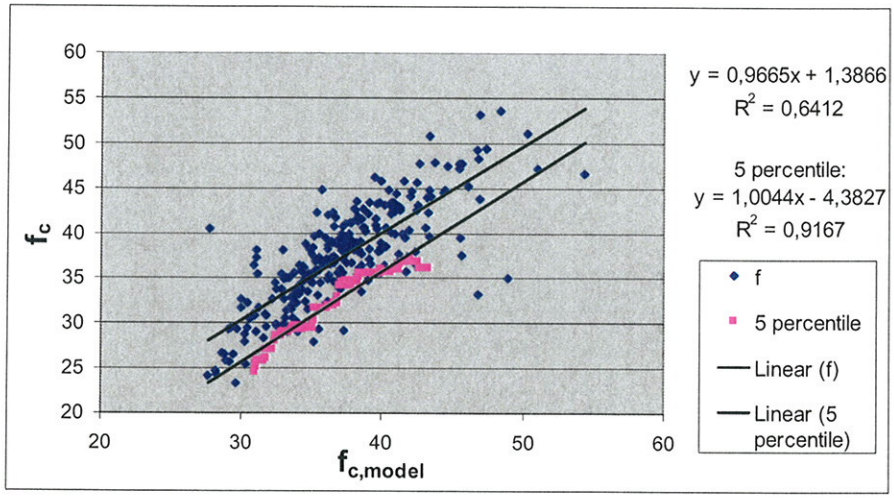

Figure 2. Modelling of compression strength by eqn. (4).

3.2 Compression perpendicular to grain

Compression tests perpendicular to grain were made according to EN408 and ASTM D143-standards. Additional beam-tests were also made and setups are shown in Fig. 3. Tested specimens are listed in Tables 3 and 4. Obtained results are shown in Table 5.

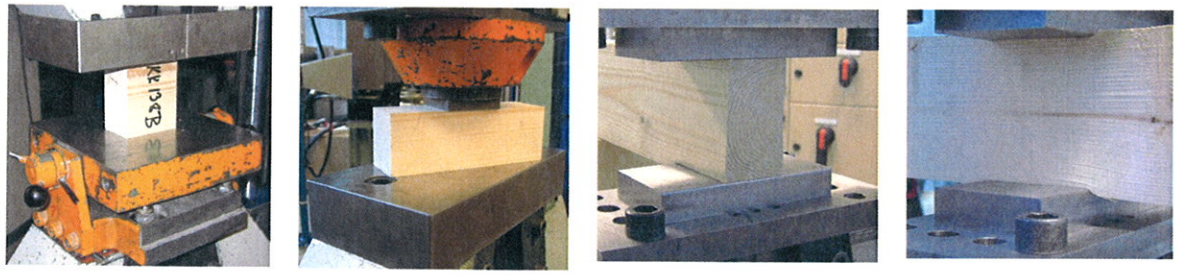

Figure 3. Perpendicular to grain tests. From left to right: EN408, ASTM D 143, beam end, and continuous beam.

Table 3. Perpendicular to grain standard tests

Test	Species	Pcs.	Specimen a x b x length [mm]	Standard	Loading program	Gauge length [mm]
COMPRESSION 90 DEG, Small size	Spruce	200	45x90x70	EN408	Deformation controlled. 300±120s	90
COMPRESSION 90 DEG, Small size	Spruce	200	45x50x150	ASTM-D143	Deformation controlled. max. 2,5mm	50

Table 4. Perpendicular to grain tests for spruce beams.

Test	Pcs.	Specimen, a x b x length [mm]	Standard	Loading program	Free distance to beam-end [mm]	Gauge length [mm]
CONTINUOUS BEAM COMPRESSION 90 DEG,	27	45x90x400	applied EN408	Deformation controlled. 300±120s	165	90
BEAM END COMPRESSION 90 DEG, Small size	27	45x90x400	applied EN408	Deformation controlled. 300±120s	330	90

Table 5. Summary of results in compression perpendicular to grain.

Test		ASTM D143	EN408	BEAM-END	CONTIN. BEAM
N		200	200	27	27
minimum (MPa)		4,8	1,9	2,8	3,7
mean (MPa)		7,0	2,8	3,9	4,7
maximum(MPa)		10,5	4,1	5,0	5,7
characteristic value (MPa)	by ranking	5,2	2,2	-	-
characteristic value (MPa)	by use of prEN14358	5,3	2,2	2,9	3,7
stand. deviation		1,1	0,4	0,5	0,6
coeff. of variation		0,16	0,14	0,14	0,12
av. density (kg/m3)		441,3	443,0	439,4	434,4
coeff. of variation of density		0,09	0,09	0,10	0,11
av. deformation (mm)		2,5	2,3	2,5	2,4

ASTM standard gave mean strength value 7 MPa, that is 2,5 times larger than the value 2,8 MPa given by EN-standard. Ratio of characteristic values is nearly as big. An obvious reason for higher values in ASTM-test is that surface of test specimen is loaded partially. Test material used has mean density meeting requirement of C24. Characteristic value 2,2 MPa is lower than 2,5MPa given in EN338 for C24.

Relation of compression strengths determined according to EN408 and ASTM D143 was studied. Specimens are knotless and taken from the same piece next to each other. Correlation analysis between EN and ASTM results gave coefficient of determination 0,49. Figure 4 shows correlation between density and perpendicular to grain compression strength measured according to both standards. Coefficient of determination is higher for ASTM-results (0,43) than for EN-results (0,29).

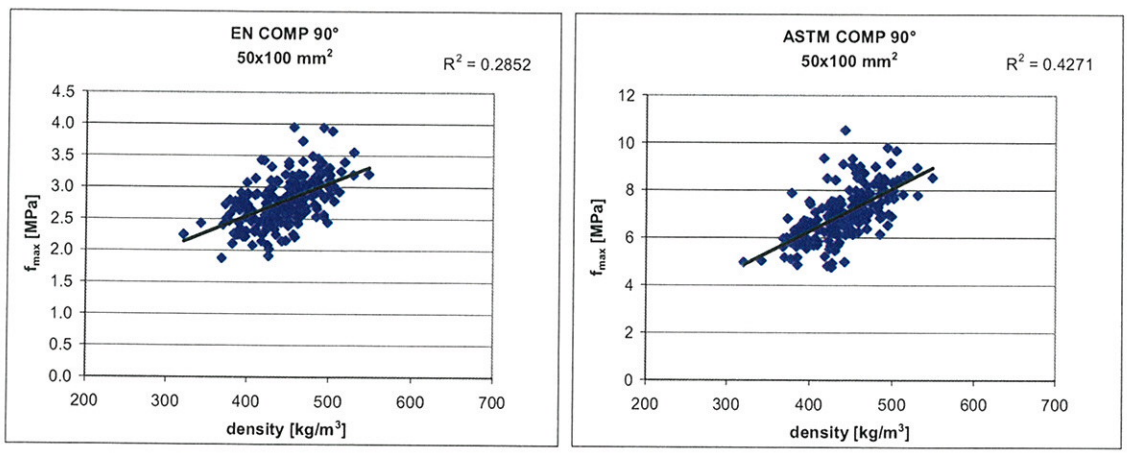

Figure 4. Compression strength perpendicular to grain vs. density for spruce.

In EN408 compression perpendicular to grain strength value is determined using small specimen, which are loaded on the total area. In an actual structural situation, the compressed beam has more load bearing capacity because the adjacent part of beam is not

loaded and supports the loaded part. Therefore when designing structures the compression capacity of the beam can be increased. In the old Eurocode pre-standard ENV1995-1-1 factor $k_{c,90}$ is used. The present version EN1995-1-1:2004 and suggested prEN1995-1-1:A1 use effective area A_{ef} which is larger than the actual area.

The ratio of strength capacity of the tested beams to compression strength determined by the standard-test EN408 was calculated by using the mean values, because amount of beams tested was only 27 pieces.

Comparison of the obtained ratios when comparing factors of different Eurocode 5 versions with test results is presented in Table 6.

Table 6. Comparison of A_{ef}/A- ratios obtained from test results and different versions of Eurocode.

TEST SETUPS	Test results $\frac{f_{mean,beam}}{f_{mean,EN408}}$	prEN1995-1-1:A1 new proposal $\frac{A_{ef}}{A}$	EN1995-1-1:2004 $\frac{A_{ef}}{A}$	ENV1995-1-1 $k_{c,90}$
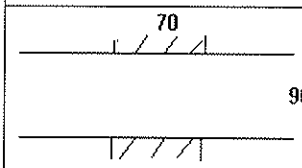	$\frac{4,7MPa}{2,8MPa}$ =1,68	1,85	1,43	1,47
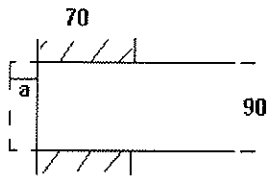	$\frac{3,9MPa}{2,8MPa}$ =1,40	1,43	1,21	1,0

According to the comparison of ratios presented in Table 6 it is concluded that our results support the suggested changes in prEN1995-1-1:A1. In case of continuous beam, the suggested design capacity of the beam is, however, ten percent higher than our test result. (1,85/1,68=1,10).

5 Shear strength

Both spruce and pine (Scots pine) were used in shear tests. The tests were made according to EN408-standard and also by the use of I-beam. Test setups are shown in Figs. 5 and 6. Tested specimens are characterised in Table 7. Obtained results are shown in Table 14. We obtained 3,9 MPa for characteristic value of shear strength of spruce in standard test, and 4,2 MPa for pine. Value for spruce is very well in line with earlier result of Glos and Denzler, 3,8 MPa [2]. I-beams gave at least 60% higher shear strength for both spruce and pine. Figure 7 shows that parallel to grain shear strength has no correlation with density. Similar result was obtained for I-beam tests.

Although the test setup was optimized for occurrence of shear-failure, 10 percent of spruce and 30 percent of pine beam failures were still bending failures. Bending failures occurred because, avoiding knots at lower flange high-moment area was not possible.

In many cases shear failure took place along the annual rings in web or in flange.

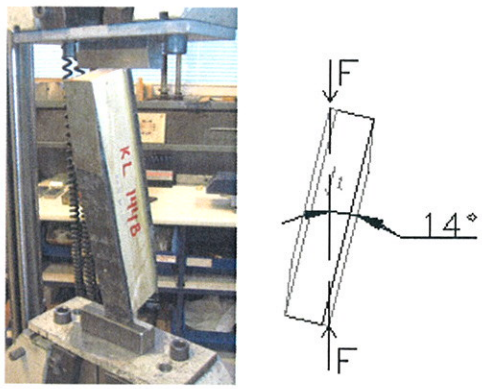

Figure 5. EN408 shear strength parallel to grain test.

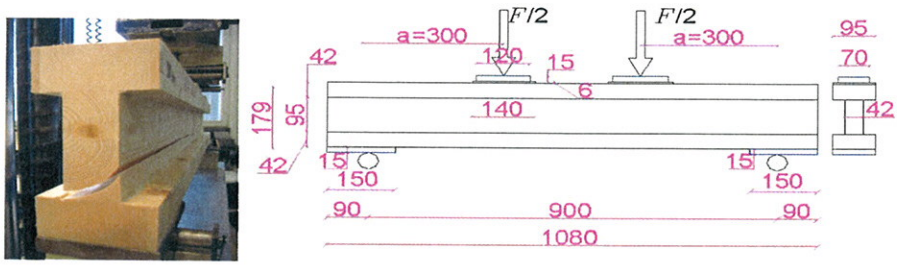

Figure. 6. I-beam test for shear strength parallel to grain of web. 4-point bending.

Table 7. Test information.

Test	Species	Pcs.	Specimen a x b x length [mm]	Standard	Loading program
SHEAR 0 DEG, Small size	Spruce	100	32x55x300	EN408	Deformation controlled. 300±120s
	Pine	100			
SHEAR I-BEAM 0 DEG, Structural size	Spruce	40	web 42x95x1080 flange 42x95x1080		Deformation controlled. 300±120s
	Pine	40			

Table 8. Summary of results.

Test		EN408-shear	EN408-shear	I-BEAM-shear	I-BEAM-shear
species		spruce	pine	spruce	pine
N		100	119	40	40
minimum (MPa)		3,2	3,3	6,6	6,4
mean (MPa)		5,2	5,6	8,3	8,6
maximum(MPa)		6,7	8,6	9,6	9,9
characteristic value (MPa)	by ranking	3,9	4,2	-	-
characteristic value (MPa)	by use of prEN14358	3,9	4,1	7,2	7,2
stand. deviation		0,8	0,9	0,6	0,8
coeff. of variation		0,15	0,16	0,08	0,09
av. density (kg/m3)		445,9	443,5	417,2	443,7
coeff. of variation of density		0,15	0,11	0,14	0,09

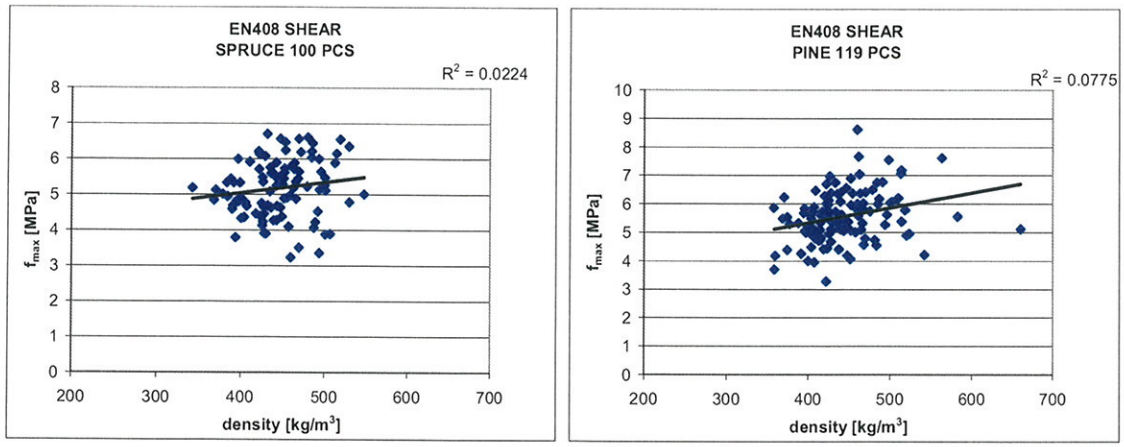

Figure 7. Shear strength vs. density for spruce (left) and pine (right).

6 Suggestions for standardisation

Obtained results partly support existing standards, partly suggest a revision. Main results are compiled in Table 9.

Compression strength values parallel to grain were 30% higher than those given in EN338. It is suggested that higher values are considered when EN338 is revised. However, it has to be kept in mind that low visual grades were not included in compression test material.

Compression strength perpendicular to grain when tested according to EN408 was lower than values given in EN338. Comparison with ASTM shows an expected difference: same material which gives 5.2 MPa characteristic value in ASTM test, gives 2.2 MPa in EN408 test.

The beam tests support the suggested changes in calculation of effective area in compression perpendicular to grain calculation of Eurocode 5.

Shear results support the idea of having one shear strength value, not dependent on grade. This value could be taken as 3,8 MPa as given as maximum value in EN338.

Table 9. Comparison of test results with EN338 values (MPa)

	Visual grade	Test result EN408	EN338	Alternative test result
$f_{c,0,k}$	C18 C24 C30 all	22,5 26,2 29,8 27,9	18 21 23	
$f_{c,90,k}$	all	2,2	2,6 (C27)	2,9 beam end, both edges loaded 3,7 middle support, both edges loaded 5,2 ASTM D 143
$f_{v,k}$	all	3,9	2,8 (C27)	7,2 I-beam

Acknowledgements

This work was financed by TEKES, Finnish glulam association, Finnforest Oyj, Stora Enso Timber, UPM-Kymmene Wood Products and VTT which is gratefully acknowledged.

References

[1] Hanhijärvi, A., Ranta-Maunus, A., Sarkama, H., Poussa, M., Mitsuhashi K., Puttonen, J. (2007). Analysis of tension and bending strength of graded spruce timber. CIB W18 paper 40-6-3.

[2] Glos, P., Denzler, J. (2003). Characteristic Shear Strength Values Based on Tests according to EN 1193.CIB W 18/36-6-1.

[3] Hanhijärvi, A., Ranta-Maunus, A. (2007). Development of strength grading of timber using combined measurement techniques. Report of the Combigrade-project – phase 2. VTT Publications, manuscript. Espoo

[4] Poussa, M., Tukiainen, P., Mitsuhashi, K., Andersin, P. (2007). COMBI T – Destructive tension, shear, and compression (0° and 90°) strength tests for Finnish sawn timber. Helsinki University of Technology, Laboratory of Structural Engineering and Building Physics Publication TKK-TRT-130. (http://www.tkk.fi/Yksikot/Talo/projektit/COMBI_T.pdf)

[5] Ranta-Maunus A. (2007). Strength of Finnish timber. VTT Publications. Manuscript.

[6] Ehlbeck, J., Colling, F., Görlacher R. (1985). Einfluss keilgezinkter Lamellen auf die Biegefestigkeit von Brettschichtholzträgern. Holz als Roh- und Werkstoff 43, 369-373.

INTERNATIONAL COUNCIL FOR RESEARCH AND INNOVATION
IN BUILDING AND CONSTRUCTION

WORKING COMMISSION W18 - TIMBER STRUCTURES

ANALYSIS OF TENSION AND BENDING STRENGTH OF GRADED SPRUCE TIMBER

A Hanhijärvi
A Ranta-Maunus
H Sarkama
VTT, Technical Research Centre of Finland

M Poussa
M Kohsaku
J Puttonen
TKK, Helsinki University of Technology, Finland

FINLAND

MEETING FORTY
BLED
SLOVENIA
AUGUST 2007

Presented b A. Ranta-Maunus
R. Steiger commented that the fb/ft relationship is similar to the results presented by Steiger in the Florence CIBW18 meeting last year.
A. Jorissen asked why 50 specimens were used to establish the 5th percentile values. A. Ranta-Maunus replied that 100 was also used but showed the results were not sensitive and he clarified coefficients used in equation for size effect.
J. Köhler and A. Ranta-Maunus discussed the point that one could use grading machines values to conduct similar studies.
I. Smith wondered about using the laboratory based test values to establish the floating fb/ft values in relation to the issue of actual structural system. As members may be subjected to combined stresses, one should exercise caution. A. Ranta-Maunus commented in Europe we use 0.6 which is lower than other countries. This seems to be too conservative.
E. Gehri agreed with I. Smith and commented that C40 did not achieve the values based on his test results.

Analysis of tension and bending strength of graded spruce timber

Antti Hanhijärvi, Alpo Ranta-Maunus, Heidi Sarkama
VTT, Technical Research Centre of Finland

Matti Poussa, Kohsaku Mitsuhashi, Jari Puttonen
TKK, Helsinki University of Technology, Finland

1 Introduction

The European standards EN 338 and EN 384 provide a strength class system for structural timber and strength profiles (characteristic strength values for bending, tension, compression and shear stresses) for each strength class. Basis of the system, when placing a piece of timber to a strength class, is bending strength supported by modulus of elasticity and density which are also grade determining properties. All other characteristic values are determined by calculation from bending strength or density.

Characteristic value (5^{th} percentile) of tension strength parallel to grain is defined in EN 338 to be 60% of bending strength. This is in good agreement with an American study based on in-grade testing data [1]. In a Nordic study it was, however, concluded that this ratio lies in range from 70% to 80% and is rather independent of grade [2]. This was partly in conflict with a German study [3] which concluded that ratio of tension to bending strength increases with increasing bending strength of machine graded (MOE flatwise) timber. The ratio was grade independent when visual grading was used. In this paper, dynamic modulus of elasticity is used as grading method and ratio of tension and bending strength is reported.

The objective of this paper is to report new experimental results on strength values of graded European spruce timber. Test material is characterised by the use of different NDT-methods. Ratio of tension strength to bending strength is determined for different grades when grading is based on dynamic modulus of elasticity.

2 Materials and methods

Sampling of test material (Norway spruce, *Picea abies*) was made from five regions of which three were in Finland and two in North-Western Russia. The three areas in Finland were: Western Finland, Eastern Finland and Kainuu. The two in Russia were East Carelia and Vologda. All logs were gathered during winter 2005-2006 from six sawmills in Finland – also including the logs from the Russian sampling areas. The Russian logs were chosen from railway car loads or truck loads, whose origin was known with the accuracy of the province ("oblast"), which was enough for the purposes of this study. Logs were taken completely randomly: no quality assessment of logs was done at selection.

The sizes of the logs were chosen so that they corresponded to the normal sawing practise in the Nordic countries, which means that the log sizes used in this study for production of different sized sawn timber cross-sections were the same as are used in normal production of the same sizes. Logs were not larger than needed for production of the planned sawn dimensions.

Table 1. Sawn dimensions and sawing pattern.

Sawn dimension	Log numbers	Sawing pattern
38 mm x 100 mm	1–44	2 ex log
50 mm x 100 mm	101–144	2 ex log
50 mm x 150 mm	201–244	2 ex log
44 mm x 200 mm	401–444	4 ex log
63 mm x 200 mm	301–344	2 ex log

Test material and non-destructive testing performed for logs and sawn timber as well as bending tests are described in detail by Hanhijärvi and Ranta-Maunus [4]. All destructive tests are made according to standard EN408, unless otherwise reported. In tension tests the free length was 2m corresponding the European method of testing glulam lamellae. Test material was conditioned to 12% MC. Tension tests are reported in detail by Poussa et al [5].

3 Tension tests

3.1 Strength of ungraded sample

A qualitative observation of the tension failure behaviour is that the length of damaged area is long in many cases, sometimes even longer that the free length. Length of damaged area was measured, and all results are shown on Fig. 1. Average of the length of damaged area was 460mm. For grading with worst knot-clusters and calculating of KAR-value, length of 150mm is commonly used. These results indicate that a longer area should be considered when evaluating the effect of knots to tension strength. However, use of 300 or 900mm long areas for KAR calculation produces lower R^2-values than 150mm when using KAR as strength predicting variable.

Tension specimens had the same free length 2000mm for all four dimensions tested. In results, no length adjustment has been made. In some analyses tension strength has been adjusted to the European reference width 150mm according to EN 408. In those cases term "adjusted strength" is used.

Correlation of tension strength to annual growth was studied and results are illustrated in Fig. 2. R^2=0,25…0,4 were obtained.

Destructive test results are summarised in Table 2. Quite some difference can be observed between pith side timber of size 44x200 and other cases. Logs used for 44x200 planks were largest used in this study, and had on average 5% lower density than others, which explains the lower strength. There is also a clear difference in strength of pith and bark side

material. However, when graded by E_{dyn}, no difference is observed in strength of graded material between bark and pith side.

Part of this test material was used for development of a new method to predict tension capacity of sawn timber considering slope of grain around knots. The method is in process to be published [7]. The original work is documented in [8].

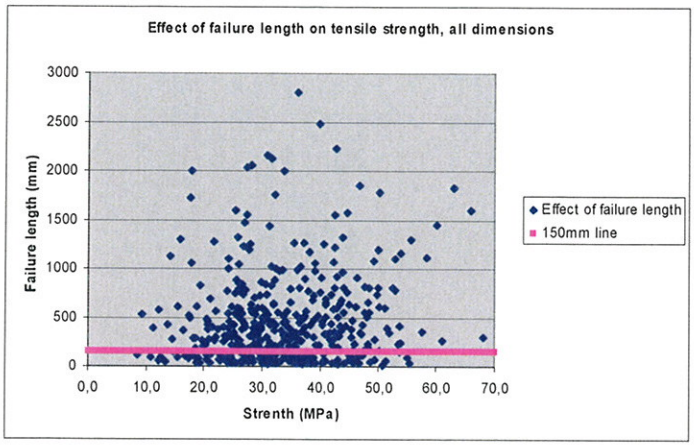

Figure 1. Failure area length vs. tensile strength.

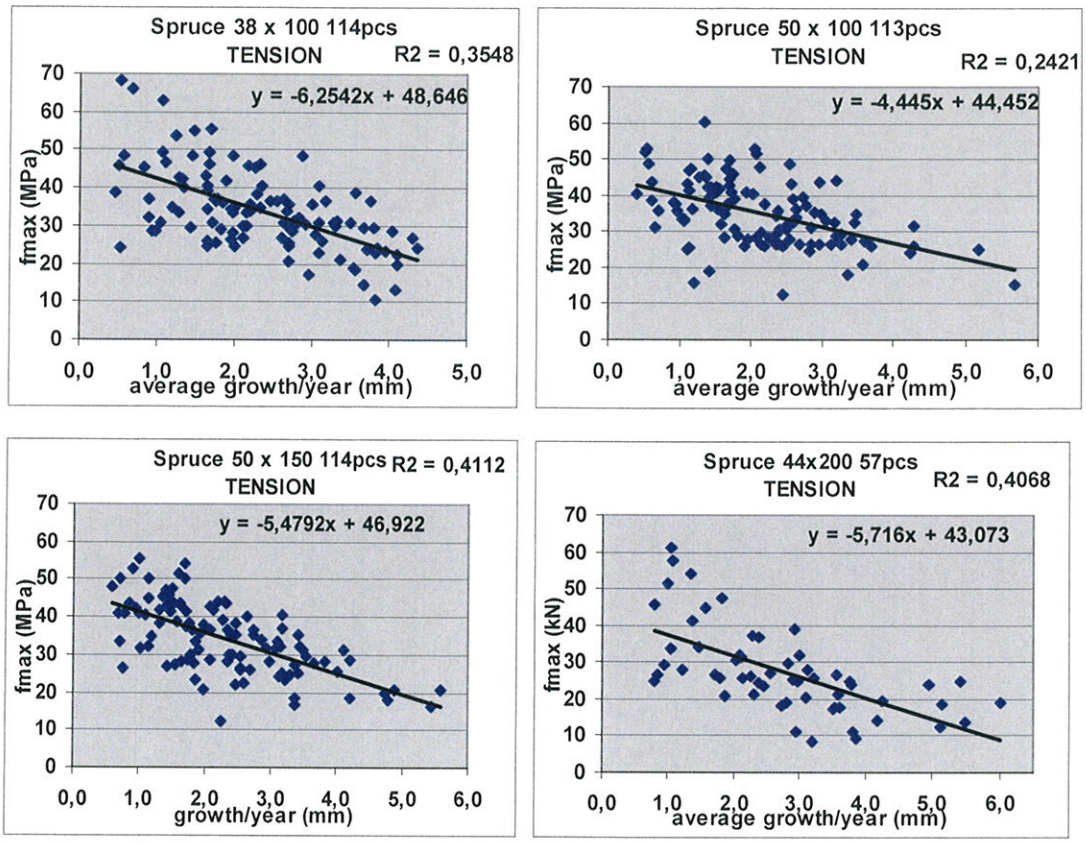

Figure 2. Tension strength vs. annual ring width.

Table 2. Result summary of tension parallel to grain tests of ungraded material

Dimension and sawing pattern	38x100 2 ex log	50x100 2 ex log	50x150 2 ex log	44x200 4 ex log		
	A, B	A, B	A, B	pith-side B, C	bark-side A, D	all four A, B, C, D
N	114	113	114	57	57	114
minimum (MPa)	10,6	12,6	12,3	8,5	14,7	8,5
mean (MPa)	34,3	35,1	34,6	27,5	32,1	29,8
maximum (MPa)	65,9	60,2	58,4	61,1	59,9	61,1
characteristic value (MPa)	19,0	21,1	18,9	11,0	17,7	13,8
stand. deviation	10,2	9,1	9,6	11,8	10,1	11,1
coeff. of variation	0,30	0,26	0,28	0,43	0,31	0,37
av. density (kg/m3)	433,3	446,4	439,3	420,1	425,4	422,8
COV of density	0,11	0,10	0,09	0,09	0,10	0,10
av. MC (%)	12,2	12,7	12,5	12,3	12,4	12,3

3.1 Graded timber

Timber material was graded by the use of different grading methods in industry and in laboratory. At the moment only part of the results are available.

Visual grading according to the Nordic INSTA rules was made in laboratory. Strength values of visually graded timber are given in Table 3. Characteristic values are calculated by ranking method, and by the prEN14358 which is based on lognormal distribution. In all 3 grades in which sample size was reasonable, obtained 5 percentile values were 30 to 40% higher than the present values in EN338.

Table 3. INSTA T-grading results compared to EN338 strength values. All characteristic values were calculated also with EN14358:2006 -method.

	T0/C14	T1/C18	T2/C24	T3/C30
N	13	96	210	136
mean [MPa]	26,7	26,2	31,8	38,9
standard dev. (MPa)	12,2	7,4	8,7	9,8
$f_{t,0,k}$ by ranking method	-	15,1	18,8	24,9
$f_{t,0,k}$ by prEN14358	8,3	15,1	18,5	23,7
$f_{t,0,k}$ present values of EN338	8	11	14	18

In order to obtain comparable values for tension and bending strength, dynamic modulus of elasticity (based on measurement of natural frequency and density) was used as grading parameter. Figure 3 shows tension strength vs. dynamic modulus of elasticity. An estimate for 5 percentile value was calculated by using sliding 5 percentile of 50 specimens around the E_{dyn} value of concern. Trendline of these sliding 5 percentile values is shown in Figure 3. Equation of the trendline is

$$f_{t,k} = 0{,}00286 E_{dyn} - 12{,}565 \qquad (1)$$

More detailed analysis of the strength results will be published in [6].

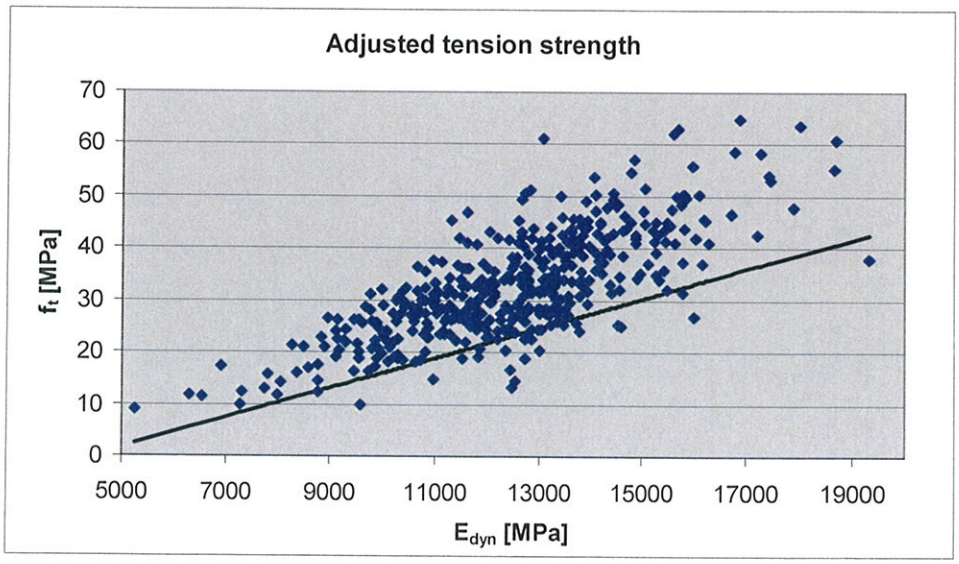

Figure 3. Size adjusted tension strength vs. E_{dyn}, also trend line for 5 percentile is shown.

4 Bending tests

4.1 Strength of ungraded sample

Statistical summary of bending strength results is shown in Table 4. Interestingly, a positive thickness effect can be observed. Dimension 44x200 includes material sawn from two different distances from pith and therefore results are given also separately.

Table 4. Result summary of bending parallel to grain tests of ungraded material

Dimension and sawing pattern	38x100 2 ex log	50x100 2 ex log	50x150 2 ex log	44x200 4 ex log			63x200 2 ex log
	A, B	A, B	A, B	pith-side B, C	bark-side A, D	all four A, B, C, D	pith-side A, B
N	195	208	211	57	82	139	156
minimum (MPa)	11,71	21,58	17,16	5,33	13,24	5,33	11,93
mean (MPa)	45,72	48,30	46,26	30,91	38,81	35,57	41,25
maximum (MPa)	67,22	75,85	75,59	53,87	63,23	63,23	62,19
characteristic value (MPa)	28,32	32,89	28,07	16,20	20,46	17,98	26,42
stand. deviation	10,12	10,01	11,55	9,74	11,16	11,26	9,95
coeff. of variation	0,22	0,21	0,25	0,32	0,29	0,32	0,24
av. density (kg/m^3)	437,65	442,23	443,35	418,12	435,53	428,39	434,10
COV of density	0,10	0,09	0,11	0,07	0,10	0,09	0,09
av. MC (%)	10,60	11,08	11,05	10,75	10,85	10,81	11,48

4.2 Strength of graded timber

Bending strength was first modelled by using dynamic modulus of elasticity as strength indicator. Determination of E_{dyn} was based on measurement of natural frequency and density. Regression analysis gave for strength adjusted to 150 mm reference size

$$f_{m,adj} = 0{,}00395E_{dyn} - 6{,}373 \qquad R^2 = 0{,}58735 \tag{2}$$

and for predicted 5th percentile

$$f_{m,k} = 0{,}00357E_{dyn} - 12{,}645 \tag{3}$$

which is shown in Fig. 4. These equations are based on strength data of same sizes as was available for tension strength in chapter 3 (38x100, 50x100, 50x150 and 44x200).

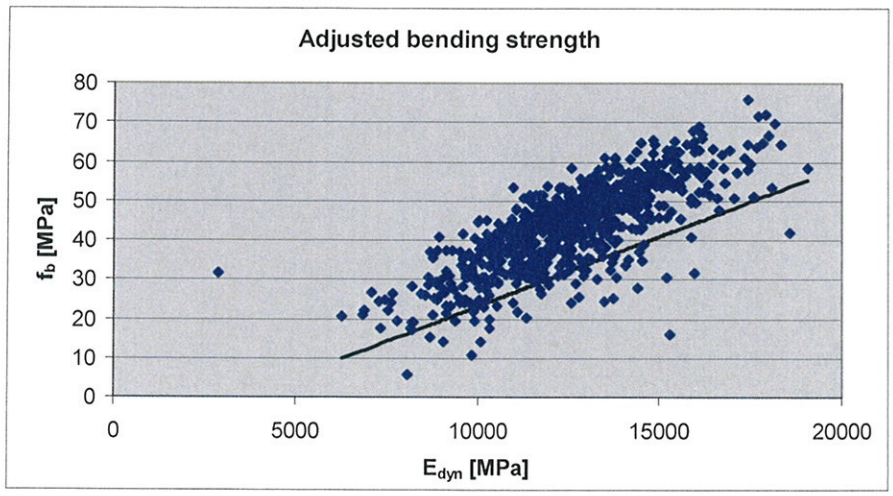

Figure 4. Size adjusted bending strength vs. E_{dyn}, also trend line for 5 percentile (eqn(3)) is shown.

Data from all five tested dimensions were used for analysis of size effect by application of regression equation

$$f_{m,adj,model} = e^{a_0} * \left(\frac{h}{h_{ref}}\right)^{a_1} * \left(\frac{b}{b_{ref}}\right)^{a_2} * \left(\frac{E_{dyn}}{E_{dyn,ref}}\right)^{a_3} \quad (4)$$

where h_{ref} = 150, b_{ref} = 50, $E_{dyn,ref}$ = 12500 and E_{dyn} is based on measurement of natural frequency and density.

Following values were obtained in regression analysis

a_0	a_1	a_2	a_3
3,788515365	-0,01843	0,167005	1,440592493

Observed bending strength vs. modelled strength is shown in Figure 5. Coefficient of determination is r^2= 0,70 while it was 0,59 when size was not variable in eqn (2).

Model for characteristic strength based on sliding 5 percentiles is

$$f_{m,k} = 0{,}8638 f_{model} - 4{,}5858 \quad (5)$$

Values obtained for eqn (4) indicate that size factor exponent 0.2 in EN384 for depth of beam is quite precise for this material. Instead, a_2=0.17 indicates a positive size factor for thickness which is not considered in EN-standards.

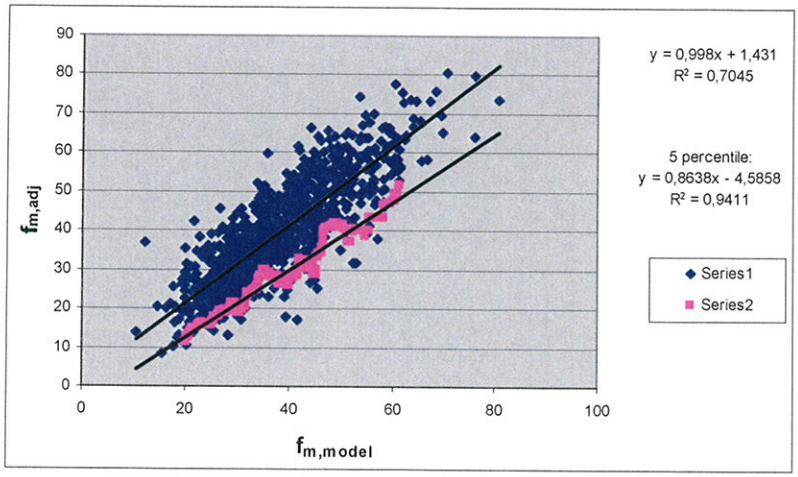

Figure 5. Observed bending strength vs. modelled according to eqn(4). Series 2 is for sliding 5 percentile.

5 Ratio of tension and bending strength

Because bending strength is the primary grade determining property, it is interesting to check the values of other grade determining properties and tension strength as function of bending strength, based on this test material.

Ratio of tension and bending strength is determined based on 5 percentile values determined by equations (1) and (3). Values from 0,65 for C16 to 0,75 for C50 are obtained. These are in good agreement with an earlier Nordic study [2].

In similar manner as relation of tension and bending strength was studied, also relation of mean modulus of elasticity and characteristic density to characteristic bending strength was calculated. Result is shown in Fig. 6.

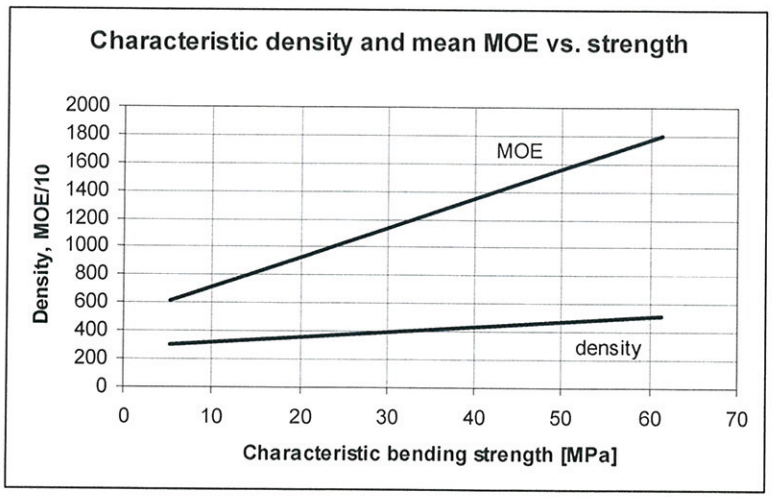

Figure 6. Relation of modulus of elasticity and density to bending strength based on sliding 5 percentiles for bending strength and density and on sliding mean values for modulus of elasticity.

6 Summary and suggestions for standardisation

Tension strength of spruce was compared to EN 338 values by using two methods: direct comparison of strength values of visually graded timber, and by comparing tension and bending strengths of material graded by use of E_{dyn}.

Visual strength-grading was performed to study connection between knot-data and tension strength. Results with graded timber show that in all strength classes characteristic tension strength value of Nordic spruce is on average 30% higher than soft-wood strength-values in the EN338-standard. This is, however, not basis for suggestions for standardisation, because visual grading was made in laboratory, not in industrial production.

Based on results from graded material by use of E_{dyn} we conclude that tension strength parallel to grain is conservative in EN 338. Based on this study and on an earlier Nordic study [2] it is suggested that characteristic tension strength should be increased. A detailed suggestion is given in Table 5. Values for other grades can be interpolated.

Size effect is considered in European standardisation in an inconsistent way. Grading standards request that bending and tension strength is given adjusted to 150 mm width of cross-section, but structural design code do not require any reduction of strength of larger dimensions than 150 mm. It is suggested that size effect in bending and tension strengths should be handled in grading standards in such a way that strength of any size is the same when material belongs to the same grade. This would include that strength models used in grading should include also the smaller dimension of cross-section as variable. According to this study, size effect in bending related to width is nearly as big as the effect of depth, but opposite: wider beam has higher strength when beam widths are in range from 44 to 63 mm. This can and should be considered in settings of grading machines.

Table 5. Suggestion for new tension strength values for some European grades.

	suggested tension to bending ratio	suggested f_{tk}	present EN338
C16	0,65	10	10
C20	0,68	14	12
C24	0,70	17	14
C30	0,72	22	18
C40	0,74	30	24
C50	0,75	37	30

Acknowledgements

This work was financed by TEKES, Woodfocus Finland, Finnish glulam association, Finnforest Oyj, Stora Enso Timber, UPM-Kymmene Wood Products and VTT which is gratefully acknowledged.

References

[1] Green, D.W.; Kretschmann, D. E. (1989). A discussion of lumber property relationships in Eurocode 5. CIB W18, Meeting Twenty Two. Paper 22-6-3.

[2] Johansson, C.J.; Boström, L.; Bräuner, L.; Hoffmeyer, P.; Holmqvist, Ch.; Solli, K.J. (1998). Laminations for glued laminated timber - Establishment of strength classes for visual strength grades and machine settings for glulam laminations of Nordic origin. SP Report 1998:38. 70p+app. ISBN 91-7848-744-7

[3] Burger, G.; Glos, P. (1997). Strength relationships in structural timber subjected to bending and tension. CIB W18, Meeting Thirty. Paper 30-6-1.

[4] Hanhijärvi, A., Ranta-Maunus, A. (2007). Development of strength grading of timber using combined measurement techniques. Report of the Combigrade-project – phase 2. VTT Publications, manuscript. Espoo

[5] Poussa, M., Tukiainen, P., Mitsuhashi, K., Andersin, P. (2007). COMBI T – Destructive tension, shear, and compression (0° and 90°) strength tests for Finnish sawn timber. Helsinki University of Technology, Laboratory of Structural Engineering and Building Physics Publication TKK-TRT-130. (http://www.tkk.fi/Yksikot/Talo/projektit/COMBI_T.pdf)

[6] Ranta-Maunus A. (2007). Strength of Finnish timber. VTT Publications. Manuscript.

[7] Mitsuhashi K., Poussa M., Puttonen J. (2007). Method to predict tension capacity of sawn timber considering slope of grain around knots. Submitted to Journal of Wood Science, Japan Wood Research Society.

[8] Mitsuhashi K. (2007). A method for predicting the tension strength of structural timber, M.Sc. thesis, Laboratory of Structural Engineering and Building Physics, TKK Helsinki University of Technology.

INTERNATIONAL COUNCIL FOR RESEARCH AND INNOVATION
IN BUILDING AND CONSTRUCTION

WORKING COMMISSION W18 - TIMBER STRUCTURES

PREDICTING THE STRENGTH OF BOLTED TIMBER CONNECTIONS SUBJECTED TO FIRE

M Fragiacomo
University of Sassari, Alghero
ITALY

A Buchanan
P Moss
D Carshalton
University of Canterbury, Christchurch
NEW ZEALAND

C Austruy
Ecole normale superieure de Cachan
FRANCE

MEETING FORTY
BLED
SLOVENIA
AUGUST 2007

Presented by M. Fragiacomo
A. Frangi commented that heated tests are completely different from fire test as there are strong temperature and moisture gradients in fire tests. One cannot use material properties to predict fire test results. M. Fragiacomo disagrees as this work is a strong starting point.
S. Thelandersson commented that this work is interesting as it shows it is most critical to keep down the temperature rise in the bolt; therefore, protecting the steel is most important.
J. König commented this presentation deals with 12 mm bolts. This is okay to restrict to this diameter. Steel-Wood-Steel failure in 8 minutes is okay. Temperature of the bolt is 350° C at 8 minutes and the temperature of the interface and wood is the same; therefore, temperature of the bolt is constant. The influence of moisture content is not important here. If there is temperature gradient along the bolt or material then this work does not apply.
H. Blass commented that if charring were observed between the steel plate and wood then Johansen formula in the code would not be valid.
G. Schickhofer received confirmation that the yield moment was measured according to the principles of EN40 (3 versus 4 point in EN 409).

Predicting the strength of bolted timber connections subjected to fire

Massimo Fragiacomo
University of Sassari, Alghero, Italy

Andrew Buchanan, Peter Moss, and David Carshalton
University of Canterbury, Christchurch, New Zealand

Carla Austruy
Ecole normale superieure de Cachan, France

1 Introduction

Fire is unpredictable and dangerous, especially in residential buildings. The effects of fire on structural members are very complex because of the large number of variables involved. Once ignition has occurred, then a layer of char forms as the wood burns. A structural wood member will lose load capacity as the wood is converted to charcoal which has no strength. The thickening char layer protects the remaining wood, resulting in a predictable rate of charring below the surface. The rate of development of this charred layer determines how long the member can continue to carry load before the strength of the remaining unburned wood material is exceeded. A thin layer of heat-affected wood below the char layer will have reduced strength and stiffness.

Wood cells consist basically of cellulose (40-50%), hemi-cellulose (20-35%), lignin (20-35%), and other products (less than 10%), together with moisture. The tension strength of wood comes from the cellulose chains in the fibrils in the cell walls while the compressive strength comes from the lignin which forms the outer skin of the fibrils. The cellulose chains degrade substantially at temperatures above 200°C while the lignin softens considerably at about 80-100°C but rehardens at higher temperatures.

In recent years, a number of research papers have been published on the influence of temperature on the mechanical properties of wood [e.g. 1, 2, 3, 4]. Research has also been carried out into the performance of joints in timber members when subjected to fire temperatures [e.g. 5, 6, 7, 8, 9]. Particular research into the embedment strength of wood at elevated temperatures has also been carried out [10, 11].

Moraes et al [10] carried out embedment tests at temperatures ranging from 20°C to 240°C. The 8 mm diameter dowel specimens were heated for 2 hours before testing to a maximum displacement of 5 mm. They found that the embedding strength at 80°C was 30% lower than at 20°C but then rose to a peak at 140°C where it was 15% lower than at 20°C and then decreased to 40-50% at 240°C. The tested specimens showed that the moisture content decreases linearly with increase in the test temperature. The specimens had a moisture content of about 5% at 80°C and were found to be almost oven dry at 140°C. Above this value, the wood lost mass in addition to the surface bound water or water bound in the molecular layer.

For some time now, the European timber code [12] has used formulae based on Johansen's yield equations [13] to predict the strength of timber connections under ambient conditions. The EC5 code [14] gives some guidance for predicting the strength of connections during fire conditions. Carling [15] defined failure as occurring when the rate of displacement exceeds 10 mm/min, or the total displacement exceeds 15 mm. He also proposed a formula for calculating the time to failure for bolted connections, based on his experimental testing.

This paper describes an experimental investigation carried out to determine the axial tensile strength of a bolted connection that utilised steel splice plates to connect the LVL members. Single-bolted connections were tested under constant temperature conditions to determine the embedment strength of the LVL over a range of temperatures. The variation in the embedment strength was then used in Johansen's equations (as presented in EC5 [14]). The purpose of the research was to investigate the relationship between the embedmenst strength of LVL timber and the time to failure of the connections when exposed to fire.

2 Background to the Testing

The design for the connection tested previously by Lau [16], Chuo [17] and Moss et al [18] was based on a tensile member in the bottom chord of a floor or roof truss. The timber (LVL) members being joined were 150 x 63 mm. The design properties of the LVL are shown in Table 1. The steel side plates were 6 mm thick. The bolts were 12 mm diameter and were made of Grade 4.6 steel.

Table 1 Limit state properties for design with NelsonPine LVL [19].

Elastic Moduli		
Modulus of elasticity	E	10700 MPa
Modulus of rigidity	G	660 MPa
Characteristic Strength		
Bending	f'_b	42 MPa
Tension parallel to grain	f'_t	22 MPa
Compression parallel to grain	f'_c	35 MPa
Shear in beams	f'_s	6.0 MPa
Compression perpendicular to grain	f'_p	12 MPa

The design load on the joint was taken to be 40% of the ultimate tensile strength of the LVL in cold conditions (i.e. a load of 40% of 221 kN = 88kN) by assuming that other design conditions will be more critical than the tensile strength of the member. With a calculated load factor of 0.33 for fire conditions, this gave an expected fire load of 29kN. Six bolts were used for the Wood-Wood-Wood (W-W-W) joint, four bolts for the Steel-Wood-Steel (S-W-S) joint, and five bolts for the Wood-Steel-Wood (W-S-W) joint. The different connections are illustrated in Figure 1.

The same size timber and steel members with the 12 mm diameter bolts were used to fabricate single-bolt joints. The bolts were placed on the member centreline with an end distance of 100 mm, i.e. eight bolt diameters, as shown in Figure 1.

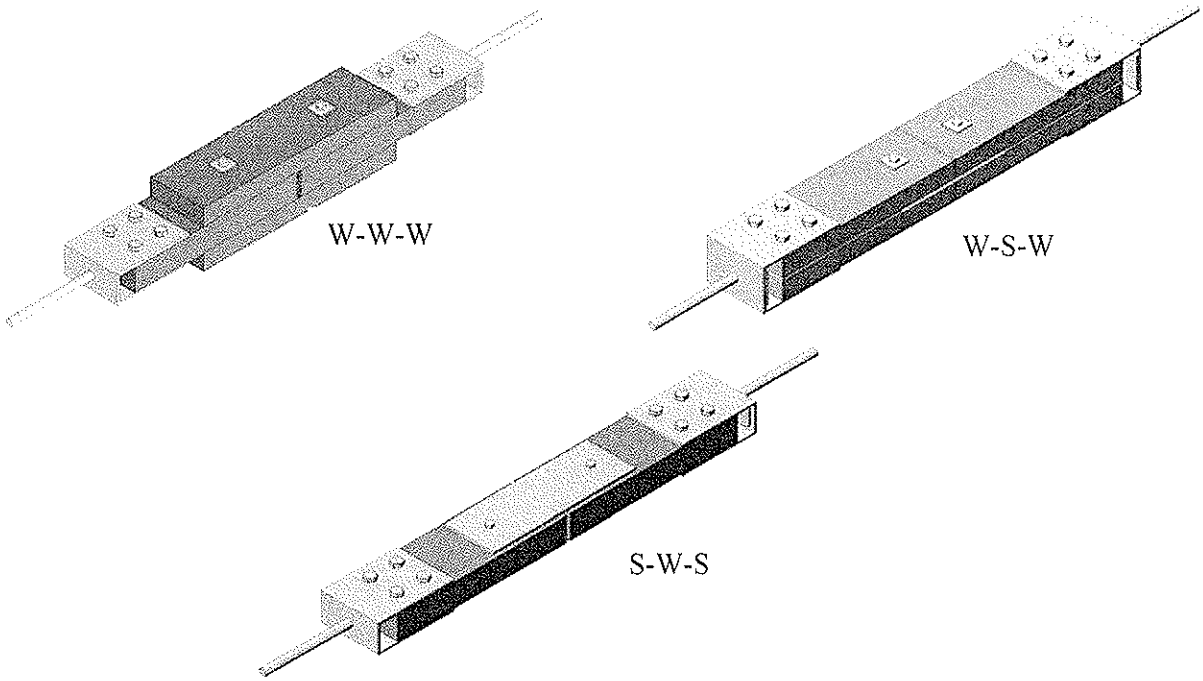

Figure 1 The three types of connection tested. Multi-bolted specimens were also used in fire tests.

3 Heated testing

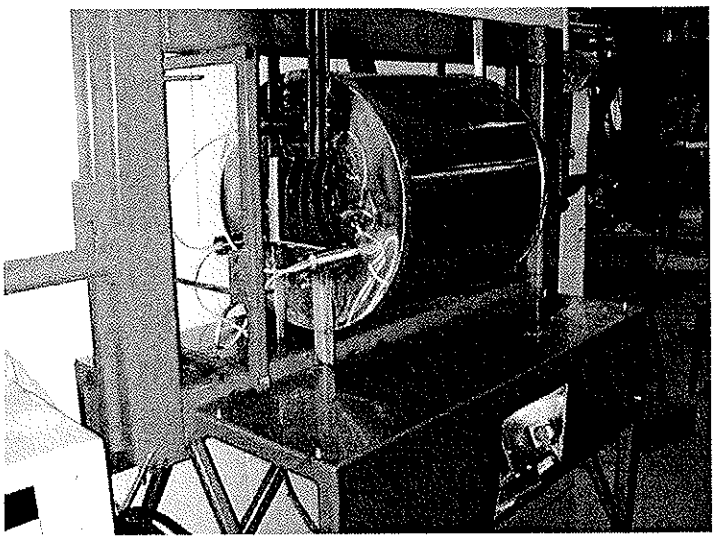

Figure 2 The test frame and furnace used for the heated and fire testing.

In order to develop a simple method of predicting the load capacity and deformation of connections in timber structures when exposed to known heat flux, a series of tests were carried out at known temperatures in a similar manner to that outlined in previous research [10, 11]. For this testing, a series of single-bolt joints were heated in the furnace for two hours at a constant temperature with no applied load under temperatures ranging from ambient to 280°C. The test specimens were then quickly loaded to failure in accordance with the loading protocol suggested by ISO 10984-2 [20]. The furnace used for both the heated tests and the fire tests is shown in Figure 2. The air temperatures measured in the furnace during tests were lower than the constant temperatures set for the furnace heating elements.

3.1 Embedment Strength

Since the S-W-S connections were similar to standard embedment test specimens, the results from these tests were used to evaluate a form of embedding strength for the LVL at elevated temperatures. The main differences between the single-bolt joints tested and the testing apparatus as required by ISO 10984-2 [20] are outlined in Table 2.

Table 2 Comparison of single-bolt connection and ISO standard embedment test [20]

	Single-bolted SWS connection	ISO Standard Embedment Test
1.	Steel members tightly bolted to timber member (Fig. 1).	No contact between steel members and test specimen.
2.	Two fasteners were used in each test (i.e. one at each member end).	Only one fastener used in test.

The "embedding strength" is based on either the maximum load or the load carried at 5 mm displacement, depending on which occurs first. As the bolted connection contained two bolts (one at each member end as shown in Figure 1) and the maximum load occurred at a large displacement, the embedding strength was calculated by dividing either the load at 10 mm displacement, or the maximum load, by the bolt diameter and the thickness of the member. Since the joints tested at ambient temperatures failed in mode k (see Figure 7), the joint strength was substituted into the relevant Johansen yield formula as given in EC5 [12] to determine the embedment strength. Other information required included the bending strength of the bolt at the various temperatures, the timber thickness, and the experimental failure mode. The results are shown in Figure 3 where it can be seen that the embedment strength decreases as the temperature increases, reaching a minimum at about 110°C and then increasing as the temperature increases further to 180-200°C, followed by a decrease with further temperature increase. The data points shown by triangles in Figure 3 are the embedment strengths determined later using 45 mm thick LVL and 12 mm thick splice plates, where the thinner thickness of LVL fully complies with the thickness to bolt diameter ratio recommended by the ISO standard [20] for embedment strength tests. The top graph of Figure 3 shows the embedment strength based on the load at 10 mm displacement while the middle graph shows the embedment strength based on the maximum load. The bottom graph is the same as the top one, except that the embedment strength is now taken as independent of temperature for all temperatures above 260 °C and below 20 °C.

3.2 Prediction of fire resistance

The temperatures of the air, the steel plate-wood interfaces, and at several points on the bolts were measured using thermocouples and are shown in Figure 4 for the S-W-S connection during a typical fire test. It can be seen that the temperatures of the steel side plates and the bolts are effectively the same. Figure 5 shows typical temperature-time relationships for the W-S-W connection. Figure 6 for the W-W-W connections on the other hand, shows that it takes longer for the bolt at the centre of the centre member to heat up than it does for the bolt head which is exposed to the fire.

For the S-W-S connections, the experimental failure mode for the bolts at ambient temperatures was mode k whereas for temperatures above 50°C the failure mode was mode j/l (see Figures 7 to 9 for sketches of these failure modes). The comparison between the

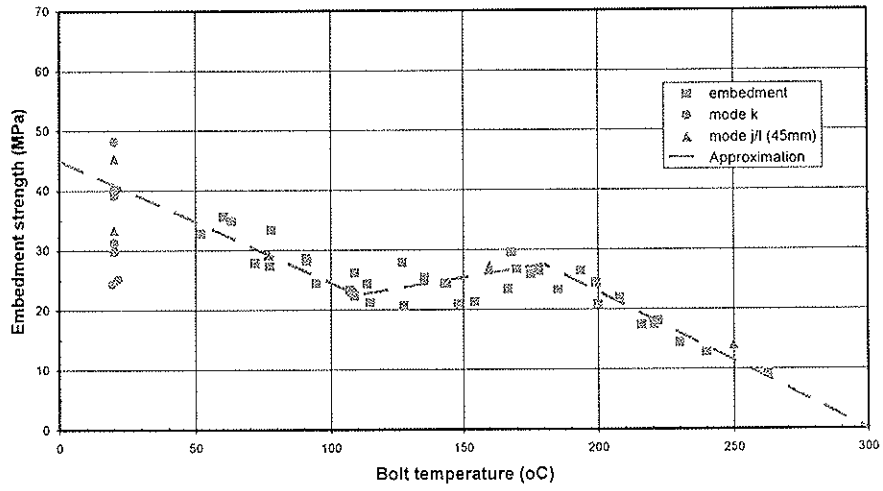

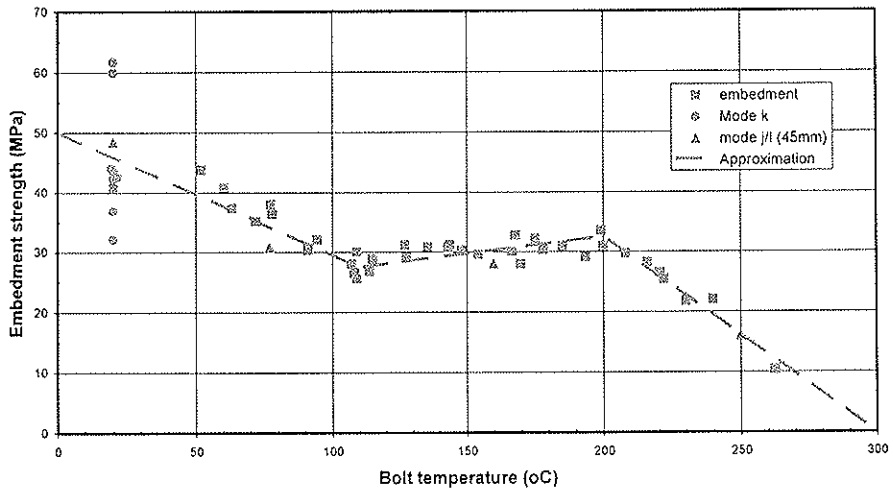

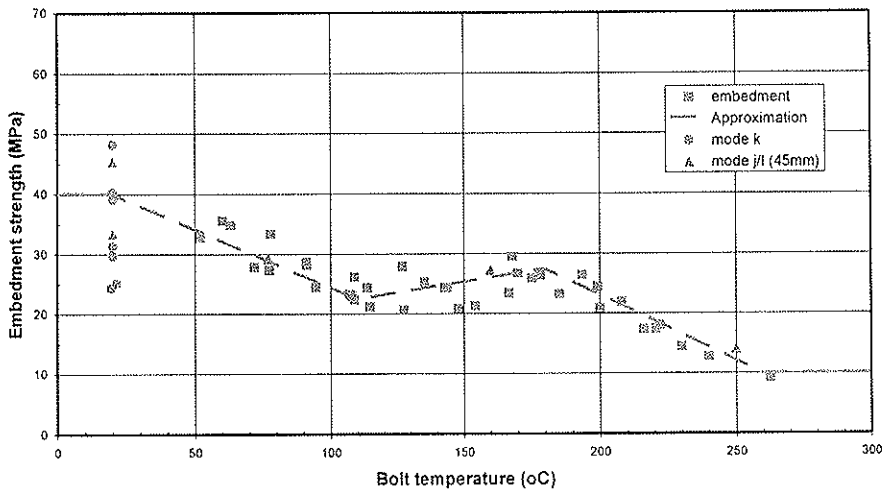

Figure 3 LVL embedment strength based on (top) load at 10 mm displacement, (middle) maximum load, and (bottom) same as top figure, with cut-off below 20°C and above 260°C.

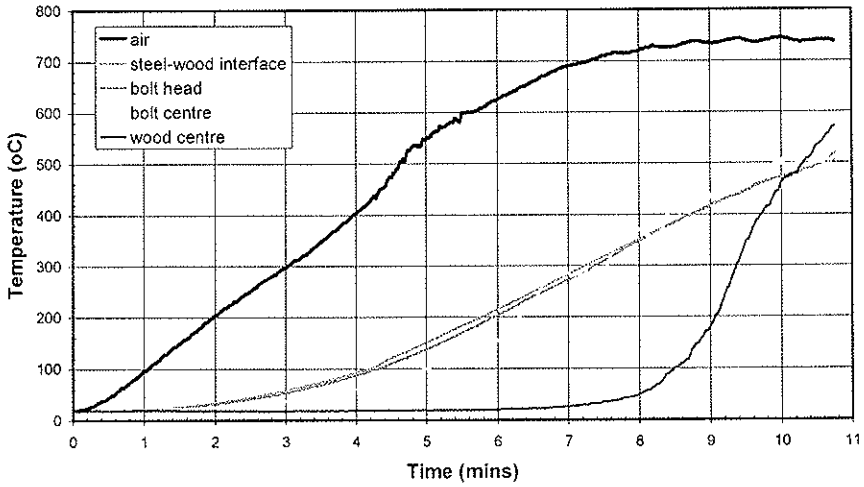

Figure 4 Temperatures measured within the S-W-S connection during the fire test.

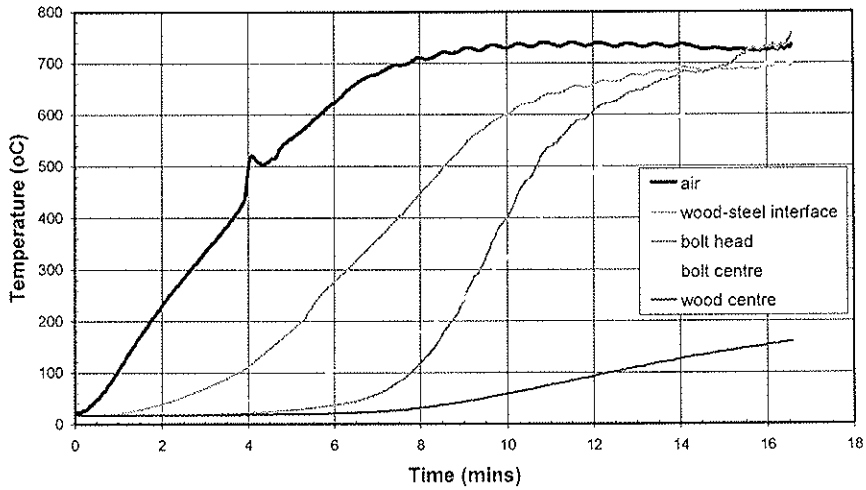

Figure 5 Temperatures measured within the W-S-W connection during the fire test.

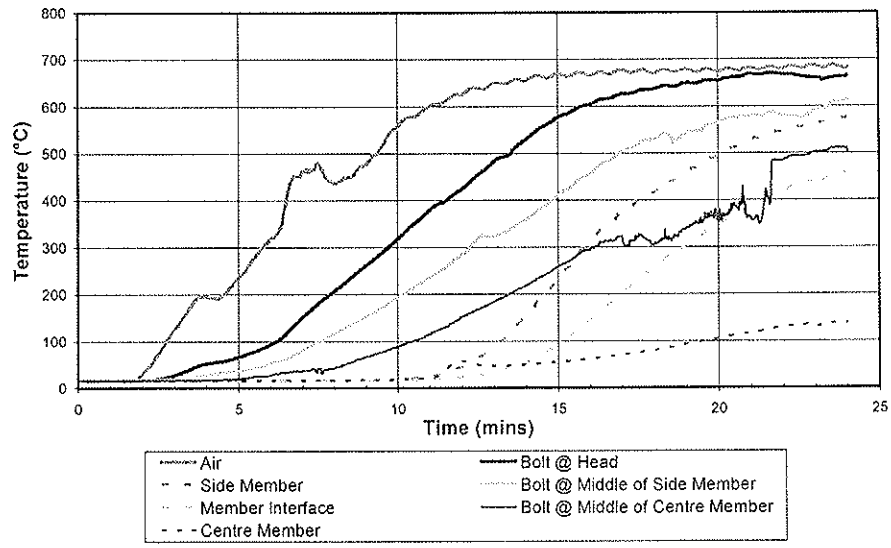

Figure 6 Temperatures measured within the W-W-W connection during the fire test.

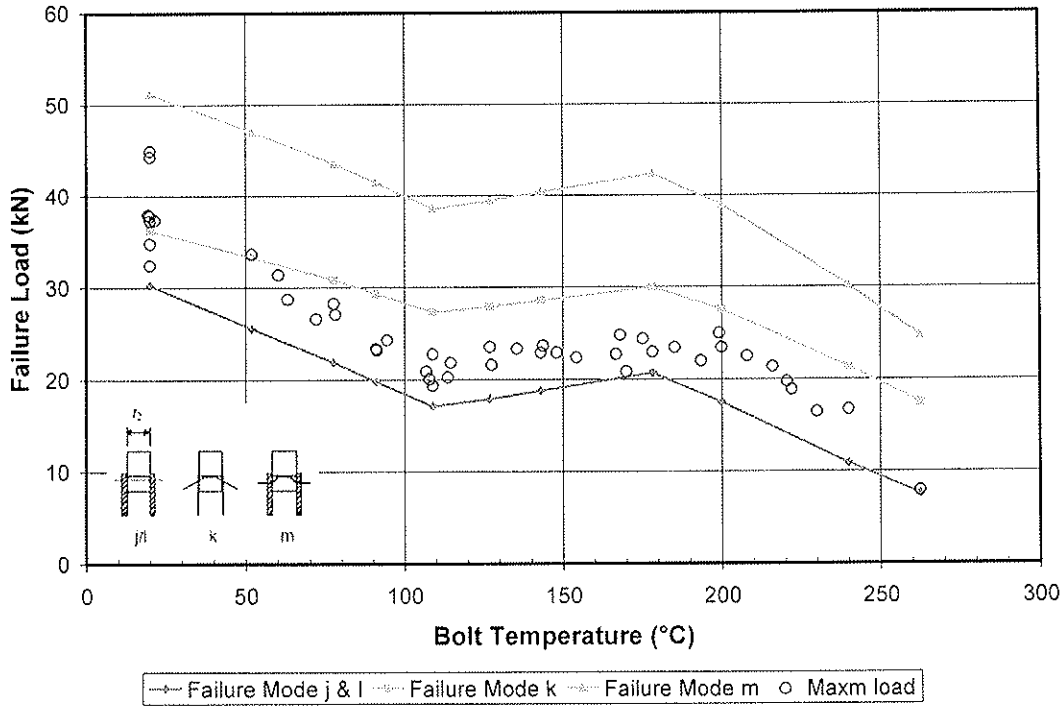

Figure 7 Predicted and experimental failure loads for single-bolt S-W-S connections tested at constant temperature.

experimental results and the predicted failure loads using Johansen's equations, and the approximation for the embedment strength shown in Figure 3(top), for modes j/l, k and m is plotted in Figure 7 together with the maximum experimental failure loads. It can be seen that, in general, almost all the maximum experimental loads fall on or above the predicted values for failure mode j/l except at 20°C where the experimental failure loads are scattered about the predicted value for mode k.

4 Failure prediction for fire tested connections

Using the experimental embedment strength calculated from the single bolt S-W-S connection tests, the predicted failure loads in fire for the three connections tested are shown in Figures 8-11. The contact thickness between the bolt and the timber members was taken as the original thickness less the thickness of the charred surface as indicated in Equation 1.

$$t_{contact} = t - (n \times D \times \theta) \qquad [1]$$

where t = Timber thickness (mm)

n = Number of charring surfaces (-) (for SWS, n = 2, otherwise n = 1)

D = Experimental charring rate (mm/min)

θ = Charring duration (min)

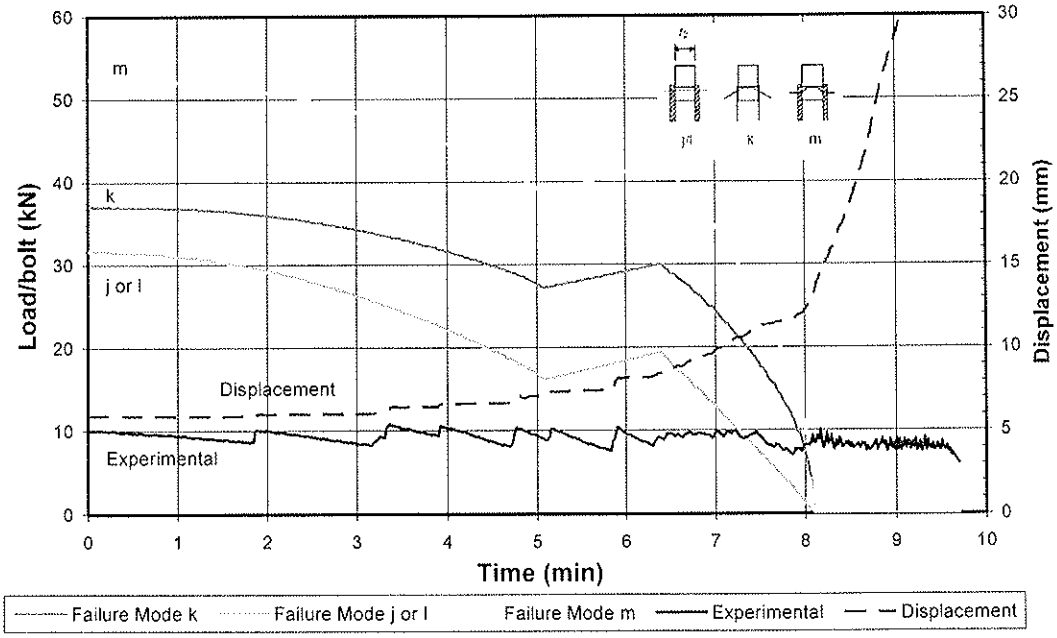

Figure 8 Predicted failure loads for S-W-S connection based on Figure 3(top) approximation).

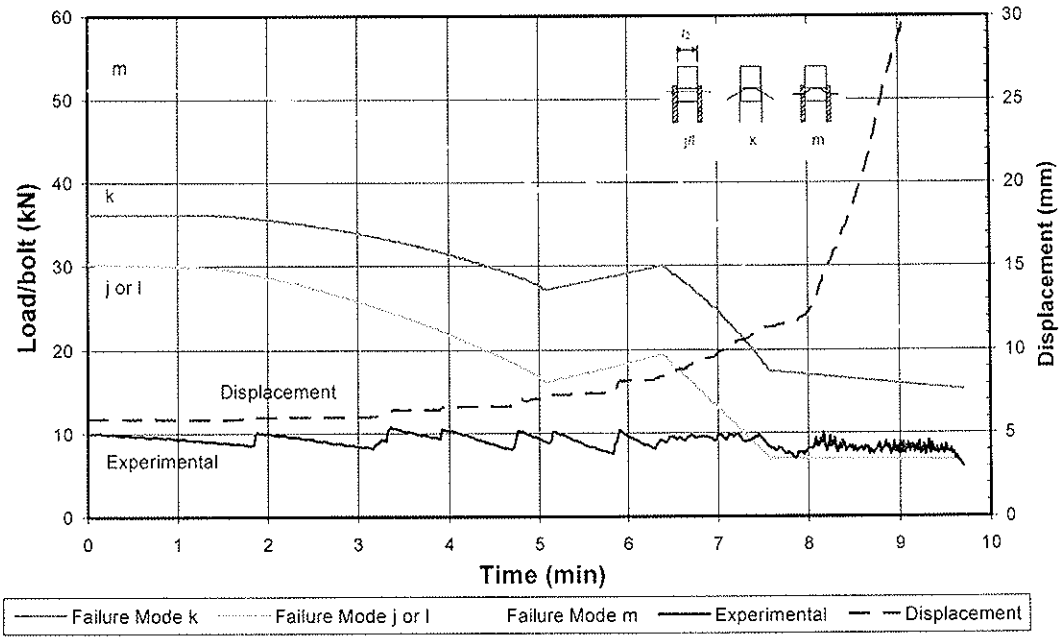

Figure 9 Predicted failure loads for S-W-S connection based on Figure 3(bottom) approximation.

In order to derive the curves for the various failure modes shown in Figures 8-11 it is necessary to know the temperature in the bolt over time, T(t), then determine the embedding strength, $f_h(T(t))$ using the approximation depicted in Figure 3(bottom), and the yielding moment for the bolt, $M_y(T(t))$. These are then substituted into the Johansen equations. Numerical studies are presently under way to predict T=T(t) during a fire, depending on the geometry of the joint. These studies, along with the more limited results

of fire tests, should enable a relationship to be established between the temperature of the air during the fire and the temperature in the bolts.

The prediction of the failure mode and the failure load per bolt for the S-W-S connection using the tri-linear embedment strength curve of Figure 3(top) (Figure 8), together with the experimental charring rate and steel strength reduction factor for temperature, was reasonably accurate. The tests were stopped when the total displacement reached 30-40 mm and the rate of displacement was increasing rapidly. However, the estimation of the failure time was too early compared to the experimental failure time; this is because after the LVL has reached its zero embedment strength, the load carrying capacity of the connection is zero, though experimentally it was still able to carry load. On the other hand, if Figure 3(bottom) is used to determine the failure time (Figure 9), the prediction seems more accurate. Nevertheless, once the LVL reaches its constant embedment strength, the load carrying capacity of the connection reduces only slightly as the timber chars and therefore the predicted failure time is very sensitive to the predicted load level.

The predicted failure loads per bolt for the W-S-W connection using the approximation of Figure 3(bottom) are shown in Figure 10. For this particular connection the predicted failure mode is always mode f. While the prediction looks reasonably accurate, it more clearly indicates a range of time over which failure could take place. For the W-W-W connection, Figure 11 shows the predicted failure loads using the approximation of Figure 3(bottom) and how they vary throughout the duration of the fire with mode g being the predicted failure mode. Again, the predicted time to failure looks reasonably accurate.

5 Discussion

The decrease of embedment strength from 50°C to about 110°C is possibly due to softening of the lignin in the cell walls, while the increase in the range between 110°C and 180-200°C is caused by the timber drying and releasing the bound water from the cells, together with possible rehardening of lignin over this temperature range. The embedding strength results described herein are similar to the results reported by Moraes et al [10]. The results are also similar to those reported by Young and Clancy [1] and Jong and Clancy [3] for the compression parallel to the grain strength of timber.

Since timber chars at around 300 °C and the char layer has negligible strength, it would seem reasonable for the embedment strength values shown in Figure 3 to reduce to zero at about 300 °C. However, in a connection that is transferring load, the char layer is displaced as it forms and the bolt continues to heat the wood in contact with it. The result is that the bolt cuts an elongated hole in the wood member; this causes movement in the joint but does not necessarily lead to failure and the joint continues to carry load. For this reason, it is suggested that the approximation of Figure 3(bottom) should be used instead of that of Figure 3(top).

If we take failure as occurring when the rate of displacement exceeds 10 mm/min, or the total displacement exceeds 15 mm [15], then Figure 8 for the S-W-S connection gives a good prediction of failure since the rate of deflection increases markedly at about 8 minutes and the total displacement exceeds 15 mm shortly after. However, for the W-S-W (Figure 10) and the W-W-W (Figure 11) connections, there is not the same close agreement between the prediction and the definition of failure based on the displacement and its rate of increase.

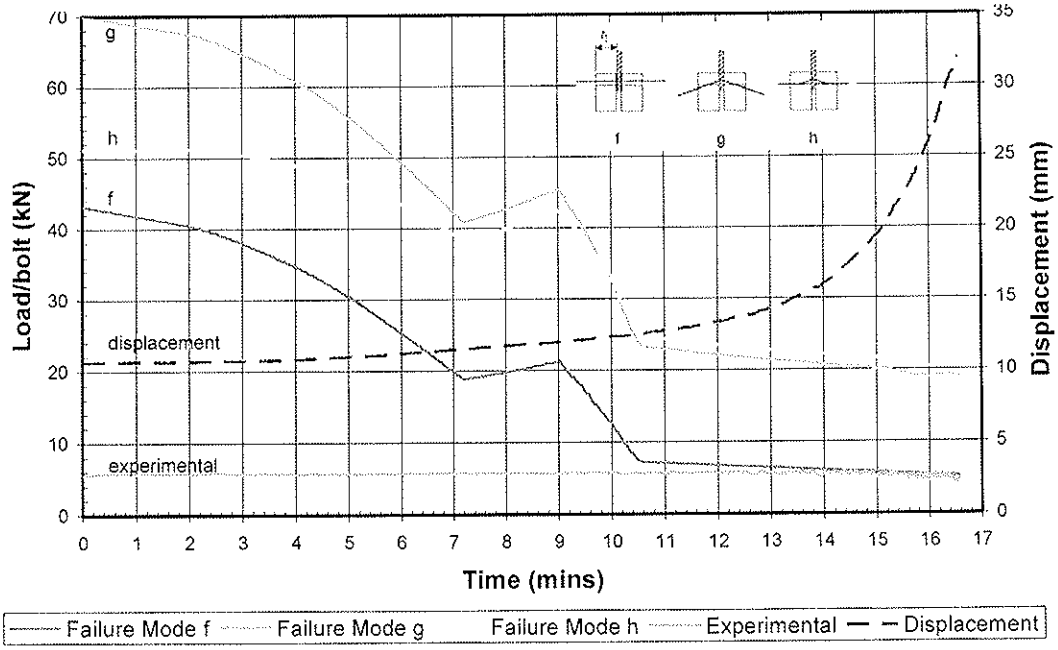

Figure 10 Predicted failure loads for W-S-W connection based on Figure 3(bottom) approximation.

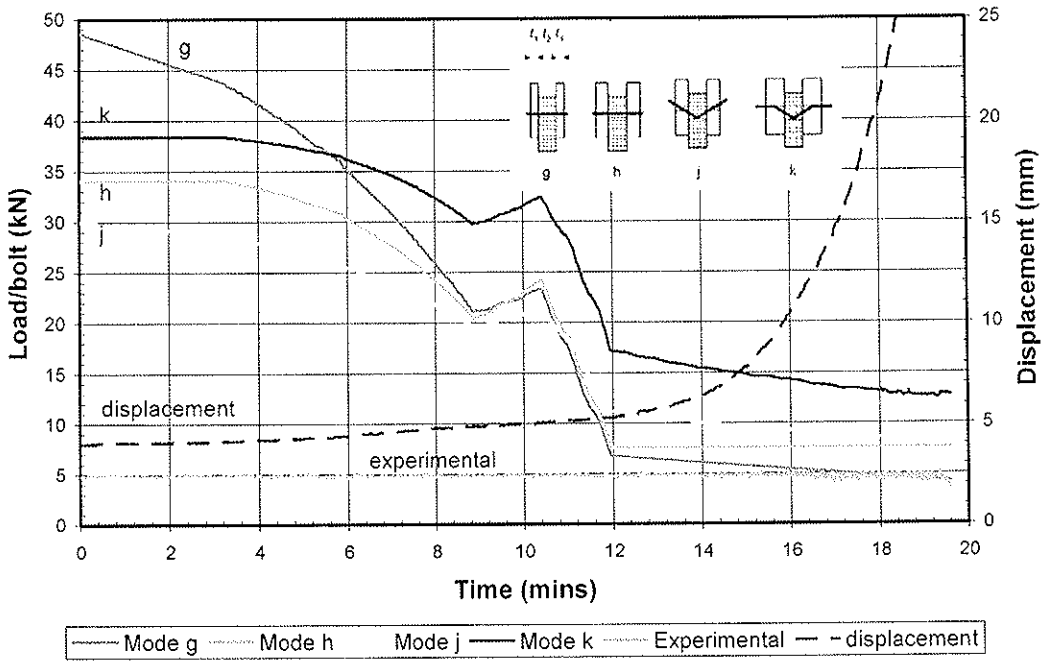

Figure 11 Predicted failure loads for W-W-W connection based on Figure 3(bottom) approximation.

6 Conclusions

The embedment strength of radiate pine LVL can be described by a tri-linear relationship that varies linearly from 40 MPa at 20°C to 25 MPa at 110°C, rises to 27.5 MPa at 180°C, then falls to 10 MPa at 260°C.

This tri-linear embedment strength was used in conjunction with Johansen's yield equations to predict the failure load and the results showed reasonable agreement with the experimental values.

Due to the good heat conduction properties of steel, there is very little difference in temperature at different locations on the bolts when a S-W-S connection is exposed to high temperatures. There is, however, some variation in temperature along the bolts for a W-W-W connection. The average timber member temperatures were generally lower than the bolt temperatures due to the poor heat conduction of wood. The exception is the S-W-S connection where the timber and bolt temperatures are comparable after some time.

7 Acknowledgements

Thanks to Nelson Pine for the supply of all the LVL which was tested. Thanks also to Bob Wilsea-Smith and Grant Dunlop for laboratory support.

8 References

1 Young, S.A. and Clancy, P. 2001. Compression mechanical properties of wood at temperatures simulating fire conditions, *Fire and Materials*, 25: 83-93.

2 Reszka, P. and Torero, J. L. 2006. *In Depth Temperature Measurements of Timber in Fires*, Proc. 4th International Workshop on Structures in Fire, Aveiro, Portugal.

3 Jong, F. and Clancy, P. 2002. *Compression properties of wood as functions of moisture, stress, and temperature*, Proc. 2nd International Workshop on Structures in Fire, Christchurch, New Zealand, 223-242.

4 Janssens, M. 2002. *Modelling of the thermal degradation of structural wood members exposed to fire*, Proc. 2nd International Workshop on Structures in Fire, Christchurch, New Zealand, 211-222.

5 Frangi, A. and Mischler, A. 2004. *Fire Tests on Timber Connections with Dowel type Fasteners*, International Council for Research and Innovation in Building and Construction, Working Commission W18 – Timber Structures, Meeting 37, Edinburgh, United Kingdom, August 2004.

6 Erchinger, C., Frangi, A., and Mischler, A. 2005. *Fire Behaviour of Multiple Shear Steel-to-timber Connections with Dowels*, International Council for Research and Innovation in Building and Construction – Working Commission W18 – Timber Structure, Meeting 38, Karlsruhe, Germany.

7 Erchinger, C., Frangi, A. and Mischler, A. 2006. *Thermal investigations on multiple shear steel-to-timber connections,* Proc. World Conference on Timber Engineering, Portland, Oregon, USA.

8 Laplanche, K., Dhima, D. and Racher, P. 2006. *Thermo-mechanical modelling of the timber connection under fire using 3D finite element model*, Proc. World Conference on Timber Engineering, Portland, Oregon, USA.

9 Schabl, S. and Turk, G. 2006. *Coupled heat and moisture transfer in timber beams exposed to fire*, Proc. World Conference on Timber Engineering, Portland, Oregon, USA.

10 Moraes, P.D., Rogaume, Y., Bocquet, J.F., and Triboulot, P. 2005. Influence of temperature on the embedding strength, *Holz als Roh- und Werkstoff*, 63: 297-302.

11 Chapuis, S., Moraes, P.D., Rogaume, Y., and Torero, J.L. (private communication, 2005). *Evaluation of in-depth temperature distributions and embedding resistance of timber in a fire.*

12 EC5 2004. Eurocode 5 – Part 1-1: *Design of Timber Structures. EN 1995-1-1:2004: General – Common Rules and Rules for Buildings*, European Committee for Standardization, Brussels, Belgium.

13 Johansen, K.W. 1949. *Theory of Timber Connections*, Int. Assn of Bridge & Struct. Eng., Publ. no. 9:249-262, Bern, Switzerland.

14 EC5 2004. Eurocode 5 – Part 1-2: *Design of Timber Structures. EN 1995-1-2:2004: General – Structural Fire Design*, European Committee for Standardization, Brussels, Belgium.

15 Carling, O. 1991. *Fire Behaviour of Metal Connectors on Wood Structures*, Proc. 1991 Int. Conf. on Timber Engineering, London, 4:106-113.

16 Lau, P.H. 2006. *Fire Resistance of Connections in Laminated Veneer Lumber*, Fire Engineering Research Report 06/3, Dept of Civil Engineering, University of Canterbury, New Zealand.
http://www.civil.canterbury.ac.nz/fire/fe_resrch_reps.shtml

17 Chuo, T.C.B. 2007. *Fire performance of Connections in LVL Structures*, Fire Engineering Research Report 07/4, Dept of Civil Engineering, University of Canterbury, New Zealand.
http://www.civil.canterbury.ac.nz/fire/fe_resrch_reps.shtml

18 Moss, P.J., Buchanan, A.H., Fragiacomo, M., Lau, P.H. and Chuo, T. Submitted for publication. Fire Performance of Bolted Connections in Laminated Veneer Lumber, *Fire and Materials.*

19 NelsonPine NZ LVL10. 2003. Design Guides and Span Tables, Nelson Pine Industries Ltd, Richmond, Nelson, New Zealand.

20 ISO 10984-2 1999, *Timber structures – Dowel-type fasteners – Part 2: Determination of embedding strength and foundation values*, International Standards Organization, Geneva.

INTERNATIONAL COUNCIL FOR RESEARCH AND INNOVATION
IN BUILDING AND CONSTRUCTION

WORKING COMMISSION W18 - TIMBER STRUCTURES

EDGE JOINTS WITH DOWEL TYPE FASTENERS IN CROSS LAMINATED TIMBER

T Uibel

H J Blaß

Universität Karlsruhe

Germany

MEETING FORTY

BLED

SLOVENIA

AUGUST 2007

Presented by T. Uibel

I. Smith questioned how to calculate the forces these types of connectors see. T. Uibel said the walls are considered as rigid body and forces are equally distributed to the fasteners and there are no data on creep tests yet. I. Smith asked about why the pull-out tests are conducted at lower load level. T. Uibel answered that the screws loaded parallel to grain of solid timber has low capacity. Capacity under permanent load for these screws would be low, therefore, the chosen low load level.

A. Jorissen received clarification of the density values used in the model.

B.J. Yeh asked if the dowel located at a gap would get lower results. H. Blass answered yes but one would not be sure how large is the difference. Therefore, it was decided not to consider this as individual case but combined the various modes together.

Edge Joints with Dowel Type Fasteners in Cross Laminated Timber

T. Uibel, H.J. Blaß
Lehrstuhl für Ingenieurholzbau und Baukonstruktionen
Universität Karlsruhe, Germany

1 Introduction

During the 39th meeting of CIB-W18 the authors presented proposals for the calculation of the load carrying capacity of joints with dowel type fasteners positioned perpendicular to the plane of cross laminated timber (CLT) [4]. In continuation of the research project [1] the load carrying capacity of edge joints with dowels and screws in CLT was examined. To calculate the load carrying capacity of dowel-type fasteners according to Johansen's yield theory [2], [3] the yield moment of the fasteners and the embedding strength are needed. The withdrawal strength is necessary to calculate the load carrying capacity of axially loaded screws. In addition, the withdrawal strength is important for estimating the rope effect of laterally loaded connections. In the narrow sides of CLT the fasteners can be positioned parallel to the grain direction. The embedment strength and the withdrawal strength are also influenced by gaps and grooves.

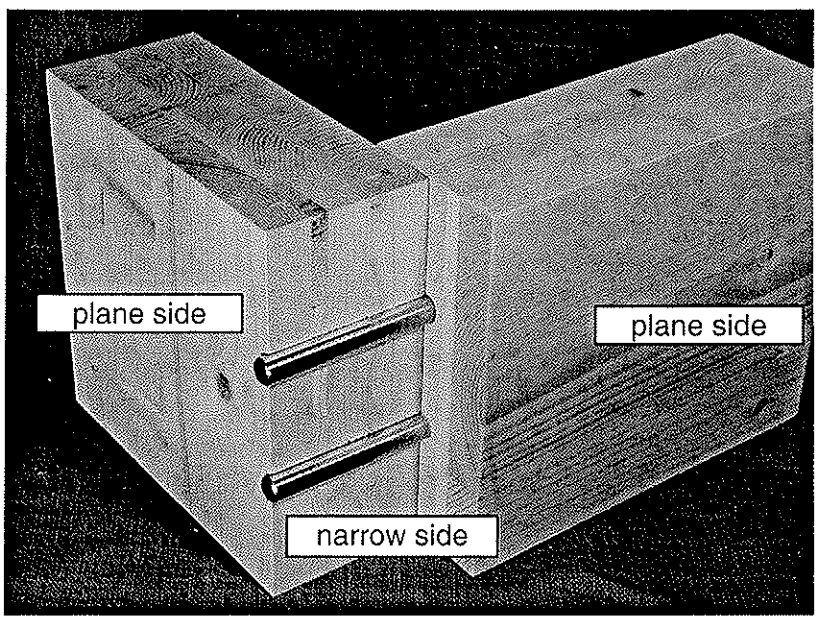

Fig. 1: Opened connection with dowels in cross laminated timber

2 Embedding strength

2.1 Test set-up and test material

The embedment tests with dowels, screws and nails in CLT were carried out according to EN 383 [5]. To avoid splitting of test specimens tensile reinforcements were required in some cases. For this purpose stripes of plywood were glued onto the surface of the test specimen, as shown in Fig. 2. The stripes were placed in some distance to the fastener to exclude influences on the embedment strength and on the stress distribution within close range of the fastener.

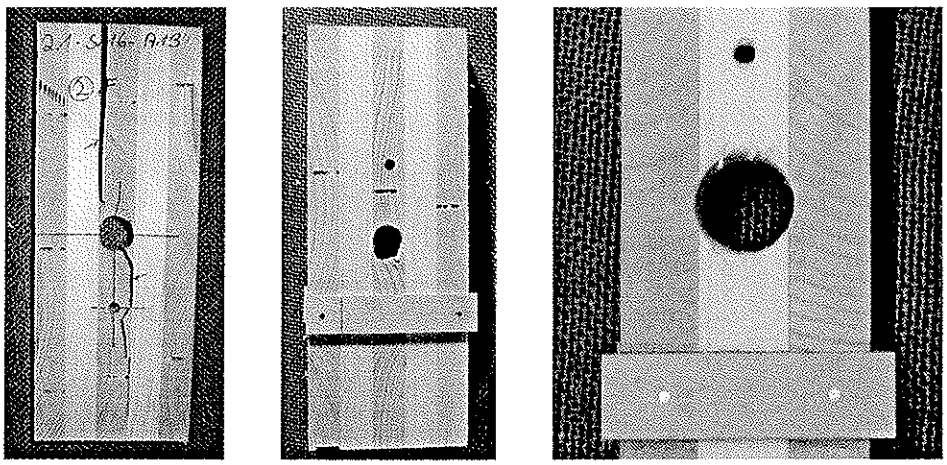

Fig. 2: Splitting failure of test specimen and tensile reinforcements to avoid splitting

The test programme includes tests with two different load directions as shown in Fig. 3 (direction A and B). In the narrow sides of CLT many positions of fasteners are possible. Fig. 4 shows five possible positions of fasteners with different diameters in relation to the thickness of the layers and in relation to the grain direction. The examined positions of fasteners in relation to gaps and grooves are displayed in Fig. 5. It was not possible to determine the relevant configuration before the tests. Thirteen different combinations of load direction and fastener positions were considered in the tests with dowels while in the tests with screws and nails seven combinations were included.

For the tests CLT made of European spruce (*Picea abies*) from four different manufacturers with seven different build-ups were used. Table 1 gives some statistical information about the density of the test specimens.

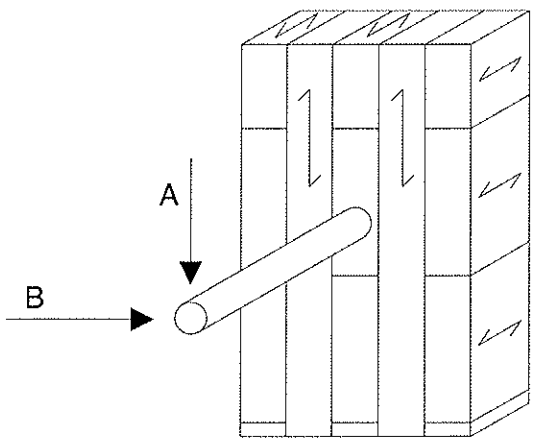

Fig. 3: Tested load directions, schematic sketch of a test specimen

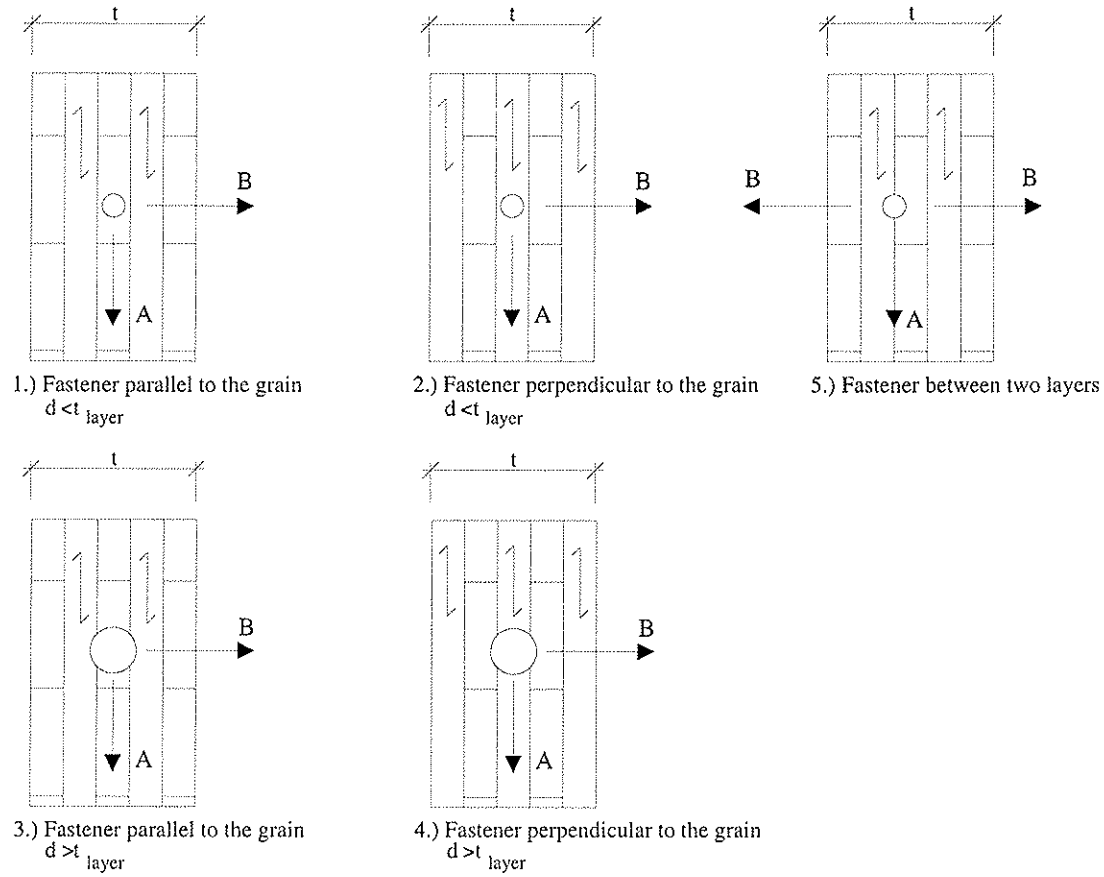

Fig. 4: Possible positions of fasteners in the narrow sides, schematic sketch

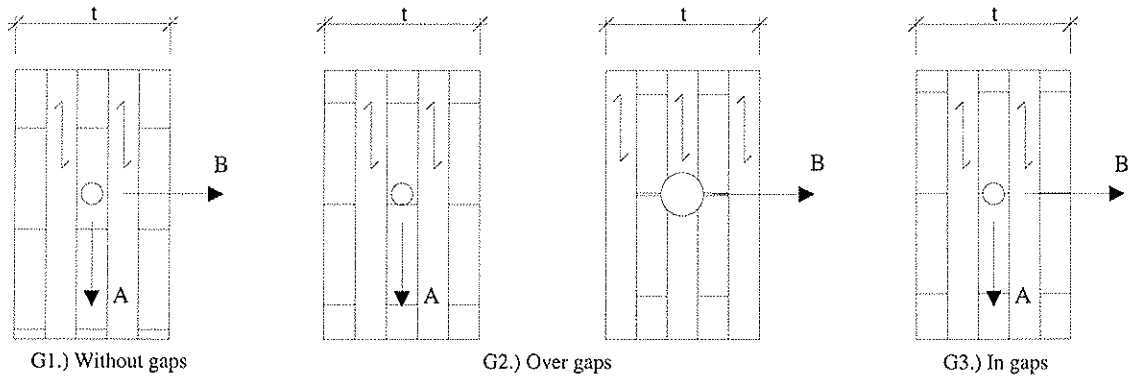

Fig. 5: Possible positions of the fasteners in relation to gaps, schematic sketch

Table 1: Density of the specimens at normal climate, 20°C/65% RH

Manufacturer/ product	n	Density of the whole cross section			Density of the relevant layers		
		ρ_{mean} kg/m³	Coefficient of variation	$\rho_{0,05}$ kg/m³	ρ_{mean} kg/m³	Coefficient of variation	$\rho_{0,05}$ kg/m³
1	184	474	5,76 %	434	481	9,54 %	412
2	292	439	7,65 %	391	417	12,2 %	345
3, 4	233	452	5,55 %	413	461	9,89 %	401

2.2 Results for dowels

To determine the embedding strength of cross laminated timber 390 tests with dowels were evaluated. For the tests dowels with 24, 16, 12, 8 and 6 mm in diameter were used. The test results in the different test configurations were analysed to reveal the relevant position.
Fig. 6 shows the ratio $f_{h,test}/\rho$ over the diameter for the tested dowel positions. The test configurations are named after the combination of load direction (A, B as shown in Fig. 3) and the position of the fasteners (1 to 5 as shown in Fig. 4). The tests carried out in position A1 result in the lowest values for the embedment strength.

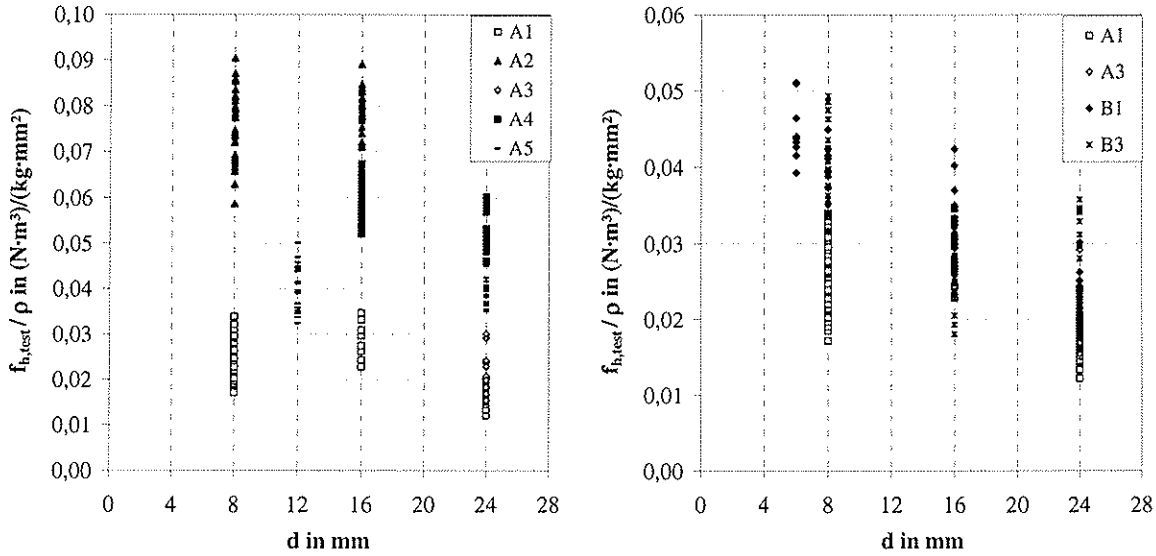

Fig. 6: Ratio $f_{h,test}/\rho$ over diameter d for the different tested positions of dowels

For dowels it was possible to develop the model for the embedment strength given in equation (1). It is based on a multiple regression analysis of 100 embedment tests carried out in the relevant test position A1. The embedment strength depends on the diameter d of the dowel and the density ρ_{layer} of the layer or the layers in which the dowel is placed.

$$f_{h,pred} = 0,049 \cdot (1 - 0,017 \cdot d) \cdot \rho_{layer}^{0,91} \quad \text{in N/mm}^2 \qquad (1)$$

$$r = 0,63$$

with

d diameter of the fastener

ρ_{layer} density of the relevant layer(s)

A comparison of predicted values and test results is shown in Fig. 7. The correlation coefficient r is equal to 0,63. The diagram shows also the results for the non-relevant positions. By inserting the characteristic density of the relevant layer which complies with the density of the raw material (350 kg/m³ for C24) in equation (1) the characteristic embedment strength can be proposed as:

$$f_{h,k} = 0,0435 \cdot (1 - 0,017 \cdot d) \cdot \rho_{layer,k}^{0,91} = 9 \cdot (1 - 0,017 \cdot d) \quad \text{in N/mm}^2 \qquad (2)$$

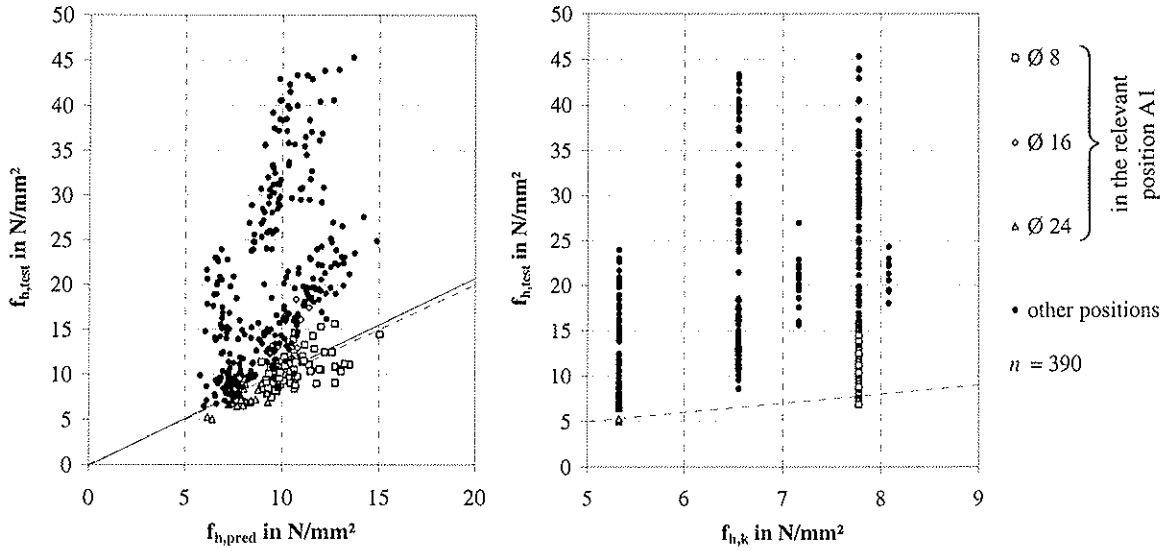

Fig. 7: Comparison of test results and predicted values resp. characteristic values of the embedment strength, influence of the dowel position

2.3 Results for screws and nails

Altogether 319 embedment tests with nails (d = 4,2 mm) and screws (d = 6, 8, 12 mm) in seven different combinations of load direction and fastener positions were carried out. On the basis of a regression analysis of 117 tests with screws and nails in the relevant test configuration A1 the embedment strength can be derived as:

$$f_{h,pred} = 0,8622 \cdot d^{-0,46} \cdot \rho_{layer}^{0,56} \quad \text{in N/mm}^2 \qquad (3)$$

$$r = 0,68$$

A comparison of predicted values and test results is shown in Fig. 8. The correlation coefficient was determined as r = 0,68. Having inserted the characteristic density of the layers ($\rho_{layer,k}$ = 350 kg/m³) in (3), simplified and adapted the equation the characteristic embedment strength can be proposed as:

$$f_{h,k} = 0,862 \cdot d^{-0,5} \cdot \rho_{layer,k}^{0,56} = 20 \cdot d^{-0,5} \quad \text{in N/mm}^2 \qquad (4)$$

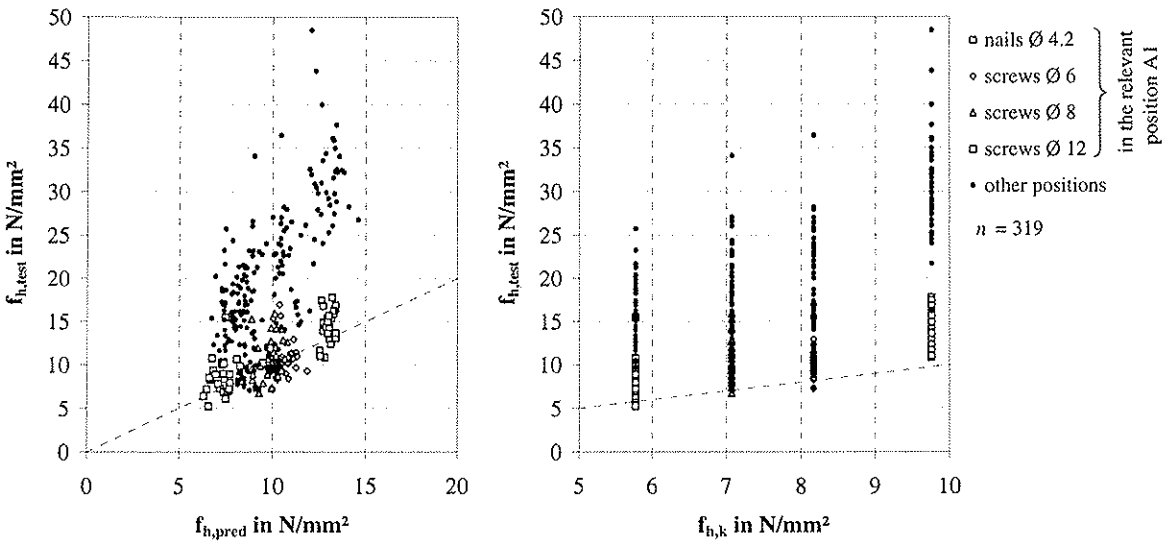

Fig. 8: Comparison of test results and predicted or characteristic values (screws/nails) resp.

3 Withdrawal strength of self-tapping screws in CLT

3.1 Test set-up and test material

To determine the withdrawal strength of self-tapping screws in CLT 119 tests with screws placed perpendicular to the plane of CLT and 268 tests with screws in the edges of CLT were carried out according to EN 1382 [6]. In the tests the positions of screws were varied, as shown in Fig. 9 and 10. In the plane side they were positioned in areas without gaps (position 1.1) and placed in gaps (position 1.2 to 1.4). Screws driven perpendicular (position C) and parallel (positions A, B) to the grain were considered in the edge withdrawal tests. Furthermore, tests with screws placed in gaps (positions B.1, B.2) were taken into consideration to derive the withdrawal capacity. Table 3 shows the statistical summary of the specimen density.

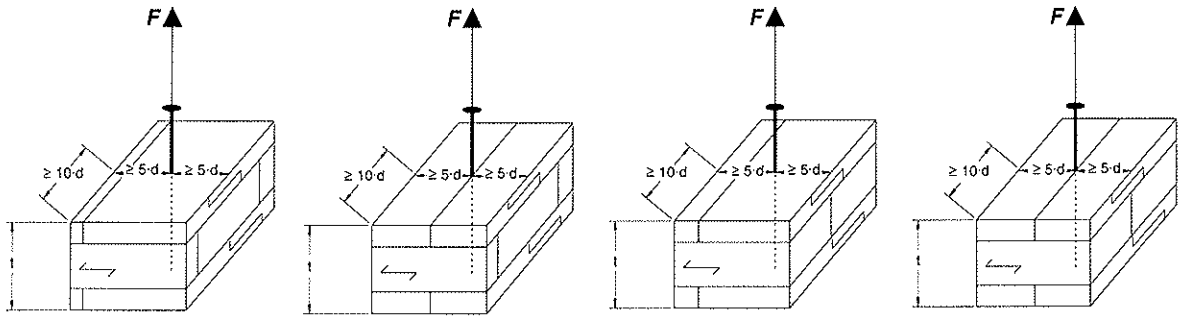

Position 1.1 1.2 1.3 1.4

Fig. 9: Set-up for withdrawal tests with screws positioned perp. to the plane of CLT

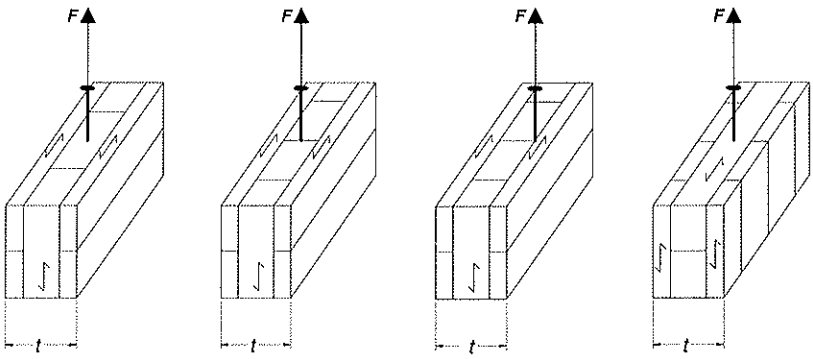

Position A B.1 B.2 C

Fig. 10: Set-up for edge withdrawal tests with screws in CLT

Table 2: Density of the specimens at normal climate, 20°C/65% RH

Manufacturer/ product	Density of the specimen for withdrawal tests							
	Plane side (hole cross section)				Narrow side (relevant layers)			
	n	ρ_{mean} kg/m³	Coefficient of variation	$\rho_{0,05}$ kg/m³	n	ρ_{mean} kg/m³	Coefficient of variation	$\rho_{0,05}$ kg/m³
1	24	454	4,48 %	423	57	448	8,21 %	374
2	73	426	5,44 %	384	159	404	11,9 %	335
3, 4	22	445	3,34 %	420	52	435	8,29 %	382

3.2 Test results

The best correlation between test results and predicted values can be achieved if the withdrawal capacity of self-tapping screws in CLT is calculated according to the following expression:

$$R_{ax,s,pred} = \frac{0,44 \cdot d^{0,8} \cdot \ell_{ef}^{0,9} \cdot \rho^{0,75}}{1,25 \cdot \cos^2\varepsilon + \sin^2\varepsilon} \quad \text{in N} \qquad (5)$$

$r = 0,91$

with

d nominal or outer diameter of the screw in mm

ℓ_{ef} effective pointside penetration length in mm

ε angle between screw axis and grain direction

ρ for joints in the plane side of CLT: density of CLT (whole cross section) in kg/m³

for edge joints in CLT: density of the relevant layer(s) in kg/m³

Fig. 11 (left) shows the test results vs. the predicted values. The correlation coefficient r is equal to 0,91. To simplify equation (5) the characteristic density of CLT is inserted and the denominator is increased up to 1,5. A further adaptation results in equation (6) for the characteristic withdrawal capacity. The right diagram in Fig. 11 shows the verification of the characteristic values.

$$R_{ax,s,k} = \frac{0,35 \cdot d^{0,8} \cdot \ell_{ef}^{0,9} \cdot \rho^{0,75}}{1,5 \cdot \cos^2\varepsilon + \sin^2\varepsilon} = \frac{31 \cdot d^{0,8} \cdot \ell_{ef}^{0,9}}{1,5 \cdot \cos^2\varepsilon + \sin^2\varepsilon} \quad \text{in N} \qquad (6)$$

with

ε joints in the plane side of CLT: $\varepsilon = 90°$, edge joints: $\varepsilon = 0°$

ρ characteristic density of CLT (400 kg/m³)

The given equations are only valid for self-tapping screws, for which the characteristic withdrawal strength in solid wood (C24) exceeds $f_{ax,k} = 80 \cdot \rho_k^2 \cdot 10^{-6} = 9,8$ N/mm².

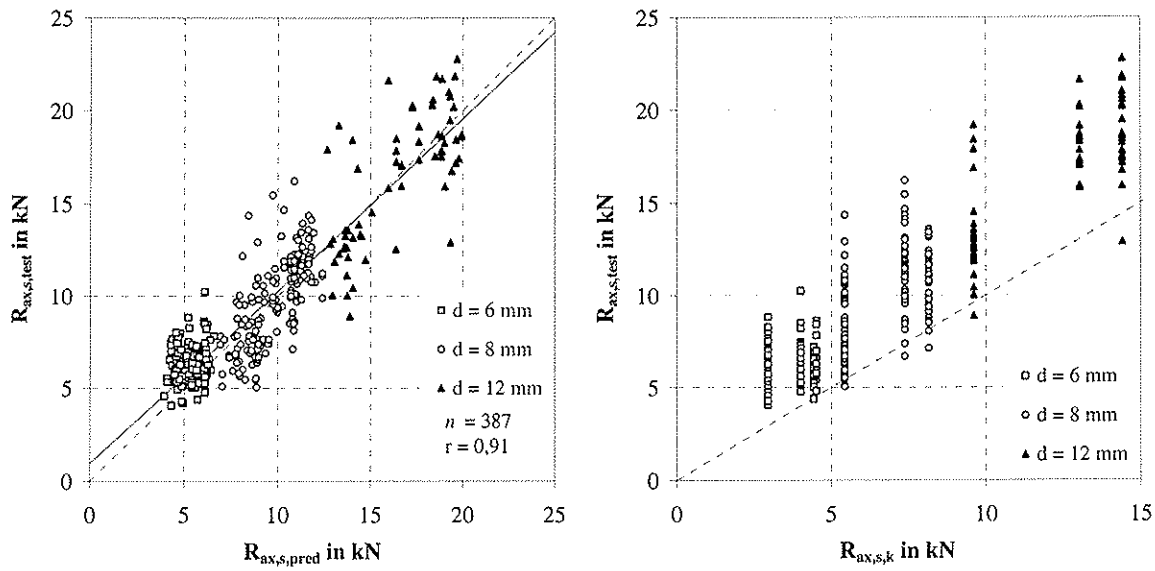

Fig. 11: Withdrawal strength - test results over predicted or characteristic values resp.

4 Load carrying capacity of edge joints

4.1 Short-term tests

In order to confirm the calculation of the load carrying capacities of edge joints in CLT 49 tests with dowels and screws were carried out. The tests also provide a basis for determining the required spacing, edge and end distances for the fasteners, which are defined in Fig. 14. Table 3 shows the specimen parameters while table 4 shows the results of the tests. Connections with fasteners placed parallel to the grain (configuration B) and perpendicular to the grain (configuration A) were considered in the tests. Furthermore, joints with fasteners placed between two layers of different grain direction were tested in configuration C. Comparisons between test results and calculated load carrying capacities are given in Fig. 12 and Fig. 13.

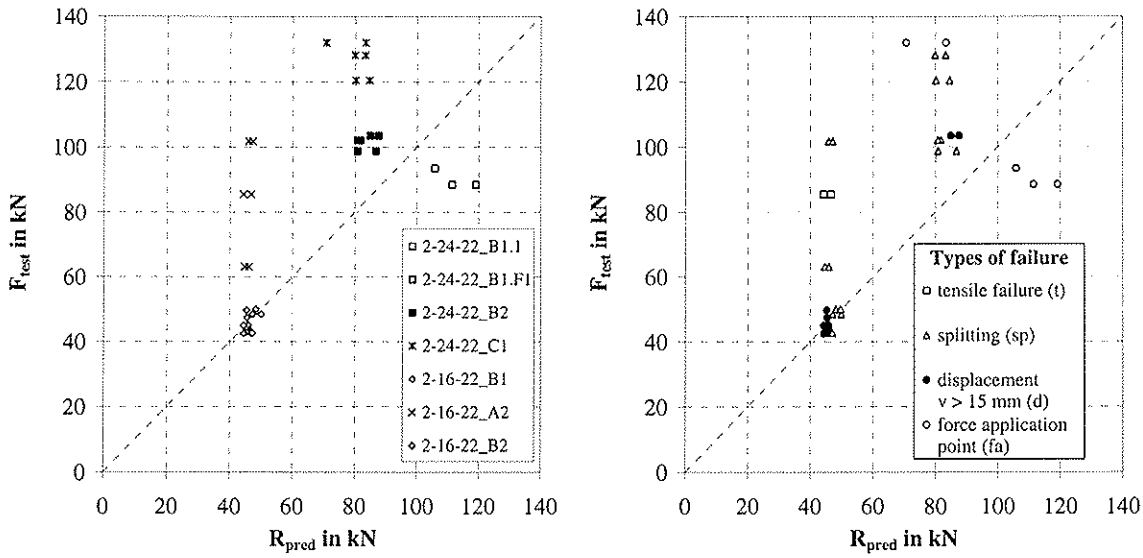

Fig. 12: Test results for edge joints with dowels vs. predicted load carrying capacities

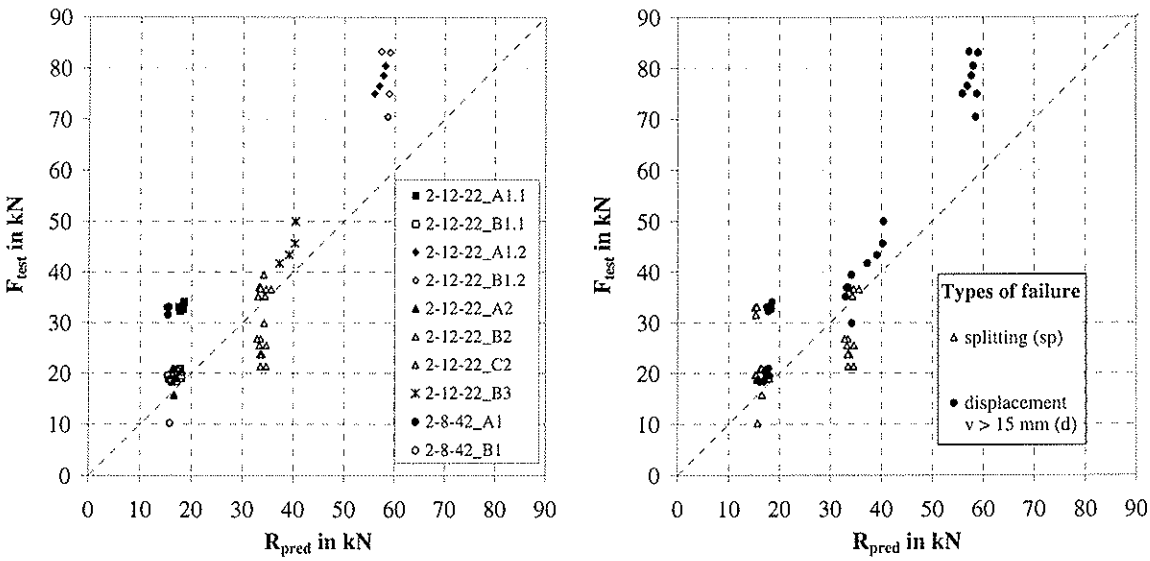

Fig. 13: Test results for edge joints with screws vs. predicted load carrying capacities

Table 3: Specimen parameters

Specimen	n_{test}	Conf.	Fasteners											Build-up of CLT
			Type	d mm	M_y Nm	t_1 mm	t_2 mm	$a_{3,t}$ mm	a_1 mm	$a_{4,c}$ mm	s	m	n	Side and middle members
2-24-22_B1	1	B	dowels	24	1224	96	160	5·d	4·d	64	2	1	5	34-13-34-13-34
2-24-22_B1.F1	1	B	dowels	24	1224	96	160	5·d	4·d	64	2	1	4	34-13-34-13-34
2-24-22_C1	3	C	dowels	24	1224	96	160	5·d	4·d	89	2	1	3	34-22-34-22-34-22-34 (reduced to 178 mm)
2-24-22_B2	3	B	dowels	24	1224	96	160	5·d	4·d	101	2	1	3	34-22-34-22-34-22-34
2-16-22_B1	3	B	dowels	16	400	80	160	5·d	4·d	30	2	1	3	19-22-19
2-16-22_A2	3	A	dowels	16	400	80	160	5·d	5·d	64	2	1	3	34-13-34-13-34
2-16-22_B2	4	B	dowels	16	400	80	160	5·d	5·d	64	2	1	3	34-13-34-13-34
2-12-22_A1.1	3	A	screws	12	63,7[1)]/100,8[2)]	120	120	12·d	10·d	64	1	1	2	34-13-34-13-34
2-12-22_B1.1	4	B	screws	12	63,7[1)]/100,8[2)]	60	120	12·d	4·d	30	2	1	2	19-22-19
2-12-22_A1.2	2	A/B	screws	12	63,7[1)]/100,8[2)]	120	120	12·d	10·d	36,5	1	3	2	34-22-34-22-34
2-12-22_B1.2	2	B/A	screws	12	63,7[1)]/100,8[2)]	120	120	12·d	10·d	36,5	1	3	2	34-22-34-22-34
2-12-22_A2	3	A	screws	12	63,7[1)]/100,8[2)]	60	120	7·d	4·d	64	2	1	2	34-13-34-13-34
2-12-22_B2	6	B	screws	12	63,7[1)]/100,8[2)]	60	120	7·d	4·d	30	2	1	4	19-22-19
2-12-22_C2	3	C	screws	12	63,7[1)]/100,8[2)]	60	120	7·d	4·d	48	2	1	4	34-13-34-13-34 (reduced to 96 mm)
2-12-22_B3	2	B	screws	12	63,7[1)]/100,8[2)]	120	120	10·d	5·d	30	1	1	4	19-22-19
2-8-42_A1	3	A	screws	8	24,1	120	80	10·d	7·d	21	1	1	2	8,5-7,5-10-7,5-8,5
2-8-42_B1	3	B	screws	8	24,1	80	120	7·d	5·d	21	1	1	2	8,5-7,5-10-7,5-8,5

s: Number of shear planes per fastener m: Number of fastener rows n: Number of fasteners per row
1) Yield moment of the thread of the screw 2) Yield moment of the shank of the screw

Table 4: Results of the tests

Specimen	Number of specimens n	Mean density $\rho_{layer,m}$ in kg/m³		Load carrying capacity per fastener and shear plane $F_{u,mean}$ in kN	Type of failure
		Side members	Middle members		
2-24-22_B1	1	408	410	9,35	1 x fa
2-24-22_B1.F1	1	405	355	11,1	1 x fa
2-24-22_C1	3	441	416	21,2	1 x fa, 2 x sp
2-24-22_B2	3	456	449	16,9	2 x d, 1 x sp+d
2-16-22_B1	3	451	482	7,85	3 x sp
2-16-22_A2	3	438	391	13,9	2 x sp, 1 x t
2-16-22_B2	4	397	433	7,52	4 x d
2-12-22_A1.1	3	400	399	8,28	3 x d
2-12-22_B1.1	4	464	442	4,88	4 x d
2-12-22_A1.2	2	431	392	6,47	2 x d
2-12-22_B1.2	2	436	446	6,50	2 x d
2-12-22_A2	3	430	388	4,64	3 x sp
2-12-22_B2	6	449	428	3,93	2 x sp, 2 x d 2 x sp+d
2-12-22_C2	3	428	428	3,68	2 x sp, 1 x d
2-12-22_B3	2	439	439	5,65	2 x d
2-8-42_A1	3	474	492	8,15	3 x sp
2-8-42_B1	3	477	518	4,06	3 x sp

fa: failure at the force application point sp: splitting of the layers d: displacement v >15 mm t: tensile failure

For most of the test series with fasteners placed parallel to the grain (configuration B) the calculated loads and the test results correspond. In the other configurations the load carrying capacity is underestimated. The reason for this discrepancy is the conservatively assumed embedment strength, which also has to cover fasteners positioned parallel to the grain. Besides, differences between the calculated load carrying capacity and the test results are determined for connections with small spacings and end distances. In these tests splitting occurred. To avoid this failure the requirements given in Fig. 14 and Table 5 have to be fulfilled. For the design of multiple fastener joints it is suggested to consider the effective number of fasteners.

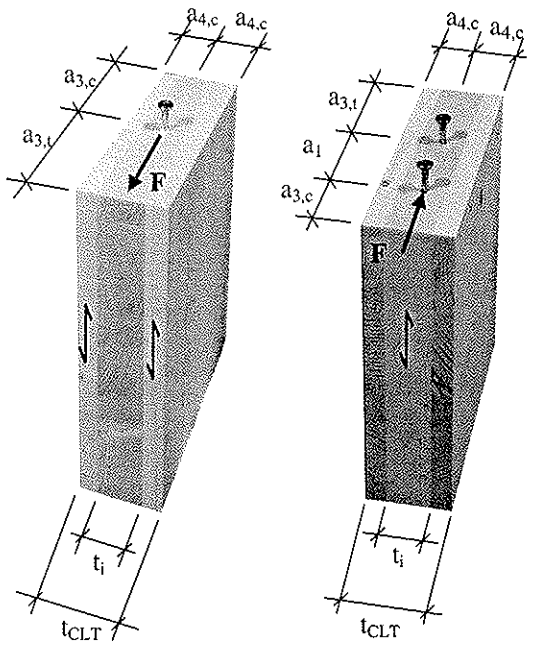

	Type of fastener	
	Self-tapping screws	Dowels
a_1	10 · d	4 · d
a_2	3 · d	4 · d
$a_{3,t}$	12 · d	5 · d
$a_{3,c}$	7 · d	3 · d
$a_{4,c}$	5 · d	3 · d

Fig. 14: Spacings, end distances and edge distances of fasteners in CLT

Table 5: Requirements for the geometry of edge joints in CLT with dowel type fasteners

Type of fastener	Minimum thickness of the relevant layer t_i in mm	Minimum thickness of CLT t_{CLT} in mm	Minimum thickness/ minimum embedded length $t_{1,req}$, $t_{2,req}$ in mm
Self-tapping screws	d > 8 mm: 3 · d d ≤ 8 mm: 2 · d	10 · d	10 · d
Dowels	d	6 · d	5 · d

4.2 Long-term tests

To examine the influence of load duration and climate variation on the load carrying capacity of edge joints with screws in CLT long-term tests were set up. The test programme contains 48 tests with axially loaded self-tapping screws driven into the middle layer of the test specimens parallel to the grain. The long-term behaviour of laterally loaded edge joints with self-tapping screws is also examined. To this purpose, tests with single and double shear CLT-to-CLT-connections are included in the test programme. The test set-up is documented in Fig. 15. The environmental conditions comply with Service Class 2. The design resistance of the test specimens was determined from the characteristic values with the modification factor k_{mod} = 0,8 and the partial factor γ_M = 1,3. The laterally loaded screws were loaded with the full design resistance while the axially loaded screws were loaded with 70 % of the design resistance. During the test duration the displacements

are measured periodically and the climate is recorded. After three years the specimens will be unloaded and the remaining load carrying capacity will be determined in short-term tests.

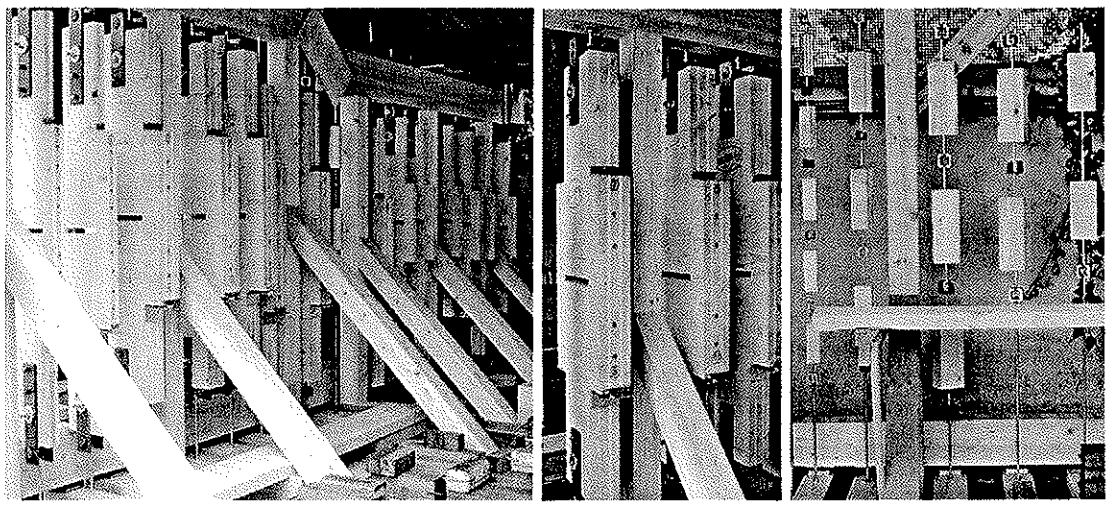

Fig. 15: Long term tests with screwed edge joints in CLT under lateral load and axial load

5 Conclusions

For calculating the load carrying capacity of edge joints in CLT the parameters embedment strength and withdrawal capacity were examined. On the basis of statistical analysis of a multitude of test results it was possible to develop functions for predicted values of these parameters. Proposals for characteristic values are also given. The validity of the presented equations is limited to CLT with a characteristic density of 400 kg/m³ made of spruce. In tests with connections the required minimum edge and end distances and spacings of fasteners were determined. In addition the tests verify the calculation of the load carrying capacities. To determine the long-term behaviour of edge joints with self-tapping screws in CLT tests are performed.

6 References

[1] Blaß, H. J.; Uibel, T.: Tragfähigkeit von stiftförmigen Verbindungsmitteln in Brettsperrholz, *Karlsruher Berichte zum Ingenieurholzbau*, Band 8, Lehrstuhl für Ingenieurholzbau und Baukonstruktionen (Ed.), Universität Karlsruhe (TH), 2007

[2] Hilson, B. O. : Verbindungen mit stiftförmigen Verbindungsmitteln – Theorie. In: Blaß, H. J.; Görlacher, R.; Steck, G. (Ed.): *Holzbauwerke STEP1 – Bemessung und Baustoffe*, Fachverlag Holz, Düsseldorf, 1995

[3] Johansen, K. W.: Theory of timber connections. International Association of bridge and structural Engineering, Bern, 1949, p. 249-262

[4] Uibel, T.; Blaß, H. J.: Load carrying capacity of joints with dowel type fasteners in solid wood panels. In: Proceedings. CIB-W18 Meeting, Florence, Italy 2006, Paper 39-7-5

[5] EN 383: 1993 - Timber structures; Test methods; Determination of embedding strength and foundation values for dowel type fasteners

[6] EN 1382: 1999 - Timber structures - Test methods - Withdrawal capacity of timber fasteners

INTERNATIONAL COUNCIL FOR RESEARCH AND INNOVATION
IN BUILDING AND CONSTRUCTION

WORKING COMMISSION W18 - TIMBER STRUCTURES

DESIGN METHOD AGAINST TIMBER FAILURE MECHANISMS OF DOWELLED STEEL-TO-TIMBER CONNECTIONS

A Hanhijärvi
A Kevarinmäki

VTT

FINLAND

MEETING FORTY
BLED
SLOVENIA
AUGUST 2007

Presented by A. Hanhijärvi
H. Blass asked in the new model which conditions would lead to the governing Johansen formula (embedment failure). A. Hanhijärvi said that it only add complication. Embedment failures could be included for the sake of completeness. He also stated that row shear failure was not considered in Annex A of Eurocode 5; therefore, this study is important. H. Blass questioned the factor of two associated with tensile strength and the splitting effects in other rows of dowel. A. Hanhijärvi suggested there is small volume in joint area; therefore, increased factor for tension strength also failure would occur at centre line. P. Quenneville commented that the glulam specimens are all brittle failures. A. Hanhijärvi said that there are no embedment failures even though experiment had different end distances and spacing.
A. Jorissen received confirmation about spacing and end distances per explained in paper. A. Jorissen also commented that the work by H. Johnsson on block shear should have been considered. A. Jorissen and A. Hanhijärvi discussed the differences between this approach and the current Eurocode 5 Annex A approach. A. Hanhijärvi further clarified that the interaction between shear and tension comes from A. Ranta-Maunus presented work of tension and tension failure length,
I. Smith mentioned that UNB students did work with lower quality wood and engineered wood products. He commented this work is good but may not be universal. He wondered how much better the proposed procedure is in terms of a regression relationship. A. Hanhijärvi commented that row shear is considered beyond the current Eurocode.

Design method against timber failure mechanisms of dowelled steel-to-timber connections

Antti Hanhijärvi, Ari Kevarinmäki
VTT, Finland

1 Introduction

The design of dowel type joints of timber is well established in the Eurocode 5 by the use of the Johansen (1949) theory. It has shown to perform well with small diameter slender fasteners (e.g. Hilson 1995). In large structures, with the increase of span length, the use of high capacity connections is necessary. High capacity dowelled connections are often implemented by slotted–in steel plates and large diameter dowels or bolts. With increasing diameter, the rigidity of the dowel increases more than the embedment capacity. Thus, the failure of timber at the connection area becomes more easily critical for the capacity of the connection – not only as embedment failure but through failure of the whole joint area by tension or shear. These shear failure mechanisms are known as block shear, plug shear or row shear. The design for these failure mechanisms is not yet sufficiently well established as reported by Ranta-Maunus and Kevarinmäki (2003).

The aim of the present work was to improve the grounds for design of heavy-duty dowelled connections by a large experimental program and consequent development of design model against the timber failure mechanisms in connections implemented by steel plates and loaded in tension. The experimental program which consisted of more than 150 tension tests on glulam and LVL-specimens was reported in Hanhijärvi et al. (2006). This paper deals with the design method that was developed based on the experimental results.

2 Symbols

a_1, a_2, a_3, a_4, dowel spacing parallel and perpend. to grain, end and edge distance, resp.
$A_{h,j}$, $A_{v,j}$, $A_{t,j}$ area of possible embedment, shear, tension failure surface of part j, resp.
B specimen height
b block shear failure mechanism
b-r, b-t block shear failure mechanism with calculational shear failure capacity > tension failure capacity, tension failure capacity > shear failure capacity, resp.
cnctr as subscript means coefficient due to stress concentration effect
CoV coefficient of variation
d dowel diameter
DF design failure mode (critical failure mechanism according to design)

f_t tension strength of timber (parallel-to-grain)
f_{t90} tension strength of timber (perpendicular-to-grain)
f_h embedment strength of timber
f_y yield strength of dowels
F_{max} failure load in tests
F_{Bk}, F_{Bm} calculated characteristic load-carrying capacity of connection according to EC5 Annex A (block/plug shear), same using mean material properties, resp.
$F_{j,k}$ calculated capacity of j'th part according to the proposed method
F_{Rk}, F_{Rm} calculated characteristic load-carrying capacity of connection according to EC5 assuming $n_{ef} = n$, same using mean properties of the test material, resp.
F_{Sk}, F_{Sm} calculated characteristic load-carrying capacity according to EC5 assuming splitting etc. ($n_{ef} \neq n$) but not block/plug shear, same using mean properties, resp.
F_{Tm} calculated capacity according to the EC5 assuming only tension failure and using mean properties of the test material and cross-section reduction due to dowel holes
$F_{TFM,k}$ calculated characteristic capacity against timber failure mechanisms according to the proposed method
j index number of part j according to possible failure surfaces in connection
k coefficient
k as subscript: characteristic value
n number of dowels in a row
n_{ef} effective number of dowels in a row
m number of dowel rows
m as subscript: average value
p plug shear failure
row row shear failure
s/r splitting or row shear failure
T tension failure mechanism (of cross-section)
TF test failure mode (prevailing failure mechanism in test)
TFM timber failure mechanisms
t_1, t_2 thickness of side and middle timber member, resp.
$t_{1,red}$, $t_{2,red}$ reduced thickness of side, middle timber member due to dowel slenderness, resp.
t_S thickness of steel plate
ρ_m mean density of the test material

3 Background

3.1 Conclusions from the test program

The experimental test program (Hanhijärvi et al. 2006) gave reason for the following conclusions in regard to the improvement of the design against timber failure mechanisms:

- The plug shear failure mechanism does not occur in the connection area contrarily to what the design equations in EC5 (EN 1995-1-1:2004; Annex A) suggest. This is due to the fact that the rigid dowels remain straight or bend very little before failure, which is then mostly due to the block shear mechanism. Failure by plug shear seems to require the development of fully developed plastic hinges.
- Connections with cross-veneered Kerto-Q-LVL showed much higher experimental capacities than could be anticipated from the design calculations of EC5. This is due to the fact that the plug shear failure does not occur because of rigid dowels even if the

lower flatwise shear strength reduces the calculational capacity for plug shear. This further affirms the conclusion that plug-shear failure requires that the plastic hinges must develop to high degree before plug shear is possible.

- When the calculational failure mode of EC5 is block shear, it could be concluded that the formulas result usually in clearly conservative design for glulam, but they are approximately on the right level for Kerto-S-LVL.

3.2 Present design method in EC 5

The basis for the design of dowelled steel-to-timber connections with slotted in steel plates against timber failure mechanisms as instructed by the formulas of Eurocode 5 and its Annex A (EC5, EN 1995-1-1:2004) are presented briefly in the following.

The load-carrying capacity in case of splitting or rowshear is calculated by a reduction of the number of dowels n and capacity given by Johansen theory (EC5, Eqs. 8.1, 8.34):

$$F_{Sk} = \frac{n_{ef}}{n} F_{Rk}, \quad where \quad n_{ef} = \min\left(n, n^{0.9} \left(\frac{a_1}{13d} \right)^{0.25} \right) \tag{1}$$

where F_{Rk} is the capacity by the Johansen theory.

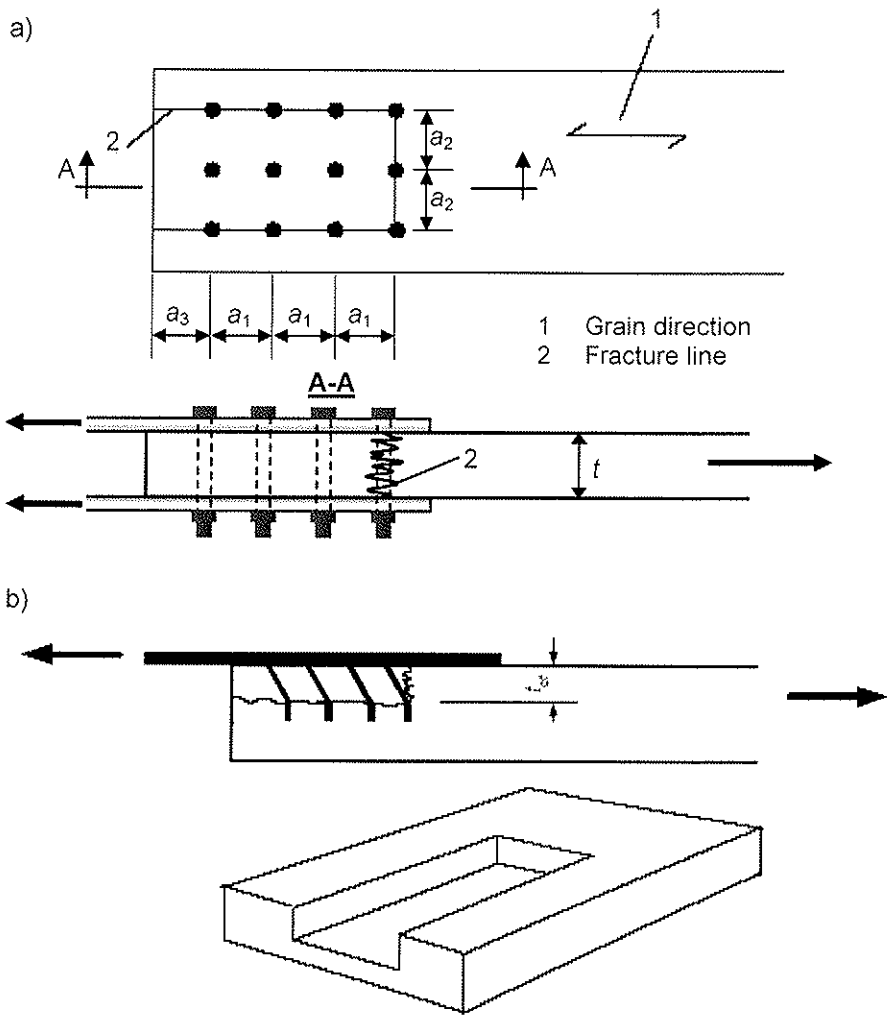

Figure 1. a) Block shear failure and b) plug shear failure of a dowelled connection.

The load-carrying capacity in case of block or plug shear failure is calculated by the formula (A.1) in the Annex A of EC5:

$$F_{bs,Rk} = F_{Bk} = \max\begin{cases} 1.5A_{net,t} f_{t,0,k} \\ 0.7A_{net,v} f_{v,k} \end{cases} \quad (2)$$

where $f_{t,0,k}$ and $f_{v,k}$ are the tensile and shear strengths of the material, respectively, and $A_{net,t}$ and $A_{net,v}$ are the areas along the assumed failure surface that are under tension and shear stress, respectively. The areas are calculated as (Annex A Eq. A.2, A.3):

$$A_{net,t} = L_{net,t} t_1 \quad (3)$$

$$A_{net,v} = \begin{cases} L_{net,v} t_1 & \text{embedment fail. or steel - timber - steel connection} \\ \frac{L_{net,v}}{2}\left(L_{net,t} + 2t_{ef}\right) & \text{other cases} \end{cases} \quad (4)$$

where t_{ef} is the calculational distance from the surface to the dowel plastic hinge according to the Johansen theory. The magnitudes of $L_{net,t} = (m\text{-}1)*(a_2\text{-}d)$ and $L_{net,v} = (n\text{-}1)*(a_1\text{-}d)+(a3\text{–}d)$ (see Fig. 1).

4 Proposal for improvement of design

4.1 Principles of the method

The proposed design method is based on the following principles:

- The method concerns only the timber failure mechanisms, the dowel yielding is assumed to be taken care by the Johansen theory as instructed in EC5. The timber failure mechanisms contain: (1) embedment failure, (2) tension failure at the connection area, (3) block shear and (4) row shear. (Note: embedment failure is also covered by the Johansen theory.)
- Plug shear failure mechanism is assumed not to be relevant, if the dowels extend through the whole thickness of all timber members. However, effect of dowel deformation (elastic or plastic bending) on timber failure mechanisms is considered through a slenderness ratio based reduction of timber thickness, when shear and splitting failure modes are considered.
- The different failure modes are considered separately, i.e. the method pursues to make the design against the different stress components (tension, shear, splitting, embedment) transparent, and so that no parameter is assigned to cover more than one failure type. However, the interaction between the stress components is considered.

The design calculation procedure goes as follows:

1) The connection area is divided into parts according to the possible failure surfaces. (In the end, the capacity of the connection is assumed to be calculable as sum)
2) The effect of load distribution between dowels is calculated in terms of effective number of dowels, which is applied when calculating the capacities of individual parts.
3) The effect of dowel slenderness on capacity is calculated in terms of reduced thickness which is applied when calculating the capacities of individual parts.
4) Each part is assigned with possible failure modes and the capacity against all modes is calculated (effect of load distribution and dowel slenderness are taken into account).

5) Interaction effects between different failure modes (stress components) are considered.
6) The smallest obtained capacity (strength) determines the capacity of each part.
7) The total capacity of the connection against tension is obtained as the sum of the capacities of the parts.

The capacities against different failure modes at the part level are derived below by combination of theoretical and empirical reasoning.

4.2 Division of connection area to parts

As a first step, the connection area is divided into parts according to the possible failure surfaces. The failure surfaces pass along the dowel rows on both sides of the dowels (shear an splitting failure) and along the line that passes through the dowel column that is farthest from the end of timber (tension failure), an example is shown in Fig. 2. (Besides these surfaces, the compressed areas of the dowel holes must be understood as the failure surface for the embedment failure capacity.) The parts are indexes as j = 0...m, so that parts 0 and m are located by the edge and are named as *outer parts*, where as the parts from 1 to m-1 are called the *inner parts*.

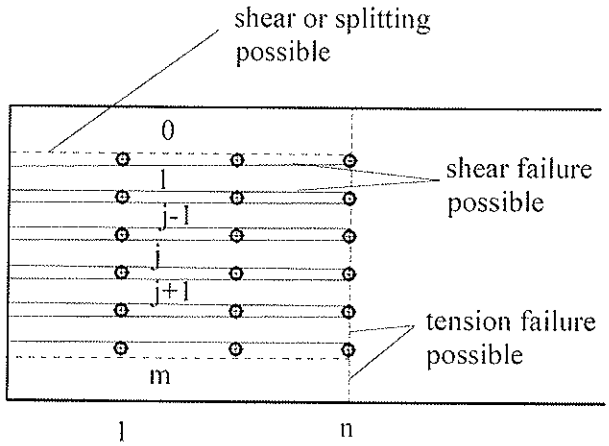

Figure 2. Division of connection area to parts by determining the possible failure surfaces.

4.3 Effect of load distribution between dowels

When there are several dowels in a row, the load per fastener cannot exceed the strength of a single fastener connection, and can reach it only, if plasticity type ductile phenomena with large deformations occur. The large deformations are possible when embedment failure occurs with strong crushing of timber under the compression of the dowels. However, the other timber failure mechanisms show brittle failure and do not permit large deformations. In the case of brittle failure modes, the need for reduction of capacity due to several dowels in a row is quite obvious even as consequence of the different stress level and thus different deformation of the areas between the dowels. (Jorissen 1998)

In EC 5 this kind of reduction is applied by the definition of effective number of fasteners in a row n_{ef}, which is dependent on the number of dowels, spacing and dowel diameter. Here a similar approach is adopted, but dependent on only the number of dowels in a row:

$$n_{ef} = n^{0.9} \tag{5}$$

The reduction is applied to all brittle failure modes: tension, shear and splitting, but *not* to embedment failure.

4.4 Effect of dowel deformations (slenderness)

As stated above, the plug shear failure was not observed in the experimental test program. The conclusion was made that it is not relevant, if the dowels extend through the whole thickness of all timber members, because the plug shear failure would require the plastic hinges to develop to high degree. However, some dowels were observed to be bent slightly and all dowels do bend a least a little due to elastic deformation. It was found that if the slenderness of the dowels is taken into account, the model fit is improved. It was therefore concluded that even the slight bending of the dowels has an effect on the load carrying capacity. The slenderness of the dowels is taken into account by reducing the timber thickness, but only when considering shear and splitting, not parallel-to-grain tension:

$$\begin{aligned} t_{1,\mathrm{red}} &= \min\left(1, \frac{d}{0.6 d_{\mathrm{gr},1}}\right) \cdot t_1 \text{, where } d_{\mathrm{gr},1} = 2.45 \sqrt{\frac{f_{\mathrm{h,m}}}{f_{\mathrm{y,m}}}}\, t_1 \text{ (side members)} \\ t_{2,\mathrm{red}} &= \min\left(1, \frac{d}{0.5 d_{\mathrm{gr},2}}\right) \cdot t_2 \text{, where } d_{\mathrm{gr},2} = 1.23 \sqrt{\frac{f_{\mathrm{h,m}}}{f_{\mathrm{y,m}}}}\, t_2 \text{ (middle members)} \end{aligned} \qquad (6,7)$$

d_{gr} is the limit above which the dowel is rigid according to the Johansen theory.

4.5 Principle of interaction effect between stress components

The stress state in the connection area is complex and all directions and components of stresses are present. Above all, the timber failure mechanisms are dependent on the parallel-to-grain tension, parallel-to-grain shear and perpendicular-to-grain tension stress components. Sjödin and Serrano (2006) and Sjödin et al. (2006) have studied the distributions of these stresses both computationally and by contact free measurements. The calculations and measurements both show that highly stressed areas of the different stress components overlap. It can be assumed that in such a complex stress state the different stresses affect the strength in a combined way, which was also indirectly concluded based on the experimental results. It is reasonable to assume an interaction effect for the stress components in the design.

In many design applications, interaction of stress components is modelled by assuming that the sum of the utilisation rates of the different components must not exceed 1 = 100%. Here, a slightly different parameterized approach is taken. It is assumed that, because the maxima of the stress components do not act in exactly the same location, the above mentioned condition is relaxed and parameterized as follows:

$$F_{1+2} = \begin{cases} F_1\left(1 - k_{\mathrm{interaction}} \dfrac{F_1}{F_2}\right), \text{if } F_1 \le F_2 \\ F_2\left(1 - k_{\mathrm{interaction}} \dfrac{F_2}{F_1}\right), \text{if } F_2 < F_1 \end{cases} \text{, with } k_{\mathrm{interaction}} = 0.3 \qquad (8)$$

Eq. (8) essentially states that when two stress components affect the capacity of a part, the interaction is taken into account by reducing the lower capacity by subtracting an amount

which is proportional to the ratio of the lower capacity to the higher. $k_{\text{interaction}}$ is a parameter, which could be varied depending on interaction type, but is here given value 0.3 for all cases. Eq. (8) is illustrated graphically in Fig. 3a.

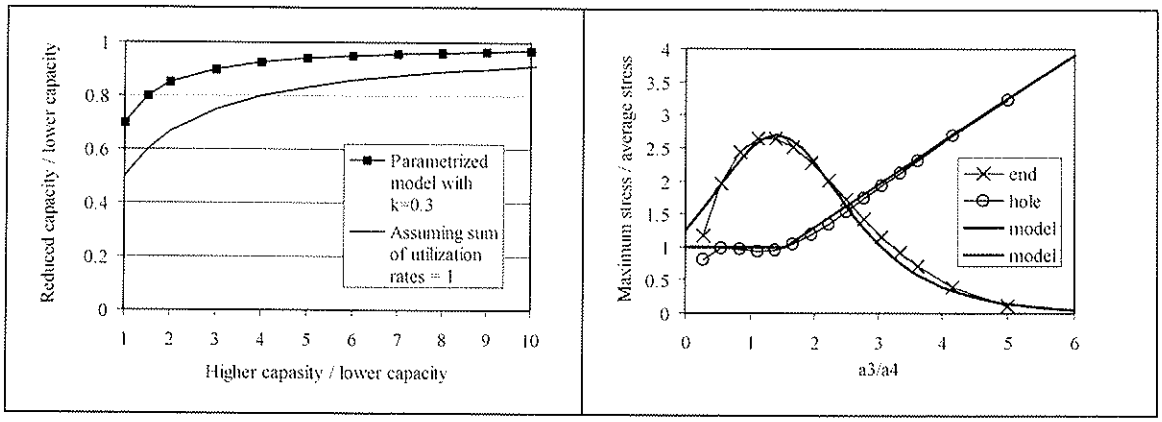

Figure 3. a) Left – Reduction of capacity due to the interaction of two stress components. Comparison of the effect of a classical model which assumes the sum of utilization rates to be 100% and relaxed parameterized model Eq. (8), which does not cause so strong reduction (interaction parameter = 0.3). b) Right– The ratio between maximum and average splitting stress (perpendicular to grain) vs. geometry parameter a_3/a_4.

4.6 Calculation of capacity of inner parts

When calculating the capacity of the inner parts ($j = 1 \ldots m\text{-}1$), the failure phenomena to be considered include:

- embedment strength at the area $A_{\text{h,j}} = n\, d\, t$
- tension failure at the area $A_{\text{t,j}} = (a_2 - d)\, t$
- shear failure at the area $A_{\text{v,j}} = 2\,[(n-1)a_1 + a_3]\, t$
- interaction effect of tension and shear

4.6.1 Embedment failure

The embedment capacity is calculated in harmony with the rigid dowel case in the Johansen theory [EC 5 Equations (8.10e), (8.11f), (8.12j) and (8.13l), however, without effect of n_{ef}]:

$$F_{\text{h,j,k}} = A_{\text{h,j}} f_{\text{h,k}} = n\, d\, t\, f_{\text{h,k}} \tag{9}$$

4.6.2 Tension failure

The tension capacity is calculated simply as tension strength times tensioned area multiplied by a stress concentration factor $k_{\text{t,cnctr}}$. and the effect of load distribution taken into account (n_{ef}). $k_{\text{t,cnctr}}$ in fact becomes higher than 1, which can be justified by arguing that the tension stress acts on a small volume only and due to the high size effect of tension strength allows tension strength to have a higher value than in general (Note: a corresponding factor has the value of 1.5 in EC 5 Annex A).

$$F_{\text{t,j,k}} = k_{t,cnctr}\,(n_{\text{ef}}/n) A_{\text{t,j}} f_{t,0,k} = k_{t,cnctr}\,(n_{\text{ef}}/n)(a_2 - d)\, t\, f_{t,0,k} \tag{10}$$

4.6.3 Shear failure

The shear capacity is calculated also in a similar simple manner. Now, both load distribution effect (n_{ef}) and dowel deformation effect (t_{red}) are taken into account. The stress concentration factor $k_{v,cnctr}$ has a value lower than 1 in order take into account the unevenness of the shear stress distribution. (Note: a corresponding factor has a value of 0.7 in EC 5 Annex A):

$$F_{v,j,k} = k_{v,cnctr}(n_{ef}/n)A_{v,j}f_{v,k} = k_{v,cnctr}(n_{ef}/n)\cdot 2((n-1)a_1 + a_3)t_{red}f_{v,k} \qquad (11)$$

4.6.4 Interaction of tension and shear

The tension stresses and shear stresses are assumed to have an interaction effect on capacity, which is taken into account in the way described above [Eq. (8), subscripts 1 => t, 2 => v].

4.6.5 Capacity of the inner part

The capacity of the j'th inner part is obtained as the smaller of the embedment strength and the combined effect of tension and shear:

$$F_{j,k} = \min\left(F_{h,j,k}, F_{t+v,j,k}\right) \qquad (12)$$

4.7 Calculation of capacity of outer parts

When calculating the capacity of the outer parts ($j = 0$ or m), the failure phenomena to be considered include:

- embedment strength at the area $A_{h,j} = 0.5\, n\, d\, t$
- tension failure at the area $A_{t,j} = (a_4 - d/2)\, t$
- shear failure at the area $A_{v,j} = [(n-1)a_1 + a_3]\, t$
- interaction effect of tension and shear
- splitting failure originating either at the end of timber or at the hole nearest to the end
- interaction effect of shear and splitting originating at the hole nearest to the end

4.7.1 Embedment failure

The embedment capacity is again calculated in accordance with the case of rigid dowel of the Johansen theory (without effect of n_{ef}).

$$F_{h,j,k} = A_{h,j}f_{h,k} = 0.5\, n\, d\, t\, f_{h,k} \qquad (13)$$

4.7.2 Tension failure

The tension capacity is obtained in a similar manner as for the inner parts (Eq. 10 above), except that a reduction factor $k_{t,outer} = 1/(1+A_{t,j}/A_{v,j})$ is used to take into account the asymmetry of the tensile stress distribution:

$$F_{t,j,k} = k_{t,cnctr}(n_{ef}/n)A_{t,j}f_{t,0,k}k_{t,outer} = k_{t,cnctr}(n_{ef}/n)(a_2 - d)t\, f_{t,0,k}k_{t,outer} \qquad (14)$$

4.7.3 Shear failure

The shear capacity is also obtained in a similar manner as for the inner parts (Eq. 11 above, however, the area under shear is only half of that of the inner parts):

$$F_{v,j,k} = k_{v,cnctr}(n_{ef}/n)A_{v,j}f_{v,k} = k_{v,cnctr}(n_{ef}/n)\cdot((n-1)a_1 + a_3)t_{red}f_{v,k} \qquad (15)$$

4.7.4 Interaction of tension and shear

The interaction of tension and shear stresses are taken into account exactly as for the inner parts Eq. (8).

4.7.5 Splitting failure

For consideration of the splitting of the outer parts, two different ways of splitting are considered:

- splitting originating at the end of the timber
- splitting originating at the dowel hole nearest to the end of the timber

This idea is based on the work of Jorissen (1998) who derived a model for the perpendicular-to-grain stresses on a plane parallel to the dowel row. The model is based on the analytical solution of a beam on an elastic foundation. His model is used here to develop an approximate mathematical expression between the splitting (maximum perpendicular-to-grain) stress and the geometry of the joint. It was applied assuming only one dowel and used to calculate the ratio between the maximum and average perpendicular-to-grain stress in the area between the dowel and the timber end. The average perpendicular to grain stress was calculated as the wedging force divided by $a_3 \cdot t$. (The peak stress in the very vicinity of the hole as well as the effect of timber thickness were not considered here.)

To study the effect of the geometry of the connection, the ratio a_3/a_4 was varied in calculations, and it was found that – for practical purposes – either the stress at the timber end or the stress at the hole corresponds to the maximum, so that it is enough to consider only these two locations. The results of the geometry effect, viz., the ratio between maximum and average perpendicular-to-grain stress at the end and at the hole as function of a_3/a_4 is plotted in Fig. 3b. By curve fitting, the ratio between the maximum and average perpendicular to grain stress is approximately expressed by at hole and at end by:

$$s_{t90,hole} = \max\left(1\,,\, 0.65\, a_3 / a_4\right)$$
$$s_{t90,end} = 2.7 / \cosh\left(a_3 / a_4 - 1.4\right) \qquad (16,17)$$

Jorissen (1998) estimated that the wedging force is of the order of 0.1 times the axial force transmitted by the dowel. A stress concentration factor $k_{t90,cnctr}$ is assumed also for the splitting failure. Thus the splitting capacity can be expressed as (effect of load distribution and dowel deformation taken into account by n_{ef} and t_{red}):

$$F_{splhole,j,k} = k_{t90,cnctr}\, n_{ef}\, 10 f_{t,90,k}\, t_{red}\, a_3 / s_{t90,hole}$$
$$F_{splend,j,k} = k_{t90,cnctr}\, n_{ef}\, 10 f_{t,90,k}\, t_{red}\, a_3 / s_{t90,end} \qquad (18,19)$$

4.7.6 Interaction of shear and splitting at the dowel hole

The shear stress and splitting stress at the dowel hole are assumed to have an interaction effect on capacity, which is taken into account in the way described above in Eq. (8) [subscripts 1 => v, 2 => splhole]

The splitting failure originating at the end of the timber is not assumed to interact with shear, because the shear stress must vanish at the end.

4.7.7 Capacity of the outer part

The capacity of the outer part (j = 0, m) is obtained as the smallest capacity:

$$F_{j,k} = \min\left(F_{h,j,k}, F_{t+v,j,k}, F_{v+splhole,j,k}, F_{splend,j,k}\right) \quad (20)$$

4.6 Capacity of whole connection against timber failure

Finally, the capacity of the connection against timber failure is obtained in case of double shear connections simply as the sum of the capacities of the parts:

$$F_{TFMk} = \sum_{j} F_{j,k} \quad (21)$$

In case of 4-shear connections (timber-steel-timber-steel-timber), the capacity is first calculated as for two double shear connections and the total capacity is then obtained as the sum.

$$F_{TFMk}^{4-shear} = F_{TFMk}^{Timber-steel-timber} + F_{TFMk}^{Steel-timber-steel} \quad (22)$$

5 Results and analysis

The design method was developed based on the observations and results obtained in the experimental program reported in Hanhijärvi et al. (2006). Simultaneously, it was verified against the results of the approximately 150 tension tests carried out in the test program. The results are presented in Tables 1 and 2 for double shear tests and multiple shear tests in Tables 3 and 4 for glulam and LVL, respectively. For better comparison of the results to the design formulas of Eurocode 5 some calculated values based on EC5 equations are also added to Tables 1-4. The observed failure mechanism as well as the critical failure mechanism of design are also reported. The calculated values represent mean values (subscript m) and are explained in the list of symbols (Chapter 2). The mean values are based on the measured values of density of timber and tensile yield strength of dowels.

All calculation have been made using mean properties. If the properties have been measured, then the mean measured values are used in calculations (reported in the corresponding Tables). The mean values of non-measured properties have been assumed the following values (Hanhijärvi et al 2006):

– Glulam: $f_{tm} = 1.3 * f_{tk} = 29$ N/mm^2, $f_{vm} = 1.3 * f_{vk} = 4.9$ N/mm^2 , $f_{t90m} = 1.0$ N/mm^2

– Kerto-S: $f_{tm} = 43$ N/mm^2, $f_{vm,edge} = 4.9$ N/mm^2, $f_{vm,flat} = 3.0$ N/mm^2 , $f_{t90m} = 1.4$ N/mm^2

The following values have been used for the stress concentration factors:

– Glulam: $k_{t,cnctr} = 2.0$, $k_{v,cnctr} = 1.0$, $k_{t90,cnctr} = 0.7$

– Kerto-S: $k_{t,cnctr} = 1.7$, $k_{v,cnctr} = 0.7$, $k_{t90,cnctr} = 0.7$

Table 1. The calculated capacities and test results of the glulam series with double-shear dowelled connections. Symbols: see Chapter 2.

Series name	ρ_m kg/m^3	DF EC5	F_{Rm} kN	F_{Sm} kN	F_{Bm} kN	F_{Tm} kN	$F_{NEW,m}$ kN	DF New	F_{max} mean kN	F_{max} CoV %	TF	F_{max} / F_{NEW}	F_{max} / F_{Bm}
Timber-Steel-Timber, Dowel diameter 12mm													
GL28h, t_1 = 42 mm, d = 12 mm, Dowel strength cl. 8.8, measured f_{ym} = 720 MPa, F_{Rk} = 520 kN													
GL_TST_d12_12x2	466	p	579	397	385	459	**393**	sple,t	424	8.3	b	**1.08**	1.10
GL_TST_d12_8x3	460	p	574	422	409	487	**414**	sple,t	504	11.6	b	**1.22**	1.23
GL_TST_d12_6x4	474	p	585	452	430	511	**473**	sple,t	529	4.4	b	**1.12**	1.23
GL_TST_d12_4x6	464	p	577	464	415	525	**644**	sh,t	571	6.2	b	**0.89**	1.38
Steel-Timber-Steel, Dowel diameter 12mm													
GL28h, t_2 = 90 mm, d = 12 mm, dowel strength cl. 8.8, measured f_{ym} = 720 MPa, F_{Rk} = 576 kN													
GL_STS_d12_12x2	462	b-r	635	424	459	567	**490**	spe,t	537	2.8	b	**1.10**	1.17
GL_STS_d12_8x3	475	b-r	644	490	459	567	**579**	spe,t	646	7.4	b	**1.11**	1.41
GL_STS_d12_6x4	447	b-t	625	411	472	572	**624**	sh,t	606	10.1	b	**0.97**	1.28
GL_STS_d12_4x6	467	b-t	638	438	479	582	**609**	sh,t	552	6.0	b	**0.91**	1.15
GL_STS_d12_3x8	466	b-t	638	490	575	693	**716**	sple,t	660	1.5	row	**0.92**	1.17
Timber-Steel-Timber, Dowel diameter 8mm													
GL28h, t_1 = 28 mm, d = 8 mm, dowel strength cl. 10.9, measured f_{ym} = 1010 MPa, F_{Rk} = 279 kN													
GL_TST_d8_12x2	472	p	314	217	191	222	**243**	sh,t	266	5.6	b	**1.09**	1.39
GL_TST_d8_6x4	425	p	296	232	214	250	**248**	spe,t	238	17.7	b	**0.96**	1.11
Steel-Timber-Steel, Dowel diameter 8mm													
GL28h, t_2 = 60 mm, d = 8 mm, dowel strength cl. 10.9, measured f_{ym} = 1010 MPa, F_{Rk} = 318 kN													
GL_STS_d8_12x2	468	b-r	355	237	212	264	**273**	sh,t	295	21.6	b	**1.08**	1.39
GL_STS_d8_6x4	462	b-t	353	232	219	264	**307**	sh,t	299	4.8	(*	**0.97**	1.37

*) the dominating failure mode is unclear

Table 2. The calculated capacities and test results of the LVL series with double-shear dowelled connections. Symbols: see Chapter 2.

Series name	ρ_m kg/m^3	DF EC5	F_{Rm} kN	F_{Sm} kN	F_{Bm} kN	F_{Tm} kN	F_{NEWm} kN	DF NEW	F_{max} mean kN	F_{max} CoV %	TF	F_{max} / F_{NEW}	F_{max} / F_{Bm}
Timber-Steel-Timber, Dowel diameter 12mm													
Kerto-S, t_1 = 39 mm, d = 12 mm, Dowel strength cl. 8.8, measured f_{ym} = 720 MPa, F_{Rk} = 563 kN													
KS_TST_d12_12x2	499	p	594	397	395	506	**361**	sh,t	400	7.9	b	**1.11**	1.01
KS_TST_d12_8x3	492	p	588	420	414	528	**408**	sh,t	460	6.8	b	**1.13**	1.11
KS_TST_d12_6x4	512	p	603	456	449	572	**477**	sh,t	507	6.1	b	**1.06**	1.13
KS_TST_d12_4x6	488	s/r	586	462	649	711	**599**	sh,t	598	0.8	b	**1.00**	0.92
Steel-Timber-Steel, Dowel diameter 12mm													
Kerto-S, t_2 = 75 mm, d = 12 mm, Dowel strength cl. 8.8, measured f_{ym} = 720 MPa, F_{Rk} = 665 kN													
KS_STS_d12_12x2	523	b-r	722	483	459	719	**450**	sh,t	500	5.2	b	**1.11**	1.09
KS_STS_d12_8x3	527	b-r	726	534	387	662	**530**	sh,t	568	0.8	b	**1.07**	1.47
KS_STS_d12_6x4	537	s/r	736	527	692	719	**600**	sh,t	591	7.1	b	**0.98**	0.85
KS_STS_d12_4x6	556	s/r	753	562	673	705	**599**	sh,t	570	4.9	b	**0.95**	0.85
KS_STS_d12_3x8	518	s/r	717	551	807	803	**671**	sh,t	561	7.3	b	**0.84**	0.70
Timber-Steel-Timber, Dowel diameter 8mm													
Kerto-S, t_1 = 27 mm, d = 8 mm, Dowel strength cl. 10.9, measured f_{ym} = 1010 MPa, F_{Rk} = 303 kN													
KS_TST_d8_12x2	502	p	324	216	199	254	**187**	sh,t	200	7.6	b	**1.07**	1.01
KS_TST_d8_6x4	514	p	328	243	214	269	**236**	sh,t	241	13.0	b	**1.02**	1.13
Steel-Timber-Steel, Dowel diameter 8mm													
Kerto-S, t_2 = 51 mm, d = 8 mm, Dowel strength cl. 10.9, measured f_{ym} = 1010 MPa, F_{Rk} = 344 kN													
KS_STS_d8_12x2	524	b-r	374	250	220	345	**223**	sh,t	296	2.0	b	**1.34**	1.35
KS_STS_d8_6x4	518	s/r	380	272	333	340	**306**	sh,t	336	2.3	b	**1.10**	1.01

Table 3. The calculated capacities and test results of the Glulam series with multiple-shear dowelled connections. Symbols: see Chapter 2.

Series name	ρ_m kg/m³	DF EC5	F_{Rm} kN	F_{Sm} kN	F_{Bm} kN	F_{Tm} kN	F_{NEWm} kg/m³	DF NEW mm	F_{max} mean kN	F_{max} CoV %	TF	F_{max} / F_{NEW}	F_{max} / F_{Bm}
4-Shear, Dowel diameter 12mm													
GL28h, d = 12 mm, dowel str. cl. 10.9, measured f_{vm} = 933 MPa, t_s = 12 mm, F_{Rk} = 1040 kN (A), 1122 kN													
GL_4Sh_d12_12x2A	447	p,b-r	1216	833	910	1096	**1008**	spe,t	968	6.9	b,b	**0.96**	1.06
GL_4Sh_d12_12x2B	449	p,b-r	1196	820	965	1096	**999**	spe,t	1084	5.7	b,b	**1.09**	1.12
GL_4Sh_d12_6x4A	463	p,b-r	1240	958	762	1106	**1073**	spe,t	856	5.9	b,b	**0.80**	1.12
GL_4Sh_d12_6x4B	462	p,b-r	1592	1230	798	1106	**1071**	spe,t	1069	6.3	b,b	**1.00**	1.34
4-Shear, Dowel diameter 8mm													
GL28h, d = 8 mm, dowel strength class10.9, measured f_{vm} = 950 MPa, t_s = 8 mm, F_{Rk} = 558 kN (A), 689 kN													
GL_4Sh_d8_12x2A	447	p,b-r	598	413	435	511	**514**	sh,t	501	20.3	b,b	**0.97**	1.15
GL_4Sh_d8_12x2B	471	b-r,b-r	791	546	468	511	**495**	sh,t	530	4.3	b,b	**1.07**	1.13
GL_4Sh_d8_6x4AZ	458	p,b-r	606	474	366	518	**497**	spe,t	586	6.1	b,b	**1.18**	1.60
GL_4Sh_d8_6x4B	455	b-r,b-r	765	599	388	517	**491**	spe,t	478	15.9	b,b	**0.97**	1.23
GL_4Sh_d8_6x4A	444	p,b-r	596	467	366	518	**500**	spe,t	546	4.5	b,b	**1.09**	1.49
6-Shear, Dowel diameter 8mm													
GL28h, d = 8 mm, dowel strength class10.9, measured f_{vm} = 950 MPa, t_s = 8 mm, F_{Rk} = 837 kN													
GL_6Sh_d8_12x2	431	p,b-r	879	688	521	786	**798**	sh,t	765	11.7	b,b	**0.96**	1.47

Table 4. The calculated capacities and test results of the LVL series with multiple-shear dowelled connections. Symbols: see Chapter 2.

Series name	ρ_m kg/m³	DF EC5	F_{Rm} kN	F_{Sm} kN	F_{Bm} kN	F_{Tm} kN	F_{NEWm} kg/m³	DF NEW mm	F_{max} mean kN	F_{max} CoV %	TF	F_{max} / F_{NEW}	F_{max} / F_{Bm}
4-Shear, Dowel diameter 12mm													
Kerto-S, d = 12 mm, Dowel strength class 10.9, measured f_{vm} = 933 MPa, F_{Rk} = 1226kN													
KS_4Sh_d12_12x2	525	p,b-r	1314	878	898	1418	**890**	sh,t	898	7.6	b,b	**1.01**	1.00
KS_4Sh_d12_6x4	523	b-t,b-t	1312	993	1065	1418	**1185**	sh,t	1157	1.2	b,b	**0.98**	1.09
4-Shear, Dowel diameter 8mm													
Kerto-S, d = 8 mm, Dowel strength class 10.9, measured f_{vm} = 950 MPa, F_{Rk} =604kN (A), F_{Rk} = 702 kN (B)													
KS_4Sh_d8_12x2A	538	p,b-r	658	440	431	683	**415**	sh,t	460	8.8	b,b	**1.11**	1.07
KS_4Sh_d8_12x2B	540	b-r,b-r	790	528	468	684	**413**	sh,t	511	2.5	b,b	**1.24**	1.09
KS_4Sh_d8_6x4A	541	b-t,b-t	660	473	466	683	**516**	sh,t	492	1.1	b,b	**0.95**	1.06
KS_4Sh_d8_6x4B	528	b-t,b-t	772	553	504	684	**517**	sh,t	528	2.8	b,b	**1.02**	1.05
6-Shear, Dowel diameter 8mm													
Kerto-S, d = 8 mm, Dowel strength class 10.9, measured f_{vm} = 950 MPa, F_{Rk} = 906 kN													
KS_6Sh_d8_12x2	550	b-t,b-t	876	627	462	670	**623**	sh,t	729	8.8	b,b	**1.17**	1.58

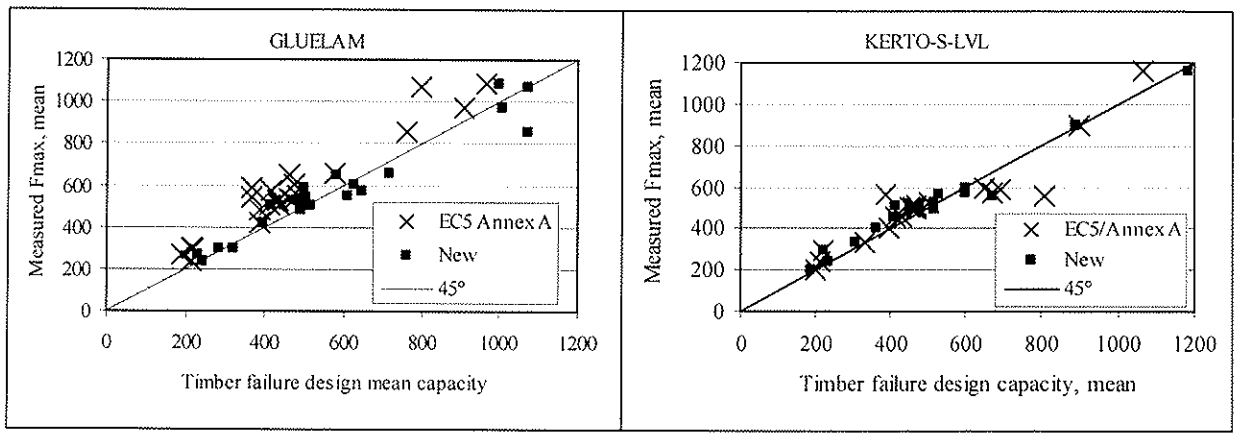

Figure 4. F_{max} plotted against block shear design capacity for Gluelam (left) and LVL (right). Each point is the mean result of one series. (Note that in all four LVL series which are under 45 degree line for the EC5 value, the critical design is not due to block shear but splitting or rowshear.)

6 Discussion and conclusions

The proposed design procedure presents a method to design dowelled timber-to-steel connections against timber failure mechanisms. The method pursues to distinguish all failure modes and present a sufficiently accurate equation for each one. This methodology chops up the complex failure phenomenon to many rather simple equations which all have reasonable purpose and derivation. Although the method is suitable for hand calculation, the best way to apply it is through a calculation spreadsheet or a small computer program, for which it is extremely suitable, since the method does not require iteration or interpolation.

The method has so far been verified only against the test results of this project for which is fits surprisingly well. More verification calculations would be advantageous but are limited by the small amount of experimental data available. However, the model should be verified properly against situations with only one row of dowels (not included in this project), which would give more insight to its performance in modelling the splitting behaviour.

Acknowledgements

This work was financed by The Technology Agency of Finland, Finnforest Oyj, Versowood Oyj, SPU-Systems Oy, LATE-Rakenteet Oy, Exel Oyj and VTT which is gratefully acknowledged.

References

Anon. 2004. Tutkintaselostus. Messuhallin katon romahtaminen Jyväskylässä 1.2.2003. (Fair centre roof collapsing in Jyväskylä, Finland, on 1 Feb 2003.). Accident Investigation Board of Finland Report B 2/2003Y

Hanhijärvi A., Kevarinmäki A., Yli-Koski. R. 2006. Block shear failure at dowelled steel-to-timber connections. CIB-W18 Meeting, Florence.

Hilson B.O. 1995. Joints with dowel type fasteners – Theory. STEP Lecture C3. In: Blass H.J., Aune P., Choo B.S., Görlacher R., Griffiths D.R., Hilson B.O., Racher P., Steck G. (Eds.): Timber Engineering STEP 1. Basis of design, material properties, structural components and joints. Centrum Hout, The Netherlands.

Johansen K.W. 1949. Theory of timber connections. International Association of Bridge and Structural Engineering. Publication No. 9:249-262. Bern.

Jorissen A. 1998. Double shear timber connections with dowel type connections. Delft University Press, Delft

Ranta-Maunus A., Kevarinmäki A. 2003. Reliability of timber structures, theory and dowel-type connection failures. CIB-W18/36-7-11, Colorado, USA, Aug. 2003.

Sjödin J., Serrano E., Enquist B. 2007. Contact free measurements and numerical analyses of the stress distribution in the joint area of steel-to-timber dowel joints. Accepted in Holz als Roh- und Werkstoff

Sjödin J., Serrano E. 2007. A numerical study of the effects of stresses induced by moisture gradients in steel-to-timber dowel joints. Accepte Holz als Roh- und Werkstoff

INTERNATIONAL COUNCIL FOR RESEARCH AND INNOVATION
IN BUILDING AND CONSTRUCTION

WORKING COMMISSION W18 - TIMBER STRUCTURES

A EYM BASED SIMPLIFIED DESIGN FORMULA FOR THE LOAD CARRYING CAPACITY OF DOWEL-TYPE CONNECTIONS

M Ballerini

Department of Mechanics & Structural Engineering, University of Trento

ITALY

MEETING FORTY

BLED

SLOVENIA

AUGUST 2007

Presented by M. Ballerini
H. Larsen commented that the exact formulae are easier to use than the proposed simplified ones. M. Ballerini suggested the reliance on computers to use the exact formulae may lead to human errors.
I. Smith asked in terms of rope effect and what type of deformation levels is assumed and suggested that in Canadian approach rope effects were ignored as large deformation are needed to develop it. M. Ballerini said that it depends on different cases. H. Blass stated that rope effect does not require large deformation. H. Larsen added that rope and friction effects are provided by the tension action of the fastener. H. Blass clarified the number 4 in the denominator comes from the friction. H. Larsen concluded that the deformation is there anyway why doesn't one take into account the added capacity due to the deformation regardless one likes the deformation or not.

A EYM based simplified design formula for the load-carrying capacity of dowel-type connections

Marco Ballerini
DIMS - Department of Mechanics & Structural Engineering, University of Trento, Italy

Abstract:
The most recent European timber design codes make use of the rigid-plastic Johansen's theory (known as the European Yield Model – EYM), for the definition of the design strength of joints with dowel-type fasteners. Beside the effectiveness of Johansen's approach, the complexity of derived equations make the design of timber joints quite difficult and not well accepted by practising engineers. However, EYM formulae are susceptible to be considerably simplified. Moreover, some failure modes can be disregarded since they cannot take place in most practical joint configurations.
The paper presents a simplified format for the design of timber dowel-type connections. It is based on the linearization of some design equations, the simplification of the equation related to failure mode Ic in timber-to-timber joints with fasteners in single shear, the demonstration of failure modes which can be disregarded.
The formulae are derived directly from the Johansen's design equations; consequently, they can be applied to dowel-type joints in any combination of grain directions between timber elements. The simplified formulae are compared and discussed with the original ones of the EYM approach.

1. INTRODUCTION

The most recent European design codes for timber structures (the EN 1995-1-1, 2004, [1], and the DIN 1052, 2004, [2]) make use of the Johansen's plastic theory (Johansen, 1949, [3]), also well-known as European Yield Model (EYM), to define the design strength of timber dowel-type connections.
It has been shown that the Johansen's equations are able to predict very well the load-carrying capacity of dowel-type joints with single fastener (see Ballerini et al., 2006, [1]). However, in joints with multiple fasteners, their prediction ability is less good due to the group effect and to the tendency of timber elements with thin thickness to split (the splitting failure is not considered in Johansen's theory). The group effect is taken into account by means of the effective number of fasteners (n_{ef}); the tendency of splitting is prevented by appropriate limits on the minimum spacing between fasteners and of minimum end and side distances.
In spite of the good prediction ability of the EYM, practising engineers do not like this new way for the evaluation of the load-carrying capacity of joints. This is due to the complexity of design equations which makes the EYM difficult to understand and manage. In order to make the Johansen's theory more friendly, different simplified approaches have been already proposed: Kangas and Kurkela (1996, [5]) and Blass et al. (1999, [6]). Particularly the latter one, developed for people unskilled in the design of timber structures, gives always a conservative design, is extremely simple and is embodied in the new German timber design code together with the original EYM.

In the following, new simplified design equations are derived and proposed. They are developed by means of the approximation and of the linearization of some equations, and highlighting the needless of others. With respect to the simplification proposed by Blass, this new simplified set of design equations gives a more advantageous design but also less simple equations.
The formulae are derived directly from Johansen's equations; consequently, they can be applied to joints in any combination of grain directions between timber elements.

2. DESIGN EQUATIONS FOR TIMBER-TO-TIMBER DOWEL-TYPE JOINTS

According to Johansen's plastic theory, the strength of dowel-type joints is governed by the failure mode which has the lower load-carrying capacity.

The failure modes which can take place in dowel-type joints are different for joints with fasteners with 1 or with 2 shear planes. They are also different for timber-to-timber and steel-to-timber joints. In this paper, since the approach is the same for timber-to-timber and steel-to-timber joints, only the former ones will be considered.

Whatever the case, in dowel-type joints, provided that brittle failures are prevented by adequate choices of end and side distances, the load-carrying capacity is governed by the following mechanical and geometrical parameters:

- $f_{h,i,k}$ the characteristic embedding strength of timber element *i*;
- $M_{y,Rk}$ the characteristic fastener yield moment;
- t_i the embedded fastener length in timber element *i*;
- d the fastener diameter.

Timber-to-timber joints with fasteners in single shear can collapse according to the 6 different failure modes shown in Figure 1; timber-to-timber connections with fasteners with 2 shear planes, can only collapse according to the 4 failure modes of Figure 2. In same Figures, for each failure mode the related characteristic load-carrying capacity, according to the new Eurocode 5 is also reported.

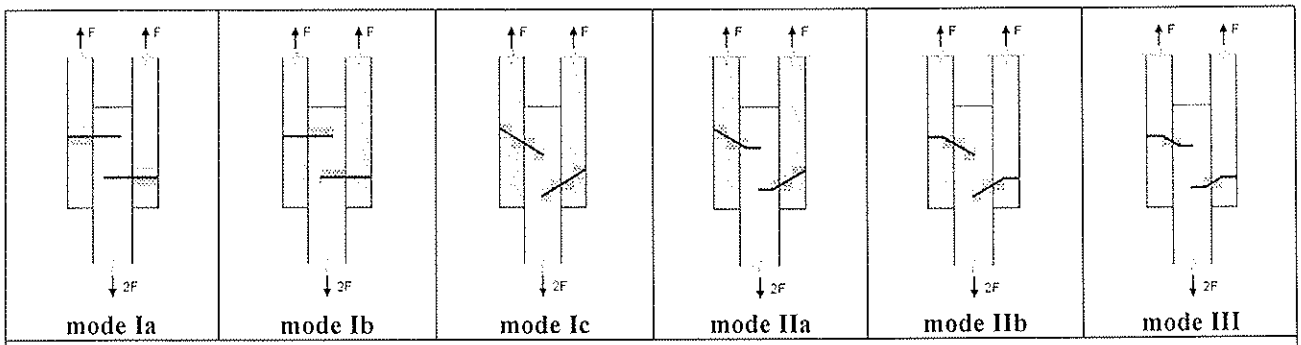

$f_{h,1,k} t_1 d$	**mode Ia**
$f_{h,2,k} t_2 d$	**mode Ib**
$\frac{f_{h,1,k} t_1 d}{(1+\beta)} \left[\sqrt{\beta + 2\beta^2 \left(1 + \frac{t_2}{t_1} + \left(\frac{t_2}{t_1} \right)^2 \right) + \beta^3 \left(\frac{t_2}{t_1} \right)^2} - \beta \left(1 + \frac{t_2}{t_1} \right) \right] + \frac{F_{ax,Rk}}{4}$	**mode Ic**
$\frac{f_{h,1,k} t_1 d}{(2+\beta)} \left[\sqrt{2\beta(1+\beta) + \frac{4\beta(2+\beta) M_{y,Rk}}{f_{h,1,k} d t_1^2}} - \beta \right] + \frac{F_{ax,Rk}}{4}$	**mode IIa**
$\frac{f_{h,1,k} t_2 d}{(1+2\beta)} \left[\sqrt{2\beta^2(1+\beta) + \frac{4\beta(1+2\beta) M_{y,Rk}}{f_{h,1,k} d t_2^2}} - \beta \right] + \frac{F_{ax,Rk}}{4}$	**mode IIb**
$\sqrt{\frac{2\beta}{1+\beta}} \sqrt{2 M_{y,Rk} f_{h,1,k} d} + \frac{F_{ax,Rk}}{4}$	**mode III**

Figure 1. Failure modes of timber-to-timber joints with fasteners in single shear and related EYM design equations

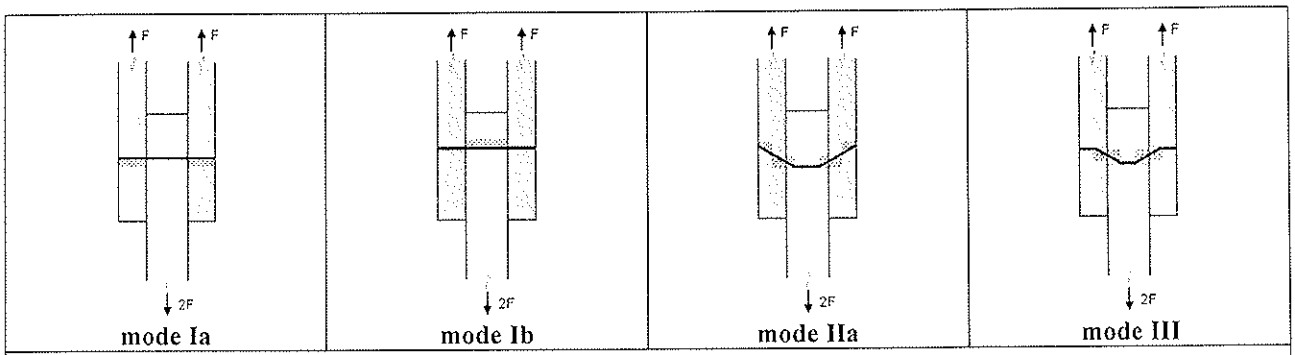

$f_{h,1,k} t_1 d$	**mode Ia**
$\frac{1}{2} f_{h,2,k} t_2 d$	**mode Ib**
$\frac{f_{h,1,k} t_1 d}{(2+\beta)} \left[\sqrt{2\beta(1+\beta) + 4\beta(2+\beta)\frac{M_{y,Rk}}{f_{h,1,k} d t_1^2}} - \beta \right] + \frac{F_{ax,Rk}}{4}$	**mode IIa**
$\sqrt{\frac{2\beta}{1+\beta}} \sqrt{2 M_{y,Rk} f_{h,1,k} d} + \frac{F_{ax,Rk}}{4}$	**mode III**

Figure 2. Failure modes of timber-to-timber joints with fasteners with 2 shear planes and related EYM design equations

In the equations, β is the ratio between the characteristic embedding strengths of timber members

$$\beta = f_{h,2,k} / f_{h,1,k}$$

while the second term in equations Ic, II (a and b) and III, represents the strength increase due to the so-called *"rope effect"*. This term, that as maximum can double the original Johansen's term, is proportional to the axial force which occurs in fasteners and can take place only if fasteners don't remain perpendicular to the shear planes at collapse.
The physical meaning of equations reported in Figures 1 and 2 is shown respectively in Figure 3 (the strength increase due to the *"rope effect"* is not represented). From graphs it is possible to notice that equations related to failure modes I provide linear relationships between load-carrying capacity and embedded fastener length λ (t_1/d, see later). On the contrary, failure mode III it is not affected by λ, and failure modes II gives non linear relationships.

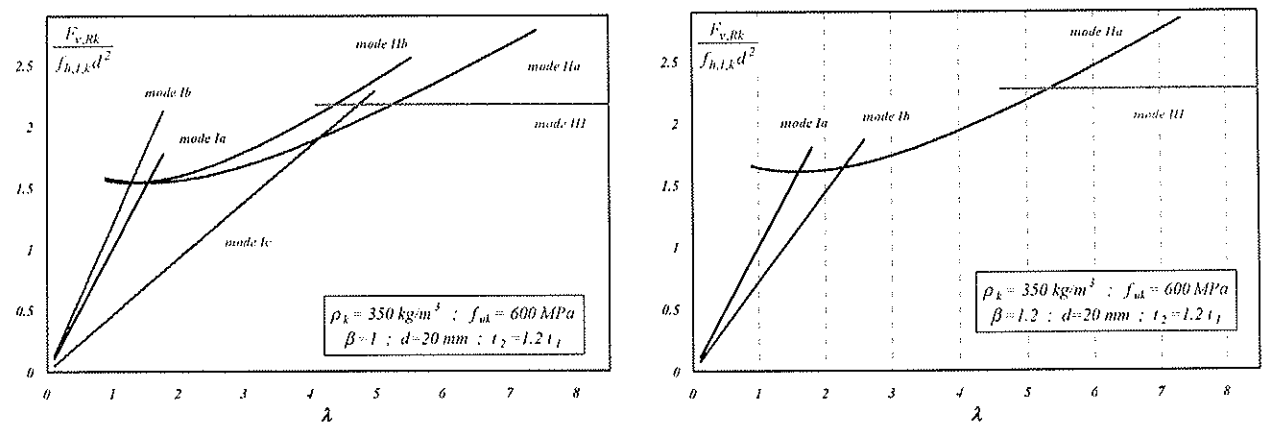

Figure 3. No-dimensional characteristic strength of timber-to-timber joints with fasteners in single shear (left) and with fasteners with 2 shear planes (right)

For the joint plotted in Figure 3 left, only failure modes Ic, IIa and III are decisive for the joint design; the others 3 failure modes don't play any role since they provide higher design loads. Moreover, mode IIa is crucial only in a little range of λ. For the joint plotted in Figure 3 right, only failure modes Ib, IIa and III are decisive.

3. SIMPLIFIED EQUATIONS FOR JOINTS WITH FASTENERS IN SINGLE SHEAR

In order to better manage design equations, they can be rewritten conveniently as follows (the strength increase of the *"rope effect"* term is not included):

$$F_{v,Rk} = f_{h,1,k} d^2 \min \xi_i$$

where:

$$\xi_i = \begin{cases} \lambda \\ \beta\theta\lambda \\ \frac{\lambda}{1+\beta}\left[\sqrt{\beta + 2\beta^2(1+\theta+\theta^2) + \beta^3\theta^2} - \beta(1+\theta)\right] \\ \frac{1}{2+\beta}\left[\sqrt{2\beta(1+\beta)\lambda^2 + 4\beta(2+\beta)\mu^2} - \beta\lambda\right] \\ \frac{1}{1+2\beta}\left[\sqrt{2(1+\beta)(\beta\theta\lambda)^2 + 4\beta(1+2\beta)\mu^2} - \beta\theta\lambda\right] \\ \sqrt{\frac{2\beta}{1+\beta}}\sqrt{2}\mu \end{cases}$$

and:

$$\lambda = \frac{t_1}{d} \quad ; \quad \theta = \frac{t_2}{t_1} \quad ; \quad \mu = \sqrt{\frac{M_{y,Rk}}{f_{h,1,k} d^3}}$$

The non-dimensional parameters λ, θ, μ, are respectively the fastener embedded slenderness in outer elements, the ratio between embedded slenderness in timber elements, the non dimensional fastener yielding moment.

Parameters β and θ have a range of variation which can be defined right away.

Concerning β, usually timber joints are made with elements of the same strength class. This implies that β can differ from 1 only if timber members are loaded by fasteners at different angles with grain direction. Consequently, extreme values of β agree with following conditions:

$$\beta_{min} = \frac{f_{h,90,k}}{f_{h,0,k}} = \frac{1}{k_{90}} \quad ; \quad \beta_{max} = \frac{f_{h,0,k}}{f_{h,90,k}} = k_{90}$$

According to Eurocode 5, k_{90} is maximum for softwood species. Since it increases with fastener diameter, assuming d_{max} of 30mm it can be concluded that β can range from 0.55 to 1.8.

Parameter θ (fastener embedded length in member *"2"* compared with the one in member *"1"*) usually ranges between 0.75-1.5. However in the following, to cover also unusual configurations, it will be investigated from 0.5 to 2.5.

Simplification of failure modes I

Simplify failure modes I means specify if there are failure modes which can be disregarded for design and get a simplification for mode Ic.

With respect to former subject, mode Ic has been compared with modes Ia and Ib. The results are shown respectively in Figure 4 (left and right).

From Figure 4 it is evident that mode Ic is decisive on the most part of parameters range. In detail, Figure 4 left shows that mode Ia became crucial only on a little part of parameters range with β and θ close to their maximum values. Figure 4 right shows that mode Ib is significant in a very little portion of the investigated range, much smaller that previous one, with β and θ close to their minimum values.

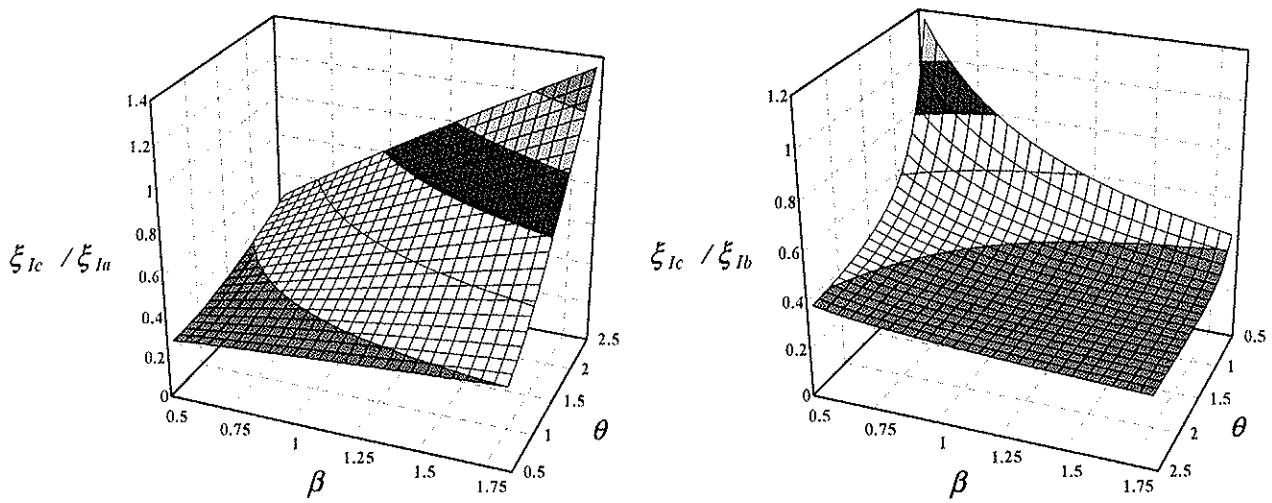

Figure 4. Failure mode Ic versus failure mode Ia (left) and failure mode Ic versus failure mode Ib (right)

It is possible to work out the conditions that rule the decisive failure modes. Mode Ia is crucial when:

$$\theta > \frac{1}{k\beta}\left[1+\sqrt{2(1+\beta)-\beta(k-1)^2}\right] \tag{1}$$

while mode Ib is central if:

$$\theta < \frac{k}{\beta}\frac{\sqrt{2\beta(1+\beta)-\beta(k-1)^2}-\beta}{(2+\beta)-(k-1)^2} \tag{2}$$

In above relations, k concerns the strength increase due to the *"rope effect"*; its range is 1-2.

Equations (1) and (2) are plotted in Figure 5 with reference to β and θ parameters (left) and with reference to β and $\beta\theta$ parameters (right). From Figure 5 left it is possible to see that rarely mode Ib can be decisive. Indeed, this requires θ values lower than about 0.5 if *"rope effect"* is not taken into account, or lower than about 1 if on the contrary it is considered at its maximum value (dashed curve). Concerning mode Ia, about same conclusions can be drawn if *"rope effect"* is not considered (θ values are out of common practice). However, if *"rope effect"* is considered at its maximum, θ values fall in the common range at least for larger β values.

From Figure 5 right it is evident that both modes Ia and Ib are without of any practical interest if the *"rope effect"* is not taken into account in mode Ic. On the contrary, if the *"rope effect"* is considered at its maximum value, both failure modes Ia and Ib can became decisive (dashed curves).

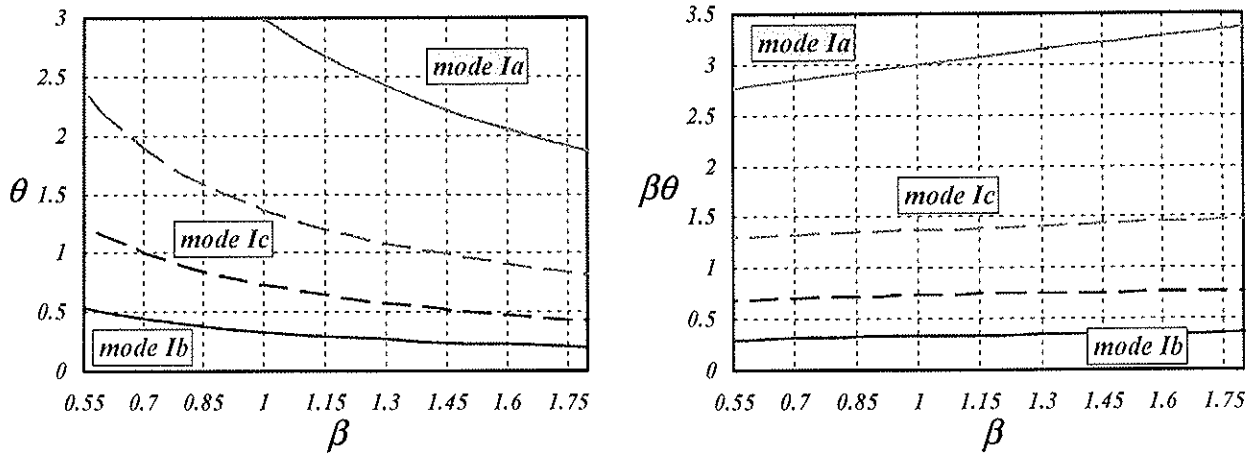

Figure 5. Decisive failure modes I vs β and (left) and decisive failure modes I vs β and βθ (right)

More helpful conclusion can be drawn if the effect of terming *"1"* the outer timber members and *"2"* the inner one is analysed.

In timber joints with fasteners in single shear (usually nails or screws), it is tradition term *"1"* the timber element which receives the fastener head and term *"2"* the one that accepts the fastener point. However, this choice is subjective. Terming *"1"* the timber element which has the lower strength between modes Ia and Ib ($f_{h,1,k}\, t_1 < f_{h,2,k}\, t_2$) allows considerable simplifications.

First of all, equation Ib is not more significant since this failure mode cannot take place ($\beta\theta > 1$).

Equation Ic can be simplified according to both following equations:

$$\xi'_{Ic} = \left(\sqrt{2} - 1\right) \frac{(\beta + \beta\theta)}{(1 + \beta)}\, \lambda \tag{3}$$

$$\xi'_{Ic} = \left(\sqrt{2} - 1\right) \frac{(\beta + \beta\theta)}{(1 + \beta)} \left(1 + 0.06(\beta\theta - 1)^2\right) \lambda \tag{3'}$$

Equation (3) is very simple and always conservative. The comparison with the original formula is plotted in Figure 6 left with reference to θ. From graph, it is possible to see that errors are in between +0/-15% in a

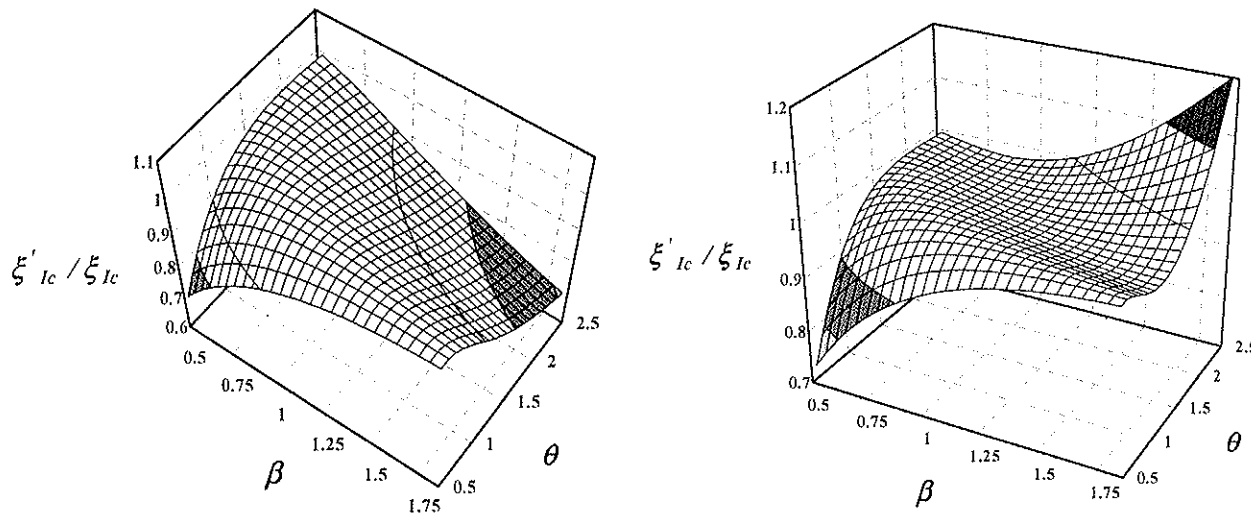

Figure 6. Mode Ic - comparison with approximated equation (3) (left) and with approximated equation (3') (right)

wide range of β and θ ($0.5 < \beta\theta < 2.5$), while they grow up to -30% on the whole investigated range. Equation (3') is less simple and not on the safe side for β and θ close to their maximum values. However, the comparison with the original formula, Figure 6 right, shows that errors are in between +0/-8% if $0.5 < \beta\theta < 2.5$ while they are in between +20/-26% on the whole investigated range.

Simplification of failure modes II

Equations related to failure modes IIa and IIb have a hard appearance; however also these equations can be simplified considerably.

Looking at Figure 3, it is possible to notice that equations related to modes IIa and IIb are quite linear close to the intersections with the equation of mode III. Moreover, due to the lower strength shown by mode Ic, equations IIa and IIb are not crucial for lower λ values.

From the above considerations, it is natural to think at a linearization of equations IIa and IIb at the intersection points with equation III.

Developing the calculations, following approximating relations can be proposed:

$$\xi_{IIa} \cong \frac{\sqrt{\beta}}{\sqrt{\beta} + 2\sqrt{1+\beta}} (2\mu + \lambda) \tag{4}$$

$$\xi_{IIb} \cong \frac{1}{1 + 2\sqrt{1+\beta}} \left(2\mu\sqrt{\beta} + \beta\theta\lambda\right) \tag{5}$$

Equations (4) and (5) are always conservative with respect to the original formulae of modes IIa and IIb. Errors are quite negligible for λ values close to ones of the intersections with mode III, but they are of about -20% at the intersections with mode Ia.

Previous work has provided simplified rules but has not show in which circumstances equation concerning mode IIb can be crucial with respect to equation IIa.

If the original equation for mode IIb is compared with the one of mode IIa with respect to β and θ separately, plots show that mode IIb is decisive for a wide range of β and θ.

However, if the same comparison is carried out with reference to values of $\beta\theta$ lager than 1, same plots show that mode IIb is crucial with respect to mode IIa only if $\beta > 1$ and $\beta\theta \leq 1.2$.

This result is illustrated in Figure 7 for the case of β at its maximum value. In this situation indeed, mode IIb shows the minimum strength with respect to mode IIa (about -12% for $\beta\theta = 1$ and $\lambda/\mu = 4.5$). The same result can be found if approximated equations are compared.

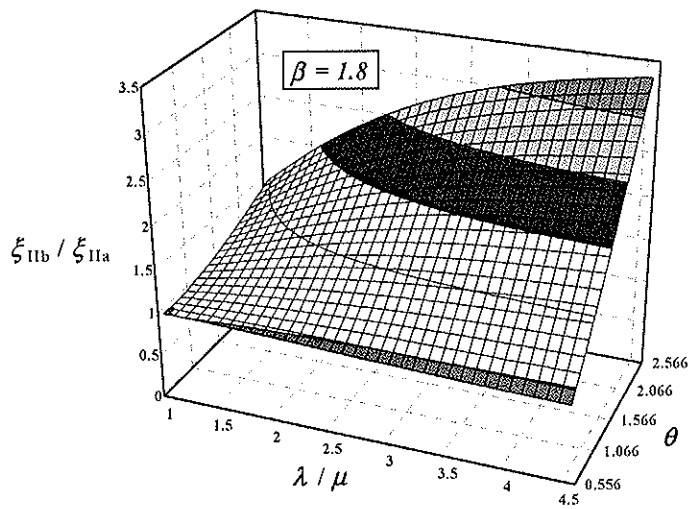

Figure 7. Comparison between equations of modes IIb and IIa for $\beta = 1.8$

4. TIMBER-TO-TIMBER JOINTS WITH FASTENERS WITH TWO SHEAR PLANES

In case of timber–to–timber dowel-type joints with 2 shear planes, only the four failure modes illustrated in Figure 2 can take place. Equations Ia, II and III of Figure 2 are totally identical to equations Ia, IIa and III of Figure 1. Equation Ib differs from the related one of joints with fasteners in single shear due to the factor 0.5; this is because equations of Figure 2 give the strength of each shear plane of fasteners.

For these joints, only the approximated formula already developed for mode IIa (4) can be proposed. When $\beta\theta$ is larger than 2, mode Ib is not crucial and the simplified formula for mode II, equation (4), gives the maximum underestimation of the actual strength: about -22%.

In this area timber joints are particularly prone to splitting. By this point of view, the conservative design of simplified formula is not so negative.

If $\beta\theta$ is smaller than 2, mode Ib became decisive and the underestimation is less significant.

5. CONCLUSIONS

A set of simplified design equations have been developed and analyzed for timber-to-timber joints with dowel-type fasteners.

For joints with fasteners in single shear, if no assumptions are done on β and θ, equations of modes Ic, IIa and IIb can be replaced by approximate relations (3), (4) and (5) which give in any case a conservative design. As an alternative, mode Ic can be better approximated by equation (3'). If the timber element with the lower embedding strength is termed *"1"*, the set of governing equations can be further simplified. In this case indeed, since $\beta\theta$ is larger than 1, mode Ib can be disregarded. Moreover, if $\beta\theta$ is larger than 1.2 also mode IIb can be omitted.

For joints with fasteners in double shear, the equation of mode II can be simplified according to the already developed equation (4).

Developed simplification maintains the classical Johansen's approach but with very simpler formulae.

If compared with Blass simplification, this set of design equations is less simple but more accurate.

REFERENCES

[1] EN 1995-1-1:2004-11, Eurocode 5 – Design of timber structures – Part 1-1: General rules and rules for buildings. *CEN: European Committee for Standardization*, Brussels

[2] DIN 1052:2004-08, Entwurf, Berechnung und Bemessung von Holzbauwerken – Allgemeine Bemessungsregeln und Bemessungsregeln für den Hochbau

[3] Johansen, K. W. (1949), Theory of timber connections. *International Association of Bridge and Structural Engineering*, Bern, Publication No. 9, pp. 249-262

[4] Ballerini, M. et. al. (2006), Dowel timber connections with two shear planes loaded parallel-to-the-grain: reliability of the new European design code by means experimental tests. *Proc. of WCTE 2006, 9th World Conference on Timber Engineering*, Portland, Oregon, USA, CD

[5] Kangas, J. and Kurkela, J. (1996), A simple method for lateral load-carrying capacity of dowel-type fasteners. *Proc. of CIB-W18 Timber Structures, Meeting 29*, Bordeaux, France, ISSN 0945-6996

[6] Blass, H. J. et. al. (1999), Simplified design of joints with dowel-type fasteners. *Proc. of PTEC'99, Pacific Timber Engineering Conference*, Rotorua, New Zealand, ISSN 1174-5096

INTERNATIONAL COUNCIL FOR RESEARCH AND INNOVATION
IN BUILDING AND CONSTRUCTION

WORKING COMMISSION W18 - TIMBER STRUCTURES

EVALUATION OF THE SLIP MODULUS FOR ULTIMATE LIMIT STATE VERIFICATIONS OF TIMBER-CONCRETE COMPOSITE STRUCTURES

E Lukaszewska
Luleå University of Technology
SWEDEN

M Fragiacomo
University of Sassari
ITALY

A Frangi
Institute of Structural Engineering, ETH Zürich
SWITZERLAND

MEETING FORTY
BLED
SLOVENIA
AUGUST 2007

Presented by M. Fragiacomo
H. Blass pointed out that the term non-conservative for the slip modulus is incorrect because non-conservative could mean either too high or too low. M. Fragiacomo agreed and will revise Table 5.
S. Thelandersson questioned how slip modulus compared to stress level between experiment and FEM at ultimate and serviceability limit state. M. Fragiacomo responded that failure loads were not compared which may not be that sensitive.
H. Larsen commented that these stiffness values are confusing and questioned why one doesn't just use the theory of plasticity for the composite beam. M. Fragiacomo responded that the brittleness of some cases show the proposed equations are important.

Evaluation of the slip modulus for ultimate limit state verifications of timber-concrete composite structures

Elzbieta Lukaszewska[1], Massimo Fragiacomo[2] and Andrea Frangi[3]

[1] *Division of Timber Structures, Luleå University of Technology, Luleå, Sweden*
[2] *Department of Architecture and Planning, University of Sassari, Italy*
[3] *Institute of Structural Engineering, ETH Zurich, Switzerland*

1 Introduction

The timber-concrete composite structure consists of timber joists and beams effectively interconnected to a concrete slab cast on top of the timber members. This type of structure was developed as an effective method for strength and stiffness upgrading of existing timber floors. Thanks to the several advantages over traditional timber floors such as increased strength and stiffness under gravity load, better seismic resistance, effective acoustic separation and improved fire resistance, the composite structure is also used in new construction.

The structural behaviour of timber-concrete composite members is mainly governed by the shear connection between timber and concrete. Almost all connection systems are flexible, i.e. they cannot prevent a relative slip between the bottom fibre of the concrete slab and the top fibre of the timber beam. As a consequence of that, conventional principles of structural analysis cannot be applied to solve the composite beam. The Eurocode 5-Part 1-1, Annex B [1] provides a simplified calculation method for mechanically jointed beams with flexible elastic connection. This method is based on the approximate solution of the differential equation for beams with partial composite action. As the shear connection is usually characterised by non-linear load-slip relationship, two different slip moduli are considered for design purposes: k_{ser} for the serviceability limit state (SLS) and k_u for the ultimate limit state (ULS) design. The slip modulus k_{ser}, which corresponds to the secant value at 40% of the load-carrying capacity of the connection ($k_{0.4}$), is usually evaluated by push-out tests according to EN 26891 [2]. For the slip modulus k_u, the use of the secant value at 60% ($k_{0.6}$) is recommended (see for example STEP 2 [3]). However, if experimental data are unavailable, the Eurocode 5-Part 1-1 suggests the use of the formulae for timber-to-timber connections by multiplying the corresponding values of slip modulus k_{ser} by two. The slip modulus k_u may then be taken as 2/3 of k_{ser} [1]. Depending on the type of connection, this assumption may or may not be adequate, leading in some cases to too conservative or not conservative results. Ceccotti et al. [4], for example, reported a significant (50%) discrepancy between experimental and analytical properties of the connection, and recommended the use of the actual connection properties obtained from push-out tests for the design of timber-concrete composite systems.

As shear connections markedly affect the efficiency of timber-concrete composite structures, a large number of shear tests on different connection systems as well as

bending tests on composite beams have been performed worldwide [4-17]. Test results can be used in conjunction with finite element (FE) numerical simulations [18] to check whether the hypothesis of assuming the slip modulus for ULS as two-thirds of the slip modulus for SLS is adequate.

The first part of the paper presents the values of the slip moduli $k_{0.4}$ and $k_{0.6}$ as well as the ratios $k_{0.6}/k_{0.4}$ measured in experimental shear tests for different connection systems. The slip moduli $k_{0.4}$ and $k_{0.6}$ are also compared with the analytical values computed using the approximate formulae suggested by Eurocode 5. In the second part of the paper, analytical calculations are compared with bending test results and numerical simulations for different timber-concrete composite beams. The analytical calculations are carried out for loads at SLS and ULS using the formulas in Annex B of Eurocode 5 and the slip moduli $k_{0.4}$ and $k_{0.6}$, respectively. The aim of the analysis is to check whether the use of the aforementioned secant shear moduli leads to accurate results for SLS and ULS design. Finally, based on the values of the ratios $k_{0.6}/k_{0.4}$ calculated from experimental tests, the assumption of the Eurocode that k_u may be taken as 2/3 of k_{ser} is verified and if necessary improved.

2 Description of the connectors tested

The choice of an effective shear connection is the key to achieve strong and stiff composite structures. Many different connectors have been proposed thus far [4-17]. Lots of research has been performed on systems with steel fasteners such as nails, screws, dowels, etc. which are generally ductile but provide only limited composite efficiency. Steel meshes epoxy-glued into the timber and notched details cut from the timber beam were found to be very effective [5,6]. This paragraph presents some of the laboratory tests performed on connection systems in different European universities.

Table 1 Shear connector description

Type	Description of the connection system
SNP	Toothed metal plate, folded at an angle of 90°, moulded into the slab
SST+S (A)	One steel tube inserted into the concrete slab with one Ø20×120mm hexagon head coach screw
SST+S (B)	One steel tube inserted into the concrete slab with one Ø20×160mm hexagon head coach screw
SP+N (A)	Two folded steel plates embedded into the concrete slab and nailed to both sides of the glulam beam with 8 ϕ4.5×75mm nails
SP+N (B)	A single folded steel plate welded onto a long punched metal plate embedded into the concrete slab and nailed to both sides of the glulam beam with 8 ϕ4.5×75mm nails
GSP	Folded steel plate embedded into the slab and epoxy-glued into a slot milled in the glulam beam
ST+S+N	One steel tube inserted into the concrete slab and connected to the glulam beam with one Ø20×160mm hexagon head coach screw and one notch cut from the glulam beam
GDF	ϕ20×120mm dowel with flanges embedded into the concrete slab and epoxy-glued into a hole drilled in the glulam beam

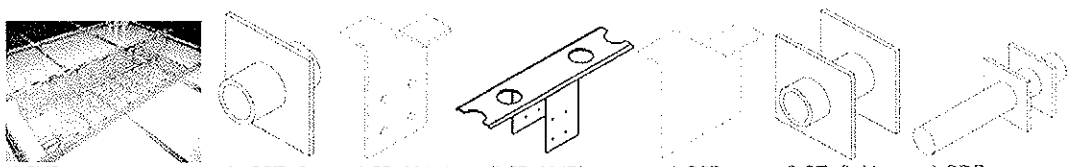

a) SNP b) SST+S (A&B) c) SP+N (A) d) SP+N (B) e) GSP f) ST+S+N g) GDF

Figure 1 Shear connectors inserted in prefabricated concrete slabs

At Luleå University of Technology, Sweden shear tests were performed on seven series of different connector types in order to assess their mechanical performance. An overall total of 30 specimens (four samples in each test batch, two samples only for the SP+N (B) connector type) were tested. Table 1 describes the type of connectors, which are displayed in Fig. 1. Full description of the test programme can be found in [7-8]. The feature of the connectors tested was that they were already embedded into prefabricated concrete slabs.

Dowel type connectors were investigated at the University of Coimbra, Portugal and at Delft University, The Netherlands. The dowel type connector consisted of a rod fabricated from steel reinforcing bars. Smooth bars were used in four tests series and corrugated bars in the rest of the tests. Three different types of timber were used: Spruce, Maritime Pine and Chestnut. Three different concrete strengths were used: a low strength/lightweight concrete, a normal strength concrete and a high strength concrete. More detailed description of the whole test programme is reported in [9]. Table 2 summarizes the push-out test programme.

Table 2 Experimental programme of push-out tests performed at the University of Coimbra, Portugal and at Delft University, The Netherlands

Type	Number of specimens	Description of the connection system
10mm A	21	ϕ10×140mm smooth bar with glulam spruce and normal strength concrete C25/30
HSC	21	ϕ10×140mm smooth bar with glulam spruce and high strength concrete C50/60
LWAC	21	ϕ10×140mm smooth bar with glulam spruce and lightweight concrete LC16/18-D1,6
C	21	ϕ10×140mm smooth bar with chestnut timber and normal strength concrete C25/30
MP	21	ϕ10×140mm smooth bar with maritime pine timber and normal strength concrete C25/30
8mm	21	ϕ8×120mm smooth bar with glulam spruce and normal strength concrete C25/30
10mm B	10	ϕ10×180mm corrugated bar with glulam spruce and normal strength concrete C30/37
INT	10	ϕ10×200mm corrugated bar with glulam spruce and normal strength concrete C30/37, with a 20mm thick timber interlayer
dVWN	10	100×100×15mm densified veneer notches and normal strength concrete C30/37
dvwNI	10	100×100×35mm densified veneer notches and normal strength concrete C30/37, with a 20mm thick timber interlayer

At the University of Coimbra, a parallel research programme was undertaken on different connector types. The push-out test programme is summarized in Table 3. A full description of the research project is presented in [10]. The experimental programmes included SFS screws (see Fig. 2), toothed metal plates and castellated profile of the timber-to-concrete interface, where the notches are constructed from high density timber pieces glued on top of the main beams (see photos in Table 3).

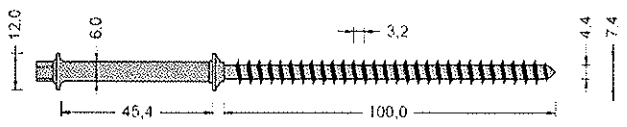

Figure 2 SFS VB 48-7.5×100 screw connector (measures in mm)

Table 3 Test programme at the University of Coimbra with screws, toothed metal plates and notch type connectors

Type	Number of specimens	Description of the connection system	Photo	Timber interlayer
B H C I V Q	39 39 24 20 23 20	SFS screws cross arranged at ±45°	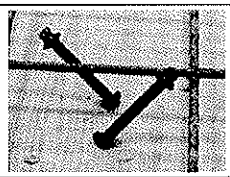	no no yes no yes no
T P S U	24 20 24 24	SFS parallel screws arranged at 45°	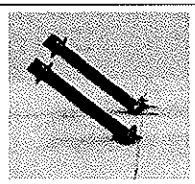	yes no yes no
A G D J	20 19 18 39	SFS screws cross arranged at ±45° with washer	-	yes no yes no
F E	6 6	20 mm notches	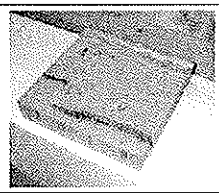	no no
M	10	Toothed metal plates		no

The laboratory test programme performed at the University of Karlsruhe, Germany included a series of direct shear tests as well as a series of short and long-term bending tests. The following connection systems were investigated:

- SFS screws cross arranged at ±45°. A total of 46 specimens characterised by different thickness of the interlayer between the concrete slab and the timber beam (0mm for type A-SCH, 19mm for type C-SCH and 28mm for type D-SCH) were tested. Fig. 3a displays the specimen type D-SCH. In the beam tests, the SFS screws were equally spaced at 200mm centre.
- Nailplates (NAG) type MNP-A with dimensions of 114×266mm, folded at an angle of 90° and moulded into the slab. A total of 46 specimens were tested. The specimen is displayed in Fig. 3b. In the beam tests, the nailplates were equally spaced at 540mm centre.
- Steel dowels and concrete notches (N+S). The 70mm diameter notches were drilled to a 30mm depth into the timber beam. The steel dowels (20mm diameter rebars) were driven in 80mm deep predrilled holes. A total of 46 specimens were tested. The specimen is shown in Fig. 3c. In the beam tests, the connectors were equally spaced at 300mm centre.

More information can be found in the report of the experimental programme [11-12].

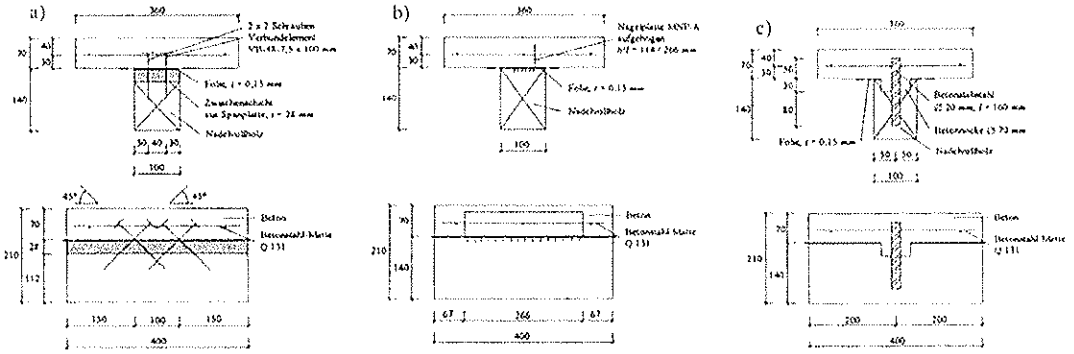

Figure 3 Direct shear test programme performed at the University of Karlsruhe: a) Screws (SCH), b) Nailplates (NAG), c) Steel dowels and concrete notches (N+S) (measures in mm)

A timber-concrete composite beam was tested for 5 years under sustained load in outdoor condition and then tested to failure at the University of Florence, Italy. The description of the experimental programme is reported in [4]. Glued-in connectors made from 18mm diameter corrugated rebars were used. The rebars were placed inside larger predrilled holes, and the gaps between the holes and the connectors were filled with epoxy resin. Two direct shear tests were performed on specimens cut from the end of the composite beam upon completion of the test to failure.

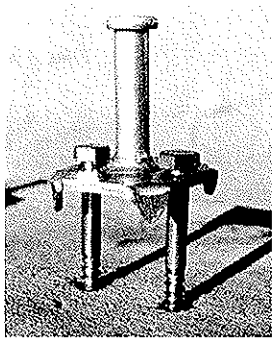

Figure 4 "Tecnaria" connector

The "Tecnaria" stud connector, see Fig. 4, was experimentally investigated at the University of Trieste, Italy. The connector is made from a 12mm diameter, 40mm long steel stud welded to a 50 mm square plate connected to the timber beam with two 10×120mm screws. Detailed report of the short- and long-term tests performed on this connector can be found in [13]. In total 18 push-out tests were performed, 9 of which with C20/25 class normal concrete slabs (NW) and 9 with concrete slabs made of L9/11 class lightweight concrete (LW).

Screw-type connectors were tested at the University of Leipzig, Germany. Detailed description of the push-out tests carried out can be found in [14]. The test configurations were as follows:

- Types A&B: two ϕ6mm diameter, 156mm long slender screws, installed at an angle of 45°. Type A screws were SFS connectors (Fig. 2) cross arranged at ±45°. Type B connector had screws with shaped shank installed in the direction of shear.
- Type C: "Tecnaria" connector (see above, Fig. 4).
- Type D: connector made from an upright steel sheet 40mm wide and 30mm high anchored in the timber beam through two 6×150mm screws at 45° angle.
- Type E: 16mm diameter connector specifically produced for the tests. The connector was a 180mm long screw with a 50mm diameter washer welded under the head.

At the University of Stuttgart, Germany, timber-concrete composite slabs with notches cut from the slab and reinforced with screws were investigated [6]. A total of 30 push-out specimens with different connection configurations were tested under short- and long-term loading. Some strips of floor were also tested to failure. The tested configurations

included connections with notches cut from the timber deck reinforced with hexagon head screws of 12mm and 16mm diameter, notches reinforced with 12mm diameter self-drilling timber screws, and notches without screws. Concrete strength classes C12/15 and C20/25 were used.

3 Shear test outcomes

The outcomes of the shear tests performed on the connectors described above are reported in this Section in terms of average shear strengths F_{max}, secant slip moduli $k_{0.4}$ and $k_{0.6}$, and ratios α between the experimental slip moduli $k_{0.6}$ and $k_{0.4}$. The analytical values of the secant slip moduli $k_{0.6}$ are also presented for those connectors where the analytical formulae suggested by the Eurocode 5 are applicable.

Table 4 Results of the direct shear tests performed at Luleå University of Technology

Type	Test results					EC5			Error
	F_{max} [kN]	$k_{0.4}$ [kN/mm]	$k_{0.6}$ [kN/mm]	α -	density [kg/m^3]	$k_{0.4,anal}$ [kN/mm]	$2k_{0.4,anal}$ [kN/mm]	$k_{0.6}$=2/3($2k_{0.4,anal}$) [kN/mm]	$k_{0.6,test}$&$k_{0.6,EC5}$ %
SNP	37.32	121.4	99.0	**0.82**	427.8	-	-	-	-
SST+S (A)	33.90	5.9	6.8	**1.15**	405.5	7.10*	14.20*	9.47*	39.3*
SST+S (B)	38.25	8.5	8.3	**0.98**	405.5	7.10*	14.20*	9.47*	14.1*
SP+N (A)	42.27	258.8	113.1	**0.43**	426.6	13.79**	27.59**	18.39**	-83.7**
SP+N (B)	39.97	5.3	3.3	**0.62**	-	-	-	-	-
GSP	64.39	248.5	183.4	**0.74**	432.7	-	-	-	-
ST+S+N	40.63	235.7	234.4	**1.01**	431.0	-	-	-	-
GDF	52.52	135.1	96.8	**0.72**	435.1	7.90*	15.80*	10.53*	-89.1*

* - $k_{0.4,anal}$ *calculated for one fastener in the connection,* ** - $k_{0.4,anal}$ *calculated for eight fasteners in the conn.*

Table 4 reports the results of the direct shear tests performed at Luleå University of Technology. The slip moduli vary from 5.3 to 258.8 kN/mm at 40% of the collapse shear load and from 3.3 to 234.4 kN/mm at 60% of the collapse shear load. The α ratios are in the range 0.43-1.15. The analytical (EC5 formulae) values of secant slip moduli $k_{0.6}$, only applicable for connectors with nails (SP+N), screws (SST+S) and glued-in dowels (GDF), are markedly different from the experimental ones (differences in the range -89.1% to 39.3%).

Table 5 Results of dowel type and notched connectors tested at the University of Coimbra and at Delft University

Type	Test results					EC5			Error
	F_{max} [kN]	$k_{0.4}$ [kN/mm]	$k_{0.6}$ [kN/mm]	α -	density [kg/m^3]	$k_{0.4,anal}$ [kN/mm]	$2k_{0.4,anal}$ [kN/mm]	$k_{0.6}$=2/3($2k_{0.4,anal}$) [kN/mm]	$k_{0.6,test}$&$k_{0.6,EC5}$ %
8mm	13.7	11.5	8.80	**0.77**	453	6.7*	13.4*	8.9*	1.6*
10mm A	22.6	15.2	11.9	**0.79**	460	8.6*	17.2*	11.5*	-3.7*
HSC	23.6	13.8	10.9	**0.80**	453	8.3*	16.7*	11.2*	2.3*
MP	25.5	24.4	20.0	**0.84**	610	13.1*	26.2*	17.5*	-12.7*
C	26.2	30.5	19.5	**0.66**	559	11.5*	23.0*	15.3*	-21.4*
LWAC	18.5	14.5	12.8	**0.79**	451	8.3*	16.7*	11.1*	-13.3*
10mm B	41.1	34.2	23.4	**0.69**	436	15.8**	31.7**	21.1**	-9.8**
INT	63.3	22.3	15.8	**0.71**	436	15.8**	31.7**	21.1**	33.6**
dvwN	138.6	304.8	318.8	**1.04**	436	-	-	-	-
dvwNl	116.2	199.9	186.9	**0.94**	436	-	-	-	-

* - $k_{0.4,anal}$ *calculated for two dowels in the connection,* ** - $k_{0.4,anal}$ *calculated for four dowels in the conn.*

Table 5 reports the results of the tests performed on notched connectors, smooth and corrugated bar fasteners investigated at the University of Coimbra, Portugal and at Delft

University, The Netherlands. For C and 10mm B connector types where, respectively, 10mm smooth and corrugated bars were used in conjunction with normal strength class concrete, the α ratio varies from 0.66 to 0.69 proving the assumption that $k_{0.6}$ can be taken as 2/3 of $k_{0.4}$. The comparison between analytical and experimental secant slip moduli $k_{0.6}$ for the aforementioned connector types leads to -21.4% and -9.8% errors, respectively. For the other configurations tested, the α ratio is higher than 2/3, and the difference between analytical and experimental values of $k_{0.6}$ is in the range -13.3% to 33.6%.

Table 6 Results of tests on screws, toothed metal plates and notched connectors performed at the University of Coimbra

Type	Test results				
	F_{max} [kN]	$k_{0.4}$ [kN/mm]	$k_{0.6}$ [kN/mm]	α -	density [kg/m^3]
B	15.4	21.0	19.5	0.93	429
H	16.4	31.8	28.0	0.88	432/429
C	15.6	19.1	18.6	0.97	430
I	14.6	31.1	29.5	0.94	430
V	17.0	20.2	18.6	0.92	430
Q	15.3	29.2	27.4	0.94	433
T	24.8	23.7	21.9	0.93	433
P	23.4	31.4	28.6	0.91	428
S	22.1	23.8	23.5	0.99	430
U	22.9	34.6	31.6	0.91	426
A	14.9	17.7	17.2	0.98	431
G	16.9	25.6	24.3	0.95	430
D	17.6	14.9	14.2	0.96	430
J	14.6	24.7	21.1	0.87	430
F	35.1	63.9	57.0	0.89	429
E	42.1	66.6	57.8	0.87	433
M	53.0	114.1	103.9	0.92	-

Table 7 Results of tests performed at the University of Karlsruhe

Type	Test results				
	F_{max} [kN]	$k_{0.4}$ [kN/mm]	$k_{0.6}$ [kN/mm]	α -	density [kg/m^3]
A-SCH	21.5	26.1	24.6	0.94	415
C-SCH	15.3	12.9	12.5	0.97	393
D-SCH	15.0	15.6	15.9	1.02	438
NAG	47.9	48.8	31.8	0.65	463
N+S	51.1	79.5	71.6	0.90	472

Push-out test results presented in Table 6 refer to connections with inclined screws, notches and toothed metal plates. The ratios α between experimental values of the secant slip moduli $k_{0.6}$ and $k_{0.4}$ varies from 0.88 to 0.99 which indicates that the shear force-slip relationship is almost linear up to failure or before significant plasticization occurs in the connection. Table 7 reports the results of the direct shear tests performed at the University of Karlsruhe, Germany. For the screwed connection (SCH) and the connection with steel dowels and concrete notches (N+S) the observed shear force-slip relationship was almost linear up to failure. For these connections the α ratio varies from 0.9 to 1.0 and is in good agreement with the tests performed at the University of Coimbra. The connection with nailplates showed an evident non-linear shear force-slip relationship. For this type of connection the α ratio was 0.65 proving the assumption that $k_{0.6}$ can be taken as 2/3 of $k_{0.4}$.

Table 8 reports the results of the push-out tests performed on the "Tecnaria" connector. The ratios α vary in the range 0.22-0.31, well below the value of 2/3 suggested by the Eurocode 5. The type of concrete did not markedly affect either the strength or to the slip moduli.

Table 8 Outcomes of the push-out tests performed on the Tecnaria connector

Type of specimen	Test results			
	F_{max} [kN]	$k_{0.4}$ [N/mm]	$k_{0.6}$ [N/mm]	α -
NW	35.1	16208	5018	0.31
LW	32.4	22138	4875	0.22
NW+LW	33.6	19442	4940	0.25

Table 9 Experimental-analytical comparison for the push-out test on the glued-in connection tested in Florence (Italy)

	Experimental	Analytical	Error %
$k_{0.4}$ [kN/mm]	25.0	14.9	-40.2
$k_{0.6}$ [kN/mm]	20.0	10.0	-50.2
α	0.80	0.67	-19.2
F_{max} [kN]	39.7	23.0	-42.2

The results of the direct shear tests performed in Florence on a specimen cut from beam No. 2 at the completion of the collapse test are presented in Table 9 together with the comparison with the analytical values. The analytical values of the glued-in rebar connection are significantly different from the experimental outcomes of the test (40-50% less). The use of the Eurocode 5 analytical formulae would therefore lead to an underestimation of the connection stiffness and strength and, consequently, to larger resistance but possible brittle failure of the composite structure [4].

Table 10 Results of the push-out tests performed at University of Leipzig

Type	F_{max} [kN]	$k_{0.4}$ [kN/mm]	$k_{0.6}$ [kN/mm]	α -
A	15.05	15.076	13.957	0.93
B	21.66	9.933	9.310	0.94
C	17.85	20.979	13.947	0.66
D	21.49	18.608	17.258	0.93
E	12.60	6.831	4.969	0.73

The results of the push-out tests performed at the University of Leipzig, Germany are reported in Table 10. Connector type E with vertical screws achieved a low stiffness even with large diameters. The ratio α is 0.73. Connector types A, B and D with inclined screws in tension were more efficient. The α ratio is larger than 0.9 confirming the outcomes of the Karlsruhe and Coimbra tests.

The outcomes of the tests performed at the University of Stuttgart on notched connections with different geometry and type of screw showed no difference if the notch edge is cut perpendicular or at an angle to the bottom of the notch. The additional insertion of a screw in the notch was found not to affect either the shear strength or the slip modulus. The shear vs. slip relationship was found to be linear almost up to failure, leading to a coefficient α equal to one. This result is also consistent with the outcomes of other tests performed on notched connectors; see for example Gutkowski et al. [5].

The outcomes of the shear tests performed on the most common shear connectors used in timber-concrete composite structures indicate that in many cases the secant slip modulus $k_{0.6}$ is significantly different from 2/3 of the $k_{0.4}$ value as suggested by the Eurocode 5 for connections between timber members. The extension of the analytical formulas for the slip modulus of timber-timber connection to timber-concrete connection suggested by the Eurocode 5 leads to fairly large differences with the experimental results, and is non conservative in some cases.

4 Experimental-analytical comparisons

This Section reports the outcomes of a number of experimental tests and numerical simulations carried out on timber-concrete composite beams with different connection systems. The purpose is to compare those values with the analytical results obtained using the Annex B formulas of the Eurocode 5-Part 1-1.

Five full-scale timber-concrete composite beams were subjected to four-point bending loading and tested to failure at Luleå University, Sweden. Both mid-span deflection v_{max} and relative slip over the support s_{max} were measured. Two beam specimens had the connection system type SST+S (B) made from inserted steel tubes (see Fig. 1b and Table 1) spaced at 250mm, while another specimen had the same type of connectors but spaced at 500mm center. The other two beams had shear connectors type SP+N (B) made from steel plates embedded in the concrete slab and nailed on the glulam beams (see Fig. 1d and Table 1) at 600mm centre. The test specimens had a span length of 4800mm. They were made from 60×1600mm prefabricated concrete slab with strength class C20/25 and

three 90×270mm glulam beams strength class GL28c spaced at 600mm centre. The collapse test results are presented in Fig. 5 for one of the beam specimens with connection type SST+S (B) and spacing 250mm. The figure illustrates the experimental total load $2P$ vs. mid-span deflection curve. In the same figure, the numerical curve obtained using a finite element model for collapse and long-term analysis of timber-concrete composite beams is also reported. In such a model, the actual non-linear shear force-relative slip relationship measured in the direct shear tests of the connection system was implemented. The detailed description of FE model used in the numerical analyses is reported in [18]. The approximating analytical curves obtained using the Annex B formulae of the Eurocode 5-Part 1-1 are plotted as well. Those curves were obtained using the experimental secant shear moduli of the connection, $k_{0.4exp}$ and $k_{0.6exp}$, at 40% and 60%, respectively, of the ultimate shear load measured in direct shear tests of the connection. The curves represent the secant stiffness of the whole composite beams, and should be used for SLS and ULS verifications as suggested by Ceccotti [3] and Ceccotti et al. [4]. The results are inside two limit curves representing the behaviour of the timber-concrete system with no connection and with rigid connection. The experimental collapse load was $2P_c$=308.17kN with a corresponding mid-span deflection of 54.53 mm. The collapse of the system occurred due to fracture in tension of the glulam beam in a cross-section with evident defects (knots).

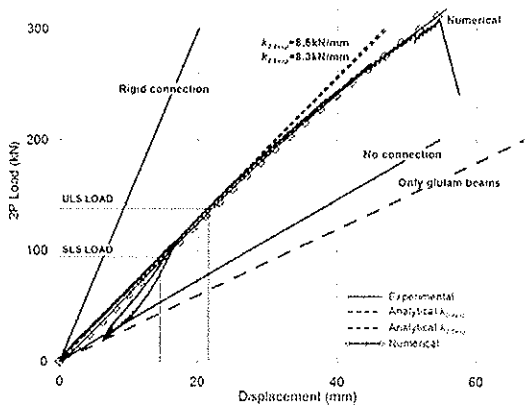

Figure 5 Total load vs. mid-span deflection during the collapse test of the beam with SST+S (A) connectors at 250 mm centre

Based on the experimental value of the collapse load, the ULS load level can be calculated using the formula [4] $2P_u=(f_k/f_m)\cdot 2P_c\cdot k_{mod}/\gamma_M$ while the SLS load level is given by $2P_s=2P_u/\gamma_Q$. The obtained load levels would be: $2P_u$=138.06kN and $2P_s$=92.04kN if the properties are assumed according to the following: characteristic strength of the glulam f_k equal to 70% of the mean strength f_m, strength modification factor k_{mod}=0.8, partial factor for material strength γ_M=1.25, and partial factor for variable actions γ_Q=1.5.

The comparison among experimental, analytical and numerical values is reported in Table 11 for both the SLS and ULS design loads. The numerical solution is very close to the experimental values, and can effectively be used to extend the experimental results to composite beams with other geometrical and mechanical properties. The numerical solution can also be used to predict quantities which were not measured during the experimental test but are needed in the design of composite beams, such as the maximum shear force in the connection, F_{conn}, the maximum stresses at the bottom fibre of the glulam beam, σ_{glulam}, and at the top fibre of the concrete slab, $\sigma_{concrete}$. The use of the analytical approach leads to accurate results since the differences with respect to the experimental and, where unavailable, numerical values (bold values in Table 11) do not exceed 10% for both SLS and ULS load levels. Table 11 reports also the analytical predictions when the slip moduli $k_{0.4EC5}$ and $k_{0.6EC5}$ calculated using the Eurocode 5

formulas are used. In this case the errors are larger (almost doubled). It is interesting to notice that the larger errors introduced by the Eurocode 5 formulas in the evaluation of the $k_{0.4EC5}$ and $k_{0.6EC5}$ values, 67% and 14% respectively (see Table 4), do not induce errors of the same magnitude on the composite beam (maximum 15%). This outcome, however, might be different in composite beams with stiffer connection system where the influence of the slip moduli on the global beam behavior is more significant.

Table 11 Analytical-experimental-numerical comparison for the beam with SST+S (B) connectors at 250 mm centre

Quantity	SLS load=92.04kN						ULS load=138.06kN					
	Exp.	Num.	Anal. $k_{0.4exp}$	Error %	Anal. $k_{0.4EC5}$	Error %	Exp.	Num.	Anal. $k_{0.6exp}$	Error %	Anal. $k_{0.6EC5}$	Error %
v_{max} [mm]	**14.41**	14.90	14.44	0.2	12.19	-15.4	**21.74**	22.14	21.82	0.4	20.91	-3.8
s_{max} [mm]	**1.23**	1.34	1.18	-4.1	1.26	2.4	**1.89**	1.98	1.76	-6.9	1.63	-13.8
$F_{conn.}$ [kN]	-	**10.40**	9.38	-9.8	11.92	14.6	-	**15.89**	14.61	-8.1	15.44	-2.8
σ_{glulam} [MPa]	-	**12.44**	12.34	-0.8	11.29	-9.2	-	**18.60**	18.57	-0.2	18.15	-2.4
$\sigma_{concrete}$ [MPa]	-	**8.47**	7.81	-7.8	7.19	-15.1	-	**12.06**	11.76	-2.5	11.29	-6.4

Table 12 Analytical-experimental-numerical comparison for the other beam specimens tested at Luleå University (Sweden), and beams with different connection systems

Connector type	Quantity	SLS				ULS			
		Exp.	Num.	Anal. $k_{0.4exp}$	Error %	Exp.	Num.	Anal. $k_{0.6exp}$	Error %
SP+N (B)* Spacing=600mm SLS=70.24kN ULS=105.37kN	v_{max} [mm]	**14.65**	14.63	15.48	5.7	**23.14**	23.70	24.92	7.7
	s_{max} [mm]	**1.47**	1.54	2.43	65.3	**2.40**	2.58	2.51	4.6
	$F_{conn.}$ [kN]	-	**9.95**	8.08	-18.8	-	**13.17**	8.35	-36.6
	σ_{glulam} [MPa]	-	**10.88**	11.48	5.5	-	**17.39**	18.00	3.5
	$\sigma_{concrete}$ [MPa]	-	**7.29**	7.19	-1.4	-	**10.39**	11.26	8.4
SST+ S (B)* Spacing=500mm SLS=88.36kN ULS=132.54kN	v_{max} [mm]	**16.85**	17.38	16.96	0.7	**23.36**	26.49	25.57	-3.5
	s_{max} [mm]	**1.60**	1.70	1.58	-1.3	**2.05**	2.62	2.34	-10.7
	$F_{conn.}$ [kN]	-	**13.56**	13.15	-3.0	-	**20.53**	19.47	-5.2
	σ_{glulam} [MPa]	-	**13.06**	13.27	1.6	-	**20.53**	19.97	-2.7
	$\sigma_{concrete}$ [MPa]	-	**8.76**	8.35	-4.7	-	**12.29**	12.57	2.3
GDF** Spacing=250mm SLS=112.90kN ULS=169.34kN	v_{max} [mm]	-	**8.02**	8.75	9.1	-	**12.67**	13.72	8.3
	s_{max} [mm]	-	**0.10**	0.21	110.0	-	**0.26**	0.31	19.2
	$F_{conn.}$ [kN]	-	**21.11**	20.39	-3.4	-	**30.84**	30.03	-2.6
	σ_{glulam} [MPa]	-	**10.32**	10.99	6.5	-	**15.53**	16.76	7.9
	$\sigma_{concrete}$ [MPa]	-	**7.08**	7.10	0.3	-	**10.50**	10.82	3.0
GDF** Spacing=500mm SLS=89.60kN ULS=134.40kN	v_{max} [mm]	-	**7.41**	7.71	4.0	-	**12.88**	12.41	-3.6
	s_{max} [mm]	-	**0.25**	0.32	28.0	-	**0.65**	0.46	-29.2
	$F_{conn.}$ [kN]	-	**30.40**	30.92	1.7	-	**41.08**	44.82	9.1
	σ_{glulam} [MPa]	-	**8.29**	9.07	9.4	-	**12.94**	14.0	8.2
	$\sigma_{concrete}$ [MPa]	-	**5.69**	5.85	2.8	-	**8.86**	9.07	2.4
GSP** Spacing=500mm SLS=84.22kN ULS=126.34kN	v_{max} [mm]	-	**8.25**	6.59	-20.1	-	**9.65**	10.32	6.9
	s_{max} [mm]	-	**0.11**	0.17	54.5	-	**0.21**	0.24	14.3
	$F_{conn.}$ [kN]	-	**31.09**	30.30	-2.5	-	**45.78**	44.66	-2.4
	σ_{glulam} [MPa]	-	**7.78**	8.23	5.8	-	**11.73**	12.54	6.9
	$\sigma_{concrete}$ [MPa]	-	**5.35**	5.32	-0.6	-	**8.01**	8.23	2.7
SNP** Spacing=600mm SLS=80.64kN ULS=120.96kN	v_{max} [mm]	-	**8.13**	7.37	-9.3	-	**14.93**	11.62	-22.2
	s_{max} [mm]	-	**0.46**	0.33	-28.3	-	**1.13**	0.48	-57.5
	$F_{conn.}$ [kN]	-	**29.92**	32.44	8.4	-	**36.20**	47.43	31.0
	σ_{glulam} [MPa]	-	**8.16**	8.37	2.6	-	**13.18**	12.81	-2.8
	$\sigma_{concrete}$ [MPa]	-	**5.66**	5.38	-4.9	-	**9.11**	8.23	-9.7
ST+S+N** Spacing=600mm SLS=110.10kN ULS=166.66kN	v_{max} [mm]	-	**8.52**	8.98	5.4	-	**13.09**	13.45	2.8
	s_{max} [mm]	-	**0.19**	0.20	5.3	-	**0.32**	0.30	-6.3
	$F_{conn.}$ [kN]	-	**49.16**	47.34	-3.7	-	**73.48**	71.05	-3.3
	σ_{glulam} [MPa]	-	**10.41**	10.98	5.5	-	**15.77**	16.47	4.4
	$\sigma_{concrete}$ [MPa]	-	**7.14**	7.09	-0.7	-	**10.72**	10.63	-0.8

**SLS and ULS design load calculated from experimental results*
***SLS and ULS design load calculated from FE numerical analysis*

Table 12 presents additional comparisons for the other beam specimens tested at Luleå University of Technology (connection types SP+N (B) and SST+S (B)). In addition, some numerical simulations were carried out in order to find the collapse loads for composite beams with the same geometrical and mechanical properties of the beam tested, but different connection systems. The ULS and SLS design loads were calculated using the same formulas introduced above. The analytical values were calculated using the slip moduli $k_{0.4exp}$ and $k_{0.6exp}$ measured in the direct shear tests and the Annex B, Eurocode 5 formulae. The comparisons confirm the accuracy of the numerical and analytical results, the latter suffering from errors generally lower than 10%. Larger errors are detected for the slip and shear forces in the connection (maximum 110% for the slip and 37% for the shear force in the connector). This is consistent with the theory on the base of the Eurocode 5-Annex B formulae, where the sinusoidal approximation of the vertical load is generally fairly good for the deflection and bending moments, but may lead to larger errors for the slip and shear force.

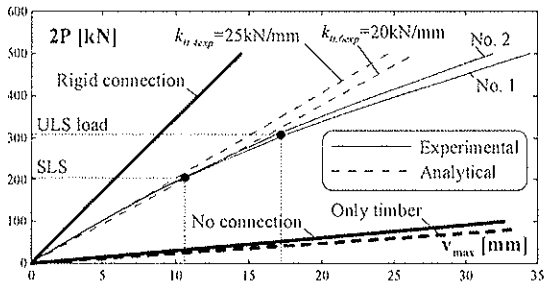

Figure 6 Total load vs. mid-span deflection during the collapse test

A 6m long timber-concrete composite beam with glued-in connectors and two glulam beams class GL24h was tested to failure in Florence (Italy). The concrete slab was characterized by a mean value of cylindrical compressive strength f_{cm}=30.4 MPa. Connector spacing was 150mm over the supports, 300mm from the support to the third points, and 450mm between the third points. The collapse occurred under a total load $2P$=500kN due to fracture in tension of the timber beam.

Fig. 6 displays the total load $2P$ vs. midspan deflection together with the theoretical limits of rigid and no connection between timber and concrete slab. The design loads for ULS and SLS, $2P_u$=307.4kN and $2P_s$=204.9kN, obtained from the collapse load as described above, are reported as well. The shear moduli of the connection as measured in the direct shear tests, $k_{0.4exp}$ and $k_{0.6exp}$ (see Table 9), were used to calculate the analytical curves based on the use of the Annex B formulas of the Eurocode 5. Those curves are used for the design at SLS and ULS. The values of the slip moduli calculated with the Eurocode 5 formulas, $k_{0.4EC5}$ and $k_{0.6EC5}$ (see Table 9) were also used to calculate the deflection, slips and stresses at SLS and ULS. The comparison is reported in Table 13. The use of the experimental shear moduli $k_{0.4exp}$ and $k_{0.6exp}$ leads to maximum errors of 30%, whereas the analytical shear moduli $k_{0.4EC5}$ and $k_{0.6EC5}$ would lead to errors of up to 50% (doubled) on deflection an stresses, and even more in terms of slips (180%).

Table 13 Experimental-analytical comparison for the collapse test of the composite beam with glued-in connectors

Quantity	SLS load 2P=204.9kN					ULS load 2P=307.4kN				
	Exp.	Anal. $k_{0.4exp}$	Error %	Anal. $k_{0.4EC5}$	Error %	Exp.	Anal. $k_{0.6exp}$	Error %	Anal. $k_{0.6EC5}$	Error %
v_{max} [mm]	10.6	10.1	-4.7	11.8	11.3	17.2	16.3	-5.2	20.4	18.6
s_{max} [mm]	0.45	0.58	28.9	1.26	180.0	0.85	1.03	21.2	1.64	92.9
σ_{glulam} [MPa]	7.9	10.3	30.4	11.1	40.5	12.2	15.5	27.0	18.1	48.4
$\sigma_{concrete}$ [MPa]	6.8	7.6	11.8	7.2	5.9	9.9	11.3	14.1	10.7	8.1

Four-point short-term bending tests to failure were performed at the University of Karlsruhe on timber-concrete composite beams with the connection systems shown in Fig. 3. The span length of the simply supported beams was 5.4 m, while the spacing between the support and the point load was 1.8 m. The timber beams consisted of 100mm wide and 200mm deep glulam beams class GL24h. The strength class C20/25 concrete slab was 600mm wide and 70mm deep. The moisture content varied between 10 and 12%. All test specimens showed a linear-elastic behaviour under service loads. At higher load levels, a non-linear behaviour due to plastic deformations of the shear connections was observed. All beam specimens failed due to fracture of the timber beams subjected to combined bending and tension. The design load for SLS and ULS was calculated using the same procedure detailed above. The connection properties $k_{0.4exp}$ and $k_{0.6exp}$ measured from direct shear tests were employed in the Eurocode 5 Annex B formulas to obtain the analytical values. The experimental-analytical comparison is summarized in Table 12 for the SLS and ULS design loads. The maximum errors on the deflection are around 25%, while the slip suffers from a larger error (up to 49%). The outcomes of the previous analyses are therefore confirmed also for these experimental tests.

Table 14 Experimental-analytical comparison for the collapse tests performed at the University of Karlsruhe

Connector type	Quantity	SLS			ULS		
		Exp.	Anal. $k_{0.4exp}$	Error %	Exp.	Anal. $k_{0.6exp}$	Error %
SCH-1 SLS=6.96kN ULS=9.48kN	v_{max} [mm]	**8.9**	11.13	25.1	**14.1**	15.25	8.2
	s_{max} [mm]	**0.31**	0.41	32.3	**0.54**	0.55	1.9
NAG-3 SLS=8.14kN ULS=11.24kN	v_{max} [mm]	**16.0**	12.78	-20.1	**26.5**	19.98	-24.6
	s_{max} [mm]	**0.79**	0.62	-21.5	**1.55**	0.79	-49.0
N+S-8 SLS=11.57kN ULS=16.38kN	v_{max} [mm]	**14.2**	15.38	8.3	**22.4**	22.31	-0.4
	s_{max} [mm]	**0.42**	0.42	0.0	**0.70**	0.59	-15.7

5 Concluding remarks

The structural behaviour of timber-concrete composite members is mainly governed by the shear connection between timber and concrete. As the shear connection is usually characterised by non-linear load-slip relationship, different values of slip moduli are adopted for SLS and ULS verifications. The slip modulus k_{ser} for SLS is usually evaluated by means of push-out tests and corresponds to the secant value at 40% of the connection shear strength. The slip modulus k_u for ULS verifications should be assumed as the secant value at 60% of the connection shear strength. For connection between timber members, however, the Eurocode 5 recommends assuming it as 2/3 of the k_{ser} value. If experimental shear test data are unavailable, the Eurocode 5 suggests the use of the formulae for timber-to-timber connections by multiplying the values of slip modulus at SLS, k_{ser}, by two. The slip modulus k_u for ULS verifications should then be taken as 2/3 of k_{ser}. The slip moduli k_{ser} and k_u are employed to design the timber-concrete composite beam at SLS and ULS using the formulae of the Eurocode 5-Part 1-1, Annex B, for composite beams with flexible connection.

In the first part of the paper, the results of shear tests performed on different types of connection systems in a number of European institutions are analysed and compared with

the simplified analytical formulae suggested by Eurocode 5 for dowel type fasteners. The second part of the paper presents a wide comparison among analytical, numerical and/or experimental outcomes for a number of composite beams. The analytical calculations are based on the use of the Annex B formulas with the shear moduli k_{ser} and k_u, whilst the numerical results were carried out using finite element software purposely developed which allows the user to implement the actual shear force-relative slip relationship for the connection. The primary conclusions are reported in the following:

- The ratios α between the experimental values of secant slip moduli $k_{0.6}$ and $k_{0.4}$ for ULS and SLS verifications varied between 0.2 and 1.15, showing significant differences from the value of 2/3 recommended by the Eurocode 5 for timber joints.
- The ratio α should be assumed equal to one for notched connection details characterized by linear shear force-relative slip relationship, and in the range 0.9 to 1 for stiff connectors such as inclined screws. The value of 2/3 seems to be appropriate for vertical screws and dowels, even though in some cases it may drop significantly (for example to 0.25 for the "Tecnaria" stud connector).
- The use of the Eurocode 5 formulae for the evaluation of $k_{0.4}$ and $k_{0.6}$ ($k_{0.4EC5}$ and $k_{0.6EC5}$) may lead to significant underestimation (up to 90%) or overestimation (up to 40%) of the experimental values.
- The use of the Annex B formulas of Eurocode 5 for composite beam with flexible connections leads to reasonably accurate solutions when the slip moduli at 40% and 60% of the shear strength evaluated in shear tests are used. The errors on deflection and stresses at both SLS and ULS design loads, in fact, do not generally exceed 10-20%. The slip and shear forces suffer from a larger error.
- The use in the Annex B formulas of the slip moduli $k_{0.4EC5}$ and $k_{0.6EC5}$ analytically evaluated leads to larger differences (20-40%, almost doubled) on deflection and stresses at both SLS and ULS.

Based on these outcomes, it is therefore recommended that the design of timber-concrete composite beams at SLS and ULS be carried out using the experimental values of the slip moduli at 40% and 60% of the shear strength, $k_{0.4}$ and $k_{0.6}$. The latter values, in fact, could be significantly different from the value of $2/3k_{0.4}$ recommended by the Eurocode 5 for connections between timber members. The analytical formulae for the evaluation of $k_{0.4}$ and $k_{0.6}$ should be used only for preliminary design since they leads to significant differences on the experimental values of slip moduli and, therefore, on the deflection, slip and stresses of the composite beam.

6 Acknowledgements

Thanks to Dr. A. Dias and Dr. L. Jorge for providing the experimental data of the shear tests performed at the University of Coimbra and University of Delft.

7 References

[1] Comité Européen de Normalisation (2003). Eurocode 5 – Design of timber structures – Part 1-1: General rules and rules for buildings, prEN 1995-1-1. Bruxelles, Belgium.

[2] Comité Européen de Normalisation (1991). Timber structures – Joints made with mechanical fasteners – General principles for the determination of strength and deformation characteristics, EN 26891. Bruxelles, Belgium
[3] Ceccotti, A. (1995). Timber-Concrete Composite Structures. In: Blass HJ et al. (ed) Timber Engineering, Step 2, 1st edn. Centrum Hout, The Netherlands.
[4] Ceccotti, A., Fragiacomo, M., Giordano, S. (2006). "Long-term and collapse tests on a timber-concrete composite beam with glued-in connection". RILEM, Materials and Structures Journal 40(1), pp. 15-25.
[5] Gutkowski, M. R., Brown, K., Shigidi, A., Natterer, J. (2004). "Investigation of notched composite wood-concrete connections". Journal of Structural engineering 130(10), pp.1553-1561.
[6] Kuhlmann U., Michelfelder, B. (2004). Grooves as shear-connectors in timber-concrete composite structures. In: 8th World Conference on Timber Engineering WCTE 2004, Lahti, Finland, 14-17 June 2004, Vol. 1, pp. 311-316.
[7] Lukaszewska, E., Johnsson, H., Stehn L. (2006). "Performance of connections for prefabricated timber-concrete composite floors". WCTE 2006, Portland OR, USA, 6-10 August 2006, CD, Paper No. 2.7.2.
[8] Lukaszewska, E., Johnsson, H., Fragiacomo M. (2007). "Performance of connections for prefabricated timber-concrete composite floors". Submitted for possible publication on RILEM, Materials and Structures Journal.
[9] Dias, A. M. P. G. (2005). "Mechanical behaviour of timber-concrete joints". Doctoral thesis, University of Coimbra, ISBN 90-9019214-X.
[10] Jorge, L. F. C. (2005). "Estruturas mistas madeira-betão com a utilização de betões de agregados leves". Doctoral thesis, University of Coimbra.
[11] Blass, H.J., Ehlbeck, J., van der Linden, M-L.R., Schlager, M. (1995). "Trag- und Verformungsverhalten von Holz-Beton-Verbundkonstruktionen". Bericht T 2710. Universität Karlsruhe.
[12] van der Linden MLR (1999) Timber-concrete composite floor systems. Doctoral thesis. Technical University of Delft, I-XVII, 1-364.
[13] Fragiacomo, M., Amadio, C., Macorini, L. (2006). "Short- and long-term performance of the "Tecnaria" stud connector for timber-concrete composite beams". RILEM, Materials and Structures Journal, Published Online.
[14] Steinberg, E., Selle, E., Faust, T. (2003). "Connectors for timber-lightweight concrete composite structures". Journal of Structural Engineering 129(11), pp. 1538-1545.
[15] Ceccotti, A. (2002). "Composite concrete-timber structures". Prog. Struct. Engng Mater. 2002; 4:264-275.
[16] Frangi, A., Fontana, M. (2000) "Versuche zum Tragverhalten von Holz-Beton-Verbunddecken bei Raumtemperatur und Normbrandbedingungen". Institut für Baustatik und Konstruktion (IBK). ETH Zürich. IBK Bericht Nr. 249.
[17] Timmermann, K, Meierhofer, U. (1993) "Holz-Beton-Verbundkonstruktionen, Untersuchungen und Entwicklungen zum mechanischen Verbund von Holz und Beton". Forschungsbericht 115/30. EMPA, Abteilung Holz.
[18] Fragiacomo, M., Amadio, C., Macorini, L. (2004). "A finite element model for collapse and long-term analysis of steel-concrete composite beams". Journal of Structural Engineering, 130(3), pp. 489-497.

INTERNATIONAL COUNCIL FOR RESEARCH AND INNOVATION
IN BUILDING AND CONSTRUCTION

WORKING COMMISSION W18 - TIMBER STRUCTURES

MODEL FOR THE PREDICTIONS OF THE DUCTILE AND BRITTLE FAILURE MODES (PARALLEL-TO-GRAIN) OF TIMBER RIVET CONNECTIONS

M Marjerrison
Department of Civil Engineering, Royal Military College of Canada

CANADA

P Quenneville
University of Auckland

NEW ZEALAND

MEETING FORTY

BLED

SLOVENIA

AUGUST 2007

Presented by P. Quenneville
E. Gehri questioned about the stiffness of timber rivet connection as the member width is wide and would have considerable moment. He questioned the ductility of the connection in relation to its low moment capacity as the uni-tension capacity is rather large. P. Quenneville said that the moment capacity of these connections is not considered in design.
H. Blass discussed the ductile failure mode. In the timber to timber failure implied limited embedment strength for the steel is considered whereas in Eurocode 5 the embedment strength of steel plate is considered as infinite. H. Blass commented that both loads parallel and perpendicular to grain need to be considered. P. Quenneville agreed.
I. Smith commented that in Saskatchewan one building had connections where over 1000 rivets were used and it carried moment successfully. P. Quenneville discussed that they might have behaved like a punch metal plate.
A. Jorissen received clarification that the Canadian code is on the unsafe side.
V. Rajcic received clarification about current Canadian design procedures with timber rivets.

MODEL FOR THE PREDICTIONS OF THE DUCTILE AND BRITTLE FAILURE MODES (PARALLEL-TO-GRAIN) OF TIMBER RIVET CONNECTIONS

Matthew Marjerrison[1] and Pierre Quenneville[2]

[1] MScA. graduate, Department of Civil Engineering, Royal Military College of Canada, P.O. BOX 17000, STN FORCES, Kingston (ON) K7K 7B4, Canada.

[2] Professor of Timber Design, Department of Civil and Environmental Engineering, University of Auckland, Auckland, New Zealand. p.quenneville@auckland.ac.nz

1 Introduction

The timber rivet is the only fastener within the Canadian design standard for which a set of design equations for both ductile and brittle failure modes is given. Available to the designers are two design equations: one for the brittle failures due to a combination of longitudinal shear and tension stresses, and the other one for the ductile failure mode. To cover the wood failure modes, design tables are provided to determine the brittle failure resistance for a variety of possible timber rivet group configurations. Over the years, the introduction of new factors such as the wood species or the thickness of the steel plates has resulted into the addition of modification factors to the design equations. Recently, with the introduction of the timber rivets on the American market, US researchers have proposed a rational design approach to predict the resistance for both ductile and brittle failure modes. The design equations to predict the ductile failures is a truncated set of the EYM equations. The design equations for the prediction of the brittle failures in the wood are based on the material shear and tension resistances and on their failure corresponding areas.

In parallel to the timber rivet studies, work in Europe on the brittle failure of nailed timber connections has resulted in similar failure modes. Based on all of the previous work and extrapolating from work done on bolted connections for brittle failure modes, a rational approach has being developed. In this paper, comparison of the various methods is made and differences in assumptions and results are highlighted.

2 Background

One of the fasteners covered in the Canadian wood design standard CAN\CSA O86 [3] is the timber rivet. The rivet is a hardened nail, ranging in lengths of 40, 65 and 90 mm and with an oval cross-section of 3.2x6.4 mm and a head shaped as a wedge. Rivets are used exclusively with perforated steel plates (holes of 7 mm) with a minimum thickness of 3.2 mm. Rivets are nailed with their flat side parallel to the grain to minimize wood fibres damage. They offer the main advantages that their installation can be done on site to accommodate final adjustments and that no pre-drilling is necessary. Because of their shape, the rivet connection is very stiff and a ductile failure can be easily achieved. Figure 1 below illustrates the shape and use of the rivet.

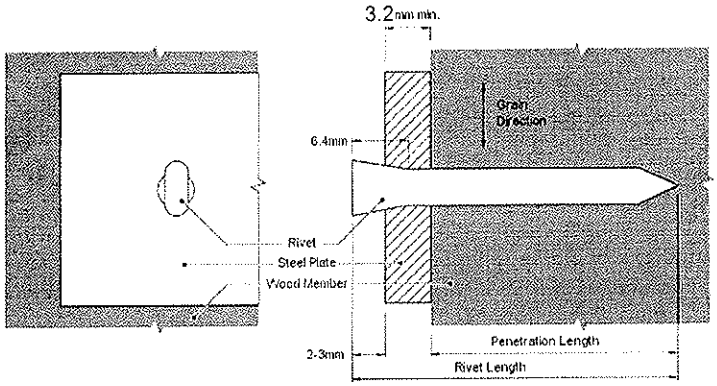

Figure 1 – Timber rivet and parameters

Much of the development work has been carried by Foschi [4] on rivet connections using 6.4 mm side plates. Foschi and Longworth [5] then provided the required design equations to predict the resistances of ductile and brittle failure modes. These equations were first developped for rivets in Douglas Fir glulam. Fox and Lincoln [6] then proposed a modification factor to account for the potential use of 3.2 mm thick steel side plates.

Karacabeily and Fraser [8] then investigated the use of rivets in spruce glulam and in Douglas Fir sawn lumber. They observed a difference in the ductile failure resistance for the Spruce glulam in comparison to the Douglas Fir one. They proposed to account for this difference through a material modification factor. Then, Karacabeyli et al. [9] further looked at the effect of material by testing rivets in sawn lumber. Following their proposal, the design procedure for rivet connections was updated and remained unchanged since.

Essentially, designers have two equations to check; one for a ductile failure mode and another one for brittle. The one for the ductile failure is simply:

$$P_y = (1.09 L_p^{0.32}\ n_R n_C)\ J_Y H \qquad (1)$$

Where L_p is the rivet penetration in the wood, n_r and n_c are the number of rivet rows and rivets per row respectively, J_y is the side plate thickness modification factor and H is the material factor. The equation to determine the resistance of the brittle failures is:

$$P_w = p_w H \qquad (2)$$

Where p_w is the resistance value obtained from tables within the standard. There are over 9 pages of tabulated values to account for the various rivet connection configurations. These values were obtained from finite element analysis by Foschi and Longworth [5]. Although numerical spreadsheet manipulations allow designers to obtain design values readily for various connection configurations, designers do not get the feeling of the effect of each variables involved in the design.;

Buchanan and Lai [2] set out to investigate the behaviour of the connections using Radiata pine from New Zealand. They compared their results with other wood species and the predictions of the Canadian, US, and European codes. They found that the European yield theory gave excellent predictions of glulam rivet strength for ductile failure modes.

The research by Stahl et al. [13] was done to improve on three shortcomings of the analysis of timber connections adopted by the Canadian and U.S. wood codes: first, the complexity of the wood failure mode analysis requires using tabular data resulting in no closed form

design equations; second some of the results of the wood failure mode analysis have not been adequately verified with sufficient testing and third, the European yield model (EYM) describing failure as a combination of fastener yield and wood bearing has been accepted for use with all other dowel type fasteners. They improved on the EYM analysis of ductile failures suggested by Buchanan and Lai [2], and followed the design laid out by Quenneville and Mohammad [12] for the wood failure of bolted timber connections. Their design procedure predicts how a block of wood bound by the array of fasteners will be torn away from the timber. Stahl et al. [13] proposed 3 modes of wood block failure.

The capacity of each block is determined by multiplying the shear and tensile strength values of wood by their corresponding areas. The overall connection would be taken as the minimum strength of the three modes. Stahl et al. assumed that only three of the EYM failure modes apply to timber rivet connections. Their assumption was that if the minimum plate thickness requirements were followed, the rivet head would always remain fixed. Although this may be true, the EYM can be adjusted to calculate the reduction in strength due to the thinner plates instead of enforcing a thickness minimum. The 3 modes utilized in Stahl's method are illustrated below in Figure 2. The upper member represents the steel plate, and the bottom represents the wood member.

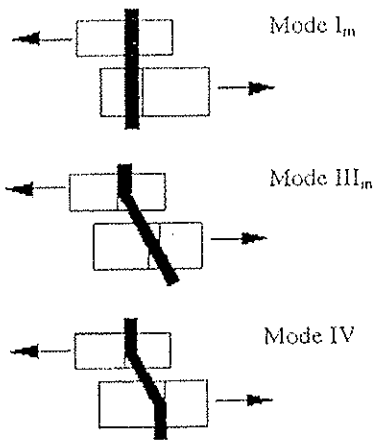

Figure 2 - Potential ductile EYM failure modes in Stahl et al. [13] approach

The wotk by Stahl et al. [13] has shown that a simple and rational method can be developed for the design of timber rivet connections; using the EYM to predict ductile failure modes and material shear and tension resistances multiplied by their corresponding areas for the prediction of brittle failures. Concurrently, Johnsson [7] studied the occurrence of brittle failures in nailed steel-to-wood connections. She used 4 mm diameter annular ringed shank nails with a penetration of 40 mm. Her conection configurations were such that the brittle failure modes were forced in order to observed them. She proposed a set of design equations to predict the plug shear failures, which are :

For p/H <0.5: $$R_{plug} = \max\begin{cases} b \cdot l \cdot f_v & \text{where } f_v = K \cdot (b \cdot l)^{-0.25} \\ b \cdot p_{ef} \cdot f_t \end{cases} \quad (3)$$

For p/H ≥0.5: $$R_{plug} = b \cdot p_{ef} \cdot f_t$$

Where p is the penetration depth, H is the member thickness, R_{plug} is the resistance, b is the plug width, l is the joint length, p_{ef} is the effective penetration depth, f_v and f_t are the shear and tensile strengths and K is a constant. Eventhough the stiffness of the fasteners are different, the wood failure modes are similar and resistances will be compared.

In order to improve on the method proposed by Stahl et al. [13], the following modifications are proposed in an attempt to provide an improved approach, consistent with the other dowel-type fasteners of the Canadian code [xx]. These modifications are:

a. Using the full version of the EYM to account for oval shaped rivets and reduction in plate thickness to estimate ductile failure resistances;
b. Calculation of effective end distance for brittle wood failures; and
c. The addition of a fourth brittle failure mode to account for a full tension failure of the member.

To assess the effectiveness of the proposed method in comparison to O86-01, Stahl et al. and Johnsson equations, all of the available tests results from the litterature were used. Marjerrison [11] lists all of the various sources, connection configurations, resistances and failure modes. Also, in order to complement on the available test data, 8 groups of rivet connections (5 replicates per group) were tested by Marjerrison. They were essentially of 40 and 65 mm rivets with a grid spacing of 25 mm. Details of the testing can be obtained from Marjerrison [11].

3 Proposed Approach

The proposed method of calculating brittle wood capacities using tensile and shear strengths multiplied by the corresponding areas as proposed by Stahl et al. [13] is a simple and rational approach. It has also been shown to work effectively with the limited testing available. Alterations made to both of the brittle and ductile design equations proposed by Stahl et al. [13] in order to best suit test data and adapt them for use in the Canadian standard are explained in detail in the next sections.

3.1 Calculation of Ductile Capacity

To cover all ductile modes, including the ones where the rivet head may rotate, the full set of the EYM equations are used. These are then modified to account for the rivet cross-section. Thus, the ductile resistance of a rivet connection is given by equation (4), which is:

$$P_y = \min \begin{cases} P_{ua} = f_s d t_s \\ P_{ub} = f_w d L_p \\ P_{uc} = \dfrac{f_s d L_p}{(1+2\beta)}\left(\sqrt{2\beta^2(1+\beta)+\dfrac{4\beta(1+2\beta)M_y}{f_s d L_p{}^2}}-\beta\right) \\ P_{ud} = \dfrac{f_s d t_s}{(2+\beta)}\left(\sqrt{2\beta^2(1+\beta)+\dfrac{4\beta(2+\beta)M_y}{f_s d t_s{}^2}}-\beta\right) \\ P_{ue} = \dfrac{f_s d t_s}{(1+\beta)}\left(\sqrt{\beta+2\beta^2\left[1+\dfrac{L_p}{t_s}+\left(\dfrac{L_p}{t_s}\right)^2\right]+\beta^3\left(\dfrac{L_p}{t_s}\right)^2}-\beta\left(1+\dfrac{L_p}{t_s}\right)\right) \\ P_{uf} = \sqrt{\dfrac{2\beta}{1+\beta}}\sqrt{2M_y f_s d} \end{cases} \quad (4)$$

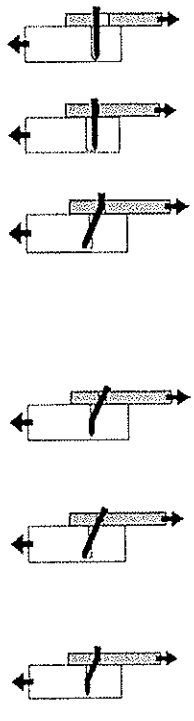

* Each equation must be multiplied by $\frac{n_r n_c n_p}{1000}$ to obtain full connection strength in kN.

Where: f_s = embedment strength of the steel plate (MPa) = $3.0 F_u$

f_w = embedment strength of the wood member (MPa) = 120 G $d^{-0.3}$

d = dimension of timber rivet perpendicular to the load component (mm)

t_s = thickness of the steel plate (mm)

β = ratio of f_w/f_s

M_y = fastener yield moment (N·mm) = $\sigma_y Z$

F_u = ultimate tensile strength of side plate (MPa)

σ_y = apparent yield strength of the rivet in bending = 900 MPa

Z = plastic section modulus (mm^3) = $\frac{db_r^2}{4}$

b_r = dimension of timber rivet parallel to load component (mm)

The complete set of equations has been shown to predict the effect of reducing the thickness of the steel side plate. For thin steel plates, the rivet head is no longer fixed rotationally, as observed by Fox and Lincoln [xx] and modes *d* or *e* govern the resistance.

3.2 Calculation of Brittle Capacity

The brittle design method proposed by Stahl et al. [13] has been modified slightly in the new proposed method. The calculation of areas has changed. The areas for the new method are outlined in Figure 4. The white areas represent the area in tension while the lightly shaded areas represent the resisting area in shear.

An extra mode (Mode 4) describing failure of the timber specimen entirely in tension has been added. The effective loading area in shear has also been reduced to reflect the results of from research in the field of bolted connections as reported by Bickerdike and Quenneville [1], and on the observation that Stahl et al.'s predictions overestimate the strength for connections with large end distances. As for bolted connections, shear forces are assumed to extend past the last rivet only for a distance of 1 rivet row spacing instead of to the end of the member. Shear forces from each rivet can be considered to be taken up by 1 rivet spacing worth of wood. The neglected wood in the end section will only experience loading after a shear redistribution takes place due to failure around the rivets. Much like Stahl et al.'s method, the capacity of each block is determined by multiplying the shear and tensile strength values of wood by their corresponding areas. The overall connection is still taken as the minimum resultant strength of the 4 modes. The capacity of the rivet group P_w in the timber is taken as the minimum of P_1, P_2, P_3, and P_4.

$$P_1, P_2, P_3, P_4 = \frac{\tau_{ult} A_v}{C_v} + \frac{\sigma_{ult} A_t}{C_t} \qquad (5)$$

Where: τ_{ult} = ultimate strength in shear parallel to grain = $16600G^{0.85}/1000$

σ_{ult} = ultimate strength in tension parallel to grain = $170700G^{1.01}/1000$

$A_{v,t}$ = area in shear, and area in tension for Modes 1, 2, 3 and 4, as determined in Figure 4.

P_1, P_2, P_3, P_4 = capacity of each mode to resist shear and tension forces according to the diagrams in Figure 4.

C_v, C_t = shear and tension factor

Mode 1

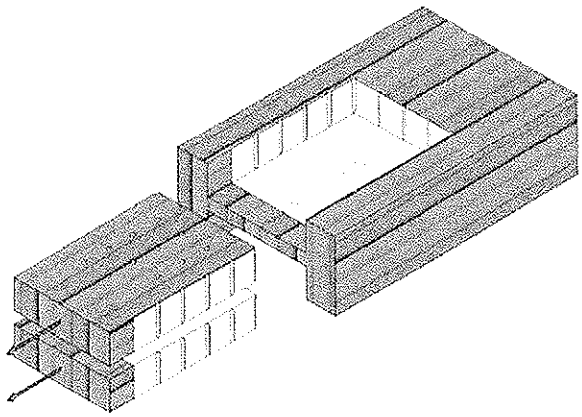

$$A_v = \{[(n_r\text{-}1)s_q n_c s_p]+2L_p(n_c s_p\text{-}6.4n_c)\}$$

$$A_t = n_p\{L_p[(n_r\text{-}1)(s_p\text{-}3.2)]\}$$

Mode 2

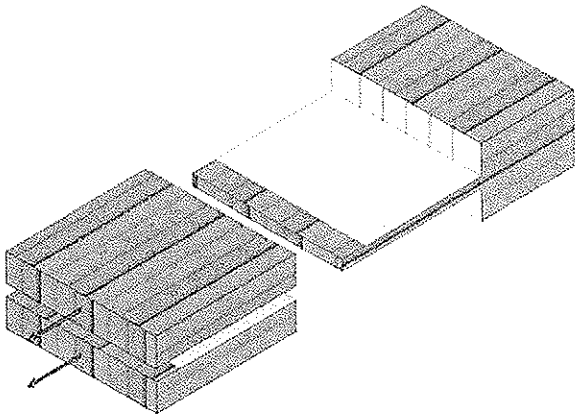

$$A_v = n_p w n_c s_p$$

$$A_t = n_p[L_p(w\text{-}3.2n_r)]$$

Mode 3

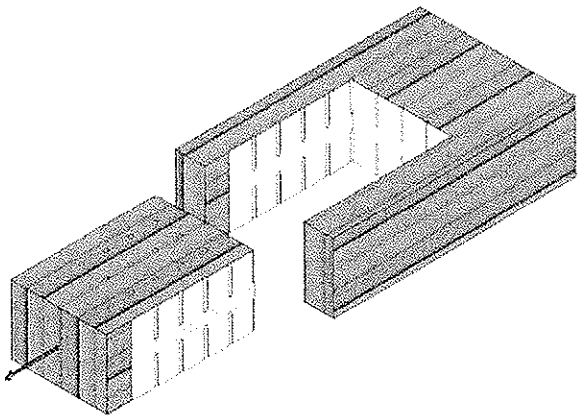

$$A_v = 2(bn_c s_p\text{-}6.4n_p L_p n_c)$$

$$A_t = (n_r\text{-}1)[bs_q\text{-}3.2L_p n_p(n_r\text{-}1)]\}$$

Mode 4

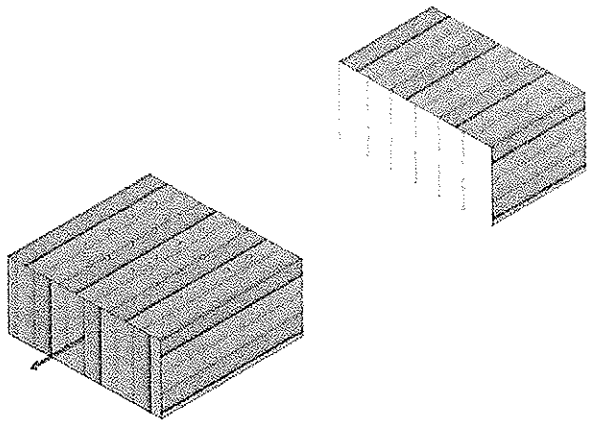

$$A_v = 0$$

$$A_t = bw$$

Figure 4 – Diagrams of possible brittle failure modes in proposed approach

4 Analysis and Discussion

To date, limited test data has made it difficult to evaluate the effectiveness of newly proposed rivet connection design methods. The equations developed by Foschi [4] have

stood the test of time. The constants and factors, which have been applied over decades, have safely enabled the engineers to obtain a good estimate of the connection strength. The proposed design method however is able to accurately predict the strength and failure mode of timber rivet connections in a simpler, more understandable way without requiring the use of tables taking up pages of the code. Using the proposed design method, predictions of the mean ultimate strength and type of failure mode were made for all of the tested group configurations, including the new test data available, as reported in Marjerrison [11]. The results were compared with predictions made using the O86-01 Standard [3] and predictions made by the method developed by Stahl et al [13].

The available tests data (Marjerrison, [11]) were separated into two groups: those that had definite brittle failures, and those that had definite ductile failures. The tests exhibiting mixed failures (including all of the new RMC test data) were set aside at this point. These data points were used to determine the effectiveness of the EYM in predicting the ductile failures. Shown in Figure 5 is a comparison of resistance predictions made using O86-01, Stahl et al.'s use of the truncated EYM and the proposed use of the full set of EYM equations. All strength predictions are for test duration and mean values assuming a normal distribution and a COV of 0.1 for ductile failures.

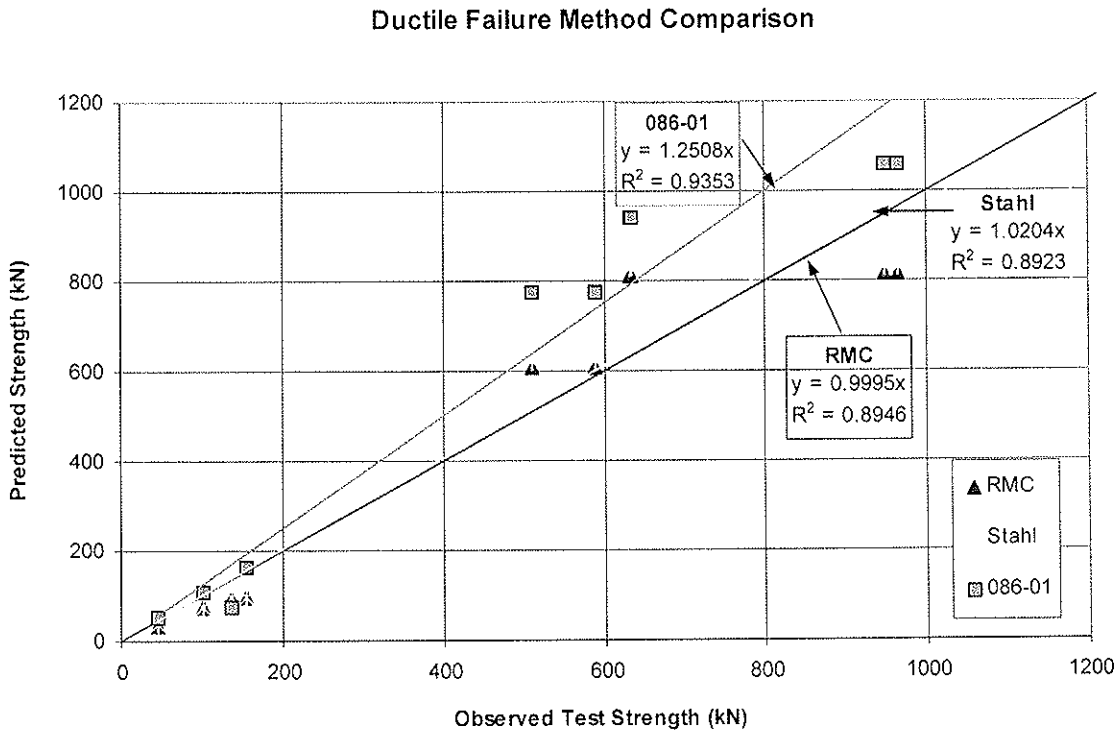

Figure 5 - Comparison of Ductile Failure Methods

Using these coefficients of variation, the O86-01 standard has a correlation coefficient of 0.935 but an average absolute error of 18.1%. Stahl et al.'s method performs very similarly to the proposed method for ductile predictions and the difference is insignificant.

The proposed design approach was also used to predict the strength of 20 available test groups exhibiting brittle failures. Predicted strengths are plotted against the observed strengths from testing in Figure 6. To optimize the predictions of the specimens that failed in a brittle manner, a value of 4 has been used for C_v and C_t. The use of this value resulted in σ_{ult} and τ_{ult} average values of 20.8 MPa and 2.26 MPa respectively for Douglas-fir. Assuming a normal distribution and COV values of 0.2 for brittle failures, the resulting apparent specified values of σ_{ult} and τ_{ult} would be 14.0 MPa and 1.52 MPa. The O86-01

specified values for D-fir glulam are 15.3 MPa and 2.0 MPa. This graph is only used to show the adequacy of the predictions using any rationale method vs. the predictions using O86-01. It should be noted that to optimize the O86-01 predictions, a COV of 0.05 would be required, making it very unlikely. Thus, the O86-01 wood failure predictions should be used with caution as they are on the un-safe side.

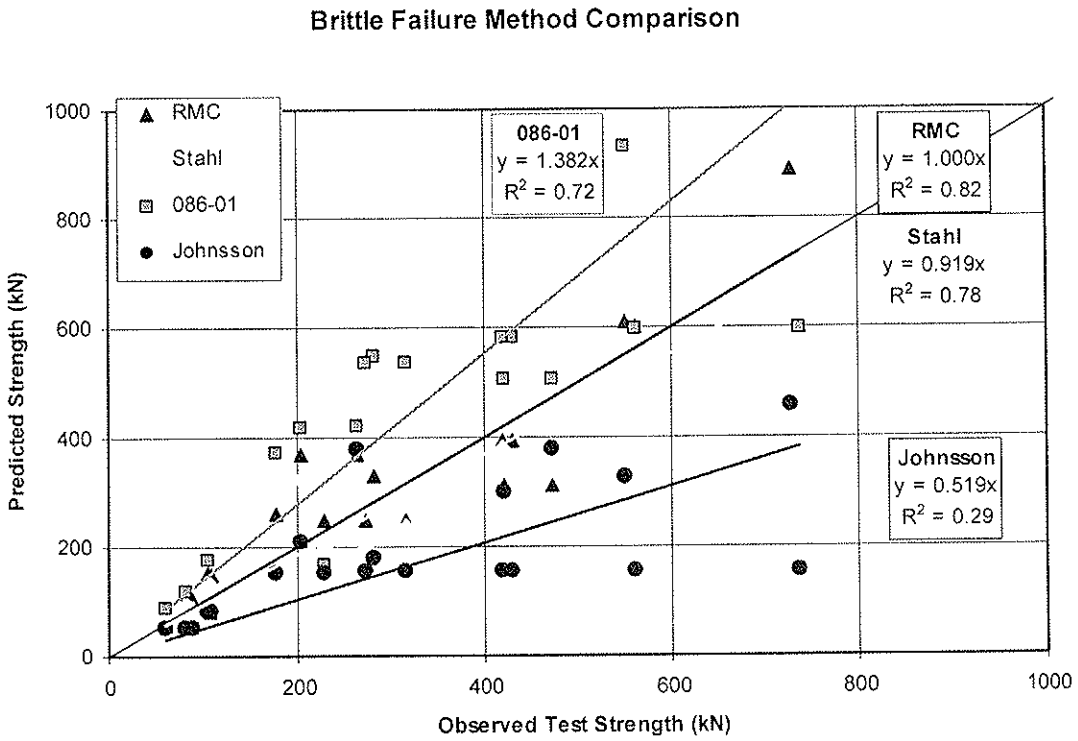

Figure 6 - Comparison of Brittle Failure Modes

The predictions using Johnsson's [7] equations yielded predictions that were generally 50% lower than test values. For most of the connections configurations, Johnsson's shear stress equation governed the resistance. It did not have the flexibility required for a lot of the cases where the only variable was the length of the rivet. Thus the entire effect of the penetration of the fastener (and of this rigid one specially), is not taken into account.

4.1 Combination of ductile and brittle

By combining the two sets of ductile and brittle equations together, a full connection design verification becomes possible. Each method must now be capable of predicting the type of failure mode in addition to the ultimate strength. The omitted tests available in the litterature (all the groups in which some specimens failed in either a ductile or brittle manner) have been introduced for a comprehensive comparison. The configurations that have been added are reported by Marjerrison [11]. Shown on Figure 7 are the minimum strength predictions (of brittle and ductile) vs. test results using the proposed approach.

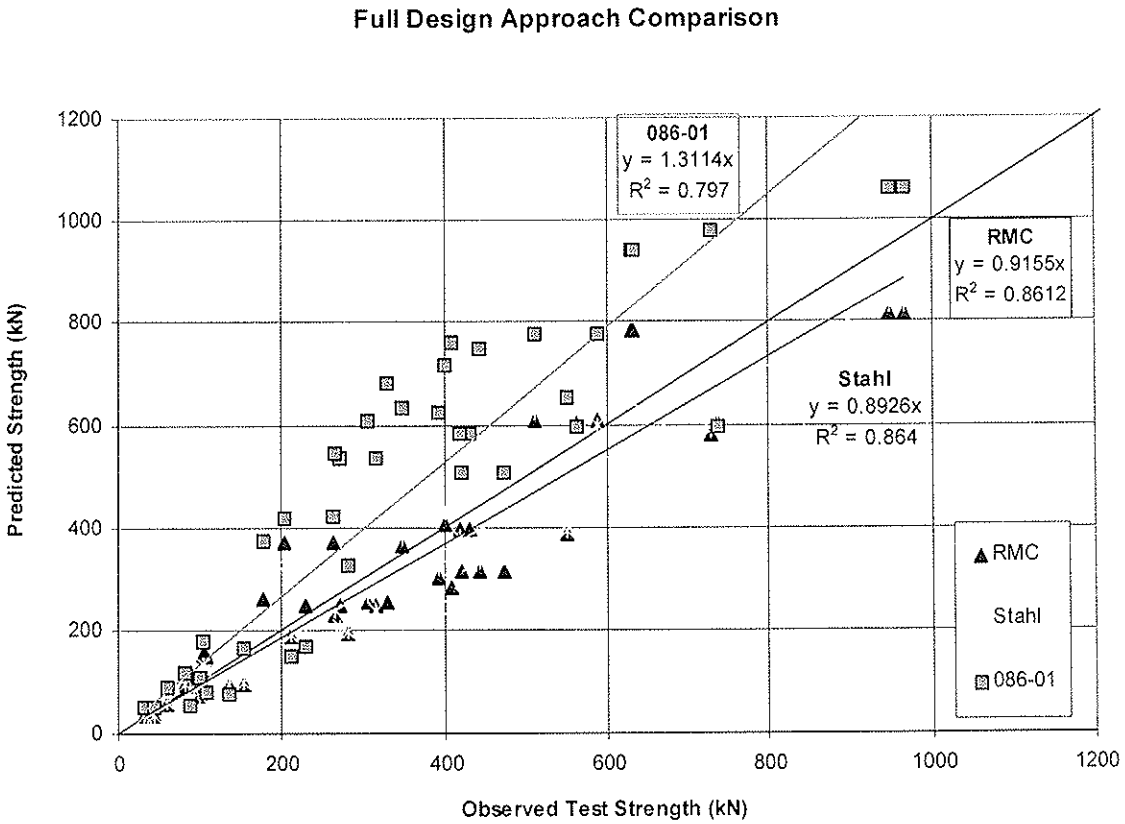

Figure 7 - Comparison of O86-01, Stahl et al.'s and the proposed method predictions

One last comparison is made by arbitrarily choosing a selection of design examples and comparing the outcomes using the current code with the newly proposed analysis. This can provide a general idea of how similar the methods are in practice. The chosen rivet configurations are shown in Table 1 below.

Table 1 - Design Examples of two plates connections in D-fir glulam

Design example	member size	# of rows	row spacing	# of columns	column spacing	rivet length	plate thickness	Predictions Proposed Method		O86-01 Predictions	Ratio
Symbol	*bxd*	n_R	s_q	n_C	s_p	L_r	w_p	5th% Brittle	5th% Ductile	5th % Strength	
Units	(mm)		(mm)		(mm)	(mm)	(mm)	(kN)	(kN)	(kN)	
1	80x228	6	25	6	25	40	6.4	**124.2**	136.9	141.0 D[1]	0.88
2	80x228	6	25	6	40	40	6.4	141.7	**136.9**	141.0 D	0.97
3	130x456	4	25	4	40	65	6.4	140.5	**79.4**	75.7 D	1.05
4	130x456	10	25	10	25	65	6.4	**352.4**	496.0	420.0 W	0.84
5	130x456	10	25	10	40	65	6.4	**399.8**	496.0	468.0 D	0.85
6	215x456	10	25	10	25	90	6.4	561.0	**515.0**	480.0 W	1.07
7	215x456	6	25	16	40	65	6.4	**473.7**	476.1	454.0 D	1.04
8	215x456	16	25	6	25	65	6.4	570.5	**476.1**	408.0 W	1.17
9	215x456	10	25	10	25	65	3.2	445.9	**410.7**	384.0 W	1.07
10	215x456	10	25	10	25	65	9.6	**412.1**	478.1	480.0 W	0.86

(1) W is for wood failure and D is for ductile failure governing the connection resistance.

In this comparison, 5th percentile strength values were computed. Of the example analyzed by Marjerrison [11], an average absolute error of -3.8% was obtained between the two methods, while 20/26 of the samples experienced the same failure mode. Three of the resulting brittle wood failure predictions (examples 9, 10, and 16) were governed by full tension through the member. A ratio of the proposed method strength predictions divided by the O86-01 predictions was calculated. Values are only used to show the variability of the two predictions. Ultimately, the method that best predicts the tests results should be used in the standard.

5 Conclusions

The proposed design method accomplishes the goals initially set.. A simple and rational design approach is proposed and which has been shown to give adequate predictions of mean test duration ultimate strengths, while improving on the proposal of Stahl et al. [13] in in the prediction of the potential ductile failures. This method eliminates the need to design using tabulated values and has been created in such a way that it should be easily implemented into future code standards. In addition, the proposed method takes into consideration many factors such as plate thickness and specific gravity of various wood species allowing it to be used over a broad spectrum of connection configurations. In the future, more testing should be done using various grades and species of sawn timbers to verify the effect of the material.

6 References

[1] Bickerdike, M., and Quenneville, J.H.P. 2006. Predicting row shear failure mode in parallel-to-grain bolted connections. Proceedings of the 9th World Conference on Timber Engineering, Portland, Oregon, 8 p.

[2] Buchanan, A.H. and Lai, J.C. 1994. "Glulam rivets in radiata pine", Canadian Journal of Civil Engineering. 21. pp. 240-250.

[3] CSA O86-01. 2001. Engineering design in wood. Canadian Standards Association, Canada.

[4] Foschi, R.O. 1973. "Stress analysis and design of Glulam rivet connections for parallel-to-grain loading of wood", Report VP-X-116. Western Forest Products Laboratory, Vancouver, B.C.

[5] Foschi, R.O., and Longworth, J. 1975. "Analysis and design of griplam nailed connections", Journal of the Structural Division, 101(ST12) pp. 2537-2555.

[6] Fox, S.P., and Lincoln, R.G. 1979. "Effect of plate and hole size on griplam nail load capacity", Canadian Journal of Civil Engineering, 6(3) pp. 390-393.

[7] Johnsson, H. 2004. "Plug Shear Failure in Nailed Timber Connections – Avoiding Brittle and Promoting Ductile Failures", Doctoral Thesis, Lulea University of Technology, pp. 182.

[8] Karacabeyli, E., and Fraser, H. 1990 "Short-term strength of Glulam rivet connections made with Spruce and Douglas fir Glulam and Douglas fir solid timber", Canadian Journal of Civil Engineering, 17 pp. 166-172.

[9] Karacabeyli, E., Fraser, H. and Deacon, W. 1998. "Lateral and withdrawal load resistance of glulum rivet connections made with sawn lumber", Canadian Journal of Civil Engineering, 25 pp. 128-138.

[10] NDS-1997. 1997. National Design Specification (NDS) for wood construction. American Forest & Paper Association, Inc., United States of America.

[11] Marjerrison, M. 2007. "Analysis of Timber Rivet Connections Loaded Parallel-to-grain". MscA Thesis, Civil Engineering Dept, Royal Military College of Canada, Kingston, Canada, 116 p.

[12] Quenneville, J.H.P., and Mohammad, M. 2000. On the failure modes and strength of steel-wood-steel bolted timber connections loaded parallel-to-grain. Canadian Journal of Civil Engineering. Vol. 27, pp. 761-773.

[13] Stahl, D.C., Wolfe, R.W. and Begel, M. 2004. "Improved analysis of timber rivet connections", Journal of Structural Engineering, Vol 130(8) pp.1272-1279.

INTERNATIONAL COUNCIL FOR RESEARCH AND INNOVATION
IN BUILDING AND CONSTRUCTION

WORKING COMMISSION W18 - TIMBER STRUCTURES

CREEP OF TIMBER AND TIMBER-CONCRETE JOINTS

J W G van de Kuilen
Delft University of Technology
THE NETHERLANDS
CNR Trees and Timber Research Institute
ITALY

A P M G Dias
Coimbra University

PORTUGAL

MEETING FORTY

BLED

SLOVENIA

AUGUST 2007

Presented by J. W. G. van de Kuilen
V. Rajcic commented that on the concrete timber structure testing and suggested that may be one should consider cyclic loading. J.W. van de Kuilen replied that it would complicate matters.
S. Thelandersson commented about designing for permanent loads and the concept of time averaging of load to predict creep behaviour.
I. Smith asked where are these creep factors used. J.W. van de Kuilen responded that the factors can be used with MOE for both concrete connections and timber.

Creep of timber and timber-concrete joints

J.W.G. van de Kuilen
Delft University of Technology NL / CNR Trees and Timber Research Institute IT
A.P.M.G. Dias, Coimbra University, PT.

Abstract
According to the EC5, the additional deformation of joints at long term shall be calculated as the short term deformation multiplied by the deformation factor (k_{def}). The short term deformation shall be determined based on the slip modulus of the joint (K_{ser}). The slip modulus of the joints may be obtained either from the models given in Eurocode 5 for some types of joints, or alternatively, from experimental tests in accordance with EN26891. In experimental tests the long term deformation is related to the short term deformation through the creep factor of the joints, and is determined relative to the initial deformation. In this situation the deformation factor from Eurocode 5 and the creep factor of the joints have an equivalent meaning. An essential difference is the determination of the short term deformation. In EC5 it is based on the joint slip modulus, while in the creep tests it is usually taken the initial deformation. In the tests considered here, the initial displacement was taken after 10 minutes after the loads are applied.
In this paper a detailed analysis is made on the determination of joints long term deformations in both situations: based on the creep factor determined from creep tests and based on the Eurocode method. These results are available from a large number of long term tests on timber-timber and timber-concrete joints. These tests have been performed at Delft University of Technology and at the University of Coimbra. Various types of fasteners have been used and both climate controlled and uncontrolled conditions have been considered. The influence of climatic aspects on the long term deformations is also discussed and a proposal for creep factors for different duration of load classes is made.

1. Introduction

In this paper test results of creep tests with nailed, toothed-plate, split-ring timber joints and timber-concrete joints with dowel-type fasteners are presented. Tests in a varying climate were initiated by Kuipers in 1983. The specimen codes mentioned in this paper relate to the specimen number and location according to Kuipers and Kurstjens [1986] and Van de Kuilen [1999]. The tests made with dowel-type-fastener timber concrete joints were carried out in Delft Technology University and Coimbra University, further details on the specimens sizes and geometries can be found in Dias [2005].

The results from these tests will be used to determine the creep rate and how and to what extent the climate variations lead to additional creep, the so called mechano-sorptive creep. Mechano-sorptive creep is defined as the additional deformations induced during the combined action of environmental (mainly moisture) actions and mechanical loads.

Finally, a derivation method is given to relate the creep factors measured in the tests to creep factors which can be used in design codes such as Eurocode 5. The creep factor k_{def} is defined as:

$$k_{def} = \frac{\varepsilon - \varepsilon_0}{\varepsilon_0} \quad (1)$$

Consequently, the total deformation or slip can be calculated as:

$$\varepsilon = \varepsilon_0 (1 + k_{def}) \quad (2)$$

2 Creep tests

Nailed joints in an uncontrolled environment

The basic analysis and parameter estimation is performed with the results of the tests which were

started in 1984 [Kuipers and Kurstjens, 1986]. The creep results that are reported here are creep tests running for almost 5000 days by 1997 at constant load levels of 30%, 40% and 50% of the average short term strength. The creep factor for nailed joints after 4800 days varies for the 30% between 2.6 and 3.8, for the 40% joints between 3.3 and 4.4, and between 3.4 and 4.6 for the 50% loaded joints. It can be concluded that there is no conclusive evidence that the creep can be considered non-linear as a result of the mechanical load. The small non-linearity could easily have been caused by the variations in relative humidity, causing a shift of the creep function to the left. Since there is a difference of about a month between the start of each string, it is likely that the time difference between the start and the first moisture change has resulted in a small shift. It is however known that at higher load levels (above 60%) the non-linearity becomes no longer negligible, since a fracture process in the form of split formation along nail rows, leads to accelerated creep on logarithmic time scale [Van de Kuilen, 1992]. The creep curve is then no longer straight, eventually leading to failure. Figures 2.1 and 2.2 show the average creep curves of nailed joints loaded at 30%, 40% and 50% of the average short term strength for a period of up to 3000 days. On log-time scale, it can be seen that the creep curve develops slowly from a line with a small slope into a line with a steep constant slope. Neglecting mechano-sorptive effects offers the possibility of describing the creep with only two parameters, which have to be determined from experiments. The displacements of the joints after 10 minutes of creep on which the creep factor is based are summarized in table 2.1.

Table.2.1 Displacements after 10 minutes for nailed joints loaded to 30%, 40% and 50%.

Series:	Specimen number and 10 minutes displacement in mm				
30%	DNb 01	DNb 02	DNb 03	DNb 04	DNb 05
	0.255	0.283	0.299	0.280	0.371
40%	SND 31	SND 32	SND 33	SND 34	SND 35
	0.445	0.547	0.456	0.387	0.544
50%	SND 36	SND 37	SND 38	SND 39	SND 40
	0.834	0.781	0.728	0.837	0.836

These displacements show that there is a small non-linearity in the relationship between load level and 10 minutes displacement. The average values for the three load levels are 0.298, 0.476 and 0.803 mm respectively. The test series of 1962 has 8 nailed joints that still had not failed in 1997. The load levels of these joints are 60% and 65% each with 4 specimens. The creep curve of the average values is shown in figure 2.2. The average 10 minutes displacement was determined at 1.65 and 2.22 mm for the 60% and 65% load level respectively. With creep factors of 3.4 and 4.2 the average displacement after 34 years of creep are 7.1 and 11.5 mm. After 13 years the creep factors were about 2.5 and 3.1 which is slightly less than observed in the newer tests. This is most probably caused by the fact that these tests were started in September at high moisture season, while the newer tests were started in the dry season with changes in relative humidity quite soon after the start of the test.

Toothed-plate joints in an uncontrolled environment

The average creep curve of three series of 5 toothed-plate joints is shown in figure 2.3 on a logarithmic time scale for 30%, 40% and 50% load level. The creep curve is steeper for 30% than for 40% and 50%. Partial failures have occurred at load levels of 40% and 50% and these have been excluded from the average creep curves after the failure had initiated. Generally, a shear plug failure under the bolt initiates an increase in creep rate. Sometimes, a single split in the centre of the middle member can be observed. Two main increases in creep factor can be determined due to the mechano-sorptive effect, with some smaller changes affecting the creep factor in later stages of the tests. An important conclusion is that the higher the load level, the lower the increase in creep factor. The main increases in creep factor occur during severe decreases in relative humidity in the laboratory. The average values have been determined without the contribution of partially failed joints. The creep rate seems to be dependent on the load level, which disagrees with the findings of the nailed joints, where the creep rate seems to be the same for the load levels presented. The displacements of the joints on which the creep factor is based are summarized

in table 2.2. The average values for the different load levels are 0.445, 0.755 and 1.176 mm respectively. The displacements reached by the 30% loaded joints vary between 2.0 and 2.4 mm. The largest displacement of a 40% joint without split formation is 3.4 mm displacement (DKa 37). The displacement of joint DKa 36 at the start of tertiary creep was approximately 4.4 mm after a loading period of 2500 days. Specimen DKa 40, with a single split in the middle member has a displacement of about 2.3 mm after 4800 days. The displacement at which tertiary creep at 50% load was initiated was about 3 mm for SKD 21 and 4.5 mm for SKD 23. The fact that the initiation of visible cracks starts from a displacement of about 2.3 mm until about 4.5 mm indicates that in future even joints at 30% load level could show partial failures and possibly even total failures.

Table 2.2 Displacements after 10 minutes for toothed-plate joints loaded to 30%, 40% and 50%.

Series:	Specimen number and 10 minutes displacement in mm.				
30%	SKD 36	SKD 37	SKD 38	SKD 39	SKD 40
	0.327	0.392	0.268	0.639	0.599
40%	DKa 36	DKa 37	DKa 38	DKa 39	DKa 40
	0.607	0.977	0.981	0.704	0.505
50%	SKD 21	SKD 22	SKD 23	SKD 24	SKD 25
	1.213	1.216	1.206	0.954	1.293

Split-ring joints in an uncontrolled environment

The creep curves of the split-ring joints are presented in figure 2.4. Besides the large increases in short time spans due to variations in relative humidity, a yearly influence is also present in the form of a shrinkage and swelling effect. Apparently the influence of the moisture variation is such that the diameter of the split-ring varies over the year. The amount of the yearly variation in diameter is discussed in paragraph 4. A further similarity to the toothed-plate joints is found in the fact that the 30% joints show the highest creep values. At 50% load level two joints have failed so far, but none at lower load levels. The remaining three joints at 50% load level have a creep factor between 3.6 and 5.4, where the creep of one of these has been influenced by the repair activities of the test set-up after failure of a joint. The displacements of the joints on which the creep factor is based are summarised in Table 2.3.

Table 2.3 Displacements in mm after 10 minutes for joints loaded to 30%, 40% and 50%.

Series:	Specimen number and 10 minutes displacement in mm.				
30%	DRa 39	DRb 08	DRb 09	DRb 10	DRb 11
	0.117	0.291	0.304	0.383	0.122
40%	DRb 16	DRb 17	DRb 18	DRb 19	DRb 20
	0.667	0.422	0.268	0.369	0.198
50%	SRD 31	SRD 32	SRD 33	SRD 34	SRD 35
	0.343	0.311	0.389	0.430	0.317

The average values for the different load levels are 0.243, 0.385 and 0.358 mm respectively. The last figure is rather small compared to the 0.385 mm of the 40% joints. Other split-ring series loaded at 50% of the average short term strength showed average values of the 10 minute displacement between 0.47 mm and 0.76 mm (average of 5 specimens each). This shows the wide scatter of results, but also indicates that the average value at 50% load level of table 2.3 is small. The creep factors for the 30% joints vary between 2.9 and 7.9 after 4800 days (≈13 years) as can be seen from figure 2.5, where the individual results are shown, together with the yearly variation in relative humidity. For the 40% joints the creep factor varies between 2.1 and 5.8. The two failed joints indicate a start of failure at a creep factor of about 4.2 for SRD 34 and 5.0 for SRD 32 giving a displacement of about 2.2 and 1.9 mm respectively. These two values can be used to predict the expected remaining time to failure of the other specimens.

Timber-concrete joints in an uncontrolled environment

The creep results for timber-concrete joints in an uncontrolled environment reported here are running for around 600 days by 2006 at constant load level of 30% of the average short term strength. The environment conditions of the laboratory correspond approximately to the Service Class 2 from Eurocode 5. The displacements of the joints after 10 minutes of creep on which the creep factor is based are summarized in table 2.4.
The creep factor obtained in these conditions after 600 days, varied between, 0.87 and 1.37 for the dowel-type fasteners without interlayer and between 0.92 and 1.33 for dowel-type fasteners with interlayer. These results show a large variation of the short and long term deformations measured in the tests.
The creep factors obtained for the notched joints are particularly high, that results from the high stiffness in the short-term but relative high long-term deformations. Two of the test specimens from test series dvwNI have failed after 117 days of loading. After that no other failures have occurred in spite of the relatively high deformations that have already been achieved for most of the test specimens from test series with notches. These results need future confirmation taking into consideration longer loading periods. Nevertheless, it is already possible to conclude that the short-term high stiffness do not result in corresponding small deformations for long-term loadings.
The average creep factors obtained for the dowel-type fasteners joints were from 1.107 and 1.083 for the test series without and with interlayer respectively. For the test series with notched joints those values were 2.749 and 4.275 for the test series without and with interlayer, respectively. The notched joints show smaller creep factors without interlayer in contrast to the joints made with dowel-type fasteners for which the specimens with interlayer showed smaller creep factors.

Table 2.4 Displacements in mm after 10 minutes for timber-concrete joints in uncontrolled environment.

Series:	Specimen number and 10 minutes displacement in mm.									
10mmB	Test1	Test2	Test3	Test4	Test5	Test6	Test7	Test8	Test9	Test10
	1.291	0.656	1.068	1.096	1.504	0.931	1.001	0.909	1.001	0.967
INT	Test1	Test2	Test3	Test4	Test5	Test6	Test7	Test8	Test9	Test10
	1.757	1.550	1.534	1.441	1.780	1.381	1.679	1.195	1.318	1.214
dvwN	Test1	Test2	Test3	Test4	Test5	Test6	Test7	Test8	Test9	Test10
	0.428	0.277	0.362	0.271	0.969	0.308	0.503	0.374	0.596	0.331
dvwNI	Test1	Test2	Test3	Test4	Test5	Test6	Test7	Test8	Test9	Test10
	0.292	0.223	0.371	0.309	0.819	0.391	0.974	0.346	1.273	0.385

Timber-concrete joints in a controlled environment

The average creep factor obtained in the experimental tests for constant climatic conditions for a minimum period of 1000 days was 0.919. The minimum creep factor obtained was 0.574 for the 10mmA test series (spruce and normal concrete) and the maximum was 1.583 for C test series (chestnut and normal concrete). The differences between those two values are significant and are related not only with the long-term behavior of the materials but also with the short-term deformations measured. In the C test series the initial deformations are small, therefore, even with long-term deformations similar to the other series the creep factors are much higher. The corrosion caused in the steel by the timber was probably a reason for that. In a short period of time the bond caused by the corrosion take part of the load, resulting in smaller slip values, in the long-term that bond is lost and thus the deformations tend to values similar to the ones obtained in the other test series. The displacements of the joints after 10 minutes of creep are

summarized in table 2.5.
The mean creep factor obtained after 1060 days of load for the test series 10mmA (constant climatic conditions) was 0.574, while for the test series 10mmB (variable climatic conditions) was 1.070.
Table 2.5 Displacements after 10 minutes for timber-concrete joints in controlled environment.

Series:	Specimen number and 10 minutes displacement.			
8mm	Test1	Test2	Test3	Test4
	0.428	0.438	0.369	0.281
10mmA	Test1	Test2	Test3	Test4
	1.282	0.985	0.745	1.018
C	Test1	Test2	Test3	Test4
	0.235	0.263	0.215	0.245
HSC	Test1	Test2	Test3	Test4
	0.351	0.545	0.508	0.535
MP	Test1	Test2	Test3	Test4
	0.414	0.294	0.447	0.393

These results show that in constant climatic conditions the creep factors are much lower (around half) than the values obtained with similar test configurations in variable climatic conditions. Furthermore the predictions for 10 and 50 years for this two test configurations showed that the differences tend to increase with the load duration.

3. Moisture content variations

In order to be able to study the influence of the varying moisture content in more detail both the relative humidity was measured as well as the mass of a control specimen. The mass of this control specimen was measured on the same regular basis as the temperature and the relative humidity. The variation in relative humidity and mass could be described by a sine function. The measurements of the first 3000 days for timber joints are shown in figure 3.1.
The density at 12% moisture content was determined at 455 kg/m^3 which is 3% more than the average density of 440 kg/m^3 of the timber used. Because of this small difference it is assumed that the moisture content function is in close agreement with the actual moisture content of the creep specimens.
In order to show the influence of moisture variations on the creep factor, the creep curves of the nailed, toothed-plate and split-ring joints at 30% load level are shown for each individual specimen. It was found that the lower the load level, the higher the influence of a moisture variation on the creep factor.

4. Creep factors for joints

The creep values obtained for joints seem high compared to those for timber, see for instance [Leicester, 1983, 1992], [Morlier, 1992]. However, the creep values measured on joints are not directly applicable as design values. This is because of a major difference in creep research between timber and joints. From each individual piece of timber the modulus of elasticity can be determined prior to the creep test or in the uploading stage of the test. Furthermore, this modulus of elasticity is the same as used in the design stage of a construction. A creep factor determined on timber can thus be used directly in the design process. This procedure cannot be applied in the case of joints. A prior loading of a joint means that initial slip has been removed from the actual creep test. This slip will not or only partly be recovered after unloading and a difference will be found if the same joint is used in the creep test. Additionally, the design value of the joint stiffness K_s should be determined in accordance with EN 26891 (ISO 6891). This stiffness value K_s is used to determine the "instantaneous slip" u_{inst} and is quite different from the stiffness measured by simply dividing the applied load by the measured initial slip.
The initial slip in a creep test is generally taken as the slip after 1 minute, 10 minutes, 1 hour or even 12 hours. Often, the 10 minutes value is taken, but no effect on the definition of "initial stiffness" has previously been reported.
As a consequence, the reported creep factors in the previous paragraph of up to 5 and of up to 20 by Leicester, [1992] cannot be used without modification. A method for modification is presented here in order to create a table with design creep factors for the three joint types.

This derivation was done assuming that the final deformation calculated with the joint stiffness from a design code and a load duration class had to be same as the final deformation measured in the creep test.

Additionally, the comparison was performed using the average values of the measurements, which is the same procedure as for timber beams. The following requirement must be fulfilled:

$$u_{\infty,calc} = u_{\infty,meas} \tag{8}$$

in which:

$$u_{\infty,calc} = u_{inst}(1 + k_{def,EC5}) \tag{9}$$

where:

$$u_{inst} = \frac{F_d}{K_s} \tag{10}$$

according to the method in EC5.
The measured final displacement using the theory applied here results in:

$$u_{\infty,meas} = u_{10\min}(1 + k_{def,meas}) = \frac{F_d}{K_{10\min}}(1 + k_{def,meas}) \tag{11}$$

with the initial displacement u_{inst} determined after 10 minutes of testing which is equal to the load F_d/K_{10min}. For the value of $k_{def;meas}$ the creep model was taken, including the mechano-sorptive parameters. The value of $K_{10\,min}$ is determined on the basis of the tests with 30% load level. The values found were 45 kN/mm, 21 kN/mm and 35 kN/mm for the nailed, toothed-plate and split-ring respectively.
Substituting equations 9, 10 and 11 in 8 and solving for the creep factor $k_{def,EC5}$ for timber joints is found as:

$$k_{def,EC5} = \frac{K_s}{K_{10\min}}(1 + k_{def,meas}) - 1 \tag{12}$$

In table 5.1 a proposal has been made for k_{def} factors for nailed, toothed-plate, split-ring and timber-concrete joints, to be incorporated into Eurocode 5. Calculations are made for the maximum time in a load-duration class i.e. for permanent loads a value of 50 years is used for $k_{def;meas.}$. The C_1 values used are: 0.6, 0.5 and 0.7 for the nailed, toothed-plate and split-ring joints respectively. Similar joint types in a controlled environment showed values which were about one-third [Van de Kuilen, 1999]. For C_2 a value of 0.011 is taken, or 90 days time for the creep curve bend. This will be the average period before seasons change from dry to wet or from wet to dry. For the mechano-sorptive creep the difference is taken between the model prediction with and without the mechano-sorptive effect after 4800 days. It is assumed that after these 13 years most of the mechano-sorptive creep has taken place and very rapid and large moisture variations have a small chance of occurring. These values are given for various test series together with the model and experimental creep curves from figure 4.1 until figure 4.6.
K_s values are derived as 51 kN/mm, 20 kN/mm, 39 kN/mm, 31.7 kN/mm and 22.2 kN/mm for the respective joint types. These values are derived in accordance with Eurocode 5 and the equations given in Blass [1995]. The value for the timber-concrete joint with interlayer was considered as 30% lower than the Eurocode value for the same joint without interlayer. The values correspond reasonably with those determined in the short term tests program, except for the toothed-plate joints. The theoretical stiffness of the toothed-plate joints is double that reported in Kurstjens [1989], which were based on the results of 34 short term tests per joint type.

Table 5.1 Proposal for deformation factors k_{def} in service class 1/2 environments

Load duration class	Time	Creep factor k_{def}				
		Timber joints			Timber-concrete joints	
		Nailed joints	Toothed-plate joints	Slip-ring joints	dowel-type fasteners	dowel-type fasteners with interlayer
Permanent	50 years	4.3	4.4	6.5	2.1	2.9
Long term	10 years	3.2	3.6	5.2	1.9	2.6
Medium term	6 months	1.1	1.0	1.5	0.66	0.76

The values in table 5.1 are based on the average values as measured in the creep tests. However, the scatter in test results is very large as shown in paragraph 2. The scatter is such that for the load

duration classes long term and permanent a variation in creep factor of ± 50% may be assumed. The contribution of the mechano-sorptive effect to the creep factor after 10 and 50 years is estimated at 0.5 for nailed joints and 2 for toothed-plate and split-ring joints. For the medium term load duration class the mechano-sorptive contribution is estimated at 0.2 for the nailed and 0.5 for toothed-plate and split-ring joints.

Literature

Blass, H.J., Ehlbeck, J. and Schlager, M., Characteristic strength of tooth-plate connector joints. Holz als Roh- und Werkstoff 51, 1993, pp. 395-399.
Dias, A.M.P.G., Mechanical behaviour of timber-concrete joints. Ph.D thesis, Delft University of Technology, Delft, 2005.
Hoffmeyer, P., Failure of wood as influenced by moisture and duration of load. Ph.D. thesis, State University of New York, Syracuse, New York, 1990.
Leicester, R.H, Lhuede, E.P., Mechano-sorptive effects on toothed-plate connectors. IUFRO S5.02, Bordeaux, France, 1992.
Krausz, A.S., Eyring, H., Deformation Kinetics, John Wiley & Sons, 1975
Kuipers, J, Kurstjens, P.B.J., Creep and Damage Research on Timber Joints - Part One. Stevin report 4-86-15/HD-23 Delft University of Technology, 1986.
Kurstjens, P.B.J., Creep and Damage Research on Timber Joints - Part Two. Stevin report 25.4-89-15/C/HD-24 Delft University of Technology, 1989
Morlier, P., Valentin, G., Toratti, T., Review of the theories on long term strength and time to failure. COST 508 Wood Mechanics Workshop on service life assessment of wooden structures, Espoo Finland, 1994.
Van de Kuilen, J-W.G., Determination of k_{def} for nailed joints. CIB-W18 Meeting 25, Ahus, Sweden, 1992.
Van de Kuilen, J-W.G., Duration of load effects in timber joints. Ph.D thesis, Delft University of Technology, Delft, 1999.
Van der Put, T.A.C.M., Deformation and damage processes in wood. Ph.D. thesis 1989.

Figures

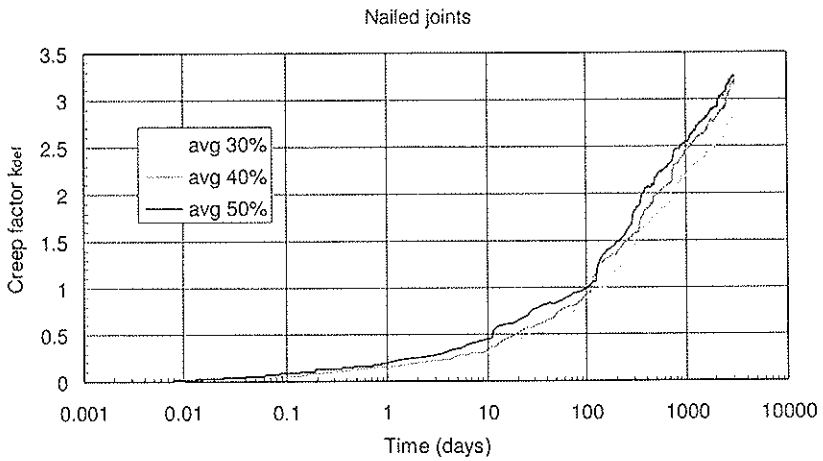

Figure 2.1 Average creep curves of nailed joints at 30%, 40% and 50% load level on logarithmic time scale.

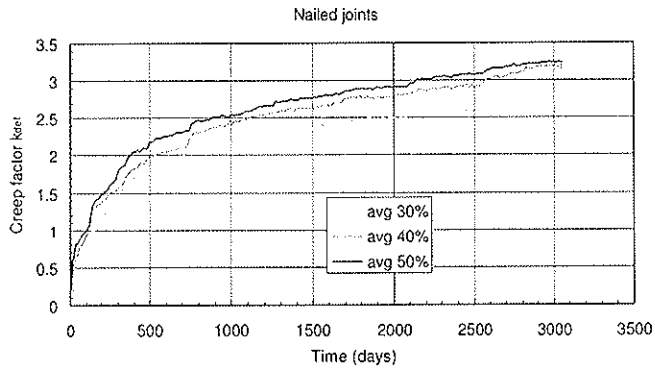

Figure 2.2 Average creep curves of nailed joints at 30%, 40% and 50% load level on linear time scale.

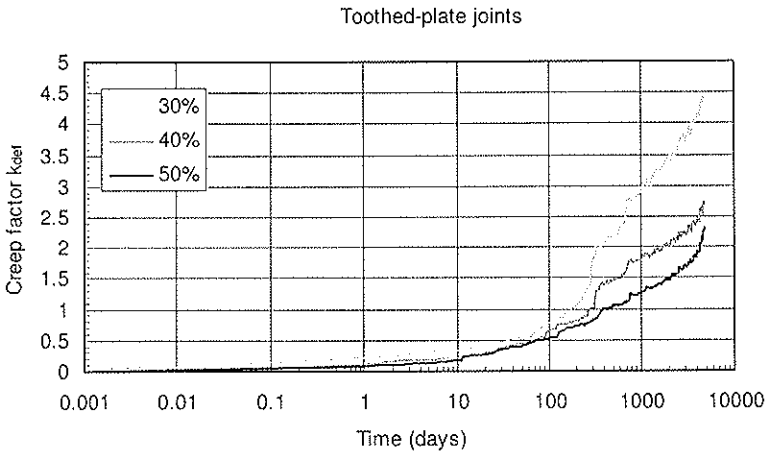

Figure 2.3 Average creep curves of toothed-plate joints at 30%, 40% and 50% load level on logarithmic time scale.

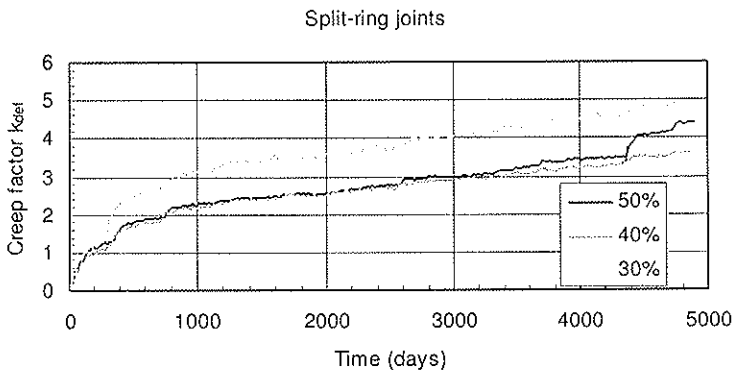

Figure 2.4 Average creep curves of split-ring joints at 30%, 40% and 50% load level at linear time scale.

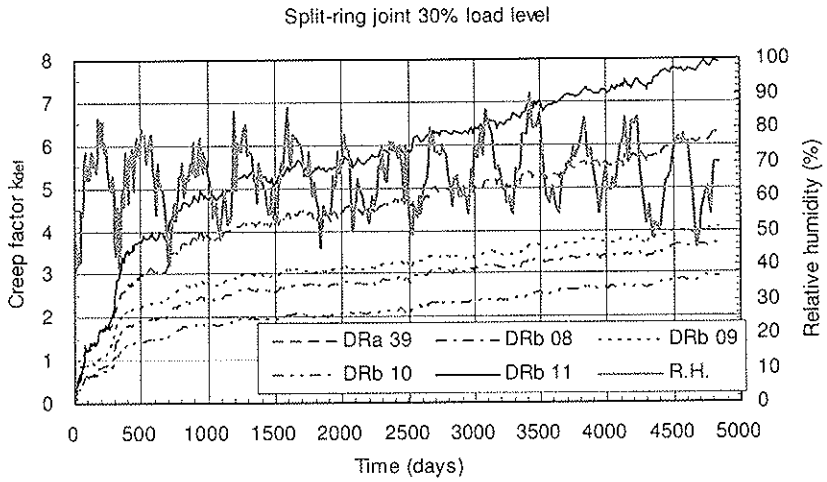

Figure 2.5 Creep of split-ring joints as influenced by relative humidity variations.

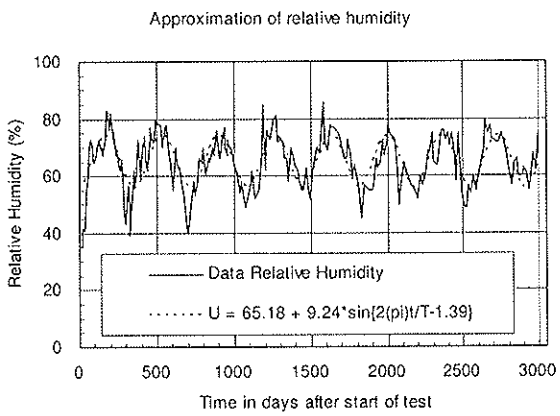

Figure 3.1 Variation of relative humidity.

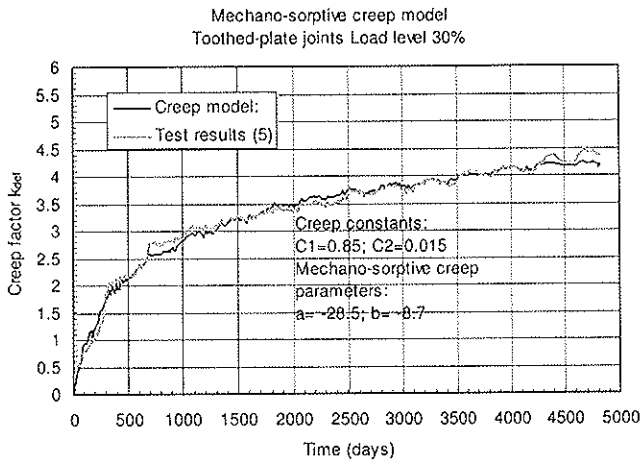

Figure 4.1 Creep model applied to toothed-plate joints at 30% load level

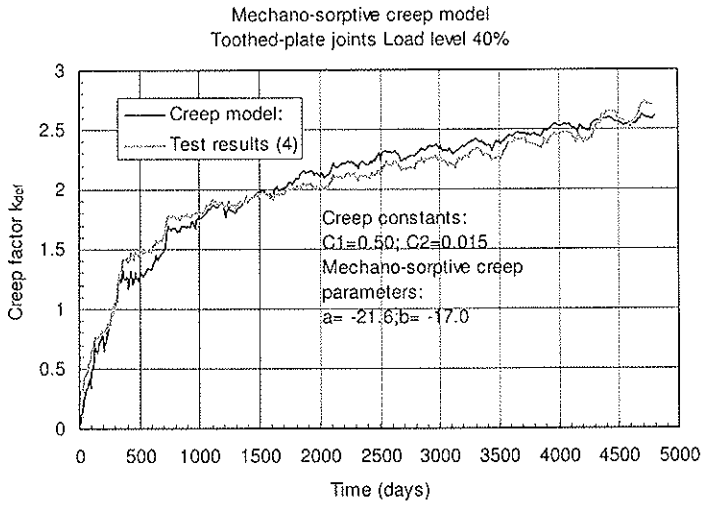

Figure 4.2 Creep model applied to toothed-plate joints at 40% load level

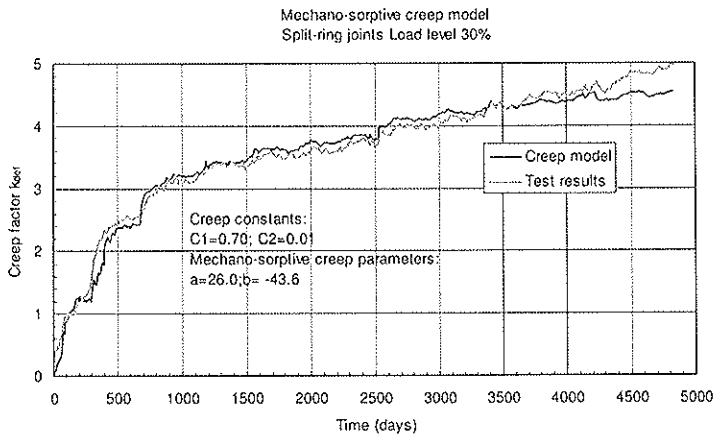

Figure 4.3 Creep model applied to split-ring joints at 30% load level

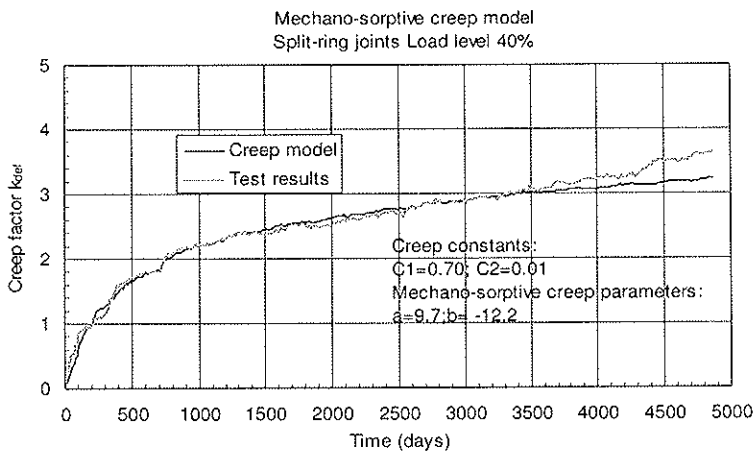

Figure 4.4 Creep model applied to split-ring joints at 30% load level.

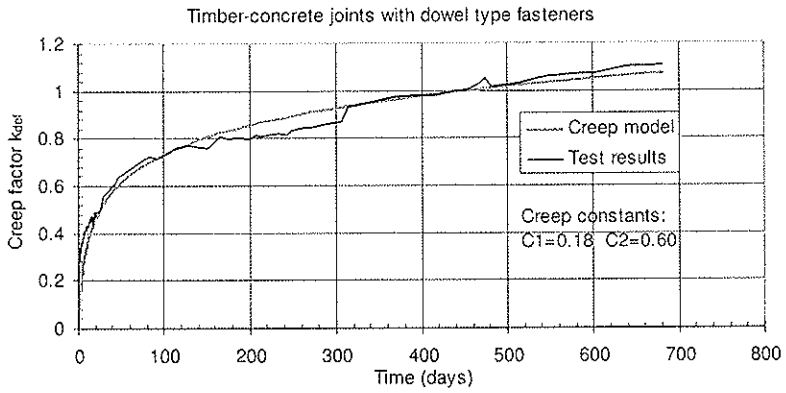

Figure 4.5 Average test results and correspondent model for timber-concrete joints with dowel-type fasteners.

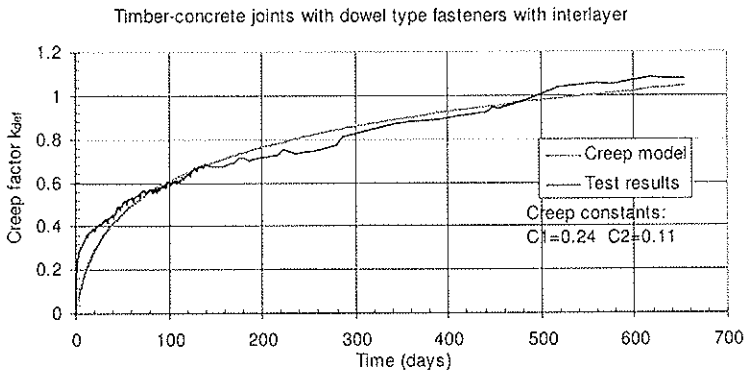

Figure 4.6 Average test results and correspondent model for timber-concrete joints with dowel-type fasteners with interlayer.

INTERNATIONAL COUNCIL FOR RESEARCH AND INNOVATION
IN BUILDING AND CONSTRUCTION

WORKING COMMISSION W18 - TIMBER STRUCTURES

LAG SCREWED TIMBER JOINTS WITH TIMBER SIDE MEMBERS

by

Kohei Komatsu
Shinjiro Takino
Research Institute for Sustainable Humanosphere, Kyoto University

Hajime Tateishi
Tateishi Architectural Design Office, Kyoto

JAPAN

MEETING FORTY
BLED
SLOVENIA
AUGUST 2007

Presented by K. Komatsu
F. Lam asked whether the difference detected between sawn timber and glulam is species effect as connection in glulam is shown to be weaker than the connection in sawn timber. K. Komatsu said that the members are intended for girders. In Japan both types of wood (Douglas fir and Redwood glulam) are recognized and therefore tested. For the Douglas fir if MOE is high then strength would be high but some low MOE Douglas fir would exhibit low strength. F. Lam commented that the grade of the material would be important and asked if these members were intended for girders why cyclic testing was conducted. K. Komatsu stated that Japan is earthquake important. This may apply to connections in girders.
H. Larsen received confirmation that lags screws were not allowed in Japan but small diameter screw were okay. He received further clarification about allowable strength proposal in AIJ and shank versus screw diameter.
H. Blass commented that the group action factor of 2 to 10 screws shown in diagram should be 1 to 5 screws. K. Komatsu agreed.

Lag Screwed Timber Joints with Timber Side Members

by

Kohei Komatsu[1], Shinjiro Takino[2] and Hajime Tateishi[3]

1:Corresponding author: Professor, Research Institute for Sustainable Humanosphere, Kyoto University, Uji, Kyoto, 611-0012 Japan, kkomatsu@rish.kyoto-u.ac.jp
2: Assistant Professor, Research Institute for Sustainable Humanosphere, Kyoto University, Uji, Kyoto, Japan
3:President: Tateishi Architectural Design Office, Kyoto, Japan

Abstract

In Japan until December 2006, lag screw could not be used in timber joints with timber side members, because lag screw has been mainly used for large cross sectional glulam members using steel side plates. However, recently demands for wishing to use lag screws also to timber-to-timber joint has been increasing mainly in the field of wooden dwelling houses, so that we have been engaged in obtaining strength and stiffness of lag screwed timber joints with timber side members for making clear whether this fastener could be used safely in timber-to-timber joints. We conducted a series of double single shear lag screwed timber-to-timber joints by setting number of lag screws in a row as an experimental parameter. Consequently, we found out that the apparent strength of timber lag screwed joint per connector showed decreasing trend as the number of lag screw increased. Finally we proposed allowable shear strength of timber-to-timber lag screwed joint based on our experimental result. At present, however, the allowable strength of timber-to-timber lag screwed joint is ought to be given by so-called 'EYT' in Japanese 'Standard for Structural Design of Timber Structures'.

1. INTRODUCTION

One of the advantageous points of using lag screws in timber structures is that it can be fastened from the one-sided external surface. Due to this convenience, demand for wishing to use lag screw has been increased in recent Japan especially in the field of wooden dwelling houses.
In our timber design standards [1], however, lag screws have been used mainly for glulam structures where only steel plates have been used for the side members. Therefore a special permission was required if lag screws were used for timber-to-timber joints, thus this limitation has been demanded to be released by the peoples who wished to use this convenience fastener also for timber-to-timber joints. From these backgrounds, we did a series of experiment to evaluate joint performance of timber-to-timber lag screwed joints and also proposed allowable strength of lag screwed timber-to-timber joints.

2. EXPERIMENT

2.1 Test Specimen and Materials

Table 1 shows configuration and specification of test specimen used in this study. Basically, kiln dried Douglas fir sawn timber or/and European red wood glulam were used for the main members because these two kinds of materials have been represented main structural beams in Japanese wooden dwelling houses. While for the side members, kiln dried western hemlock sawn timber was used which

has been extensively used up to recently for sub-structural members such as sill. Densities of wooden materials used in this experiment were tabulated in Table.2 .

Table 1 Configuration and specification of test specimens (Replications =3)

Number of lagscrews in a row	End distance e_e (mm)	Space between fasteners S (mm)	Main member and cross section (mm)	Side member and cross section (mm)	Lag screw used (mm)
1	500 (41.7d)	–	Douglas fir sawn timber or/and European red wood glulam 120 x 210	Western hemlock sawn timber 40 x 120	d=12, l=125 Bearing plate : 40 x 40 t = 4.5
2	230 (19.2d)	540 (41.7d)			
3	230 (19.2d)	270 (22.5d)			
4	230 (19.2d)	180 (15d)			
5	140 (11.7d)	180 (15d)			

Table 2 Physical properties of materials used in this study

Part in the specimen	Main member				Side member-1		Side member-2	
Species	Douglas fir sawn timber		European red wood Glulam		Western hemlock sawn timber			
Item	Mean	C.V.	Mean	C.V.	Mean	C.V.	Mean	C.V.
Moisture content at test	19.7%	0.17	15.1%	0.23	10.4%	0.23	10.3%	0.26
Density at test	529kg/m^3	0.10	533kg/m^3	0.06	438kg/m^3	0.10	439kg/m^3	0.08
Number of measuments n	30		32		62		62	

The specification of lag screws used in this experiment were as follows:
diameter d = 12 mm and length l =125 mm with square steel bearing plates of 4.5 x 40 x 40 mm.
Figure 1 shows configuration of each test specimen used in this experiment.

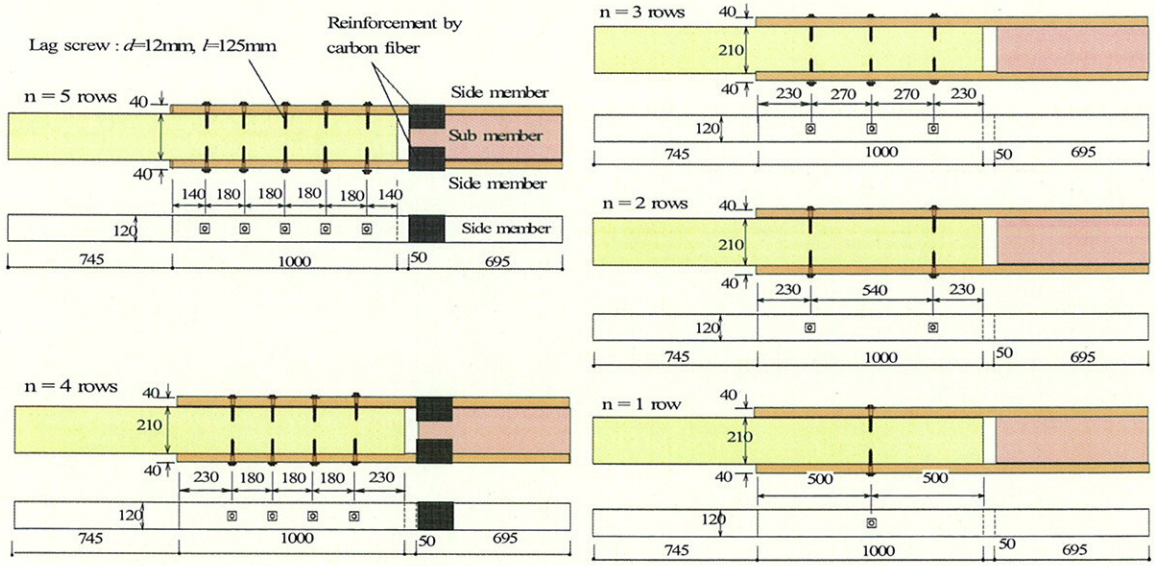

Fig.1 Test specimens for lag screwed timber to timber joints

In this experiment, one specimen among three replications was loaded in monotonic tensile load, while the rest of two specimens were loaded in cyclic push-pull loading schedule based on the movement of cylinder of servo-actuator of testing machine as shown below:

1st cycle : 0→ +5 mm → 0 → -5 mm → 0
2nd cycle : 0→+10 mm → 0 →-10 mm → 0
3rd cycle : 0→+15 mm → 0 →-15 mm → 0
Last cycle : 0 → P_{max}

Photograph 1 shows a feature of tensile shear test done in an Instron servo-actuator type testing machine of capacity 1000kN (Instron model 8050). We preliminary confirmed that there were negligibly small differences among slip displacements measured at each fattener point, thus we set a pair of relatively large deflection measuring devices at mid point in a row of fattener to measure a pair of representative slip displacement between main member and side members as shown in photo.1.

Photo.1 Lag screwed timber-to-timber joint with a pair of deflection measuring devices at middle of a fasteners.

3. RESULTS AND DISCUSSION

3.1 Examples of Load per Fastener(*P*)-Slip(*S*) Relationship

Figure 3 show typical examples of load per lag screw(*P*)-slip(*S*) relationships of multiple lag screwed timber-to-timber joints. From these figures, it can be seen that a trend of decreasing in joint performance as the numbers of lag screws in a row increase.

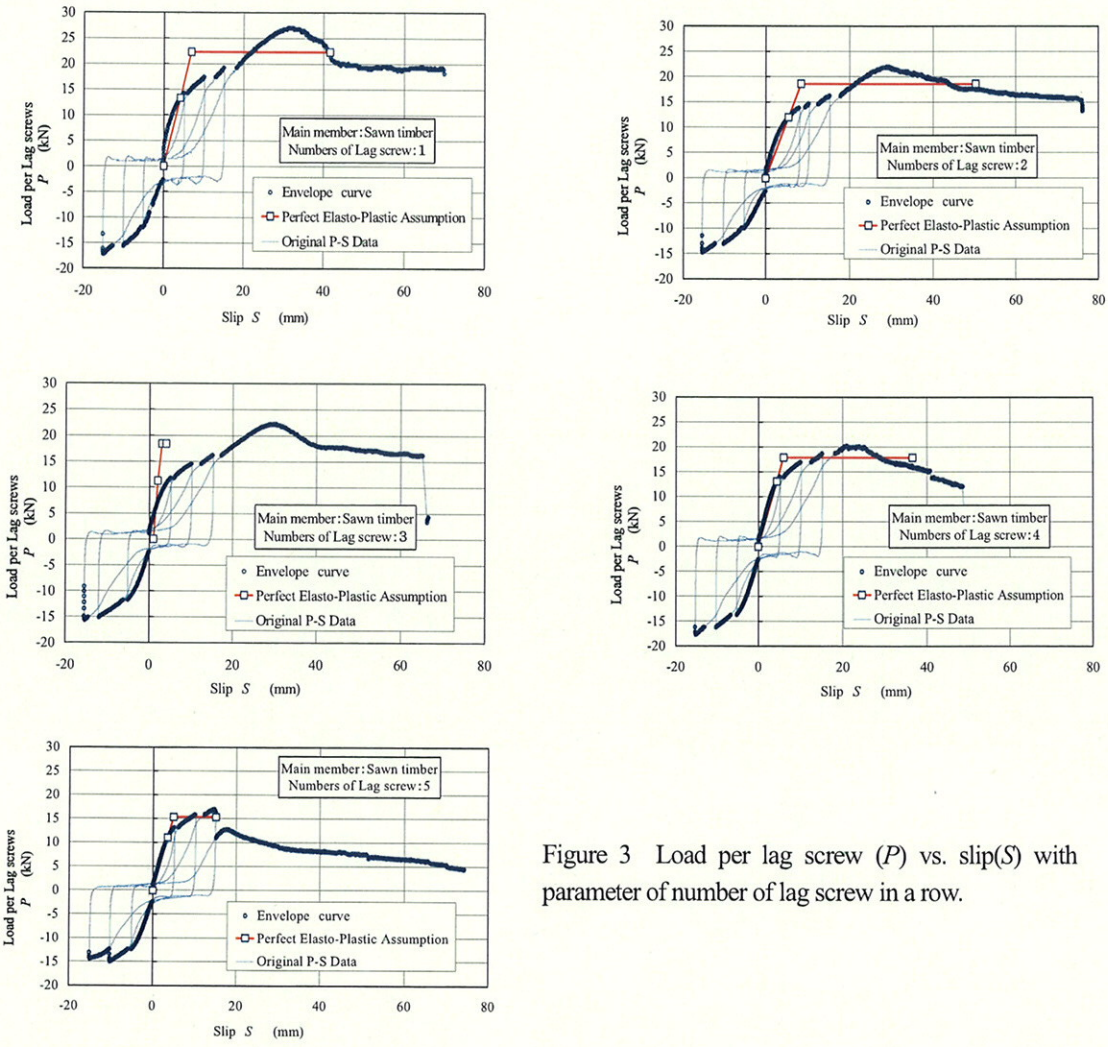

Figure 3 Load per lag screw (*P*) vs. slip(*S*) with parameter of number of lag screw in a row.

3.2 Estimation of Characteristic Quantities based on Perfect Elasto-Plastic Assumption

In figure3, bi-linear plots were obtained based on a current Japanese rule[2], which is being used for estimating performance of shear walls, stiffness and strength of various timber joints, and sub-assembly components in timber structures. Table 3 summarizes the estimated characteristic values of lag screwed timber-to-timer joints tested in this study. Figure 4 shows definitions of each characteristic points used in table 3.

Table 3 Estimated results (mean value of 3) based on a current Japanese rule [2]

Number of lag screw in a row	S_{pmax} (mm)	P_{max} (kN)	S_y (mm)	P_y (kN)	K (kN/mm)	S_v (mm)	P_u (kN)	S_u (mm)	$\mu = S_u/S_v$
(a)Main member =Glulam									
1	28.64	21.22	4.52	11.48	2.614	7.37	18.08	41.33	5.57
2	28.60	22.22	4.39	11.98	2.736	6.92	18.84	48.73	7.07
3	15.14	17.64	2.97	10.48	3.520	4.56	16.09	28.96	5.93
4	7.11	13.62	1.59	7.28	4.806	2.62	11.92	13.90	6.22
5	12.02	14.37	1.73	8.04	5.056	2.74	12.75	23.00	9.34
(b)Main member = Sawn timber									
1	28.52	25.12	4.60	12.66	2.843	7.60	21.05	45.46	6.04
2	29.91	21.83	4.56	12.04	2.691	7.10	18.69	52.17	7.57
3	24.78	18.71	3.29	9.83	3.237	5.40	16.13	41.46	8.77
4	19.89	19.10	3.72	11.61	3.150	5.43	17.01	33.41	6.16
5	20.38	17.58	3.29	10.79	3.321	4.74	15.58	29.90	6.52

here;

S_{pmax} : Slip at P_{max}.
P_{max} : Maximum load.
K : Stiffness defined in [2]
S_v : Slip at P_u
P_u : Ultimate load defined in [2]
S_y : Slip at P_y
P_y : Yield load defined in [2]
S_u : Slip at $0.8P_{max}$ defined after P_{max}
μ :ductility factor defined as Su/Sv

Principle: Area painted in Fig.4 = Area surrounded by bi-linear lines, S_u line and Slip S line.

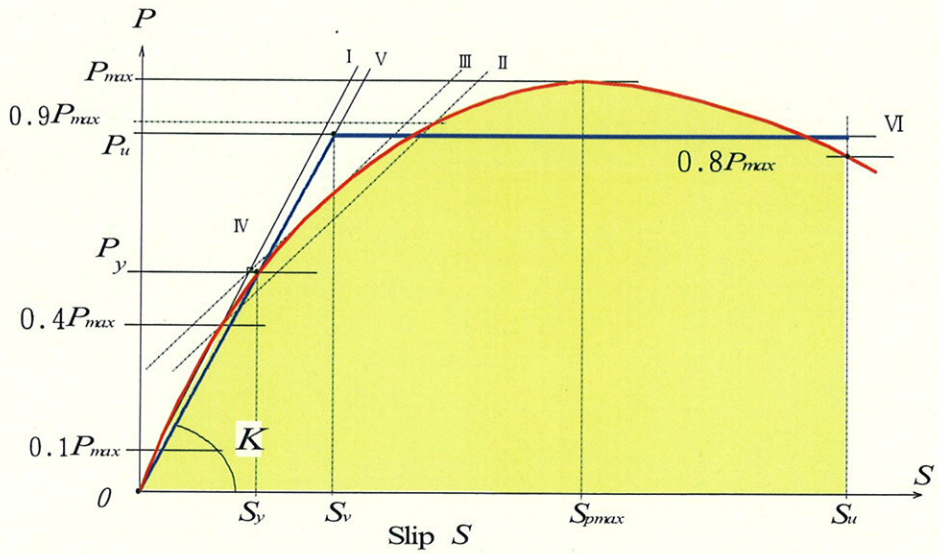

Fig.4 Definitions of each characteristic points used in Table 3.

3.3 Joint Performance as a Function of Number of Fastener in a Row

Figure 5 shows a clear decreasing tendency of joint's strength per fastener as number of lag screw in a row increases. This kind of decreasing tendency might be common to most multiple timber joints [3], and implication of this phenomenon might be able to be done by employing, for example, Lantos's classical theory [4].

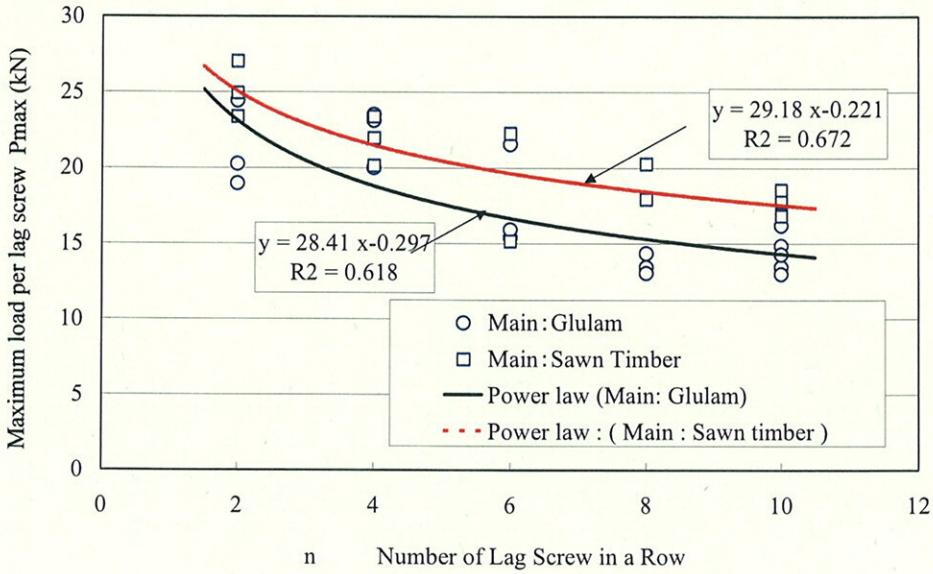

Figure 5 Joint strength per fastener vs. number of lag screw

Figure 6 shows a tendency of slip modulus per fastener as a function of numbers of lag screw in a row. It is interesting to know that initial stiffness per fastener tends to increase due to the effect of friction between main member and side member as number of lag screw increases. And this tendency becomes clearer in the case of glulam than the case of sawn timber, probably because rough surface on sawn timber gives less friction than smooth surface on glulam.

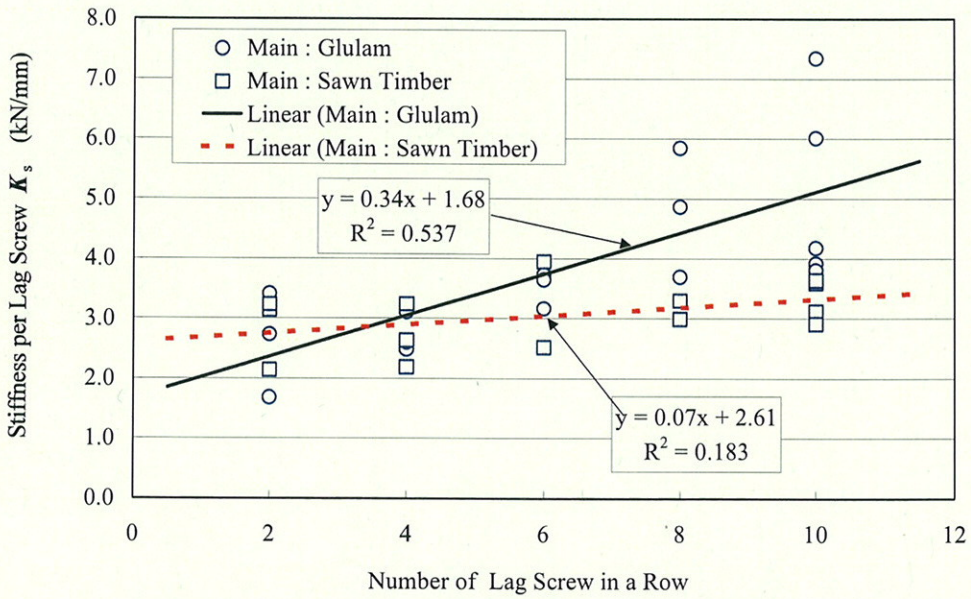

Figure 6 Joint stiffness per fastener vs. number of lag screw

3.4 Allowable Strength Derived from Experimental Results

According to the US timber design code [5], the design strength of timber joint composed of multiple fasteners F_m is estimated in equation (1) by applying the "group action factor C_g" and number of fastener "**n**" to the allowable strength of single fastener f_1. That is;

$$F_m = f_1 \times n \times C_g \Rightarrow C_g = \frac{\frac{F_m}{n}}{f_1} \quad \cdots\cdots (1)$$

In Japan, allowable strength of single fastener f_1 can be derived by multiplying 'scatter factor' to the 'estimated value P_e', which might be determined from equation (2).

$$P_e = \text{Min.}\left\{ \begin{array}{l} P_y \\ \\ \dfrac{2}{3} P_{max} \end{array} \right. \quad \cdots\cdots (2)$$

where,

P_y and P_{max} are experimental values evaluated from full-scale test, and in this study, they could be obtained from the bi-linear approximation [2] as shown in Table 3. or/and Fig.4. In case of this study 'estimated value P_e' was always determined from the yield load P_y. Here, we would like to consider P_y obtained from test specimens with one lag screw in a row as the value of f_1. Then by applying a regression analysis on the other test results, a series of regression equation between "group action factor C_g" and number of fastener "**n**" was obtained as shown in Figs.7-(a),(b).

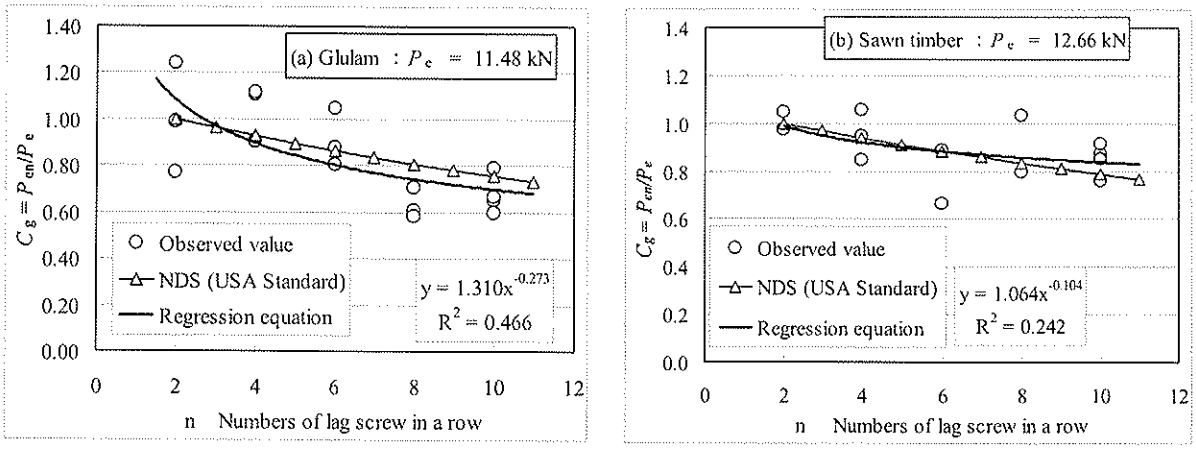

Fig.7 Relationship between "group action factor Cg" and number of fastener "n"

Finally, by using regression equations shown in each figures 6-(a),(b), 'estimated value P_e' for each specimen could be inversely evaluated as shown in equation (3).

$$P_e = \left(\frac{P_{en}}{A} \right) n^{\alpha} \quad \cdots\cdots (3)$$

Table 4 shows the evaluated allowable strength values for timber-to-timber lag screwed joints.

Table 4 Allowable strength value of ltimber to timber lag screwed joints

Main member	Sawn timber	Glulam
Evaluated P_e by eq.(3) (kN)	12.75	11.64
C.V.	0.110	0.169
Scatter factor	0.778	0.668
Allowable strength for short term loading P_1 (kN)	9.92	7.77
Number of specimen	14	17

3.5 Allowable Strength Proposed in AIJ standard[1]

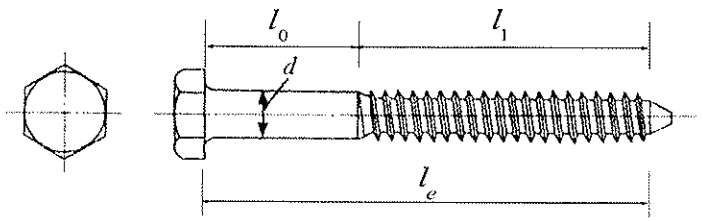

$l \geq 8d \quad l' \geq 3d$

If $l_0 \leq (2d + l)$, then valley diameter at threaded part should be 'd'

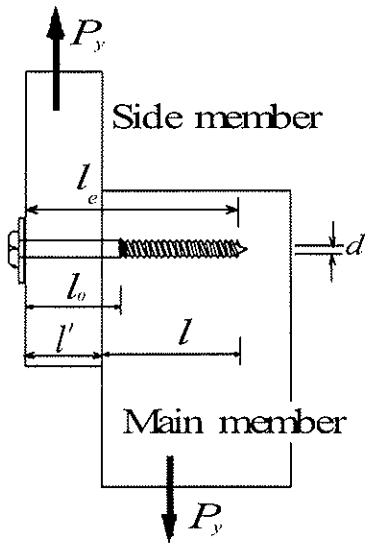

Fig.8 Definition of lag screwed timber-to-timber joint and configuration of lag screw [1].

Figure 8
shows a generalized configuration of lag screwed timber-to-timber single joint issued in the latest Standard for Structural Design of Timber Structures published by Architectural Institute of Japan [1]. In this standard, it was proposed that allowable strength of lag screwed timber joint should be estimated using so-called "European Yield Theory". The final estimation equations will be written as follows.

3.5.1 Design allowable strength (p_a)

Allowable strength (p_a) of single lag screwed joint for design should be estimated by equation (4)

$$p_a = \frac{1}{3} \times {}_j K_d \times {}_j K_m \times r_u \times p_y \qquad \ldots\ (4)$$

where,

p_y : yield strength of single lag screw (N)

${}_j K_d$: factor for DOL (long = 1.1, medium long = 1.43, medium short = 1.6, short = 2.0)

${}_j K_m$: moisture content factor (always wet or initial MC higher than 20% = 0.7, occational wet = 0.85, dry = 1.0)

r_u : ultimate strength factor (yield mode I = 1.0, yield mode II or III = 1.1, yield mode IV = 1.2)
but in the case of lag screwed timber - to - timber joint, r_u = 1.0

1/3 : this is composed of safety factor (2/3) and adusting factor from short to long (1/2)

(a) Yield strength (p_y)

Yield strength (p_y) of single lag screwed timber –to-timber joint is to be estimated by equation (5).

$$p_y = C \times F_e \times d \times l \qquad \ldots. (5)$$

where,

C : coefficient depends on joint configulation and failure mode

F_e : basic bearing strength of main member (N/mm^2)

d : diameter of fastener (mm).

l : effective length of fastener in main member (mm).

(b) Coefficient *C*

Coefficient C should be determined from the minimum value of equation (6).

$$\text{Mode - Ia} : C = \alpha\beta$$

$$\text{Mode - Ib} : C = 1$$

$$\text{Mode - II} : C = \frac{\sqrt{\beta + 2\beta^2(1+\alpha+\alpha^2)+\alpha^2\beta^3} - \beta(1+\alpha)}{1+\beta}$$

$$\text{Mode - IIIa} : C = \sqrt{\frac{2\beta(1+\beta)}{(2+\beta)^2} + \frac{2\beta\gamma\left(\frac{d}{l}\right)^2}{3(2+\beta)}} - \frac{\beta}{2+\beta}$$

$$\text{Mode - IIIb} : C = \sqrt{\frac{2\alpha^2\beta^2(1+\beta)}{(2\beta+1)^2} + \frac{2\beta\gamma\left(\frac{d}{l}\right)^2}{3(2\beta+1)}} - \frac{\alpha\beta}{2\beta+1}$$

$$\text{Mode - IV} : C = \frac{d}{l}\sqrt{\frac{2\beta\gamma}{3(1+\beta)}}$$

.... (6)

where,

α: width of side member/ effective length of fastener in main member (l'/l)

l': width of side member (mm)

β: ratio of bearing strength of side member and that of main member (F_e'/F_e)

F_e : bearing strength of main member (N/mm^2)

F_e' : bearing strength of side member (N/mm^2)

γ: ratio of basic material strength of fastener and that of basic bearing strength of main member (F/F_e)

F : basic material strength of fastener (N/mm^2)

Figure 9 shows yielding modes for lag screwed timber-to-timber joint which are the corresponded to each case defined in equation (6).

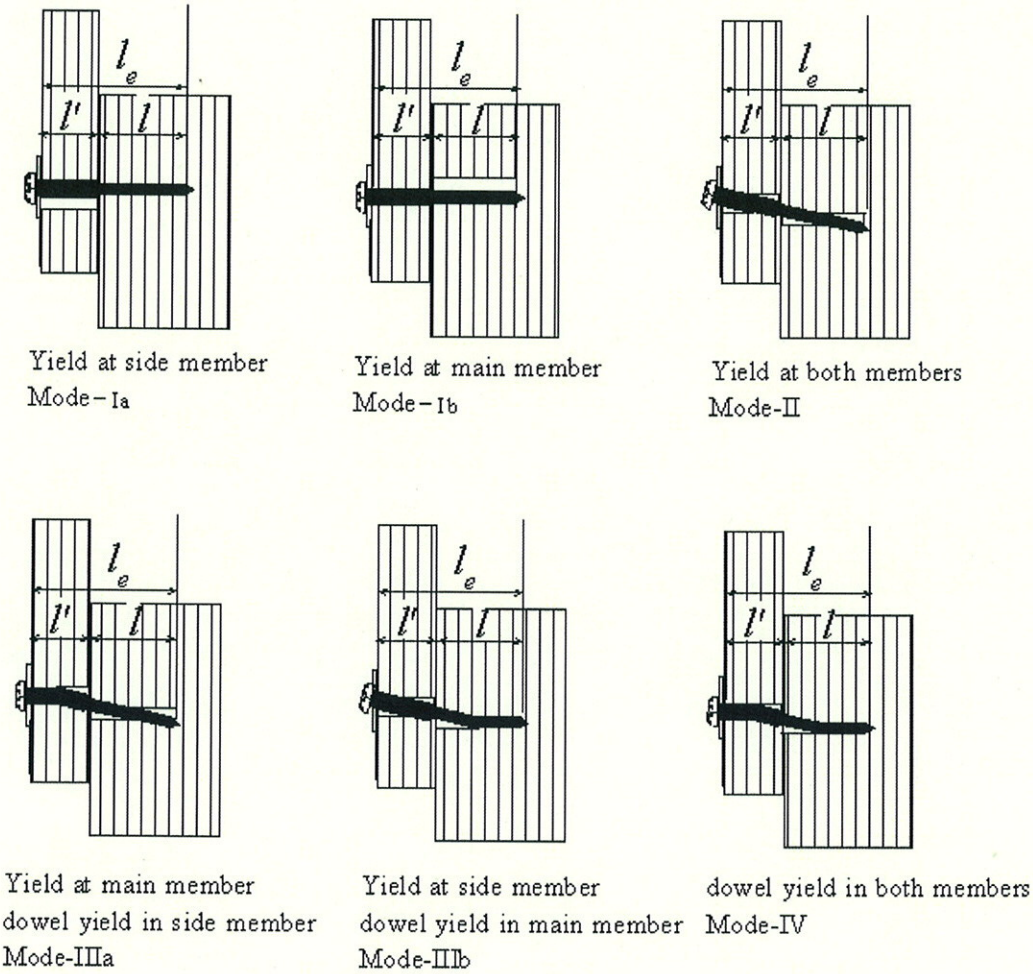

Fig.9 Yielding modes for lag screwed timber-to-timber joint

(c) Comparisons between AIJ allowable strength and experimentally derived ones

Table 5 shows comparisons between allowable strength of lag screwed timber-to-timber joint derived from AIJ equations (4) and (5) and experimental values shown in Table 4.

Table 5 Comparisons between allowable strength by AIJ assignment and experimental values

F	Fe	Fe'	d	l'	l	α	β	γ
N/mm^2			mm					
490	25.4	22.4	12	40	85	0.4705882	0.88189	19.29134

Yield mode	Mode-Ia	Mode-Ib	Mode-II	Mode-IIIa	Mode-IIIb	Mode-IV		
C	0.415	1.000	0.331	0.385	0.258	0.347		
Min. C	0.258					Glulam	Sawn timber	
$p_y = C \times F_e \times d \times l$		6.69		Experimental value		7.77	9.92	(kN)
$p_a = (1/3) \times 2 \times 1 \times 1 \times p_y = (2/3)\, p_y$		4.46	(kN)					

here, ${}_jK_d = 2.0$, ${}_jK_m = 1.0$, and $r_u = 1.0$ were adopted for calculating equation (4). Value of F for shank of lag screw was quoted from the value assigned to the screws whose diameter is larger than 5mm in AIJ standard.

4. CONCLUSION

From Table 5, it is appeared that AIJ allowable strength for lag screwed timber-to-timber joint seems to be so conservative compared with those derived from current practical method based on experimental values [2]. Of course, the current practical method shown in equations (2) is not authorized by AIJ, however, this method tends to be used more widely in the field of corresponding sectors relating to wooden residential houses, thus it will be necessary in near future to make AIJ standard estimation method for wooden fasteners harmonize with current practical method [2].

REFERENCES

[1] Architectural Institute of Japan (edited): Standard for Structural Design of Timber Structures, Maruzen, 2006. (in Japanese)

[2] Japan Housing and Wood Technology Center (edited): Allowable stress design for wooden post & beam residential houses, 145-146, 2002. (in Japanese)

[3] For example; A. Jorissen: "Double Shear Timber Connections with Dowel Type Fasteners", Delft University Press, 264 pages, 1998.

[4] G. Lantos: "Load Distribution in a Row of Fasteners Subjected to Lateral Load", Wood Science, 1(3), 129-136, 1969.

[5] National Forest Products Association (edited.): National Design Specification for Wood Construction 1991 Edition, Part VII "Mechanical Connections", 27-125, Washington, D.C., 1999.

INTERNATIONAL COUNCIL FOR RESEARCH AND INNOVATION
IN BUILDING AND CONSTRUCTION

WORKING COMMISSION W18 - TIMBER STRUCTURES

EXTENSION OF EC5 ANNEX B FORMULAS FOR THE DESIGN OF TIMBER-CONCRETE COMPOSITE STRUCTURES

J Schänzlin
Institute of Structural Design, University of Stuttgart

GERMANY

M Fragiacomo
Department of Architecture and Planning, University of Sassari
ITALY

MEETING FORTY

BLED

SLOVENIA

AUGUST 2007

Presented by J. Schänzlin
A. Ceccotti asked which problems are anticipated with shrinkage of concrete. J. Schänzlin said that bending failure of the timber may be possible. This will depend on span where over 5 m serviceability governs and less than 5 m ultimate limit state governs. A. Ceccotti suggested that one should survey existing concrete timber systems of over 10 years old to see if there are indeed issues as he has not heard of any problem. M. Fragiacomo replies that University of Colorado has experience with a case of 3.5 m span where excessive deformation was encountered.

Extension of EC5 Annex B formulas for the design of timber-concrete composite structures

Jörg Schänzlin
Institute of Structural Design, University of Stuttgart, Germany

Massimo Fragiacomo
Department of Architecture and Planning, University of Sassari, Italy

Abstract

The design of timber concrete composite slabs is currently carried out using the EC5 Annex B formulas for timber-timber composite beams with flexible connections. Since timber, concrete and connection are all characterised by time-dependent phenomena such as creep and inelastic strains due to different thermal expansion or shrinkage of concrete and timber, the most critical design condition is often the limitation of the deflection in the long-term. In order to determine the effect of inelastic strains in terms of deformation and eigenstresses, the design method based on the EC5 formulas has to be extended. Furthermore, the effective creep coefficients in the composite beam differ from the pure material creep coefficients due to the stress redistribution taking place over the service time. Some modified creep values for composite structures should therefore be proposed. The paper presents two possible approaches to extend the EC5 method in order to account for the aforementioned phenomena. The two approaches are compared to each other and with rigorous solutions. They can both be proposed for an improvement of the current design procedure of timber-concrete composite slabs and beams in accordance with the EC5 provisions.

1 Introduction

Timber-concrete composite beams and slabs are a type of construction used both for upgrading of existing timber floors and for new buildings. Advantages over timber floors include larger strength and stiffness under vertical and lateral loads, effective acoustic separation, larger thermal mass and greater fire resistance.

The design for vertical loads can be carried out using the EC 5 Annex B formulas, as suggested by Ceccotti (1995). Those formulas, proposed for timber-timber composite beams with flexible connectors, can be effectively used for the design of composite beams and slabs in the short-term. For the design in the long-term, the same formulas can be used in conjunction with the effective modulus method, where the elastic moduli of timber, concrete and connection are reduced to account for creep (Ceccotti 1995). However, there are a number of time-dependent phenomena taking place in the concrete slab which make the behaviour of timber-concrete composite structures quite different from that of timber-timber composite beams. The main differences are listed in the following:

- The inelastic strains developing over time in the concrete slab are markedly different from those in the timber beam. The former ones are due to drying shrinkage and thermal expansion, whereas the latter ones are caused by moisture variations and thermal expansions. The difference in inelastic strains causes deflection and eigenstresses in the timber-concrete composite beam, whereas none of these effects occurs in timber-timber composite beams (Fragiacomo (2006), Ceccotti et al. (2007), Schänzlin (2003), Schänzlin and Kuhlmann (2004)).
- The creep coefficient of concrete is different from that of timber and from that of connection

both as final value in the long-term and as trend over time. This difference causes the effective creep coefficients of the timber beam, concrete slab, and connection system being different from the pure material creep coefficients of these elements (see Schänzlin and Kuhlmann (2004)).

- There is an interaction between creep and shrinkage for both concrete and timber which should be accounted for.

Due to such differences, the use of the EC5 Annex B formulas in conjunction with the effective modulus method may lead to significant approximations for timber-concrete composite beams subjected to long-term loading. Some research has recently been performed in order to investigate the influence of the aforementioned phenomena on the long-term behaviour of the composite structure and to incorporate them in a user-friendly design approach. Within the following sections the results of two of these studies are compared to one another and summarized in a jointed design proposal.

2 Consideration of inelastic strains in the design method

2.1 General approach

The internal forces and deflection of a timber-concrete composite beam resulting from inelastic strains due to different thermal expansion or different shrinkage of concrete and timber cannot be computed using the EC5 Annex B formulas. Since recent investigations pointed out that their influence is significant (Fragiacomo (2006), Schänzlin (2003)), it is quite important to propose a method for their evaluation.

The elastic solution of a simply supported composite beam with smeared flexible connection subjected to vertical load and different inelastic strains in the concrete slab and timber beam can be obtained by solving a differential equation. Since the problem is quite complex, simplified approaches have been developed and proposed:

- Superposition of the effects (deflection and internal forces) of vertical load with the effects of inelastic strains. For the former effects, the EC5 Annex B formulas can be used. For the latter effects, closed form formulas derived by integrating the differential equation of the composite beam with flexible connection are employed (Fragiacomo (2006), Fragiacomo and Ceccotti (2006)).
- Transformation of the inelastic strains into a fictitious vertical load and modification of the effective bending stiffness suggested by the EC5 Annex B (see Schänzlin (2003)). In this case all effects (deflection, internal forces) are evaluated using the EC5 Annex B formulas with the modification of the effective bending stiffness and the addition of a fictitious load equivalent to the inelastic strains.

2.2 Superposition of the effects according to Fragiacomo (2006)

In elastic phase, the principle of superposition can be used to separate the effects of vertical loads and inelastic strains. The effects (deflection, internal forces) of vertical loads can be computed using any design method which considers the flexibility of connection, such as the EC5 Annex B approach. The effects of inelastic strains in the concrete slab and timber beam of a simply supported composite beam with flexible connection can be computed using the rigorous formulas reported in the following:

- Input values
  - Difference of inelastic strains between concrete (subscript 1) and timber (subscript 2)
    $$\Delta\varepsilon = \Delta\varepsilon_2 - \Delta\varepsilon_1 \quad (1)$$
  - Geometrical properties (lever arm z, area A, second moment of area I, b and h being the breadth and depth of the i^{th} component, t being the distance between the top fibre of the

timber beam and the bottom fibre of the concrete slab)

$$z = 0.5 \cdot h_1 + t + 0.5 \cdot h_2\,,\ A_i = b_i \cdot h_i\,;\ I_i = \frac{b_i \cdot h_i^3}{12};\ i = 1,2 \tag{2}$$

- Stiffness (Young's modulus E)

$$(EA)^* = \frac{E_1 \cdot A_1 \cdot E_2 \cdot A_2}{E_1 \cdot A_1 + E_2 \cdot A_2}\ ;\ (EI)_{abs} = E_1 \cdot I_1 + E_2 \cdot I_2 \tag{3}$$

$$(EI)_{full} = (EI)_{abs} + (EA)^* \cdot z^2 \tag{4}$$

- Coefficient (Slip modulus of connection K_{ser}, connector spacing s_{ef}, span length L, distance from the left support to the cross-section x)

$$\alpha = \sqrt{\frac{K}{s_{ef}(EA)^*} \cdot \frac{(EI)_{full}}{(EI)_{abs}}} \tag{5}$$

$$\gamma_g(x) = 1 + \tanh(0.5\alpha L) \cdot \sinh(\alpha x) - \cosh(\alpha x) \tag{6}$$

- Mid-span deflection due to inelastic strains

$$u_{\max} = u_{\max,full} \cdot \gamma_u \qquad \text{where} \tag{7}$$

$$u_{\max,full} = \frac{\Delta\varepsilon}{z} \cdot \frac{(EI)_{full} - (EI)_{abs}}{(EI)_{full}} \cdot \frac{L^2}{8} \qquad \gamma_u = 1 - \frac{8}{(\alpha \cdot L)^2} \cdot \left[1 - \frac{1}{\cosh(0.5 \cdot \alpha \cdot L)}\right] \tag{8}$$

- Internal forces due to inelastic strains

$$N_2(x) = -N_1(x) = N_{2,\max,full} \cdot \gamma_g(x) \qquad \text{and} \qquad M_i(x) = M_{i,\max,full} \cdot \gamma_g(x) \tag{9}$$

$$\text{where} \qquad N_{2,\max,full} = -\frac{\Delta\varepsilon}{z} \cdot \frac{(EI)_{full} - (EI)_{abs}}{(EI)_{full}} \cdot \frac{(EI)_{abs}}{z}\ , \tag{10}$$

$$M_{i,\max,full} = \frac{\Delta\varepsilon}{z} \cdot \frac{(EI)_{full} - (EI)_{abs}}{(EI)_{full}} \cdot E_i \cdot I_i \qquad \text{and} \tag{11}$$

$$\gamma_g(x) = 1 + \tanh(0.5 \cdot \alpha \cdot L) \cdot \sinh(\alpha \cdot x) - \cosh(\alpha \cdot x) \tag{12}$$

- Shear forces in the connection due to inelastic strains

$$F(x) = K \cdot s_f(x) \qquad \text{where} \tag{13}$$

$$s_f(x) = s_{f,\max,abs} \cdot \gamma_s(x), \qquad s_{f,\max,abs} = -\Delta\varepsilon \cdot \frac{L}{2}, \tag{14}$$

$$\text{and} \qquad \gamma_s(x) = \frac{1}{0.5\alpha L} \cdot [\tanh(0.5 \cdot \alpha \cdot L) \cdot \cosh(\alpha \cdot x) - \sinh(\alpha \cdot x)] \tag{15}$$

The design procedure is summarized in the flowchart of Fig. 1

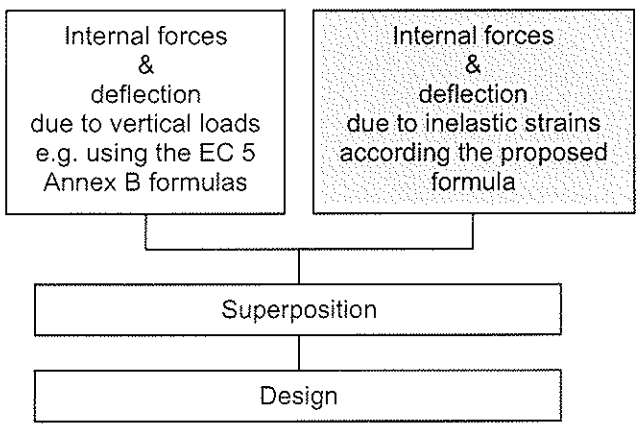

Fig. 1 Design procedure using the superposition of effects according to Fragiacomo (2006)

2.3 Consideration of inelastic strains using a fictitious load according to Schänzlin (2003)

The determination of the fictitious vertical load producing the same effects as the inelastic strains was performed in a first step by comparing the deflection of a composite beam subjected to both a sinusoidal loading and a sinusoidal inelastic strain along the beam length with the deflection of a homogenous beam with an unknown effective bending stiffness and the same loading (see Fig. 2).

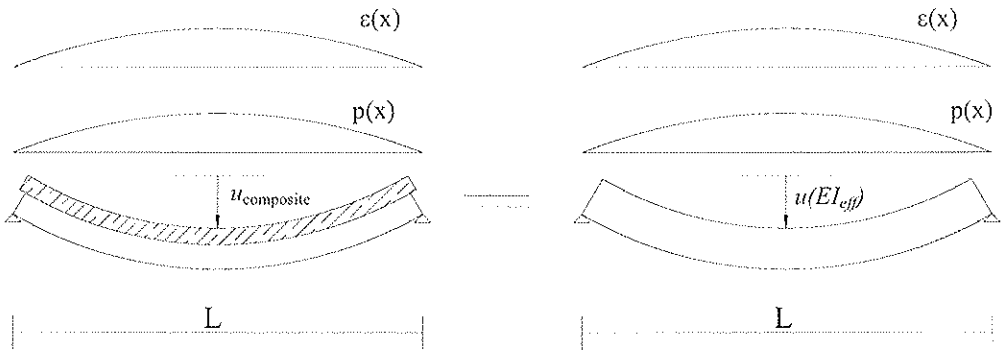

Fig. 2 Comparison of the deflection for the evaluation of the effective bending stiffness

Then the value of the effective stiffness EI_{eff} which makes the curvatures of both beams equal is calculated. Final formulas similar to those suggested by the EC 5 Annex B are obtained. Such formulas are listed below.

- Fictitious vertical load equivalent to the inelastic strains

$$p_{sls} = C_{p,sls} \cdot \Delta\varepsilon \tag{16}$$

where p_{sls} Fictitious vertical load, which represents the effects of inelastic strains on the structure

$C_{p,sls}$ Coefficient

$$= k_N \cdot \frac{E_1 \cdot A_1 \cdot E_2 \cdot A_2 \cdot z \cdot \gamma_1}{\left(E_1 \cdot A_1 + E_2 \cdot A_2\right) \cdot L^2} \tag{17}$$

$\Delta\varepsilon$ Difference in the inelastic strain between the timber beam (sub. 2) and the concrete slab (sub. 1)

$= \varepsilon_2 - \varepsilon_1$

k_N $= \pi^2$

- Effective bending stiffness

$$EI_{eff,sls} = C_{1,sls} \cdot EI_{EC5\ Annex\ B} \tag{18}$$

where $EI_{EC5\ Annex\ B}$ Effective bending stiffness according to EC5 Annex B

$C_{1,sls}$ Coefficient, which considers the interaction between vertical load q_d and inelastic strains in terms of slip in the joint

$$= \frac{p_{sls} + q_d}{\frac{E_1 \cdot A_1 + E_2 \cdot A_2}{\gamma_1 \cdot E_1 \cdot A_1 + E_2 \cdot A_2} \cdot p_{sls} + q_d} \tag{19}$$

γ_1 Coefficient calculated according to EC5 Annex B

- Bending moment of the concrete slab (sub. 1) and timber beam (sub. 2): since the curvature is assumed to be the same in both beams, the bending moment can be calculated with

$$M_i = \frac{E_i \cdot I_i}{EI_{eff,sls}} \cdot M\left(q_d + 0.8 \cdot p_{sls}\right) \tag{20}$$

where $EI_{eff,sls}$ Effective bending stiffness according to EC5 Annex B which accounts for the interaction between vertical load and inelastic strains (see Eq. (18))

M_i Bending moment of the i component

$M(q_d + 0.8 \cdot p_{sls})$ Resulting bending moment due to vertical load and part (80%) of the fictitious load equivalent to inelastic strains

- Axial forces: the axial forces are determined using the equilibrium equation:

$$N_i = \frac{M(q_d) - \sum_{i=1}^{2} M_i}{z} \tag{21}$$

where $M(q_d)$ Resulting bending moment due to vertical load only

z Distance between the centroids of the concrete slab and timber beam

- Shear forces F in the connection due to
  - shrinkage of the concrete slab:

$$V_{\max,res} = -\pi \cdot E_2 \cdot A_2 \cdot \frac{E_1 \cdot I_1 + E_2 \cdot I_2}{(\gamma_1 \cdot E_1 \cdot A_1 + E_2 \cdot A_2) \cdot L \cdot a_2} \cdot \Delta\varepsilon + V(q_d) \tag{22}$$

where $V(q_d)$ Resulting shear force due to vertical load only, calculated using the formulas (Eq. B.10) suggested by the Annex B of the EC5.

  - shrinkage of the timber beam

$$F = \frac{K}{s_{eff}} \cdot L \cdot \left[\frac{M_{\max,2} \cdot z}{\pi \cdot E_2 \cdot I_2} - \frac{E_1 \cdot A_1 + E_2 \cdot A_2}{\pi \cdot E_1 \cdot A_1 \cdot E_2 \cdot A_2} \cdot N_{\max,2} - \frac{\Delta\varepsilon}{2} \right] \tag{23}$$

The flowchart of the design procedure is displayed in Fig. 3.

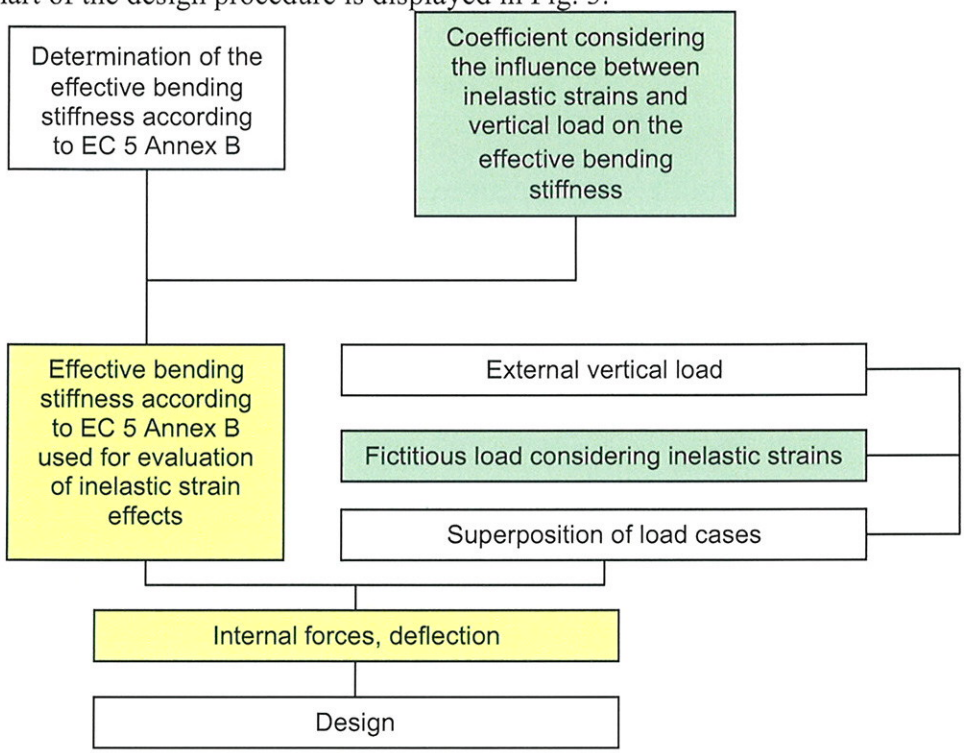

Fig. 3: Design procedure based on transformation of the inelastic strains into a fictitious load (Schänzlin 2003)

As visible, the proposed design approach is directly linked to the EC5 Annex B formulas where only some modifications such as the effective bending stiffness, the introduction of a new load case,

and some changes in the way of calculating the internal forces are introduced.

2.4 Comparison with the exact theoretical solution

Within the proposed design methods, some simplifications such as a sinusoidal distribution along the beam length of both the external vertical load and inelastic strain have been done. It is therefore important to assess the accuracy of the proposed approximated design methods against the theoretical exact solution obtained by Daboan et. al. (1993). About 2700 cases representing composite beams with different span lengths, concrete breadths and depths, timber breadths and depths, connection slip modulus, vertical load, and concrete shrinkage have been analysed (see Tab. 1).

Tab. 1: Range of parameters varied in the parametric analysis

	Minimum	Maximum
Climate	Indoor (SC1)	Sheltered, outdoor (SC2)
Elastic deflection limit	L/800	L/3000
γ coefficient according to EC5 Annex B	0.1	0.95
Span length in m	5.00	10.00
Timber beam (depth by breadth in cm)	18×10	44×10
Timber slab (depth by breadth in cm)	6×100	16×100
Concrete flange (beam) (depth by breadth in cm)	6×65	14×10
Concrete flange (slab) (depth by breadth in cm)	11×100	28×100
Difference in inelastic strains	0	60×10^{-6}

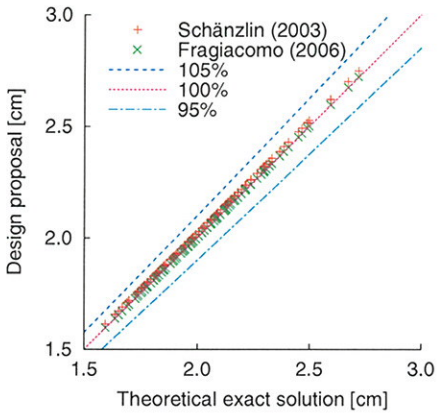

Fig. 4: Comparison of the mid-span deflections

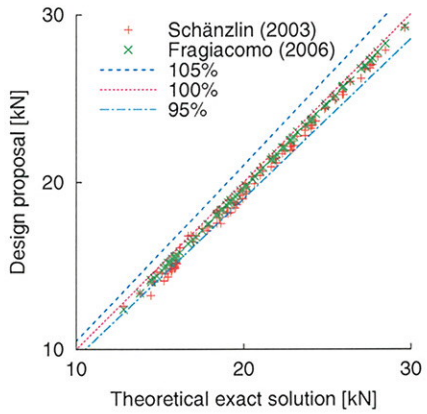

Fig. 5: Comparison of the timber and concrete axial forces at mid-span

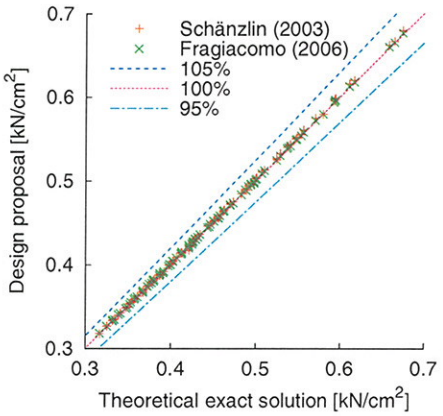

Fig. 6: Comparison of the bottom fibre timber stresses at mid-span

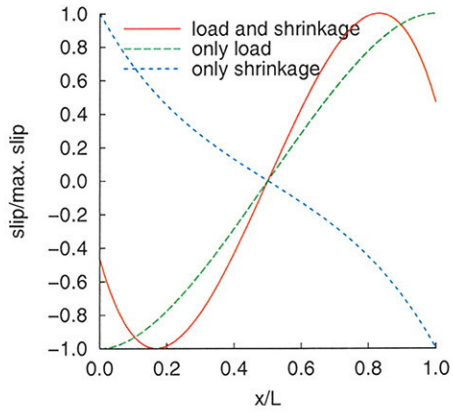

Fig. 7: Trend of the slip along the beam length

The outcomes of this extensive parametric analysis, displayed in Fig. 4 to Fig. 6, show that the differences among rigorous and simplified formulas do not exceed 5% on deflection, internal forces (bending moment and axial forces), and normal stresses.
However, some larger discrepancies can be recognized for the maximum shear forces in the connection. The reason for such differences in both design methods is the non-linear trend of the slip between concrete and timber due to vertical load and concrete shrinkage. Since the slip resulting from the vertical load is different and opposite from that caused by concrete shrinkage, the superposition results in a trend where the peak value is not at the support but at a cross-section between the support and mid-span (Fig. 7). Therefore differences appear between the theoretical exact solution and the design proposals. At the support, the approach according to Fragiacomo (2006) provides good approximation for slips and shear forces, whereas the approach according to Schänzlin (2003) overestimates the maximum shear flow in the joint. Since concrete shrinkage causes slip and shear opposite to those due to external vertical load, the concrete shrinkage can be ignored in the design of the connectors. The most critical condition for the connection will be, in fact, in the short-term ($t = 0$) when shrinkage has not appeared yet. On the other hand an increase in temperature will result in positive slips and shear forces which will increase the slip and shear due to external load. In this case the effect of inelastic strains cannot be neglected. However, since the maximum value will be at the support, in this case both approaches lead to good approximations and can be used.

3 Effective creep coefficients in timber-concrete composite structures

Creep coefficients are defined as the ratio between delayed and elastic deformation under constant loading:

$$\varphi = \frac{u_{creep}}{u_{elastic}} = \frac{\varepsilon_{creep}}{\varepsilon_{elastic}} = \frac{u_{total} - u_{elastic}}{u_{elastic}} = \frac{\varepsilon_{total} - \varepsilon_{elastic}}{\varepsilon_{elastic}} \tag{24}$$

where φ, u, ε are the creep coefficient, displacement and strain, respectively. The effective modulus method is a simplified method that can be used to consider the influence of the creep strain in the determination of the internal forces. Such a method is based on the introduction of a fictitious reduced elastic modulus (the "effective modulus") obtained by dividing the elastic modulus by one plus the creep coefficient of the material:

$$\varepsilon_{total} = \varepsilon_{elastic} + \varepsilon_{creep} = \varepsilon_{elastic} + \varphi \cdot \varepsilon_{elastic} = (1+\varphi) \cdot \frac{\sigma}{E} = \frac{\sigma}{E_{eff}} \text{ where } E_{eff} = \frac{E}{(1+\varphi)} \tag{25}$$

By means of the effective modulus, the creep coefficient directly affects the stress distribution and the deflection of the structure.

In composite beams, where the creep strains in the component materials (concrete, timber and connection) differ from each other, the elastic strain is not constant over time due to the compatibility of the deformation (see Fig. 8).

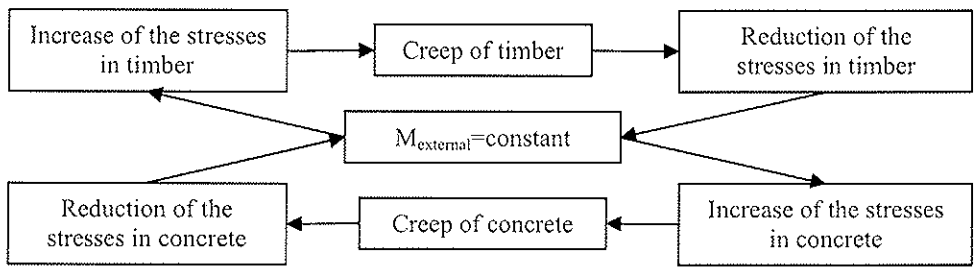

Fig. 8: Stress redistribution taking place in timber-concrete composite structures

Therefore a modification of the creep coefficients should be introduced in order to account for the compatibility of deformation and therefore improve the accuracy of deflection and stresses. In order to investigate the influence in the long-term of the interaction between the cross sections in composite slabs, Ruesch and Jungwirth (1976) derived effective creep coefficients in statically indeterminate composite systems made from two different concrete cross sections rigidly connected to each other. Kreuzinger (1994) extended the formulas in order to account for the flexibility of the connectors. Both approaches hypothesize an affine temporal development of the creep strains. In the case of a timber-concrete composite structure, however, the temporal development of the creep coefficients of timber, concrete and connection significantly differ from each other.

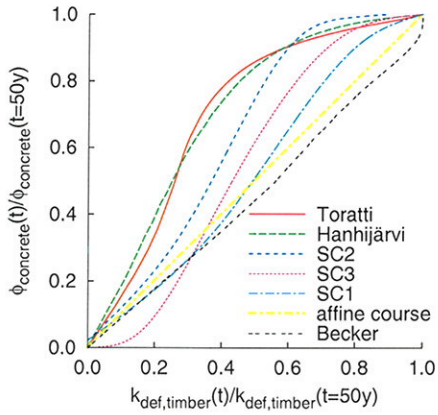

Fig. 9: Comparison among different creep coefficients of timber relative to concrete (SC=Service Class)

Tab. 2: Intervals for consideration of the different temporal development of creep coefficients based on the rheological model developed by Hanhijärvi (1995)

Interval	Timber	Concrete
	$\Delta\varphi_{t,Mat,i} / \varphi_{t,Mat}(t=\infty)$	$\Delta\varphi_{c,Mat,i} / \varphi_{c,Mat}(t=\infty)$
1	40%	85%
2	20%	15%
3	40%	0%

Fig. 9 compares different rheological models used for timber, showing a large scatter in results. However, in most of the models and according to EC5 (1995), timber creeps at a slower rate than concrete. Therefore concrete reduces its stresses and timber increases its stresses over time. Even though this tendency is reduced by the creep taking place in the connection system, not only are the initial and the final point in time of interest for the design of the composite beam, but also the period of time between $t = 3$ and $t = 7$ years. Within this period, in fact, concrete has reached about 95% of its final creep strain, whereas timber has reached only about 60% of its final creep value according to the models of Hanhijärvi (1995) and Toratti (1992). This will cause the highest peak of stresses over the entire service life to occur in timber during the period of time between $t = 3$ and $t = 7$ years.

Since there is no affine development of the creep strain among concrete, timber and connection, the different temporal development of the creep strain should be considered in the determination of the effective creep coefficients. To this purpose, the entire service life can be divided into time intervals where an affine trend can approximately be assumed. The effective creep coefficients can then be determined using the equation:

$$\Delta\varphi_{u,Comp,i} = \frac{\Delta\varphi_{u,Mat,i}}{\Delta\Psi_i} \cdot \frac{\left(\frac{\Delta\varphi_{w,Mat,i}}{\Delta\Psi_i} - 1\right) \cdot e^{-\Delta\Psi_i} - \frac{\Delta\varphi_{w,Mat,i}}{\Delta\Psi_i} - \Delta\varphi_{w,Mat,i} - 1}{\prod_{j=i}^{n}\left(\left(1 - \frac{\Delta\varphi_{w,Mat,j}}{\Delta\Psi_j}\right) \cdot e^{-\Delta\Psi_j} + \frac{\Delta\varphi_{w,Mat,j}}{\Delta\Psi_j}\right)} \tag{26}$$

where
- n Numbers of time intervals in which the entire service life has been divided into
- i Current time interval
- $\Delta\varphi$ Variation of the material creep coefficient in the time interval (see Tab. 2)
- $\Delta\Psi$ Variation of the creep coefficient of the system (see Ruesch and Jungwirth (1976))
- $Comp$ Composite beam

Mat Material

$u,,w$ Component of the composite beam, e.g. timber and concrete

Since this formula is too complex for design purposes, a parametric analysis has been carried out in order to determine the increase of the creep coefficients of timber (subscript t) and concrete (subscript c) due to the load redistribution. In this parametric analysis, different parameters have been varied (see Tab. 1). The effective creep coefficients can therefore be determined using the equation

$$k_{def,composite} = \psi_t \cdot k_{def,EC5} \text{ and } \varphi_{composite} = \psi_c \cdot \varphi_{EC2} \quad (27)$$

The increase in creep coefficient due to the stress redistribution in simply supported composite beams subjected to vertical load can be determined using the formulas reported in Table 3.

Tab. 3: ψ coefficients for the evaluation of the effective creep coefficient due to the influence of composite action and different temporal development of the creep strain (subscript t= timber, subscript c= concrete, γ_1 calculated according to EC5 Annex B, Eq. (B.5))

$\psi_{c,\text{indoor-climate}} = 2.59 - 0.75 \cdot \gamma_1^{3.32}$ $\psi_{c,\text{outoor-climate}} = 1.82 - 0.24 \cdot \gamma_1^{3.51}$	for slab systems ($b_t = b_c$, $1/3 \leq A_c/A_t \leq 1$), and for beam systems ($b_t << b_c$, $1 \leq A_c/A_t \leq 3$) for $t = 50$y
$\psi_{c,\text{indoor-climate}} = 2.47 - 1.05 \cdot \gamma_1^{1.70}$ $\psi_{c,\text{outdoor-climate}} = 1.72 - 0.45 \cdot \gamma_1^{1.73}$	for slab systems ($b_t = b_c$, $1/3 \leq A_c/A_t \leq 1$), and for beam systems ($b_t << b_c$, $1 \leq A_c/A_t \leq 3$) for $t = 3$-7y
$\psi_t(t = 3-7y) = 0.5$; $\psi_t(t = 50y) = 1.0$	For beam and slab systems

The increase in creep coefficients due to the stress redistribution can then be considered in the design using the formulas:

$$E_{t,eff} = \frac{1}{1+\psi_t \cdot k_{def}} \cdot E_t(t=0), E_{c,eff} = \frac{1}{1+\psi_c \cdot \varphi} \cdot E_c(t=28d) \text{ and } K_{eff} = \frac{1}{1+2 \cdot k_{def}} \cdot K(t=0) \quad (28)$$

Since the determination of the effective creep coefficients depends on the type of loading, shrinkage would lead to a different effective creep coefficient. An effective shrinkage has then been introduced to simplify the evaluation of the long-term effects. The effective shrinkage takes into account the different creep behaviour due to a constant vertical loading or an imposed displacement/strain such as inelastic strains. The creep of material, in fact, reduces the eigenstresses in statically indeterminate systems subjected to imposed displacements/strains. Based on the outcomes of an extensive parametric analysis, the value of the effective shrinkage was computed as

$$\varepsilon_{eff}(t = 3-7y) = 0.5 \cdot \varepsilon_{Material} \text{ and } \varepsilon_{eff}(t = 50y) = 0.8 \cdot \varepsilon_{Material} \quad (29)$$

4 Concluding remarks

In this paper, two different design approaches for the evaluation of the influence of inelastic strains on the behaviour of timber-concrete composite beams have been introduced and discussed. One approach is directly linked to the EC5 Annex B and based on the evaluation of an external fictitious load equivalent to the effect of inelastic strains. In the other proposal, the internal forces and deflections due to inelastic strains and vertical load are separately evaluated and then superimposed. Therefore such proposal can be used in conjunction with any design method for composite beams under vertical load accounting for the flexibility of the connection system.

In addition, effective creep coefficients have been introduced since the redistribution of the internal forces during the service life affects the relationship between creep strain and elastic strains. The different temporal development of the creep strains has also to be considered, since normally

concrete creeps faster than timber. As a consequence of that, the stresses in timber can reach their maximum value within the period between 3 to 7 years, especially if concrete shrinkage is avoided or reduced by using special admixtures.

However several questions are still open for the design of timber-concrete composite structures, such as the value of the factored load coefficient γ_F for shrinkage to be used in ultimate limit state design. Only in DIN Fachbericht 104 (2003) on composite bridges a γ_F value of 1.0 is proposed. The use of this proposal for timber-concrete structures is questionable, since the steel profile provides a ductile behaviour for the steel-concrete composite beam. Additional stresses due to increasing concrete shrinkage can then be resisted by plasticization of the steel leading to an increase in deflection but with very little reduction in load-bearing capacity. However timber is not as ductile as steel, and the increase in stresses due to concrete shrinkage and difference in creep coefficient may lead to brittle failure of the timber beam in tension.

5 References

Becker, P. (2002). „Modellierung des zeit- und feuchteabhängigen Materialverhaltens zur Untersuchung des Langzeitverhaltens von Druckstäben aus Holz", Bauhaus-Universität Weimar, *Ph.D Thesis*.

Ceccotti, A. (1995). "Timber-concrete composite structures." *Timber Engineering, Step 2*, First Edition, Centrum Hout, The Netherlands, E13/1-E13/12.

Ceccotti, A., Fragiacomo, M., and Giordano, S. (2007). "Long-term and collapse tests on a timber-concrete composite beam with glued-in connection." *Materials and Structures, RILEM, Special Volume "Research for Reliable Timber Structures"*, 40(1), 15-25.

Dabaon, M., Tschemmernegg, F., Hassen, K., and Lateef, T. A. (1993). "Zur Tragfähigkeit von Verbundträgern bei teilweiser Verdübelung." *Stahlbau*, 62, 3–9.

DIN Fachbericht 104 (2003) Verbundbrücken.

EC 5 (2005) Design of timber structures Part 1-1 General Rules General rules and rules for buildings.

Fragiacomo, M. (2006). "Long-term behavior of timber-concrete composite beams. II: Numerical analysis and simplified evaluation." *Journal of Structural Engineering*, 132(1), 23-33.

Fragiacomo, M., and Ceccotti, A. (2006). "Simplified approach for the long-term behaviour of timber-concrete composite beams according to the Eurocode 5 provisions." *Meeting thirty-nine of the Working Commission W18-Timber Structures, CIB, International Council for Research and Innovation*, Florence (Italy), August 28-31, paper No. 39-9-1, 12 pp.

Hanhijärvi, A. (1995). "Modelling of creep deformation mechanisms in wood." Helsinki University of Technology. Technical Research Centre of Finland. VTT Publications. Espoo (SF), *Ph.D Thesis*.

Kreuzinger, H. (1994). *Verbundkonstruktionen Holz / Beton*.

Ruesch, H. and Jungwirth, D. (1976). *Stahlbeton, Spannbeton - Berücksichtigung der Einflüsse von Kriechen und Schwinden auf das Verhalten der Tragwerke*. Bd. 2. Werner-Verlag.

Schänzlin, J. (2003). "Zum Langzeitverhalten von Brettstapel-Beton-Verbunddecken.", Institut für Konstruktion und Entwurf, University of Stuttgart, *Ph.D Thesis*.

Schänzlin, J. and Kuhlmann, U. (2004) "Time dependent behaviour of timber-concrete-composite structures" In: *Proceedings of the 8th World Conference on Timber Engineering, WCTE 2004, Lahti, Finland*, June 14-17, 2004, pp. 313-318.

Toratti, T. (1992). "Creep of timber beams in variable environment." Helsinki University of Technology, Laboratory of Structural Engineering and Building Physics, *Ph.D Thesis*.

INTERNATIONAL COUNCIL FOR RESEARCH AND INNOVATION
IN BUILDING AND CONSTRUCTION

WORKING COMMISSION W18 - TIMBER STRUCTURES

SIMPLIFIED DESIGN METHOD FOR MECHANICALLY JOINTED BEAMS

U A Girhammar

Civil Engineering, Faculty of Science and Technology
Umeå University

SWEDEN

MEETING FORTY

BLED

SLOVENIA

AUGUST 2007

Presented by U.A. Girhammar
H. Blass commented on the choice of buckling length to come close to exact solution.
A. Frangi questioned the influence of variability of the material properties which is more important than the calculation work. U.A. Girhammar agreed but stated why not use a better method.

Simplified design method for mechanically jointed beams

Ulf Arne Girhammar
Department of TFE – Civil Engineering, Faculty of Science and Technology,
Umeå University, Sweden

Abstract

A simplified analysis and design method for composite beams with partial interaction that predicts the deflections and internal actions and stresses is proposed. The method is general in nature and can be applied to arbitrary boundary and loading conditions, and material and geometry parameters. A corresponding approximate method for mechanically jointed beams is given in Eurocode 5, Annex B. This method was originally developed on the basis of only simply supported end conditions. However, for other boundary conditions Eurocode 5 gives recommendations that generally are not as accurate as those obtained from the method presented in this paper. An effective bending stiffness is introduced that reflects the influence of the interlayer slip and depends on the partial composite action (or shear connector) parameter and the relative bending stiffness parameter, which also are defined in the paper. The effective beam length of the problem equals the buckling length for the corresponding column buckling problem. The proposed method is applied to a number of practical cases and the approximate results are compared with the exact values. The results of the approximate analysis procedure are found to be extremely good for beam deflections and usually very good for internal actions and stresses, except for interlayer slip forces. For the simply supported beam case where the Eurocode 5 method is applicable all values coincide. For other boundary conditions, the error in the Eurocode 5 procedure can be up to 36 % depending on the recommended value for the effective beam length.

The proposed method was derived independently and is presented in a somewhat different way, but is basically the same as the present Eurocode 5 method. Except for, in the author's opinion, being simpler to apply, the proposed method clarifies the "correct" way to choose, for different boundary conditions, the effective beam length to be used in either procedure.

1 Introduction

Common types of composite constructions are built up of different combinations of beams and plates. These members are used in building constructions as floor and wall components and in bridge construction. Often the beams and plates are attached to each other by different kinds of shear connectors as studs, screws and nails. These mechanical connectors usually permit interlayer slip between the constituents and, therefore, only partial composite action will develop. A typical interlayer shear load (V_s) – interlayer slip (Δu) relationship for a flexible shear connection is usually non-linear, but frequently approximated by a linear relationship, $V_s = K \cdot \Delta u$, i.e. by using a constant slip modulus (K).

The one-dimensional, linear elastic, partial composite action theory is well established. Exact methods for composite beams and beam-columns have been developed, e.g. by Girhammar & Gopu (1993) and Girhammar & Pan (2007). However, for a general case this theory is complex and often very cumbersome to apply. Therefore, these refined procedures are not suitable for practical design work. This paper presents approximate static analysis

procedure for designing composite beams with interlayer slip. The proposed method is parallel to the Eurocode 5 method, but it is general in nature and can be applied to arbitrary boundary and loading conditions.

Based on this theory, the author presented a simplified analysis method for composite beams with partial interaction to the Swedish and European civil engineering community, Girhammar (1985, 1992). An effective bending stiffness was introduced that accounted for the effective beam length depending on the boundary conditions. The methods were used to calculate the deflection as well as the internal actions of the beam. Independently, McCutcheon (1986) proposed an 'emperical' composite bending stiffness for partially composite simply supported beams. He also suggested a procedure to evaluate the interlayer slip (and hence the interlayer shear stresses), but it was proved not to be correct or too simplified by Kumar & Gopu (1987). In fact, it will be shown in this paper that the McCutcheon procedure to calculate the composite bending stiffness is an approximate expression of a special case of the general method proposed by the author. The McCutcheon formula has been utilized in a number of subsequent studies.

Wang (1998) developed a simple approach for calculating maximum deflections in composite steel-concrete composite beams with partial interaction based on the theoretical results presented by Girhammar & Gopu (1993). On the basis of the solution for a special case of a simply supported beam with uniformly distributed load, he extended on intuitive grounds the applicability of this solution to more general arrangements of beam loading and boundary conditions. The validation of this extension was checked by comparisons with results obtained from finite element analyses and with experimental results. He found very good agreements between these results and the approximate predictions. However, the good agreement was due to the fact that his "intuitive" choice of effective beam length was very close to the "correct" effective length taken as the corresponding "buckling length" as demonstrated in this paper.

Eurocode 5 summarizes a simplified method to calculate an effective bending stiffness and to predict the internal actions. The method is based on the exact solution for a simply supported partially composite Euler-Bernoulli beam subjected to a sinusoidal distributed load, cf. e.g. Cecotti (2003). This solution is used to define an effective bending stiffness that, as usual, depends on the length of the beam. The basis for this method is probably the works of Möhler (1956), Schelling (1968), and Heimeshoff (1987). Even though the method is restricted to simply supported beams, Eurocode 5 allows for extensions to beams with other boundary conditions. The code recommends an effective beam length of 0.8 times the relevant span for continuous beams and of twice the length for cantilever beams. Cecotti (2003) indicates that the effective beam length to be used in the effective bending stiffness equation should be the distance between two zero-moment points. As shown in this paper, this is not the most accurate choice for the effective beam length.

Eurocode 5 suggests an approximate expression for the maximum shear stress that is not theoretically correct or accurate. It can be regarded as an upper bound for the shear stress. This formula is repeated in Cecotti (2003) (unfortunately with a minor misprint). However, a theoretically exact way of calculating the maximum shear stress is found in earlier versions of the code, CIB (1983) and CEN (1993), or in the text book by Larsen & Riberholt (2005). In these publications (except CEN, 1993), also the distance to the neutral axis of the sub-element, where the normal stresses are zero and the maximum shear stresses occur, are found. In this paper, an alternative expression is given.

The purpose of this paper is to present an approximate static analysis procedure for

partially composite beams with arbitrary boundary, loading and geometrical conditions based on the exact static analysis methods for beams and beam-columns presented by Girhammar & Gopu (1993) and Girhammar & Pan (2007). The method is illustrated for two-layered partially composite beams. Extension to a three-layered beam is straight forward, but will not be treated here. Multi-layered beams are the object of another study.

1 Theoretical background on exact analysis

1.1 Basic assumptions

The partial composite action theory for Euler-Bernoulli beams with interlayer slip is based on the Stüssi-Granholm-Newmark-Pleshkov model, see Girhammar & Pan (2007). The mechanical fasteners are evenly spaced and assumed to produce uniformly distributed slip forces or interlayer shear stresses with a constant slip modulus K [N/m^2]. Full composite action (infinite slip stiffness, $K \rightarrow \infty$) and non-composite action (zero slip stiffness, $K \rightarrow 0$) represent upper and lower bounds for the partial composite action.

The geometric parameters defining a typical composite beam with two sub-elements of different materials are shown in Fig. 1. The subscripts '1' and '2' refer to the top and bottom elements of the cross-section, respectively. The x-axis of the coordinate system is located in the centroid of the fully composite section.

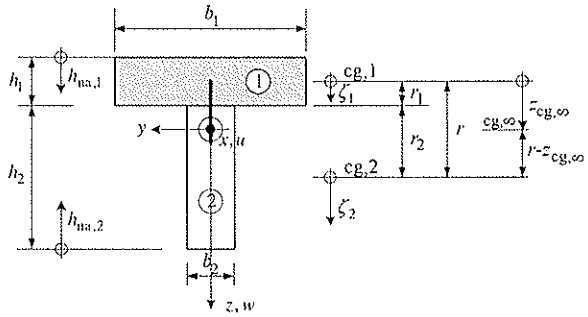

Figure 1. Geometric parameters of composite beam (cg = centre of gravity).

A free-body diagram of a differential element in the composite beam subjected to a distributed transverse loading (q) and an axial load (P) acting in the centriod of the fully composite section ($z_{cg,\infty}$) is shown in Fig. 2, where moments (M, M_1, M_2), shear forces (V, V_1, V_2), normal forces (N, N_1, N_2), slip force per unit length (V_s) are defined. The location

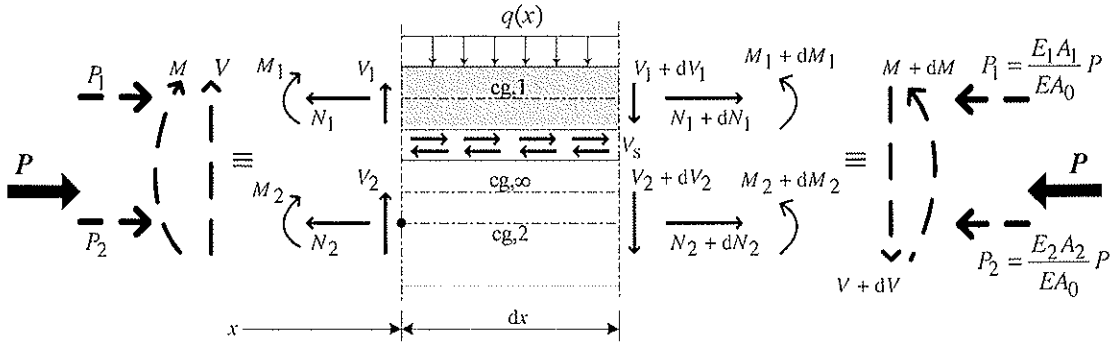

Figure 2. Differential element in the composite beam-column subjected to a distributed transverse load and axial loading. Definition of internal forces and moments as shown.

of P at the centroid implies that P_1 and P_2 are proportioned in accordance with the relative axial stiffnesses of the elements they are acting on. This type of axial load application ensures that the axial loads induce uniform axial strain in the member and do not contribute to the bending of the member. The total axial stiffness of the member, $(EA)_0 = E_1A_1 + E_2A_2$, is for convenience denoted simply EA_0. The same kind of notation will be used for the bending stiffness, $(EI) = EI$. The interlayer slip is denoted by Δu. The length of the composite beam is denoted L.

1.2 Beams subjected to transverse loading

Girhammar & Gopu (1993) and Girhammar & Pan (2007) derived for a partial composite beam subjected to transverse loads the differential equation and the general solution in terms of the displacement w. By knowing the solution w for a given set of boundary conditions, the various internal actions can be obtained. They introduced two parameters that govern the behaviour of composite beams with interlayer slip; the non-dimensional partial composite action (or shear connector) parameter, αL, and the non-dimensional relative bending stiffness parameter, EI_0/EI_∞, as

$$\alpha L = \sqrt{\frac{Kr^2}{EI_0(1-\frac{EI_0}{EI_\infty})}}\,L; \qquad \frac{EI_0}{EI_\infty} = \frac{1}{1+\frac{EA_p\,r^2}{EA_0\,EI_0}} \tag{1)-(2)}$$

where

$$\begin{cases} EI_0 = E_1I_1 + E_2I_2 \\ EI_\infty = EI_0 + \dfrac{EA_p r^2}{EA_0} \end{cases}; \qquad \begin{cases} EA_0 = E_1A_1 + E_2A_2 \\ EA_p = E_1A_1 \cdot E_2A_2 \end{cases} \tag{3)-(4)}$$

where E_iI_i, EI_0, EI_∞ = bending stiffness of the i^{th} sub-element, of the non-composite section ($K \to 0$), and of the fully composite section ($K \to \infty$) and E_iA_i, EA_0, EA_p = axial stiffness of the i^{th} sub-element, sum, and product of the axial stiffness of sub-elements.

The practical range for the composite action parameter is of the order of $0.1 < \alpha L < 100$ or often even more narrow, $1 < \alpha L < 10$, for many applications. For rectangular sub-elements, the interval for the relative bending stiffness parameter is $0.25 \le EI_0/EI_\infty < 1$. For further details, see Girhammar & Pan (2007).

The exact solutions for the partially composite beams with the different boundary and loading conditions discussed in this paper are not presented here.

1.3 Beam-columns subjected to both transverse and axial loading

Girhammar et al. (1993, 2007) also derived for a partial composite beam-column subjected to both transverse and axial loads the differential equation and the general solution in terms of the displacement w. If $q = 0$, that equation and solution reduces to that valid for a pure column. The critical buckling load, P_{cr}, was obtained as

$$P_{cr} = \theta_{cr}^2 \frac{EI_\infty}{1+\frac{\frac{EI_\infty}{EI_0}-1}{1+\frac{\alpha^2}{\theta_{cr}^2}}} = \frac{\theta_{cr}^2}{\theta_{cr,\infty}^2} \frac{1}{1+\frac{\frac{EI_\infty}{EI_0}-1}{1+\frac{\alpha^2}{\theta_{cr}^2}}} P_{cr,\infty} \tag{5}$$

where $\theta_{cr} = \pi/\mu L$ is the (fundamental) eigenvalue that depends on the boundary conditions or the buckling length coefficient (μ), and $P_{cr,\infty} = \theta_{cr,\infty}^2 EI_\infty$ the (fundamental) buckling load for a fully composite section. It was shown by Girhammar & Pan (2007) that the buckling length coefficients for partially composite columns with boundary conditions according to the four Euler cases can, from a practical point of view, be taken the same as those valid for fully composite or ordinary solid columns, i.e. $\mu \approx \mu_\infty$. The coefficients, μ_∞, are readily available in engineering handbooks.

1.4 Effective bending stiffness for partially composite beams

Based on eqn (5) and using the fact that $\mu \approx \mu_\infty$, they introduced an effective bending stiffness, EI_{eff}, for partially composite beams as

$$EI_{eff} = \frac{EI_\infty}{1 + \dfrac{\dfrac{EI_\infty}{EI_0} - 1}{1 + \dfrac{\mu^2}{\pi^2}(\alpha L)^2}} \tag{6}$$

For a simply supported member ($\mu = 1$), eqn (6) gives $EI_{eff} = EI_\infty/[1 + f_\Delta(EI_\infty/EI_0 - 1)]$, where $f_\Delta = \pi^2/[(\alpha L)^2 + \pi^2]$. McCutcheon (1986) proposed a composite bending stiffness for simply supported members with the parameter given by $f_\Delta = 10/[(\alpha L)^2 + 10]$. His parameter was established by evaluating a number pinned-pinned beams subjected to various loading conditions. It is obvious that the general effective bending stiffness proposed in this paper reduces to the approximate composite bending stiffness for simply supported beams as proposed by McCutcheon (1986).

In Appendix A, an alternative way of expressing the effective bending stiffness is given. This is done for reasons of comparison with the effective bending stiffness presented in Eurocode 5 as discussed in later sections.

2 Simplified analysis and design method

2.1 General

The exact procedure for computing deflections and internal actions in partially composite beams is very cumbersome and not well suited for design applications. For this reason, an approximate procedure for determining these quantities, which correspond to the exact analysis results, is presented here. A comparison of the results obtained from the exact and approximate procedures for a number of practical cases will be made in section 4.

2.2 Deflections in partially composite beams

An approximate solution to the deflection of partially composite members can be obtained by replacing the fully composite bending stiffness (EI_∞) with the effective bending stiffness (EI_{eff}) in the expressions for the deflection of corresponding fully composite members, i.e.

$$w_{eff} = \frac{EI_\infty}{EI_{eff}} \cdot w_\infty \tag{7}$$

where w_{eff} is the approximate deflection in a partially composite beam and w_∞ the exact one in a fully composite member (usually readily available in structural handbooks). The approximate solutions for partially composite beams with the different boundary and loading conditions discussed in this paper are not presented here.

2.3 Internal actions and stresses in partially composite beams

An approximate value of the internal actions and stresses in partially composite members can in a corresponding way be obtained by replacing EI_∞ with EI_{eff} in the expressions for the internal actions and stresses in fully composite beams. For the internal actions we arrive at

$$N_{i,\text{eff}} = \mp(1-\frac{EI_0}{EI_{\text{eff}}})\frac{M}{r}; \qquad M_{i,\text{eff}} = \frac{E_i I_i}{EI_{\text{eff}}}M; \qquad V_{\text{s,eff}} = (1-\frac{EI_0}{EI_{\text{eff}}})\frac{V}{r} \qquad (8)\text{-}(10)$$

where the minus sign in eqn (8) refers to $i = 1$ and plus sign to $i = 2$. The maximum normal stresses from the internal normal force and moment, respectively, are then given by

$$\sigma_{i,\text{eff,n}} = (1-\frac{EI_0}{EI_{\text{eff}}})\frac{M}{A_i r}; \qquad \sigma_{i,\text{eff,m,max}} = \frac{E_i h_i}{EI_{\text{eff}}}\frac{M}{2} \qquad (11)\text{-}(12)$$

The maximum shear stress occurs where the normal stress is zero or at the location of the neutral axis of the sub-element. Introducing the effective bending stiffness in the expression for maximum shear stresses in the individual sub-components in ordinary fully composite beams we arrive at

$$\tau_{i,\text{eff,max}} = \frac{V ES_{\text{na},i}}{EI_{\text{eff}} b_i} = \frac{E_i h_{\text{na},i}^2}{EI_{\text{eff}}}\frac{V}{2} \qquad (13)$$

where $ES_{\text{na},i}$ is the first moment of the axial stiffness of the sheared area with respect to the neutral axis of the i^{th} sub-element. For a rectangular cross-section, this parameter is given by $ES_{\text{na},i} = E_i h_{\text{na},i}^2/2$, where according to eqn (B.2) in Appendix B,

$$h_{\text{na},i} = r_i + (1-\frac{EI_0}{EI_{\text{eff}}})\frac{EI_{\text{eff}}}{E_i A_i r} \qquad (14)$$

Hence, the last expression in eqn (13) and eqn (14) is only valid for rectangular cross-sections. The interlayer shear or slip force per unit length is given by eqn (10). The load on a fastener is then obtained by multiplying that interlayer slip force with the (effective) spacing of the fasteners, s, i.e.,

$$F_{\text{s,eff}} = V_s s = (1-\frac{EI_0}{EI_{\text{eff}}})\frac{s}{r}V \qquad (15)$$

The interlayer slip is given by $\Delta u = V_{s,\text{eff}}/K$. It is clear from eqns (8)–(10) that in a partially composite beam the internal normal forces are always less, the internal bending moments always greater, and the interlayer shear stresses always less than their corresponding values in a fully composite beam.

3 Illustrative examples

3.1 Evaluation of approximate deflections – Different effective beam lengths

The exact and approximate expressions for the deflections of partially composite beams with the four different Euler boundary conditions and subjected to a uniformly distributed (q_0) and a midspan loading (Q), respectively, have been derived (but is not presented here). For a cross-section according to Figure 3, the exact and approximate deflections are presented in Table 1. In the table, the deflection for a corresponding fully composite beam ($w_{\infty,\max}$) is also given. The approximate deflections are calculated according to the method presented in this paper and also according to the procedure given in Eurocode 5 (2004).

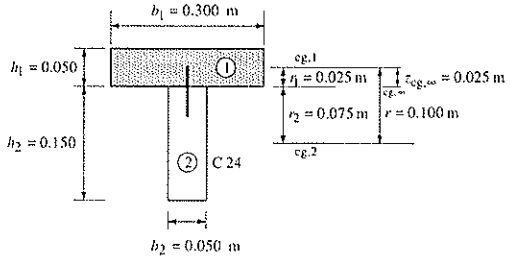

Modulus [GPa]	Axial Stiffness [MN]	Bending Stiffness [MNm^2]	Parameters
K = 0.05	E_1A_1 = 180	E_1I_1 = 0.0375	q_0 = 1 kN/m
E_1 = 12	E_2A_2 = 60	E_2I_2 = 0.113	L = 4 m
E_2 = 8	EA_0 = 240	EI_0 = 0.150	α = 2.11 /m
		EI_∞ = 0.600	αL = 8.43
		EI_{eff} = 0.439	θ_{cr} = 0.785 /m

(Uncracked concrete plate in compression.)

Fig. 3. Simply supported composite timber-concrete beam.

Table 1. Comparisons of maximum deflections obtained from exact and approximate analysis for partially composite beams with different boundary conditions — Composite timber-concrete beam according to Figure 3.

Boundary and loading Conditions	Exact $w_{\infty,\max}$ [mm]	Exact $w_{\max}$ [mm]	Approximate, $w_{\text{eff},\max}$ [mm]			
			Present method	Error %	Euro-code 5	Error %
Clamped-free (μ = 2); L = 2 m						
• Distributed load (q_0 = 1 kN/m)	3.33	4.76	4.55	-4.6	4.54[1)]	-4.9
• Point load (Q = 1 kN)	4.44	6.16	6.07	-1.5	6.07	-1.5
Pinned-pinned (μ = 1); L = 4 m						
• Distributed load (q_0 = 1 kN/m)	5.56	7.56	7.59	+0.4	7.59	+0.4
• Point load (Q = 1 kN)	2.22	3.08	3.03	-1.5	3.03	-1.5
Pinned-clamped (μ = 0.7); L = 4 m						
• Distributed load (q_0 = 1 kN/m)	2.30	3.86	3.83	-0.6	3.53[2)]	-9.3
					3.67[3)]	-5.1
Clamped-clamped (μ = 0.5); L = 4 m						
• Distributed load (q_0 = 1 kN/m)	1.11	2.32	2.30	-1.0	1.70[2)]	-36.0
					2.09[4)]	-11.2

1) For cantilevered beams, Eurocode 5 recommends that the effective beam length equals twice the actual length.

2) For continuous beams, Eurocode 5 recommends that the effective beam length equals 0.8 of the relevant length.

3) The effective beam length chosen as the distance between the two zero-moment points in the propped beam, i.e. L = 0.75 × 4 = 3 m.

4) The effective beam length chosen as the distance between the two zero-moment points in the clamped beam, i.e. L = 0.5794 × 4 = 2.32 m.

It is evident from Table 1 that the present method predicts (extremely) well the deflections for various boundary conditions. For simply supported beams, the values obtained from the present method and from Eurocode 5 coincide as they should. Also, there is full agreement between the two methods for the cantilever case. This is due to the fact that Eurocode 5 recommends an effective beam length that is equal to the "correct" corresponding buckling length. However, for the propped and fixed beams, there is a big difference in the results due to the big difference between the recommended effective beam length and the "correct" corresponding buckling length. If an effective beam length equal to the distance between the zero-moment points is chosen, the difference between exact and approximate values is reduced considerably, but far from as close as those obtained from the present method.

3.2 Evaluation of approximate stresses — Different geometrical designs

The deflections and internal stresses in five partial composite beams (details not shown here) with different support and loading conditions and different material and geometry parameters are computed by using the expressions obtained from the exact and approximate analysis procedures. The results obtained from the two procedures are compared in terms of their maximum values in Table 2. The five different cases treated are the following:

1. Pinned-pinned partially composite beams ($\mu = 1$)
   a) Timber-concrete beam — Uniform distributed load
      - Non-cracked concrete plate in compression: ($L = 4$ m; $q_0 = 1$ kN/m)
      - Fully cracked concrete plate in tension: ($L = 4$ m; $q_0 = 1.66$ kN/m)

Table 2. Comparison of results from exact and approximate analysis for different composite members (concr. in compression assumed non-cracked; cases 1a$_1$, 1b, and 2a).

Case	Exact analysis (Maximum values)				Approximate analysis (Maximum values)							
	w mm	σ MPa	τ MPa	V_s kN/m	w mm	Error %	σ MPa	Error %	τ MPa	Error %	V_s kN/m	Error %
1a$_1$	7.56	Concr 2.22 Wood 4.44	Concr. 0.0447 Wood 0.268	11.4 15.0[1)]	7.59	+0 .4	Concr 2.24 Wood 4.49	0 + 1.1	Concr. 0.0461 Wood 0.276	+3.1 +3.1	13.2	+16
1a$_2$	14.6	Wood 9.0 Reinf. 113	Wood 0.485	11.0 14.9[1)]	14.6	0	Wood 29.1 Reinf. 112	+1.1 -0.5	Wood 0.474	-2.3	12.7	+16
1b	16.1	Concr 3.19 Steel 123	Concr. 0.0835 Steel 5.42	116 183[1)]	16.1	0	Concr 3.19 Steel 124	0 + 0.7	Concr. 0.0929 Steel 5.65	+11 + 4.2	136	+18
1c	13.0	6.08	0.104	9.92 11.2[1)]	12.8	- 1.5	5.56	- 7.6	0.101	- 2.9	8.59	-13
2a	5.43	Concr 3.99 Wood 3.89	Concr. 0.0238 Wood 0.0892	5.99 13.2[1)]	5.41	-0 .4	Concr 3.82 Wood 3.82	-4.3 -1.8	Concr. 0.0249 Wood 0.0866	+4.8 -2.3	4.93	-18

[1)] Slip force for a fully composite section ($V_{s,\infty}$).

b) Steel-concrete beam — Uniform distributed load: (L = 6 m; q_0 = 15 kN/m)
c) Wood-wood beam (symmetric) — Point load at midspan: (L = 4 m; Q = 3 kN)

2. Free-clamped partially composite beams (μ = 2)
   a) Timber-concrete beam — Point load at free end: (L = 2 m; Q = 2 kN)

It is evident from Table 2 that the present method predicts (extremely) well the deflections for various composite beam designs. It is also clear that there is generally a good agreement between exact and approximate internal stresses, except for interlayer slip forces. The difference for slip forces is of the order of 15 %. With a few exceptions, the error in approximate normal and shear stresses is less than 5 %. All values were also calculated using the procedure in Eurocode 5 (2004) (however, for the maximum shear stresses the equations given in CIB Structural Timber Design Code (1983) were used) and were found to be exactly the same. In both simply supported (case 1) and cantilevered beams (case 2), the Eurocode 5 recommends the "correct" effective beam length.

It is to be expected that the values for shear stress and interlayer forces are less accurate than those for the normal stresses and deflections, since they are obtained by differentiating the moment and the normal force, respectively. For interlayer shear forces, correction factors could be developed. Also, the shear connectors can conservatively be designed for the interlayer shear forces obtained for a fully composite section ($V_{s,\infty}$) (note that this does not result in zero interlayer slip). Then, the influence of the resulting increased slip modulus on the remaining internal actions and deflections should be evaluated. Tentatively, an increase of, say, 20% in the shear connector strength will result in about 10% increase in the shear connector stiffness (if the shear connector strength is proportional to the square of the connector diameter and the stiffness (slip modulus) is directly proportional to the connector diameter). A 10 % increase of the slip modulus will also result in about 10 % change in the deflection and internal forces and stresses.

4 Summary and conclusions

A simplified analysis and design method for composite members with partial interaction that predicts the deflections and internal actions and stresses has been proposed. The principle of the approximate method for partially composite beams is to replace the fully composite bending stiffness (EI_∞) with the partially (effective) composite bending stiffness (EI_{eff}) in the expressions for deflections and internal actions and stresses in the corresponding fully composite beam. The effective bending stiffness reflects the influence of the interlayer slip and depends on the partial composite action (or shear connector) parameter (slip modulus, cross-section material and geometry, and beam length) and relative bending stiffness parameter (relation between the non- and fully composite bending stiffnesses of the beam). The effective beam length of the problem equals the buckling length for the corresponding column buckling problem. The methods are general in nature and can be applied to arbitrary support and loading conditions, and material and geometry parameters.

The proposed approximate method has been applied to a number of simple practical cases and the results obtained have been compared with the exact values. The applicability of the simplified analysis procedure was found to be very good (usually an error less than 5 %), except for the interlayer shear stresses (an error of about 10-20 %). The proposed method gives identical results for composite beams with interlayer slip as the approximate method given in Eurocode 5 (2004) for simply supported members.

This approximate analysis procedure for designing composite beams with interlayer slip is well suited for designers and should be considered for inclusion in Eurocode 5. Specifically, the principle for the choice of the most accurate effective beam length should be introduced in the code.

The derived approximate analysis procedure can also be extended to include multi-layered composite beams, in particular three-layered members, multiple stringer or joist systems with decking or sheathing, and to include gaps in the decking or sheathing.

Appendix A: Alternative expression for effective bending stiffness

The effective bending stiffness is given by eqn (6). Alternatively, this equation can be written as

$$EI_{\text{eff}} = EI_0 + \gamma(EI_\infty - EI_0) \tag{A.1}$$

where

$$\gamma = \frac{1}{1 + \frac{EI_\infty}{EI_0}\frac{\theta_{\text{cr}}^2}{\alpha^2}} = \frac{1}{1 + \frac{\pi^2}{K\mu^2 L^2}\frac{EA_{\text{p}}}{EA_0}} \tag{A.2}$$

For a simply supported beam ($\mu = 1$), eqn (A.2) reduces to the γ-value given in Eurocode 5 (2004). The parameter γ can also be written as

$$\gamma = \frac{\frac{EI_{\text{eff}}}{EI_0} - 1}{\frac{EI_\infty}{EI_0} - 1} = \left(\frac{EI_{\text{eff}}}{EI_0} - 1\right)\frac{EA_0\, EI_0}{EA_{\text{p}}\, r^2} \tag{A.3}$$

Appendix B: Shear stresses in sub-components

Shear stress distribution, τ_i, in the i^{th} sub-element can be derived in the following way. The differential equations of equilibrium for a small rectangular block without body forces in a two-dimensional body is given by $\partial\sigma_i/\partial x + \partial\tau_i/\partial\zeta_i$. The boundary conditions for the shear stresses is given by $\tau_i(\mp d_i/2) = 0$ and $\tau_i(\pm r_i) = V_s/b_i$. Then using the normal stress, the internal moment, and the slip force distributions, we finally obtain for the rectangular cross-section

$$\tau_i = \frac{V_s(r_i + \zeta_i)}{A_i} + \frac{(V - V_s r)E_i(r_i^2 - \zeta_i^2)}{2EI_0} \tag{B.1}$$

Maximum shear stresses ($\tau_{i,\max}$) occur at the neutral axis of the sub-element ($\zeta_{\text{na},i}$). Differentiating eqn (B.1), we arrive at

$$\zeta_{\text{na},i} = \frac{V_s EI_0}{E_i A_i (V - V_s r)} = \left(1 - \frac{EI_0}{EI_{\text{eff}}}\right)\frac{EI_{\text{eff}}}{E_i A_i r} \tag{B.2}$$

where the last expression in eqn (B.2) follows from eqn (10).

Acknowledgements

The author expresses sincere appreciation for the financial support from The County Construction Federation of Västerbotten, The Foundation for Technology Transfer in Umeå, The County Administrative Board of Västerbotten and The European Union's Structural Funds – Regional Fund: Goal 1.

References

Cecotti, A. (2003). "Composite Structures." Chapter 21 in *"Timber Engineering,"* S. Thelandersson and H. J. Larsen, eds., John Wiley & Sons, Ltd.

CEN (1993). "Eurocode 5 – Design of timber structures – Part 1-1: General rules and rules for buildings." ENV 1995-1-1, European Committee for Standardisation (CEN), Brussels, Belgium.

CEN (2004). "Eurocode 5 — Design of timber structures - Part 1-1: General – Common rules and rules for buildings, EN 1995-1-1, European Committee for Standardisation (CEN), Brussels, Belgium.

CIB (1983) "Structural Timber Design Code". CIB-W18 Timber Structures, Publ. 66, 6th Ed., Int. Council for Building Research Studies and Documentation (CIB).

Girhammar, U. A. (1985). "Composite Wood Structures." *J. Swed. Soc. Civ. Engrs,* (3), 37-42 (in Swedish).

Girhammar, U. A. (1992). "General Analysis – Continuous Shear Connectors" and "Simplified Analysis". In: "Timber-Concrete Composite Load-Bearing Structures – From Theory to Applications", Rep. of Tech. Comm. 111-CST RILEM, Ed. A. Ceccotti, Dept. of Civ. Eng., Univ. of Florence, Italy (unpubl. rep.). Cf. also: RILEM TC 111 CST (1992). "Behaviour of timber-concrete load-bearing structures." *Proc. ACMAR-Ravenna Int. Symp.*, Dept. of Civ. Eng., Univ. of Florence, Italy.

Girhammar, U. A., and Gopu, V. K. A. (1993). "Composite Beam-Columns with Interlayer Slip — Exact Analysis." *J. Struct. Eng.*, 119 (4), 1265-1282.

Girhammar, U. A., and Pan, D. (2007). "Exact static analysis of partially composite beams and beam-columns." *Int. J. Mech. Sci.* 49 (2007) 239-255.

Heimeshoff, B. (1987). "Zur Berechnung von Biegeträgern aus nachgiebig miteinander verbunden Querschnittsteilen im Ingenieurholzbau." *Holz als Roh- und Werkstoff*, 45, 237-241.

Kumar, N., and Gopu, V. K. A. (1987). "Stiffness of Framing Members with Partial Composite Action." Discussion, *J. Struct. Eng.*, 113 (12), 2522-2524.

Larsen, H. J., and Riberholt, H. (2005). "Timber Structures – Design." SBi-anvisning 210, Danish Building Research Institute, Horsholm, Denmark (in Danish).

McCutcheon, W. J. (1986). "Stiffness of Framing Members with Partial Composite Action." *J. Struct. Eng.*, 112 (7), 1623-1637.

Möhler, K., (1956). "Über das Tragverhalten von Biegeträgern und Druckstäben mit zusammengesetztem Querschnitt und nachgiebigen Verbindungsmitteln." Habilitationsschrift, Technische Hochschule Karlsruhe, Germany.

Schelling, W. (1968). "Die Berchnung nachgiebig verbundener, zusammengesetzter Biegeträger im Ingenieurholzbau." Dissertation, Teschnische Hochschule Karlsruhe, Germany.

Wang, Y. C. (1998). "Deflections of Steel-Concrete Composite Beams with Partial Shear Interaction." *J. Struct. Eng.*, 124 (10), 1159-1165.

INTERNATIONAL COUNCIL FOR RESEARCH AND INNOVATION
IN BUILDING AND CONSTRUCTION

WORKING COMMISSION W18 - TIMBER STRUCTURES

DEVELOPMENT OF NEW CONSTRUCTIONS OF GLULAM BEAMS IN CANADA

F Lam

N Mohadevan

University of British Columbia

CANADA

MEETING FORTY

BLED

SLOVENIA

AUGUST 2007

Presented by F. Lam

H. Blass asked how the laminating factors were developed. F. Lam replied that they were obtained via a model calibration procedure where the smaller (0.3 m) beams were used in the calibration and the deeper (0.6 m) confirmed the factors. Also this type of factor was reported by Falk.

J. Köhler asked about the correlation between the tension strength of the laminae and the finger joints considered. F. Lam replied that it was not considered; even though there might be some correlations, the program still gives good results when it was ignored.

DEVELOPMENT OF NEW CONSTRUCTIONS OF GLULAM BEAMS IN CANADA

Frank Lam and Nahulesalingam Mohadevan
University of British Columbia

In Canada the manufacturing of Glulam beams and the grading rules of laminating stock are stipulated under Canadian Standards CSA 0122. This paper reports on procedures undertaken to develop new constructions of Canadian Glulam beams that can fit well with the characteristics of the wood resource. Detailed study of the lam-stock was first conducted via a series of grading analysis and testing. The lam-stock was testing non-destructively for modulus of elasticity and then destructively for tension strength. Grading rules were modified to establish new grades of lam-stock. Subsequently, a detailed knot database was developed to study the performance of these grades based on the US-GAP program. Tension testing was also conducted to establish the strength of finger joints for various new grades of lam-stock. A stochastic finite element program was used to evaluate different prototype construction of glulam beams. An experimental program was then conducted to test full size glulam beams in bending and shear to verify program predictions including size effects issues. Excellent agreement between program predictions and test results was observed.

1. INTRODUCTION

In North America the minimum requirements for the manufacturing of Glued laminated timber (Glulam) beams are specified in CSA O122 M89 (Canada) and ANSI/AITC AI90.1 (US). CSA O122 M89 uses visual grading and modulus of elasticity (MOE) assessment to build different grades of glulam while ANSI additionally requires the knot distribution of the material to be considered. CAN/CSA 0122 M89 specifies four grades of lam-stock B-F, B, C and D. B-F is the highest grade designated for the extreme tension zones of 20f and 24f beams. For this grade, knots or other similar defects exceeding 10 mm and local slope of grain steeper than 1:16 shall not be permitted within 13 mm of the edge of the outer tension face lamination after finishing. D is the weakest grade, generally placed at the mid zone of the beam. The laminating boards of this grade are allowed to have knot sizes up to 50% of the board width.

The current Canadian specifications generally deal with pre-established lamina grades and specify whether the given beam lay-up is admissible. The US procedures require tedious knot assessments to qualify the material grade. It is recognized that there is a need for more efficient beam design procedures which will increase the performance of the glulam beams as well as improving the efficient use of timber resource. One of the key-issues from the glulam manufacturers' point of view is the available supply of the high grade material needed for the extreme tension zone of the 24f beams. Here the interest is to investigate the possibility to modify some of the knot size restrictions at the extreme tension zone of the 24f beams in order to match the strength requirements to the knot size characteristics of the lamina resource for the tension lamina-grades. In this way the current research has been formulated to developed/validate new procedures to construct more efficient glulam beams and to optimize the lamina grade specifications for the construction of 24f Douglas fir glulam beams. The study consists of a series of laboratory investigations to test the strength characteristics of lamina and full scale glulam beams coupled with computer

analysis using ULAG, a stochastic finite element program developed at the University of British Columbia (UBC). The program can simulate virtual construction of glulam beams/columns with progressive loading until collapse to investigate the bending capacities and failure behaviors of the glulam.

2. DEVELOPMENT OF NEW LAMINA GRADES

The initial guidelines for the new lamina grades were proposed by Western Archrib - Structural Wood Systems. This consists of the specifications for a set of seven laminating grades T1, T2, Cc, B, C, Dc, and D. Here T1 and T2 are tension lamina grades and Cc and Dc are compression lamina grades.

Douglas fir 38 mm x 140 mm laminae were used for all the grade assessment and verifications. Lamina samples were randomly selected from the mills and delivered to UBC in batches. The first four batches of materials were used for the primary grade development process and verification. These batches consist of one hundred and eighty-nine 2.44 m long boards and five hundred and nine 4.88 m long boards.

The development process involves a series of grading analysis and testing. Grading was conducted by the combination of E rating and visual grading as specified in the new guidelines. Initially the grade yield and the grade distribution across the samples were analyzed. Then the guidelines were modified to improve the grade yield. Based on this a set of five lamina grades with potential grade turnout was chosen for further assessments. Then the samples were tested in tension. The finalized grade set was inspected and verified by National Lumber Grades Authorities (NLGA) personnel and the results were reviewed by experts from the industry and UBC. Some of the key grading factors of the modified guidelines are given in Table 1 and the corresponding grade turnout and MOE data are given in Table 2.

Table 1. Key grading factors considered for the resource assessment

Parameter	T1	B	C_c	C	D
$MOE_{(min)}$, MPa	13,100	12,400	12,400	11,000	-
$MOE_{(average)}$, MPa	15,400			12,000	-
Knot size, mm	35	35	55	55	70
Edge knot, mm	23	-	-	-	-
SOG, all four sides	1:16	1:16	1:12	1:12	1:08
Pith (maximum allowed)[1]	1/8				
Clear wood(minimum requirement), %	67				
SRC spacing, mm	600				
Knot spacing near finger joint[2]	2Φ				

[1]As a ratio of the cross section of the lamina

[2]Any knots over 10 mm in diameter not permitted within 2 knot diameter of any finger joint.

Table 2. Grade turnout

	T1	Cc	B	C	D
Grade turnout, m	419	119	402	885	1,068
MOE, Mean, MPa	15,226	14,155	13,683	11,774	9,992
COV, %	12	7	9	6	17
Total number of boards tested	184	44	223	201	138

Subsequently tension tests were conducted to determine the strengths of the laminae and the finger joints. The lamina tension tests were carried out at two gauge lengths 3.66 m and 1.22 m with a 0.61 m grip length at each end. For each grade the

speed of loading was adjusted to maintain an average time-to-failure of 10 minutes. A Metriguard tension testing machine with full resistant grips and a capacity of about 450 kN was used for the testing.

The mean tensile strength values corresponding to the T1 grade tested at 3.66 m and 1.22 m gauge length are 42.9 MPa and 52.6 MPa, respectively. Based on these values a length effect factor k of 5.4 was established for the material tested. The relationship between the strength values and the corresponding material volume (Lam 2000) used in the assessment of k factor is given in equation 1. In the equation (1) τ and V corresponds to the tensile strength and the volume of the material, respectively. The subscripts 1 and 2 refer to the samples corresponding to the two different lengths considered. Then all the lamina strength values were size adjusted to a 2.44 m gauge length in order to establish a unique set of reference strength data. This database was used as input for the ULAG analysis.

$$\frac{\tau_1}{\tau_2} = \left(\frac{V_2}{V_1}\right)^{\left(\frac{1}{k}\right)} \qquad (1)$$

Approximately four hundred finger jointed lamina specimens of the four grades, T1, B, C and D were tested in tension. Here the gauge length and the grip lengths were kept at 0.66 m and 1.22 m, respectively. Again the speed of loading was kept to achieve a time to failure of approximately 10 minutes. As expected, both lamina and finger joint failures were observed during the tests. This resulted in two sets of strength data: one corresponding to the finger joint failure cases and the other corresponding to the lamina failure cases where the finger joint strength is higher than that of the failure load of the specimen. This issue of mixed failure modes was addressed using the Maximum Likelihood Evaluation (MLE) theory to isolate the strength of finger joints from a censored database. The summary statistics of the lamina and finger joint tensile strength test results are given in Table 3.

Table 3. Summary statistics of the lamina and finger joint tensile strength test results

	Lamina				Finger Joint (MLE)			
Material Grade	T1	B	C	D	T1	B	C	D
Mean strength, MPa	50	35	29	24	42	40	33	28
COV, %	24	23	32	27	21	21	19	22
Number of specimens tested	184	223	201	138	126	100	104	100
Number of finger joint failures					110	67	46	31

As expected, in T1 grade's case, the lamina strength is much higher than that of the finger joint's. In B grade's case, both strength values come closer and in C grade's and D grade's cases, the finger joint's strength is higher than that of the lamina.

3 ULAG ANALYSIS

During the ULAG assessments, the finite element glulam beam models were simulated with 0.05 m segments along the beam length. The models were subjected to a virtual progressive loading until collapse yielding the corresponding failure loads, deflections and failure types. For each of the beam case investigated, the beam strength statistics were determined based on a set of one thousand glulam beam simulations and loading data.

The ULAG study deals with two main aspects: fine tuning and validating the ULAG program for glulam strength assessments to confirm code requirements and to assess the performance of the new lamina grades. The basic input material for the ULAG analysis were the tensile strength and the MOE test databases of the lamina and finger joints and the length distribution of the lamina. Another characteristic of interest is the laminating effect between the lamina which is not considered in the original ULAG program. During the current analysis a trial set of laminating factors were proposed for the new lamina grades (Table 4). These factors were used in subsequent ULAG analysis to determine the beam configuration and loading setup for the calibration tests. It is noted that laminating factors are not only grade dependent. Additional considerations are needed to establish laminating factors: 1) the position of the lamina within the member, 2) whether the lamina is supported by adjacent laminae on one side or both; and 3) the relative stiffness of the lamina in comparison to the adjacent laminae. Care must be taken when applying the trial laminating factors to unconventional lay-ups that differ significantly from the material tested in this research program.

Table 4. Trial sets of laminating factors proposed for the new lamina grades and beam lay-ups

Material grade	T1	B	C	D
Laminating factor	1.1	1.2	1.3	1.4

A series of ULAG simulations were performed to assess the performance of the lamina grades. For these analyses, glulam beams were simulated with a span to depth ratio of 15:1 assuming that the lamina consist of 75% 4.88 m and 25% 2.44 m long members. The beam lay-ups used for the assessments are given in Table 5 and the corresponding characteristics (5^{th} percentile) strength and specified strength values predicted are given in Table 6. The target specified strength of these beams is 30.6 MPa. All of the beams except #1 (8) and #4(8) met the target level.

Table 5. Glulam lay-ups used for the ULAG assessments

Lamina number(from the bottom of the beam)		20	19	18	17	16	15	14	13	12	11	10	9	8	7	6	5	4	3	2	1
Beam lay-up cases	#1(8)													Cc	C	D	D	D	D	B	T1
	#4(8)													Cc	C	D	D	D	D	C	T1
	U1(10)											Cc	Cc	C	D	D	D	D	C	B	T1
	U2(10)											Cc	C	C	D	D	D	D	C	C	T1
	U1(20)	Cc	Cc	Cc	C	C	D	D	D	D	D	D	D	D	D	D	C	C	B	T1	T1
	U2(20)	Cc	Cc	C	C	C	D	D	D	D	D	D	D	D	D	D	C	C	C	T1	T1
	#4(20)	Cc	Cc	Cc	C	C	D	D	D	D	D	D	D	D	D	D	C	C	B	B	T1

Table 6. ULAG predicted specified strength values

Parameter	Beam lay-up cases						
	#1(8)	#4(8)	U1(10)	U2(10)	U1(20)	U2(20)	#4(20)
Depth, m	0.30	0.30	0.38	0.38	0.76	0.76	0.76
Width, m	0.13	0.13	0.13	0.13	0.13	0.13	0.13
Number of laminations	8	8	10	10	20	20	20
Characteristic strength, ULAG, MPa	37.2	35.6	38.5	38.0	34.8	34.7	32.5
Specified strength, ULAG, MPa	30.1	28.3	32.8	32.6	35.3	35.2	32.8

4 GAP ASSESMENTS

The knot database on the new lamina grades developed in this study was provided to Dr. Borjen Yeh (APA) to conduct a parallel assessment using the U.S. code approved program GAP. The lamina lay-ups given in Table 5 were used for this assessment as well for comparison purposes. GAP program predicts the allowable strength capacities equivalent to a standard glulam beam of 0.13 m x 0.30 m x 6.40 m for the U.S. These values are converted to specified strengths for the Canadian Code corresponding to a standard beam size of 0.13 m x 0.61 m x 9.10 m. Comparisons between GAP and ULAG predicted glulam specified strengths are given in Table 7.

Table 7. Comparisons between the ULAG and GAP predicted specified strength

Parameter	Beam lay-up cases						
	#1(8)	#4(8)	U1(10)	U2(10)	U1(20)	U2(20)	#4(20)
Allowable strength predicted by GAP, MPa	17.8	17.2	17.8	16.9	18.4	18.0	17.7
Specified strength, GAP, MPa (1)	32.8	31.2	33.3	31.8	36.0	35.1	34.5
Specified strength, ULAG, MPa (2)	30.1	28.3	32.8	32.6	35.3	35.2	32.8
Ratio (1)/((2)	0.92	0.91	0.98	1.03	0.98	1.00	0.95

The GAP predicted specified strength values are above 30.6 MPa indicating satisfactory performance for all the lay-ups considered. In all cases GAP predictions tend to higher than ULAG except for U2(10) and U2(20). It is noted that the GAP procedure does not consider finger joint strengths which may partially explain why it seems to be less conservative than ULAG.

5 BENDING SIMULATIONS

Initially ULAG bending simulations were carried out to identify the beam lay-ups satisfying a 24f 1.8 E grade. For this purpose a series of trial analysis were carried out using trial beam lay-ups. Beam lay-ups and dimensions of the finalized beam sets selected for the bending tests are given in Table 8.

Table 8. Beam Lay-ups selected for bending simulation

Lay-up ID	Lamina number from top of the beam															
	1	2	3	4	5	6	7	8	9	10	11	12	13	14	15	16
A8U	Cc	C	D	D	D	D	C	T1								
A5U	Cc	B	C	C	D	D	D	D	D	D	D	D	C	C	B	T1

Two sets of twenty four 0.30 m and 0.61 m deep glulam beams manufactured according to the proposed beam lay-up (Table 8) were used for the bending calibration and verification tests respectively. The tests were carried out with a third point loading (Figure 1). The test apparatus consists of two end supports, two loading heads attached to a loading bar and the machine head. The advancement of the machine head and the corresponding load is monitored and controlled by a computerized data acquisition system. The 0.3 m deep beams were tested at 21:1 span to depth ratio and 0.61 m deep beams were tested at 18:1 span to depth ratio. The loading rates of these sets were kept at 10 mm/min and 13 mm/min respectively to maintain an average failure time of 10 minutes.

MOE values for all the bending beams were evaluated from load-deformation curves obtained prior to the ultimate loading. A specially designed cable yoke system was used to obtain the required load-deflection data with a loading level of 25% of the ULAG predicted mean failure load.

The summary of the bending test results is given in Table 9 and a comparison between the ULAG predicted strength distribution and the laboratory test results are given in Figure 2.

Figure 1. Typical third point loading configuration used for the bending test

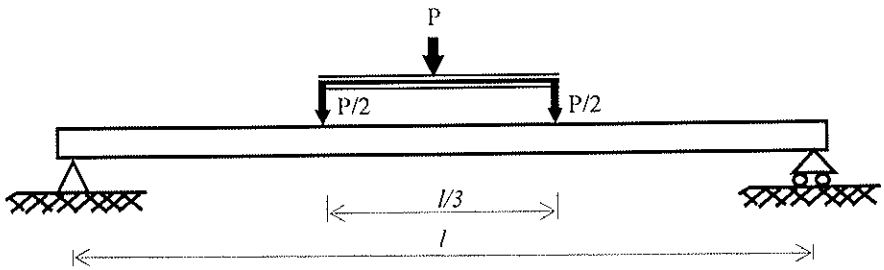

l - test span
P- total load on the beam

Table 9. Summary of the bending test results

		Tested		Predicted		Error, %	
Beam depth, m		0.30	0.61	0.30	0.61	0.30	0.61
MOR	Mean, MPa	48.3	41.8	49.0	42.0		
	COV	11	14	14	13		
MOE	Mean, MPa	13,326	12,923	12,484	12,278	-6.3	-5.0
Specified strength, MPa		34.5	32.2	34.5	32.7	-0.2	1.6

Figure 2. Comparisons between the ULAG predicted strength distribution and the laboratory test results

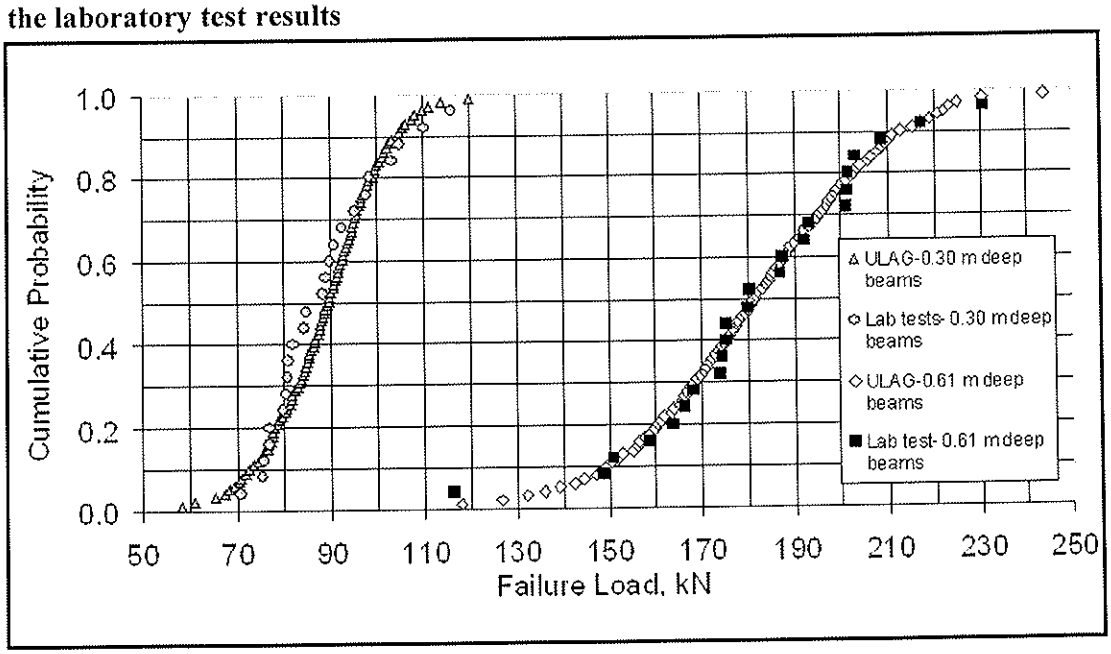

6 GLULAM SHEAR

A finite element model volume integration scheme of Foschi & Barrett (1976) and Lam et al. (1997) was followed to perform the shear strength predictions. This model predicts the failure load of a full scale beam that has a common probability of failure as a clear wood block shear specimen. The shear strain distribution was extracted from the ULAG predicted nodal displacements. The corresponding shear stress distribution in the member was determined. Now based on the weakest link theory the mean shear failure load $P_{0.5}$ can be written as:

$$P_{0.5} = \frac{P\tau^*_{0.5}}{I^{1/K}} \qquad (2)$$

where,

$\tau^*_{0.5}$ - mean shear strength of a unit volume 1.64E-05 m^3

I - shear stress field integrated over the volume under the applied load P

k - Weibull shape parameter.

$\tau^*_{0.5}$ can be determined based on the following relationship (Foschi & Barrett 1976) :

$$\tau^*_{0.5} = \beta_t \tau_{ASTM} \qquad (3)$$

where,

$\beta_t = 1.333+0.336(k-4) \quad if\ 4 \le k \le 8$

$\beta_t = 2.678+0.251(k-8) \quad if\ 8 \le k \le 10$

τ_{ASTM} is the ASTM block shear strength at the probability of interest.

The D grade Douglas fir clear wood mean-shear strength value of 8.98 MPa with 16% COV reported by Lam et al. (1997) was used for the assessments of the beam-lay-up given in Table 10. The results are given in Table 11.

Table 10. Shear calibration beam lay-up (A1)

Lamina number (from the bottom of the beam)	8	7	6	5	4	3	2	1
Lamina grades	T1	B	D	D	D	D	B	T1

Table 11. Results of the initial shear simulations

Beam depth, m	Span to depth ratio	Predicted shear capacity, kN	Predicted shear strength, MPa
0.30	7	345	6.21
0.30	6	433	7.79

The D grade material used in the glulam shear zone (middle core of the beam) is the weakest grade, expected to be having inferior strength parameters. Therefore, the clear wood strength corresponding to the Douglas fir D grades should be weaker than that of reported by Lam et al. (1997). In this way the predicted strength values given in Table 11 can be considered as an upper bound for the shear capacity of the glulam beams considered.

Laboratory assessment consists of three sets of 0.30 m and 0.45 m deep glulam beams (without finger joints). Each of these sets consists of 24 beams. First two sets (Cases B and C) of the 0.30 m deep beams were used for model calibration and the third set (Case G) was used for the model verification. The details of the test configuration used for the shear tests are given in Table 12 and the schematic diagram of the typical shear testing arrangement used is shown in Figure 3. The shear test data was processed using the MLE technique in order to determine the uncensored

statistical parameters corresponding to the pure shear failures. The summary of the shear test results is given in Table 13. Without consideration of stress volume effect, the mean load in case G is expected to be 1.5 times higher than that of case C. The clear observed disagreement can be explained by stress volume effect in shear as shown in the analysis following Equations 2 and 3.

Table 12. Shear test configuration

Beam depth	0.30 m (1 ft)	0.30 m (1 ft)	0.46 m (1.5 ft)
Beam width	0.129 m (5 ¼ in.)		
Span to depth ratio	7	6	6
Test span, *l*	2.13 m (7')	1.83 m (6')	2.74 m (9 ft)
Beam length	2.44 m (8')	2.13 m (7')	3.1 m (10 ft and 2 in.)
Loading type	Four point loading		

Table 13. Summary of the shear test results

Beam Case	Depth, m	Span to depth ratio	Failure load		Number of shear failures	Based on MLE Simulation	
			Mean (kN)	COV (%)		Mean Load, (kN)	COV (%)
C	0.3	6	311	9	20	313	13
B	0.3	7	263	10	17	275	8
G	0.46	6	389	10	18	397	11

Figure 3. Configuration of the typical shear testing arrangement

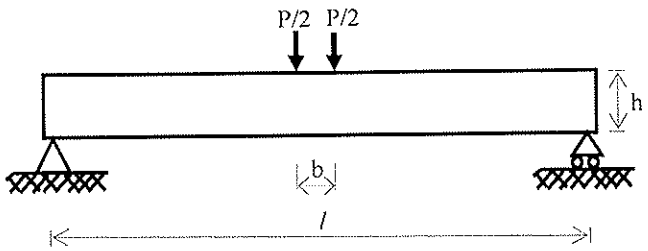

l - test span
b = 0.46 m, the spacing between the pair of loading heads at the center
h= beam depth
P- total load on the beam

After the shear beam testing the clear wood strength parameters used in the shear-stress volume model were fine-tuned based on the test results. This was done by a series of trial and error assessments using different sets of the clear wood strength parameters which are close to the values given in Lam et al. (1997). The selected clear wood strength set which produce the minimum errors between the tested and predicted average shear loads is given in Table 14. This is the predicted clear wood strength values for the Douglas fir D grade material. About 25% of the beams broke in bending mode. In a couple of cases the failures were initiated by the tensile cracks and the ultimate failure occurred in shear. The results of this analysis considering stress volume effect in shear compared with the shear test results are given in Table 15.

Table 14. Predicted clear wood shear strength values corresponding to Douglas fir D grade laminae

Parameter	Mean, MPa	COV, %
τ_{ASTM}	9.0	18

Table 15. A comparison of predicted and tested shear capacity of the glulam beams

Beam Case	Tested shear capacity (mean), kN	Predicted shear capacity (mean), kN	Error, %
C	313	330	5.4
B	275	266	-3.4
G	397	385	-2.9

7 CONCLUSIONS

The characteristics of Douglas fir lamina were studied based on visual grading, defect mapping, MOE and tensile testing, and finger joint testing. Based on these investigations an optimized set of five Douglas fir lamina grades T1, Cc, B, C and D were developed. Their strength properties assessed and the grade turnout was established.

Various combination of the beam lay-ups built with the new lamina grades was analyzed using the computer models ULAG and GAP to develop new lay up of 24f Dogulas fir glulam beams. ULAG tend to give more conservative results compared to GAP. Subsequently the performance of the new beam construction was demonstrated through full size testing of two sets of 0.30 m deep and 0.61 m deep glulam beam in bending. The target specified strength and MOE requirements for the 24f glulam beams were confirmed and excellent accuracy of ULAG in simulating the flexural strength distribution of glulam was demonstrated. The enhanced ULAG also predicts the shear capacities of glulam with good agreement explaining the observed influenced of stress volume on the shear strength of glulam.

The procedures established from this study demonstrate a new method for glulam beam lay-up design and assessment by using ULAG to predict the flexural capacity of Glulam beams as well as using the tensile strength and the corresponding MOE values of the lamina and the tensile strength of the finger joints as input.

8 ACKNOWLEDGEMENTS

The authors express their sincere thanks to the Natural Resources of Canada Value to Wood program and the industrial partners, specially the Western Archrib-Structural Wood Systems for their financial and material support during the study. Authors also acknowledge Mr. Kent Fargey, Mr. Travis Van De Vliert, and Dr. Borjen Yeh for their technical supports during the study.

9 REFERENCES

AITC. 2004. Standard specifications for structural glued laminated timber of softwood species. AITC 117-2004, American Institute of Timber Construction, Centennial.

ASTM. 2006. Practice for Establishing allowable properties for structural glued laminated timber (Glulam). Standard ASTM D 3737, American Society for Testing Materials, West Conshohocken, Pa.

CSA. 1989. Engineering design in wood (limit states design). Standard CAN/CSA O86.1-M89, Canadian Standards Association, Rexdale, Ont.

CSA. 1989. Qualification code for manufacturers of structural glued-laminated timber. Standard CAN/CSA-O177-M89, Canadian Standards Association, Rexdale, Ont.

CSA. 1989. Structural glued-laminated timber. Standard CAN/CSA-O122-M89, Canadian Standards Association, Rexdale, Ont.

Falk, R. and Colling, F. 1994 Laminating effects in glued-laminated timber beams. Journal of Structural Engineering, ASCE, 121(12): 1857-1863.

Folz, B. and Foschi, R.O. 1993. ULAG: Ultimate load analysis of glulam-user's manual. Version 1.0, Department of Civil Engineering, The University of British Columbia, Vancouver, Canada. 23p.

Folz, B.R. 1997. Stochastic finite element analysis of the load-carrying capacity of laminated wood Beam-Columns. Ph.D. Thesis, The University of British Columbia, Vancouver, Canada. 163 p.

Foschi, R. O. and Barrett, J.D. 1976. Longitudinal Shear in Wood Beams: a design method. Canadian Journal of Civil Engineering, NRC Canada, 3: 199-208.

Klapp, H. and Brüninghoff, H. 2005. Shear Strength of Glued Laminated Timber. Proceedings of the International Council for Research and Innovation in building and Construction, Working Commission W18- Timber Structures. 38th meeting, Karlsruhe, Germany, August 2005.

Lam, F. 2000. Length effect on the tensile strength of truss chord members. Can. J. Civ. Eng. NRC Canada, 27: 481-489.

Lam, F., Yee, H. and Barrett, J.D. 1997. Shear strength of canadian softwood structural lumber. Can. J. Civ. Eng. NRC Canada, 24: 419-430.

Marx, C.M. and Evans, J.W. 1988. Tensile strength of laminating grades of lumber. Forest Prod. J. 38(7/8): 6-14

Steiger, R. and Köhler, J. 2005. Analysis of censored data-examples in timber engineering research. Proceedings of the International Council for Research and Innovation in building and Construction, Working Commission W18- Timber Structures. 38th meeting, Karlsruhe, Germany, August 2005.

Timusk, P.C. 1997. Experimental evaluation of the ULAG glulam beam simulation program. M.Sc. Thesis, The University of British Columbia, Vancouver, Canada. 80 p.

Yeh, B. and Williamson, T.G. 2001. Evaluation of glulam shear strength using a full-size four-point test method. Proceedings of the International Council for Research and Innovation in building and Construction, Working Commission W18- Timber Structures. 34th meeting, Venice, Italy, August 2001.

INTERNATIONAL COUNCIL FOR RESEARCH AND INNOVATION
IN BUILDING AND CONSTRUCTION

WORKING COMMISSION W18 - TIMBER STRUCTURES

DETERMINATION OF MODULUS OF SHEAR AND ELASTICITY OF GLUED LAMINATED TIMBER AND RELATED EXAMINATIONS

R Brandner
Competence Center holz.bau forschungs gmbh
AUSTRIA

E Gehri
ETH - Swiss Federal Institute of Technology Zurich
SWITZERLAND

T Bogensperger
G Schickhofer
Graz University of Technology

AUSTRIA

MEETING FORTY

BLED

SLOVENIA

AUGUST 2007

Presented by R. Brandner
H. Blass commented that the factor for one lamination has no meaning and this is only important for beams greater than 600 mm. He asked whether it would be possible to use the mean rather than the 5th percentile. R. Brandner agreed in general but replied that for other markets where thin beams are considered this is also important. This factor is also important for buckling not just lateral torsional buckling.
I. Smith commented that vibration data from UNB can be made available.

Determination of modulus of shear and elasticity of glued laminated timber and related examinations

R BRANDNER
Competence Center holz.bau forschungs gmbh
Austria

E GEHRI
ETH - Swiss Federal Institute of Technology Zurich
Switzerland

T BOGENSPERGER, G SCHICKHOFER
Graz University of Technology, Institute for Timber Engineering and Wood Technology
Austria

Abstract

This paper deals with the determination of the modulus of elasticity of boards, finger joints in tension and hence builds up glued laminated timber (GLT). Emphasize has been taken on determination of G-modulus of GLT by execution of both standardized test methods acc. EN 408, by torsion tests and application of shear-fields in constant transverse force areas during destructive four-point bending tests acc. EN 408. Comprehensive evaluations of relationships between G- and E-module and related mechanical properties have been carried out. Furthermore product of (E · G) has been examined as relevant value for lateral torsional buckling based on test results and simulations. A proposal for further standardization for determination of G-modulus of GLT acc. EN 408 will be presented. Simulations evaluate the influence of selected parameters on expectable G-modulus. The data states as bases for further regulations concerning lateral torsional buckling of GLT in dependence of size in comparison to solid wood beams and should be considered for standardization.

1 Introduction

The elastic characteristics of isotropic materials can be described on the bases of two independent parameters. The relationships between the modulus of elasticity E and shear G are directly linked. Wood, as an anisotropic but describable orthotropic material, requires nine independent parameters to link the tensors of stress and strain. The module of elasticity of structural lumber parallel and perpendicular to the grain are relative simple to determine and well known. In contrast, shear module make some troubles in determination within static tests, and often underlie a certain bias due to minor deflections in combination with high loads and influences in regard to load configuration. General, the knowledge of the material inherent module is necessary for design and modelling of structures. To enable the determination of relevant paramters and comparison to publications standardized and robust testing procedures are necessary. So far it is ambitious to define relationships between G and easy to handle and dependent material properties to enable estimation of G-values through

calculations. In current standards, the relationship between E and G is general utilized as constant ratio, for example $E_{m,mean}$ / G_{mean} = 16 acc. EN 338 or $E_{t,0,l,mean}$ / G_{mean} = 15.4 acc. EN 1194.This constant ratio assumes, that material properties like density and knottiness have no or equal influence on both, E and G (Görlacher and Kürth 1999). Furthermore it has to be mentioned, E derived by different methods are not general equal. The knowledge for accurate G values is of increasing importance with decreasing span-to-depth ratio (l / d) (Skaggs and Bender 1995, Gehri 2005) and in case of lateral-torsional buckling (Harrison 2006). As given in Kollmann 1951, following important influences on the shear modulus are given:

- density, share of late wood (positive relationship)
- moisture content (negative relationship)
- knottiness, grain deviations (up to seven-times of strain on the border between knot and surrounding 'clear wood')
- temperature (negative relationship)
- load direction (highly pronounced anisotropy)

Kollmann 1951 annotated that the ratio E / G can not be constant due to the anisotropic behaviour of wood. A literature study offer wide ranges of E / G (see Tab. 1).

Tab. 1: Literature review concerning E / G

Literature source [--]	**E / G** [--]
Niemz 1993	12 ÷ 35
Divos et al. 1998	8 ÷ 24
Harrison 2006	11.6 ÷ 36.6

Görlacher and Kürth 1999 reported linear regression models for G vers. E and G vers. ρ, based on dynamical examined values determined on 1188 # board segments with l / w / d = 150 / 150 / 30 (35) mm and confirmed on the one hand the dependency of G from density, on the other hand the increasing ratio E / G with increasing E and hence increasing strength class and closed with a proposal for EN 338. As given, the increase of G is rather low, even G for main range of strength classes C18 to C40 acc. the proposal for EN 338 can be seen as more or less constant (increase from proposed G = 580 N/mm² to 660 N/mm² → + 14 %) in comparison to the increase of E = 9000 N/mm² to 14000 N/mm² (→ + 56 %).

Emphasize of this paper is to present and compare static test procedures for the determination of shear modulus of GLT with the background knowledge of E from boards in tension and hence build up GLT, tested flatwise and edgewise. To get as much information of E and G main parts of GLT have been part of examination. $E_{t,0,l}$ and E_{dyn} of boards and E_{dyn} of both parts of finger joint specimens have been determined. Hence homogenous build up GLT GL24h has been tested edgewise and flatwise in 4p.- and 3p.-bending acc. EN 408, and a sub sample of 10 # of GLT has been tested in torsion and by application of measurements of shear deflections in constant transverse force areas during standard 4p.-bending test acc. EN 408. Due to cutting pattern of halved roundwood it has not been possible to determine G_{LR} and G_{LT} accurately. Determined G-values gained from bending tests are in that case, according to torsion tests, smeared G-values, influenced by loading direction of the system structure GLT.

2 Materials and Methods

2.1 Materials

Boards of one breakdown, spruce (picea Abies karst.) with provenience Middle Europe, have been visual graded under industrial environment to grading classes S10, S13 and reject acc. DIN 4074. The lot of S10 has been used for further applications to produce glued laminated timber (GLT) of strength class GL24h acc. EN 1194. Specimens for tension tests of boards and finger joints have been selected randomly. Static tests have been carried out with boards, finger joints and hence build up GLT. The dimensions, tested quantity and carried out tests are given in Tab. 2.

Tab. 2: Overview of tested material, dimensions, carried out tests and examined properties

material	quantity	dimension			tests	examined properties
		l	w	d		
[--]	[--]	[mm]	[mm]	[mm]	[--]	[--]
boards	100 #	3000	150	40	tension	u, ρ, E_{dyn}, $f_{t,0,l}$, $E_{t,0}$
finger joints	50 #	1750	150	40	tension	u, ρ, $E_{dyn,parts}$, $f_{t,j}$
GLT-GL24h	25 #	3040	150	160	4-p. bending	u, ρ, $f_{m,g,ew}$, $E_{m,g,l\text{-}g,ew}$
	25 #	6080	150	320	4-p. bending (25 #, 10 # shear field)	u, ρ, $f_{m,g,ew}$, $E_{m,g,l\text{-}g,ew\text{-}fw}$, $G_{m,g,ew\text{-}fw}$, $G_{SF,ew}$
					3-p. bending (25 #)	u, ρ, $E_{m,g,l\text{-}g,app,ew\text{-}fw}$, $G_{m,g,ew\text{-}fw}$
					torsion (10 #)	u, ρ, $G_{t,1600\text{-}2950\text{-}5000}$

'l-g' ... tested local and global; 'ew-fw' ... tested edgewise and flatwise

2.2 Methods

All tests have been carried out with continuous measurement of time, deflections and forces. Bending- and torsion tests have been derived by application of hysteresis with peaks of deflections at 50 % of calculated average maximum stress level.

2.2.1 Tension tests of boards and finger joints

The tension tests of boards parallel to the grain have been done acc. EN 408 with free testing length $l_{test} > 9 \cdot w = 1420$ mm (= 9.5 · w), by measurement of local- (acc. to EN 408 $l_{0,EN\,408} = 5 \cdot w = 750$ mm) and global deflections ($l_{0,maschine} = 1645$ mm). Tension tests on finger joints have been accomplished at the Holzforschung Austria / Vienna, with free testing length of $l_{test} = 200$ mm acc. EN 1194. The tension strengths $f_{t,0,l}$, $f_{t,j}$ and modulus of elasticity $E_{t,0,l}$ have been calculated acc. EN 408.

2.2.2 Applied test methods for the determination of modulus of elasticity and shear of GLT GL24h

For the determination of E-, G-module and bending strength $f_{m,g}$ various static test configurations have been applied on glued laminated timber GLT GL24h which are given in detail afterwards. All deflections at bending tests have been measured by application of yokes to delete bias due to local indentations at loading points.

2.2.2.1 Single span method acc. EN 408

Acc. to EN 408 method for the determination of G by ‚single span' has been applied on GLT, loaded edgewise and flatwise. This method enables calculation of G by confrontation of $E_{m,g,l}$ calculated out of deflections over $l_1 = 5 \cdot w$ in middle section free of transverse force and $E_{m,g,app}$ – including bending and shear deflection – of 3p.-bending tests with span $l = l_1 = 5 \cdot w$. The formulations for calculation of G are given in EN 408.

2.2.2.2 Variable span method acc. EN 408

‚Variable span method' acc. EN 408 has been applied on all 25 # GLT-beams, edgewise and flatwise loaded, by variation of $(d / l)^2$ within $0.0028 \leq (d / l)^2 \leq 0.030$ (edgewise) and $0.0025 \leq (d / l)^2 \leq 0.030$ (flatwise). Calculation scheme is given in EN 408.

2.2.2.3 Torsion tests

Torsion tests have been carried out acc. to ASTM D 198, but with some adaptations. Free testing length has been $l_{test} = 18 \cdot w = 5760$ mm, whereby six gages have been placed with distances of 1600, 2950 and 5000 mm, but reduced minimal distance to clamps of $1.2 \cdot w = 380$ mm. Rotations have been recorded by extensometers, placed on both sides of each gage point, and averaged (Fig. 1). Due to lack of deeper knowledge of G_{LR} and G_{LT} – small differences are published by Keunecke et al. 2007 ($G_{LR,mean} = 617$ N/mm² (COV-$G_{LR} = 12.1$ %), $G_{LT,mean} = 587$ N/mm² (COV-$G_{LT} = 12.1$ %) – calculation of G_{tor}, as smeared G_{LR} and G_{LT}, has been accomplished under assumption of isotropic material acc. to Möhler and Hemmer 1977. Formulations are given in [1], [2]; some impressions are given in Fig. 2.

$$I_{tor} = \eta_1 \cdot d \cdot w^3 \qquad [1]$$

$$\vartheta = \frac{M_{tor}}{G_{tor} \cdot I_{tor}} \rightarrow G_{tor} = \frac{M_{tor}}{\vartheta \cdot I_{tor}} = \frac{dM_{tor}}{d\vartheta} \cdot \frac{1}{\eta_1 \cdot d \cdot w^3} \qquad [2]$$

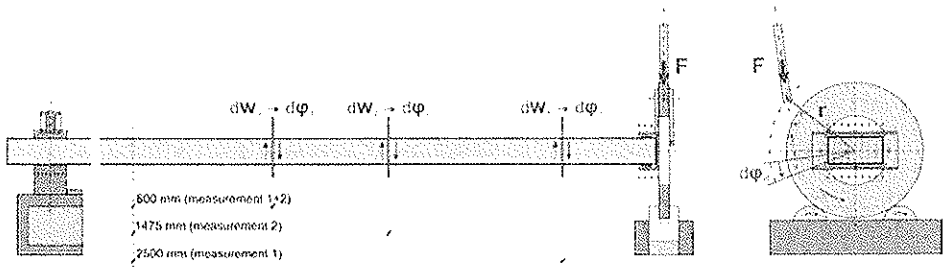

Fig. 1: Test configuration for the examination of G_{tor} of GLT GL24h

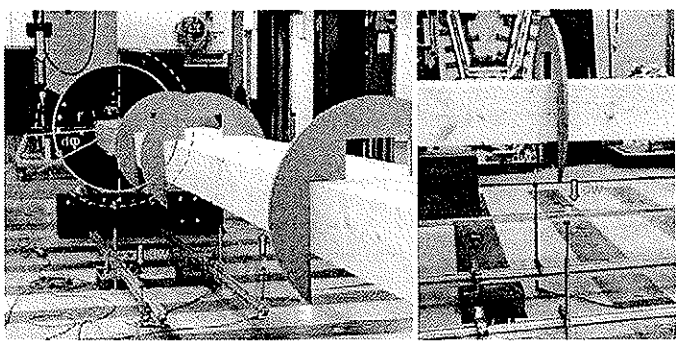

Fig. 2: Test configuration for the examination of G_{tor} of GLT GL24h: transfer of force for torque (left), local measurement of torque by extensometers on both sides (right)

2.2.2.4 Shear field tests during destructive 4-point bending tests

Measurements of shear deflection in area of constant transverse force during bending tests have already been accomplished in the past by FMPA 1983 and Gehri 2005. The idea has been to adjust this test configuration, generally applied in shear tests, for the standard 4p.-bending test acc. EN 408 (see Fig. 3). Due to minor induced shear deflection precise measurement device has been applied on total four shear fields per each GLT-beam, placed on both sides of constant shear force and opposite each side of the beam, tested edgewise in 4p.-bending. Due to the squared parabola shape of shear strength over the cross section but reduced monitoring field of shear deflection over the depth of the beam, general applied shear correction factor $\kappa = 6 / 5$ has to be adjusted and replaced by α acc. to Gehri 2005 (see [3]).

$$\alpha = \frac{\tau_{SF}}{\tau_0} + \frac{2}{3} \cdot \left(\frac{\tau_{max}}{\tau_0} - \frac{\tau_{SF}}{\tau_0} \right) \quad \text{with } \tau_0 = G \cdot \gamma = \frac{Q}{w \cdot d},\ \tau_{SF} = \tau\left(z = \frac{L}{2} \right) = \frac{Q \cdot S(z)}{I_y \cdot w} \qquad [3]$$

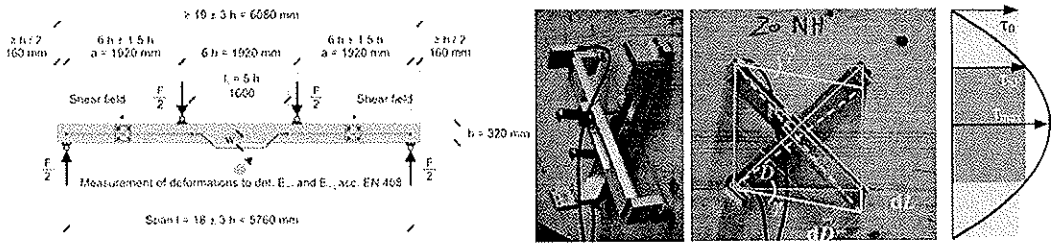

Fig. 3: Test configuration for the examination of G_{SF} of GLT GL24h during 4p.-bending tests acc. EN 408 (left), measurement device and shear deflection as basis for calculation of G_{SF} (middle), scheme for declaration of τ_0, τ_{max} and τ_{SF} (right)

The calculation procedure for G_{SF} is given in [4], [5].

$$\gamma = \frac{1}{2} \cdot \left(|dD_1| + |dD_2| \right) \cdot \frac{\sqrt{2}}{L} = dD_{mean} \cdot \frac{\sqrt{2}}{L} \qquad [4]$$

$$G_{SF} = \alpha \cdot \frac{\tau_0}{\gamma} = \alpha \cdot \frac{L}{A \cdot \sqrt{2}} \cdot \frac{dQ}{dD_{mean}} \qquad [5]$$

Exact determination of α by FEM acc. Bogensperger 2007 has shown good agreement of method proposed by Gehri 2005 [3], with $\alpha_{FEM} = 1.390$ versus $\alpha_{Gehri} = 1.375$ acc. given test configuration with L = 160 mm, placed in the middle of the d_{GLT} and middle of constant shear force sections.

2.2.3 Modelling

The product (E · G) has been modelled by application of Monte-Carlo simulation method, introduction of stochastic and selected parameters for sensitivity analysis. For simulation, virtually GLT-beams have been generated. The lamellas and boards itself have been build-up of elements with l_{seg} = 150 mm, width of w_{board} = 150 mm and thickness of d_{board} = 40 mm, referencing standard dimensions of boards cut in pieces lengthwise. Data concerning E and G for boards with definite length of $l_{board} = c \cdot l_{seg}$ (c for number of serial board segments lengthwise per each board: $c_{ref} = 27$ # → l_{board} = 4050 mm) have been generated, based on equal distributed random numbers and transformed by inverse transformation method. E and G have been assumed to be normal distributed (ND). Correlation between E and G is under discussion. Skaggs and Bender 1995 published values for r (E, G) between - 0.342 ≤ r (E, G)

$\leq$ + 0.554, depending on lumber grade. For modelling, correlation r (E, G) has been accomplished by bivariate statistics. The E and G-values for the segments have been generated by the same method as for E and G for board totally, under assumption that E_{board} and G_{board} represent the mean value of the segments, with assumed COV-E = COV-G, whereby the segments itself have been divided into 'segments free of strength reducing properties' (F) and segments including strength reducing properties' (P), which have been also distributed randomly – within distribution constraints and without autocorrelation – over the length of the boards. Values for E and G of intermediate segments (between F's and P's) represent averaged neighbouring values. The dimension of virtually GLT-beams has been chosen equal to 4p.-bending test configuration of EN 408, with $l_{GLT} = 19 \cdot d_{GLT}$, $l_{span} = 18 \cdot d_{GLT}$, and loading at third points. Module of elasticity E_y, E_z and shear G_{xz}, G_{xy}, G_{tor} have been calculated acc. Blaß 2005 by first creation of packages with length = l_{seg} = 150 mm of (E · G) over the beam depth by calculating the average value, and second, calculating the (E · G) of each beam under assumption of a serial system of packages. Due to main interest in E and G concerning lateral torsional buckling of edgewise loaded GLT-beams, E_z and G_{tor} (respective E_{fw} and G_{tor}) have been applied for calculation of (E · G).

3 Results

3.1 Tensile test results of boards and finger joints

Results of tension test parallel to the grain of boards and finger joints are given in Tab. 3. Data of density ρ and modulus of elasticity ($E_{t,0,l}$ and E_{dyn}) have been adjusted to u = 12 % moisture content acc. EN 384.

Tab. 3: Test results of tension tests on boards and finger joints, graded S10 acc. DIN 4074

	Tension tests – boards				**Finger joints**		
	ρ_l [kg/m³]	E_{dyn} [N/mm²]	$E_{t,0,l}$ [N/mm²]	$f_{t,0,l}$ [N/mm²]	$\rho_{l,i}$ [kg/m³]	E_{dyn} [N/mm²]	$f_{t,i}$ [N/mm²]
Quantity	100 #	100 #	100 #	100 #	49 #	49 #	49 #
mean	**423**	**13650**	**10550**	**27.3**	**422**	**13540**	**26.5**
COV	**10.8 %**	**16.9 %**	**19.0 %**	**39.5 %**	**7.3 %**	**13.2 %**	**18.6 %**
5 % qu. acc. CM	351	10000	7550	14.0	380	10290	19.4
5 % qu. acc. DM	352 (3pWD)	10210 (2pLND)	7580 (2pLND)	14.0 (2pLND)	375 (3pWD)	10200 (2pWD)	18.7 (3pWD)
5 % qu. (DM, k_{size})	--	--	--	13.7	--	--	18.7

Statistical analysis give high COV-$f_{t,0,l} \approx$ 40 % and COV-$f_{t,j} \approx$ 20 %. Nevertheless, demands for strength class C24 acc. EN 338 have been reached with $f_{t,0,l,05,DM}$ = 13.7 N/mm², $E_{t,0,l,mean}$ = 10550 N/mm² (COV-$E_{t,0,l} \approx$ 19 %) and $\rho_{l,05}$ = 380 kg/m³ (COV-$\rho_l \approx$ 11 %). Requirement on tension strength of finger joints acc. EN 1194, with $f_{t,j,05} \geq 5 + f_{t,0,l,05} \rightarrow f_{t,j,05} = 13.7 + 5 = 18.7$ N/mm², has been fulfilled.

3.2 Tests results of determined modulus of elasticity and shear of GLT

3.2.1 Single span method acc. EN 408

The test results for the local and global modulus of elasticity ($E_{m,g,l,ew\text{-}fw}$, $E_{m,g,g,ew\text{-}fw}$) of 4p.-bending tests and of 3p.-bending tests ($E_{m,g,app,ew\text{-}fw}$) are given, together with $G_{ew\text{-}fw}$, in Tab. 4 and 5. Comparison of $E_{t,0,l,mean}$ = 10600 N/mm² (COV-$E_{t,0,l}$ = 19 %) of boards with $E_{m,g,l,ew,mean}$ = 10800 N/mm² (COV-$E_{m,g,l,ew}$ = 10 %) gives nearly the same mean value. $E_{m,g,l,fw,mean}$ = 11900 N/mm² (COV-$E_{m,g,l,fw}$ = 6 %) reflects an increase of around 1000 N/mm² (+ 12 %) due to parallel loading of boards and predominant mature wood in the high stressed outer zones

of GLT in flatwise bending. Due to homogenisation the COV-E decreases significantly. G-modulus with $G_{ew,mean}$ = 820 N/mm² (COV-G_{ew} = 12 %) and $G_{fw,mean}$ = 790 N/mm² (COV-G_{fw} = 12 %) appears rather high in comparison to literature (Görlacher and Kürth 1994: $G_{mean,C24}$ = 620 N/mm²). Also the COV-$G_{ew\text{-}fw}$ = 12 % show up non expectable high dispersion.

Tab. 4: Test results of G of GLT GL24h tested edgewise acc. EN 408 – 'single span method'

	$E_{m,g,l,ew}$ [N/mm²]	$E_{m,g,g,ew}$ [N/mm²]	$E_{m,g,app,3pB,ew,1600}$ [N/mm²]	$G_{3pB,ew\text{-}4pB,ew,1600}$ [N/mm²]
quantity	25 #	25 #	25 #	25 #
mean	**10800**	**9870**	**6580**	**823**
COV	**9.5 %**	**8.2 %**	**6.2 %**	**12.2 %**
5 %-qu. acc. CM	9130	8130	6030	713
5 %-qu. (CM) / mean	0.85	0.82	0.92	0.87

Tab. 5: Test results of G of GLT GL24h tested flatwise acc. EN 408 – 'single span method'

	$E_{m,g,l,fw}$ [N/mm²]	$E_{m,g,g,fw}$ [N/mm²]	$E_{m,g,app,3pB,fw,750}$ [N/mm²]	$G_{3pB,fw\text{-}4pB,fw,750}$ [N/mm²]
quantity	25 #	25 #	24 #	24 #
mean	**11940**	**11610**	**6890**	**790**
COV	**6.3 %**	**5.1 %**	**6.3 %**	**11.5 %**
5 %-qu. acc. CM	10780	10740	6240	656
5 %-qu. (CM) / mean	0.90	0.93	0.91	0.83

3.2.2 Variable span method acc. EN 408

Tab. 6 and 7 contain particular test results gained from accomplished 'variable span method' to determine G of GLT. Corresponding $E_{m,g,app,ew\text{-}fw}$ values for all spans edgewise and flatwise are given and reflect clearly the increasing influence of shear (due to increasing shear deflection) with decreasing span. Calculated data for $E_{m,g,3pB,ew\text{-}fw}$ is given.

Tab. 6: Test results of G of GLT GL24h tested edgewise acc. EN 408 – 'variable span method'

	$E_{m,g,app,6000}$ [N/mm²]	$E_{m,g,app,2948}$ [N/mm²]	$E_{m,g,app,2204}$ [N/mm²]	$E_{m,g,app,1836}$ [N/mm²]	$E_{m,g,3pB,ew}$ [N/mm²]	$G_{3pB,ew}$ [N/mm²]
quantity	25 #	25 #	25 #	25 #	25 #	25 #
mean	**10450**	**9100**	**7990**	**7190**	**10950**	**767**
COV	**7.1 %**	**6.7 %**	**6.9 %**	**6.3 %**	**7.5 %**	**11.7 %**
5 %-qu. acc. CM	9200	8180	7130	6560	9630	629
5 %-qu.(CM) / mean	0.88	0.90	0.89	0.91	0.88	0.82

Tab. 7: Test results of G of GLT GL24h tested flatwise acc. EN 408 – 'variable span method'

	$E_{m,g,app,3000}$ [N/mm²]	$E_{m,g,app,1382}$ [N/mm²]	$E_{m,g,app,1034}$ [N/mm²]	$E_{m,g,app,860}$ [N/mm²]	$E_{m,g,3pB,fw}$ [N/mm²]	$G_{3pB,fw}$ [N/mm²]
quantity	25 #	25 #	25 #	25 #	25 #	24 #
mean	**11410**	**9680**	**8470**	**7580**	**11840**	**752**
COV	**5.4 %**	**5.5 %**	**5.4 %**	**5.8 %**	**6.4 %**	**10.7 %**
5 %-qu. acc. CM	10440	8850	7660	6880	10540	650
5 %-qu.(CM) / mean	0.91	0.91	0.90	0.91	0.89	0.86

Compared to the test results of 'constant span method' COV-$E_{m,app}$ confirm COV-$E_{m,g}$ with around 6 %. Also the data for $G_{ew,mean}$ = 770 N/mm² (COV-G_{ew} = 12 %) and $G_{fw,mean}$ = 750 N/mm² (COV-G_{fw} = 11 %) are a bit lower but confirm more or less the foregoing presented results. Calculated values of $E_{m,g,3pB}$, with $E_{m,g,3pB,ew,mean}$ = 10950 N/mm² (COV-$E_{m,g,3pB,ew}$ = 8

%) and $E_{m,g,3pB,fw,mean}$ = 11840 N/mm² (COV-$E_{m,g,3pB,fw}$ = 6 %), are on the same level as $E_{m,g,l,ew\text{-}fw,mean}$, gained from 4p-bending tests.

3.2.3 Torsion tests

Tab. 8 reflects data of carried out torsion tests by testing each beam twice, first running with gage points at distances 1600 mm and 2950 mm, second running with gage points at 5000 mm and second time at 1600 mm. Calculated $G_{tor,mean}$ show a slight increasing trend with decreasing distance to the clamps, combined with a slight decrease of COV-G_{tor}. Last observation can be explained by the averaging effect of local G-values with increasing measurement length. Test results of $G_{tor,mean}$ = 620 N/mm² (COV-G_{tor} = 4 %) contradict the G-values gained with bending tests on the mean- and COV-basis, but confirm test data of Görlacher and Kürth 1994. As given in Tab. 8, test results for the measurement distance of 1600 mm of running's express high stability, accuracy and robustness of this simple to apply test method.

Tab. 8: Torsion test results for G_{tor} of GLT GL24h

	$G_{tor,1600,1}$ [N/mm²]	$G_{tor,1600,2}$ [N/mm²]	$G_{tor,1600,mean}$ [N/mm²]	$G_{tor,2950}$ [N/mm²]	$G_{tor,5000}$ [N/mm²]
quantity	10 #	10 #	10 #	10 #	10 #
mean	**606**	**606**	**606**	**616**	**627**
COV	**4.6 %**	**4.1 %**	**4.3 %**	**4.2 %**	**3.4 %**
5 %-qu. acc. CM	564	566	565	583	597
5 %-qu. (CM) / mean	0.93	0.93	0.93	0.95	0.95

2.2.4 Shear field tests during destructive 4-point bending tests

Enforced recording of shear deflections in four observation fields with L / L = 160 / 160 mm placed in constant transverse force sections enable calculation of G as additional characteristic, determined during standard 4p.-bending tests acc. EN 408. The results of calculated G-module of the same 10 # GLT-beams as for torsion tests of averaged measured deflections within opposite paced shear fields (SF) of each side of the beam ($G_{SF,left,mean}$, $G_{SF,right,mean}$) and statistics of mean G-values of both sides are given in Tab. 9.

Tab. 9: Test results of shear field tests for G of GLT GL24h, during 4p-bending tests acc. EN 408

	$G_{SF,left,mean}$ [N/mm²]	$G_{SF,right,mean}$ [N/mm²]	$G_{SF,mean}$ [N/mm²]
quantity	10 #	10 #	10 #
mean	**654**	**705**	**694**
COV	**12.2 %**	**12.8 %**	**8.4 %**
5 %-qu. acc. ND	525	554	603
5 %-qu. (ND) / mean	0.80	0.79	0.87

It has to be remarked, calculated average expectable shear deflection of the diagonal within observation field with D = L · √2 = 226.3 mm has been calculated with dD = 0.1 mm. This underlines the high requirements concerning accuracy of measurement device.

3.3 Modelling

Based on computer code written by Bogensperger in Java®, sensitivity analyses for (E · G) have been accomplished. The reference values for modelling are given with: $E_{board,mean}$ = 12500 N/mm², $G_{board,mean}$ = 650 N/mm², COV-E,G_{boards} = 20 %, COV-E,$G_{board\_segments}$ = 20 %, l_{board} = 27 # board-segments · $l_{board\_segment\ =\ 150\ mm}$ = 4050 mm, l_{GLT} = 19 · d_{GLT} = 19 · $d_{GLT\ =\ 40\ mm}$

· 15 # = 600 mm = 11400 mm, $DM_{E,G}$ ~ ND and r (E, G) = 0.00. Neither variation of COV-E,G_{boards}, COV-$E,G_{board\_segments}$ nor quantity of segments per each board had a significant impact on results of $(E \cdot G)_{mean}$ or $(E \cdot G)_{05}$. Significant influence is only present on COV-(E · G). The minor influence on $(E \cdot G)_{05}$ despite variation of COV-(E · G) can be explained by the low reference value of COV-$(E \cdot G)_{ref}$ = 4.5 %.

Emphasize of this study has been to evaluate the product $(E \cdot G)_{05}$ by taken into account E_z and G_{tor} of the same GLT-beam, which is of importance for judgement of lateral torsional buckling. The product $(E \cdot G)_{05}$ defines a kind of material value and contradicts the current calculation schema with $(E_{05} \cdot G_{05})$ (see [6]). Generally, $(E \cdot G)_{05} \neq (E_{05} \cdot G_{05})$, only in case of r (E · G) = 1.00 this relationship lead to an equation. By assumption of a positive correlation between E and G, $(E_{05} \cdot G_{05})$ compared to $(E \cdot G)_{05}$ is on the conservative and hence safe side for stability calculations. In case of negative correlation of E and G, as mentioned by Skaggs and Bender 1995, the maximum failure is given with 5 %.

$$\sigma_{m,crit} = \frac{M_{y,crit}}{W_y} = \frac{\pi \cdot \sqrt{E_{0,05} \cdot I_z \cdot G_{05} \cdot I_{tor}}}{l_{ef} \cdot W_y} \qquad [6]$$

Significant increase of $(E \cdot G)_{05}$ is given with increasing quantity of interacting lamellas in the GLT-beam. Further examinations, by considering variation of COV-E,G_{boards}, reflect a high impact of system size on $(E \cdot G)_{05}$, up to a level of around 15 # laminations, representing the reference GLT-beam with $d_{GLT,ref}$ = 15 · $d_{board,ref}$ = 15 · 40 mm = 600 mm. The relative and absolute decrease of COV-(E · G) can be described by application of a power function, whereby the power itself appears high influenced by the parameters COV-E,G_{board}. Variation of COV-E,G_{board} further influences the expectable relative value of $(E \cdot G)_{05}$. Due to interaction of parallel and serial elements the relative relationship between COV-E,G_{board} and d_{GLT} appears like the behaviour of the 'system factor', with constant $(E \cdot G)_{mean}$, decreasing COV-(E · G) and nonlinear increase of $(E \cdot G)_{05}$, and can be expressed by the herein introduced factor $k_{EG} = (E \cdot G)_{05,n} / (E \cdot G)_{05,1}$.

4 Discussion

4.1 Dependency of G from selected mechanical and physical properties

General, correlation between E and ρ can be expected on a level of r = 0.7 ÷ 0.8. Because of constricted spectrum of examined test series a relationship between E and ρ cannot be supported neither negated. The same holds true for G vers. ρ, which leads to limited explanatory power for G vers. E. Nevertheless, there has to be a lack of relationship between E and G expressed by an observable decreasing coefficient of determination r^2 with increasing share of shear deflection of $E_{m,app}$ is given. Together with results of modelling with minor influence of r (E, G) on (E · G) for stability considerations, the importance of correct r (E, G) is not of great importance, but due to apparent difficulties in determination of G by static tests it would be helpful.

4.2 Differences between E-modulus, gained by flatwise and edgewise bending

As given in Tab. 4-5 and Tab. 6-7, $E_{m,g,fw}$ reflects a bit lower COV as $E_{m,g,ew}$, due to increasing homogenisation potential with increasing quantity of interacting laminations in loading situation. Furthermore, $E_{m,g,fw,mean}$ is generally about 1000 N/mm² higher than

$E_{m,g,ew,mean}$ which can be explained by predominant occurrence of mature wood in high stressed regions in case of flatwise bending.

4.3 Evaluation of applied static test methods for the determination of G-modulus

Fig. 4 reflects derived G-values in dependence of applied test method. Test methods regulated in EN 408 lead to high G_{mean} and unexpected high COV-G if compared to COV-G_{tor}. The higher dispersion may be explained by the difficulty of deriving share of shear-deflection out of total deflection whereby test method of 'constant span' appears more appropriate due to determined deflections within the same material area and equal measurement length. In case of 'variable span method' additional bias is given by calculation of the gradient of linear regression model between $1 / E_{m,app}$ and $(d / l)^2$ due to overestimation of boarder pairs of variates. Additional, by variation of span a certain dispersion of gained E- and G-values can be expected due to material inhomogeneities. The dispersion of G-values gained from torsion tests with COV-G_{tor} = 4 % nearly thirds the COV-G_m = 12 % and confirms the assumption of COV-E ≈ COV-G. The test results for G_{SF} gained from shear fields are about in the middle of G_m and G_{tor}, on the mean level and by attracting COV-G_{SF}. Higher COV-G_{SF}, compared to COV-G_{tor}, can be explained by bias in measurement of minor shear deflections under influence of local material inhomogeneities.

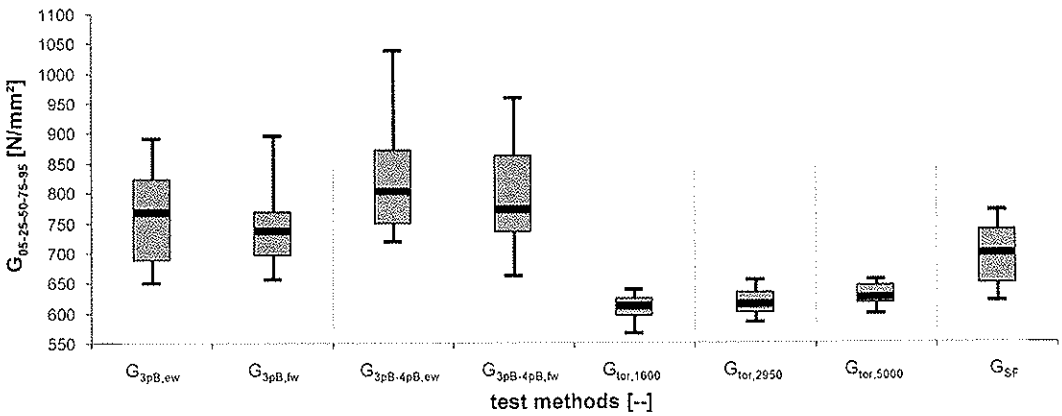

Fig. 7: Box-plots of calculated G-values, gained from applied static test methods

The differences of various G-values on the mean-level can be interpreted as a result of interacting different material characteristics G_{LR} and G_{LT}, together with different loading situations combined with differences between high stressed regions, system actions, and the influence of shear warping in the symmetry of GLT-beam in 3p-bending and general in every discontinuity of transverse force. In case of 'variable span method' every deformation underlies blocking due to shear warping and this may lead to higher G-values than expectable as material property. By application of 'constant span method' $E_{m,app}$ based on 3p-bending is influenced by shear warping combined with reduced deflections, in contrast to $E_{m,g,l}$ based on local and free of shear warping measured bending deflection. The differences between 'blocked' and 'not blocked' deformations may lead to higher G-values than in case of 'variable span method'. In contrast, measurements of shear deflection within shear fields during 4p-bending test is placed in high stressed shear region and thereby lead to higher deflections as by averaging the shear deflection over the whole beam. This may explain the lower $G_{SF,mean}$ compared to $G_{3pB,ew}$ and $G_{3pB-4pB,ew}$. Shear warping in case of edgewise loading situation can be expected higher than in flatwise bending. This may also explain the higher $G_{ew,mean}$ compared to $G_{fw,mean}$.

Due to ongoing discussion of ratio E / G, values concerning this test series are given with $E_{m,g,g,ew,mean}$ / $G_{3pB\text{-}4pB,ew,mean}$ = 12.0 in contrast to $E_{m,g,g,ew,mean}$ / $G_{tor,5000,mean}$ = 15.7, which reflects the influence of applied test method for the determination of G. For comparison Görlacher and Kürth 1999 published for strength class C24 a ratio of E / G = 18.

Considering the importance of robustness of applied test methods for determination of material characteristics and by taken into account economic aspects current test methods given in EN 408 can not be proposed for further application. Due to bias in measuring minor shear deflections within shear fields in 4p-bending tests this test method seems first appropriate for shear tests or in case of standard 4p-bending tests acc. EN 408 on beams with d ≥ 600 mm (L ≥ 300 mm) or second for beams with high homogenisation factor like plywood, with d ≥ 300 mm (L ≥ 150 mm). The big advantage of this method is given by additional measurement of a material property during standardized tests. The disadvantage lies in low proportion of tested material in shear compared to test methods like torsion or 'variable span'. The torsion tests itself can be proposed as simple to apply static test configuration with low requirements on test equipment, low forces and well measurable torque. Advantage of torsion is given by testing a high proportion of the beam volume and robustness of gained values. Further advantage of torsion is given in case of stability examinations and the necessity of knowledge of G_{tor}. The disadvantage of torsion test is given by only determination of one material property in contrast to 4p-bending tests with measurements in shear fields, whereby characteristics like $f_{m,g}$, $E_{m,g,l}$, $E_{m,g,g}$ and G_{SF} can be calculated out of data of one single test.

4.4 Handling of $(E \cdot G)_{05}$ for the design of GLT under lateral torsional buckling

General and under assumption of statistical normal distributed data 5 %-quantiles of material parameters are derived in dependency of a statistical parameter of location (e. g. mean) and dispersion (e. g. COV) [7].

$$x_{05} = \bar{x} - 1.645 \cdot s = \bar{x} \cdot (1 - 1.645 \cdot COV) = \bar{x} \cdot k_{05} \quad \text{with} \quad k_{05} = (1 - 1.645 \cdot COV) \qquad [7]$$

The factor k_{05}, as multiplier for x_{mean} to derive x_{05}, is hence only dependent on COV. Acc. to EN 338 k_{05} for calculation of $E_{0,05}$ is given with k_{05} = 0.67, comprising COV-E = 20 %. EN 1194 regulates calculation of $E_{0,g,05}$ in dependence of $E_{0,l,mean}$ with k_{05} = 0.85 or k_{05} = 0.81 if $E_{0,g,05}$ is derived in relation to $E_{0,g,mean}$, representing COV-$E_{0,g}$ = 12 %. Based on presented test series and simulation results it can be demonstrated, that COV-E,G – by assumption of COV-G ≈ COV-E – depends predominately on the system size and thus on the quantity of interacting lamellas, boards and board segments in the system GLT.

Fig. 5 gives the relationship between (E · G) vers. d_{GLT} for the reference input parameters of the simulations. In addition data of test series, with $(E \cdot G)_{mean} = 7.33 \cdot 10^6$, $(E \cdot G)_{05} = 6.55 \cdot 10^6$ and COV-(E · G) = 7.1 % are included. The dispersion of static tests confirm the simulation results, deviation on the mean- and 5 %-quantile level follow from lower $E_{m,g,g,mean,fw}$ of practical tests. The reference $d_{GLT,ref}$ = 600 mm and assumed $d_{board,ref}$ = 40 mm leads to n = 15 # laminations within one beam and to COV-$(E \cdot G)_{ref}$ = 4.5 %. As result a k_{05} for deriving $E_{0,g,05}$ and $G_{g,05}$, based on mean values $E_{0,g,mean}$ and $G_{g,mean}$, for n = 15, representing reference GLT-beam, of k_{05} = 0.9 can be proposed. For n < 15, k_{05} has to be decreased in dependence of n to k_{05} = 0.67 in case of n = 1, as given in EN 338 for structural timber.

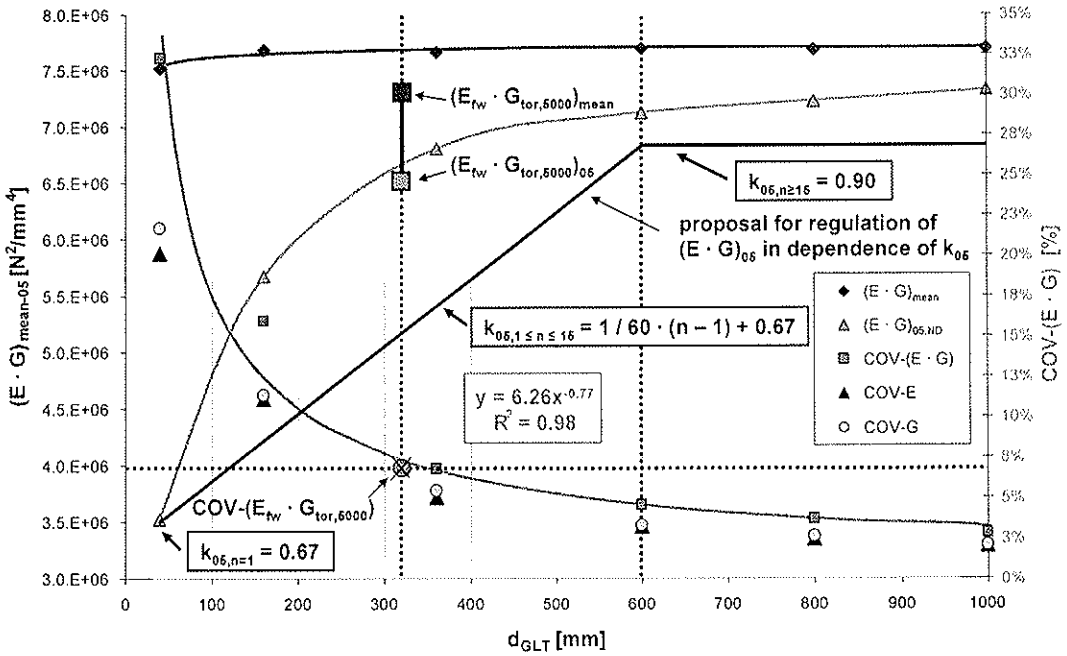

Fig. 5: Relationship between $(E \cdot G)_{mean\text{-}05}$ and COV-$(E \cdot G)$ vers. d_{GLT}: Comparison of test results and data gained from simulation, including a proposal for further regulation of $(E \cdot G)_{05}$ for GLT

5 Conclusion

Emphasize of presented research project has been to examine various static test configurations for the determination of G of glued laminated timber GLT GL24h. Both test configurations given in EN 408 – 'single span method' and 'variable span method' – have been applied and compared to torsion tests and G_{SF} derived from measurements of shear deflections in 'shear fields'. As discussed, both methods of EN 408 cannot be proposed for further application due to lack of robustness and by consideration of economic aspects. Measurement of shear deflections during standardized 4p-bending tests acc. EN 408 enables enlarged knowledge of tested beam and may reflect robustness in case of consideration of constraints concerning size and material inhomogeneities. The torsion method, in contrast, enables simple, robust and cost efficient determination of G-values, relevant for stability considerations. Both methods torsion test and measurement of shear deflections in shear fields are proposed for implementation in EN 408, torsion in regard to ASTM D 198 and shear field method in regard to standard 4p.-bending test of EN 408 by consideration of discussed constraints!

Additional accomplished simulations of E, G and $(E \cdot G)$ for the design process concerning lateral torsional buckling reflect perfect agreement with data of practical tests and enables an advanced further regulation and derivation of $E_{0,g,05}$ and $G_{g,05}$ in EN 1194 (see Tab. 10). In regard to $G_{tor,mean}$ = 620 N/mm² and G_{SF} = 690 N/mm², gained from static tests, and by consideration of minor variation of G_{mean} compared to $E_{0,mean}$ (see Görlacher and Kürth 1999) a constant value of $G_{g,mean}$ = 650 N/mm² can be proposed for all strength classes of homogeneous and heterogeneous GLT out of softwood. This confirms a proposal of Blaß 2005. Based on data gained from simulations a higher k_{05} = 0.9 for GLT with $d_{GLT} \geq 600$ mm and / or $n \geq 15$ # can be proposed in contrast to current k_{05} = 0.81 acc. EN 1194. This leads to an increase of + 11 % of I_{ef} in the design of lateral torsional buckling ($\sqrt{E_{0,g,mean}} \cdot 0.81 \cdot I_z \cdot G_{g,mean} \cdot 0.81 \cdot I_{tor}$ = **0.81** · $\sqrt{E_{0,g,mean}} \cdot I_z \cdot G_{g,mean} \cdot I_{tor}$ vers. $\sqrt{E_{0,g,mean}} \cdot 0.90 \cdot I_z \cdot G_{g,mean} \cdot 0.90 \cdot I_{tor}$ = **0.90** · $\sqrt{E_{0,g,mean}} \cdot I_z \cdot G_{g,mean} \cdot I_{tor}$ → **increase of I_{ef} = + 11.1 %**) and in contrast to structural timber to an increase of + 34 %, based on k_{05} = 0.67. For example in case of d_{GLT} = 300 mm

and n = 8 # k_{05} has to calculated with $k_{05} = 1 / 60 \cdot (n - 1) + 0.67 = 1 / 60 \cdot (8 - 1) + 0.67 = 0.78$.

Tab. 10: Proposed models for $E_{0,g,mean}$, $E_{0,g,05}$, $G_{g,mean}$ and $G_{g,05}$ for the regulation of glued laminated timber in EN 1194

Modulus of elasticity	$E_{t,0,g,mean}$	$= E_{t,0,l,mean}$
	$E_{t,0,g,05}$	$= E_{0,g,mean} \cdot \min\left\{\frac{1}{60} \cdot (n-1) + 0.67 \right.$ $\left. 0.9 \right.$
Shear modulus	$G_{g,mean}$	$= 650$ N/mm²
	$G_{g,05}$	$= G_{g,mean} \cdot \min\left\{\frac{1}{60} \cdot (n-1) + 0.67 \right.$ $\left. 0.9 \right.$

n ... quantity of laminations

6 Acknowledgement

The research work within the project P05 grading is financed by the competence centre holz.bau forschungs gmbh and performed in collaboration with the Institute of Timber Engineering and Wood Technology of the Graz University of Technology and partners from industry.
The project is fostered through the funds of the Federal Ministry of Economics and Labour, the Styrian Business Promotion Agency Association, the province of Styria and the city of Graz.

7 References

7.1 Papers and reports

Blaß H J (2005) Ermittlung des 5 %-Quantils des Produktes aus Elastizitätsmodul und Torsionsschubmodul für Brettschichtholz. Forschungsbericht der Versuchsanstalt für Stahl, Holz und Steine der Universität Karlsruhe, 11 Seiten.

Bogensperger T (2007) Auswertung von Schubverformungen über die Längenänderungen von Diagonalen. Interner Forschungsbericht des Kompetenzzentrums holz.bau forschungs GmbH, Projekt P05 grading, 9 Seiten.

Burger N, Glos P (1995) Verhältnis zwischen Zug- und Biege-Elastizitätsmoduln von Vollholz. Holz als Roh- und Werkstoff 53 (1995) 73-74.

Divos F, Tanaka T, Nagao H, Kato H (1998) Determination of shear modulus on construction size timber. Wood Science and Technology, 32 (1998) 393-402.

FMPA (1983) FMPA – Prüfung von Furnierschichtholz „Kertopuu". Bericht I.4-34523.

Gehri E (2005) Zur Schubfestigkeit von Brettschichtholz aus Fichte und Esche. Versuchsbericht, Rüschlikon, 9 Seiten.

Gehri E (2005) Verformung unter Schub – Bestimmung des Schubmoduls. Theoretische Betrachtungen und Versuchsbericht, Rüschlikon, 10 Seiten.

Gehri E (2005) Zur Erfassung des Schubmoduls über die Schiebung. Versuchsbericht, Rüschlikon, 7 Seiten.

Görlacher R, Kürth J (1994) Determination of shear modulus. CIB W18/27-10-1, Sidney, 6 pages.

Harrison S K (2006) Comparison of Shear Modulus Test Methods. Master thesis, Faculty of Virginia Polytechnic and State University, 106 pages.

Keunecke D, Sonderegger W, Pereteaunu K, Lüthi T, Niemz P (2007) Determination of Young's and shear moduli of common yew and Norway spruce by means of ultrasonic waves. Wood Science and Technology, 41 (2007) 309-327.

Kollmann F (1951) Technologie des Holzes und der Holzwerkstoffe. Springer-Verlag – Berlin-Göttingen-Heidelberg, Zweite Auflage, Erster Band.

Möhler K, Hemmer K (1977) Verformungs- und Festigkeitsverhalten von Nadelvoll- und Brettschichtholz bei Torsionsbeanspruchung. Holz als Roh- und Werkstoff 35 (1977) 473-478.

Niemz P (1993) Physik des Holzes und der Holzwerkstoffe. DRW-Verlag, ISBN 3-87181-324-9.

Skaggs T D, Bender D A (1995) Shear deflection of composite wood beams. Wood and Fiber Science, 27(3), 327-338.

7.2 Standards

ASTM D 198:2003-05 Standard Tst Methods of Static Tests of Lumber in Structural Sizes

DIN 4074-1:2004-01-19 Strength grading of wood – Part 1: Ciniferous sawn timber

EN 338:2003-07-01 Structural timber – Strength classes

EN 384:2004-05-01 Structural timber – Determination of characteristic values of mechanical properties and density

EN 385:2002-05-01 Finger jointed structural timber – Performance requirements and minimum production requirements

EN 408:2005-04-01 Timber structures – Structural timber and glued laminated timber – Determination of some physical and mechanical properties

EN 1194:1999-09-01 Timber structures – Glued laminated timber – Strength classes and determination of characteristic values

INTERNATIONAL COUNCIL FOR RESEARCH AND INNOVATION
IN BUILDING AND CONSTRUCTION

WORKING COMMISSION W18 - TIMBER STRUCTURES

COMPARATIVE EXAMINATION OF CREEP OF GLT- AND CLT-SLABS IN BENDING

R A Jöbstl
G Schickhofer

Institute for Timber Engineering and Wood Technology
Graz University of Technology

AUSTRIA

MEETING FORTY

BLED

SLOVENIA

AUGUST 2007

Presented by R. A. Jöbstl
J.W. van de Kuilen asked how constant was the constant climate and what would happen if variable climate was used? R. A. Jöbstl replied that the condition was mostly constant except in one case where the specimen was near the door and there may be some issue. R. A. Jöbstl said that for non-constant climate there is no information about the shear behaviour. There are examples of 19 laminate CLT used in bridge plate behaving well.

Comparative examination of creep of GLT- and CLT-slabs in bending

R A Jöbstl, G Schickhofer

Institute for Timber Engineering and Wood Technology

Graz University of Technology, Austria

1 Abstract

Cross laminated timber (CLT) is – comparable with plywood – build up of orthogonal layers. The base materials are boards or in further steps the lamella, which match the requirements of glued laminated timber (GLT). Concerning standardisation, CLT is only regulated nationally in DIN 1052 and SIA 265. The main current application lies in residential buildings. Because of high slenderness in case of ceilings – span to depth ratios of 25 to 35 – serviceability design is generally decisive.

As a result – beside of short-term-deformations – long-term-deformations and related creep of discussed structures has to be kept in attention. According the current European design reglementations long-time-deformation has to be derived by reducing stiffness characteristic which is regulated by deformation factor k_{def}. The k_{def} for CLT has still to be identified.

For that long-term four-point-bending-tests on five-layered CLT slab elements acc. EN 408 have been carried out at the Graz University of Technology. To reduce the sample size, parallel tests on GLT slab elements have been done with same testing configuration to enable direct comparison of test results of CLT with a well examined and known structure. By testing, loading (approx. 9 % and approx. 25 % of failure load) and climate (approx. SC1 and SC2) have been varied.

The results for CLT lead to about 30 ÷ 40 % higher creep value k_c compared to GLT, which nearly conforms the difference between unidirectional build up GLT and comparable to CLT orthogonal build up plywood.

Data gained from total deformation demonstrate smeared creep value $k_{c,CLT,5s}$ over the five-layered cross section. Furthermore, based on these results and by some additional assumptions creep value $k_{c,9090}$ for rolling shear G_{9090} has been derived. This has enabled calculation of CLT-elements with various number of layers, which demonstrate relative low difference to five-layered build up. By application of this method a practice relevant and smeared creep value for the whole structure – as possible for other layered wood-structures like plywood and OSB – can be derived by the engineer.

2 Introduction

Cross laminated timber (CLT) is a multi-layered shell product, whereby orthogonal board layers lead to blocking each other. So CLT is familiar to two further products well introduced in timber engineering – with the product glued laminated timber (GLT) concerning base material board and dimensions, to product plywood comparable due to dimensional stability and slab-like character.

For application in timber engineering as slab loaded in bending, up to now lack of knowledge concerning expectable system- and laminating effect for economic ultimate limit design and creep values respectively deformation factors for serviceability have been given. Both questions have been addressed in a common project on the Graz University of Technology, whereby system-structural behaviour has been presented in [1] and theme concerning long-term-deformations will be discussed in on hand report. Based on short-term four-point bending tests (see [1]) and long-term bending tests on five-layered CLT-elements creep values and deformation factors are proposed. Parallel identical accomplished long-term-tests on GLT-plate-elements, a well known and standardized product, have enabled direct comparison with CLT.

3 Current knowledge and status of research

3.1 Creep in design codes

The long-term-behaviour, and hence serviceability, are deeply influenced by the creep-behaviour of the material itself. The description and design is derived by enlargement of static short-term-deformations through introduced k_{def}. In design codes these deformation factors are regulated in dependence on product and climate, respective service class (SC). For building sector up to know most relevant are the unidirectional structures – like solid timber, solid structural timber and glued laminated timber – which show lowest creep effect, examined by numerous tests on specimens in structural size. All further products are characterised by higher creep-deformations, in dependence of:

- Quantity of cross section with fibre direction perpendicular to loading direction (like CLT and plywood: share of layers lengthwise and perpendicular),
- Dispartment factor of base material (board – veneer – chip – fibre)
- Quantity of adhesive

The product CLT is up to now not defined in EN 1995-1-1:2004. Hence no deformation factor is given but due to comparable build up of cross section CLT can be classified akin to plywood. In contrast national standards DIN 1052:2004 and SIA 265:2003 rate CLT to class of unidirectional wood products. Acc. EN 1995-1-1:2004 by 'connection of two wood-based elements' with deviating deformation factors calculation of long-term deformation has to be derived based on smeared total deformation factor acc. (1).

$$k_{def} = 2 \cdot \sqrt{k_{def,1} \cdot k_{def,2}} \qquad (1)$$

In EN 1995-1-1:2004 no deformation factor for layers perpendicular is given. Nevertheless it can be assumed that formulation (1) may lead to values on significant too conservative bases.

3.2 Research and creep

The layers perpendicular, which are the major principle of cross section build up of CLT, accept higher creep deformation for CLT compared to GLT and hence a supposed wise classification in the group of plywood. Niemz describes in [2] a creep value of 0.1 to 0.3 for wood parallel to grain, but 0.8 to 1.6 for wood perpendicular to grain. Also Madson suggests in [3] a significant higher creep influence in loading perpendicular to grain, whereby no quantification but qualitative assessment in diagrams is given. These reflect around 50 % higher long-term deformations in loading perpendicular to grain compared to loading parallel to grain – but already after fiftieth of time.

4 Aim of this work

The aim of presented project ‚creep of CLT' has been derivation of creep value $k_{c,CLT}$ for CLT by practical tests for product relevant (and due to general approval) service classes SC1 and SC2 under loading in bending out of plane. In first line guiding values for design of long-term behaviour of constructions out of CLT-elements should be derived to enable reliable declaration by the engineer. Because of this, examination of the difference between CLT and GLT, as numerous examined and well known engineered product, for practical relevant cross sections has been the main target.

On this basis derivation of creep values $k_{c,90|90}$ for cross layers have been aspired to enable conclusion of changes in dependence of CLT cross sections of various quantity of layers.

In the end a proposal for deformation factors $k_{def,CLT}$ for CLT should be possible.

5 Method

5.1 Test variations

Application of CLT-elements as roof- or ceiling-elements requires mostly high slenderness of around $l / d = 25 \div 35$. This leads to most relevant design in serviceability. For these general uniaxial spanned elements a testing program for enabling direct comparison of CLT with GLT has been established. The variation in the product states as first variation parameter.

Tab. 1 Variation parameter 1 – Product CLT and GLT

VP 1: Product	Cross Laminated Timber	Glued Laminated Timber

As second variation parameter two stress levels have been examined. As referent destructive tests on specimens build up of the same base material have been accomplished and given in [1]. Per each variation a test-tower of five in serial linked elements has been tested, whereby loading on each specimen has been increased due to net weight of above specimen (see 5.3).

Tab. 2 Variation parameter 2 – Stress level 1 and 2

VP 2: Stress level	Cross Laminated Timber	Glued Laminated Timber
Bending strength [1]	$f_{m,c,mean}$ = 40.1 N/mm²	$f_{m,g,mean}$ = 42.3 N/mm²
	$f_{m,c,05}$ = 31.1 N/mm²	$f_{m,g,05}$ = 35.8 N/mm²
Stress level 1,	3.0 ÷ 3.9 N/mm²	2.4 ÷ 3.1 N/mm²
dead load 7 kN	7.5 % ÷ 9.6 % ($f_{m,c,mean}$)	5.6 % ÷ 7.2 % ($f_{m,g,mean}$)
	9.7 % ÷ 12.4 % ($f_{m,c,05}$)	6.7 % ÷ 8.6 % ($f_{m,g,05}$)
Stress level 2,	8.6 ÷ 9.4 N/mm²	6.8 ÷ 7.5 N/mm²
dead load 20 kN	21.4 % ÷ 23.5 % ($f_{m,c,mean}$)	16.1 % ÷ 17.7 % ($f_{m,g,mean}$)
	27.6 % ÷ 30.4 % ($f_{m,c,05}$)	19.1 % ÷ 21.0 % ($f_{m,g,05}$)

The third variation parameter deals with two climates approx. according SC1 and SC2.

Tab. 3 Variation parameter 3 – Climate 1 and 2

VP 3: Climate	Climate 1	Climate 2
Condition: humidity / temp	55 % / 20°C	78 % / 20°C
Masured equilibrium moisture content	11.6 %	14.2 %

This leads to 2 · 2 · 2 = 8 variations. Per variation five specimens have been combined in one testing tower (see 5.3), whereby totally 40 elements have been tested.

5.2 Test material

Based on identical base material of boards, wood species spruce (strength class C24 with cross section 120 / 22 mm) groups of random selected boards have been defined to build up first CLT-elements and second GLT-elements as quasi unidirectional slab-elements (see [1] for data concerning third group of boards for tension tests). The cross sections of both element-types had a width of 480 mm (four boards in parallel in outer layers) and thickness of 110 mm (five-layered build up), as given in Fig. 1.

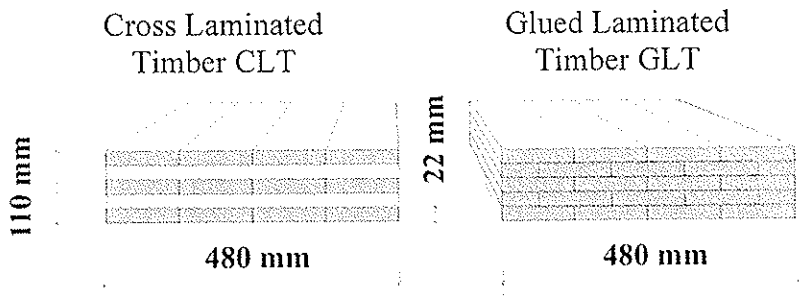

Fig. 1 Cross sections of testing material Cross Laminiated Timber CLT and Glued Laminiated Timber GLT

5.3 Test setup

Four-point bending test configuration has been applied acc. EN 408:2005 and identical to [1]. All five-layered elements have been build up of boards with cross section 120 / 22 mm which lead to nominal thickness of d = 110 mm. Due to testing configuration acc. Fig. 2 this lead to span of 1980 mm and loading in third points.

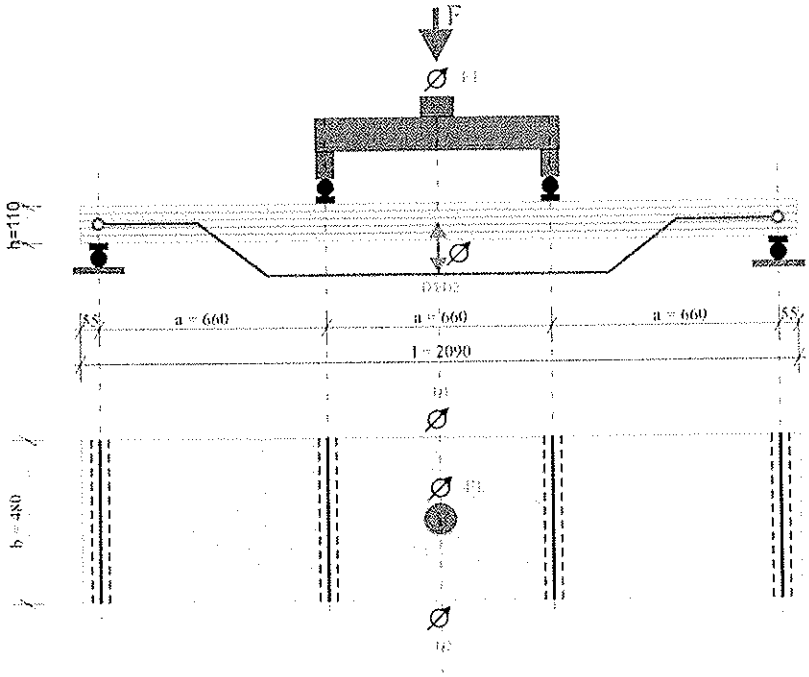

Fig. 2 Test setup: 4-point-bending test according to EN 408:2005

For accuracy measurement of global deformation of elements reference beams have been applied, placed on both sides and in centre line.

As already given in 5.1, for all 8 variations 5 specimens have been combined in one tower (see Fig. 3). In Fig. 4 for creep-towers in climate chamber are presented. Load introduction and alternating support of specimens on the outer points and third points is visible. More over five-layered build up can be imagined.

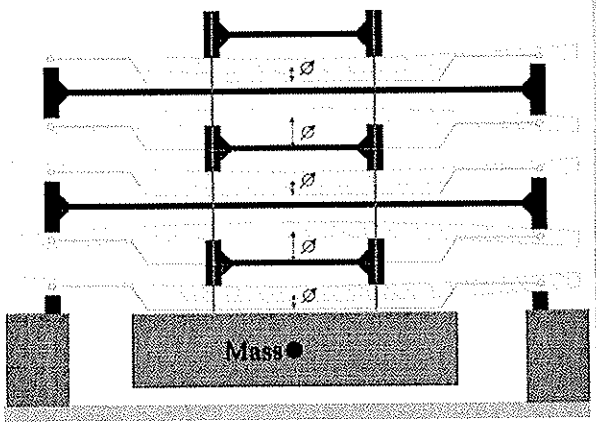

Fig. 3 Test setup: Deformation drawing of one creep tower per each variation paramter

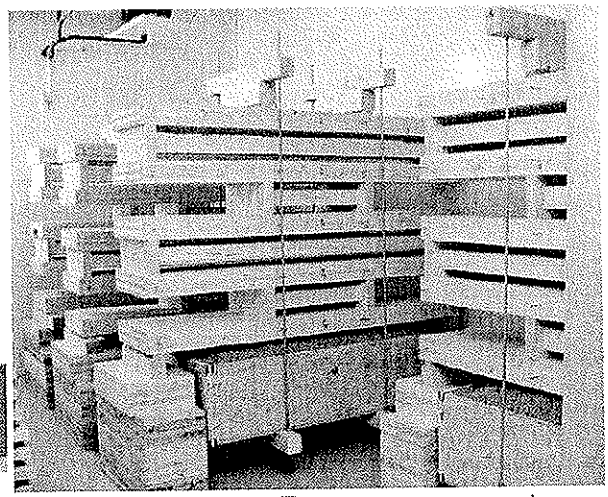

Fig. 4 Test setup: Four creep towers in one climate chamber

6 Discussion

6.1 Results of creep tests

The creep towers have been exposured to loading, as described above, for one year, whereby global deformations have been measured and recorded continuously. In Fig. 5 mean-values for deformations of in each case five linked specimens in relationship to time are given. The coefficient of variation of global deformation within the same tower is given between 2.2 % ÷ 6.1 % for load level 2 (20 kN) and 4.8 % ÷ 11.1 % for load level 1 (7 kN). Higher COV for lower load level may be a result of minor deformations and combined lower measurement accuracy. In Fig. 5 creep value k_c has been compared with time in years.

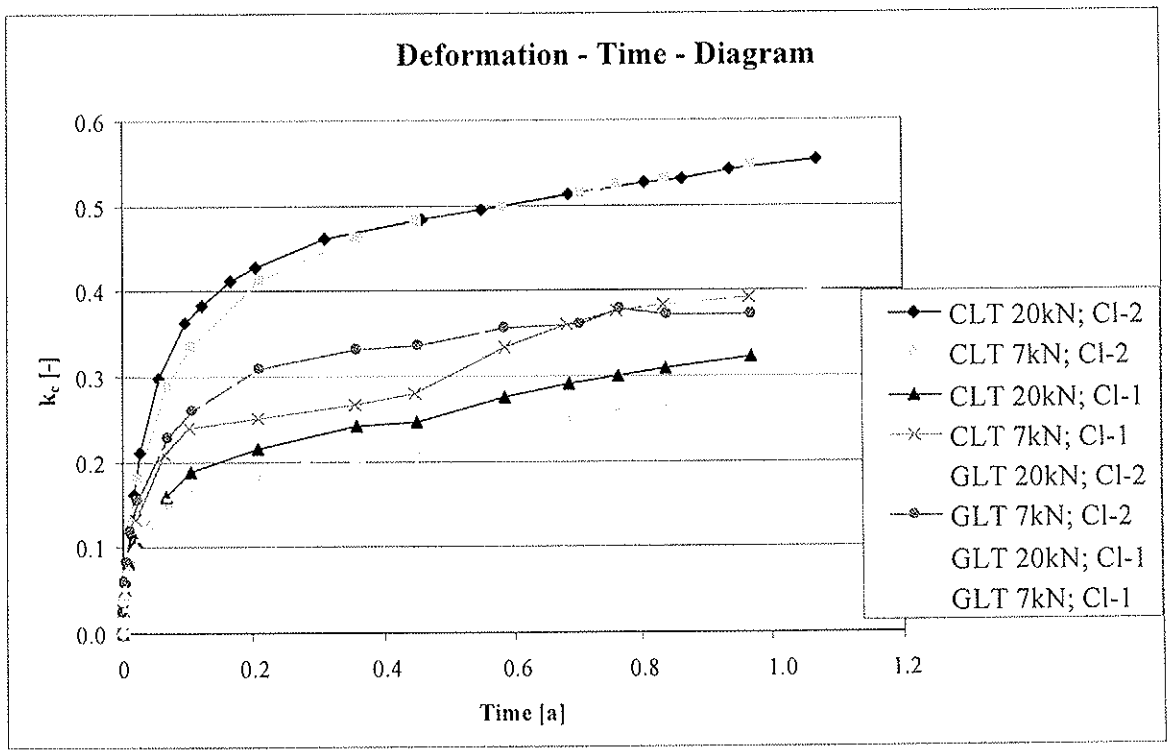

Fig. 5 Results of creep tests of Cross Laminated Timber CLT and Glued Laminated Timber GLT

Time-dependent graphs of creep reflects nearly perfect accordance of towers of same cross section and same climate. Only exception is given by CLT-towers of climate 1 (55% / 20°C), whereby tower with higher load level leads to unexpected low deformation values – up to now no explanation has been found. General, creep-graphs of climate 1 reflect more discontinuity. The reason for that may be often induced climate variations due to opening the climate chamber.

By comparison of latest measurement results of CLT- with GLT-element-towers, in dependence of climate and load level, a 37 % to 47 % higher increase of deformation of orthogonal build up cross sections due to creep is determinable. In contrast, deformation factors k_{def} for plywood – compared with unidirectional wooden structures acc. EN 1995-1-1:2004 – are about 33.3 % (SC1) and 25.0 % (SC2) higher. Values are listed in Tab. 4.

Tab. 4 Difference between creep - deformation of GLT to CLT

Climate	Load level	Increase GLT ⇨ CLT
Climate 1 (quasi SC1)	LL 1 (7 kN)	+ 41.9 %
	LL 2 (20 kN)	+ 19.3 %
	EN 1995-1-1	+ 33.3 %
Climate 2 (quasi SC2)	LL 1 (7 kN)	+ 46.5 %
	LL 2 (20 kN)	+ 38.5 %
	EN 1995-1-1	+ 25.0 %

6.2 Comparison between GLT and CLT

An additional possibility to derive a deformation factor $k_{def,CLT}$ for CLT based on current creep data is given by direct comparison of creep graphs of GLT and CLT. For that assumptions like mathematical similar functions for creep behaviour of GLT and CLT and correct deformation factors $k_{def,GLT}$ given in EN 1995-1-1:2004 have to be made. In that case and for every load duration it is possible to derive the creep value $k_{c,CLT,t}$ for CLT and the creep value $k_{c,GLT,t}$ for GLT by the relationship

$$\frac{k_{c,CLT,t}}{k_{c,GLT,t}} = \frac{k_{def,CLT}}{k_{def,GLT}} \qquad (4)$$

and further more the deformation factor $k_{def,CLT}$.

In Fig. 6 graphs of deformation factor $k_{def,CLT}$ for all four CLT-creep-towers in dependence of time, gained by application of equation (4), are given. For comparison deformation factor k_{def} for service classes SC1 and SC2 for plywood are included.

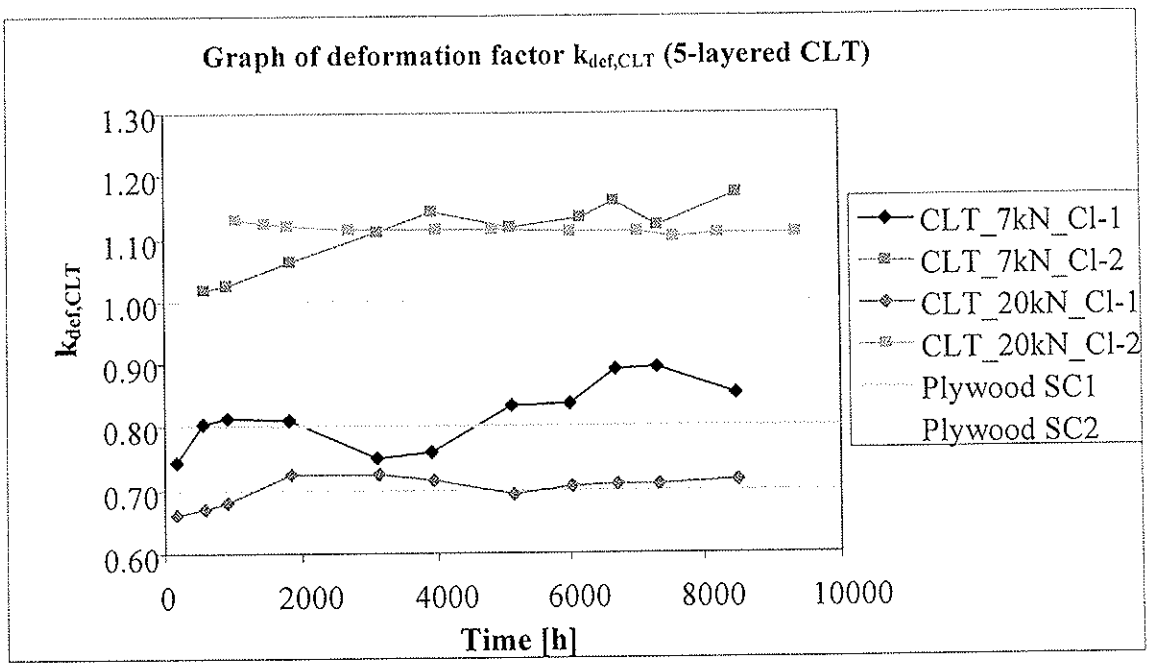

Fig. 5 Comparison between GLT and CLT

Fig. 5 clearly visualises robust and nearly constant data for extrapolations of predominant creep towers of higher load level, with $k_{def,CLT,Cl-2} \sim 1.1$ and $k_{def,CLT,Cl-1} \sim 0.7$. The deformation factor for climate 1 may be too low, as described in 6.1. Due to this graph of lower load level for climate 1 will be preferred with expected value of around 0.85.

7 Design concept (SLS)

7.1 Long term deformation of 'homogeneous' and 'heterogenous-smeared' cross sections

Deformation due to bending and shear force at time t = 0 can be calculated as given:

$$w_{t=0} = w_{M,t=0} + w_{V,t=0} = \frac{1}{E \cdot I} \int M\bar{M}dx + \frac{\kappa}{G \cdot A} \int V\bar{V}dx \tag{5}$$

The long-term deformation respective creep has to be derived by increase of short-time deformation through sum of 1.0 plus deformation factor (respective through reduction of stiffness on the same amount). For unidirectional products like GLT the same deformation factor k_{def} for all types of loading, in that case for bending E-modulus E_0 for share of moment and G_{090} for share of shear force, has to be assumed acc. to standards:

$$w_{t=\infty} = w_{t=0} \cdot (1 + k_{def}) = w_{M,t=0} \cdot (1 + k_{def}) + w_{V,t=0} \cdot (1 + k_{def}) \tag{6}$$

Equation (6) in (5) leads to:

$$w_{t=\infty} = w_{M,t=\infty} + w_{V,t=\infty} = \frac{(1 + k_{def})}{E \cdot I} \int M\bar{M}dx + \frac{(1 + k_{def}) \cdot \kappa}{G \cdot A} \int V\bar{V}dx \tag{7}$$

respective acc. to classical multi-layer Euler-Bernoulli-beam (rigid composite theory) for CLT

$$w_{t=\infty} = w_{M,t=\infty} + w_{V,t=\infty} = \frac{(1 + k_{def,CLT})}{E \cdot I_{eff}} \int M\bar{M}dx + \frac{(1 + k_{def,CLT}) \cdot \kappa}{G \cdot A_{eff}} \int V\bar{V}dx \tag{8}$$

The examinations of creep tests on CLT in chapter 6 induce over the whole cross section smeared creep value $k_{c,CLT}$, as basis for further determination of deformation factors $k_{def,CLT}$.

7.2 Refeed to a 'material-value' for $k_{def,9090}$ perpendicular to grain

Calculated creep values $k_{c,CLT}$ of chapter 6 are only guilty for five-layered cross section, as examined. On the basis of simple engineering assumptions it should be possible to calculate a smeared creep value $k_{c,9090}$ and hence a deformation factor $k_{def,9090}$ for layers perpendicular to grain, out of smeared deformation factors $k_{def,CLT}$.

Stiffness for tested five-layered CLT-cross section can be derived as following, under assumption of lack of transfer of axial force in layers perpendicular due to gaps ($E_{90} = 0$):

$$(E \cdot I_{eff})_{5S} = \frac{b \cdot h^3}{12} \cdot \frac{1}{125} \cdot (99 \cdot E_0 + 26 \cdot E_{90}) = \frac{I_{geo}}{125} \cdot 99 \cdot E_0 \tag{9}$$

$$(G \cdot A_{eff})_{5S} = b \cdot h \cdot \frac{1}{5} \cdot (3 \cdot G_{090} + 2 \cdot G_{9090}) = \frac{A_{geo}}{5} \cdot (3 \cdot G_{090} + 2 \cdot G_{9090}) \tag{10}$$

$$\kappa_{5S} = \frac{6}{5} \cdot \frac{3 + 2 \cdot \frac{G_{9090}}{G_{090}}}{99^2} \cdot \left(960 \cdot \frac{G_{090}}{G_{9090}} + 883 \right) \tag{11}$$

Furthermore following assumptions are given:

$$E_{90,t=0} = E_{90,t=\infty} = 0 \tag{12}$$

$$E_{0,t=\infty} = \frac{E_{0,t=0}}{(1 + k_{def,0})} \tag{13}$$

$$G_{090,t=\infty} = \frac{G_{090,t=0}}{(1 + k_{def,0})} \tag{14}$$

$$G_{9090,t=\infty} = \frac{G_{9090,t=0}}{(1 + k_{def,9090})} \tag{15}$$

The deformation factor $k_{def,9090}$ in equation (15) defines the searched material characteristic for creep in shear perpendicular to the grain (directions tangential-radial respective '9090', general named as rolling shear).

The material characteristics with index-enlargement t = 0 correspond to material characteristics which are regulated in design codes.

In contradiction to consideration of smeared cross sections for calculation of deformations acc. (8) a layered cross section can be dealt with:

$$w_{t=\infty} = w_{M,t=\infty} + w_{V,t=\infty} = \frac{(1 + k_{def,0})}{E_0 \cdot I_{geo} \cdot \frac{99}{125}} \int M \bar{M} dx + \frac{\frac{6}{5} \cdot f(G_{090}, G_{9090}, k_{def,0}, k_{def,9090})}{\frac{A_{geo}}{5} \left(3 \cdot \frac{G_{090}}{1 + k_{def,0}} + 2 \cdot \frac{G_{9090}}{1 + k_{def,9090}} \right)} \int V \bar{V} dx \tag{16}$$

The numerator in share of shear deformation contains the function for the shear correction factor κ (see equation (11)) but for time t = ∞.

Through equation of deformations of (8) and (16) deformation factor $k_{def,9090}$ can be gained iteratively.

$$w_{t=\infty,smeared} = w_{t=\infty,layered} \tag{17}$$

Based on over cross section smeared deformation factors $k_{def,CLT}$ in Tab. 5 lead to deformation factor $k_{def,9090}$ for the material characteristic of strength class C24 in Tab. 6 (per ratio of shear modulus $G_{090}/G_{9090} = 10$ acc. EN 338:2003 and for the constant rolling shear modulus $G_{9090} = 50$ N/mm², as given in technical approvals):

tab. 6 Deformation factors $k_{def,9090}$ based on test results respective standardized deformation factors based on iterative method

Basis: $k_{c,10Y}$	Service Class 1		Service Class 2	
Product / Material	k_{def} acc. EC 5	k_{def} acc. 6.3	k_{def} acc. EC 5	k_{def} acc. 6.3
GLT	0.6	0.6	0.8	0.8
Plywood / CLT	0.8	0.85 (0.70)	1.0	1.1
Timber$_{9090}$ (G_{090}/G_{9090}=10)	1.95	2.27 (1.26)	2.15	2.80
Timber$_{9090}$ (G_{9090}=50N/mm²)	1.60	1.88 (1.11)	1.80	2.33

7.3 Re-calculation of over cross section smeared values of alternative build ups

For practical relevant determination of long-term-deformations it is proposed not to introduce a further material parameter. Instead and under help of now elicited deformation factors $k_{def,9090}$ (respective creep value $k_{c,9090}$) a smeared deformation factor $k_{def,CLT}$ is calculated for alternative cross section build ups and compared with data of tested five-layered elements.

For further re-calculation deformation factors, gained from comparative calculations between GLT and CLT, serve as basis.

tab. 7 Deformation values k_{def} gained from comparative calculations between GLT and CLT acc. 6.3

	SC 1	SC 2
$k_{def,CLT}$	0.85	1.1
$k_{def,0}$	0.6	0.8
$k_{def,9090}$ (G_{090}/G_{9090} = 10)	2.27	2.80
$k_{def,9090}$ (G_{9090} = 50 N/mm²)	1.88	2.33

These deformation factors used in equation (16), but converted acc. quantity of layers of desired cross section, lead to fictive deformations $w_{t=\infty}$, which again introduced in equation (8) lead to over cross section smeared deformation factor $k_{def,CLT}$ for number of layers between 3 and 19 in Fig. 6 presented.

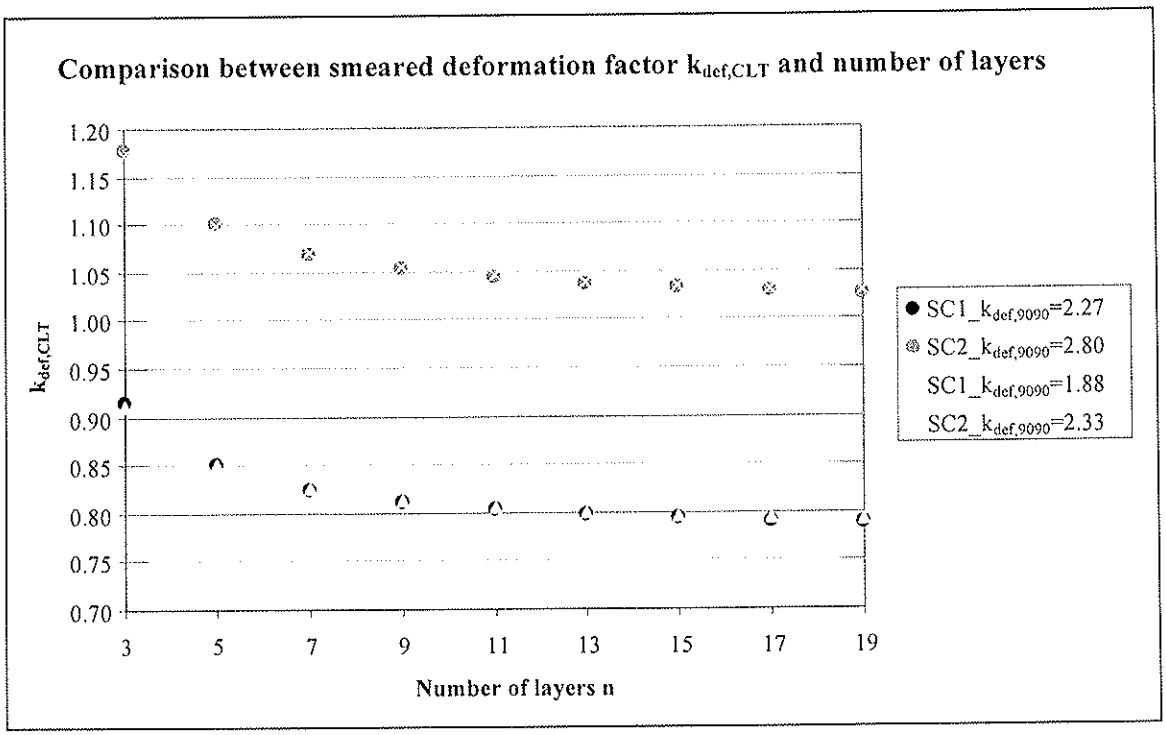

Fig. 6 Comparison between smeared deformation factor $k_{def,CLT}$ and number of layers

Acc. these findings following statements are possible:

- For calculation necessary assumption of rolling shear modulus G_{9090} (as ratio to shear modulus G_{090} or as constant value with 50 N/mm²) has only minor influence on over cross section smeared deformation factor $k_{def,CLT}$.
- With increasing number of layers the over cross section smeared deformation factor $k_{def,CLT}$ is decreasing continuously and converges to a constant value.
- The scope of deformation factors in dependence of number of layers varies around the data gained from five-layered elements ($k_{def,CLT,SC1}$ = 0.85, $k_{def,CLT,SC2}$ = 1.10) with deviation of ± 7 %.
- For 19-layered elements deformation factors are comparable with those of plywood (SC1 $k_{def,plywood}$ = 0.80 - $k_{def,CLT,19layers}$ = 0.79; SC2 $k_{def,plywood}$ = 1.00 - $k_{def,CLT,19layers}$ = 1.03)

8 Summery

At Graz University of Technology comparable creep tests on five-layered cross laminated timber- and glued laminated timber-elements have been accomplished. After about one year of loading, increase of deformation of CLT compared to GLT reached around 39 % to 47 %. By assumption of similar creep-functions for both examined products over cross section smeared deformation factors $k_{def,CLT}$ for two climates have been derived. By application of simple engineering approach a deformation factor for layers perpendicular $k_{def,9090}$ has been re-calculated for the rolling shear modulus G_{9090} (the modulus of elasticity perpendicular to the grain E_{90} has been assumed with 0) and hence concluded for over cross section smeared deformation factors $k_{def,CLT}$ for alternative cross section build ups.

Presented deformation factors for number of layers with 3 to 19 show converging function with increasing number of layers. In that way calculated deformation factors are comparable with plywood acc. EN 1995-1-1:2004. Based on these results it is proposed to consider the product CLT concerning long-term-behaviour within the group of plywood, whereby for number of layers lower or equal 7 the deformation factor has to be increased by 10 %.

9 Acknowledgement

The research work within the presented project is financed by the competence centre holz.bau forschungs gmbh and performed in collaboration with the Institute of Timber Engineering and Wood Technology of the Graz University of Technology and the industrial partner StoraEnso Timber.
The project is fostered through the funds of the Federal Ministry of Economics and Labour, the Styrian Business Promotion Agency Association, the province of Styria and the city of Graz.

10 Symbols

k_{def}	deformation factor
$k_{def,0}$	deformation factor for the material characteristic E_0
$k_{def,9090}$	deformation factor for the material characteristic G_{9090}
k_c	creep value
$k_{c,10Y}$	creep value for extrapolated load duration of 10 years
$f_{m,g}$	bending strength of GLT
$f_{m,c}$	bending strength of CLT
h, d	height, depth of a plate in bending flatwise
l	length
w	deformation
$w_{smeared}$	deformation calculated based on smeared cross-section-values
$w_{layered}$	deformation calculated based on discrete layered cross-section-values
E_0	modulus of elasticity parallel to the grain
E_{90}	modulus of elasticity perpendicular to the grain
G_{090}	shear modulus acting in the plane of grain-direction and perpendicular to the grain
G_{9090}	shear modulus acting in the plane perpendicular to the grain; known as 'rolling shear modulus'
I	moment of inertia
I_{geo}	moment of inertia based on geometric, cross section surrounding dimension
$E \cdot I_{eff}$	effective bending stiffness

A	cross section
A_{geo}	cross section based on geometric, cross section surrounding dimension
$G \cdot A_{eff}$	effective shear stiffness (without shear correction factor)
κ	shear correction factor
κ_{5S}	shear correction factor of 5-layered CLT of constant layer thickness
Cl-1	climate 1
Cl-2	climate 2
LI-1	load level 1
LI-2	load level 2
SC 1	service class 1 according EN 1995-1-1:2004
SC 2	service class 2 according EN 1995-1-1:2004

Additional indices

X_{GLT}	... of the product GLT
X_{CLT}	... of the product CLT
X_{5s}	... of 5-layred cross section
X_t	... at particular time t
$X_{t=0}$	... at particular time t = 0
$X_{t=\infty}$	... at particular time t = ∞
X_{mean}	... mean of ...
X_{05}	... 5 %-quantile of ...
X_M	... due to moment
X_V	... due to shear force

11 References

[1] Jöbstl, R. A., Moosbrugger, Th., Bogensperger, Th., Schickhofer, G.: A Contribution to the Design and System Effect of Cross Laminated Timber (CLT). Proceedings of CIB W18/39-12-4, Florence, Italy, 2006

[2] Niemz, P.: Physik des Holzes und der Holzwerkstoffe. DRW-Verlag, ISBN 3-87181-324-9, 1993

[3] Madsen, B.: Structural Behaviour of Timber. Timber Engineering Ltd., ISBN 0-9696162-0-1, 1992

INTERNATIONAL COUNCIL FOR RESEARCH AND INNOVATION
IN BUILDING AND CONSTRUCTION

WORKING COMMISSION W18 - TIMBER STRUCTURES

STANDARD PRACTICE FOR THE DERIVATION OF DESIGN PROPERTIES OF STRUCTURAL GLUED LAMINATED TIMBER IN THE UNITED STATES

T G Williamson
Borjen Yeh

APA – The Engineered Wood Association

U.S.A.

MEETING FORTY

BLED

SLOVENIA

AUGUST 2007

Presented by T. Williamson
H. Larsen mentioned he was confused by the paper and asked if the test results for thousands of beams tested are available. T. Williamson replied that the results are available in reports.
A. Ranta-Maunus commented that this type of information is needed.

Standard Practice for the Derivation of Design Properties of Structural Glued Laminated Timber in the United States

Thomas G. Williamson, P.E.
Borjen Yeh, Ph.D., P.E.
APA - The Engineered Wood Association, U.S.A.

Abstract

Structural glued laminated timber (Glulam) has been used in North America for more than 70 years. The design properties for glulam when manufactured with a recognized manufacturing standard, such as the *American National Standard for Structural Glued Laminated Timber*, ANSI AI90.1, are typically derived in accordance with ASTM D 3737, *Standard Practice for Establishing Allowable Properties for Structural Glued Laminated Timber.*

ASTM D 3737 itself is an analytical model based on the "I_K/I_G" model established in 1954 through extensive research conducted by the US Forest Products Laboratory in Madison, Wisconsin. In addition to the bending strength, other design properties of glulam, such as modulus of elasticity, shear, compression parallel to grain, and compression perpendicular to grain, can be calculated using ASTM D 3737 when the glulam layup (grade combination) is defined. As compared to European practice, ASTM D 3737 represents a different perspective in assigning glulam design values, which is well supported by years of practical experience in North America and thousands of confirming full-scale beam tests. One of the differences is the fact that ASTM D 3737 and ANSI A190.1 are based on using the strength reducing characteristics of the laminating grades as the basis for assigning design properties and then requiring the use of an equivalent end joint strength to support these properties.

In addition, the ASTM D07 Committee on Wood is currently balloting a new standard that will permit the establishment of design bending stress and stiffness based on full-scale flexural tests. This paper describes the standard practice for the derivation of design properties of glulam in the United States based on both analytical and empirical approaches. This information provides alternative methods to the existing European practice in assigning glulam design values. Understanding the differences between the European and US practice could help facilitate the development and harmonization of glulam standards that are being developed in countries such as China and Taiwan as well as for ISO standards currently under development.

1. Introduction

While structural glued laminated timber (glulam) has been used in Europe for over 100 years, it was first introduced into the United States (U.S.) in 1935 with the first structure being a research laboratory at the U.S. Forest Products Laboratory in Madison WI. This structure used Tudor arches as the primary structural framing elements and is still in service today, even enduring the effects of a serious fire.

Since this first application, glulam has grown to be an approximately 500 million board foot per year industry in the U.S. Approximately 60% of all glulam produced in the U.S. is used in residential framing as shown in Figure 1. Residential framing applications include glulam headers over door and window openings, garage door headers, floor beams, roof rafters and ridge beams. While some of these applications take advantage of the aesthetics associated with glulam by exposing them, the majority of these end uses are in concealed applications. Nonresidential uses include churches, schools, warehouses, recreational facilities, retail, office buildings, chemical storage plants and others and are often exposed in the finished structure. Therefore, while the use of glulam is often predicated on its inherent aesthetic features, in all cases, the key to the final selection of glulam is its inherent strength, durability, integrity and unquestioned quality.

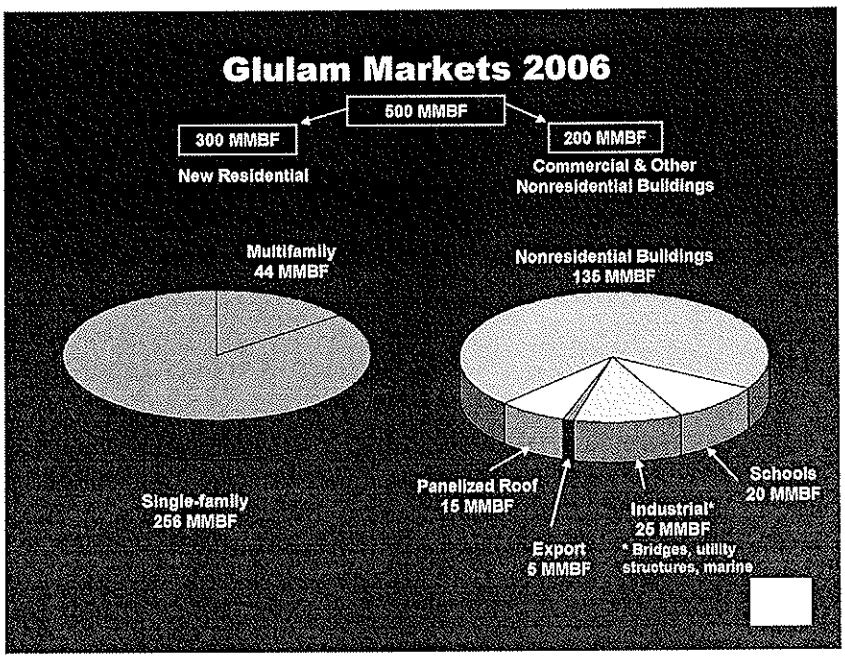

Figure 1

In 2000, the U.S. combined its three regional building codes into the International Building Code, IBC (primarily applicable to engineered construction such as non-residential) and the International Residential Code, IRC (primarily applicable to prescriptive residential construction). Both of these codes require that all glulam be trademarked as being in conformance with ANSI A190.1, "Structural Glued Laminated Timber" [1] and Section 4.3.6 of this standard requires that grade combinations for glulam be developed in accordance with ASTM D3737 "Standard Practice for Establishing Allowable Properties for Structural Glued Laminated Timber" [2] or shall be obtained by performance testing and analysis in accordance with recognized standards.

2. Early Glulam Research

Since glulam was a new product in the U.S., the US Forest Products Laboratory (FPL) in Madison, WI undertook a series of extensive tests on glulam arches beginning in 1934. This included tests of glulam to check for such factors as design formulas, working stresses and the effect on strength of curvature, end joints and knots and was reported in USDA Technical Bulletin 691, "The Glued Wooden Arch" [3]. With the great demand during

World War II for heavy timbers, the development of glued laminated timbers was greatly hastened and significant research was conducted in the areas of adhesives, lumber quality and the testing of full-size laminated beams and columns to supplement and confirm the work reported in Technical Bulletin 691. This work was published in USDA Technical Bulletin 1069, "Fabrication and Design of Glued laminated Wood Structural Members" [4] and formed the basis for the development of characteristic design stresses for glulam which is still used today.

The basic premise of Technical Bulletin 1069 is that the strength of glued laminated timber is dependent on the knot characteristics and their distribution in the glulam member. This led to the development of the "I_K/I_G" model that forms the basis for ASTM D3737 This standard has undergone numerous changes over the years including (a) incorporating provisions for using full-scale beams tests to determine flexural and horizontal shear properties, (b) adding special provisions for tension laminations and (c) introducing the volume effect factor with the current version of the standard being D3737-06.

It is important to note that in addition to being the basis for D3737, Technical Bulletin 1069 was also the predecessor of the manufacturing and fabrication requirements for glulam used today in the U.S. The first manufacturing standard for glulam was U.S. Department of Commerce Commercial Standard CS 253-63 published in 1963 and it was subsequently revised and published as Department of Commerce Standard, PS 56-73. At the same time it was also promulgated as ANSI Standard A190.1-1973, and this has been superseded by A190.1-1983, A190.1-1992 and the current version of A190.1-2002.

3. ASTM D3737

3.1 Introduction

Since ASTM D373 is relatively complicated, this paper will only address the determination of allowable bending stresses for a glulam member loaded on the X-X axis. The basic concept of D3737 is that clear wood strength properties and their expected variation for small clear, straight-grained specimens of green lumber based on ASTM D 2555 [5] can be used to develop stress index values for the various strength properties. For example, for a bending member loaded on the X-X axis, the bending stress index can be determined by calculating the fifth percentile of modulus of rupture in accordance with Test Methods D 2555, multiplying by an appropriate adjustment factor and multiplying by 0.743 to adjust to a 12-in. (30 cm) deep, uniformly loaded simple beam with a 21:1 span-to-depth ratio. As an alternative, results of testing and analysis of large glued laminated timber beams of Douglas Fir-Larch, Southern Pine and Hem-Fir are also used to establish stress indexes.

These stress indexes are then multiplied by stress modification factors developed based on the effects of strength reducing characteristics of knots, slope of grain and density. For example, the bending stress modification factor for knots, ($SMF_{bx\ knots}$) is given by the equation,

$$SMF_{bx\ knots} = (1 + 3\frac{I_K}{I_G})\,(1 - \frac{I_K}{I_G})^3\,(1 - \frac{I_K}{2I_G}) \qquad (1)$$

3.2 I_K/I_G Analysis

The "I_K/I_G" analysis that forms the basis for D3737 is based on determining how strength reducing characteristics including knot sizes and slope of grain of the individual laminations and their distribution within the glulam member affect the overall strength of the finished glulam. The following definitions are used.

Ik is the sum of the moments of inertia of the cross sectional areas of all knots within 6 inches (150 mm) of a single cross section at the 99.5 percentile

Ig is the moment of inertia of the full of gross cross section

X-bar is defined as the average of the sum of all knot sizes within any 1-ft length along the piece of lumber

h is the difference between the 99.5 percentile knot size and X-bar

Thus, it is necessary to define the knot characteristics, X-bar and h, for all combinations of species and lumber grades to apply the "I_K/I_G" principles. Annex A6 of D3737 provides guidance on the determination of these knot dependent values. There are 8 types of knots that are measured and these are shown in Figure 2. Note that there is no knot type 8 by committee decision. All knots of 3/8" (6 mm) or greater are measured and the projected cross-sectional area for each knot type is determined.

Any linear regression routine that determines the parameters of the regression line and the value of the 99.5 percentile can be used to emulate the procedure of plotting the sum of knots cumulative frequency data on arithmetical probability paper and drawing a straight line through the data, which was the method used in USDA Bulletin 1069. The underlying assumption for using this procedure is that an analysis, which handles the knot data as normally distributed, is satisfactory.

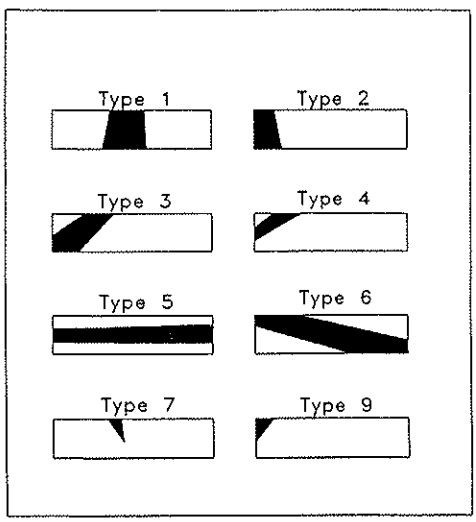

Figure 2

The following steps summarize the provisions of Annex A4 of D3737 to determine the allowable flexural design stress (F_{bx}) for horizontally laminated beams assuming the use of

several zones based on different grades and or species of laminating lumber throughout depth of the member. This can be used for symmetric layups or for unsymmetric layups such as shown in Figure 3. Note that the grade combination in Figure 3 for a six-zone beam also shows that different species as well as different lumber grades can be intermixed.

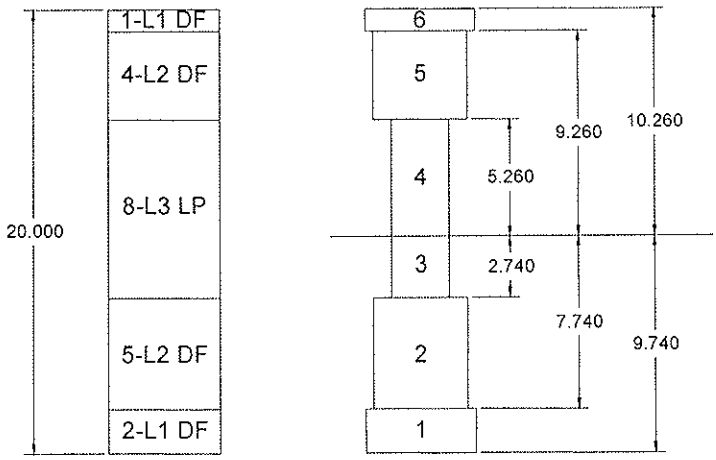

Figure 3

1. The location of the neutral axis of the transformed section is determined using Equation (2), and the distance from the neutral axis to the edges of each grade zone in the beam is determined using Equations (3) and (4).

$$\bar{y} = \frac{\sum_{j=1}^{n_l}\left[\frac{E_j}{2}\left(y_j^2 - y_{(j-1)}^2\right)\right]}{\sum_{j=1}^{n_l}\left[E_j\left(y_j - y_{(j-1)}\right)\right]} \tag{2}$$

where: $\bar{y}$ = distance from bottom of beam to neutral axis
E_j = long span modulus of elasticity for *j*th zone
y_j = distance from bottom of beam to top of *j*th zone
$y_{(j-1)}$ = distance from bottom of beam to bottom of *j*th zone
n_l = total number of zones in beam

$$N_j = \left(y_j - \bar{y}\right) \tag{3}$$

$$N_{(j-1)} = \left(y_{(j-1)} - \bar{y}\right) \tag{4}$$

where: N_j = distance from neutral axis to upper edge of *j*th zone
$N_{(j-1)}$ = distance from neutral axis to lower edge of *j*th zone

2. The transformed moment of inertia for each zone about the neutral axis is calculated using Equation (5), and the moment of inertia of the transformed section is calculated using Equation (6).

$$I_j = b\left(\frac{E_j}{E_T}\right)\frac{\left(N_j^3 - N_{(j-1)}^3\right)}{3} \tag{5}$$

where: I_j = transformed moment of inertia of *j*th lam about neutral axis

E_T = modulus of elasticity of transformed section
b = un-transformed width of laminations

$$I_T = \sum_{j=1}^{n_j} I_j \tag{6}$$

where: I_T = transformed moment of inertia of the section

3. The moment of inertia of the un-transformed (gross) section is calculated using Equation (7).

$$I_g = \frac{bD^3}{12} \tag{7}$$

where: I_g = gross moment of inertia of the section
D = depth of the section

4. An I_K/I_G ratio is calculated for each zone using Equation (8).

$$\left(\frac{I_k}{I_g}\right)_j = \frac{\sum_{i=1}^{j}\left(x_i\left(\frac{E_i}{E_j}\right)(O_i)\right) + \sqrt{\sum_{i=1}^{j}\left(h_i^2\left(\frac{E_i}{E_j}\right)^2(P_i)\right)}}{2d_j^3} \tag{8}$$

where: x_j = the average knot size, expressed in decimal fraction of width, for the grade of lamination in the *j*th zone
h_j = the difference between the 99.5 percentile and average knot size, expressed in decimal fraction of the width, for the grade of lamination in the *j*th zone
d_j = the distance between the outermost edge of the *j*th zone and the neutral axis

5. The stress modification factor for knots, $SMF_{bx\ knots\ j}$, is calculated for each zone using Equation (9).

$$SMF_{bx\ knots\ j} = \left(1+3\left(\frac{I_k}{I_g}\right)_j\right)\left(1-\left(\frac{I_k}{I_g}\right)_j\right)^3\left(1-\left(\frac{I_k}{2I_g}\right)_j\right) \geq SR_{bx\ \min\ j} \tag{9}$$

6. The stress modification factor for slope of grain, $SMF_{bx\ SOG\ j}$, is determined for each zone based on tabulated data for slope of grain values from 1:4 to 1:20 given in Table 4 of D3737.

7. The stress modification factor for each zone is determined using Equation (10).

$$SMF_{bx\ j} = \min\left\{SMF_{bx\ knots\ j}, SMF_{bx\ SOG\ j}\right\} \tag{10}$$

8. The maximum stress permitted on each zone, $F_{max,\ j}$, is calculated using Equation (11).

$$F_{max,\ j} = K\left(BSI_j\right)\left(SMF_{bx\ j}\right) \tag{11}$$

where: $F_{max,\ j}$ = maximum stress allowed at outer edge of *j*th zone
BSI_j = bending strength index of laminations in *j*th zone
$SMF_{bx\ j}$ = strength ratio for bending = Min($SR_{bx\ knots}$, $SR_{bx\ SoG}$)
K = 1.4 for flexural compression
= 1.0 for flexural tension

9. The apparent outer fiber stress on the beam corresponding to $F_{max,\,j}$ for each zone is calculated using Equation (12).

$$\sigma_{apparent,j} = F_{\max,j}\left(\frac{D/2}{d_j}\right)\left(\frac{E_T}{E_j}\right)\left(\frac{I_T}{I_g}\right) \tag{12}$$

10. The allowable flexural design stress (F_{bx}) is determined using Equation (13).

$$F_{bx} = \min\left\{\sigma_{apparent,j}\right\}(TL) \tag{13}$$

where: TL = tension lamination factor
= 1.0 if tension laminations meeting the requirements of section 4.3 of D3737 are used
= 0.85 if tension laminations meeting the requirements of section 4.3 of D3737 are not used and d ≤ 15 in. (0.38 m)
= 0.75 if tension laminations meeting the requirements of section 4.3 of D3737 are not used and d > 15 in. (0.38 m)

11. The required strength ratio of the tension lamination (SR_{TL}) is calculated using Equation 14, and the tension lamination grading requirements of section 4.3 of D3737 are determined, if a tension lamination factor of 1.0 is used in Equation (13).

$$SR_{TL} = \frac{F_{bx}\left(\frac{2d_{TL}}{D}\right)\left(\frac{E_{TL}}{E_T}\right)\left(\frac{I_g}{I_T}\right)}{BSI_{TL}} \tag{14}$$

where: d_{TL} = the distance from neutral axis to the outer edge of the T.L.
E_{TL} = the long-span modulus of elasticity of the lumber in the outermost tension zone
BSI_{TL} = the bending stress index of the lumber in the outermost tension zone

Since this analysis is calculation intensive, APA has developed a computer software program designated as GAP (glulam allowable properties) and this is recognized in ICC Evaluation Service report ESR-1940 as an alternative to using the hand calculation procedures of D3737. By knowing the knot characteristics of X-bar and h, any combination of grades and species can be input into the computer model and the resulting design properties for that grade combination are generated. It is important to note that this calculation methodology, although dating back to the 1950's, has been verified by thousands of full-size beam tests conducted at APA, the USDA Forest Products Laboratory and various North American universities. While more sophisticated probabilistic models have been developed over the years at Texas A&M and Purdue Universities, they yield essentially the same results as D3737 and require much more complicated material property inputs and thus did not achieve widespread acceptance.

It is also important to note that countries exporting glulam into the U.S. must complete this analysis to develop their claimed design properties before the glulam can be accepted under the IBC or IRC codes.

3.3 Tension Laminations

As noted in steps 10 and 11 above, the term "tension lamination" has been introduced. The results of full-size beam tests reported in references [6] and [7] yielded an empirical relationship between the size of knots in the tension zone and bending strength that was adopted into D3737 in the early 1980's. This relationship dictates that special grading considerations be applied to the laminations used in the outer 10 % of the beam depth on the tension side. This tension side may exist on the top or bottom of the beam, or both, depending upon loading and support conditions. If horizontally laminated timbers are manufactured without applying these special tension lamination-grading considerations, the allowable bending stress shall be reduced by multiplying the calculated allowable stress by 0.85 if the beam depth is 15 in. (0.38 m) or less or by 0.75 if the beam depth exceeds 15 in. (0.38 m).

The special grading provisions for maximum permissible knot characteristics in tension laminations based on the SR_{TL} calculated in accordance with equation (14) depend on the location in the beam depth (i.e., the outer 5% of the beam depth and the next inner 5% of the depth), and the actual beam depth (i.e., 4 laminations to 12" (12.5 cm), 12" (12.5cm) to 15" (38cm) and greater than 15" (38 cm)).

3.4 Volume Factor

Traditionally, the design properties generated in accordance with D3737 for bending stress were further adjusted by a size factor, $C_F = (12/d)^{1/9}$, which is similar to the European requirements for establishing flexural design properties for a depth of 12 inches (30 cm) and adjusting them for other depths. However, research involving full-size beams with a large range in sizes conducted by the glulam industry in the late 1980's and reported in reference [8] led to the adoption of the volume effect factor, C_V, in D3737 in the early 1990's. This was also adopted by the U.S. codes and is referenced in the IBC and IRC codes as a required design adjustment factor for glulam.

This research demonstrated that the flexural strength of glulam beams is not only affected by the depth of the member but also by its width and length. Therefore, for horizontally laminated bending members, the bending stress determined in accordance with D3737 must be adjusted for sizes greater than the standard size beam (as defined below) by multiplying by the volume effect factor, C_V, defined as follows:

$$C_V = [\ 5.125/w\ ]^{1/x}\ [12/d\ ]^{1/x}\ [21/L\ ]^{1/x} \leq 1.0 \qquad (15)$$

where:

d = beam depth, in.
w = beam width, in.
L = length of beam between points of zero moment, ft.
x = exponent determined by procedures outlined in Annex A8 of D3737

The standard beam is assumed to be uniformly loaded and is defined as having a depth of 12 in. (30 cm), a width of 5-1/ 8 in. (13 cm) and a length of 21 ft (6.4 m). It is noted that for Western species in the U.S., the exponent "x" is 10 and for Southern pine the exponent is 20. For other species, including imported species, it is necessary for the certification agency and manufacturer to establish the exponent "x" to be able to publish flexural design properties in accordance with U.S. building codes.

4. ANSI A190.1

While D3737 focuses on the lumber properties as they influence design properties, it is acknowledged that an equally important consideration is the strength of the end joints, particularly in highly stressed tension zones of members. ANSI A190.1 requires that all end joints be qualified using a full-size tension test with a gauge length of 2 feet (60 cm). The requirement is that the 5% tolerance limit with 75% confidence shall exceed 1.67 times the Qualification Stress Level (QSL) using 2x6 lumber. For bending members the QSL is defined as the highest published tabular design value based on normal duration of loading and dry service conditions.

As an example, for a glulam bending member having a published bending stress of 2400 psi (16.5 MPa), the end joint qualification is 2400x1.67 = 4000 psi (27.6 MPa). For a member with a published design stress of 3000 psi (20.7 MPa), the requirement is 3000x1.67 = 5010 psi (34.5 MPa). Qualification tests are required for all combinations of species, adhesives and treatments used by any manufacturer. ANSI A190.1 also sets for the requirements for daily full-size tension tests to confirm the quality of the end joints.

The premise for the 1.67 factor is based on full-scale beam tests with the end joint strength being equivalent to the tension lamination quality. Thus, in a test of 100 beams, it is hypothesized that 50 would fail at an end joint and 50 would fail due to some lumber strength-reducing characteristic and this has been generally confirmed by the large magnitude of full-scale beam tests conducted in North America.

5. Performance Based Standard

As previously noted, a provision was added to ANSI A190.1-2002 to permit the development of characteristic values for grade combinations using performance testing as an alternate to the provisions of D3737. Similarly, Table 2 of D3737 provides bending stress index values based on full-size beam tests.

However, there is no published U.S. standard describing how to conduct full-scale glulam beam tests and how to analyze the resulting data. The values in Table 2 of D3737 are based on beams designed using these values and tested in accordance with ASTM Test Methods D 198 yielding bending strength values such that the lower fifth percentile will exceed the design bending stress by a factor of 2.1 with 75 % confidence. Analysis of test data assumed a lognormal distribution but there were no definitive sample preparation and sampling requirements.

To address this need, a Task Group of the ASTM Section Committee on Glulam, D07.02.02, has drafted a new standard, "Standard Practice for Establishing Characteristic Values for Flexural Properties of Structural Glued Laminated Timber by Full-Scale Testing". The scope of the standard is to develop procedures for full-scale testing of structural glued laminated timber to determine or verify characteristic values used to calculate flexural design properties. Guidelines are given for (1) testing individual structural glued laminated timber layups (with no modeling), (2) testing individual glulam combinations (with limited modeling), and for (3) validating models used to predict characteristic values. The sample size to be evaluated is based on which of these conditions are being evaluated.

This practice is limited to procedures for establishing characteristic flexural properties (MOR and MOE) although some of the principles for sampling and analysis presented may be applicable to other properties. The characteristic value is defined as a test statistic from which design values can be derived by the application of appropriate adjustment factors. For flexural strength properties of structural glued laminated timber, this characteristic value is typically a 5th percentile estimate with 75% confidence. For deformation-based properties, such as modulus of elasticity, this value is represented by the average value. This standard is currently being balloted by ASTM and is expected to be approved at the Fall 2007 meeting of D07.

6. Conclusions

With a large number of projects underway in ISO/TC165, Timber Structures, to develop ISO standards for glued laminated timber, it is important that countries involved in the process understand various national standards and how the provisions of those national standards need to be accommodated in the ISO process. This is also true when countries such as China and Taiwan move toward developing their own national standards for products such as glulam and must consider how other national standards have been developed. In virtually all cases some compromises are required by the various countries involved to be able to work towards harmonization of glulam standards through the ISO process while acknowledging national differences.

Acknowledgements: Special thanks go to Jeffrey Linville of the American Institute of Timber Construction who took the lead for the ASTM Glulam Section Committee on revising and simplifying Annex A4 of D3737 as presented in this paper. Also, for his efforts as Chairman of the Task Group of the Glulam Section Committee that developed the draft standard for performance-based testing of full-size beams referenced in this paper.

7. References

(1) American National Standards Institute. 2002. *American National Standard for Wood Products - Structural Glued Laminated Timber.* ANSI A190.1. New York, NY.

(2) ASTM International. 2006. *Standard Practice for Establishing Allowable Properties for Structural Glued Laminated Timber (Glulam).* ASTM D3737. West Conshohocken, PA.

(3) U.S. Department of Agriculture. 1935. Technical Bulletin 691, *The Glued Laminated Wooden Arch*, Madison, WI.

(4) Freas, A. D., and Selbo, M. R. 1954. *Fabrication and Design of Glued Laminated Wood Structural Members,* Technical Bulletin No. 1069, U.S. Department of Agriculture, Madison, WI (Available only from American Institute of Timber Construction).

(5) ASTM International. 2006. *Standard Practice for Establishing Clear Wood Strength Values.* ASTM D2555. West Conshohocken, PA.

(6) Moody, R. C. 1977. *Improved Utilization of Lumber in Glued Laminated Beams,* Research Paper FPL 292, U.S. Forest Products Laboratory, Madison, WI.

(7) Marx, C. M., and Moody, R. C. 1981. *Strength and Stiffness of Shallow Glued-Laminated Beams with Different Qualities of Tension Laminations*, Research Paper FPL 381, U.S. Forest Products Laboratory, Madison, WI

(8) Moody, R., Falk, R., and Williamson, T. 1990. *Strength of Glulam Beams-Volume Effects,* Proceedings of the 1990 International Timber Engineering Conference, 1:176–182, Tokyo, Japan

INTERNATIONAL COUNCIL FOR RESEARCH AND INNOVATION
IN BUILDING AND CONSTRUCTION

WORKING COMMISSION W18 - TIMBER STRUCTURES

CREEP AND CREEP-RUPTURE BEHAVIOUR OF STRUCTURAL COMPOSITE LUMBER EVALUATED IN ACCORDANCE WITH ASTM D 6815

Borjen Yeh

T G Williamson

APA – The Engineered Wood Association

U.S.A.

MEETING FORTY

BLED

SLOVENIA

AUGUST 2007

Presented by B.J. Yeh

A. Salenikovich asked whether the LVL were tested on edge or on flat. B.J. Yeh replied that edgewise loading was considered.

H. Blass questioned whether testing at laboratory condition where climate is not controlled would be an issue. B.J. Yeh replied that the moisture content of the specimen after testing was checked to be always less than 16%.

F. Lam commented that the Madison Curve represented clear wood behaviour not lumber. Also 3 months test may not be sufficient to develop full understanding of the material behaviour especially when dealing with a very uniform product such as OSL. Different from lumber, this type of product may pass the 90 days test but it is possible that many can still break suddenly soon after 90 days.

E. Karacabeyli agreed with F. Lam that 90 days may not be enough. Products that nearly pass the test should not be used. He said that loading at 55% of the 5th percentile stress level should not fail any specimen in 30 year. May be one should not expect failure.

B.J. Yeh replied Forintek data was used and the chosen stress level should see failure. The aim is to protect against the minimal performance.

E. Karacabeyli said that the 2.0 factor comes from lumber with average at approximately 1.6. Creep recovery should be considered in future changes.

A. Hanhijärvi stated that it has been shown that inside the wood moisture gradient can affect the strength. He asked about the type of conditioning with respect to short term and longer term test. These may have influence on composites. Also this can influence creep.

B.J. Yeh replied that the specimens were preconditioned at least 30 days prior to testing. After the 90 days test the product cannot deviate from short term moisture content by more than 2%. Products will be used in unconditioned indoors condition so we are trying to simulate this. Moisture cycle is difficult to perform.

A. Hanhijärvi stated that during erection the material may get wet.

B.J. Yeh replied that in Canada there is a requirement of 3 week soaking and then re-drying to address this issue but it may be too severe and not used in the U.S.

Creep and Creep-Rupture Behaviour of Structural Composite Lumber Evaluated in Accordance with ASTM D 6815

Borjen Yeh, Ph.D., P.E. and Thomas G. Williamson, P.E.
APA – The Engineered Wood Association, U.S.A.

Abstract

Structural composite lumber (SCL), as defined in accordance with ASTM D 5456, *Standard Specification for Evaluation of Structural Composite Lumber Products*, includes laminated veneer lumber (LVL), parallel strand lumber (PSL), laminated strand lumber (LSL), and oriented strand lumber (OSL). As there is no consensus-based national or international manufacturing standard for SCL, mechanical properties of SCL products manufactured in North America are proprietary and normally derived following ASTM D 5456. One of the qualification requirements for SCL is the evaluation of its creep and creep-rupture behaviour in accordance with the 90-day long-term bending tests specified in ASTM D 6815, *Standard Specification for Evaluation of Duration of Load and Creep Effects of Wood and Wood-Based Products*.

According to ASTM D 5456, the performance of SCL is affected by many factors, such as wood species, wood element size and shape, adhesive, and manufacturing parameters. As a result, SCL products produced by each individual manufacturer are required to be evaluated separately, regardless of the similarity in product characteristics with other manufacturers. This means each SCL manufacturer is required to evaluate the creep and creep-rupture behaviour of its products individually even though the components of the finished product is similar.

Since the publication of ASTM D 6815 in 2002, APA – The Engineered Wood Association has evaluated the creep and creep-rupture behaviour of many SCL products in accordance with this standard. Therefore, there is a wealth of information in this area. This paper studies the creep and creep-rupture behaviour of SCL products manufactured with a variety of wood species, and SCL types and grades. This information may be used by SCL manufacturers, third-party inspection agencies, regulatory bodies, and standard developers in determining generic creep and creep-rupture effects on SCL products.

1. Introduction

Structural composite lumber (SCL) is a generic term used to describe a family of engineered wood composites. By the definition of ASTM D 5456 [1], *Standard Specification for Evaluation of Structural Composite Lumber Products*, SCL consists of laminated veneer lumber (LVL), parallel strand lumber (PSL), laminated strand lumber (LSL), and oriented strand lumber (OSL). The difference between these SCL products lies mostly in the type and size of the substrates, and the manufacturing processes used to manufacture the finished products.

This SCL classification system by ASTM is a physical differentiation among the subgroups of SCL, but is not necessarily based on product performance. For example, the

difference between the relatively new wood composites of LSL and OSL is simply the strand dimension. The strands used in LSL and OSL are defined by the ASTM D07.02 Subcommittee on Lumber and Engineered Wood Products as having an average length of at least 150 times and 75 times, respectively, the least dimension (usually the strand thickness). This ASTM definition is by no means scientific, but reflects the practical limitations of commercially available products at the time of the standard development. While it is true that LSL typically has higher mechanical properties than OSL, some higher grades of OSL may have higher performance characteristics than the lower grades of LSL.

Just like wood I-joists, there are no national or international manufacturing standards in existence today for SCL. However, ASTM D 5456, which was originally published in 1993, has become the basis for product qualification and code recognition in both the US and Canada. In the last 14 years, ASTM D 5456 has evolved through numerous revisions. One of the most recent changes was the adoption of ASTM D 6815 [2], *Standard Specification for Evaluation of Duration of Load and Creep Effect of Wood and Wood-Based Products*, as a requirement for evaluating the long-term performance of SCL.

It is very important to recognize that ASTM D 6815 was not developed for evaluating the true load duration and creep effects on SCL products. Instead, the procedures prescribed in ASTM D 6815 are intended to demonstrate the engineering equivalence to the duration of load and creep effects of solid-sawn lumber when used in dry service conditions. The development of product-specific duration of load or creep factors, or the long-term product performance due to a combination of load duration and changing environmental conditions is considered beyond the scope of ASTM D 6815.

According to ASTM D 5456, the performance of SCL is affected by many factors, such as wood species, wood element size and shape, adhesive, and production parameters. As a result, SCL products produced by each individual manufacturer are required to be evaluated separately, regardless of the similarity in product characteristics with other manufacturers. This means each SCL manufacturer is required to evaluate the creep and creep-rupture behaviour of its products individually even though the components of the finished product is similar.

Since the publication of ASTM D 6815 in 2002, APA – The Engineered Wood Association has evaluated the creep and creep-rupture behaviour of many SCL products as part of the ASTM D 5456 product qualification requirements. Therefore, there is a wealth of information in this area. This paper studies the creep and creep-rupture behaviour of SCL products manufactured with a variety of wood species, and SCL types and grades. This information may be used by SCL manufacturers, third-party inspection agencies, regulatory bodies, and standard developers in determining generic creep and creep-rupture effects on SCL products.

2. Materials and Test Methods

2.1 Products Description

For the purpose of this study, LVL products made with Douglas fir, Southern pine, Spruce, Maritime pine, Eucalyptus, or a mixture of these species, and LSL and OSL products made with Aspen or mixed Aspen and Poplar were conducted. These products were manufactured using a variety of manufacturing equipment and press parameters. All LVL products were manufactured with phenolic adhesives meeting the requirements of ASTM

D 2559 [3], *Standard Specification for Adhesives for Structural Laminated Wood Products for Use Under Exterior (Wet Use) Exposure Conditions*. The LSL and OSL products were made with an MDI binder system. APA does not have data on PSL, which is only produced by one manufacturer in North America. Table 1 describes the materials reported in this study.

Table 1. Product description

Test Series	Product Type	Species	Grade E [(a)]		Adhesive
			MPa	10^6 psi	
A	LVL	Maritime pine	18620	2.7	Phenolic
B	LVL	Eucalyptus/So. Pine (55:45)	17240	2.5	Phenolic
C	LVL	Spruce/D. fir (50:50)	15860	2.3	Phenolic
D	LVL	Douglas fir	15170	2.2	Phenolic
E	LVL	Southern pine	13790	2.0	Phenolic
F	LSL	Aspen	11030	1.6	MDI
G	OSL	Aspen/Poplar	10340	1.5	MDI

[(a)] Mean value from short-term bending tests using matched specimens

2.2 Test Methods

To evaluate the long-term performance of SCL products, ASTM D 6815 requires the applied load for the long-term (90-day) specimens to be based on 55% of the 5th percentile parametric point estimate of the short-term bending load using matched specimens. This load level was selected based on the review of long-term performance of solid-sawn lumber. It should be noted that the choice of the 5th percentile parametric point estimate, as opposed to the 5th percentile with 75% confidence that is commonly used for the design value derivation, was meant to be conservative because the point estimate gives a higher value (i.e., higher applied load on the long-term specimens) than the characteristic value with 75% confidence. Also, it is noted that the applied load for the long-term specimens was based on the ultimate load (i.e., the moment capacity of the specimens), instead of the bending stress, of the short-term specimens. This may be critical to specimens that would experience significant dimensional changes (e.g., thickness swell) due to fluctuations in surrounding environments.

The short-term specimens were tested edgewise in a universal testing machine using the third-point loading method, as shown in Figure 1, with an on-centre span of 1143 mm (45 inches) or 1372 mm (54 inches). The specimen depth was mostly 63.5 mm (2-1/2 inches), resulting in a span-to-depth ratio ranging from 18:1 to 27:1. The higher span-to-depth ratio (i.e., 27:1) helped to reduce the dead weight required for creep tests, but is still in compliance with ASTM D 6815. The load rate for the short-term tests was set to fail the specimen in approximately 1 minute. All specimens were preconditioned at the indoor laboratory conditions for at least 30 days prior to the long-term tests.

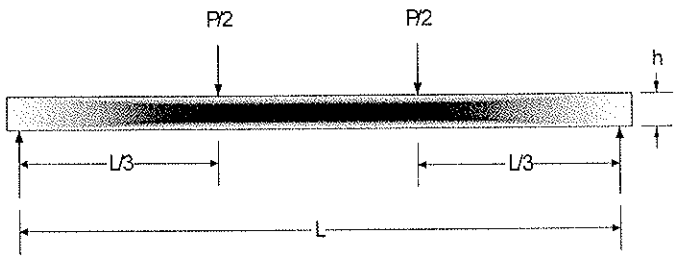

Figure 1. Bending test configuration (L/h = 18 to 27)

Long-term bending tests were performed on the specimens that were side-matched with the short-term specimens from the same production billets using a test frame designed and fabricated by APA staff. The test span and loading configuration were identical to the short-term specimens. Figures 2 and 3 are simplified schematic diagrams of the creep test frame. The dead load was independently applied to each individual specimen through a third-point loading harness. An adjustable weight was attached to a lever to magnify the load to achieve the desired dead load. Deflection was measured with a linear potentiometer mounted on a tripod placed on the top of the specimens. Deflection was continuously measured with a computerized data acquisition system.

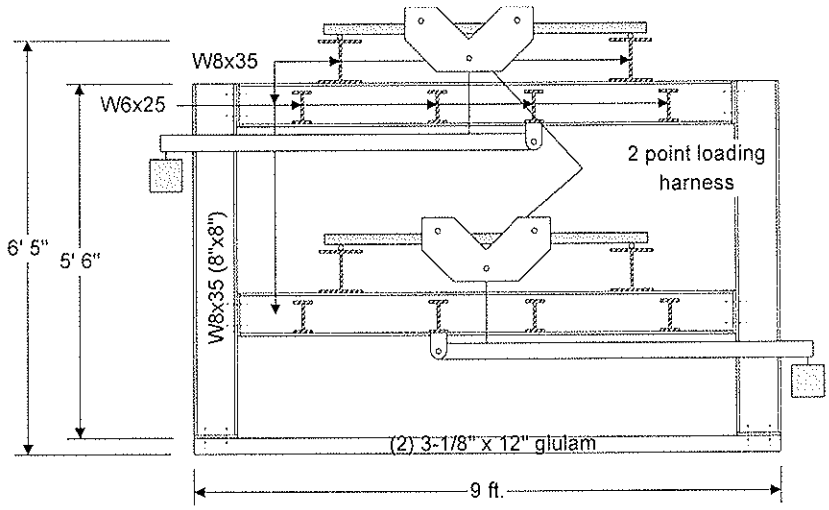

Figure 2. Schematic diagram of long-term bending frame in end elevation (1 inch = 25.4 mm; 1 foot = 305 mm)

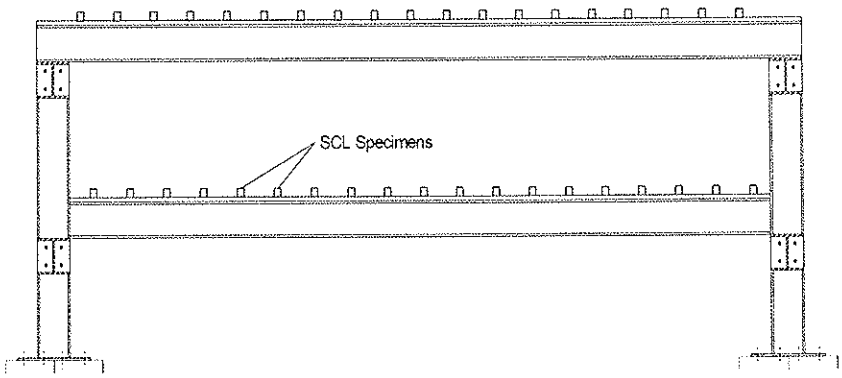

Figure 3. Schematic diagram of long-term bending frame in side elevation

The dead load was individually adjusted until the desired load was achieved on each specimen. Each weight was checked by measuring the applied load through a load cell located on the reaction of each individual specimen. Once all of the weights were adjusted, the weights were fixed to the levers and load was applied to the specimens over a 1-minute time period. All long-term tests were conducted in uncontrolled indoor laboratory conditions, which had a fluctuation of temperature between 18 and 27°C (65 to 75°F) and relative humidity between 50 to 70%. A data logger was used to measure the

environmental conditions of the area where the creep tests were conducted throughout the entire long-term test period.

Each test series is required by ASTM D 6815 to contain a minimum of 28 specimens for side-matched short-term and long-term tests (58 specimens total). However, the test results reported below are based on 28 to 32 long-term specimens. The additional specimens beyond the minimum were intended to provide a safety net in case there was a malfunction of any individual linear potentiometers during the long-term test period. Table 2 shows the specimen dimensions and test details.

Table 2. Specimen dimensions and test details

Test Series	Product	No. of Spc.	Width, b (mm)	Depth, h (mm)	Applied Load, P (kN)	Span, L (mm)	L/h	Estimated Initial Strain (mm/mm)
A	2.7E LVL	30	38.1	63.5	5.4	1372	21.6	0.0026
B	2.5E LVL	30	44.5	63.5	6.5	1143	18.0	0.0024
C	2.3E LVL	31	44.5	63.5	5.3	1372	21.6	0.0026
D	2.2E LVL	31	44.5	63.5	5.3	1372	21.6	0.0027
E	2.0E LVL	32	44.5	50.8	2.7	1372	27.0	0.0024
F	1.6E LSL	31	38.1	63.5	3.4	1143	18.0	0.0023
G	1.5E OSL	28	44.5	63.5	3.7	1143	18.0	0.0023

Assuming the bending strain at the extreme fibre of the specimen remains elastic on the application of load (55% of the 5th percentile point estimate), Table 2 also shows the estimated initial bending strain at the extreme fibre, as calculated using elastic engineering mechanics. It is interesting to note that the estimated initial bending strains for all 7 products were in the range of 0.2 to 0.3%.

3. Results and Discussions

Figures 4 through 10, as provided in the end of this paper, show the creep deflections of the LVL, LSL, and OSL products throughout the test duration. As noted from these figures, these products follow a similar trend as solid-sawn lumber under long-term loading. ASTM D 6815 prescribes the following 3 acceptance criteria for a product to demonstrate the engineering equivalence to the duration of load and creep effects on solid-sawn lumber:

1. No specimen shall be allowed to fail if the minimum sample size is 28,
2. Fractional deflection at the 90th day for each individual specimen shall not be greater than 2, and
3. All specimens shall show a decreasing creep rate over the 90-day test period.

None of the specimens failed in any of the 7 products reported in this study, which satisfied the first criterion.

3.1 Initial Deflection

ASTM D 6815 defines the initial deflection as the deflection that is measured 1 minute after the application of load. Table 3 compares the calculated deflection based on an elastic beam equation and the measured deflection at 1 minute after the application of load for Series A, B, F, and G (the calculated deflection data for Series C, D, and E are not

available because the modulus of elasticity of the long-term specimens, which is not required by ASTM D 6815, was not tested). Results shown in Table 3 suggest that the measured initial deflection per ASTM D 6815 is in good agreement with the calculated elastic deflection.

Table 3. Comparison of calculated and measured initial deflections

Test Series	Product	Mean Calculated Deflection [a] (mm)	Measured Initial Deflection [b]		Ratio [c]
			Mean (mm)	COV	
A	2.7E LVL	15.9	16.5	0.030	1.04
B	2.5E LVL	12.3	11.6	0.051	0.94
F	1.6E LSL	9.7	9.8	0.054	1.01
G	1.5E OSL	9.9	9.5	0.050	0.95

[a] Calculated based on the dimensions and MOE of each specimen for long-term loading
[b] Measured at 1 minute after the application of load
[c] The mean measured initial deflection divided by the mean calculated deflection

3.2 Fractional Deflection

Fractional deflection is defined by ASTM D 6815 as the ratio of the deflection at a test duration and the initial deflection measured 1 minute after the application of load. In the US timber design code, *National Design Specification for Wood Construction* (NDS) [4], the time-dependent deflection (creep) factor is limited to no greater than 1.5 and 2.0 times the elastic deflection due to long-term loading in dry and wet service conditions, respectively. Due to the relative high dead load specified in the standard, ASTM D 6815 prescribes the fractional deflection of each individual specimen (not the average of all specimens in a test series) to be no greater than 2.0 at a 90-day test duration. Table 4 shows the fractional deflection at the 90-day test duration for all 7 products evaluated in this study. As shown, the maximum fractional deflection for these products at the 90-day test duration was 1.38, which is lower than 1.5.

Table 4. Factional deflection at the 90-day test duration

Test Series	Product	Fractional deflection at the 90-day test duration			
		Maximum	Mean	Minimum	COV
A	2.7E LVL	1.31	1.23	1.18	0.024
B	2.5E LVL	1.21	1.19	1.16	0.013
C	2.3E LVL	1.20	1.16	1.13	0.015
D	2.2E LVL	1.20	1.15	1.11	0.020
E	2.0E LVL	1.32	1.26	1.21	0.023
F	1.6E LSL	1.31	1.26	1.23	0.013
G	1.5E OSL	1.38	1.34	1.32	0.013

3.3 Diminishing Creep Rate

It is obvious that the purpose of specifying the diminishing creep rate in ASTM D 6815 is to avoid the acceptance of a product from the tertiary creep. A typical evaluation of diminishing creep rate is to divide the test duration into 3 thirty-day periods and show that the creep deflection at the second period (30 to 60 days) is less than the first period (0 to 30 days), and the third period (60 to 90 days) is less than the second period. While this is simple, there are cases when the creep deflections in the second and third periods are both very small and therefore, it is not unusual that this criterion is violated due to the temperature and relative humidity fluctuations in the uncontrolled test environment, as

previously mentioned. In such cases, ASTM D 6815 permits the test duration to be extended for additional 30 days (total 120 days).

Among all 7 products evaluated in this study, all specimens meet the diminishing creep rate requirements except for the 2.7E LVL (Test Series A), which had a maximum creep deflection of 0.50 mm (0.020 inch) during the second period and 0.58 mm (0.023 inch) during the third period due to a significant relative humidity fluctuation in the third period. As a result, the test series was extended to 120 days and the fourth period (90 to 120 days) had a maximum creep deflection of 0.33 mm (0.013 inch), which satisfied the requirement of ASTM D 6815.

3.4 Residual Bending Strength and Modulus of Elasticity

While ASTM D 6815 does not require the residual bending strength and modulus of elasticity of each specimen be measured at the end of the long-term testing, some selected products were tested to destruction after the 90-day (120-day for the 2.7E LVL) loading using the same test setup as the matched short-term specimens. This information is helpful for the evaluation of the strength and stiffness degradation, if any, due to the long-term loading. Table 5 shows the residual MOR and MOE ratios of the 2.7E LVL, 1.6E LSL, and 1.5E OSL.

Table 5. Ratios of the mean bending strength and modulus of elasticity between the long-term and matched short-term specimens

Test Series	Product	Ratio of the Mean Residual Properties [a]	
		MOR	MOE
A	2.7E LVL	0.99	0.99
F	1.6E LSL	0.96	0.99
G	1.5E OSL	1.06	1.03

[a] The ratio between the long-tern specimens after the test duration and matched short-term specimens

In reviewing the data provided in Table 5, it should be recognized that the comparison was based on matched specimens, but not exactly the same specimens (the same specimen could not be tested to destruction twice), and therefore, the between-specimen variations should be considered. Besides, the moisture conditions were apparently not the same in the 90-day test period. With these considerations in mind, it seems reasonable to conclude that there was a negligible long-term loading effect on the bending properties of the SCL products reported in this study.

4. Conclusion

Based on the evaluation of creep and creep rupture behaviour of 7 SCL products that covered a wide range of elastic properties, product types (LVL, LSL, and OSL), and manufacturing parameters in accordance with the procedures of ASTM D 6815, it is reasonable to conclude that the SCL products, if properly manufactured, have demonstrated the engineering equivalence to the duration of load and creep effects of solid-sawn lumber when used in dry service conditions. There is strong evidence that the LVL products (5 out of 7 products evaluated in this study) manufactured with today's technology have a similar creep and creep rupture behaviour as solid-sawn lumber. In fact, there has not been a single instance, as far as APA is aware, when an LVL product failed to meet ASTM D 6815 requirements in the last 10 years. Therefore, an opportunity exists for standardizing the creep and creep rupture factors for LVL products without the expensive

and time-consuming long-term tests, provided that the LVL product is manufactured with an adhesive, wood species, and manufacturing parameters typical of those evaluated.

On the other hand, the newer generation of SCL products, such as LSL and OSL, tends to be more innovative than LVL in the use of adhesive binder systems, wood species, strand geometry, and other manufacturing parameters. Therefore, more long-term test data are needed for LSL and OSL to gain the same confidence as the LVL products on their creep and creep rupture behaviour.

At this point, ASTM D 6815 is a go-no-go standard that does not provide an alternative if a SCL product fails to meet the prescribed acceptance criteria. This may pose a challenge for the market access of newer products. In recognizing this need, the ASTM D07 Committee on Wood, which has jurisdiction over the ASTM D 5456 and D 6815 standards, has initiated the dialogue among its key members for the development of a standard that would allow the establishment of unique creep and creep rupture factors for the new generation of structural composite lumber in the future.

5. References

1. ASTM International. 2006. *Standard Specification for Evaluation of Structural Composite Lumber Products.* ASTM D5456-06. West Conshohocken, PA.

2. ASTM International. 2006. *Standard Specification for Evaluation of Duration of Load and Creep Effects of Wood and Wood-Based Products.* ASTM D6815-02a. West Conshohocken, PA.

3. ASTM International. 2006. *Standard Specification for Adhesives for Structural Laminated Wood Products for Use Under Exterior (Wet Use) Exposure Conditions.* ASTM D2559-04. West Conshohocken, PA.

4. American Forest & Paper Association. 2005. *National Design Specification for Wood Construction.* Washington, D.C.

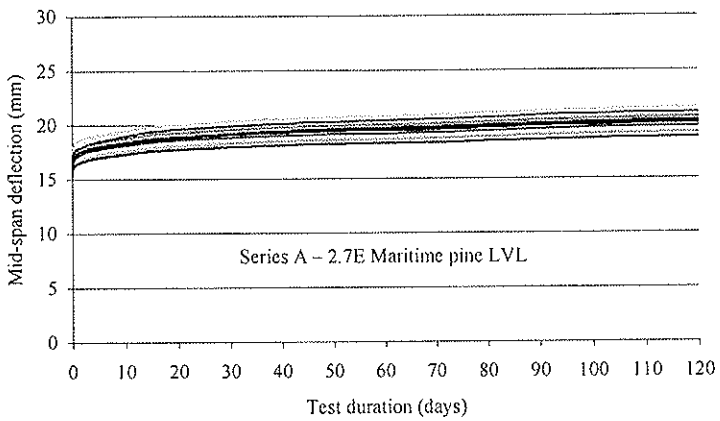

Figure 4. Series A – 2.7E Maritime pine LVL

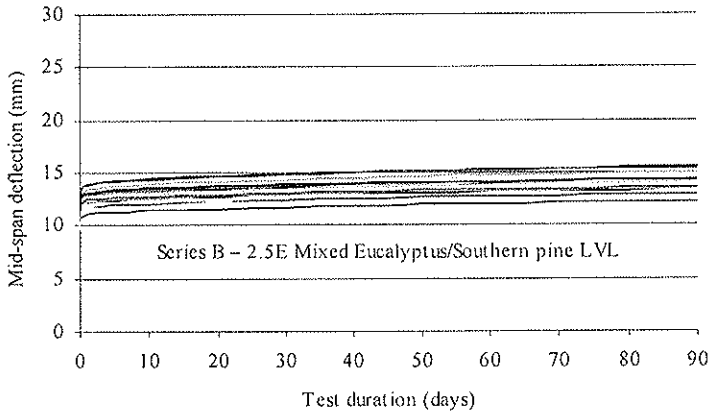

Figure 5. Series B – 2.5E Mixed Eucalyptus/Southern pine LVL

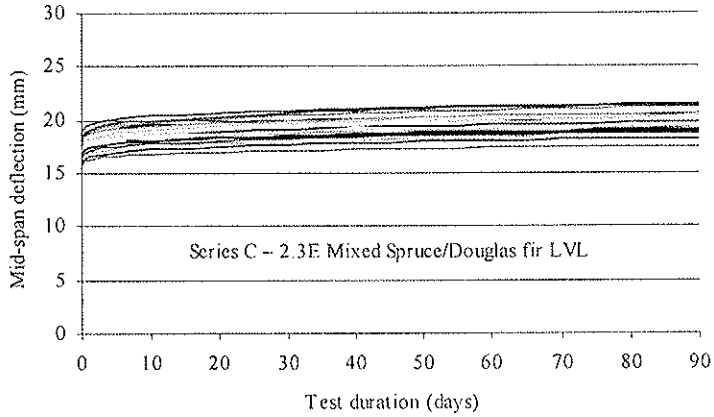

Figure 6. Series C – 2.3E Mixed Spruce/Douglas fir LVL

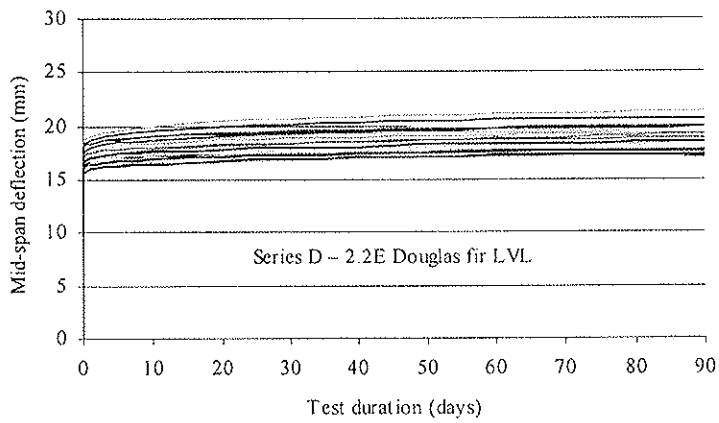

Figure 7. Series D – 2.2E Douglas fir LVL

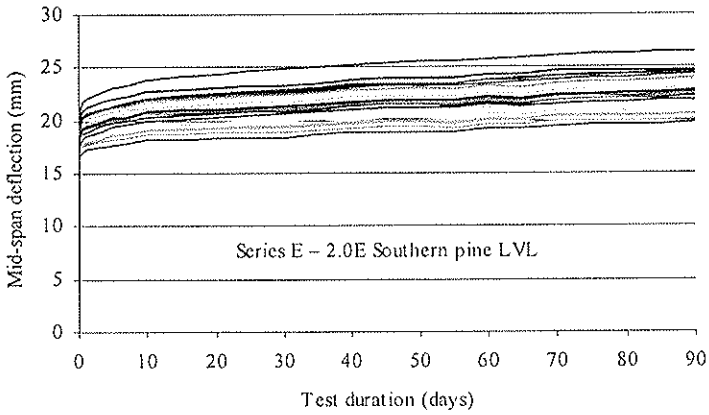

Figure 8. Series E – 2.0E Southern pine LVL

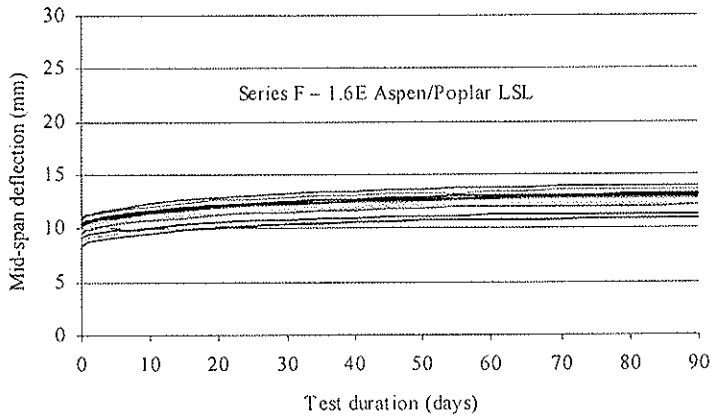

Figure 9. Series F – 1.6E Aspen LSL

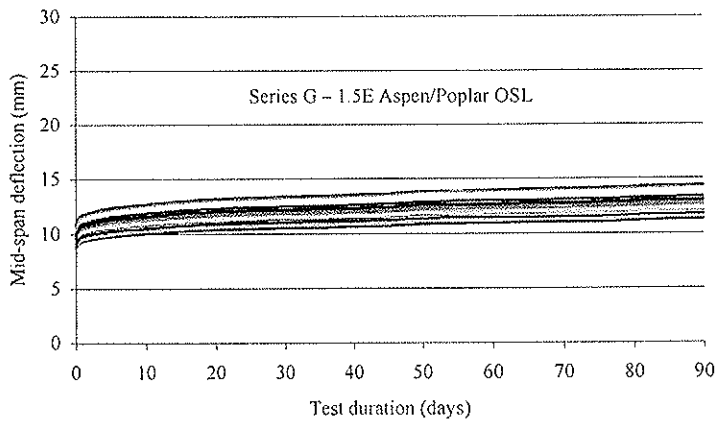

Figure 10. Series G – 1.5E Aspen/Poplar OSL

INTERNATIONAL COUNCIL FOR RESEARCH AND INNOVATION
IN BUILDING AND CONSTRUCTION

WORKING COMMISSION W18 - TIMBER STRUCTURES

BENDING STRENGTH OF COMBINED BEECH-SPRUCE GLULAM

M Frese

H J Blaß

Universität Karlsruhe

GERMANY

MEETING FORTY

BLED

SLOVENIA

AUGUST 2007

Presented by M. Frese

R. Brandner received clarification about the finger joint and the characteristic of the spruce beam as the outer laminations are the most important for bending strength.

A. Frangi asked whether it is possible to substitute with low quality material such as wind damaged wood. M. Frese stated that since the tensile strength of the low quality material is unknown may be it can be used in the middle 20% and check their shear strength. R. Steiger stated that testing of the wind damage material showed that the MOE was not affected but the strength goes down. This work was presented last year in Florence (CIB38-5-1 by Arnold and Steiger). For example for C20 and C40 bending strength is okay but tension strength drops down significantly. One should be careful with structural use of this material.

Bending strength of combined beech-spruce glulam

M. Frese, H.J. Blaß
Lehrstuhl für Ingenieurholzbau und Baukonstruktionen
Universität Karlsruhe, Germany

Abstract

This paper is the third part of an easily understandable series dealing with the bending strength of beech glulam published in CIB-W18 since 2005. It describes how to handle combined beech-spruce glulam with bottom and top lamellae of beech and middle lamellae of spruce.
The main topics of the paper are particularly stress distribution in the cross section, characteristic bending strength, MOE, beam lay-up and demands on both the strength grading of the lamellae and the characteristic finger joint bending strength.
In comparison with combined beech glulam it is to be expected that substituting middle spruce lamellae for beech decreases the cost of materials due to the higher price of beech. But the lower MOE of spruce compared to beech has to be considered causing an increase in tensile or compression edge stress, respectively, if the cross section is to be subjected to the same bending moment as a combined beech glulam beam. The use of the calculation model for the characteristic bending strength which is originally related to combined beech glulam does, therefore, necessitate some further considerations to define strength classes for combined beech-spruce glulam.

1 Introduction and reflection

The calculation model (1) for the characteristic beech glulam bending strength was introduced in the first paper of 2005 [1]. It should be pronounced that the model was exclusively developed on the basis of combined beech glulam and is, therefore, particularly suitable to predict the characteristic bending strength of combined beech glulam. Hence the effect of discontinuous stress distribution in the cross section is covered by the model. That means for instance if a combined GL48 glulam is theoretically used up to the characteristic bending strength of 48 N/mm² the effective tensile or compression edge stress is higher than 48 N/mm². And in the glue line between the various strength graded lamellae one ideally expects a discontinuation in the stress distribution. In contrast to this it would be possible to marginally increase the characteristic bending strength in case of homogeneous glulam.

$$f_{m,g,k} = -2,87 + 0,844 \cdot f_{m,j,k} - 0,0103 \cdot f_{m,j,k}^2 \\ -0,192 \cdot f_{t,\ell,k} - 0,0119 \cdot f_{t,\ell,k}^2 + 0,0237 \cdot f_{m,j,k} \cdot f_{t,\ell,k} \quad (1)$$

Fig. 1 and Fig. 2 are to more accurately explain this background. In general for design one assumes a homogeneous cross section and takes care that the stress (σ) is lower than the

strength. Unlike this, in the assumed more realistic mechanical model a totally different stress distribution is present. For that Fig. 2 shows the influence of a variable portion β_1 on the increase factor μ_1 and makes possible to calculate the effective edge stress ($\mu_1 \cdot \sigma$) of a cross section related to combined beech glulam. In Fig. 2 six different strength classes are considered which correspond in part to various $E_{1,beech}/E_{2,beech}$ ratios. Concerning the strength classes GL28 to GL48 the portion β_1 was fixed at 2/3 (compare [1]). Hence, the corresponding increase factor μ_1 in Table 1 has to be taken into account to determine the effective edge stress in case of these strength classes.
From all this one can conclude that in general both the E_1/E_2 ratio and the portion β affect the effective edge stress and, therefore, the characteristic bending strength in case of lay-ups differing from those which are related to the strength classes GL28 to GL48.

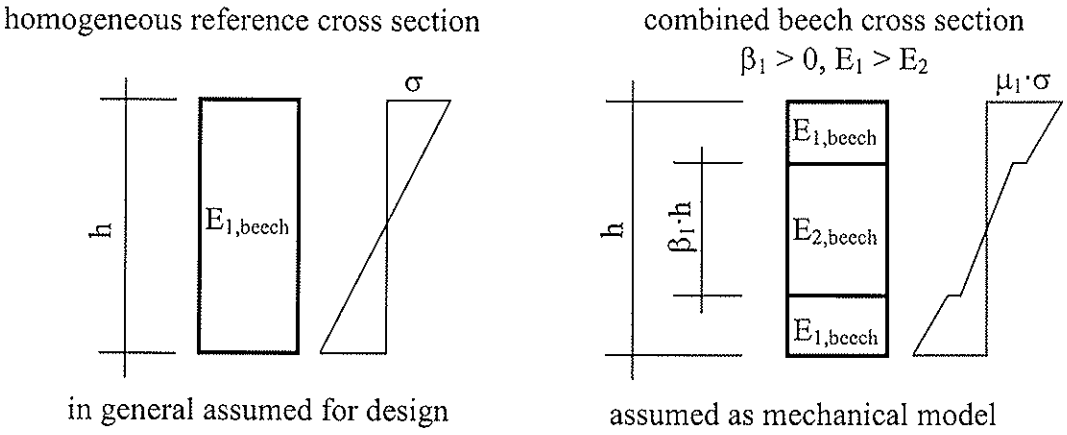

Fig. 1 Denotation for the homogeneous reference cross section and the combined beech cross section

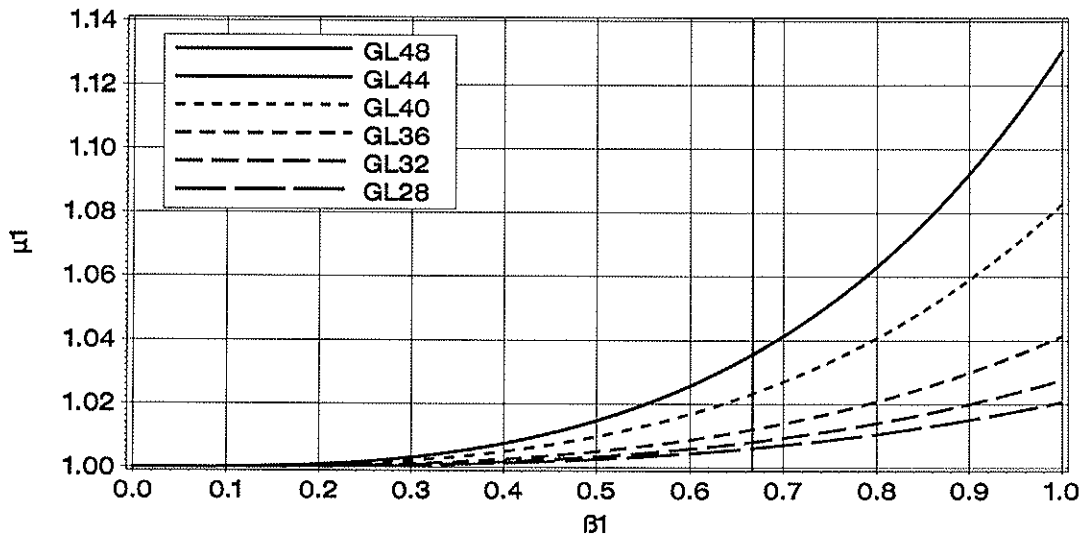

Fig. 2 Increase factor μ_1 depending on the portion β_1 related to a combined beech cross section (Fig. 1 right) in comparison with the homogeneous reference cross section (Fig. 1 left); vertical reference line at $\beta_1 = 2/3$

Table 1 $E_{1,beech}/E_{2,beech}$ ratios, increase factor μ_1 ($\beta_1 = 2/3$) and effective edge stress of the combined beech cross section

	GL28	GL32	GL36	GL40	GL44	GL48
$E_{1,beech}/E_{2,beech}$	1,021	1,028	1,041	1,083	1,13	1,13
μ_1 ($\beta_1 = 2/3$)[1]	1,006	1,008	1,011	1,023	1,036	1,036
eff. edge stress in N/mm²	28,2	32,3	36,4	40,9	45,6	49,7
[1] covered by the calculation model (1)!						

2 Considerations related to combined beech-spruce glulam

The step in this section is to substitute beech by spruce in the middle cross section. Therefore, on the basis of the conclusion above both the increase in edge stress and the corresponding unknown portion β_2 are to be determined. More about the approach and further details are published in the research report [3].

First new $E_{1,beech}/E_{2,spruce}$ ratios have to be taken into account. For that those ratios are listed in Table 2 which considers the lower MOE of spruce compared to beech in the middle of the cross section. The spruce corresponds to the visual grade S10 according to DIN 4074-1. In EN 1912 S10 is assigned to strength class C24. In order to determine the unknown portion β_2 Fig. 3 and Fig. 4 clearly show what happens when beech is substituted by spruce. The curves in Fig. 4 represent the increase factor μ_2 for the edge stress depending on a variable portion β_2. With that it is easy to determine an appropriate lay-up for beech-spruce glulam in consideration of the following aspects:

- On the one hand it is economic to have a large portion β_2 but on the other hand the increase in edge stress should be as small as possible to keep the characteristic bending strength level of the cross section originally related to the combined beam.
- Apart from this the characteristic bending strength of spruce glulam GL24 has to be considered too.

The reasons listed below validate the decision to fix the portion β_2 at 3/5:

- The increase μ_2 (third row in Table 2) does not exceed 1,03. Consequently one expects a decrease in characteristic bending strength of less than 3%. Hence it is possible to retain the strength classes GL28 to GL48 by laying down marginally higher demands on the characteristic finger joint bending strength (= $f_{m,j,k}$) . This is possible because the characteristic finger joint bending strength is one of the two variables in the calculation model (1). A suitable higher value can, therefore, be easily calculated. In addition the technical conditions make possible to produce finger joints with an appropriate strength. This was confirmed in the second paper of 2006 [2].
- With regard to the characteristic bending strength of spruce glulam GL24 the effective bending stress near the glue line must not exceed 24 N/mm². This condition is fulfilled when β_2 is 3/5. For that the stress distributions in Fig. 5 represent the effective stress if the characteristic bending strength in the homogeneous reference cross section is present. The selection of stress distributions shows that it is GL48 where the strength of spruce is nearly totally exploited.

Table 2 $E_{1,beech}/E_{2,spruce}$ ratios, increase factor μ_2 ($\beta_2 = 3/5$) and effective edge stress of the beech-spruce cross section

	GL28	GL32	GL36	GL40	GL44	GL48
$E_{1,beech}/E_{2,spruce}$	1,17	1,18	1,19	1,24	1,30	1,30
μ_2 ($\beta_2 = 3/5$)[1]	1,026	1,026	1,024	1,020	1,016	1,016
eff. edge stress in N/mm²	28,9	33,1	37,3	41,8	46,3	50,5
[1] the further increase in edge stress in consequence of μ_2 is not covered by the calculation model (1)!						

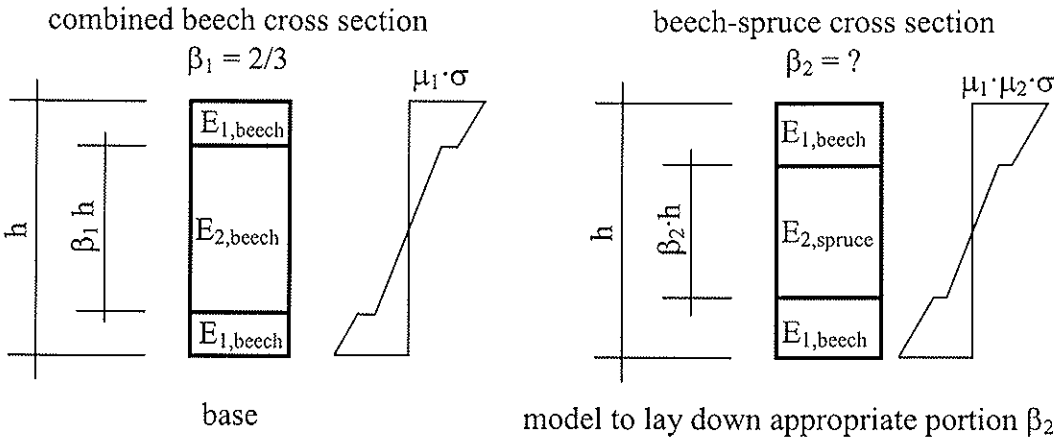

Fig. 3 Denotation for combined beech cross section and beech-spruce cross section

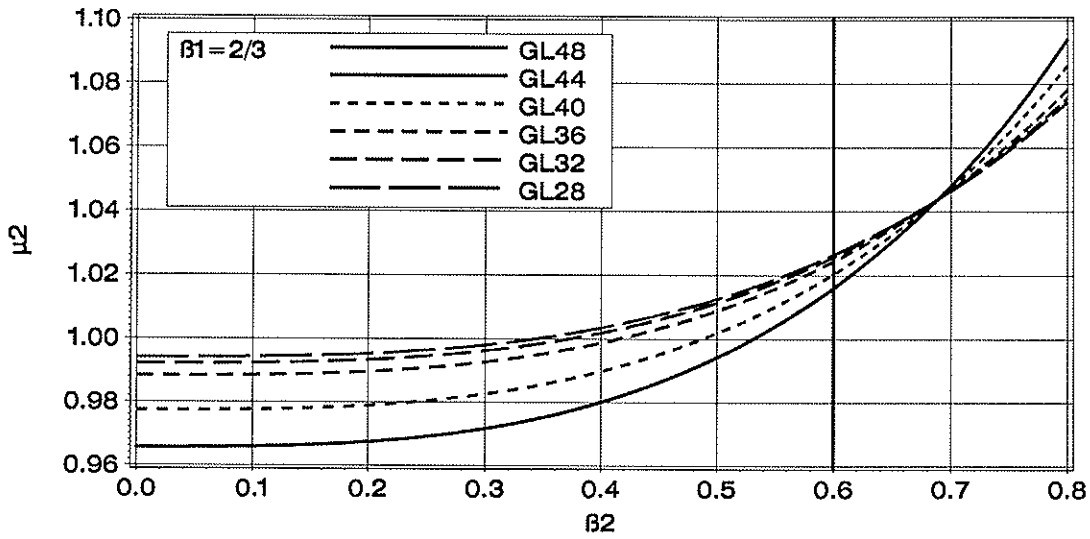

Fig. 4 Increase factor μ_2 depending on the portion β_2 related to a beech-spruce cross section (Fig. 3 right) in comparison with the combined beech cross section (Fig. 3 left); vertical reference line at $\beta_2 = 3/5$

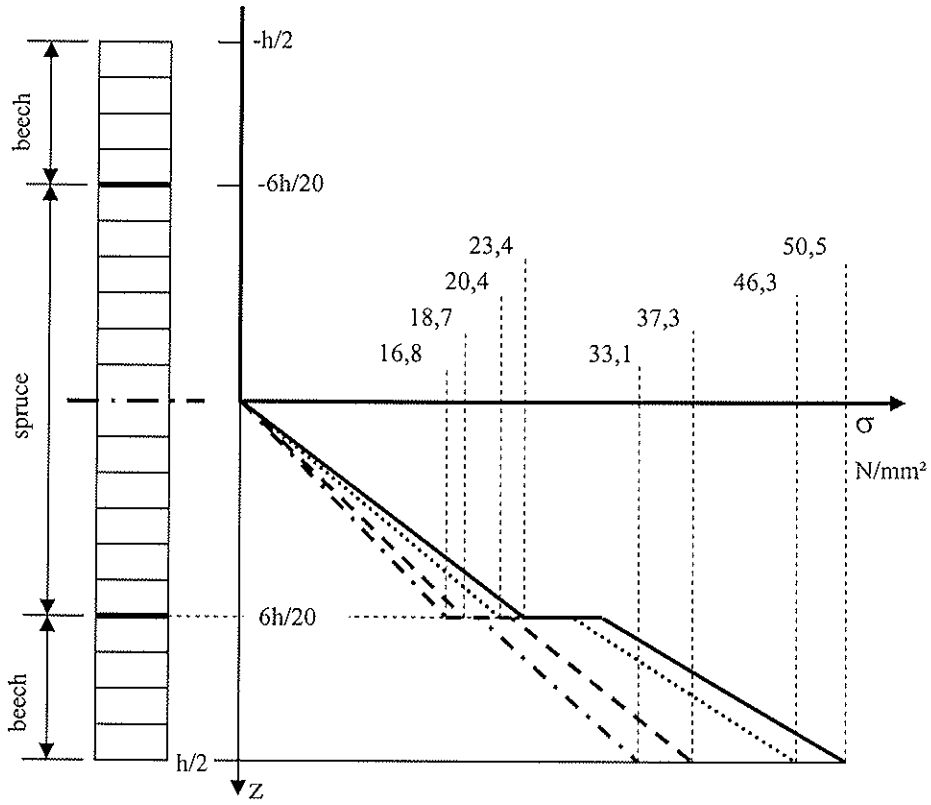

Fig. 5 Stress distribution in the cross sections related to beech-spruce glulam; selection of the strength classes GL32, GL36, GL44 und GL48

3 Comparative tests on combined beech-spruce glulam

12 bending tests on beech-spruce glulam beams were conducted in order to approximately prove the theoretical reflections above. For the following comparisons it is necessary to repeat the results of the 24 combined beech glulam beams which were already published in the paper of 2005 [1]. Fig. 6 should help to form a picture of the beech-spruce test beams versus the combined. The strength classes as well as details about the beam lay-up are presented in Table 3. Details about the test set-up of the beech-spruce beams are shown in Fig. 7. Apart from some marginal differences the beams are well comparable to each other in order to study the influence of substituting spruce (S10) for beech (grades 3 or 2) in the middle of the test beams indicated by a white area in Fig. 7.

The bending tests were conducted according to EN 408. The results can be found in Table 4 and Fig. 8. In the latter beech-spruce beams are represented by circle shaped and combined beech beams by star shaped symbols.

As expected, the exchange of beech by spruce has an insignificant influence on the mean bending strength. And this confirms the reflections in section 2 which showed a decrease in bending strength of less than 3%. Due to the lower MOE of spruce a more pronounced influence on the test beam's MOE can be in part observed.

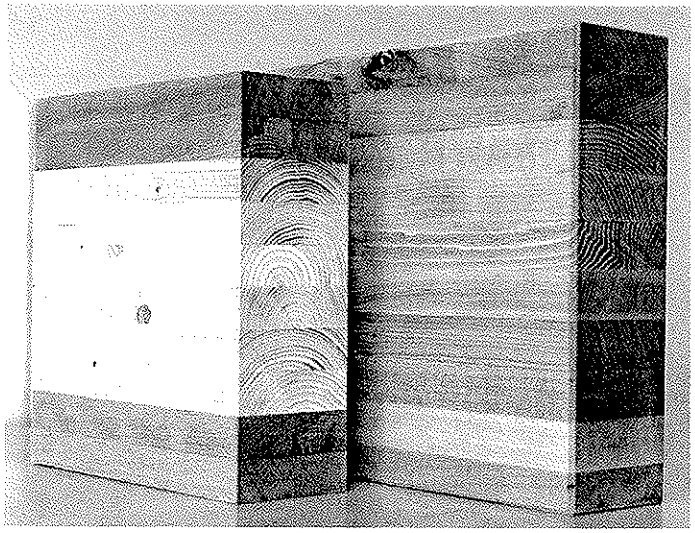

Fig. 6 On the left a section of a beech-spruce beam and on the right a section of a combined beech beam

Table 3 Strength class and beam lay-up of the beech-spruce as well as combined beams

strength class	grade of beech according to [1] and of spruce according to DIN 4074-1		span mm	height mm
	outer zone	middle zone		
very high, beech-spruce	5	spruce S10	5400	302
high, beech-spruce	4	spruce S10		302
very high, combined	5	3		340
high, combined	4	2		340

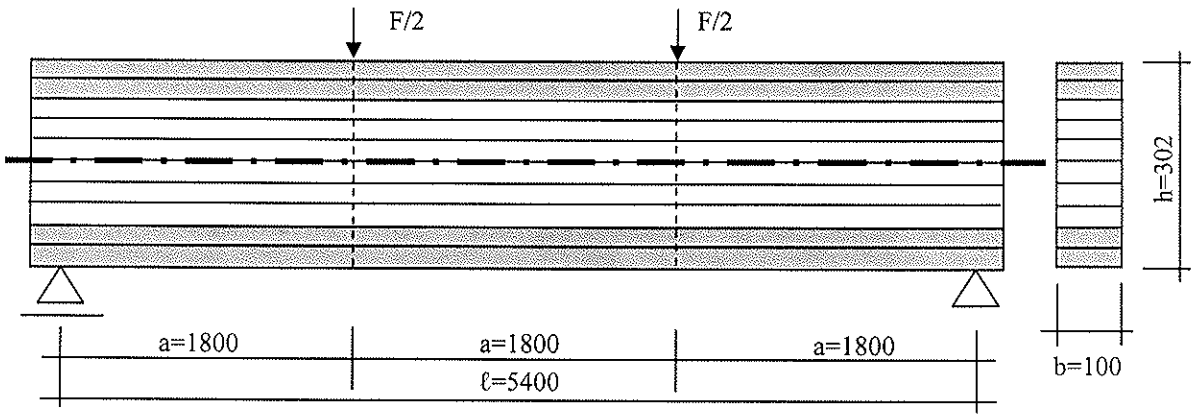

Fig. 7 Test set-up for the beech-spruce beams, 2 x 2 beech lamellae in grey and 6 spruce lamellae in white

Table 4 Bending strength and MOE statistics of the beech-spruce and combined beech test beams

	beech-spruce		combined	
	high	very high	high	very high
bending strength in N/mm²				
n	6	5[1]	12	11[1]
x	57,3	57,5	57,8	63,7
s	6	9,19	9,32	7,51
MOE in N/mm²				
n	6	6	12	12
x	14200	14400	14400	15500
s	700	735	383	490

[1] due to a poor manufactured finger joint in the outermost lamella one value is disregarded in the statistics

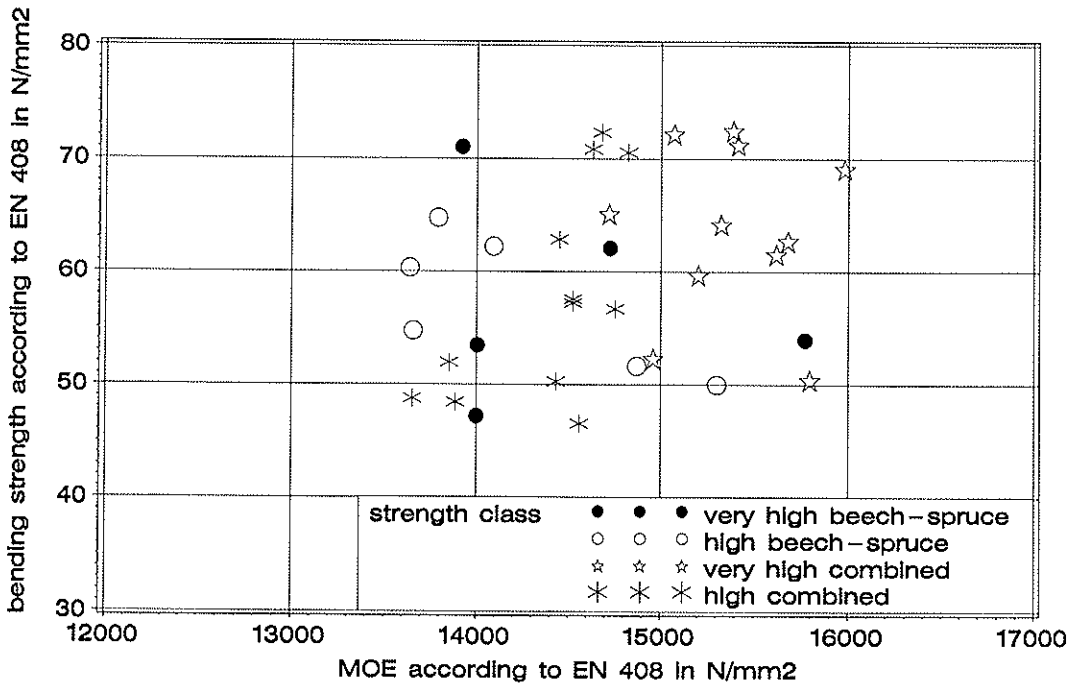

Fig. 8 Bending strength depending on MOE; comparison of 11 beech-spruce test beams and 23 combined beech test beams

4 Conclusions

Substituting beech by spruce in the middle zone of a combined beech glulam beam causes an increase in edge stress in the beech-spruce cross section of less than 3% in comparison with the combined beech cross section. The important thing about it is that the portion of the middle zone must not exceed 60 % of the beam height. By defining marginally higher

demands on the characteristic finger joint bending strength than in case of combined beech glulam it is possible to compensate for the decrease of about 3% related to the characteristic bending strength. Hence, the same strength classes are possible as in case of combined beech glulam. Table 5 gives a survey of the results and the demands on both strength grading and finger joints.

Table 5 Strength and stiffness values and requirements; reference beam height 600 mm

	GL28hyb	GL32hyb	GL36hyb	GL40hyb	GL44hyb	GL48hyb
strength values (N/mm²)						
$f_{m,k}$	28	32	36	40	44	48
stiffness values (N/mm²)						
$E_{0,mean}$	13200	13200	13200	14000	14700	14700
$E_{0,05}$	12400	12400	12400	13300	14200	14200
beech: requirements outer zone (≥h/5)						
DEB[2]	≤0,33	≤0,20	≤0,042	≤0,20[1]	≤0,20	≤0,042
E_{dyn}	-	-	-	>14000[1]	>15000	>15000
$f_{t,l,k}$	22	27	32	36	40	48
$f_{m,j,k}$	≥48	≥54	≥59	≥64	≥71	≥72
spruce: requirements middle zone (<3/5·h)						
[3]	S10	S10	S10	S10	S10	S10

[1] This grading model was in addition developed after publishing Table 5 in [1]
[2] Quantifies the single knot according to DIN 4074-5
[3] Visual grading according to DIN 4074-1

5 References

[1] Frese M, Blaß HJ (2005). Beech glulam strength classes. CIB-W18/38-6-2, Karlsruhe, Germany

[2] Frese M, Blaß HJ (2006). The influence of the grading method on the finger joint bending strength of beech. CIB-W18/39-18-2, Florence, Italy

[3] Blaß HJ, Frese M (2006). Biegefestigkeit von Brettschichtholz-Hybridträgern mit Randlamellen aus Buchenholz und Kernlamellen aus Nadelholz – The Bending strength of beech-spruce glulam with bottom and top beech lamellae and middle spruce lamellae (only available in German). Band 6. Karlsruher Berichte zum Ingenieurholzbau. Universitäts-verlag Karlsruhe: Karlsruhe

EN 408:1995. Bauholz für tragende Zwecke und Brettschichtholz – Bestimmung einiger physikalischer und mechanischer Eigenschaften – Structural timber and glued laminated timber – Determination of some physical and mechanical properties

DIN 4074-1/-5:2003. Sortierung von Holz nach der Tragfähigkeit: Nadel- und Laubschnittholz – Strength grading of wood: Coniferous sawn timber and sawn hard wood (only available in German)

EN 1912:2004. Structural timber - Strength classes - Assignment of visual grades and species

INTERNATIONAL COUNCIL FOR RESEARCH AND INNOVATION
IN BUILDING AND CONSTRUCTION

WORKING COMMISSION W18 - TIMBER STRUCTURES

QUALITY CONTROL OF GLULAM: SHEAR TESTS OF GLUE LINES

R Steiger

Swiss Federal Laboratories for Materials Testing and Research, Wood Laboratory
Dübendorf

E Gehri
ETH, Swiss Federal Institute of Technology

Zürich

SWITZERLAND

MEETING FORTY

BLED

SLOVENIA

AUGUST 2007

Presented by R. Steiger
H. Larsen commented it is interesting that the method is based on certain agreement. Part of the proposed work is based on equilibrium and part based on failure criterion. Interaction between combined stresses can influence failure load. R. Steiger stated that the equilibrium condition is valid also for orthotropic material and there are additional test results from 1930's that the failure criterion is okay. The paper will be updated. H. Larsen commented that this might be academic as the device finds higher stresses or strengths then requirement must be increased accordingly. R. Steiger agreed.

Quality control of glulam: Shear tests of glue lines

R. Steiger

Empa, Swiss Federal Laboratories for Materials Testing and Research, Wood Laboratory Duebendorf, Switzerland

E. Gehri

Prof. em. ETH, Swiss Federal Institute of Technology, Zurich, Switzerland

1 Introduction

Among other tests, shear tests of the glue lines are required in the course of quality control measures to be carried out in glulam plants. The procedures to be followed are given in various standards like for example EN 392:1995 [1], ASTM D 905-03:2003 [2] and ISO 12579:2006 [3]. In the EN as well as in the ISO standard the method of applying shear stress to the glue line is only given by a principle scheme (fig. 1). Based on this scheme a variety of test equipment has been produced and is used by laboratories, glulam manufacturers and producers of adhesives.

Depending on the actual construction of the test equipment as well as the procedure of testing, the resulting stress in the glue line is neither uniformly distributed nor pure shear but rather a combination of shear and normal stresses. In case of simultaneously acting shear stress and tensile stress perpendicular to the grain, the shear strength values drop dramatically, whereas compression stresses perpendicular to the grain lead to an overestimation of the shear strength of the bond line. The problem of the test method not being suitable to test the capacity of the glue line correctly has been addressed in several stages of the development of EN 392 ([4] as an example) but has not been solved at last. To overcome this problem, a prototype of a shear test device which ensures a clearly defined state of shear loading of the specimens has been developed in Switzerland (fig. 2).

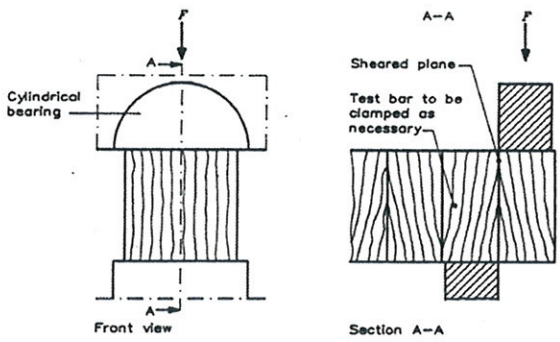

Fig. 1: Method of applying shear stress to a glue line according to EN 392:1995 [1]

Fig. 2: Prototype of shear test equipment with a defined state of shear in the glue line

2 Background

2.1 Difference between "shear" and "shearing"

Shear stress distributions depend on the type of loading (shear or shearing), and hence corresponding strength values differ. Shearing stresses $f_{v,a}$ result from a pair of parallel (shearing) forces working in opposite direction against each other with a small distance between the working lines, causing two contiguous parts of a specimen to slide relatively to each other in a direction parallel to their plane of contact. Shear stresses f_v contrarily occur simultaneously together with bending moments in beam-type members; the acting stress is applied continuously to the member. That is why shear design stresses cannot be directly derived from shearing tests. In this paper it was not possible to use the terms "shear" and "shearing" strictly correct. The original wording "shear" of literature and standards was maintained.

2.2 Test methods to derive shear properties of wood

For the determination of shear properties of wood and wood-based materials there is a wide variety of test methods. In [5] block shear tests, torsion of prismatic bars, anticlastic bending, Iosipescu shear test, multipoint bending, off-axis tension or compression and in-plane shear loading are mentioned together with relevant literature. Additionally panel shear tests [6, 7], short-span bending of rectangular or notched members [8, 9] and the Arcan shear test [10] exist. All of these methods aim at achieving a well defined and uniform state of shear stress in a well defined test zone. But this has proven to be very difficult [9, 11,12].

With regard to the quality control of glue lines in practice common one-sided block shear tests are regarded as the best method since the specimens are simple to fabricate and the test process is easy to carry out [1-3, 13]. In former days not only one-sided block shear tests but also double-sided symmetric block shear specimens of different size and shape were used [14-16] (figs. 3 and 4). Since the distribution of shear stresses is still uneven, the resulting shear strength strongly depends on the geometrical dimensions of the specimen. Besides, there are significant stresses perpendicular to the grain influenced by the actual frictional properties of the settings and the contact zone between specimen and bearing [17]. Roš [18, 19] tried to overcome this situation and to prevent the specimens from early splitting by prestressing them perpendicular to the grain.

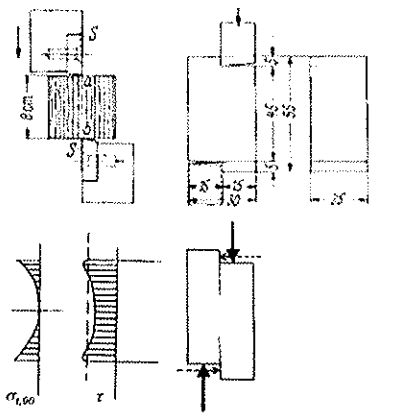

Fig. 3: One-sided block shear test (Bauschinger 1883 [13])

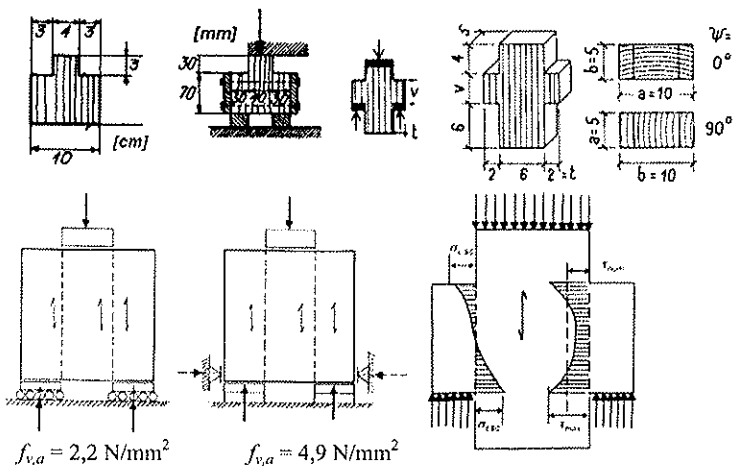

Fig. 4: Doubled-sided block shear test specimens [16-18]

3 Block shear tests of glue lines

3.1 Principles according to different standards

3.1.1 European standards

In Europe the requirements for glued-laminated timber are given in the standard EN 14080:2005 [20]. The bonding strength of glue lines shall be assessed as a glue line integrity test according to one of the test procedures defined in EN 386:2001 [21]. The EN 386:2001 asks for delamination tests according to EN 391:2001 and block shear tests according to EN 392:1995. The shear strength $f_{v,a}$ of each glue line shall be at least 6 N/mm^2. For coniferous wood and poplar lower individual values of shear strength (down to 4 N/mm^2) shall be regarded as acceptable if the wood failure reaches a certain percentage (table 1).

Table 1: Minimum wood failure percentages relating to the shear strength (EN 386:2001)

	Average values			Individual values		
Shear strength $f_{v,a}$ [N/mm^2]	6	8	$f_{v,a} \geq 11$	$4 \leq f_{v,a} < 6$	6	$f_{v,a} \geq 10$
Minimum wood failure percentage [1)]	90 %	72 %	45 %	100 %	74 %	20 %

For values in between, linear interpolation shall be used.

1) For average values the minimum wood failure percentage is: $144 - 9 \cdot f_{v,a}$
For the individual values the minimum wood failure percentage for shear strengths $f_{v,a} \geq 6$ N/mm^2 is: $153{,}3 - 13{,}3 \cdot f_{v,a}$.

The block shear test is to be carried out according to EN 392:1995 [1]. This standard is intended to be used in the field of continuous quality control of glue lines. A principle scheme for the shearing tool is given (fig. 1): The shearing force shall be applied self-aligning via a cylindrical bearing so that the specimen is loaded at the end grain with a stress field uniform in width direction and the distance between the glue line and the sheared plane nowhere exceeds 1 mm.

The specimens shall be of the form shown in figure 5 (e. g. width b and thickness t = 40 to 50 mm) with loaded surfaces to be smooth and parallel to each other as well as perpendicular to the grain direction.

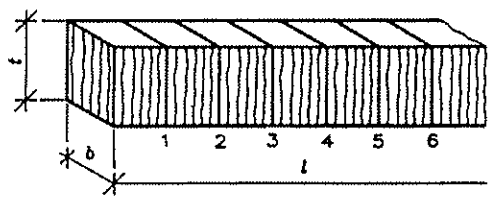

Sizes: length ℓ
width b: 40 to 50 mm
thickness t: 40 to 50 mm

Fig. 5: Test piece to derive shear strength of glue lines according to EN 392:1995 [1]

The shear(ing) strength $f_{v,a}$ is derived from

$$f_{v,a} = k \frac{F_u}{A} \quad (1)$$

with A = sheared area = $b \cdot t$, F_u = ultimate load and k being a modification factor for test pieces where the thickness in the grain direction of the sheared area is less than 50 mm.

3.1.2 American standards

In the United States glulam producers follow quality control guidelines ANSI/AITC 190.1-2002 [22] and ANSI/AITC 200-2004 [23]. Shear testing of glue lines is covered by AITC Test T107. Here, concerning shear block tests, reference is made to the American Standard ASTM D 905-03 [2]. The standard makes aware of the fact that "this test method cannot be assumed to measure the true shear strength of the adhesive bond" because "many factors interfere or bias the measurement including the strength of the wood, the specimen, the shear tool design themselves and the rate of loading". It is also mentioned, that "stress concentrations at the notches of the specimen tend to lower the measured strength", this being in contrast to the test method according to ASTM D 143 [24] where it is (by mistake) said, that "these effects are self correcting so that the measured strength is close to the true shear strength of wood". The shearing tool to be used shall have a self-aligning seat ensuring uniform lateral distribution of the load. The shearing tool shown in figure 6 has been found satisfactory. The shape and the dimensions of the specimen are given in fig. 7.

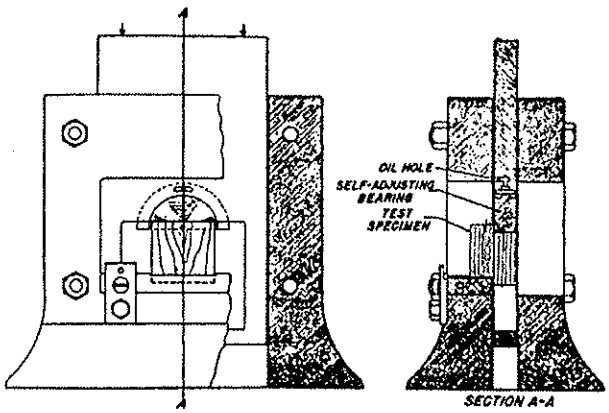

Fig. 6: ASTM D 905-03 shearing tool [2]

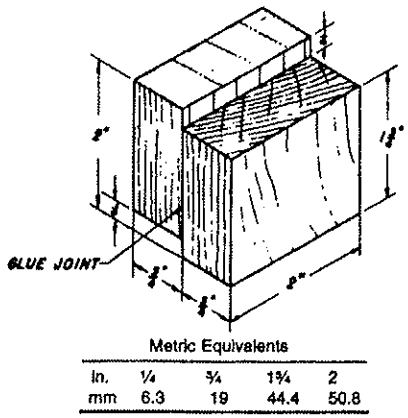

Fig. 7: ASTM D 905-03 specimen to derive shear strength of bond lines [2]

3.1.3 ISO standards

Within the ISO standards series ISO 12578 [25] deals with the component performance and the requirements for the production of glulam. The formulations in this standard are quite similar to the European pendant EN 386:2001. In analogy to the latter, one possibility of controlling glue line integrity and strength is to perform shear block tests. Here reference is made to the standard ISO 12579 [3]. ISO 12579 provides a combination of rules and specimen types taken from EN 392 and ASTM D 905. Concerning the apparatus to be used for the shear tests, the standard provides only a schematic sketch similar to EN 392 (fig. 1). In ISO 6238:2001 [26] one can find an example of a shearing tool for compressive shear block tests being identical to the one shown in figure 6 of ASTM D 905-03.

3.2 Shortcomings of the block shear test method

The block shear test method has the advantage of being simple with regard to the preparation of the test specimen, the test equipment needed, the overall procedure and the analysis of the test results. But nevertheless there are several shortcomings to be mentioned:

- The test method suffers from a non uniform shear stress distribution with a stress concentration near the corner as it was shown by experimental and theoretical stress analysis [9, 11]. Hence the derived shear strength using equation (1) is only nominal.
- The test results are influenced by the actual materialisation of the principal sketch of EN 392 (fig. 1) as well as by the person carrying out the test (see 3.3). In figure 8, as an example three different types of test devices are shown. It can easily be seen that the way of applying forces and thus the resulting stress situation in the bond line differ.

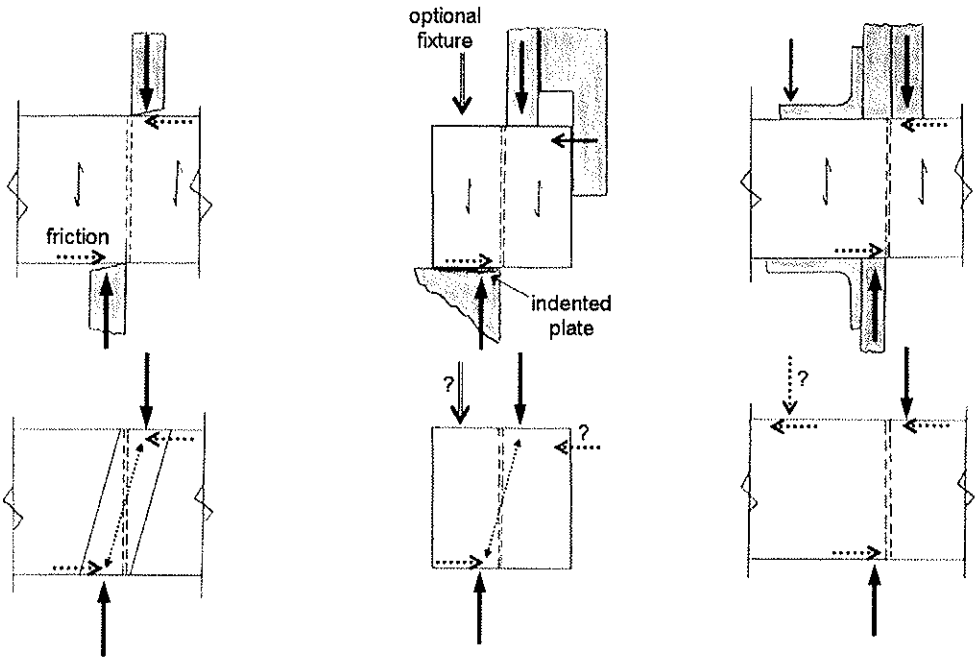

- wedge-shaped punch → carves
- stresses perpendicular to the bond line

statically indeterminate loading

- forces and stress distribution acting on glue line depend on test device (geometry, friction, stiffness) and variation of specimen geometry

Fig. 8: Three examples of shearing tools used by different labs and glulam producers

- During the shear test, the specimen is subjected to a shear strain. Most of the existing shearing devices hinder this strain. This results in unknown side effects on the test results.
- Test results derived using different test devices cannot be compared directly. Strictly said: the method only serves the glulam producer as a kind of warning sign if the test values drop below a certain threshold.

3.3 Analysis of static equilibrium

The state of static equilibrium in specimens tested according to EN 392:1995 is shown in figure 9. Being not aligned but rather eccentric (with a gap e depending on the dimensions of the stamps ℓ_A of the actual test equipment) the acting shearing forces A_v cause a moment $A_v \cdot e$, which has to be compensated by a counteracting moment $h \cdot A_h$. Both the eccentricity e and the counteracting moment are indeterminate, depending on the actual shearing device. Assuming a mean shear strength of $f_{v,a}$ = 6 N/mm^2 the shearing force in a bonded zone of 50 · 45 mm^2 is 13,5 kN and the equilibrium "frictional force" A_h has to be 3 kN.

The "frictional" stress thus is 6 N/mm^2 and the width of the punches needs to be 7 to 10 mm, assuming a maximal strength parallel to the grain of $f_{c,0}$ = 30 to 40 N/mm^2.

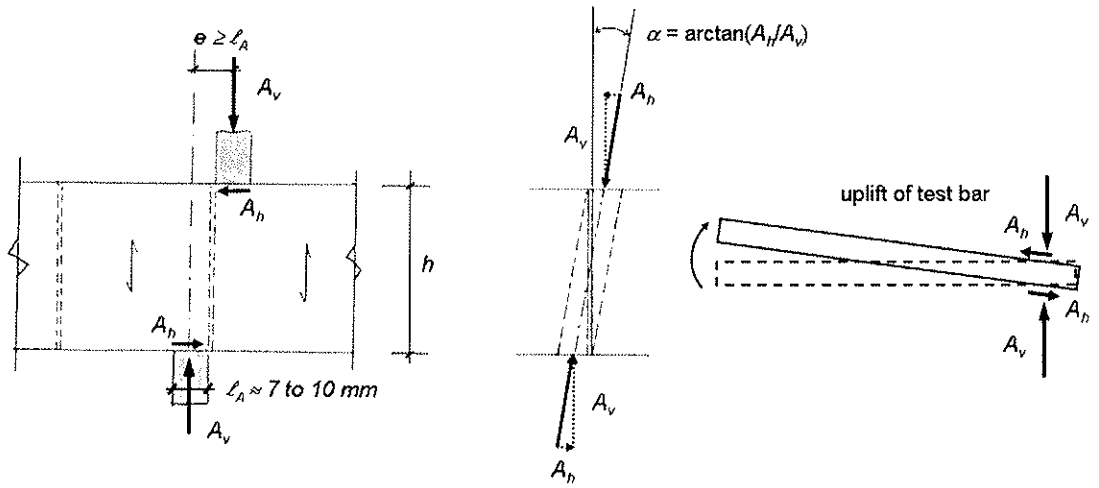

Fig. 9: Static equilibrium in shear test specimens according to EN 392:1995

Actually there is a state of compression at an angle to the grain ($\alpha \approx \arctan(A_h/A_v) = \arctan(3/13{,}5) = 12{,}5°$ and a counteracting moment is built up when the zone of maximum compression stress is deformed. The deformation leads to an uplift of the test bar. If the uplift is prevented for example by holding down the test bar, significant bending stresses are added to the acting shearing stresses and the specimen tends to fail early at low level of shear stress. This situation actually happened in a Swiss glulam plant, where the person being responsible for the shear tests of glue lines retired and was replaced by another person. After this replacement there was a drop in test results. This drop could not be explained because there was no change in production parameters. Analysing the situation in detail it was found that the new person was younger and more powerful than his predecessor, holding down the test bar with more power.

It is well known, that simultaneously acting tensile stresses perpendicular to the grain result in lower shear strength, whereas compressive forces perpendicular to the grain help to resist higher shear stresses (fig. 10). In the actual Swiss Standard for the design of timber structures [27] there is a design criteria taking account of these effects (fig. 11).

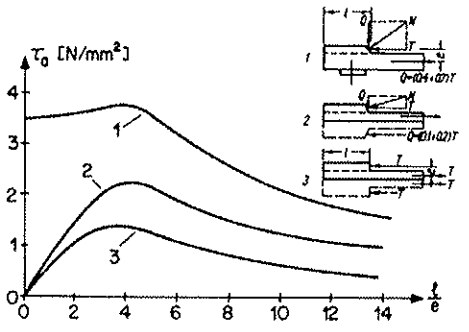

Fig. 10: Influence of compression stresses perpendicular to the grain on shear strength [28]

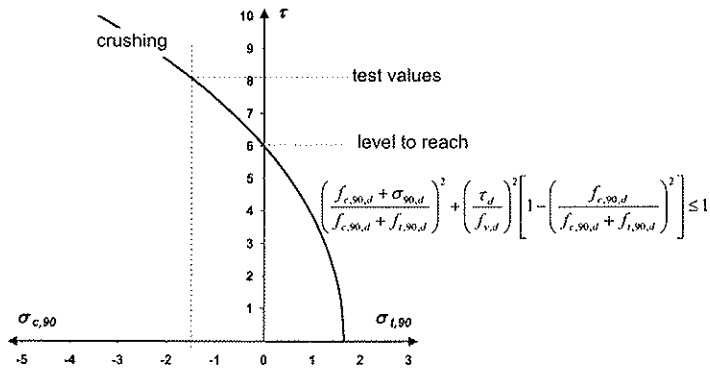

Fig. 11: Design criteria for simultaneously acting shear stress and stresses perpendicular to the grain [27]

4 Optimized block shear test

4.1 Approach

As it is well known and shortly summarized below, one can derive shear strength by carrying out compression tests not parallel to the grain but rather with a certain inclination. Panel shear tests to derive shear strength parallel to the grain according to EN 408:2003 [6] for example are based on that. There an oblique angle between the loading direction and the longitudinal axis of the specimen (which is actually the grain direction) of 14° is used. The procedure however is rather tedious and not suitable for the quality control of glue lines, since tapered steel plates have to be glued to the specimens. But the idea of carrying out a compression test at an oblique angle to the grain can be used to improve the block shear test method.

4.2 Compression and tension stresses at an angle to the grain

Different angles α between loading directions and grain can e. g. be modelled by the Hankinson-formula [29], which independently was also found by Kollmann [30] based on scientific findings in crystal physics by Hörig [31]. The Hankinson formula does not provide any information on failure modes to be expected with varying angles α.

Stüssi [32, 33] showed, that for isotropic materials a relation between normal stresses σ and shear stresses τ is determined by stress equilibrium of a plane strain element subjected to a stress σ_α inclined by an angle α with reference to the grain direction. The principle stresses σ_1 and σ_2 are:

$$\sigma_1 = \sigma_\alpha \qquad (2)$$

$$\sigma_2 = 0 \qquad (3)$$

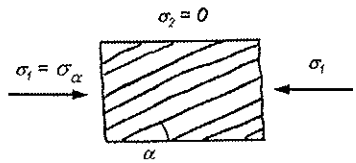

Respective stresses parallel and perpendicular to the grain and shear stresses can be calculated according to the theory of the strength of materials:

$$\sigma_0 = \sigma_\alpha \cdot \cos^2 \alpha \qquad (4)$$

$$\sigma_{90} = \sigma_\alpha \cdot \sin^2 \alpha \qquad (5)$$

$$\tau_{0,90} = \sigma_\alpha \cdot \cos\alpha \cdot \sin\alpha \qquad (6)$$

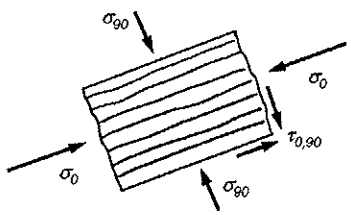

Depending on the actual angle α between loading and the grain direction there are three different failure modes possible:

- compression failure parallel to the grain: $\sigma_\alpha = \dfrac{\sigma_0}{\cos^2 \alpha}$ (7)
- shear failure: $\sigma_\alpha = \dfrac{\tau_{0,90}}{\sin\alpha \cdot \cos\alpha}$ (8)
- compression failure perpendicular to the grain: $\sigma_\alpha = \dfrac{\sigma_{90}}{\sin^2 \alpha}$ (9)

Solving Airy's stress function, Ylinen [34] found that these formulas are valid for orthotropic materials as well. The dependency of compression strength from the angle between grain and load direction is shown in figure 12. It can be concluded that:

- the shear strength $f_{v,0,90}$ can be derived from compression tests at an oblique angle α to the grain based on equation 8:
  $f_{v,0,90} = f_{c,\alpha} \cdot \cos\alpha \cdot \sin\alpha$ (10)
- shear failures can to be expected for $\alpha_1 \leq \alpha \leq \alpha_2$ (Analysing test results by Kraemer, Baumann and Stüssi it can be shown, that this assumption is valid [35].)

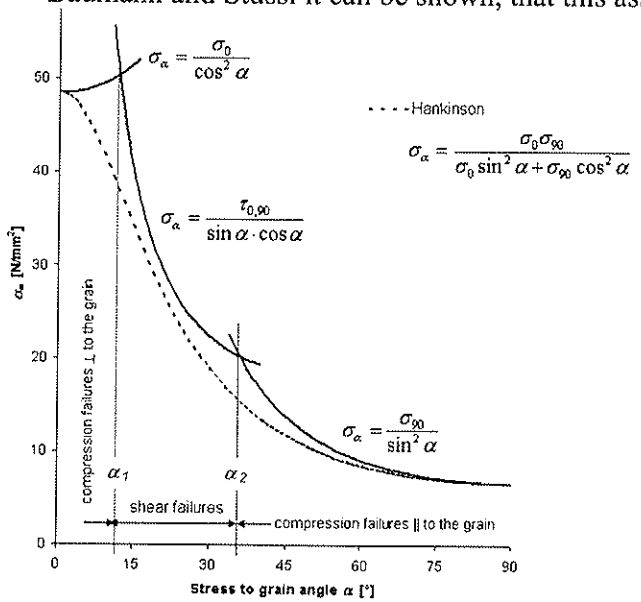

Fig. 12: Influence of the angle between loading and grain direction on compression strength according to Stüssi [32, 33]

4.3 Prototype of a new shearing tool

Owing to the fact that high compression stresses perpendicular to the grain result in higher shear stresses (fig. 10), an angle α in the range of α_1 is to be preferred. In analogy to the EN 408:2003 rules [6] for panel shear tests an angle α of 14° is chosen (fig.13), being equal to a slope of 1:4. Prototype tests and calculations showed that smaller slopes of e. g. 1:5 or 1:6 would not be possible since the specimens might crush due to exceeding compression stresses parallel to the grain in the loading zone. With a slope of 1:4 for coniferous specimens shear strengths up to 10 – 12.5 N/mm^2 were recorded resulting in compression stresses parallel to the grain of 40 to 50 N/mm^2. When testing deciduous specimens this problem is even bigger, since these species with increasing quality show a stronger increase in shear strength than in compression strength parallel to the grain.

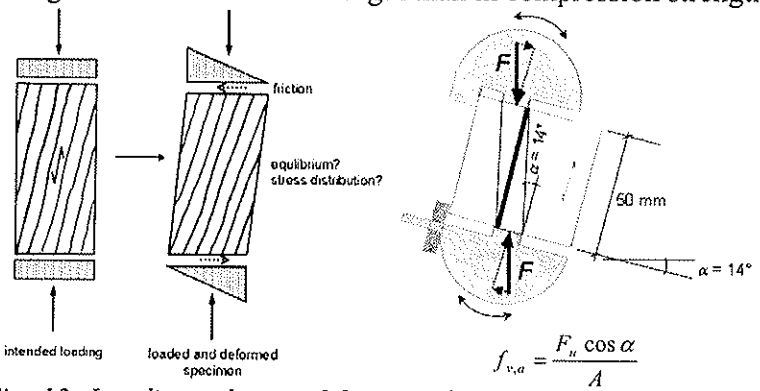

Fig. 13: Loading scheme of the new shearing tool

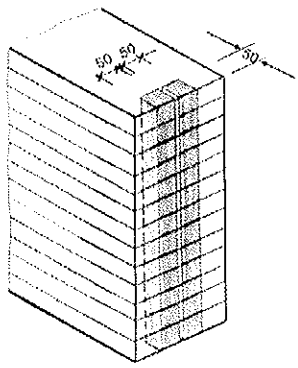

Fig. 14: Pairs of specimens

As it is shown in figure 13 (left) and experimentally proven [36], a shearing strain occurs during the shearing test. This shearing strain may not be hindered or blocked but rather be made possible. That is why the upper and the lower plungers are coupled to the loading parts by pivot bearings. To account for the specifications given by EN 392:1995 (cylindrical bearing, see fig. 1) one of the plungers has a two-way pivot bearing.

5 Test results

5.1 Comparison of existing and new test device

In a preliminary study the new test equipment was compared to the former one by carrying out tests with both devices over a time span of 5 months. Almost 160 specimens taken from approximately 40 glulam beams were tested to failure. The shear strength values as well as the percentages of failure in timber were recorded. The glulam beams were produced from Norway spruce lamellas bonded together using a melamine urea formaldehyde adhesive (MUF). A direct comparison between both test series was possible since the test bars were taken as pairs from the front ends of the beams as shown in fig. 14.

Figs. 15 to 17 give an overview of the test results. Compared to the new test equipment the shear strengths derived with the former device are considerably lower. This is due to tensile stresses perpendicular to the grain. Whereas these test results are not inline with the demands of EN 386 ($f_{v,min}$ = 3,6 N/mm^2 < 6 N/mm^2), the "same" specimens reach minimal shear strengths of 6,3 N/mm^2 with the new device and thus are ok. Concerning the percentage of wood failure there are no big differences between the two devices although the shear strengths reached with the new device are about 50% higher.

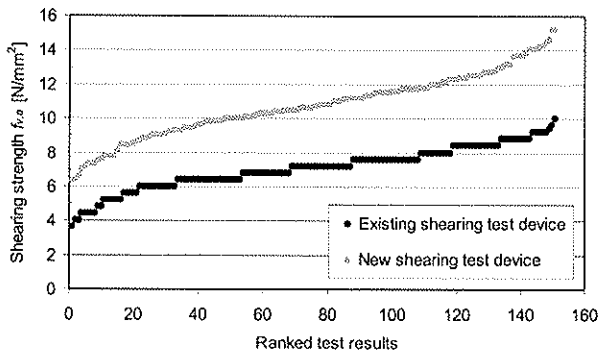

[N/mm^2]	Established device	New device
Max	10	15,2
Min	3,6	6,3
Mean	7,1	10,7
COV	18 %	18 %

Fig. 15: Comparison established / new device in terms of shear strengths of glue lines

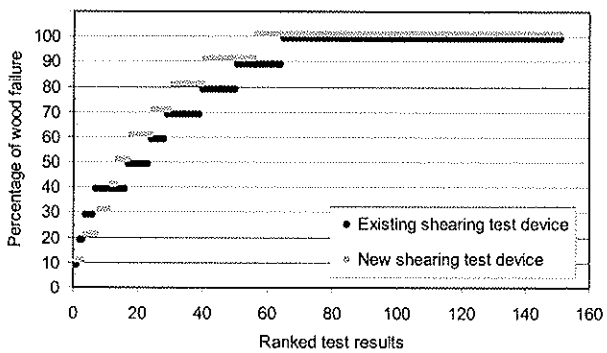

[%]	Established device	New device
Max	100	100
Min	10	10
Mean	84,8	86,7
COV	27 %	27 %

Fig. 16: Comparison established / new device in terms of percentages of wood failure

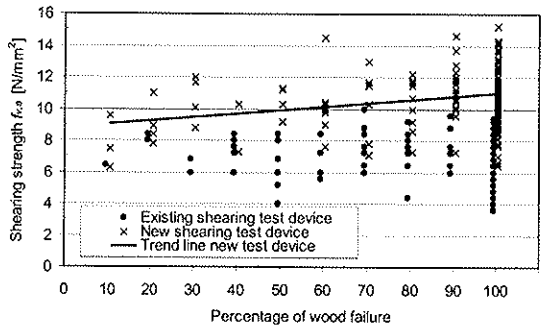

Fig. 17: Comparison of established and new shearing tool: shear strength values with regard to percentage of wood failure

In fig. 17 the shear strengths are classified according to the percentage of timber failure. When using the new prototype shearing tool, the percentages of wood failure increase with increasing shearing strength. The "same" specimens tested with the established device do neither fulfil the minimum shear strength criteria (no values below 4 N/mm^2) nor is there an adequate percentage of wood failure regarding the low values.

5.2 Handling of the new tool

The prototype is in daily use by a Swiss glulam producer and has proven to be easy to handle as well as to give reliable and reproducible test results. The preparation of the specimens does not differ from the former test method.

6 Conclusions

It was shown that:

- using established shearing tools many factors (strength of wood, shape and size of specimen, design of the shearing tool, test person, rate of loading, etc.) interfere or bias the measurements,
- instead of shear tests according to common standards used in the quality control of glue lines, axial compression tests with an oblique angle between the grain and the loading direction of 14° (slope 1:4) should be made,
- the prototype of the presented shearing tool has the potential of producing reliable and reproducible shear strength values not being influenced by the person who carries out the tests,
- test results using the new shearing tool are higher than those derived with the established one (most results are higher than 6 N/mm^2),

It is therefore suggested to:

- add the compression shear test at an oblique angle between load and grain direction to the relevant product standards
- add hints to EN 392 which make aware of the shortcomings of the actual EN 392 method (similar to the US standard ASTM D 905-03).
- make clear distinction between "shear" and "shearing" tests or stresses respectively.
- deepen the experimental research under industrial as well as laboratory conditions.

7 References

1. Comité Européen de Normalisation CEN, TC 124, 1995: EN 392: Glued laminated timber - Shear test of glue lines.
2. American Society for Testing and Materials ASTM, 2003: ASTM Standard D 905-03: Standard test method for strength properties of adhesive bonds in shear by compression loading.
3. International Organization for Standardization ISO, TC 165, 2006: Draft International Standard ISO 12579.2: Timber structures - Glued laminated timber - Method of test for shear strength of glue lines.
4. Comité Européen de Normalisation CEN, TC 124, 1990: Inquiry of prEN 392: Glue line shear test. Inquiry launched 16. 08. 1990 and closed 16. 02. 1991.
5. Yoshihara, H., Matsumoto A., 2005: Measurement of the shearing properties of wood by in-plane shear test using a thin specimen. Wood Science and Technology **39** (2): p. 141-153.
6. Comité Européen de Normalisation CEN, TC 124, 2003: EN 408: Timber structures - Structural Timber and glued laminated timber - Determination of some physical and mechanical properties.
7. Feldborg T., 1991: Determination of some mechanical properties of timber in structural sizes. In Proceedings of the 1991 International Timber Engineering Conference. London, UK. Timber Research and Development Association TRADA.
8. Larsen H.J., 1987: Determination of shear strength and strength perpendicular to grain. Paper 20-6-3 in Proceedings of CIB-W18 Meeting Twenty. Dublin, Ireland.
9. Radcliffe B.M., Suddarth S.K., 1995: The notched beam shear test for wood. Forest Products Journal 5 (2): p. 131-135.
10. Arcan M., Hashin Z., Voloshin A., 1978: Method to produce uniform plane-stress states with applications to fiber-reinforced materials. Experimental Mechanics **18** (4): p. 141-146.
11. Coker E.G., Coleman G.P., 1935: Photo-elastic investigations of shear-tests of timber. Selected Engineering Papers of the Institution of Civil Engineers. London, UK.
12. Bodig J., Jayne B.A., 1993: Mechanics of Wood and Wood Composites. Krieger Publishing Company. Malabar, USA.
13. Kollmann F.F.P., Côté Jr. W.A., 1968: Principles of wood science and technology. Vol. 1: Solid Wood. Springer. Berlin, Germany.
14. Eidgenössische Materialprüfungsanstalt an der E.T.H. in Zürich, 1924/25: S.I.A-Normen für Holzbauten - Ergebnisse der Festigkeitsuntersuchungen an der E.M.P.A. mit Bauhölzern. Zurich, Switzerland.
15. Empa, 1949/1950/1952: Richtlinien zur Untersuchung von Holz - 2. Teil: Untersuchungen zur materialtechnischen Charakterisierung von Rundholz und Schnittware. Eidg. Materialprüfungs- und Versuchsanstalt für Industrie Bauwesen und Gewerbe. Zurich, Switzerland.
16. Staudacher E., 1942: Schweizerische Bau- und Werkhölzer - Ergebnisse der an der Eidgenössischen Materialprüfungs- und Versuchsanstalt Zürich, in Zusammenarbeit mit der Eidgenössischen Anstalt für das forstliche Versuchswesen, Zürich, in den Jahren 1936 bis 1941 durchgeführten systematischen Untersuchungen über waldfrisches Holz der Fichte, Tanne, Lärche, Buche und Eiche. Zurich, Switzerland.
17. Henrici D., Scheicher U., 1988: Shear-strength of glued lap joints in test specimens with frictionless support. Holz als Roh- und Werkstoff **46** (1): p. 33.
18. Roš M., 1925: S.I.A.-Normen für Holzbauten - Ergebnisse der Festigkeitsuntersuchungen an der E.M.P.A. mit Bauhölzern, in den Jahren 1924/25 als Grundlage für die Normen des S.I.A. Eidgenössische Materialprüfungsanstalt der E.T.H. in Zürich. Zurich, Switzerland.
19. Roš M., 1936: Das Holz als Baustoff. I. Schweizerischer Kongress zur Förderung der Holzverwertung. Bern, Switzerland.
20. Comité Européen de Normalisation CEN, TC 124, 1995: EN 14080: Timber structures - Glued laminated timber - Requirements.
21. Comité Européen de Normalisation CEN, TC 124, 2001: EN 386: Glued laminated timber - Performance requirements and minimum production requirements.
22. American Institute of Timber Construction AITC, 2002: Standard 190.1-2002: American National Standard - Structural glued laminated timber.
23. American Institute of Timber Construction AITC, 2004: Standard 200-2004: Inspection manual for structural glued laminated timber.
24. American Society for Testing and Materials ASTM, 2000: ASTM Standard D 143-94: Standard test methods for small clear specimens of timber.
25. International Organization for Standardization ISO, TC 165, 2007: Draft International Standard ISO 12578.2: Timber structures - Glued laminated timber - Component performance and production requirements.
26. International Organization for Standardization ISO, TC 165., 2001: International Standard ISO 6238: Adhesives - Wood-to-wood adhesive bonds - Determination of shear strength by compressive loading.
27. Schweizerischer Ingenieur- und Architekten-Verein SIA, 2003: Norm SIA 265 - Holzbau.
28. Karlsen G.G., Goodman W.L., 1967: Wooden structures. MIR Publishers, Moscow, Russia.
29. Hankinson R.L., 1921: Investigation of crushing strength of spruce at varying angles of grain. U. S. Air Service Information Circular Vol. 3 (Circular No. 259).
30. Kollmann F., 1934: Die Abhängigkeit der Festigkeit und der Dehnungszahl der Hölzer vom Faserverlauf. Der Bauingenieur **15** (19/20): p. 198-200.
31. Hörig H., 1931: Zur Elastizität des Fichtenholzes. Zeitschrift für technische Physik **12** (8): p. 369-379.
32. Stüssi F., 1946: Holzfestigkeit bei Beanspruchung schräg zur Faser. Schweizerische Bauzeitung **128** (20): p. 251-252.
33. Stüssi F., 1949: Holzfestigkeit schräg zur Faser. Schweizerische Bauzeitung **67** (6): p. 90.
34. Ylinen A., 1963: A comparative study of different types of shear test of wood. Publication 82 of the State Institute for Technical Research. Helsinki, Finland.
35. Gehri E., Steurer T. 1979: Holzfestigkeit bei Beanspruchung schräg zur Faser. Bulletin 7/2 der Schweizerischen Arbeitsgemeinschaft für Holzforschung SAH. Zürich. p. 1-27.
36. Keylwerth R., 1951: Die anisotrope Elastizität des Holzes und der Lagenhölzer. Mitteilung aus der Bundesanstalt für Forst- und Holzwirtschaft. Reinbek, Hamburg. VDI-Forschungsheft 430. Verlag des Vereines Deutscher Ingenieure, Düsseldorf, Germany.

INTERNATIONAL COUNCIL FOR RESEARCH AND INNOVATION
IN BUILDING AND CONSTRUCTION

WORKING COMMISSION W18 - TIMBER STRUCTURES

TIMBER TRUSSES WITH PUNCHED METAL PLATE FASTENERS - DESIGN FOR TRANSPORT AND ERECTION

H J Blass

Universität Karlsruhe

GERMANY

MEETING FORTY

BLED

SLOVENIA

AUGUST 2007

Presented by H. Blass
R. Zarnic commented that this work may be applicable to consider out of plane loading of trusses due to earthquakes.
P. Paevere received clarification about controlling factors for long span and for splice joint.
H. Larsen and H. Blass discussed about the applicability of rope model. H. Blass stated that profiled teeth may perform better and the request for this type of work came from the industry. He has experienced with strong-tie product when the rope factor works well. Here continual movement due to dynamic load was not considered and the work is a rough proposal.
P. Paevere stated he has developed withdrawal test for different reasons.
T. Williamson stated that in U.S. builder tips as guidelines are available although they did not work for all cases.
There were further discussions on consequences of failure caused by damage during transport and erection. H. Blass agreed that sometimes damage cannot be easily detected.

Timber Trusses with Punched Metal Plate Fasteners - Design for Transport and Erection

H.J. Blass

Universität Karlsruhe, Germany

1 Introduction

During transport and erection of trusses with punched metal plate fasteners unintentional forces and moments may occur which are difficult to quantify but increase with increasing truss dimensions. Hence a careful handling during transport and erection becomes ever more important with increasing truss length.

Eurocode 5 stipulates in 9.2.1 (8):

All joints should be capable of transferring a force $F_{r,d}$ acting in any direction within the plane of the truss. $F_{r,d}$ should be assumed to be of short-term duration, acting on timber in service class 2, with the value:

$$F_{r,d} = 1,0 + 0,1L \tag{9.18}$$

Where $F_{r,d}$ is in kN and L is the overall length of the truss, in m.

However, this requirement does not take into account unintentional forces perpendicular to the truss plane. A design of members and connections for larger minimum forces leads to more robust members capable of better withstanding the exposure during transport and erection. This paper presents the background of a design method of trusses with punched metal plate fasteners for loads during transport and erection which is part of the German timber design code DIN 1052.

2 Background for unintentional loads

Observations during production or transport and erection of trusses with lengths between 20 m and 30 m show significant unintentional loads particularly perpendicular to the truss plane. These loads occur e. g. during lifting of the trusses from the press tables and lead to bending deformations of the narrow trusses perpendicular to the plane (see Fig. 1). Consequently, the continuous upper and lower chords are loaded in bending. Unintentional loads within the truss plane also occur, but the trusses are designed to carry large vertical loads parallel to their plane and hence are not sensitive to the latter loads.

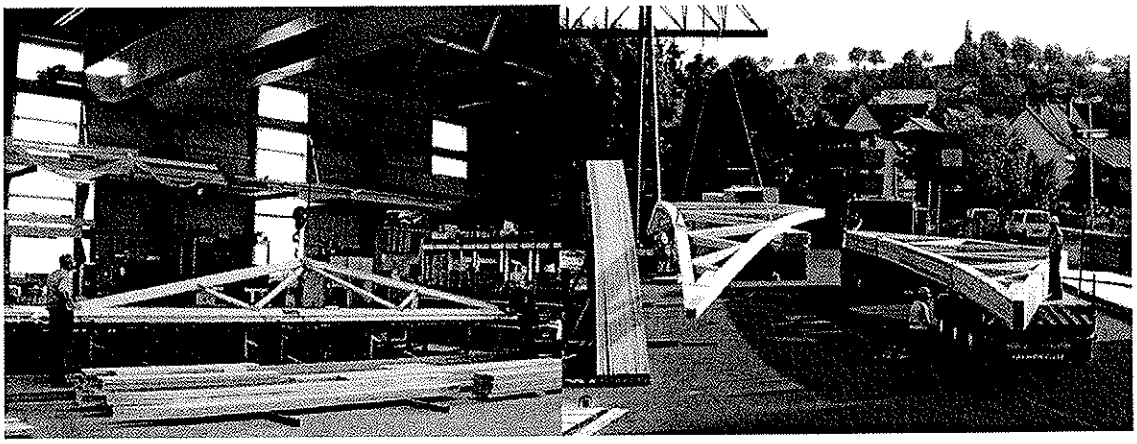

Figure 1: Truss production (left) and truss bending during lifting (right).

Once the trusses are properly erected and braced, they form a part of a three-dimensional structure and – due to the stiffness distribution within this structure - are exposed to only minor loads perpendicular to the truss plane. In order to derive the governing loads perpendicular to the truss plane, possible loads during production, transport and erection are considered. The following case of a symmetrical triangular truss is considered as a basis for assessing unintentional loads perpendicular to the truss plane:

The truss is located on a horizontal table and is lifted at the apex (see Fig. 1 left). As soon as the apex is lifted, the truss is supported continuously along the lower chord and by a simple support at the apex. Consequently, the upper chord is exposed to bending moments perpendicular to the truss plane resulting from the self weight. This load situation is considered conservative for the production process since cross-bars or multiple hangers should be used for larger spans to minimise loads and bending moments.

In order to assess the inner forces and moments resulting from the described lifting procedure, two trusses loaded by self-weight were calculated exemplarily using a three-dimensional analysis. The lower chord was assumed to be supported continuously, the apex connection was simply supported. All nodes were assumed to be able to transfer bending and torsional moments.

The configurations of the symmetrical triangular trusses with members of strength class C24 are:

Table 1: Features of the calculated trusses

	Truss 1	Truss 2
Span	24,52 m	28,56 m
Length	26 m	30 m
Upper chord cross-section	50 x 220 mm	60 x 240 mm
Lower chord cross-section	50 x 200 mm	60 x 180 mm to 60 x 220 mm
Cross-section of diagonals	50 x 80 mm to 50 x 140 mm	60 x 80 mm to 60 x 120 mm

The main results of the calculation using a timber density of 5 kN/m³ are summarised in Table 2.

Table 2: Inner forces and moments of the calculated trusses

	Truss 1	Truss 2
Maximum bending moment upper chord	0,68 kNm	1,19 kNm
Maximum torsion moment upper chord	0,41 kNm	0,59 kNm
Maximum shear force upper chord	0,37 kN	0,55 kN
Maximum shear force diagonals	0,14 kN	0,40 kN

An alternative calculation with torsion hinges at the member ends resulted in maximum bending moments of 0,89 kNm for truss 1 and 1,82 kNm for truss 2.

Since a three-dimensional analysis of trusses for each building project is much too costly, the following approximation is used to take into account unintentional loads in trusses during production, transport and erection:

Upper and lower chord are considered as continuous beams on three supports with constant span. The uniformly distributed load follows from the self weight of the chords with the maximum density according to EN 1991-1-1 for solid timber:

$$q_k = b \cdot h \cdot \rho = b \cdot h \cdot 5 \quad \text{kN/m}^3 \tag{1}$$

The maximum bending moment at the inner support results with the total truss length ℓ:

$$M_k = \frac{q_k \ell^2}{32} = \frac{b \cdot h \cdot 5 \cdot \ell^2}{32} \tag{2}$$

and the maximum shear force perpendicular to the truss plane:

$$V_k = \frac{5 \cdot q_k \ell}{16} = \frac{5 \cdot b \cdot h \cdot 5 \cdot \ell}{16} \tag{3}$$

From equation (2) maximum upper chord bending moments of 1,07 kNm result for truss 1 and 2,03 kNm for truss 2. The corresponding values from equation (3) for the shear force are 0,43 kN and 0,62 kN. These values exceed the inner forces calculated using the three-dimensional analysis and hence are considered conservative, if the upper and lower truss chords including any splices are designed for the bending moment and shear force according to equations (2) and (3).

Considering the design value of the bending moment, load duration class "very short" and service class 2, the design of the timber cross-section for bending moments yields:

$$\frac{M_d}{W} = \frac{1{,}35 \cdot b \cdot h \cdot 5 \cdot \ell^2 \cdot 6}{32 \cdot b^2 \cdot h} \le f_{m,d} = \frac{f_{m,k} \cdot 1{,}1}{1{,}3} \tag{4}$$

A minimum chord width b follows from equation (4):

$$b \ge \frac{1{,}5 \cdot \ell^2}{f_{m,k}} \quad \text{in mm} \tag{5}$$

Here, ℓ is the total truss length in m and $f_{m,k}$ the characteristic bending strength in N/mm².

For the design of the chord splices including the apex joint the bending moment is set equal to a pair of forces creating a compressive and a tensile force in the two punched

metal plate fasteners of the splice joint. The compressive or tensile force follows from the bending moment in equation (2):

$$F_{c,k} = F_{t,k} = \frac{M_k}{b} = \frac{h \cdot 5 \cdot \ell^2}{32} \tag{6}$$

If the one-sided tensile or compressive force is converted to an equivalent splice force, a minimum tensile force perpendicular to the joint line in load duration class "very short" for the design of the splice joint results:

$$F_{t,d} = 0{,}47 \cdot h \cdot \ell^2 \quad \text{in kN} \tag{7}$$

Similarly, the shear force perpendicular to the truss plane is calculated as:

$$V_d = 2{,}3 \cdot b \cdot h \cdot \ell \quad \text{in kN} \tag{8}$$

Here, b is the chord width, h is the chord depth and ℓ is the total truss length in m.

For the two trusses 1 and 2, the minimum upper chord tensile force according to equation (7) becomes 70 kN and 101 kN, compared to the minimum force according to equation (9.18) of Eurocode 5 of only 3,6 kN and 4,0 kN.

3 Tests under loads perpendicular to the truss plane

In order to study the load-deformation behaviour of connections with punched metal plate fasteners loaded perpendicular to the fastener plane and to verify the assumptions regarding the partition of the bending moment in a tensile and compressive force, tests with different punched metal plate fasteners were performed. For 12 types of fastener, five bending and five shear force tests were carried out.

3.1 Bending tests

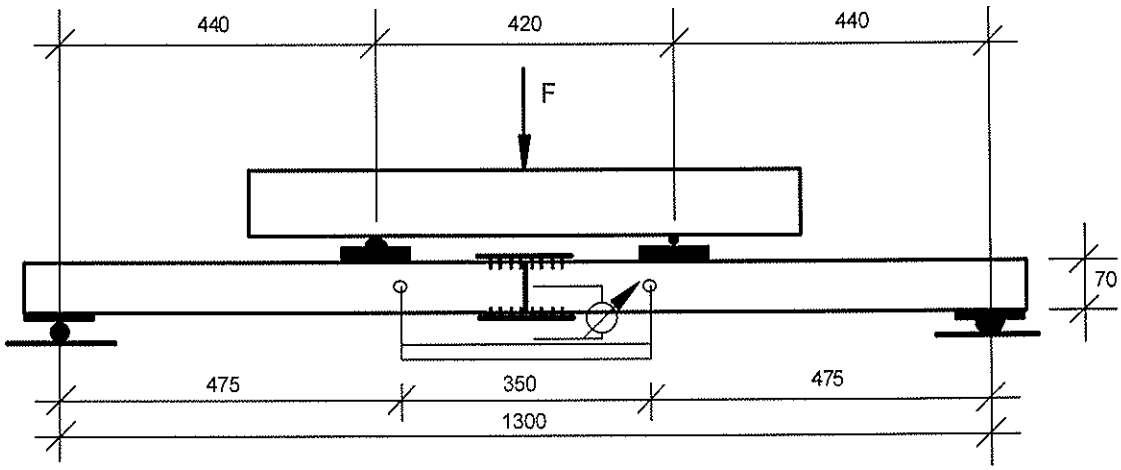

Figure 2: Chord splice bending test configuration (dimensions in mm).

The bending tests were performed with $\alpha = \beta = 0°$ and a gap of 2 mm between the end grain surfaces of the timber members. The fastener bite was between 49 mm and 74 mm. The load per fastener was calculated as the maximum bending moment in the test, divided by the timber member thickness b. In most cases, the failure was characterised by an anchorage failure in the tensile plate and a buckling failure in the compressive plate (see

Figure 3). In general, the anchorage capacity from the bending tests was up to 10 % lower than the capacity from tensile tests according to EN 1075. This decrease is caused by the reduced distance between tensile and compressive force after plate buckling. However, due to the larger bending moment and shear force based on the simplified continuous beam model compared to the results of the three-dimensional analysis of the trusses, the simplified model is still applied.

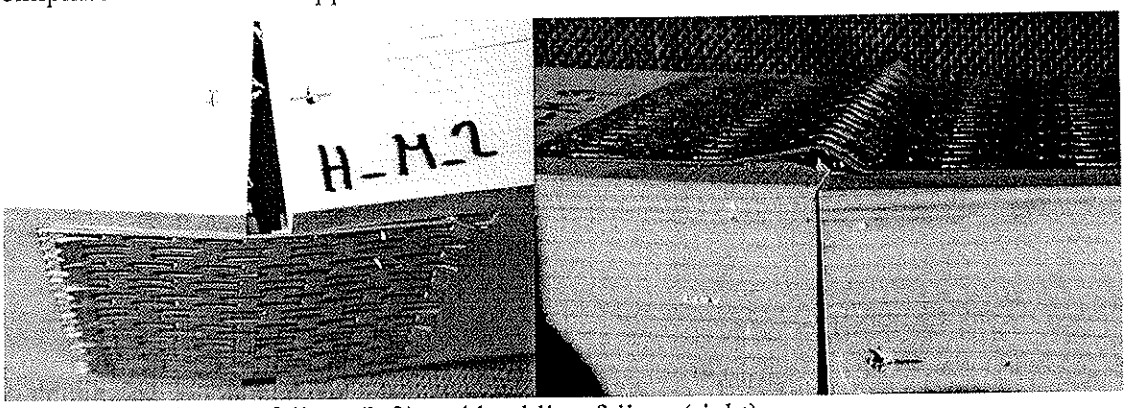

Figure 3: Anchorage failure (left) and buckling failure (right).

3.2 Shear tests

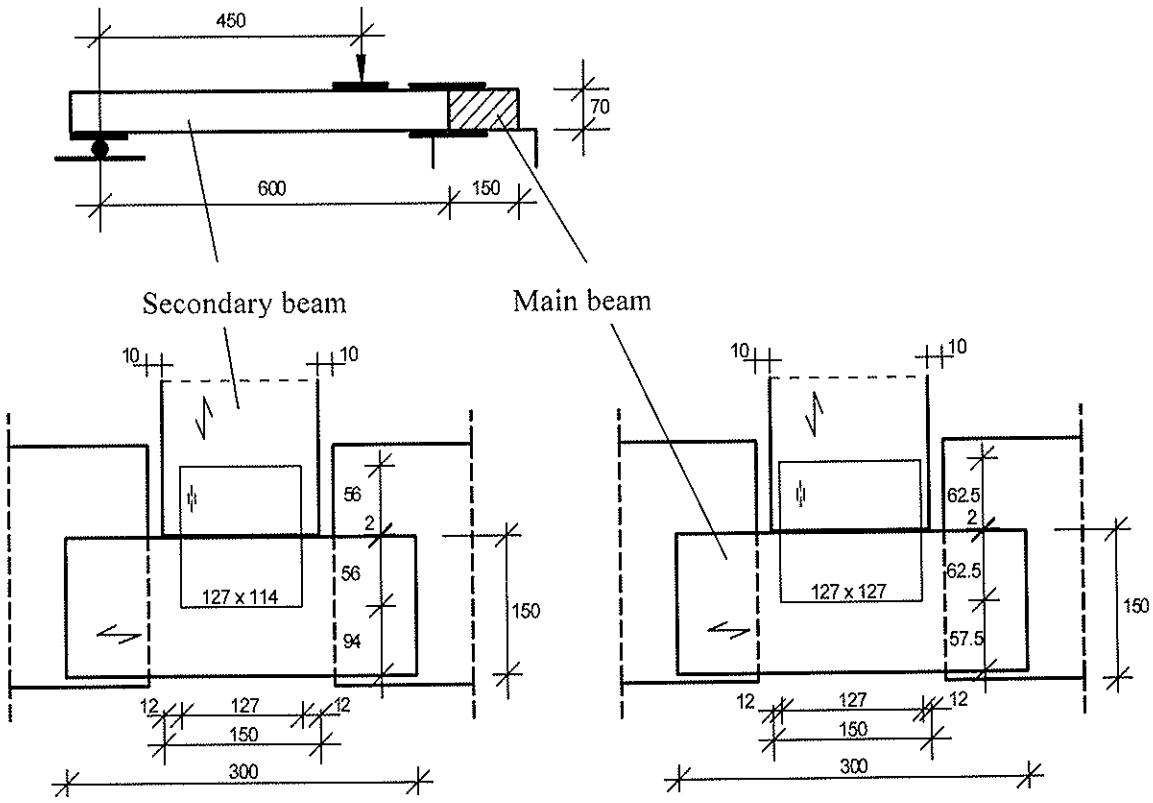

Figure 4: Example of shear test configuration (dimensions in mm).

In the shear tests the punched metal plate fasteners are loaded perpendicular to their plane. The plate main direction was perpendicular to the joint line. The failure was characterised by a fastener plate deformation with subsequent withdrawal of nails beginning close to the joint line in both timber members. With increasing deformation a first maximum in the load-deformation-curve is reached. As soon as the gap between the timber members is closed, the load generally exceeds the first maximum and sometimes reaches the double

value of the first maximum load. This strengthening effect, however, was disregarded when evaluating the test results.

The nails of the punched metal plate fasteners are hence loaded in withdrawal and the nails closest to the joint line are loaded highest. The shear capacity perpendicular of the punched metal plate fastener depends on the contribution of several nail rows, a load per nail therefore cannot be determined. Hence the capacity is determined per unit length of joint line based on the minimum fastener bite in the tests. This fastener bite is a precondition for the shear capacity f_{ax}.

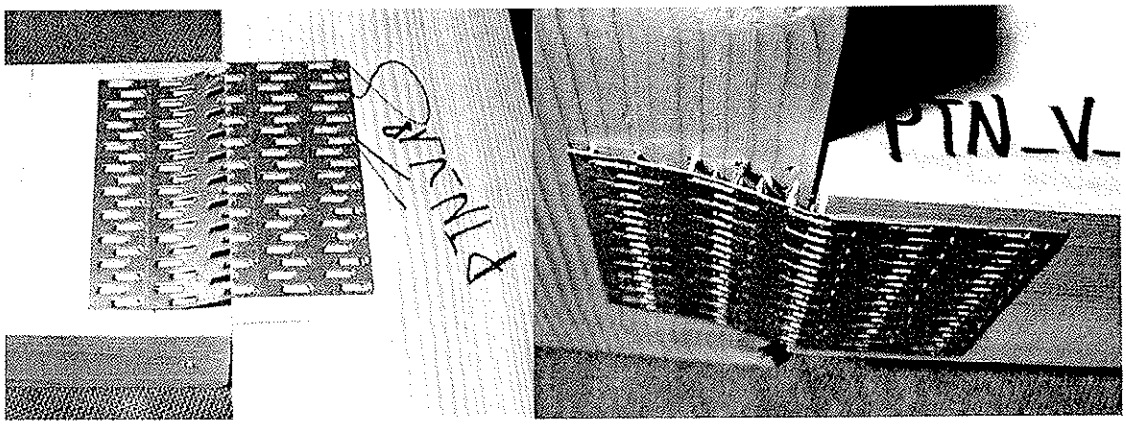

Figure 5: Truss plate deformation and subsequent withdrawal failure of nails close to the joint line.

Table 1 shows the shear capacity f_{ax} per mm joint line for different punched metal plate fasteners of different producers together with some plate properties and the bite used in the tests. The ultimate load of each test was modified with regard to a characteristic density of 350 kg/m³ by multiplying F_{max} with

$$\eta_H = (350/\rho_N)^c \tag{9}$$

ρ_N is the average normal density of the two timber members of the connection and c is a factor taking into account the influence of the density on the ultimate load. The size of c depends on the type of loading and the shape of the nails in the punched metal plate fastener. For the anchorage capacity parallel to the punched metal plate fastener (nails in shear), values between 0,25 and 0,5 are found in tests. Here, the number of tests was not sufficient to estimate c, hence c = 2 was assumed in accordance with Eurocode 5 Part 1-1 8.3.2 (6) for the withdrawal parameter of smooth nails.

Table 1 Shear test results for different punched metal plate fasteners

Nail plate	A1	A2	B1	B2	B3	C1	D1	D2	E1	E2	E3	E4
$f_{ax,mean}$ N/mm	17,0	27,3	14,0	17,5	24,0	31,6	25,3	17,2	38,2	27,1	32,3	31,1
COV	0,04	0,07	0,22	0,24	0,35	0,28	0,12	0,18	0,22	0,24	0,27	0,11
Nail length mm	8,2	14,0	8,3	9,1	21,0	19,5	20,2	8,5	20,2	20,2	8,5	13,9
Plate thickness	1,00	1,50	1,00	1,50	2,00	2,00	2,00	0,99	2,00	1,50	1,00	1,25
Area/nail mm²	81	122	88	67	350	279	317	90	315	315	81	100
Bite mm	62,5	56,0	54,5	65,5	69,0	65,5	49,0	48,5	49,0	49,0	50,0	74,0

There is no clear relation between the shear capacity per unit length perpendicular to the truss plate and nail length, plate thickness or nail density. Consequently, the shear capacity

of punched metal plate fasteners perpendicular to the truss plane has to be determined by tests for each plate.

For simultaneous loading parallel and perpendicular to the punched metal plate fastener, a linear interaction is proposed, similar to the rule for combined laterally and axially loaded smooth nails in Eurocode 5.

$$\frac{\tau_{F,d}}{f_{a,\alpha,\beta,d}} + \frac{s_{ax,d}}{f_{ax,d}} \leq 1 \qquad (10)$$

where:

$\tau_{F,d}$ design anchorage stress

$f_{a,\alpha,\beta,d}$ design anchorage capacity per unit area

$s_{ax,d}$ design shear load per unit length perpendicular to the punched metal plate fastener

$f_{ax,d}$ design shear capacity per unit length perpendicular to the punched metal plate fastener

4 Design proposal

Eurocode 5 9.2.1 should be complemented as follows:

All joints should be capable of transferring a force $F_{r,d}$ acting in any direction within the plane of the truss. $F_{r,d}$ should be assumed to be of short-term duration, acting on timber in service class 2, with the value:

$$F_{r,d} = 1,0 + 0,1\ell \qquad (9.18)$$

Where $F_{r,d}$ is in kN and ℓ is the overall length of the truss, in m.

The design situation transport and erection may be assumed to be accounted for if the conditions (9.19) to (9.22) are fulfilled.

The member width shall fulfil the following condition:

$$b \geq \frac{1,5 \cdot \ell^2}{f_{m,k}} \quad \text{in mm} \qquad (9.19)$$

where ℓ is the total truss length in m and $f_{m,k}$ the characteristic bending strength in N/mm².

The apex joint and the splice joints of upper and lower chord should have a sufficient plate capacity to transfer a tensile force $F_{t,d}$ acting perpendicular to the joint line within the plane of the truss, with the value:

$$F_{t,d} = 0,5 \cdot h \cdot \ell^2 \quad \text{in kN} \qquad (9.20)$$

where h is the chord depth and ℓ is the total truss length in m.

The apex joint and the splice joints of upper and lower chord should have a sufficient anchorage capacity to simultaneously transfer a tensile force $F_{t,d}$ acting perpendicular to the joint line within the plane of the truss and a shear force V_d acting perpendicular to the truss plane. $F_{t,d}$ and V_d should be assumed to be of very short-term duration, acting on

timber in service class 2. $F_{t,d}$ is calculated according to equation (9.20) and V_d has the value:

$$V_d = 2{,}3 \cdot b \cdot h \cdot \ell \quad \text{in kN} \tag{9.21}$$

where b is the chord width in m.

The following expression should be satisfied:

$$\frac{\tau_{F,d}}{f_{a,\alpha,\beta,d}} + \frac{s_{ax,d}}{f_{ax,d}} \leq 1 \tag{9.22}$$

where:

$\tau_{F,d}$ design anchorage stress

$f_{a,\alpha,\beta,d}$ design anchorage capacity per unit area

$s_{ax,d}$ design shear load per unit length perpendicular to the punched metal plate fastener,

$s_{ax,d}$ $= V_d/\ell_s$, where ℓ_s is the length of the joint line covered by the plate,

$f_{ax,d}$ design shear capacity per unit length perpendicular to the punched metal plate fastener

5 Summary

This paper presents a design proposal for the design situation transport and erection of trusses with punched metal plate fasteners. Although Eurocode 5 contains minimum loads within the truss plane for connections in trusses which are independent of the loads for the permanent design situation, these minimum loads are considered insufficient especially for larger span trusses. During transport and erection, unintentional loads occur, leading to bending moments and shear forces also perpendicular to the truss plane predominantly in the truss chord members.

The background of the proposed design is a situation, where a truss lying on a horizontal basis is lifted at the apex. A simplified analysis of the chords as continuous beams on three supports leads to bending moments and shear forces perpendicular to the truss plane to be considered in truss design. Apart from significantly larger minimum loads for the truss connections in the upper and lower chords, a minimum timber member width results from the design proposal.

Since the plate and anchorage capacities in Eurocode 5 do not provide load-carrying capacities for loads perpendicular to the truss plane, a test method is shown for providing the necessary capacities. While the bending moment from loads perpendicular to the truss plane only cause stresses parallel to the punched metal plate fasteners and hence may be considered in design with the capacities listed in Eurocode 5, the shear forces perpendicular to the truss plane necessitate a new resistance property f_{ax} of punched metal plate fasteners which is to be determined by tests for each type of fastener.

For the design of the connections between diagonals and chords, the design rules in Eurocode 5 are considered sufficient.

INTERNATIONAL COUNCIL FOR RESEARCH AND INNOVATION
IN BUILDING AND CONSTRUCTION

WORKING COMMISSION W18 - TIMBER STRUCTURES

DESIGN OF SAFE TIMBER STRUCTURES
HOW CAN WE LEARN FROM STRUCTURAL FAILURES?

S Thelandersson
E Frühwald

Div. of Structural Engineering
Lund University

SWEDEN

MEETING FORTY
BLED
SLOVENIA
AUGUST 2007

Presented by S. Thelandersson
R. Zarnic supposed suggestion about count of consequence as a requirement and the probability that something will be done should be higher.
U. Kuhlmann stated that Cost action started on this issue of robustness and invite interested to participate. Example includes joint ductility and redistribution of load to account for robustness. S. Thelandersson stated that he is fully aware of the Cost action.
T. Williamson stated that in US the number of statistics will be different. Largest errors are construction. Since the Northridge earthquake, the seismic part of the code has been upgraded. Wind loads have also been upgraded.
I. Smith stated that robustness consideration began in the 60's and 70's. Insurance companies do not differentiate between materials. Design code considers single member rather than system behaviour.
P. Quenneville mentioned that newspaper article on railing failures indicated not due to faulty material.
H. Gehri stated that it is good to hear no failure due to code as the code is for verification of design. There is a need to define robustness, redundancy, and ductility in code. S. Thelandersson agreed.
P. Paevere questioned whether the loads are biased which may give designers a bad name. S. Thelandersson stated one example is failure in Denmark was due to the structure's dead weight. P. Paevere said that earthquakes have not been considered. S. Thelandersson stated that they are not important for N. Europe.

Design of safe timber structures

How can we learn from structural failures?

Thelandersson S., Frühwald, E.

Div. of Structural Engineering, Lund University, Sweden

1 Introduction

When implementing Eurocode 5 the level of safety for timber structures is re-evaluated in many European countries in national application rules. This has raised the question whether the current level of safety for timber structures is appropriate in relation to e.g. steel and concrete structures. A similar debate has also been initiated as a consequence of several spectacular failures in timber buildings e.g. in the Nordic countries and Germany, during recent years.

As an example, in January 2003, the glulam truss roof of a bicycle velodrome in Denmark collapsed, see Fig. 1. Two main roof trusses fell down in spite of the fact that there was no snow load at all on the roof [1, 2]. The investigation [1] of the failure revealed that the main cause was multiple errors related to the structural analysis and conceptual modelling of the primary structure. This event created a heated debate in Denmark concerning quality assurance and control systems in the building process. Minor quality deficiencies of the glulam used in the structure were also revealed in the investigation, but these were found to be irrelevant for the occurrence of failure.

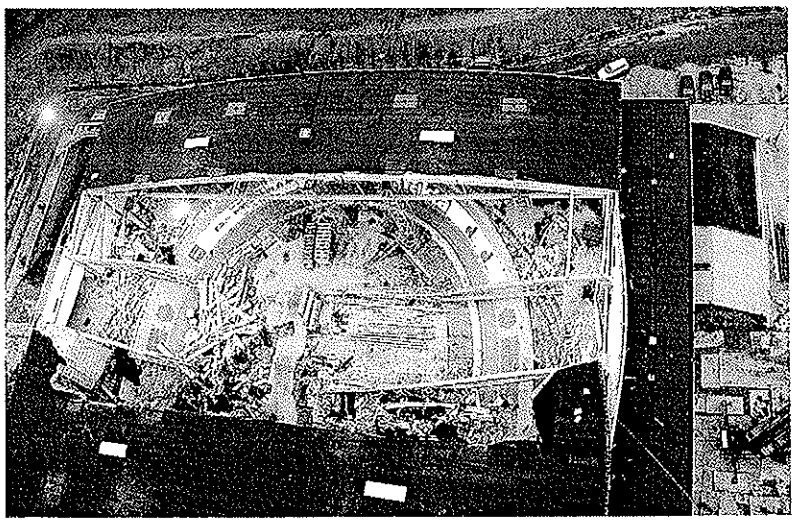

Fig. 1. Photo taken from above after the failure of bicycle arena roof.

It is clear that events of the type described above are negative for the competitiveness of timber on the construction market. The question is what can be done to reduce the risk for failure in timber structures in the future. For this purpose a comprehensive survey and analysis of failures in timber structures have been made as a part of a Swedish-Finnish research program. The main hypothesis for the work has been that quality assurance, control systems and improved training may be necessary, since previous investigations of structural failures in general conclude that structural damage is primarily related to gross human errors, ignorance and carelessness [3]. The present paper summarises the results from this survey with an analysis of the underlying causes and associated conclusions and recommendations. A full report on the survey is available, see reference [4].

More specific, the objectives for undertaking the survey of building failures were to get a picture of

- the underlying reasons for observed failures
- which type of components are most prone to failure
- which failure modes are most frequent
- what can be done to avoid or reduce failures

Many similar surveys for building structures in general and for all structural materials can be found in the literature. A general conclusion from such studies is that failure almost without exception occurs due to human errors. Kaminetzky [3] suggested that human errors can be divided into three categories:

1. Errors of knowledge (ignorance)
2. Errors of performance (carelessness and negligence)
3. Errors of intent (greed)

Ellingwood [5] compiled results from a series of investigations during the years 1979-1985 to identify where in the building process errors occur. Although the classification of errors is not fully comparable among different investigators, the results are quite revealing. The occurrence of errors are of the same order of magnitude for design/planning and construction respectively, with slightly higher frequency for the design phase. Failures due to material deficiencies or maintenance are relatively uncommon.

A comprehensive failure survey was performed by Matousek & Schneider [6], who investigated 800 cases from different sources. Among other things, they performed a further analysis of the character of the mistakes for those cases where errors were made in planning and design. The result of this is shown in Table 1. It is interesting to note that a majority of mistakes is related to conceptual errors and structural analysis. Incorrect assumptions or insufficient consideration of loads and actions was found to be a common type of error.

Rather few cases related specifically to timber structures are found among the failure investigations published in the literature. The conclusion from this is not necessarily that timber structures are "safer" than structures from other materials. A more probable explanation is that failure cases related to timber structures have been included only to limited extent in the data material collected in previous investigations.

However, special investigations of failures in timber structures are found in references [7-9], but these are rather limited and usually do not allow general conclusions to be drawn. Dröge & Dröge [7] describe 31 cases in a rather detailed manner. From their investigation

Table 1. Characteristics of errors made in the planning and design phase [6].

Type of error	Percentage by number of 295 damage cases.
Conceptual errors	34
Structural analysis	34
Drawings and specifications	19
Work planning and preparation	9
Combinations	4
Total	100

the following technical causes of damage which occur in timber structures can be identified.

- Inadequate behaviour of joints
- Effects of moisture exposure (imposed strains, shrinkage)
- Poor durability performance
- Inadequate bracing of structural system
- Inadequate performance of material and products
- Inadequate appreciation of loads

2 Methodology for present survey

The concept of failure considered in the present project is mainly related to the ultimate limit state and not to loss of serviceability. Thus, failures are defined as events which directly or indirectly have or could have implied risk for human lives. A total of 127 failure cases were included in the survey. The data material used in the project was collected in different ways. In about half of the cases, direct information on failure cases including documented investigations of the failure events and their causes were provided by project participants who had been assigned to investigate failures. The rest of the cases were taken from literature, where failure cases and analysis of their causes have been presented mostly based on investigation work performed by others. Although, this makes the information more indirect, leading to increased risk of misinterpretation, such cases were included to broaden the sample size, provided they were deemed to be sufficiently documented.

As in other failure surveys presented in the literature, the sampling process is difficult, since many failures are either not investigated or the results from investigations are not publicly available. Thus, the results from the present survey, like other failure surveys performed before this one, cannot be interpreted as a random sample representative for the building practice. The study comprises mostly failure cases from Scandinavia (Sweden, Finland and Norway) as well as Germany and United States.

A short summary of each of the investigated failure cases is given in the full report [4]. This summary gives the most basic facts about each case together with an evaluation of the main reason for the failure event as it is interpreted by the investigator or reporter.

3 Survey results and interpretation

3.1 Primary cause behind the failure event

For each case in the study, one cause or sometimes several causes of failure were identified. The different types of errors were classified with respect to the following nine categories:

1. Wood material performance:
   By this is meant that the materials used in the product have been of poor quality in relation to practice. An example is larger knots than permitted in glulam laminations.
2. Manufacturing errors in factory:
   This relates to manufacturing errors, which should have been detected in the production according to practice and internal quality control. An example is poor bonding quality of finger joints in glulam.
3. Poor manufacturing principles:
   This means that the basic principle used for manufacturing the product has been poor. However, the poor principle has been used as intended.
4. On site alterations:
   Here, alterations of the structure have been made on site. These alterations have led to the failure. Note that it is often difficult to know whether these alterations were intended from start, or made on site for practical reasons.
5. Poor design/lack of design with respect to mechanical loading:
   This means that the failure was due to errors in the strength design of the structure (design method). In this category only mechanical loading is considered.
6. Poor design/lack of design with respect to environmental actions:
   This means that the failure was due to errors in strength design but the failure was caused by mechanical loading in combination with environmental actions (e.g. drying cracks, shrinkage effects and durability damage).
7. Poor principles during erection:
   Failures, which are due to poor handling at the erection of the structure, are grouped in this category.
8. Overload in relation to building regulations
9. Other/unknown reasons

In 44 out of the 127 cases, the failure could not be related to one single error but to two or three types of errors, which sometimes could be seen as primary and secondary causes. For each case where multiple errors were identified the evaluator made an estimate of the weight of each type of error causing the failure event. As an example a certain case could be assigned with weight 0.6 to category 5, "poor design" and weight 0.4 to category 4, "on site alterations" with the sum for each case always being 1.0.

The results from the classifications of errors leading to failure are presented in Table 2. The first column shows the distribution of the nine error categories for all the 127 failure cases expressed as percentages of weighted classifications. It can be seen that the most common

Table 2. Distribution of errors causing failure in the present study.

		% of failure cases Causes classified by weight					Gross number of identified causes without weights (in % of failure cases)
Failure category		**All**	**LTH**	**VTT**	**SP**	**AE**	**All**
1	Wood material performance	1.5	1.3	3.3	0.0	0.0	3.9
2	Manufacturing errors in factory	5.4	3.0	6.0	16.7	0.0	7.9
3	Poor manufacturing principles	4.2	0.6	5.0	18.9	0.0	5.5
4	On-site alterations	12.5	9.9	26.3	7.2	0.0	19.7
5	Design (mechanical loading)	41.5	44.2	38.7	30.6	50.0	54.3
6	Design (environmental loading)	11.4	11.9	12.7	12.2	4.2	16.5
7	Poor principles during erection	14.1	20.9	3.3	7.8	12.5	19.7
8	Overload	4.4	4.8	4.7	5.6	0.0	7.1
9	Other / unknown	5.1	3.4	0.0	1.1	33.3	7.1
Total %		100	100	100	100	100	142
Number of cases		127	67	30	18	12	

cause of failure is related to design. Forty-one percent of the investigated failures are caused by poor design or lack of strength design. Other important failure causes are poor principles during erection (14.1%), on-site alterations (12.5%) and insufficient or lacking design with respect to environmental actions (11.4%). In total, about half of the failures are caused by the designer (deficiencies in design for strength and/or environmental actions). About one fourth of the failures are caused by the personnel working at the building site (on-site alterations, poor principles during erection). This means that wood quality, production methods and principles only cause a small part (together about 11%) of the failures. The problem is therefore not the wood material, but engineers and workers in the building process. This picture is similar to that found from other failure investigations for other types of structures (mostly steel and concrete), where human errors were found to be the dominating cause behind failure events. This is shown in Table 3, where the percentages of main failure causes from the present study are compared with corresponding data for steel and concrete structures found in references [10] and [11], respectively. For timber structures an additional element may be that many building professionals are less skilled in design of more advanced wood structures. However, whether this is true or not, can not be deduced from the present investigation.

Table 3: Failure causes (in % of cases) for different building materials. Data from own survey as well as from the literature.

Failure cause	**Timber [present survey]**	**Steel [10]**	**Concrete [11]**
Design	53	35	40
Construction process	27	25	40
Maintenance /reuse		35	
Material/manufacturing	11		
Other	9	5	20

The collection of failure cases originates from four main sources labelled LTH, VTT, SP and AE. The material from each of these four sources may be different since the sub-samples are different and the analysis of the cases and the classification was made by different persons. Therefore, the distribution of failure causes for these sub samples are also presented in Table 2.

A few of the 127 failure cases can be seen as typical failures representing a number of similar buildings which failed in the same way and for the same reasons. Such cases have been included as one case in the data base in order not to bias the sample. One example is a case, which describes failures in old glulam beams manufactured in the 1960ies with a cold setting acid-curing adhesive, which had insufficient durability and is sensitive to moisture. The case was classified as type 3, "Poor manufacturing principles". This single case represents 20 similar buildings in Sweden, which all were identified shortly after the first failure cases were detected. If all parallel cases were included in the study the total amount of failure cases would amount to 179. If all 179 cases are included in the data base the general picture of error types does not change, except for the category "Poor manufacturing principles". The latter is explained by the fact that the above mentioned case represents 20 similar events.

3.2 Type of structural element involved in the failure

The types of structural element or joint involved in the failures are presented in Table 4. In many cases more than one type of element is involved in a single case. Therefore, the sum of percentages in Table 4 is significantly larger than 100. Beams, trusses and bracing are the most frequent structural elements used in roof structures and also most frequent in the failure cases studied. Especially in the case of failure of trusses, almost all failures are caused by insufficient or absent bracing and poor principles during erection. Beams, especially curved beams and double-tapered beams with loads generating tension stresses perpendicular to the grain but also to large extent straight beams, are dominant in the list of failures.

Joints were involved in the failure event in 23 % of all cases. Table 5 shows which type of joints were used in the cases where joints contributed to failure. Dowel-type joints are dominant, both in terms of their use in structures and among the failure cases.

Table 4. Type of structural element that failed.

Type of structural element	Percentage of cases
Beam	47
Truss	34
Bracing	29
Joint	23
Arch	8
Column	4
Frame	2
Total %	147

Table 5. Type of joint that failed.

Type of joint	Percentage of cases
Dowel-type	57
Punched metal plate	10
Glued	7
Other	27
Total %	101

3.3 Failure modes involved in the investigated cases

In Table 6 the distribution of failure modes identified in the investigated cases are presented. It can be seen that instability is a very dominant failure mode. This means that the collapse/failure was caused by insufficient/absent bracing, which led to buckling, or material failure. Bending failures and tension perpendicular to grain failures are also common.

3.4 Age of the structure at the time of failure

There is a correlation between failure mode and the age of the structure at the time of failure. About 19 % of the failure cases compiled in this study occurred during erection, about a third (34 %) during the first three years after completion and the rest later on, see Table 7. Very remarkable is that about 21 % of the structures failed during the first year after completion. The average age at failure is 7 years. Some failures occured after 30 to 40 years, but only few cases with failures due to long-term behaviour such as duration of load behaviour, decay and corrosion were found among the cases in this investigation. Such cases are probably more frequent in practice.

Table 6. Failure modes.

Failure mode	Percentage of cases
Instability	30
Bending failure	15
Tension failure perpendicular to grain	11
Shear failure	9
Drying cracks	9
Excessive deflection	7
Tension failure	5
Corrosion of fasteners / decay	4
Withdrawal of fasteners	3
Compression	2
Other / unknown	21

Table 7. Time of failure (age known for 87 cases, i.e. 69 % of all cases).

Time of failure	Percentage of cases
During construction	18.6
During the first 3 years	33.7
After 3 years or later	47.7

4. Summary and conclusions

4.1 How can we learn from previous failures?

The majority of the failures compiled in the present study could have been avoided if available knowledge had been utilised in a correct way. About half of the failures are caused by errors in design or lack of design. One quarter of the failures was due to errors made on the building site. The study more or less confirms the conclusion made by many others that for structures of all types of materials, almost all failures occur due to gross human errors.

Failures due to human errors can not be counteracted by increasing safety factors or safety levels in structural codes. None of the failures were caused by unfavourable combinations of random events. Thus, there is no evidence from the present investigation that the safety level for timber in structural codes is inadequate.

The risk of human errors can be reduced by improving building process management, control as well as training and education. Such measures should be especially focussed on those technical aspects found to be the most common causes of failures. Training of engineers and control in the design phase should have high priority, since the present investigation shows that most errors are made in this phase. Some of the issues which should be emphasised are

- Bracing to avoid instability problems both in the finished structure and during construction.
- Situations with risk for perpendicular to grain failure
- Consideration of moisture effects
- Design of joints

It is difficult to understand why the first one, see Fig. 2 relating to bracing, should be a problem at all. Engineers should have sufficient knowledge about the basic behaviour of load bearing structures, to be able to estimate the risk for lateral stability. This issue is not specific for timber structures.

An important task for future research in timber engineering should be to develop methods to design robust structural systems, which are less sensitive to failure of single elements in the system and where the consequences of unforeseen events such as human errors and accidental loading are reduced.

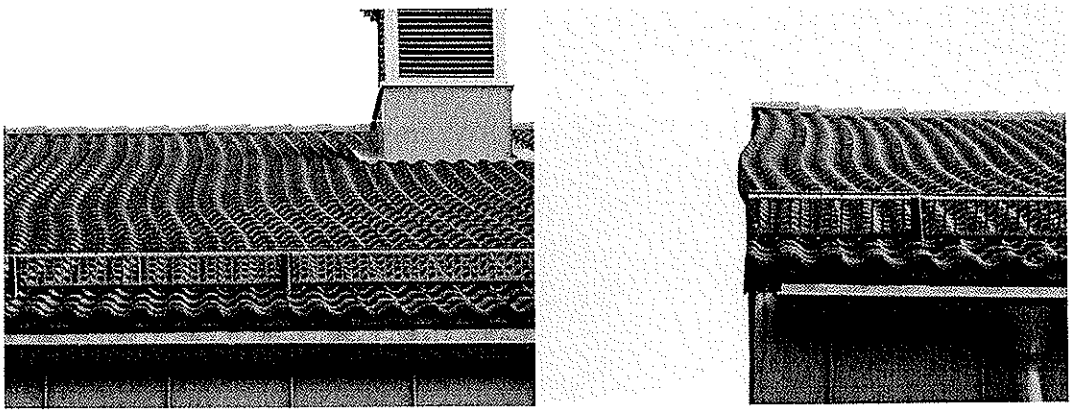

Figure 2. Deformations in roof due to lateral buckling of top chord of roof trusses

References

[1] Thorup, P.M., Larsen H.J. Skønserklæring Ballerup Superarena. In Danish. March 2003.

[2] Hansson M., Larsen H.J. Recent failures in glulam structures and their causes, Engineering Failure Analysis, Elsevier, 12(2005), pp 808-818.

[3] Kaminetzky D. Design and Construction Failures – lessons from forensic investigations. McGraw-Hill, New York, 1991.

[4] Frühwald, E., Serrano, E., Toratti, T., Emilsson A., Thelandersson, S. Design of safe timber structures – How can we learn from structural failures in concrete, steel and timber. Report TVBK-3053, Div. of Struct. Eng. Lund University, 2007.

[5] Ellingwood, B. Design and construction error effects on structural reliability. ASCE, J. of Structural Engineering, 13, no. 2, 1987, pp. 409-422.

[6] Matousek, M., Schneider J. Untersuchungen zur Struktur des Sicherheitsproblemes bei Bauwerken. Inst. für Baustatik und Konstruktion, ETH, Zurich, 1976.

[7] Dröge, G., Dröge, T. Schäden an Holztragwerken. Schadenfreies Bauen, Band 28, Fraunhofer IRB Verlag, Stuttgart 2003.

[8] Mönck, W., Erler, K. Schäden an Holzkonstruktionen. Huss-Medien GmbH, Verlag Bauwesen, 4th Ed., Berlin 2004.

[9] Colling F. Lernen aus Schäden im Holzbau - Ursachen, Vermeidung, Beispiele. Deutsche Gesellschaft für Holzforschung. Fraunhofer IRB Verlag, Stuttgart 2000.

[10] Oehme P., Vogt W. Schäden an Tragwerken aus Stahl. Schadenfreies Bauen, Band 30. Fraunhofer IRB Verlag, Stuttgart 2003.

[11] Brand, B., Glatz, G. Schäden an Tragwerken aus Stahlbeton. Schadenfreies Bauen, Band 14, 2nd Ed. Fraunhofer IRB Verlag, Stuttgart 2005.

INTERNATIONAL COUNCIL FOR RESEARCH AND INNOVATION
IN BUILDING AND CONSTRUCTION

WORKING COMMISSION W18 - TIMBER STRUCTURES

EFFECT OF TRANSVERSE WALLS ON CAPACITY OF WOOD-FRAMED WALL DIAPHRAGMS – PART 2

U A Girhammar
Civil Engineering, Faculty of Science and Technology
Umeå University

B Källsner
Växjö University
SP Trätek – Technical Research Institute of Sweden

SWEDEN

MEETING FORTY

BLED

SLOVENIA

AUGUST 2007

Presented by U.A. Girhammar
F. Lam commented that one should also consider the deformation aspect as it is important in terms of damage and drift demand in earthquake. In particular the claim that one can rely on the transverse walls to replace hold-downs needs to be refined for earthquake applications. U.A. Girhammar replied that this is intended only for monotonic loads and not for earthquakes.
I. Smith stated that test of actual building shows the importance of rigidity of upper and lower floors. He aggress with F. Lam's comment that tie down situation will need to consider both elastic end as well as plastic end. U.A. Girhammar agreed.
E. Karacabeyli received explanation from U.A. Girhammar of example of when to use fix end and when to use free end. H. Blass commented it would be safe to assume free end in design.
R. Zarnic received explanation from U.A. Girhammar about the test set up boundary condition and the real situation is a combination of both free and fix ends.
N. Chun commented that fl does not reach fp. Panel closest to one end may fail before the end panel reaches fp. U.A. Girhammar replied that the model already considered this issue.

Effect of Transverse Walls on Capacity of Wood-Framed Wall Diaphragms – Part 2

Ulf Arne Girhammar
Department of TFE – Civil Engineering, Faculty of Science and Technology,
Umeå University, Sweden

Bo Källsner
School of Technology and Design, Växjö University, Sweden
SP Wood Technology – Technical Research Institute of Sweden

Abstract

It is well known that the structural behaviour of a wood-framed wall diaphragm is to a large extent dependent on the 3-dimensional behaviour of the whole building. In this connection the influence of transverse walls is an issue of special interest.

A plastic design method capable of analyzing the behavior and capacity of partially anchored wood-framed wall diaphragms has been presented in previous papers. In a previous paper (Girhammar & Källsner, 2006), the plastic model was applied to the case where a wall diaphragm is connected to a transverse wall. The tying-down effect of the transverse wall on the vertical uplift was studied and the effect on the horizontal load-bearing capacity of the wall diaphragm was analyzed. Tests were conducted to evaluate the strength of these transverse walls when the top rail was free to displace horizontally. In this paper a corresponding study of transverse walls, but now when the top rail is fixed with respect to horizontal displacement, is presented. Also, a more general description of the analytical model is given.

The paper describes the theoretical analyses and the experimental results for sheathed wood-framed transverse walls of different number of sheet segments and with fixed top rails. The effect of the tying-down action of transverse walls on the load-carrying capacity of wall diaphragms and the agreement between theoretical and experimental results is presented.

1 Introduction

1.1 Background

The structural behaviour and capacity of wall diaphragms are primarily dependent on the sheathing-to-timber joints, the anchorage of the studs, the size and position of the vertical loads, and on the transverse walls and the inter-component connections between the wall diaphragms and the surrounding structures. Due to the conditions for stud anchoring and the action of vertical loads on the studs, the wall diaphragm will behave as fully or partially anchored. A new plastic method capable of analyzing the behaviour and capacity of both, with respect to vertical uplift, fully and partially anchored wood-framed wall diaphragms frequently used in practice has been presented in previous papers; see e.g. Källsner and Girhammar (2005). The method covers static loads and can be applied when mechanical fasteners with plastic or partially plastic characteristics are used.

It is well known that the structural behaviour of a wood-framed wall diaphragm is to a large extent dependent on the 3-dimensional behaviour of the whole building. In this connection the influence of transverse walls is an issue of special interest. These transverse walls, connected to the wall diaphragms, may have the corresponding restraining effect on the vertical uplift of the wall diaphragms as tying-down devices or vertical loads. This tying-down effect will depend on the strength and stiffness of the transverse wall itself as well as on the inter-component connection between the two walls. In this paper, attention is given to the capacity of the transverse wall itself.

1.2 Objective and scope

The overall purpose of the research project is to develop an analytical method for the design of wood-framed wall diaphragms in the ultimate limit state with different anchoring, loading and geometrical conditions and with different sheet and framing materials, and fasteners used.

The objective of the previous paper (Girhammar & Källsner, 2006) and this paper is to describe the theoretical analyses and the experimental results for sheathed wood-framed transverse walls of different geometrical configurations and with different boundary conditions. Transverse walls are studied by varying the number of sheet segments and the horizontal fixing of the top rail. The extreme case of horizontally free top rail was studied in that previous paper and the other extreme case of horizontally fixed top rail will be object of this paper. The effect of the tying-down action of transverse walls on the load-carrying capacity of wall diaphragms and the agreement between theoretical and experimental results will be presented.

The purpose of this paper is also to investigate the effect of transverse walls on the load-carrying capacity of partially anchored wood-framed wall diaphragms and to give some design recommendations.

In this paper, the plastic model is applied to the transverse wall and its tying-down effect on the vertical uplift and the effect on the horizontal load-bearing capacity of the wall diaphragm is analyzed. In an ongoing study, tests are being conducted to evaluate the strength and stiffness of these transverse walls and to enable a verification of the analytical results. Here it will be assumed that the build-up of the transverse walls and the wall diaphragms is similar. Only the tests on transverse walls with fixed top rail will be included here.

2 Testing program

2.1 Specification of transverse walls tested

Tests on sheathed wood-framed transverse walls of different geometrical configurations and with different boundary conditions subjected to a vertical uplifting force have been conducted. The testing arrangements are shown in Figure 1.

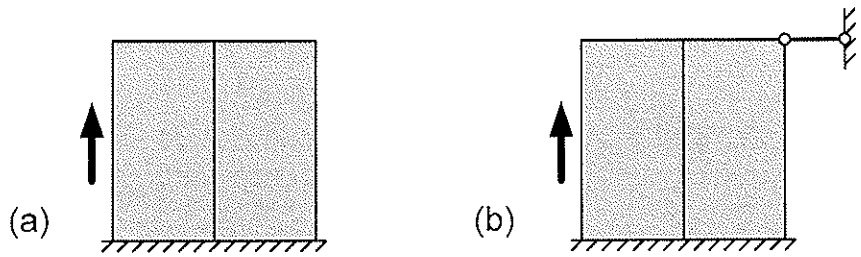

Figure 1. Testing of transverse walls subjected to vertical uplift and (a) top rail free to displace horizontally and (b) top rail fixed against horizontal displacement.

One series refers to transverse walls with different numbers of sheet segments and the top rail free to displace horizontally, series 1. That series was reported on in the previous paper (Girhammar & Källsner, 2006). The other series refers to transverse walls with different numbers of sheet segments and the top rail fixed against horizontal displacement, series 2. This series will be addressed in this paper. The free and fixed top rail, respectively, constitute the extreme cases for the behaviour of transverse walls in practice. The different tests for series 2 are summarized in Table 1.

Table 1. Specifications of transverse walls tested. Bottom rail was fully anchored to the substrate in all tests.

Series	Configuration	Boundary conditions	Number of tests
2a	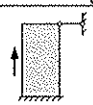	Top rail fixed against horizontal displacement	5
2b	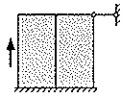		5

2.2 Specification of sheathing-to-timber joints tested

For the one segment transverse walls, the sheathing-to-timber joints were tested using the same bottom rail as used in each of the full scale wall test specimen. The tests on the plastic capacity of the sheathing-to-timber joints were performed on single nail test specimens.

For the two segment transverse walls, no detailed joint tests were performed using the same bottom rails as used in the full scale wall tests. Instead, the values for the plastic shear capacity of the sheathing-to-timber joints used were those obtained in an earlier study, see Girhammar et al. (2004).

2.3 Test specimens and testing procedure

All walls and joints tested were made of sheathing fastened to a timber frame. Only one side of the frame was sheathed. The test specimens were designed as follows:

- Frame members: Pine (Pinus Silvestris), C24, 45×120 mm, stud spacing 600 mm.
- Sheathing: Hardboard, 1200 × 2400 × 8 mm (wet process fibre board, HB.HLA2, Masonite AB).
- Sheathing-to-timber joints: Annular ringed shank nails, 50×2.1 mm (Duofast, Nordisk Kartro AB). The joints were hand-nailed and the holes were pre-drilled, 1.7 mm. Nail

spacing was 100 mm along the perimeter and 200 mm along the vertical centre line of the sheets. Edge distance was 11.25 mm along the vertical studs and 22.5 mm along the bottom and top rails.

- Framing joints: Two annular ringed shank nails of dimension 90×3.1 mm were applied in the grain direction of the vertical studs.

All wall and joint tests were performed under displacement control with a constant rate of 8 and 2 mm/min, respectively. The vertical load was applied as a tension force along the side of the leading stud of the wall. The horizontal displacement and the reaction force were measured at the centre of the top rail for the two tests series, respectively. The bottom rail was anchored against vertical uplift to the substrate along the entire length of the wall.

For each test, the density and moisture content were determined and a choice of fasteners was tested with respect to the bending yield stress. However, these results are not yet available.

3 Test results for transverse walls and sheathing-to-timber joints

3.1 Transverse walls with top rail fixed against horizontal displacement

The test results for transverse walls with one and two sheet segments and top rail fixed against horizontal displacement are summarized in Table 2. A ductile type of joint failure by yielding and withdrawal of nails from the bottom rail took place, where the main direction of the nail forces was essentially perpendicular to the bottom rail, especially the segment most to the right. The final failure mode of the wall was ductile.

Table 2. Test results for transverse walls with different number of sheet segments and top rail fixed against horizontal displacement. Aspect ratio h/b = 2.

Series 2	Maximum load in different tests [kN]	Mean value of maximum load [kN]	Coefficient of variation [%]
One segment: Wall A – E	16.1, 17.3, 14.7, 15.7, 12.9	15.3	10.7
Two segments	17.4, 25.6, 21.5, 21.6, 20.8	22.4	13.0

3.2 Sheathing-to-timber joints in one segment transverse walls

The results for the sheathing-to-timber single joint tests with bottom rails from the one segment transverse walls are summarized in Table 3. A ductile type of joint failure by yielding and withdrawal of nails from the bottom rail took place in all tests, except one failure in Wall B (1.34 kN; nail rupture).

Table 3. Test results for sheathing-to-timber joints with bottom rails from one segment transverse walls.

Series 1	Maximum load in different tests [kN]	Mean value of maximum load [kN]	Coefficient of variation [%]
Wall A	1.19, 1.14, 1.19	1.18	2.5
Wall B	1.48, 1.34, 1.51	1.43	7.7
Wall C	1.21, 1.15, 1.10	1.16	4.8
Wall D	1.07, 1.20, 1.10	1.12	6.0
Wall E	1.05, 0.840, 1.03	0.974	12.0
	Mean value of all series	1.17	14.0

The relation between the mean value of the maximum load of the sheathing-to-timber joints in the different walls in Table 3 and the corresponding maximum load for each individual one segment wall in Table 2 is shown in Figure 2.

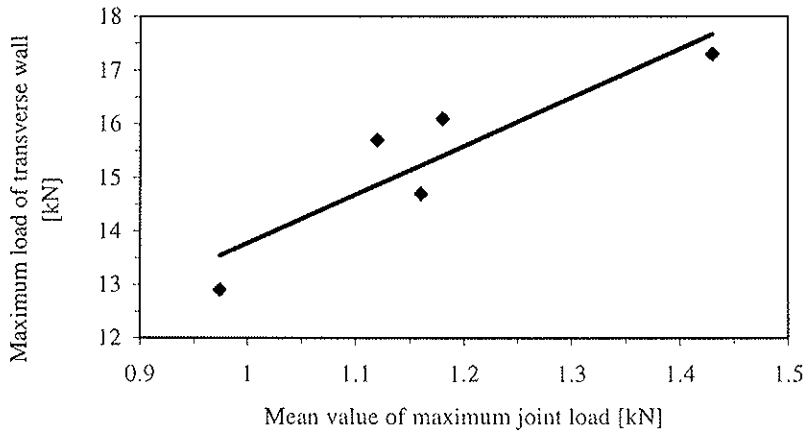

Figure 2. Relationship between load capacity of sheathing-to-timber joints and load capacity of one segment transverse walls.

4 Analytical model

4.1 Basic assumptions

For the analytical evaluation of the capacity of the partially anchored transverse walls subjected to vertical uplift a plastic lower bound method is proposed. This means that a force distribution is chosen that fulfils the conditions of force and moment equilibrium for each timber member and sheet. The analysis is based on a true plastic lower bound method and corresponds to the plastic method with the internal equilibrium regarded as presented in the previous paper, Girhammar & Källsner (2006). The influence of the framing joints is neglected.

In order to obtain simple expressions for the capacity of the transverse walls, the fastener forces are assumed continuously distributed along the timber members. The load-carrying capacity of the sheathing-to-timber joints is consequently given in force per unit length. In all the examples presented below, it is assumed that the fastener spacing around the perimeter of the sheets is constant.

4.2 Vertical load-bearing capacity

4.2.1 General

Consider the transverse wall diaphragm of three segments according to Fig. 3a. At the left end of the transverse wall, it is connected to a shear wall perpendicular to the transverse wall and subjected to a vertical load, V, due to the uplifting of the shear wall. The force equilibrium of the different segments is illustrated in Fig. 3b. The transferred force per unit length of the sheathing-to-timber joints along the bottom rail with a direction ϕ_i is denoted f_i. Its ultimate plastic capacity is denoted by f_p. The force transfer of the framing joints is neglected. The left segment is restrained by the vertical force, V_{R1}, due to the restraining effect of the other segments. The value of V_{R1} depends on the number of segments in the transverse wall. The total horizontal force along the top rail (H) equals the reaction force in the top rail fixed against horizontal displacement.

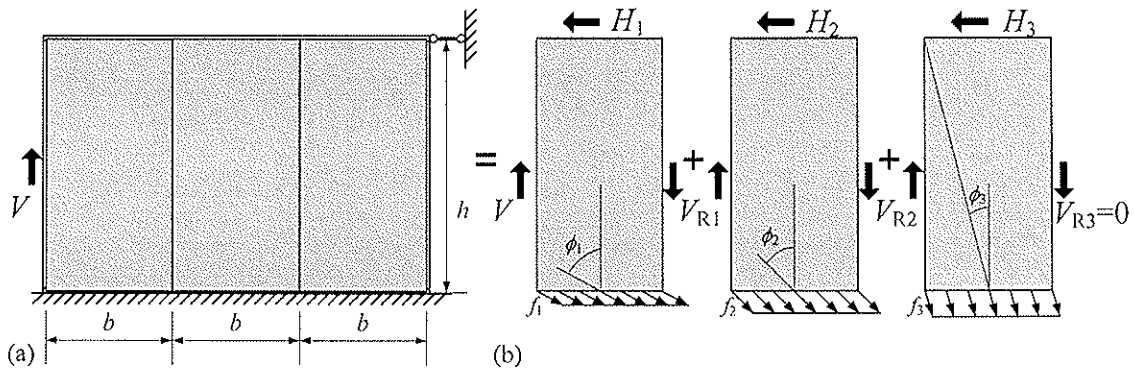

Figure 3. (a) Original transverse wall subjected to vertical uplift V; and (b) Free-body diagrams of the segments. The left segment is subjected to a vertical force, V_R, due to the restraining effect of the segments to the right. The transferred force per unit length along the bottom rail with a direction ϕ_i is denoted f_i.

4.2.2 A representative segment of transverse walls

Now, consider the left segment as a representative segment for transverse walls consisting of different numbers of segments according to Fig. 4a. According to the static theorem, this wall equals the sum of the two sub-cases according to Figure 4b.

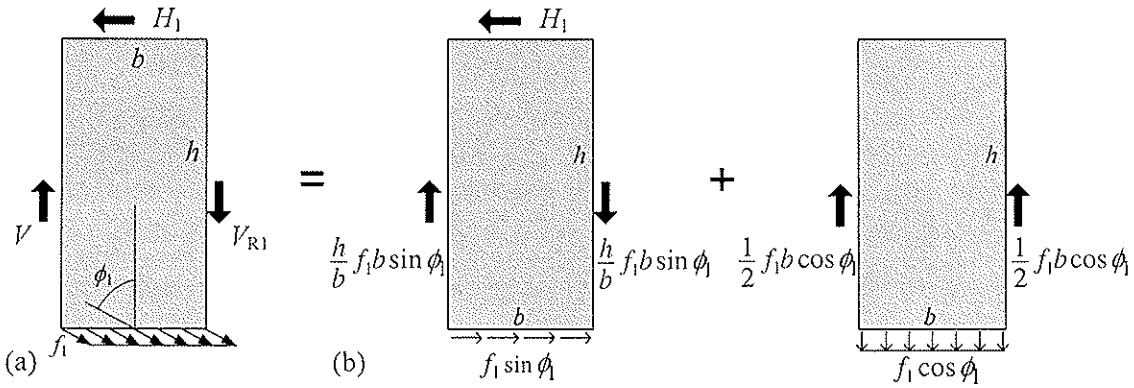

Figure 4. (a) Representative segment of a transverse wall subjected to vertical uplift V and restraining force V_{R1} is (b) divided into two sub-cases.

The resulting joint force along the bottom rail (F_1) and the horizontal force along the top rail (H_1) can be written as

$$F_1 = f_1 b \tag{1}$$

$$H_1 = F_1 \sin\phi_1 \tag{2}$$

Thus, the resulting force F_1 is independent of the angle, ϕ_1. The vertical forces are given by

$$V_{R1} = \frac{h}{b} F_1 \sin\phi_1 - \frac{1}{2} F_1 \cos\phi_1 \tag{3}$$

$$V = \frac{h}{b} F_1 \sin\phi_1 + \frac{1}{2} F_1 \cos\phi_1 \tag{4}$$

For these equations to be valid, three conditions must be fulfilled:

$$F_1 \le f_p b \tag{5}$$

$$V_{R1} \le f_p h \tag{6}$$

$$V \le f_p h \tag{7}$$

Case 1: For the condition $F_1 = f_p b$, the restraining force V_{R1} according to eqn (3) gives the following expressions for the angle of the joint force along the bottom rail

$$\phi_1 = \begin{cases} 2\arctan\left[-\dfrac{1}{\dfrac{b}{2h} - \dfrac{V_{R1}}{f_p h}} + \sqrt{\left(\dfrac{1}{\dfrac{b}{2h} - \dfrac{V_{R1}}{f_p h}} \right)^2 + \dfrac{\dfrac{b}{2h} + \dfrac{V_{R1}}{f_p h}}{\dfrac{b}{2h} - \dfrac{V_{R1}}{f_p h}}} \right] & \text{for } \dfrac{V_{R1}}{f_p h} < \dfrac{b}{2h} \\ 2\arctan\dfrac{b}{2h} & \text{for } \dfrac{V_{R1}}{f_p h} = \dfrac{b}{2h} \\ 2\arctan\left[\dfrac{1}{\dfrac{V_{R1}}{f_p h} - \dfrac{b}{2h}} - \sqrt{\left(\dfrac{1}{\dfrac{V_{R1}}{f_p h} - \dfrac{b}{2h}} \right)^2 - \dfrac{\dfrac{V_{R1}}{f_p h} + \dfrac{b}{2h}}{\dfrac{V_{R1}}{f_p h} - \dfrac{b}{2h}}} \right] & \text{for } \dfrac{V_{R1}}{f_p h} > \dfrac{b}{2h} \end{cases} \tag{8}$$

Case 2: For the condition $V = f_p h$, the restraining force V_{R1} according to eqn (3) gives the angle and the resultant joint force as

$$\phi_1 = \arctan \frac{1 + \dfrac{V_{R1}}{f_p h}}{1 - \dfrac{V_{R1}}{f_p h}} \frac{b}{2h} \tag{9}$$

$$\frac{F_1}{f_p b} = \frac{1}{2\sin\phi_1} \left(1 + \frac{V_{R1}}{f_p h}\right) \tag{10}$$

4.2.3 Application to one and two segment transverse walls

Consider transverse walls with one and two segments of dimension h/b = 2 according to Fig. 5a and Fig. 5b, respectively.

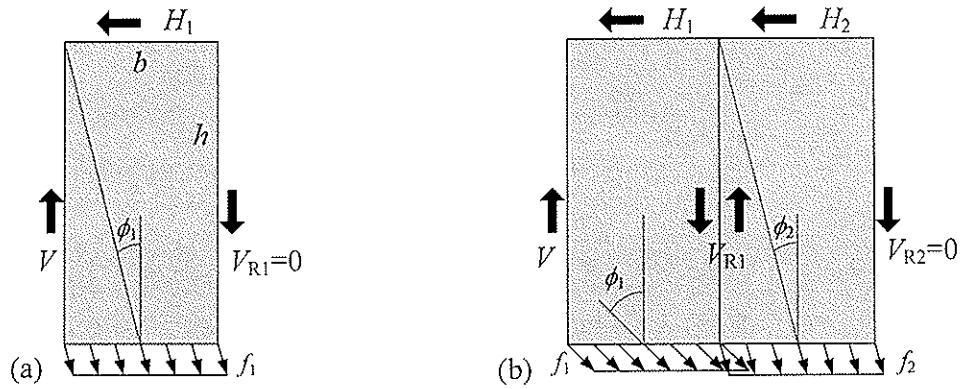

Figure 5. Plastic capacity of (a) a one segment and (b) a two segment transverse wall diaphragm in case of top rail fixed against horizontal displacement.

For the one segment wall, the vertical force V_{R1} = 0. The angle of the joint force according to eqn (8a) or directly from eqn (3) and the horizontal load and vertical capacity become

$$\phi_1 = 2\arctan\left[-\frac{2h}{b}+\sqrt{\left(\frac{2h}{b}\right)^2+1}\right]=\arctan\frac{b}{2h} \quad \rightarrow \quad \phi_1 = 14.0^\circ \text{ for } \frac{h}{b}=2 \tag{11}$$

$$H_1 = 0.243 f_p b = H \tag{12}$$

$$V_1 = 0.970 f_p b = V \tag{13}$$

For the two segment wall, the second segment (No. 2) is first evaluated and corresponds to the one segment wall according to eqns (11) - (13). Then the first segment (No. 1) is evaluated to give

$$\phi_1 = 42.1^\circ; \qquad \phi_2 = 14.0^\circ \tag{14}$$

$$V_{R1} = 0.970 f_p b; \qquad V_{R2} = 0 \tag{15}$$

$$H_1 = 0.670 f_p b; \qquad H_2 = 0.243 f_p b; \qquad H = 0.913 f_p b \tag{16}$$

$$V_1 = 0.742 f_p b; \qquad V_2 = 0.970 f_p b; \qquad V = 1.712 f_p b \tag{17}$$

5 Comparison between analytical and measured results

For the one segment transverse walls, the plastic capacity of the sheathing-to-timber joints, f_p, used to compare the experimental and theoretical values are those obtained for single sheathing-to-timber joint tests according to section 3.1, i.e. f_p = 1.17 / 0.1 = 11.7 kN/m. For the two segment transverse walls, no separate sheathing-to-timber joint tests were performed. Instead, those obtained earlier according to Girhammar et al. (2004), i.e. f_p = 10.5 kN/m.

The results obtained by the analytical method and those measured by testing are compared in Table 4.

Table 4. Comparison of theoretical and experimental results for vertical load-bearing capacity of transverse walls with different number of segments. The top rail is fixed against horizontal displacements. Aspect ratio h/b = 2.

Test wall	Load-carrying capacity V		$\frac{V_{measured}}{V_{calculated}}$
	Measured [kN]	Analytical values [kN]	
One	15.3	$0.970 f_p b = 13.6$	1.12
Two	22.4	$1.712 f_p b = 21.6$	1.04

The results according to Table 4 are preliminary. It is obvious that there is fairly good agreement between theoretical and experimental values. Also, it is noted that the effect of the framing joints is neglected.

6 Effect of transverse walls on the capacity of wall diaphragms

The horizontal load-carrying capacity and effective wall length of partially anchored wall diaphragms can be written as (Källsner & Girhammar, 2005) (full vertical shear model)

$$H = f_p l_{eff}; \qquad l_{eff} = \begin{cases} l - \frac{h}{2}\left(1 - \frac{V_0}{f_p h}\right)^2 & ; \quad l \geq h(1 - \frac{V_0}{f_p h}) \\ l\left(\frac{l}{2h} + \frac{V_0}{f_p h}\right) & ; \quad l \leq h(1 - \frac{V_0}{f_p h}) \\ l & ; \quad \frac{V_0}{f_p h} \geq 1 \end{cases} \qquad (18)\text{-}(19)$$

where V_0 is the vertical downward load on the leading stud and corresponds to the vertical capacity of the transverse walls, V.

If it is assumed that the vertical capacity of the transverse walls can be utilized in tying down the leading stud of wall diaphragms made of the same number of segments as in the

Table 5. Effect of transverse wall on the horizontal load-carrying capacity of wall diaphragms with different number of segments. The number of segments is the same in both wall diaphragms and transverse walls. Aspect ratio h/b = 2.

Wall diaphragm	Horizontal load-carrying capacity of wall diaphragm, H			Increase of H	$\frac{H_{V_0=V_{test}}}{H_{V_0=0}}$
	$V_0 = 0$	$V_0 = f_p h$	$V_0 = V_{test}$		
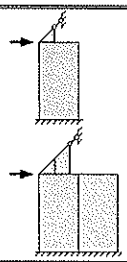	$0.250 f_p b$	$1 f_p b$	$0.793 f_p b$	$0.54 f_p b$	3.17
	$1 f_p b$	$2 f_p b$	$1.99 f_p b$	$0.99 f_p b$	1.99

transverse walls, the horizontal load-carrying capacity of these wall diaphragms will increase as shown in Table 5. $V_0 = f_p h$ corresponds to the case of fully anchored leading stud.

Table 5 clearly shows the big effect of the tying down action of the transverse walls on the load-carrying capacity of wall diaphragms with different number of segments. The geometrical configuration is assumed to be the same in both the transverse walls and the wall diaphragms. For a one segment wall diaphragm, for example, the load-bearing capacity is more than three times that of a wall diaphragm without the restraining effect of the transverse wall.

7 Design recommendations

Based on the analysis as presented above for fixed transverse walls and based on the results of the previous paper (Girhammar & Källsner, 2006) dealing with free transverse walls, the design recommendations according to Table 6 can be given. The effect of *fixed* transverse walls is the same as that of *free* transverse walls with twice as many segments as in the fixed wall.

Table 6. Design recommendations concerning the horizontal load-carrying capacity of wall diaphragms with different number of segments and with the leading stud tied down by transverse walls with different number of segments.

Number of segments in *free* transverse walls	Number of segments in *fixed* transverse walls	Horizontal load-carrying capacity H [1)]
0	0	$\begin{cases} H_{full} - 0.75 f_p b & \text{for } n_s = 1 \\ H_{full} - f_p b & \text{for } n_s \geq 2 \end{cases}$
1	0.5	$\begin{cases} H_{full} - 0.50 f_p b & \text{for } n_s = 1 \\ H_{full} - 0.55 f_p b & \text{for } n_s \geq 2 \end{cases}$
2	1	$H_{full} - 0.25 f_p b$
3	1.5	$H_{full} - 0.10 f_p b$
4	2	H_{full}

1) Notation: n_s = number of segments in wall diaphragm.

8 Conclusions

A plastic lower bound method is used to study the effect of transverse walls on the load-carrying capacity of partially anchored wood-framed wall diaphragms. The load-bearing capacity of transverse walls with various numbers of sheet segments and the top rail fixed against horizontal displacement subjected to a vertical uplifting force is derived.

The analytical values are compared to preliminary test results and are found to agree well. A more comprehensive experimental study and evaluation need to be conducted to verify the analytical models. Also, the effect of the framing forces needs to be taken into account.

The tying down effect of transverse walls with the same geometrical configurations as for the wall diaphragms is demonstrated for walls with one and two sheet segments. The effect is found to be very significant.

Acknowledgements

The authors express sincere appreciation for the financial support from The Development Fund of the Swedish Construction Industry (SBUF), The Swedish Research Council for Environment, Agricultural Sciences and Spatial Planning (FORMAS), The County Administrative Board of Västerbotten and The European Union's Structural Funds – The Regional Fund: Goal 1, together with the timber and building industry.

References

Girhammar U.A., Bovim N.I., and Källsner B., "Characteristics of sheathing-to-timber joints in wood shear walls", *8th World Conference on Timber Engineering*, Lahti, Finland, 2004.

Girhammar, U. A. and Källsner, B. "Effect of transverse walls on capacity of wood-framed wall diaphragms", *Proceedings CIB-W18 Meeting*, Florence, Italy, Paper 39-15-3, 2006.

Källsner B., and Girhammar U.A., "Plastic design of partially anchored wood-framed wall diaphragms with and without openings", *Proceedings CIB-W18 Meeting*, Karlsruhe, Germany, Paper 38-15-7, 2005.

INTERNATIONAL COUNCIL FOR RESEARCH AND INNOVATION
IN BUILDING AND CONSTRUCTION

WORKING COMMISSION W18 - TIMBER STRUCTURES

MIDPLY WOOD SHEARWALL SYSTEM: CONCEPT, PERFORMANCE AND CODE IMPLEMENTATION

Chun Ni
M Popovski
E Karacabeyli
FPInnovations, Forintek Division

E Varoglu
Intelligent Solutions

S Stiemer
University of British Columbia

CANADA

MEETING FORTY
BLED
SLOVENIA
AUGUST 2007

Presented by C. Ni
B. Dujic asked about the end stud detail with respect to the gap. C. Ni replied that the end stud will also need the 3 mm gap.
I. Smith commented that the same increase for both wind and seismic design was suggested. He asked whether one should use the same capacity for both situations. C. Ni replied in Canadian code one does not distinguish these cases in terms of base shear capacities. I. Smith stated that even though this is done in codes, it may not be acceptable and one can't just increase capacity for all situations especially when larger displacements are involved in one case.
A. Ceccotti asked if these walls were anticipated to be used with other walls. C. Ni replied that this could be done if different R factors were used. F. Lam stated that one should be careful when one combines midply with other systems as different systems have different stiffness which can influence the distribution of loads through diaphragm action.
M. Yasumura asked about the hold-downs for standard and midply walls. C. Ni replied that higher capacity hold-downs would be needed.

Midply Wood Shearwall System: Concept, Performance and Code Implementation

Chun Ni, Marjan Popovski, Erol Karacabeyli
FPInnovations, Forintek Division, Canada

Erol Varoglu
Intelligent Solutions, Canada

Siegfried Stiemer
University of British Columbia, Canada

Abstract

This paper introduces a new shearwall system referred to as "midply wall". The new wall system uses the same wall sheathing and dimension lumber as standard shearwalls used in platform-frame construction in North America. In this wall, however, the sheathing is placed in the centre of the wall between a series of pairs of studs and plates placed on both sides of the wall sheathing. As a result, nails connecting the framing members to the sheathing work in double shear in contrast to single shear in standard shearwalls. This results in substantial improvements in the overall performance of midply walls. Test results for midply walls under monotonic, cyclic and dynamic loading conditions are presented and compared with those for standard shearwalls under similar loading conditions. Implementation of the midply wall in wood design codes in North America is proposed and issues related to the code implementation are discussed.

1 Introduction

Wood frame construction is extensively used in North America for single family and low-rise multi-family dwellings. In the last few decades, wood frame construction has evolved to include 3 or 4 story multi-family residences. In some of these applications, garages at the first story, large openings in the exterior walls, large floor spans, concrete topping on floors, and heavy tiles on roofs became common practice. While wood frame construction has generally performed well during severe earthquakes and hurricanes (Rainer and Karacabeyli 1999), the evolution in construction practices at times creates additional demand on the lateral load resistant system, and consequently necessitates innovation in new designs and construction methods that increase the lateral resistance of wood frame shearwalls.

In this paper, a new wall system named Midply Wall System is introduced. Test results for midply walls under monotonic, cyclic and dynamic loading conditions are presented and compared with those for typical standard shearwalls under similar loading conditions.

Implementation of the midply wall in wood design codes in North America is proposed and issues related to the code implementation are discussed.

2 Midply Wall Concept

A standard shearwall consists of a wood frame built with studs and plates and structural sheathing panels fastened on the wood frame. Studs are generally made of 38 × 89 mm or 38 × 140 mm lumber (nominal 2 in × 4 in or 2 in × 6 in) and are spaced at 406 mm or 610 mm (16 or 24 in) on centre. At the bottom of the wall, studs are supported on a horizontal bottom plate or foundation sill plate, while at the top of the wall the studs support the horizontal double plate. Structural sheathing is fastened to the narrow faces of the framing members. The midply wall system consists of standard shearwall components used in regular shearwalls but re-arranged in such a way that the lateral resistance and the dissipated energy of the system significantly exceed that in standard wall arrangements. Figure 1 illustrates a cross section of standard shearwall and that of a Midply wall system that uses the same 38 × 89 mm lumber studs.

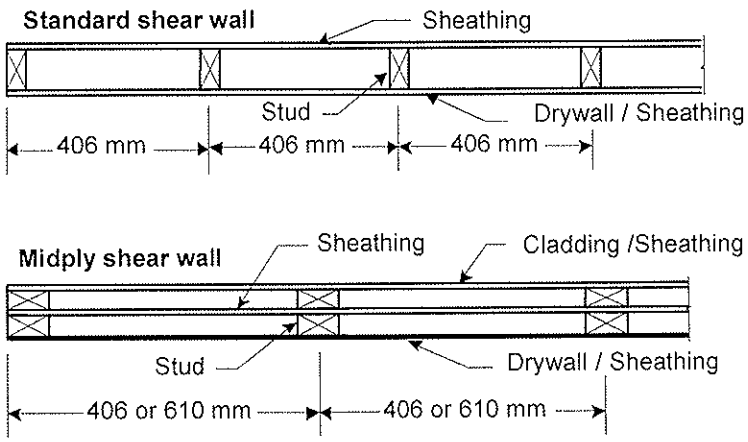

Figure 1 Cross-section of a standard shearwall (top) and a midply wall (bottom) with two exterior panels

The superior performance of midply wall under lateral loading is attained through the following means:

1. A wood based panel is used at the centre of the wall to provide the lateral resistance of the wall without increasing the nominal thickness of the wall. Nails connecting this panel to the framing work in double shear as illustrated in Figure 2 (or in triple shear if additional exterior wood based sheathing is used), providing the increased lateral load carrying capacity.
2. Studs in midply wall system are placed at a 90 degree rotated position relative to those in standard shearwalls. Sheathing material is fastened to the wide face of the studs instead of the narrow face of the studs in case of standard walls. This increases the lateral load capacity of the midply wall by providing more edge distance for fasteners on the perimeter of the sheathing panels placed in the mid plane and at the exterior face of the wall. Increased edge distance reduces the

possibility of nail tear out failures and makes it easier for framers to nail the sheathing to the studs.

3. The heads of nails are kept away from the surface of the mid-panel; consequently nail pull through failure at the mid panel is physically prevented. Also, poor construction practices such as over driven sheathing nails (SEAOSC 1997 and Jones and Fonseca 2002) and nails going through the panels missing the studs are practically avoided.

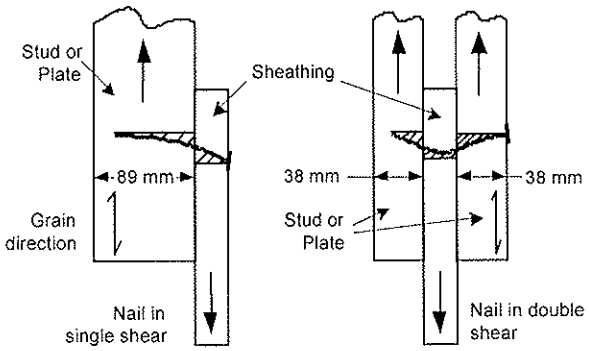

Figure 2 Nailed joints working in single shear in a standard shearwall and in double shear in a midply wall

3 Midply Wall Test Program

The test program consisted of monotonic, cyclic and shaking table tests on 2.44 m × 2.44 m midply walls. Details of the test program and test results can be found in (Varoglu et al. 2006, 2007). A summary of wall configurations, test results and comparison between midply and standard shearwalls is provided below.

All midply walls, 2.44 × 2.44 m in size were constructed with 38 × 89 mm Spruce-Pine-Fir (SPF) framing members manufactured to National Lumber Grades Authority (NLGA) standards. Except for wall M41-1 in which Oriented Strand Board (OSB) with a thickness of 10.5 mm was used, OSB or Canadian Softwood Plywood (CSP) panels with a thickness of 12.7 mm in vertical orientation were used for the middle sheathing. Power driven nails of 3.0 mm in diameter and 82 mm in length were used to connect the framing material and the mid panels. To allow the sheathing to rotate during the tests, a 12 mm gap between the bottom edge of the mid-panel and the lower edge of the plates was placed during the fabrication of the walls. The same gap was also placed between the top edge of the mid-panel and the upper edge of the top plates. All midply walls were tested within one or two days of construction.

For the purpose of comparison, results from tests on standard shearwalls are also presented here. All standard shearwalls, 2.44 × 4.88 m in size were constructed with 38 × 89 mm framing members of No. 2 and better grade SPF lumber and with 9.5 mm thick vertically placed CSP sheathing on one side. Stud members were spaced at 406 mm on centre. The top plate and the end studs consisted of double members, while the bottom plate and the interior studs consisted of single members. The sheathing panels were connected to the framing members with power driven nails (3 mm in diameter and 65 mm in length) at nail

spacing of 150 mm around the panel perimeter, and 300 mm elsewhere. Commercially available hold-downs were used in the standard shearwall tests.

A summary of the test results of midply and standard shearwalls under monotonic and cyclic testing are provided in Tables 1 and 2. Test results of midply walls during shake table tests are provided in Table 3. To compare the performance of midply and standard shearwalls, the test results of midply and standard shearwalls are presented on the basis of per unit length.

Comparisons of the performances of selected midply walls and typical standard shearwalls under monotonic and cyclic loading are illustrated in Figure 3.

From Tables 2 and 3, it was found that the midply walls with and without vertical load (M40/M41-1 and M39) have average lateral load capacities over 3 times the average load capacities of the typical standard shearwalls (S31/S51/S52 and S37/S38) under monotonic loading. In the case of cyclic loading, similar ratios of the lateral load capacities were found between the midply walls (M28/M29/M30/M14 and M31) and typical standard shearwalls (S33 and S34/S39/S40).

Table 1 Average test results of midply walls

Wall No.	Stud spacing (mm)	Load Protocol	Vertical Load (kN/m)	P_{max} [1] (kN/m)	Δ_u [2] (mm)	K [3] (kN/m/mm)	E (J/m)
M40/M41-1	610	Monotonic	18.2	31.4	121 [b]	1.66	-
M39	610	Monotonic	None	30.2	120 [b]	1.32	-
M28/M29/M30/M14	610	Cyclic [a]	18.2	28.7	95	1.65	13,655
M31	610	Cyclic [a]	None	27.9	100	1.24	15,790
M32	406	Monotonic	18.2	36.3	103 [c]	1.57	-
M46 [d]	406	Cyclic [a]	None	27.6	83	0.44	8,750

[1] P_{max} is the average value of maximum unit lateral load.
[2] Δ_u is the average value of ultimate displacement, which is defined as the displacement at 80% of maximum load on the descending portion of the load-displacement curve.
[3] K is the average value of the secant stiffness between 10% and 40% of the maximum load.
[a] The unit lateral load capacity (P_{max}), ultimate displacement (Δ_u) and the secant stiffness (K) are obtained based on first envelop curve.
[b] Test stopped when the maximum extension of actuator is reached and load was above 0.8 P_{max}.
[c] Test stopped when the load capacity of the actuator is reached.
[d] Wall was subjected to five ISO98 tests in succession with increasing maximum displacement. Results are for ISO 98 test with 125mm maximum displacement.

Table 2 Average test results of standard shearwalls

Wall No.	Load Protocol	Vertical Load	P_{max} (kN/m)	Δ_u (mm)	K (kN/m/mm)	E (J/m)
S31/S51/S52	Monotoni	18.2	8.8	105	0.58	-
S37/S38	Monotoni	None	8.7	88	0.55	-
S33	Cyclic [a]	18.2	9.6	78	0.76	3,820
S34/S39/S40	Cyclic [a]	None	9.0	77	0.68	3,210

[a] The unit lateral load capacity (P_{max}), ultimate displacement (Δ_u) and the secant stiffness (K) are obtained based on first envelop curve.

Table 3 Shake table test results of midply shearwalls

Wall No.	Stud spacing (mm)	Exterior Sheathing	Vertical Load (kN/m)	Load at Failure	Failure Mode	P_{max} (kN/m)	Δ_u (mm)	E [b] (J/m)
M48-01	610	None	none	Kobe 0.52g	End stud tension failure	26.9	53	5020
M48-02	610	None	none	Landers 0.54g	End stud tension failure	22.3	49	17847
M49-01	406	9 mm plywood	none	Kobe 0.67g	End stud tension failure	34.7	51	15833
M49-02 [c]	406	9 mm plywood	none	Kobe 0.67g	End stud tension failure	39.0	53 [a]	26579
M50-01	406	none	11.1	Kobe 0.67g	Cable failure	23.6	146	30369
M50-02	406	none	11.1	Kobe 0.67g	Cable failure	31.6	106	22896

[a] Test stopped before failure, when the load capacity of the actuator is reached.
[b] Cumulative energy dissipation of series of earthquake motions with increasing peak ground acceleration until failure occurs or test stops.
[c] Survived the first application of Kobe 0.67g and failed at second applicationof the same.

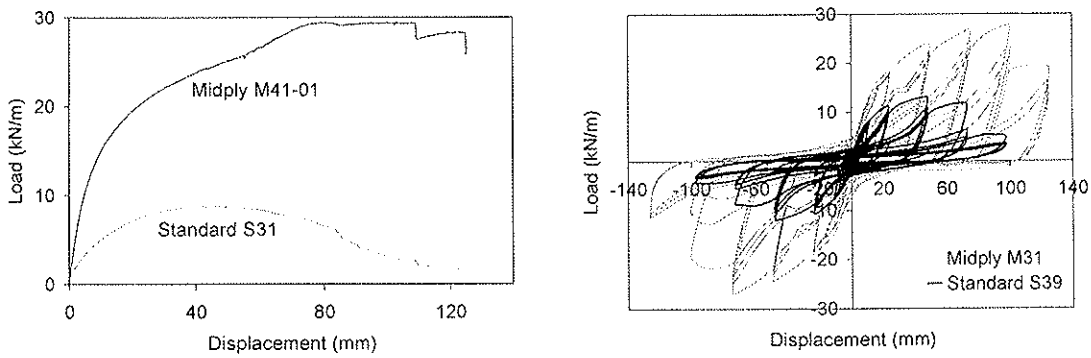

a) Monotonic test b) Cyclic test

Figure 3 Comparison of performance of Midply and standard shearwalls

The ratios between stiffness values of Midply walls (M40/M41-1 and M39) and those of typical standard shearwalls (S31/S51/S52 and S37/S38) are in the range of 2.4 to 2.8. In the case of cyclic loading, the ratios of stiffness values for midply walls and typical standard shearwalls are in the range of 1.8 to 2.2. For midply walls subjected to monotonic loading, ultimate displacements were not achieved due to the limitations of the testing equipment. At the displacement where testing was stopped, midply walls were well over 80% of their lateral load capacities on the descending portion of the load-displacement curve. In the case of cyclic loading, ultimate displacements of midply walls were at least 20% higher than those of typical standard walls. Midply walls were found to be far superior energy dissipation systems in comparison to standard shearwalls. An examination of energy dissipation data presented in Tables 2 and 3 reveals that energy dissipation values of Midply walls were from 3 to 5 times higher than those for typical standard shearwalls.

The shake table tests on midply walls were performed on the shaking table at the Department of Civil Engineering at the University of British Columbia (UBC). Each wall configuration was subjected to a series of earthquake ground motions with increasing peak ground acceleration (PGA) until failure occurred. Two replicates of each midply wall with the same configuration were tested, with one tested with Kobe earthquake and the other tested with Landers earthquake. For wall M48, one wall survived the 0.35g Kobe earthquake and the other wall survived the 0.35g and 0.52g Landers earthquake. For wall M49 (with exterior sheathing), one wall survived the Kobe earthquake at 0.35 and 0.52g and the other wall survived the Landers earthquake at 0.35, 0.52 and 0.54g. For wall M50 (with vertical load), both walls survived all three levels of Kobe (0.35, 0.52 and 0.67g) and Landers (0.35, 0.52 and 0.54g) earthquakes, respectively. In case of midply walls without vertical loading the failure mode was tension failure of the end studs. However, the tests on midply walls with vertical loading could not be completed due to the failure of the cable providing the vertical load.

Comparison of the results of shake table tests on Midply and standard shearwalls can be found in (Varoglu et al. 2007). It showed that for both Kobe and Landers earthquakes, the peak base shear of a midply wall was over 2.5 times that of a typical standard shearwall subjected to the same earthquakes.

4 Code Implementation

Comparision of average test results of midply and typical standard shearwalls is provided in Table 4. Because different panel thickness, nail size and nail spacing were used in the tests, a direct comparision of lateral load capacity cannot be made between the midply shearwall and a comparable standard shearwall which has the same panel thickness, nail size and nail spacing. Based on test results of nailed joints in Karacabeyli et al. (2000), it shows that the shear strength of a nailed joint in double shear is about 80% higher than that in single shear. In midply shearwalls, the lateral load capacity may be further increased through the elimination of failure modes observed in standard shearwalls. By providing more edge distance for fasteners on the perimeter of the sheathing panels, the possibility of nail tear out failures is greatly reduced. As the nail heads are kept away from the surface of the mid-panel, nail pull through the sheathing failure mechanism in the mid panel is physically prevented.

Table 4 Comparison of average monotonic and cyclic test results of midply and typical standard shearwalls

Wall configuration	Framing member	Sheathing thickness	Nail size (mm)	Nail spacing[a] (mm)	P_{max} (kN/m)	Δ_u (mm)	K (kN/m/mm)	E (J/m)
Standard	38 × 89 mm	9.5 mm	3.0 × 65	152/305	8.9	88.9	0.6	3363
Midply	38 × 89 mm	12.7 mm &10.5 mm	3.0 × 82	102/102	30.0	103	1.4	13193
			Midply / Standard		3.4	1.2	2.3	3.9

[a] The first and second rows represent the nail spacing around panel perimeter and elsewhere, respectively.

Based on the findings from quasi-static and shaking table tests, a code change proposal on design of Midply walls has been prepared and submitted for potential implementation in the Canadian Standard for Engineering Design in Wood - CSA O86-01 (CSA 2005). It is recommended that the specified shear capacity of a midply shearwall be taken as twice the specified shear capacity of a one-sided standard shearwall.

To ensure that the midply walls are able to reach their shear capacity, the following construction and detailing requirements are recommended:

1. The wood-based panels in the center of the wall should have a minimum thickness of 12.7 mm. There should be 3 mm gap between adjacent panels. Wood-based panels should be placed so that there is a 12 mm gap between the bottom edge and the lower end of the bottom plate (Figure 4). The same holds for the top edge of the mid panel and the upper edge of the top plate.

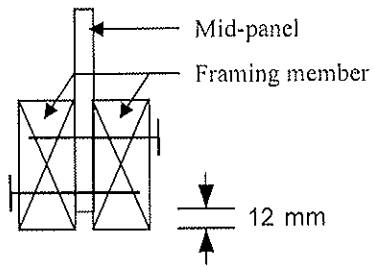

Figure 4 Cross section of a bottom plate in a midply wall

2. Framing members and the mid-panels should be nailed together using nails with adequate penetration and with the same nail spacing in all locations. Such nail spacing can be accomplished by using two rows of fasteners.
3. The end of the Midply wall should be checked for bearing strength and buckling. An additional stud may be necessary to resist the high compression forces and prevent buckling in the end studs, as shown in Figure 5.

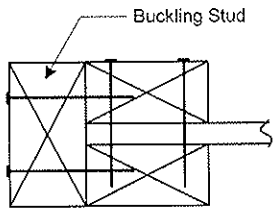

Figure 5 A detail of an end stud in a midply wall that includes the added buckling stud

4. Where the dead loads are not sufficient to prevent overturning moment, hold-down connections at the end of the Midply wall should be designed to resist the uplift forces and transfer the forces through a continuous load path to the foundation. Discussion on hold-down connections can be found in Section 5.4.
5. To prevent detachment of the intermediate studs at the panel joints during reversible earthquake loading, the pair of studs should be connected to each other.

This can be accomplished by fasteners with adequate penetration equally spaced along the height of the wall (Figure 6).

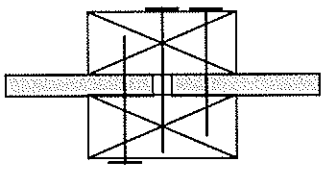

Figure 6 A detail of an intermediate stud in a midply wall where the two panels meet

5 Discussion

5.1 Deflection of Midply Walls

In the National Building Code of Canada (NBCC 2005), it is required that limit of interstorey drift be checked for wind and earthquake loads. Deflection formula of standard shearwalls was provided in the Commentary of CSA O86-01 (CSA 2005). It provides a reasonable estimate of shearwall deflection due to loads applied in the factored resistance shear range. As the stiffness of a midplay shearwalls is approximately twice that of a typical standard shearwall, the midply wall can be essentially treated as two one-sided shearwalls. As a result, it seems reasonable to presume that the deflection of midply shearwall can be estimated from deflection formula of standard shearwall. Comparison with test results is currently under way to verify this hypothesis.

5.2 Seismic Force Modification Factor (R-factor)

In the National Building Code of Canada (NBCC, 2005), the seismic force modification factor, R_d, is assigned a value of 3.0 for nailed wood shearwalls where hold-downs are used or where dead loads are sufficient to prevent overturning moment. This factor is primarily used to characterize the ability of the structure to undergo deformations beyond yielding. Test results have shown that in case of midply walls, the ultimate displacements were much bigger than those of typical standard walls. Based on this fact, it may be reasonable to assume that midply walls are assigned a minimum force modification factor R_d of 3.0. Validation of this claimis is under way through the use of a series of non-linear dynamic analyses.

5.3 Midply Walls with Multiple Layers

Test results have shown that the lateral load capacities for shearwalls are cumulative in the elastic range, when same or different sheathing is applied on both sides (Karacabeyli & Ceccotti 1996). The test results show that midply shearwalls have slightly larger displacements at maximum lateral load capacities than standard shearwalls (Varoglu et al. 2006). However, as more edge distance is available for fasteners on the perimeter of the sheathing panels, the displacement at lateral load capacity of exterior sheathing could be comparable to that of mid-panels as the possibility of nail tear out failures is greatly reduced. Although midply walls with exterior sheathing were not tested in monotonic and cyclic loads due to the limit of the test equipment, one can assume that the lateral load

capacity is cumulative for a midply wall with additional exterior panels sheathed on one or both sides. With two additional exterior panels (one on each side), a midply wall can provide much greater lateral load capacity than any standard shearwall can ever achieve.

5.4 Hold-Down Connections for Midply Walls

In the shake table tests, midply walls without vertical loading suffered premature tension failure at end studs. As a result, the lateral load capacity was much less than in walls ones tested with vertical load. Premature end stud failure can be avoided by restraining the end studs against uplift by means of continuous steel rods, in lieu of hold-downs, at each end of the wall. This idea was proved effective during the cyclic testing of two midply walls where two steel rods of 16 mm diameter were used to connect the top and bottom plates at each end of the test wall. Test results showed that these walls exhibited good ductility and the premature end stud tension failure was eliminated. The lateral load capacities of midply walls tested with this improved uplift prevention detail were similar to those achieved in shake table tests of midply walls with vertical load (Varoglu et al. 2007).

6 Concluding Remarks

A new shearwall construction system named Midply Wall System is introduced. The Midply Wall System is designed to provide superior resistance to earthquake and wind loads. The improved performance is achieved by rearrangement of wall framing components and sheathing used in standard shearwalls.

Comparison of the performance of midply and typical standard shearwalls is presented. The average lateral load capacity of midply walls was more than three times higher than in typical standard shearwalls. Test results showed that the stiffness values for midply walls were approximately two to three times the average stiffness values of typical standard shearwalls. Midply walls' energy dissipation was more than 3 times higher than in typical standard shearwalls.

Implementation of the midply walls in the Canadian wood design code CSA O86-01 is also discussed. The new wall system provides architects and engineers with more options in the design of wood frame construction in cases where the demand on the shearwalls exceeds the capacity of standard shearwalls. Besides narrow shearwalls in platform frame construction, the midply wall system can be used next to garage or window openings, in seismic upgrading of existing structures, and in prefabricated housing systems for application in areas with high risk of earthquakes and hurricanes.

References

CSA, 2005. Engineering Design in Wood. Standard CSA O86-01, Canadian Standards Association, 178 Rexdale Boulevard, Etobicoke, Ont.

Jones, S. N. and Fonseca, F.S. (2002). "Capacity of oriented strand board shearwalls with overdriven sheathing nails." J. Struct. Engrg. ASCE, 128(7), 898-907.

Karacabeyli E., Ceccotti A., "Test Results on the Lateral Resistance of Nailed Shearwalls", Proceedings of the International Wood Engineering Conference, New Orleans, USA, Vol.2, 1996, pp.179-186.

Karacabeyli, E., Ni, C., Lungu, D., Fraser, H., Stiemer, S.F., 2000. Midply Wall System – Final Report (No.3). Forintek Canada Corp. (Internal report).

NBCC, 2005. National Building Code of Canada. Institute for Research in Construction, National Research Council of Canada, Ottawa, Ont.

Rainer, J.H., Karacabeyli, E. 1999. Performance of wood-frame building construction in earthquakes, Special Publication No. SP-40, Forintek Canada Corp., Vancouver, BC.

SEAOSC. (1997). "Standard method of cyclic (reversed) load tests of framed shearwalls for buildings." Structural Engineers Association of Southern California, Whittier, Calif.

Varoglu, E.; Karacabeyli, E., Stiemer, S., and Ni, C. 2006. The Midply wood shearwall system: concept and performance in monotonic and cyclic testing. Journal of Structural Engineering, American Society of Civil Engineers. Vo. 132, No. 9. pp. 1417-1425.

Varoglu, E., Karacabeyli, E., Stiemer, S., Ni , C., Buitelaar, M., and Lungu, D. 2007. Midply wood shearwall system: Performance in dynamic testing. Journal of Structural Engineering, American Society of Civil Engineers. Vol. 1333, No. 7. pp. 1035 – 1042.

INTERNATIONAL COUNCIL FOR RESEARCH AND INNOVATION
IN BUILDING AND CONSTRUCTION

WORKING COMMISSION W18 - TIMBER STRUCTURES

SEISMIC BEHAVIOUR OF TALL WOOD-FRAME WALLS

M Popovski
E Karacabeyli

FPInnovations – Forintek Division

A Peterson

University of BC, Vancouver BC

CANADA

MEETING FORTY
BLED
SLOVENIA
AUGUST 2007

Presented by M. Popovski
B.J Yeh asked about the 1:1 aspect ratio of the walls as "tall" walls are mostly more slender. M. Popovski clarified that the actual application will involve cases when the walls will be longer so the aspect ratio of "tall" walls will not be an issue. He also explained that the application of the vertical load was applied to the bottom plate rather than the top plate.
A. Salenikovich received clarification of spiral nails versus ring shank nails. M. Popovski stated that spiral nail and common nails were used and there is significant difference between the behaviour of both connections. He also explained 1.7E LSL was used as plates for all walls and different type of studs were considered.
F. Lam asked about the possible influence of wetting and re-drying during construction if LSL was used as stud. M. Popovski said that they do not have information but walls are built with LSL in practice. Expect industry would have data on the subject and perhaps factory manufacturing can avoid the wetting and re-drying issues. F. Lam suggested one to conduct connection tests to check whether this is an issue.

Seismic Behaviour of Tall Wood-Frame Walls

Marjan Popovski[1], Anthony Peterson[2], and Erol Karacabeyli[1]

[1]FPInnovations – Forintek Division, [2]University of BC, Vancouver BC, Canada

Abstract

A series of 13 quasi-static tests were performed to determine the behaviour of tall wood-frame shearwalls subjected to seismic loads. The walls tested were 4.9 m x 4.9 m in size and included different sheathing-to-stud nailed connections, two types of studs and blocking (spruce-pine-fir dimensional lumber and laminated strand lumber), various stud spacing, various stud-to-plate connections, sheathing material and thickness. The research results showed that with efficient stud spacing, nailing pattern, stud-to-plate connection details, and appropriate sheathing thickness, both spruce-pine-fir (SPF) and laminated strand lumber (LSL) studs are viable material options for tall walls. Walls that used LSL studs spaced up to 2440 mm on centre were able to withstand large lateral forces and dissipate high amounts of hysteretic energy. Tall walls with SPF studs spaced 610 mm on centre, aside from being able to withstand large lateral forces, showed increased ability to sustain large deformations provided that close nail spacing is used. An arrangement consisting of commercially available double hurricane ties and a joist hanger was found to be an effective stud-to-plate connection resisting the shear and uplift forces.

1 Introduction

In North America, wood-frame construction has been in use since the early 19th century. Although the system has evolved and changed over time, wood-frame construction still remains simple in concept and well within the scope of the average builder. Today more than ninety percent of North American homes are constructed using this building method. Lately, efforts have been made to extend the use of this method to non-residential applications. Developments such as hotels, motels, low-rise commercial properties, and community centres are all benefiting from the advantages of the wood-frame construction. For these applications, the wood-frame construction concept can be used with little modification from its residential version. That is not the case, however, for most industrial or commercial buildings. Such buildings usually require larger open spaces and greater heights than other non-residential buildings and need walls that are usually referred to as tall walls. Tall wood-frame walls can be a viable alternative to the steel systems and concrete tilt-up construction currently being used in box-type non-residential construction in North America, especially in seismic prone areas, where some concerns regarding the seismic performance of concrete tilt-up buildings have emerged.

Previous research in the field of wood-frame walls has focused on regular residential walls. Consequently, design guidelines for these walls have been developed and introduced in North American codes and standards. On the other hand, small amount of research has

been undertaken to investigate the structural performance of tall walls. Changes in design philosophy, supported by experimental and analytical research results can help this wood-frame system to become a more attractive alternative. For these reasons, FPInnovations - Forintek Division, and the Department of Civil Engineering at the University of British Columbia, have undertaken a research project on the structural performance of tall wood-frame walls. This paper deals with one aspect of this project: Experimental testing to determine the influence of different connection detailing, anchorage, sheathing thickness, nail length, framing material, framing configuration and blocking, on the response of tall walls subjected to lateral loads.

2 Tall Wall Specimens

The 4.9 m x 4.9 m (16' x 16') walls tested in the study were divided in two distinctive wall series. The first series, referred to as the "600 series", consisted of five walls with SPF lumber studs, while the second, "700 series" included eight walls with LSL studs (Table 1). Walls 601 and 701 were subjected to monotonic lateral loading, while all other walls were subjected to reversed cyclic loading. Walls 604 and 703 were subjected to vertical loading in addition to the lateral cyclic loading. Eight 13.3 kN hydraulic actuators spaced at 610 mm were placed inside the walls to deliver the 20 kN/m of vertical loading (Figure 1d).

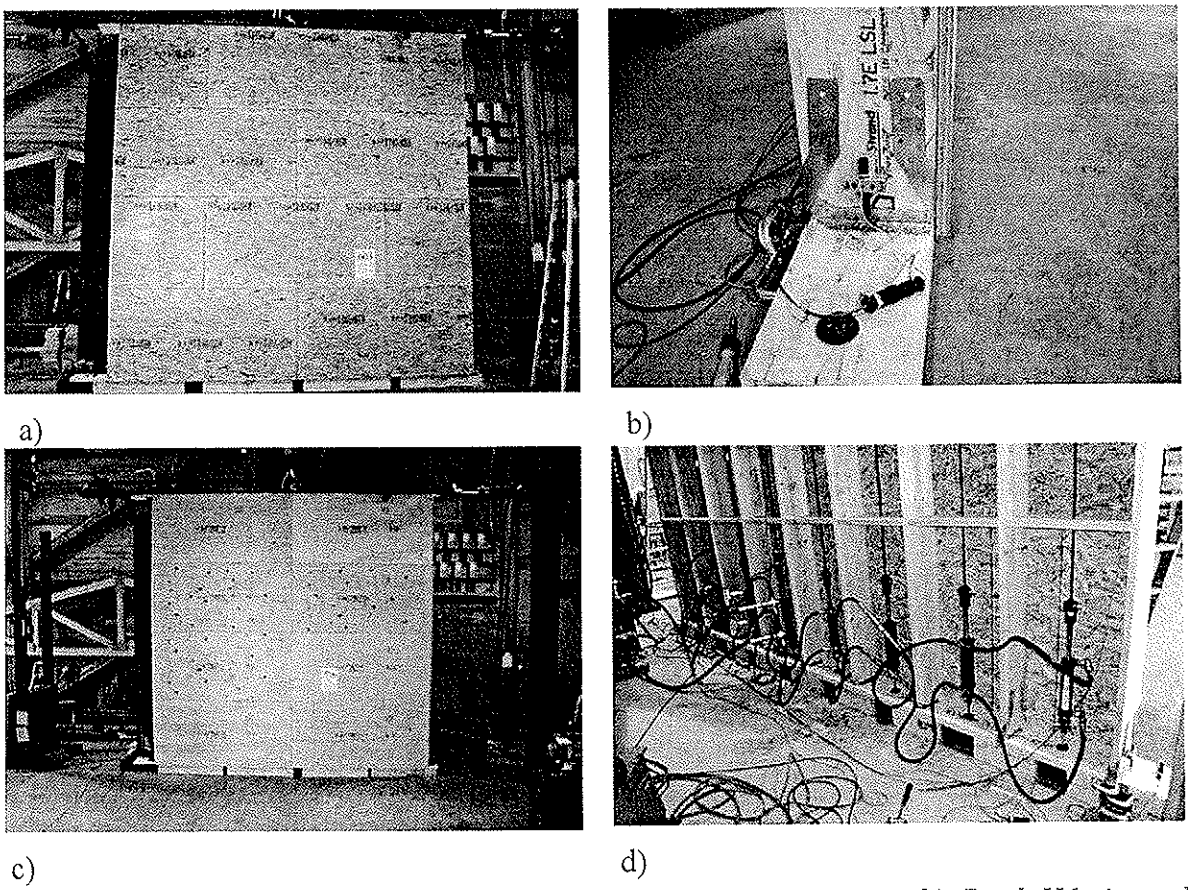

Figure 1. Tall wall with: a) Typical staggered panel orientation; b) Dual H6 tie and hanger stud to plate connection; c) Stacked panel orientation (wall 706); d) Actuator assembly used for applying vertical loads

Walls 701 to 703, and wall 708 used 15.1 mm thick OSB, while walls 704 to 707 used 25.4 mm thick Douglas-fir plywood (DFP). As a result of the 25.4 mm thick sheathing, walls 704, 706 and 707 utilized 3.0 mm diameter, 76 mm long spiral nails for sheathing application, while wall 705 used 3.75 mm diameter, 76 mm long common nails. The stud to plate connections were consistent for all 700 series walls, with two H6 ties top and bottom being used on all studs, as well as Simpson Strong Tie® (Simpson) HU9 hangers on all studs (Figure 1b). Blocking was used in all walls except wall 707. The blocking material matched the stud material in all cases and was spaced at 1220 mm on centre. The blocking connections in the 600 series were either three toenails, or three end-nails. Wall 701 used the same type of nailing scheme for the blocking as in the 600 series. Walls 702 to 705 and wall 708, however, used 6 nails per blocking connection, while wall 706 used 9 nails. All blocking used 3.3 mm diameter, 83 mm long common nails. Wall 708 also had 15.5 mm thick gypsum wallboard applied to the side opposite of that of the sheathing. All 700 series walls had scattered sheathing pattern (Figure 1a), except for the wall 706 that used stacked sheathing pattern (Figure 1c).

Table 1. Test matrix used in the study.

Wall No.	Stud		Sheathing Thickness	Nail Spacing and Properties				Load Protocol[4]
	Type	Spacing [mm]	[mm] and Type	Perimeter [mm]	Interior [mm]	Diameter [mm]	Length [mm]	
601	SPF	610	9.5 OSB	152	305	2.5	65	→
602	SPF	610	9.5 OSB	152	305	2.5	65	↔
603	SPF	610	15.1 OSB	152	305	2.5	65	↔
604	SPF	610	15.1 OSB	152	152	2.5	65	↔ + ↓
605	SPF	610	15.1 OSB	102	152	2.5	65	↔
701	1.5E LSL	1220	15.1 OSB	152	305	2.5	65	→
702	1.5E LSL	1220	15.1 OSB	152	305	2.5	65	↔
703	1.5E LSL	1220	15.1 OSB	152	305	2.5	65	↔ + ↓
704	1.7E LSL	1220	25.4 DFP	152	305	3.0	76	↔
705	1.7E LSL	1220	25.4 DFP	152	305	3.75	76	↔
706 [1]	1.7E LSL	2440	25.4 DFP	102	n/a	3.0	76	↔
707 [2]	1.7E LSL	1220	25.4 DFP	152	152	3.0	76	↔
708 [3]	1.5E LSL	1220	15.1 OSB	152	305	2.5	65	↔

[1] Sheathing placed in non-alternating pattern i.e. stacked formation; [2] Unblocked; [3] 15.5 mm thick gypsum wallboard added on the non-sheathed side. Screw spacing 203 mm c/c; [4] Symbol → indicates monotonic loading, ↔ cyclic loading, ↔ + ↓ is cyclic plus vertical loading.

The 600 wall series had 38 mm x 235 mm (2x10) No. 2 or better SPF studs and 1220 mm x 2440 mm OSB sheathing with thickness of 9.5 mm and 15.1 mm placed in staggered formation (Figure 1a). The studs were spaced at 610 mm on centre. The top and bottom plates consisted of 44 mm x 242 mm 1.7E LSL for all walls. The plate to stud connections consisted of two main components, Simpson LU28L joist hangers placed at every stud, and different configurations of Simpson H6 hurricane ties, which were the primary connector to resist the uplift forces. For wall 601, the H6 ties were placed on the top and bottom of all studs on the opposite side of the sheathing. Wall 602 used the same arrangement of ties on all studs except the last two studs on either end of the wall that had ties on both, the

sheathed and non-sheathed side of the stud (Figure 1b). Walls 603 to 605 had the dual tie formation only on the end two studs on either side of the wall and the middle stud, while the remaining studs were connected without any H6 ties. Walls 601 and 602 were sheathed with 9.5 mm OSB, while walls 603 to 605 were sheathed with 15.1 mm OSB. All 600 series walls used 2.5 mm diameter, 65 mm long spiral nails to connect the sheathing.

3 Loading Protocols and Instrumentation

A reinforced hollow steel beam provided a foundation to which the specimens were bolted down, while a hollow steel bar bolted to the top plate was used as load spreader bar. The spreader bar had attachments that allowed for lateral guides to be used to ensure a steady and consistent unidirectional movement of the walls. In all cases, anchor bolts were located on the centre line of the LSL bottom plates. The walls were subjected to monotonic or cyclic lateral loading using a 110 kN hydraulic actuator (Figure 1c).

String displacement transducers were placed at the top and at mid-height of the walls to measure lateral deflection. Six other displacement transducers were used at the both end studs and the middle stud to measure plate-to-stud uplift. In addition, two displacement transducers were used to measure bottom plate slip and its uplift from the foundation. A modified form of the loading protocol according to the ISO 16670 standard was used during the testing (ISO, 2003). Such modifications are permitted under section A.2d of the standard. Walls 601 and 701 were subjected to monotonic load pattern of 15.2 mm/min and were used to obtain the necessary parameters such as yield and ultimate displacements, later used for defining the cyclic protocol. The cycle pattern used was as follows: 1 cycle at 1.25%, 2.5%, 5%, 7.5%, and 10% of the ultimate displacement from either wall 601 or 701, and then a series of 3 cycles at 20%, 40%, 60%, 80%, 100%, and 120% of the ultimate displacements. After each set of 3 cycles, one cycle at the previous displacement level was applied.

4 Results and Discussion

Some of the most important wall properties obtained from the experimental testing are shown in Table 2. The symbols used in the table are the following: P_{max} is the maximum load attained by the wall, Δ_{max} is the wall displacement at maximum load, Δ_{ult} is the wall displacement at 80 % of the maximum load after the peak load was reached, E is the hysteretic energy dissipated by the wall, and μ is the ductility of the wall ($\mu = \Delta_u / \Delta_y$). All properties were determined according to the European Standard EN 12522 (EN 2001). All properties except, ductility, were determined based on the first envelope curve of the wall response in the initial direction (direction of the maximum load). Since there was a significant difference in ductility between the two directions of loading for most of the walls, the values in Table 2 represent the average ductility.

During the first test (wall 601), torsional failure of some of the studs was observed. The failure was attributed to the eccentricity that occurred between the plane of the sheathing and that of the single ties placed on the studs on the side opposite to the sheathing. Although this is not a problem in regular shearwalls, it should be taken into account when designing walls with increased stud depth. To mitigate this type of stud failure in the remaining tests most studs were connected with dual H6 ties, one on the back and one at the front of the stud. Wall 602 that did not utilize dual ties on the middle stud of the wall

also experienced a torsional stud failure at that particular stud. No torsional stud failures were observed in the rest of the walls tested.

Table 2. Tall wall properties obtained from quasi-static tests.

Wall	P_{max} [kN]	Δ_{max} [mm]	Δ_{max} % Drift	Δ_u [mm]	Δ_u % Drift	μ**	E [kJ]
601	38.5	152.0	3.10	161	3.29	5.0	n/a
602	38.2	94.4	1.93	97.3	1.99	5.1	25.0
603	39.6	92.5	1.89	135.8	2.77	6.0	32.3
604	42.1	93.1	1.90	131.7	2.69	6.6	34.9
605	62.6	124.8	2.55	131.7	2.69	6.0	51.6
701	49.5	105	2.14	149	3.04	8.8	n/a
702	53.4	89.8	1.83	98.7	2.01	6.0	29.6
703	48.1	90.1	1.84	98.9	2.02	6.6	29.0
704	64.6	91.1	1.86	100.3	2.05	5.6	45.8
705	77.8	90.5	1.85	105	2.14	5.2	58.4
706	83.2	91.3	1.86	100.5	2.05	5.5	51.6
707	26.2	91.7	1.87	120.9	2.47	5.6	23.0
708*	64.1	59.3	1.21	93.8	1.91	6.5	32.5

* 15.5mm thick gypsum wallboard placed on non-sheathed side; ** Average of both sides of the loop

Walls 603 to 605, which had 15.1 mm thick sheathing, had higher maximum load, ductility, maximum displacement, and energy dissipation than the walls with 9.5 mm sheathing (Table 2, Figure 2). In the walls with 15.1 mm thick sheathing, the connecting nails failed due to shear and fatigue, after being exposed to a large number of alternating cycles. This failure mode was different than that of walls with thinner 9.5 mm sheathing, where nails typically pulled through the sheathing, thus not allowing for the maximum connection resistance to develop. In general, most strength and ductility related properties of the walls were found to be proportionally related to the number of nails and the total cross-section area of the nails around the perimeter of the sheathing panels. Load-deformation hysteretic curves for walls 602, 603 and 605 are shown in Figures 2a, 2b, and 2c, respectively.

The deformed shape of the SPF walls in elevation consisted of bending (bowing) of the studs in the lower half of the wall, while the upper half of the studs remained relatively straight during the testing (Figure 3b). There was total failure of almost all plate-to-sheathing fasteners along the bottom of the wall, and up the wall sides to a height of 1.2 m. The presence of vertical load in wall 604 resulted in a switch of the failure location to that along the horizontal blocking at the mid-height of the wall. The maximum load, ductility and energy dissipation of this wall were slightly higher than those of the non-vertically loaded wall 603, which had similar properties (Figure 2b). This is in agreement with results reported from other experimental studies on regular shear walls (Dean and Shenton, 2005). In general, blocked tall walls with SPF studs spaced at 610 mm on centre were found to be effective lateral load-resisting systems. They were able to dissipate large amounts of hysteretic energy, especially when the nail spacing was reduced.

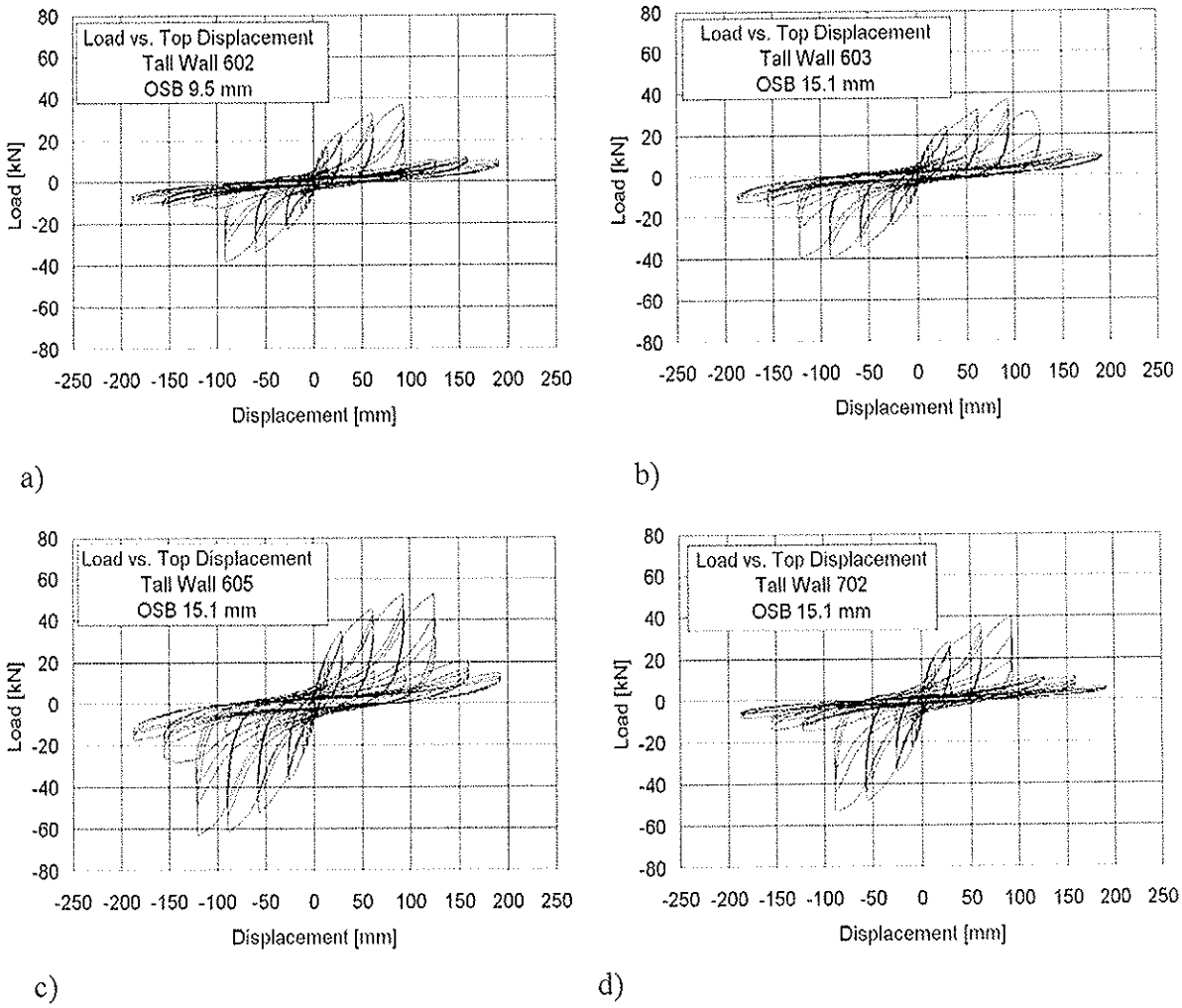

Figure 2. Hysteretic behaviour of walls: a) wall 602; b) wall 603; c) wall 605; d) wall 702.

Although not an issue with the 600 wall series, the first LSL wall tested (701) experienced a bottom plate failure on the tension side of the wall due to very high uplift forces and use of an anchor bolt not close enough to the last stud (figure 3b). It was also found that the end-nailing pattern used for the blocking of that wall was not sufficient, as nail pull-out of the studs was observed. Consequently, alternative nail patterns were introduced for the blocking in the rest of the walls. This included paired end-nailing and toe-nailing of the blocking to the studs. Similarly, changes to the anchor bolt pattern were made for all remaining walls of the 700 series.

Wall 702, which had 15.1 mm OSB sheathing, had lower maximum load and energy dissipation compared to wall 704, which had 25.4 mm DFP sheathing (Table 2, Figure 3a). The higher energy dissipation was attributed to the different failure mode of the nails. In walls with thinner OSB sheathing, the nails tended to develop only one plastic hinge along the shank length. In case of the walls with 25.4 mm thick DFP, the nails were able to develop three or more plastic hinges along the shank (Figure 4). Both values of sheathing thickness (15.1 mm and 25.4 mm) were able to prevent nail pull-through failures, thus allowing the nailed connections to develop higher load capacity. Wall 705 that utilized common nails had the highest energy dissipation of all walls (Figure 3a). The common nails used in this wall, however, experienced many withdrawals, which was not the case for other walls where spiral nails were used.

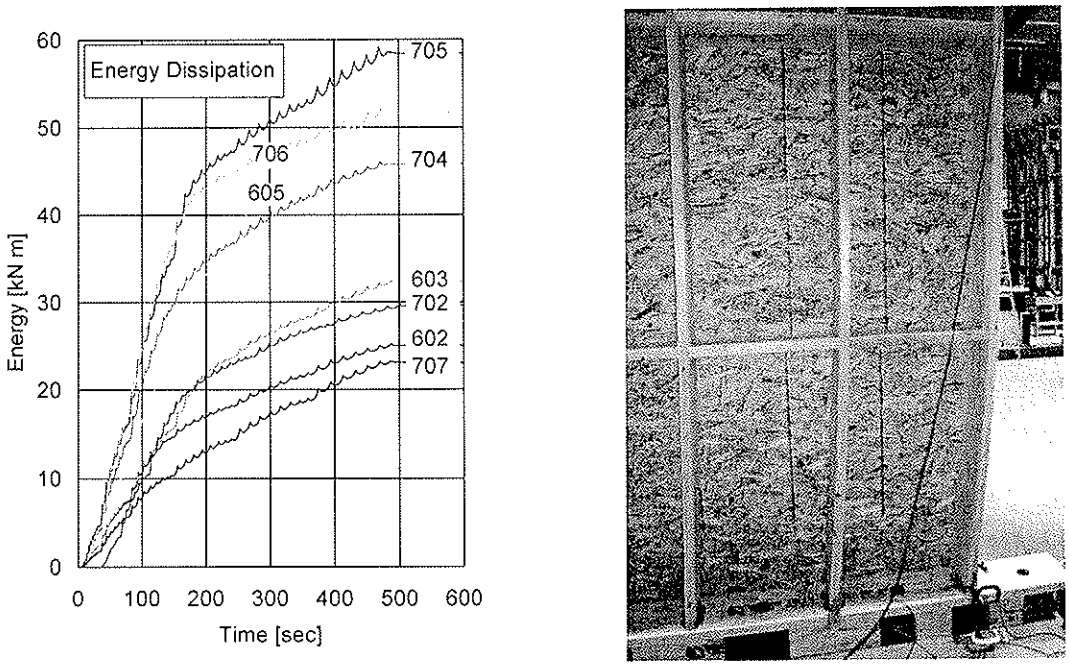

(a) (b)

Figure 3. a) Energy dissipation of various walls obtained during the testing; b) Typical deformed shape of the wall studs in the lower half of the walls.

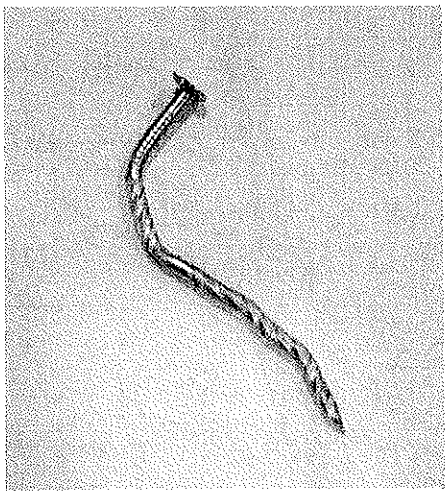

Figure 4. Typical nail failure mode exhibited in walls 704 to 706 with 25.4 mm thick plywood.

The use of larger stud spacing (1,220 mm) used for the 700 series walls did not appear to cause any detrimental effects on the tall wall behaviour under cyclic loads. Moreover, wall 706, which had the largest stud spacing of all walls (2,440 mm instead of 1,220 mm), was able to carry the highest load of all walls and exhibited a ductility level similar to that of other walls. This was attributed to the facts that this wall used 25.4 mm plywood sheathing, larger diameter nails, and smaller nail spacing. It should be noted, however, that in case of tall walls with larger stud spacing particular attention should be paid to the issues related to load transfer from the roof to the shearwall. Due to larger spans in the top plate between the studs, an increase in its deflection is to be expected from the joist or truss loads. In some cases (stud spacing of 2440 mm) use of double top plate might not be sufficient and other solutions should be sought. The only one unblocked wall tested (wall 707), experienced lower maximum load and hysteretic energy dissipation than other walls

(Table 2, Figure 3). It behaviour was in correlation with previous findings from tests on 2.44 m tall unblocked shear walls (Ni and Karacabeyli, 2002). The use of engineered wood products should not be encouraged in unblocked tall walls. The effect of using a higher strength (and relatively more expensive) product is offset by the lower wall strength and overall performance due to lack of blocking.

The deformed shape of the LSL walls in elevation was similar to that of the SPF walls and included bending of the studs in the lower half of the wall (Figure 5). The upper half of the wall remained relatively straight during the testing. The wall failure mode included connection failures of plate-to-sheathing fasteners along the bottom of the wall, and up the sides. Unlike the SPF walls, where the wall failure mode and failure location were affected by the addition of a vertical load, the same load level did not appear to have any significant effect on the 700 wall series. It seems that larger vertical loads, that unfortunately exceed the capacity of the test setup, were needed in order for LSL studded walls to have any positive effect of the vertical load.

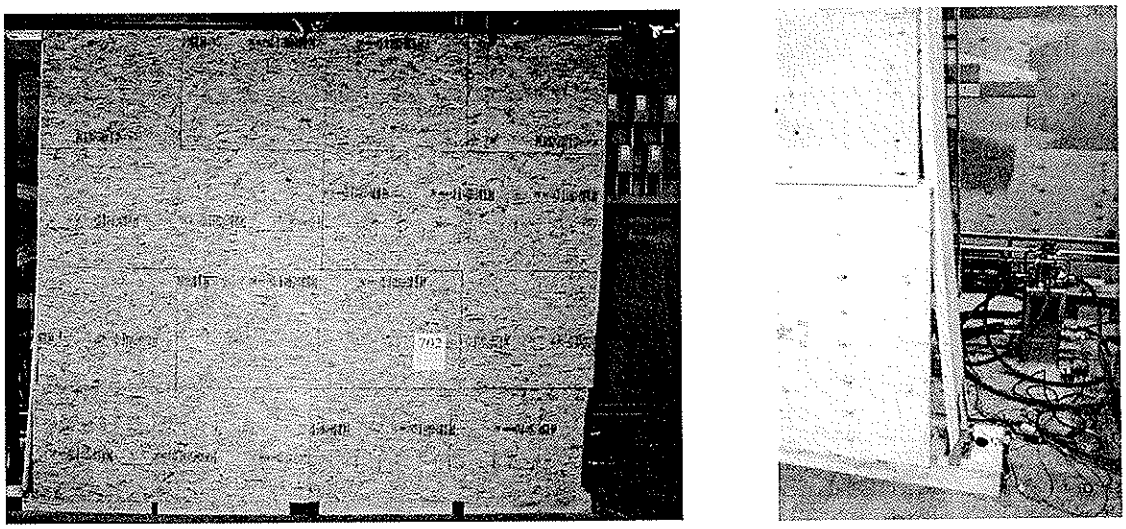

(a) (b)

Figure 5. a) Typical deformed shape of the wall during the testing; b) Stud-to-sheathing failure along the bottom plate and along the sides of the wall.

When 15.5 mm gypsum wallboard was added to the opposite side of the wall (wall 708), an increase in initial stiffness, maximum load, and energy dissipation was observed (Table 2). The maximum load, however, occurred at a lower displacement when compared to the equivalent wall with wood-based panels only (wall 702). The gypsum wallboard failure mode was screw tear-out at lower displacement levels than those for the OSB sheathing. After the gypsum wallboard failure, the OSB sheathing was able to withstand another load cycle.

The capacity and overall performance of the inexpensive off-the-shelf connectors used in the testing program was satisfactory. The dual H6 tie configuration wrapped under the bottom plate along with the joist hangers and the dense nailing pattern used, provided an effective stud-to-plate connection. No significant uplift of the studs occurred in any of the tests when such anchorage was provided. High uplift forces did cause minor transverse bowing of the bottom plate in some instances. Wider washers for the anchor bolts were used to mitigate this issue.

A simple material cost analysis showed that LSL based tall walls are more expensive than SPF based walls, even before construction time and labour factors are included. This is

significant to mention since cost issues related to the material used for the walls are often of a bigger concern than the labour related to driving few more nails in the wall. This cost and weight advantage of SPF-based walls can therefore be utilized in applications where the larger vertical and lateral load-carrying capacity of the LSL-based walls is not required. It should be noted, however, that while the SPF-based walls are easier to construct and manoeuvre, larger sizes of dimension lumber studs are susceptible to warping, which may lead to poor fitting and delays in construction. To mitigate some of these issues, these walls can be prefabricated in an assembly plant setting and then transported and tilted up on the construction site.

5 Conclusion and Design Recommendations

In this paper, results are presented from a series of quasi-static tests aimed to determine the seismic behaviour of tall wood-frame walls. Tall walls 4.9 m x 4.9 m in size were tested with a variety of sheathing-to-stud connections, stud material, stud spacing, stud-to-plate connections, as well as sheathing material and thickness. Findings and observations from this project are anticipated to be useful for development of design guidelines for tall walls subjected to seismic loads in wood design codes and standards. Some of the design recommendations are given bellow:

(a) Tall-walls with both, SPF and LSL studs can be effective lateral load resisting systems. Stud tables for dimensional lumber and some engineered wood products such as laminated veneer lumber spaced at 305 mm, 406 mm and 610 mm on center subjected to wind loads are given in the "Tall Wall Workbook" (CWC, 2007);

(b) From a cost competitive point of view, tall walls with engineered wood product studs, such as LSL, should be used with larger stud spacing (1.2 m and larger) and thicker sheathing (up to 28.6 mm). The larger stud spacing per se, was not found to be detrimental to the tall wall performance against lateral loads, without the presence of significant simultaneously applied vertical load;

(c) Use of thin (9.5 mm) sheathing should be avoided in combination with studs made of denser wood products such as LSL, due to the increased presence of nail pull-through the sheathing failure mechanism. Such mechanism doesn't allow for full potential of the nailed connections to be developed. On the other hand, nails in tall walls made with 25.4 mm thick plywood were able to develop three or more plastic hinges during testing, thus providing the wall with high lateral load capacity and energy dissipation;

(d) Tall walls may be designed as blocked or unblocked. Blocked tall walls, especially in case with engineered wood studs, are more cost effective per unit of shear resistance;

(e) For lumber stud walls, use of higher strength lumber or engineered wood products for the top and bottom plates is recommended to resist the induced uplift and anchorage loads;

(f) For walls with a stud spacing larger than 610 mm, top plate deformation between the studs shall be checked, as it may become an issue, especially when transferring large gravity loads in case when roof joists are placed perpendicular to the wall line;

(g) Stud-to-plate connections are of great importance for the overall performance of tall walls. An arrangement consisting of off-the-shelf dual hurricane ties and a hanger proved to be an efficient and cost-effective solution for the stud-to-plate connections, for both, site built and prefabricated tall walls. Use of asymmetrical stud to plate

connections, such as single tie or custom made connectors that connect the non-sheathed side of the stud only, should be avoided in high seismic zones due to susceptibility of the studs to torsional failure;

(h) Attention should be paid to the design of the anchoring devices for tall walls, so that they can efficiently transfer the load to the foundation, without damaging the bottom plate. For example large plate washers may be used to prevent splitting of the bottom plate;

(i) The effect of vertical load (in the amount of 20 kN/m) on a tall wall with dimensional lumber studs resulted in a slight increase in the lateral load capacity, ductility and energy dissipation compared to a non-vertically loaded wall with similar properties;

(j) Application of gypsum wallboard on the other side of the wall increased the stiffness and the lateral load capacity of the tall wall. The maximum load, however, occurred at displacement drifts lower than in equivalent shearwalls without gypsum boards. For walls with LSL studs for example, the maximum load occurred at a drift of 1.8% for wall without gypsum vs. 1.2 % for wall with gypsum wallboards. The ultimate displacement drifts, however, occurred at relatively similar drift levels (1.9 % vs. 2%);

(k) Test results suggest that tall walls with wood-based panel on one side and a gypsum wallboard on the other should be assigned a lower ductility-related force modification factor (R_d factor) than tall walls with wood-based panels only. A similar provision is already introduced in the Canadian Standard for Engineering Design in Wood for standard shearwalls.

6 References

CWC 2007. Tall Walls Workbook – Single Storey Commercial Wood Structures. Canadian Wood Council, Ottawa, Ontario.

Dean, P. K., and Shenton, H. W, 2005. Experimental Investigation of the Effect of Vertical Load on the Capacity of Wood Shear Walls. ASCE Journal of Structural Engineering, 131(7), 1104-1113.

EN 12512, 2001. Timber structures - Test methods - Cyclic testing of joints made with mechanical fasteners. European Committee for Standardization. Brussels, Belgium.

ISO 2003. ISO Standard 16670. Timber structures—Joints made with mechanical fasteners—Quasi-static reversed-cyclic test method. ISO Technical committee on timber structures. Geneva, Switzerland.

Ni, C., and Karacabeyli, E, 2002. Effect of Blocking in Horizontally Sheathed Shear Walls. Wood Design Focus, 12 (2), 18-24.

INTERNATIONAL COUNCIL FOR RESEARCH AND INNOVATION
IN BUILDING AND CONSTRUCTION

WORKING COMMISSION W18 - TIMBER STRUCTURES

INTERNATIONAL STANDARD DEVELOPMENT FOR LATERAL LOAD TEST METHOD FOR SHEAR WALLS

M Yasumura
Shizuoka University

JAPAN

E Karacabeyli
Forintek Canada Corporation

CANADA

MEETING FORTY

BLED

SLOVENIA

AUGUST 2007

Presented by M. Yasumura

B. Dujic asked about the recommendation for the next approach and how many specimens would be needed. I. Smith questioned what would be the implication with respect to design as different test methods lead to different results; i.e., how to interpret the results as designers should not be put in a situation to do the interpretation. M. Yasumura replied that the ISO standards should not be involved in the interpretation of results as this is the responsibility of individual nations. E. Karacabeyli explained that method A is more or less the approach used in most design codes and method B is used in the U.K. as the lower bound.

A. Ceccotti received clarification on Figure 5.

A. Salenikovich commented that this work should be coordinated with ASTM initiatives. He asked about perforated walls. M. Yasumura replied that the perforated walls were not considered but they can be tested in method two where length of specimen becomes an issue and in method 1 where standard length can be used. Method 2 has no limitation on length. A. Salenikovich commented that loading beam stiffness needs consideration. M. Yasumura agreed.

B.J. Yeh commented the ASTM initiative is considering the number of specimens and will share the information. The influence of loading beam is important based on APA experience. The reason why this research did not show a difference may be because vertical load was already applied and the aspect ratio of the walls.

International Standard development for lateral load test method for shear walls

Motoi Yasumura
Shizuoka University, Japan
and
Erol Karacabeyli
FPInnovations, Forintek Division, Canada

1 Introduction

Shear walls are widely used for resisting member against wind and seismic load in timber structures. Evaluation of the structural performance of shear walls under static and reversed-cyclic loading has become a requirement of wind and seismic design. The working group 7 of ISO-TC 165 (International Organization of Standardization, Technical Committee on Timber Structures) is preparing the International Standard to provide a test method for static and cyclic lateral loading as a basis for the development of characteristics of shear walls for use in wind and seismic design [1].

The standard is intended to provide static and cyclic test methods as a basis for the derivation of lateral load resisting parameters which are required in the wind and seismic design of shear walls in timber structures. This standard can be used to determine those parameters under the conditions that;

(1) the boundary conditions are designed to ensure that the full shear capacity of the wall is achieved (Method I), and

(2) the boundary conditions are designed to reflect the intended actual construction details (Method II).

In Method I, the full shear capacity of the wall specimen is achieved through application of sufficient vertical loads, and/or adequate hold-down connectors or tie-down rods (at both ends of the wall specimen in cyclic test). In Method II, the wall specimen is tested with representative boundary conditions (e.g. anchorage, hold-down connector details), and the vertical (compressive or tensile) loads that are expected to be used in actual construction.

In this paper, a Finite Element Model with non-linear joint elements connecting sheathing panels to wooden frames was developed for wood-framed shear walls [3] and the influence of the test methods including of the vertical restraint of the end of walls, vertical loads, and the length of walls on the shear capacity are studied.

The cyclic displacement schedule in ISO Standard 16670 [2] which was developed for cyclic testing of connections in consultation with a group of international experts, is also employed in this standard. The cyclic displacement schedule is intended to produce: (a)

data that sufficiently describe the elastic and inelastic cyclic properties of the wall specimen, and (b) demands representative of those imposed on the walls by earthquakes.

2 Racking test of shear walls

2.1 Specimens

Wood-framed shear walls of Japanese standard size were prepared for static (monotonic) and reversed cyclic lateral load tests. Specimens had wooden frames of 1.82m and 2.44m height sheathed with 9mm thick larch plywood (JAS Grade 2) on one side as shown in Fig.1. Sheathing materials were connected to frames of nominal two-by-four lumbers of S-P-F No.1 and 2 with JIS A5508 CN50 nails (50.8mm length and 2.87mm diameter). Nails were spaced 100mm in the perimeters of a sheet material and 200mm on the central support. Studs were spaced 455mm and connected to bottom and double top plates with CN90 nails (88.9mm length and 4.11mm diameter). End studs were doubled and connected each other with CN75 nails (76.2mm length and 3.76mm diameter) spaced 300mm.

2.2 Test methods

Two kinds of specimens, Walls (A) and (B) as shown in Figs. 1 (a) and 1 (b) were prepared for the racking tests. The bottom plates of Wall (A) were connected to 89mm by 89mm Western hemlock sill (MOE of 12,000N/mm^2) and steel foundation with four bolts of 16mm diameter. Double top plates were connected to 89mm by 184mm glulam girder (JAS E120-F330) with four bolts of 16mm diameter. Two hold-down connectors HDB15 were applied to both ends of wall connected to the studs with three bolts of 12mm diameter and

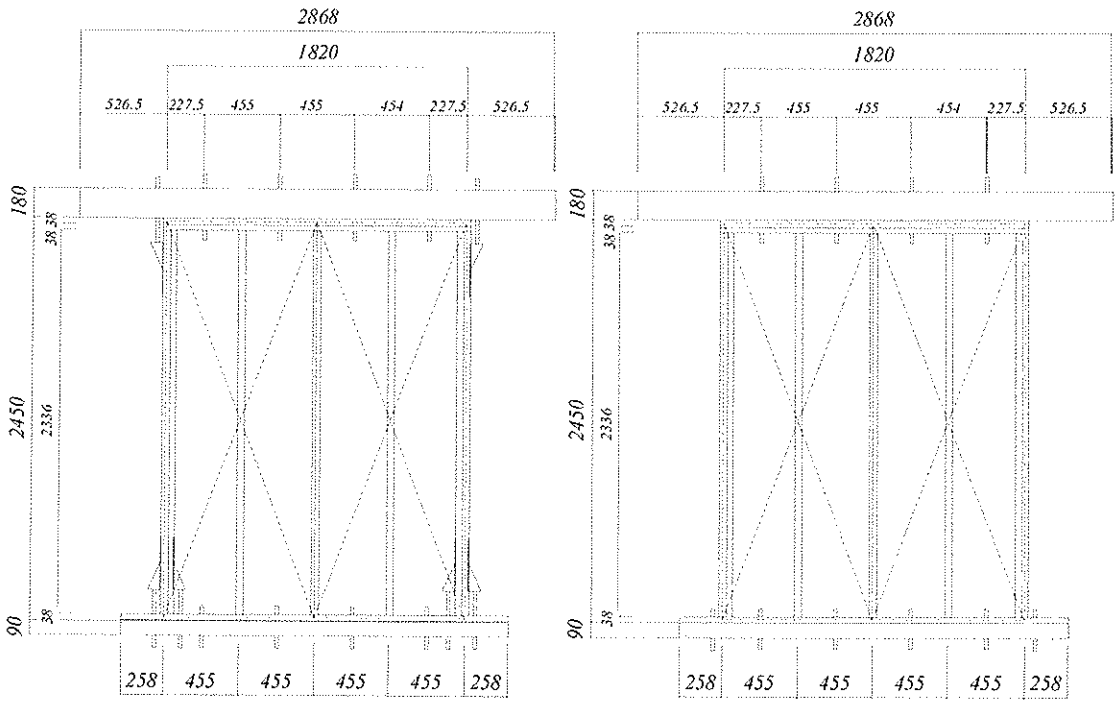

(a) Wall (A) with hold-down connectors **(b) Wall (B) without vertical restraint**

Fig. 1 Wall specimens

connected to the steel frame with a 16 mm diameter bolt. One hold-down connector HDB15 was applied at the top of end studs to connect to glulam girder located at the top of wall with a 16mm diameter bolt. The bottom plates of Wall (B) were connected to 89mm by 89mm sill and steel foundation with six bolts of 16mm diameter. Double top plates were connected to 89mm by 184mm glulam girder with four bolts of 16mm diameter. No hold-down connectors were applied either at the bottom nor at the top of the end studs.

The static (monotonic) and the reversed cyclic loads were applied at the end of girder by a computer-controlled actuator, and horizontal and vertical displacements of wall were measured by electronic transducers. One specimen was subjected to the monotonic loading, and then two were tested under the reversed cyclic loading based on the loading protocol in ISO WD21581.

2.3 Test results

Figure 2 shows the typical relationships between the lateral loads and the story drift in Walls (A) and (B). It is observed that the maximum lateral load in reversed cyclic loading test tended to be slightly lower than that in monotonic loading test. The lateral load decreased suddenly after the peak load especially in Wall (A) while the degradation in Wall (B) was more gentle. The maximum loads of Wall (A) in monotonic and reversed cyclic lateral load tests were respectively 30.2kN and 27.3kN in average, and those in Wall (B) were respectively 10.1kN and 9.1kN in average which were almost one thirds of those of Wall (A) .The ultimate displacement of Wall (A) defined by the eighty percent of the maximum load after the peak in monotonic and reversed cyclic lateral load test were respectively 126mm and 102mm in average, and those of Wall (B) were respectively 31.1mm and 27.2mm in average which were almost one forth of those of Wall (A) . These results indicate that both the maximum lateral loads and ultimate displacements decrease significantly if no hold-down connectors are applied, and it should be noted that the test results are highly influenced by the boundary conditions.

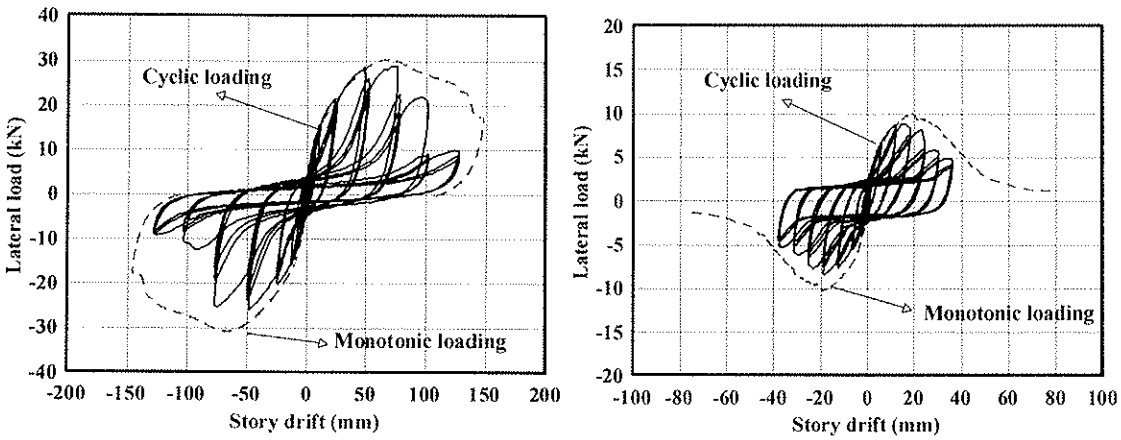

(a) Wall (A) **(b) Wall (B)**

Fig. 2 Typical load-displacement relationships

3. Modelling of walls

The effects of vertical restraint, vertical loads, wall length on the racking strength of shear walls were analysed by using Finite Element Method. Figure 3 shows the Finite Element

model for the wood-framed shear walls consisting of the beam element, plate element and joint element connecting plate element to flame element.

Single shear nail tests according to ISO 16670 were conducted to model the load-slip relationships of nail joints. A single specimen was tested by monotonic loading to determine the cyclic protocol and six specimens were subjected to the reversed cyclic loading. Figure 4 shows typical load-slip relationship of the nail joint and Fig.5 shows the tri-linear model of the envelop curves used for the simulation.

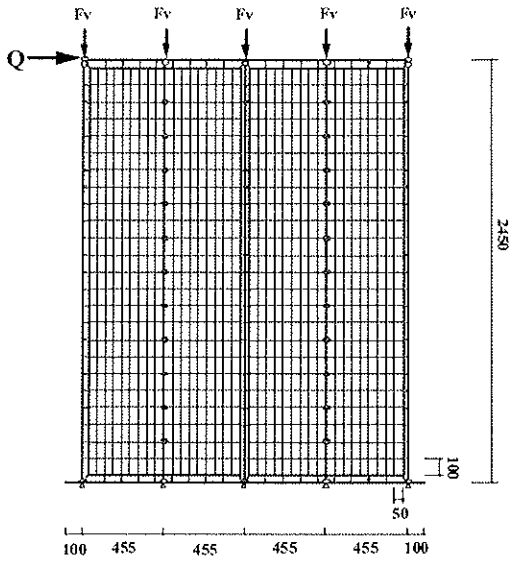

Fig.3 Finite Element Model of shear walls

CASTEM 2000 was used to simulate the load-displacement relationships of shear walls. For Wall (A) whose end studs were connected to the steel base with hold-down connectors, all the frame members were assumed to be connected with pin joints without slips, and the bottom of studs of Wall (B) was assumed to be free for the separation.

Figure 6 shows the comparison of the envelope curves of Walls (A) and (B) with the simulation. The simulation predicted quite well the strength and stiffness of Wall (A), but

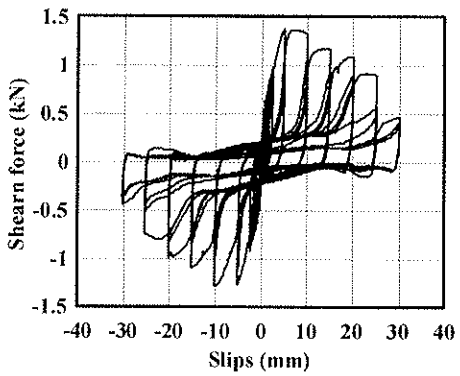

Fig. 4 Load-slip relationships of nail joint

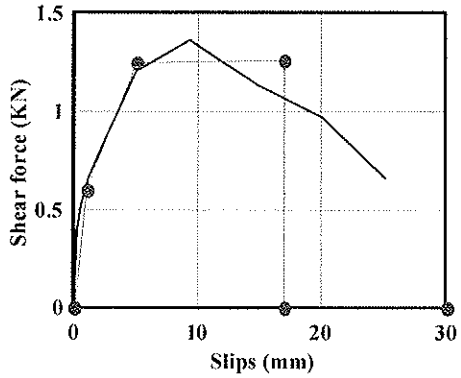

Fig.5 Tri-linear model for envelope curves

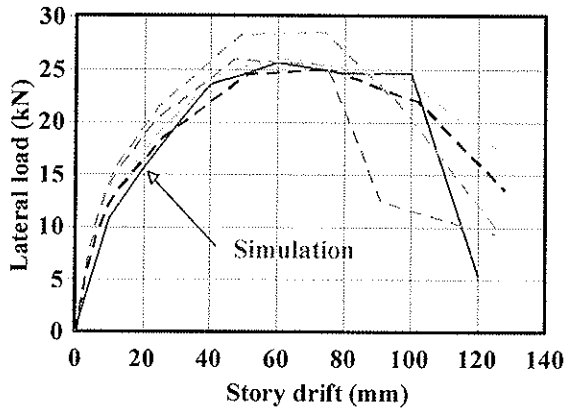

(a) Wall (A)

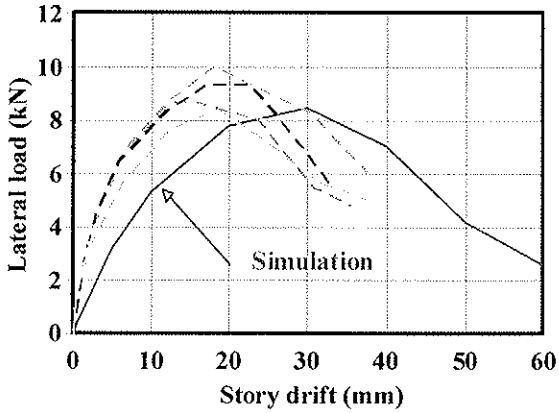

(b) Wall (B)

Fig.6 Comparison of simulation with the experimental results

it tended to underestimate the stiffness of Wall (B) which had no connections at the bottom of end studs although it predicted comparatively well the strength of the wall.

4. Parameter study

Parameter studies were done to investigate the influence of the vertical loads, wall length, vertical restraint of the end studs by using the Finite Element Model mentioned above. Table 1 shows the studied parameters. Walls with three different length of 1, 2 and 3 units (1 unit of 910mm with one sheet of plywood) were subjected to horizontal and vertical loads. The vertical loads were applied on the girder at the position of each stud (455mm apart). The vertical load per stud varied from 1 to 6kN.

Table 1 Parameter of simulation and total vertical loads

Length of wall	Vertical load per stud					
	1kN/stud	2kN/stud	3kN/stud	4kN/stud	5kN/stud	6kN/stud
1 unit (910mm)	3kN	6kN	9kN	12kN	15kN	18kN
2 units (1820mm)	5kN	10kN	15kN	20kN	25kN	30kN
3 units (2730mm)	7kN	14kN	21kN	28kN	35kN	42kN

5. Results and discussions

Figure 7 shows the simulated load-displacement relationships of wall with different vertical loads without vertical restraint and those with vertical restrains without vertical loads. It shows that the effect of vertical loads on the strength and the ductility of one unit wall (L=910mm) without vertical restraint is comparatively small, and that of two and three unit walls (L=1820mm and 2730mm) was more significant than that of one unit wall. Figure 8 shows the ratio of the maximum lateral load without vertical restraint to that in wall with full vertical restraint. It shows that the maximum lateral load of one, two and three unit wall were respectively 18% , 33% and 47% of the wall with full vertical restraint increased as the wall length increased. The maximum lateral loads increased as the vertical loads increased, and those of one, two and three unit wall attained to 44%, 70% and 85% of the wall with full vertical restraint when the vertical load per stud was 6kN (total vertical loads of 18kN, 30kN and 42kN, respectively).

Figure 9 shows the relationships between the maximum lateral load and the wall length with the vertical loads of 0kN, 2kN and 4kN/stud in the wall without vertical restraint and the wall with full vertical restraint without vertical loads. In case of wall with full vertical restraint, the maximum load increased proportionally as the wall length increased. This indicates that the length of wall does not have an important effect on the shear strength per wall length if they are tested in Method I (full vertical restraint of end studs and no vertical loads), and the structure with this type of wall can be designed with an assumption that the strength of shear wall is proportional to the total length of the wall if both ends of each shear wall are fully anchored with hold-down connectors. In case that the racking tests are

conducted according to Method II and the wall end is not fully connected to the foundation, more complicated design method may be required.

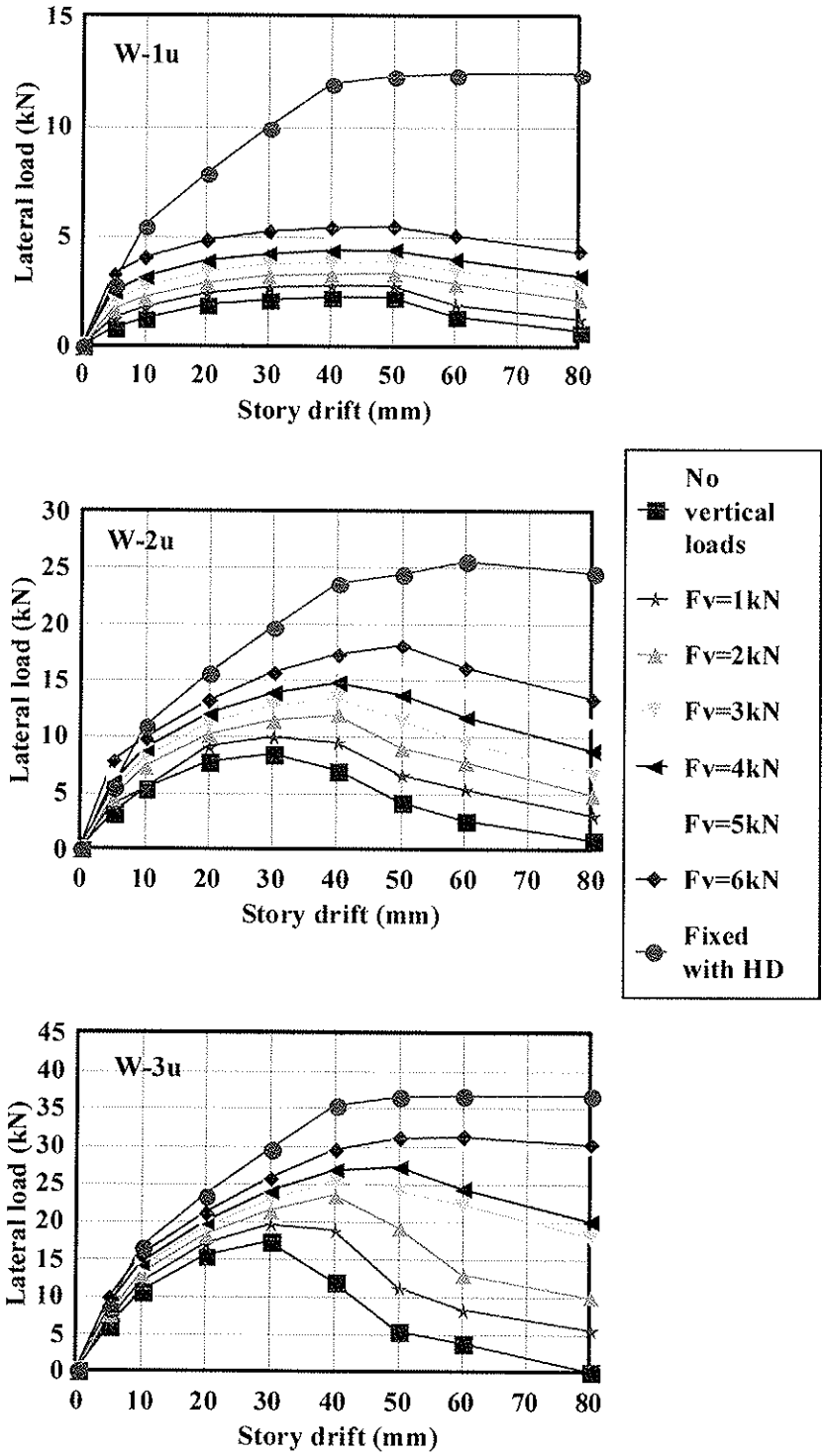

Fig. 7 Simulated lateral resistance (wall length of 1, 2, 3 units, 1 unit=910mm)

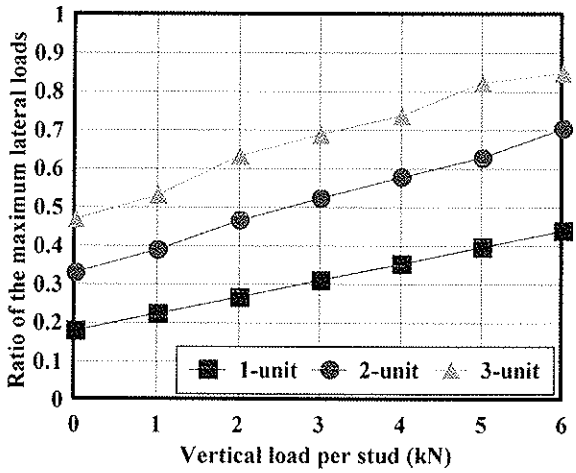

Fig. 8 Ratio of the maximum lateral load of wall without vertical restraint to that with vertical restraint

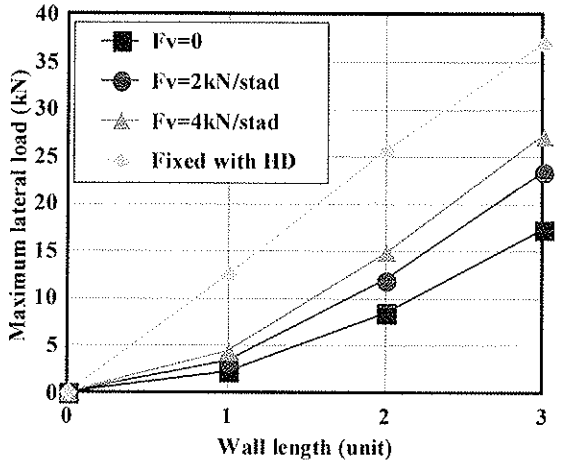

Fig. 9 Influence of wall length on the maximum lateral load of wall with and without vertical restraint

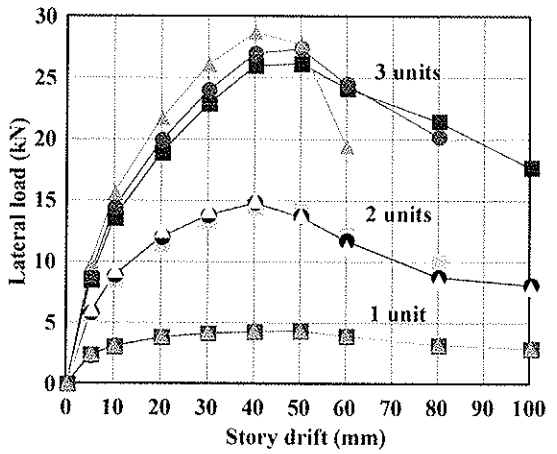

Fig.10 Influence of the stiffness of loading beam when vertical loads are 4kN/stud (stiffness of beam: 0.01EI, EI, 100EI)

Figure 10 shows the load-displacement relationships of walls of 1, 2 and 3 unit length with the vertical loads of 4kN per stud. The stiffness of loading beam of one hundredth and one hundred times was taken for simulation. It shows that the stiffness of loading beam had

very little influence on the shear resistance of wall when the wall lengths were one and two units (910mm and 1820mm), but the shear resistance increased as the stiffness of loading beam increased in the wall of three units length (2730mm). This indicates that the stiffness of loading beam has an influence on the test results when the length of wall is large and the vertical load is high. This should be noted especially when the racking test is conducted with Method II.

6. Conclusions

The following conclusions are derived from the parameter study which employed Finite Element Model that is verified against the static and reversed cyclic lateral load tests of wood-framed shear walls performed according to the draft.

(1) The vertical restraint of the wall with hold-down connectors, for example, is the most influential factor on the test results of strength and ductility in racking tests

(2) The effect of vertical loads on the strength and ductility of one unit wall (L=910mm) is comparatively small, and that of two and three unit walls (L=1820mm and 2730mm) is more significant when no vertical restraints are applied.

(3) Maximum lateral loads of the wall without vertical restrains and vertical loads whose length is one, two and three units (L=910, 1820, 2730mm) are respectively 18% , 33% and 47% of the wall with full vertical restraint.

(4) Maximum lateral loads of the wall without vertical restrains and with the vertical loads of 6kN per stud (total vertical loads of 18kN, 30kN and 42kN, respectively) whose length is one, two and three units (L=910, 1820, 2730mm) are respectively 44% , 70% and 85% of the wall with full vertical restraint.

(5) Maximum lateral loads of wall with full vertical restraint is proportional to the wall length. The length of wall does not have an important effect on the shear strength per wall length if they are tested with Method I.

(6) Maximum lateral load of wall without vertical restraint increases exponentially with the wall length. The length of wall have an important effect on the shear strength of wall if no vertical restrains are applied.

(7) Stiffness of loading beam has an influence on the test results when the length of wall is large and the vertical load is high. This should be noted especially when the racking test is conducted with Method II.

Acknowledgments

The authors would like to express their thanks to Ms. Kawasaki and Ms. Wada of Laboratory of Timber Structures and Housing Environment, Shizuoka University for their assistance of conducting racking tests of shear walls.

References

1. International Standardization Organization, TC165-WG7: ISO WD21581: Timber structures – Static and cyclic lateral load test method for shear walls, 2007.
2. Sverker Andreasson, Motoi Yasumura; Sensitivity study of the finite element model for wood-framed shear walls, J Wood Sci 48:171-178, 2002
3. International Standardization Organization: ISO 16670: Timber structures – Joints made with mechanical fasteners – Quasi-static reversed-cyclic test method, 2003

INTERNATIONAL COUNCIL FOR RESEARCH AND INNOVATION
IN BUILDING AND CONSTRUCTION

WORKING COMMISSION W18 - TIMBER STRUCTURES

INFLUENCE OF OPENINGS ON SHEAR CAPACITY OF WOODEN WALLS

B Dujic
University of Ljubljana, Faculty of Civil and Geodetic Engineering

S Klobcar
CBD Contemporary Building Design Ltd.

R Zarnic
University of Ljubljana, Faculty of Civil and Geodetic Engineering

SLOVENIA

MEETING FORTY

BLED

SLOVENIA

AUGUST 2007

Presented by B. Dujič
H. Blass comment that some systems behaved more like frames than shear walls.
G. Schickhofer received clarification on small specimen shear test configuration with respect to Figure 13 as an approach common in masonry structure research. He commented that may be other methods for shear modulus evaluation is more appropriate.
He asked whether the results can be extended to 5 layer plates. B. Dujic replied yes if anchor failures also governs but can't confirm.
B.J. Yeh questioned whether energy dissipation were compared and commented on the issue of end of wall buckling failure under compression. B. Dujic replied that hysteresis loops seemed to indicate narrower loops compared to conventional walls. B.J. Yeh commented that this is more similar to moment frame compared to conventional wall; therefore, different R factors may be warranted.
F. Lam commented that the presence of transverse wall should prevent buckling from happening and therefore would not be an issue. He mentioned that the 1/200 drift limit seems severe as a serviceability requirement compared to N. America. B. Dujic agreed with the transverse wall comment and explained the range of drift limit states considered in Europe.
A. Ceccotti commented R is a little lower than for wood frame.
R. Steiger commented for assessment of stiffness properties modal analysis and NDT methods can be used.

Influence of Openings on Shear Capacity of Wooden Walls

Bruno Dujic

University of Ljubljana, Faculty of Civil and Geodetic Engineering, Slovenia

Simona Klobcar

CBD Contemporary Building Design Ltd., Slovenia

Roko Zarnic

University of Ljubljana, Faculty of Civil and Geodetic Engineering, Slovenia

Abstract

The new generations of massive cross-laminated wooden structures are recently becoming more popular in European market. The new trends are also bringing multi-storey timber structures. Special attention is paid to buildings located in earthquake prone areas of middle and south Europe. Therefore, the appropriate guidelines for designing have to be set for existing and new timber structural systems to assure their seismic resistance. In design of wood structures, the contribution of fenestrated wall segments usually is not taken into account when calculating the wall shear capacity. Some experimental and analytical studies have shown that fenestrated wall segments may contribute to the earthquake resistance of the wood-frame plywood sheathed walls. The load-bearing capacity and stiffness of fenestrated wood walls are influenced mostly by the size and layout of the openings. To evaluate the shear strength and stiffness reduction for different size and placement of openings in the wall, development of a mathematical model verified against experimental tests, is of paramount importance.

The main goals of the experimental research and parametric study presented in this paper are to provide information on how to estimate the racking strength and stiffness of cross-laminated solid wood walls with openings, and to recognize how the shape and the area of the openings influence the shear capacity and stiffness of cross-laminated wood walls. Results form the preformed parametric study are summarised in diagrams that could serve as a practical tool for estimating the influence of fenestration on the stiffness and load-bearing capacity of cross-laminated solid wood walls. The study has concluded that openings with a total area of up to 30 % of the entire wall surface do not significantly influence the load-bearing capacity of the wall. The stiffness in such case, though, is reduced for about 50 %.

1 Introduction

Shear walls are structural elements that are frequently used to resist seismic and wind loads in timber structures. Currently, wood-frame buildings are designed for earthquake and wind loads by taking into account shear resistance of full wall segments only. Parts of wall above and bellow the openings are excluded from the calculation method (Fig.1). Although this approach may be valid for light-frame buildings, it can lead to under-estimation of shear resistance of a building with cross-laminated walls. For more accurate and economic design, parts of wall above and below the openings have to be taken into account as they transfer the loads between full wall segments and influence their boundary conditions [1]. Therefore entire wall assembly with different openings could be determined as one structural element of full length with reduced shear strength and stiffness [2]. To evaluate the shear strength and stiffness reduction for different fenestrations, development of a verified and validated mathematical model is needed to reduce number of experimental tests.

A series of racking tests on fenestrated cross-laminated (X-lam) solid wood panels were carried out at University of Ljubljana. The main objective of the testing was to understand the global response of fenestrated panels and to obtain data for verification and validation of response of the panel predicted by a numerical model [3]. The model was developed and the parametric study carried out using the commercial software SAP2000. Main parameters of interest were related to nonlinear behaviour of anchors and elastic behaviour of X-lam wall segments around openings and were determined through additional testing.

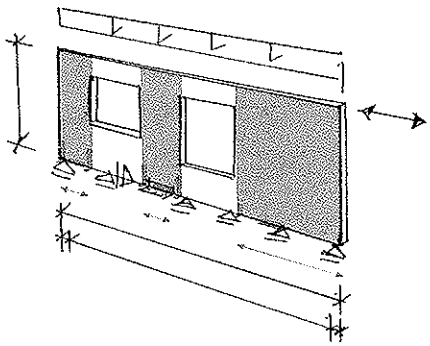

Fig.1: Example of massive wood wall with openings and principle of design with only full wall segments.

The numerical model of experimentally tested panels was used for parametric study on panels with different patterns of fenestrations. The parametric study resulted in diagrams, which show the relation between panel area ratio and ratio of racking load and stiffness of fenestrated X-lam walls against non-fenestrated one. Study of fenestrated X-lam wood walls followed the concept of previous research on light-frame walls presented in Section 2.

2 State of the art - Influence of openings in light timber frame walls

As far as we know there are no published research results concerning behaviour of X-lam fenestrated panels. However, there are published research results on fenestrated light-frame walls [4] [5] [6].

2.1 Research by H. Sugiyama and M. Yasumura

Hideo Sugiyama and Motoi Yasumura reported results of racking tests on plywood-sheathed timber frame walls of reduced scale 1:3 with various openings [4] and full-size walls [5] constructed according to standard specification of North American light-frame structures.

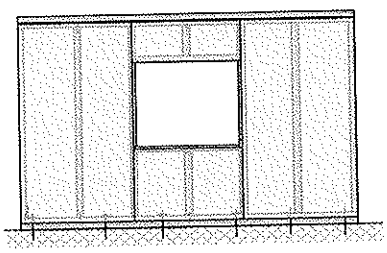

Fig.2: Fenestrated timber-frame wall with sheathing.

They defined the sheathing area ratio, r (eq.1), in order to classify walls based on the amount of openings in the wall (Fig.2). The sheathing area ratio was determined by: a) the ratio of the area of openings to the area of wall and b) the length of wall with full height sheathing to the total length of wall. Two empirical equations (eq. 2) were put forward [4] [5], which make it possible to estimate the shear strength and stiffness of any fenestrated timber frame wall if shear characteristics of a fully-sheathed wall of the same size is known.

Using the same definition, the parameter r is proposed here to be named "*panel area ratio*" of fenestrated X-lam wooden wall (Fig.3). The proposed panel area ratio r takes into account both size and shape of openings. Regarding the size aspect, the value of r is inversely proportional to the opening area. Regarding the shape of the opening, a higher value of r is associated with vertically oriented fenestration. In the case of non-fenestrated wall the value of r is equal to 1.0.

The ratios between shear strength F and shear stiffness K of fenestrated light-frame wall and non-fenestrated one, as obtained from tests, are presented in Figures 3 and 4, respectively. Ratio of shear stiffness is defined as relation between shear stiffness of the wall with openings and shear stiffness of the wall without openings of equal dimensions and at the same level of shear strain. Similarly, ratio of shear strength presents relation between shear strength of fenestrated and non-fenestrated wall.

Ratio of shear stiffness is evaluated at shear deformation of 0.01 rad of light-frame wall and is nearly constant at lower shear deformations.

Variables in equation 1 are as follows:

r panel area ratio

H height of the wall element

L length of the wall element

$\sum L_i$ length of full height wall segments

$\sum A_i$ sum area of openings

$\alpha = \frac{\sum A_i}{HL}$ ratio of openings in wall element

$\beta = \frac{\sum L_i}{L}$ ratio of full wall segments.

$$r = \frac{1}{1+\frac{\alpha}{\beta}} = \frac{H\sum L_i}{H\sum L_i + \sum A_i} \quad (1)$$

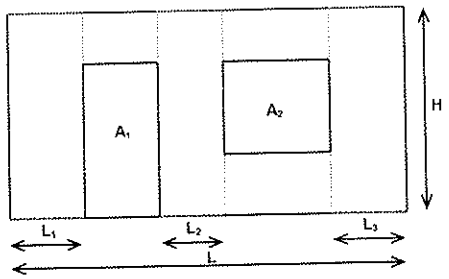

In diagrams that present the influence of openings on shear capacity of light-frame wall the same trend line was determined for evaluation of shear strength and shear stiffness ratios. The experimentally obtained empirical equations are expressed in terms of panel area ratio as shown in Equation 2:

$$K = \frac{r}{3-2r} \quad \text{and} \quad F = \frac{r}{3-2r} \quad (2)$$

Where:

F ratio of shear strength of fenestrated and non-fenestrated light-frame wall;

K ratio of shear stiffness of fenestrated and non-fenestrated light-frame wall;

r panel area ratio (or sheathing area ratio as named in the original research paper).

2.2 Research by J. D. Dolan and A. C. Johnson

In 1996 J. Daniel Dolan and A. C. Johnson published results of monotonic and cyclic tests on full-size light-frame walls with various openings. Monotonic results were compared with the trend line obtained by the Japanese research (Fig.3, Fig.4). Results obtained on full-size light-frame walls have shown slightly higher shear capacity especially at smaller ratio of openings. Shear stiffness was evaluated at shear deformation that corresponds to 40% of ultimate racking load and the following equation was proposed:

$$F = 1{,}27r - 0{,}28 \quad (3)$$

Significant differences observed between monotonic and cyclic response of shear walls were the main reason that the evaluation of the seismic response of a structure be conducted based on cyclic tests. Because the empirical equations presented were mainly based on monotonic test results, further investigation was done on full-size walls under cyclic loading defined according to sequential phased displacement protocol. Shear resistance determined by cyclic tests was up to 30% less than resistance obtained under monotonic loading. Higher difference between monotonic and cyclic responses was observed in case of non-fenestrated wall panels. With decreasing of panel area ratio r or with increasing the ratio of openings α the difference was smaller.

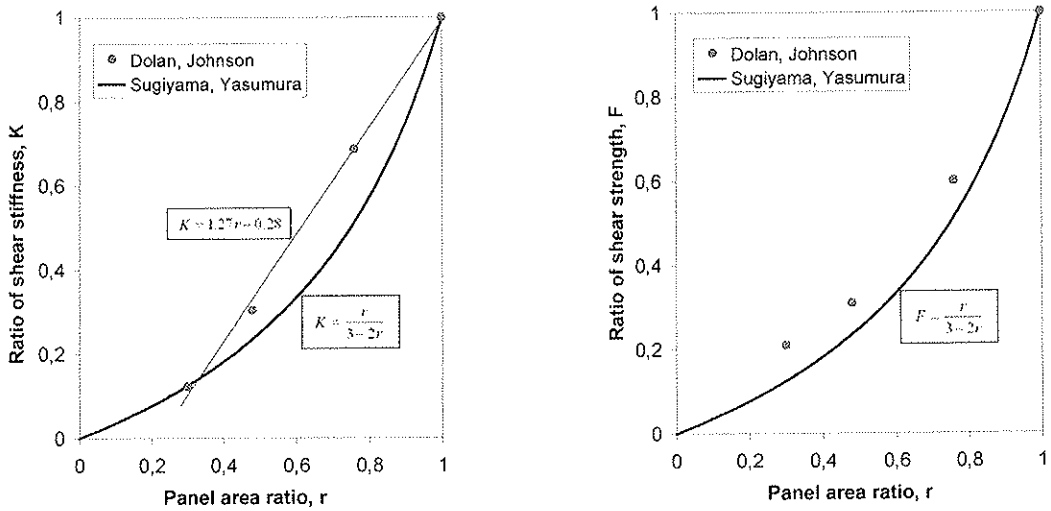

Fig.3: Trend lines obtained in past research for reduction of a) shear stiffness and b) shear strength of fenestrated walls.

3 Experimental research on X-lam solid timber walls with openings

3.1 Racking tests on X-lam timber walls with openings

Two configurations of walls of equal dimensions (320 x 272 x 9.4 cm) represented by two specimens each have been tested under the same boundary conditions. Specimens of Wall 14 were without openings while the specimens of Wall 13 had a door and a window openings (Fig.5). The tests have been preformed at the Laboratory of the Faculty of Geodesy and Civil Engineering in Ljubljana, Slovenia using the test set up specially designed and constructed for testing of panels under different boundary conditions and constant vertical loading [1] [2].

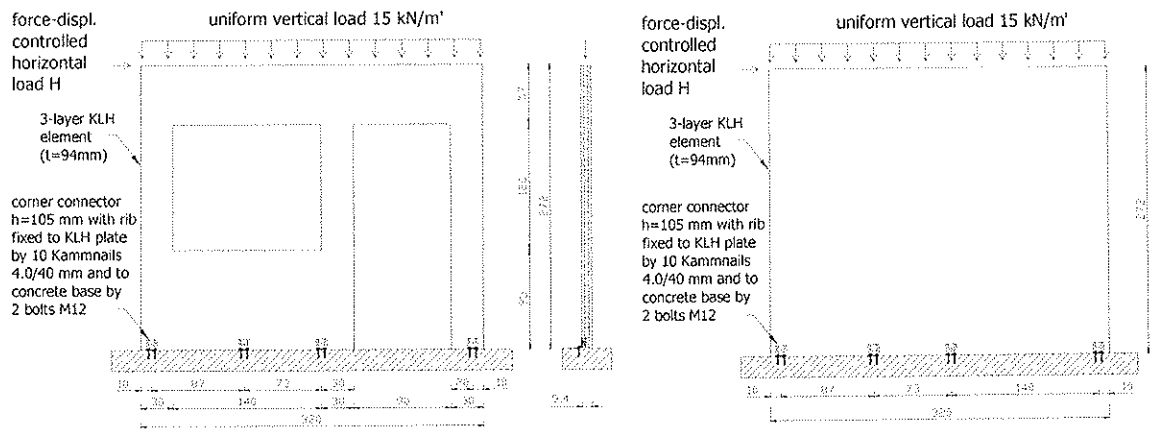

Fig.5: Configuration of Wall 13 with a door and a window openings and Wall 14 without openings.

The specimens were produced by the Austrian company KLH Massivholz GmbH as solid elements composed of three layers of cross glued laminated (X-lam) timber. Four BMF corner connectors with ribs with a height of 105 mm were installed as shown in Fig. 5. Corner connectors were placed 10 cm from the edge of the wall and attached with ten 4.0/40 mm nails with annular threads to the KLH plate and with two steel bolts M12 to reinforced concrete foundation.

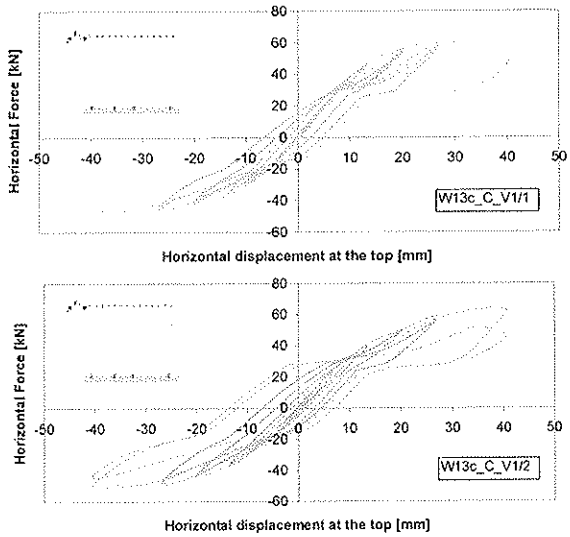

Fig.6: Hysteretic response of two tested X-lam walls with window and door openings (r=0.41).

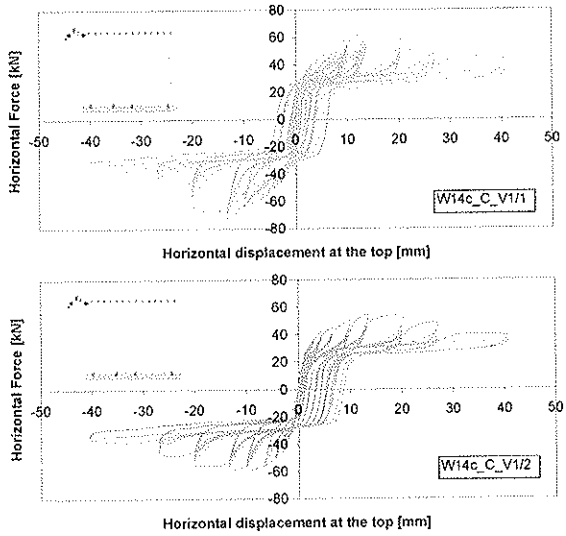

Fig.7: Hysteretic response of two tested non-fenestrated X-lam wall panels.

A total of four cyclic tests were performed to obtain the hysteretic response of fenestrated and non-fenestrated X-lam walls (Fig.6 and Fig.7). EN 12512 standard was used for determination of the cyclic loading protocol.

The hysteretic wall response showed two significant differences in stiffness and in thickness of the hysteretic loops. These differences were more visible in response of non-fenestrated wall relative to the fenestrated one. The first stage was characterized by more stiff response with tight hysteretic loops and represented shear wall response where mainly shear deformations of X-lam wood material occurred along with some initial contact slip between assembled elements. The vertical load prevented tension deformations of anchors. The second stage was characterized by lower stiffness and much wider hysteretic loops. Higher level of horizontal load caused tension forces in anchors and therefore uplift of the wall. The energy dissipation in this case was mostly due to deformation of the corner connectors and the fasteners that attached them to the wall and to the foundation.

The initial envelopes of the hysteretic response of the four cyclic tests are presented in Figure 8.

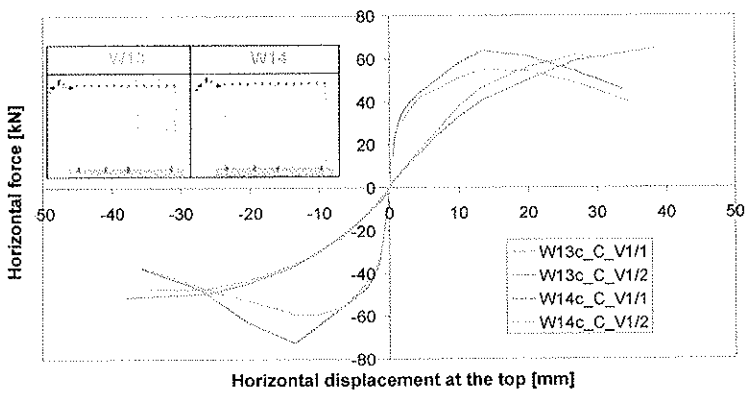

It can be observed that the openings (r=0.41) reduced shear stiffness, while the shear strength remained almost the same. The responses were not symmetric because of asymmetrical placement of anchors (Fig.5) to accommodate the door opening.

Fig.8: Envelopes of hysteretic response of X-lam walls of dimension 320/272/9.4 cm.

3.2 Accompanying experimental programs for determination of mechanical properties of constituent elements

The response of the tested wood walls depends on the boundary conditions and the magnitude of vertical load and also on the configuration and mechanical properties of the constituent elements and the assembly as a whole. Therefore, some accompanying tests were done on constituent elements of the wall to obtain their mechanical properties, which were used in the model.

3.2.1 Modulus of elasticity

The main load-bearing direction of 3-layer X-lam wooden plate is defined by direction of wood fibres in outer layers. Therefore the E-modulus in load-bearing direction was signed as $E_{p,0}$ while E-modulus in the perpendicular direction was signed as $E_{p,90}$. Moduli of elasticity in both orthogonal directions were determined using wall segments of 30 x 30 x 9.4 cm in size. X-lam timber plate consisted of strips of spruce stacked on top of each other and glued together forming large-size solid cross-laminated boards. The thickness of the strips wall was 30 mm in the main load-bearing direction and 34 mm in perpendicular direction (Fig. 9). The moisture content of these strips was 12% (±2%) to protect the product from growth of any pests, fungi as well as insects attacks.

E-moduli in plane of 3-layer X-lam timber plate were determined on three specimens for each orthogonal direction according to EN 789. Because two layers of wood strips were oriented in the main load-bearing direction with the cross section almost double that of the perpendicular one, the ratio of E-moduli in the orthogonal directions was expected to be of the same magnitude. The load was applied at a constant rate of load head displacement. The rates were 0.011 mm/s and 0.014 mm/s, which corresponded to loading rates so that failures occur within time interval of 300±120 s according to the standard requirements. Deformations in each layer were measured by extensometers (V1, V2, V3 and V4) with the gage length of 200 mm.

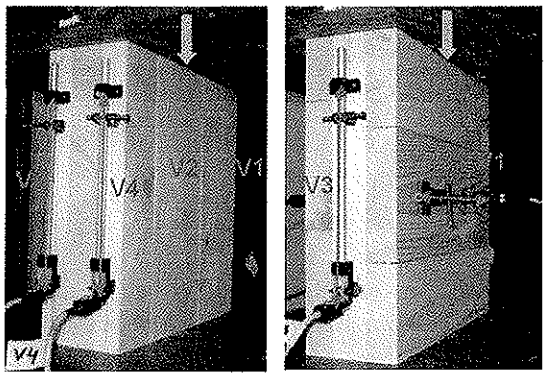

Fig.9: X-lam specimens for determination of E-modulus in plane for two orthogonal directions.

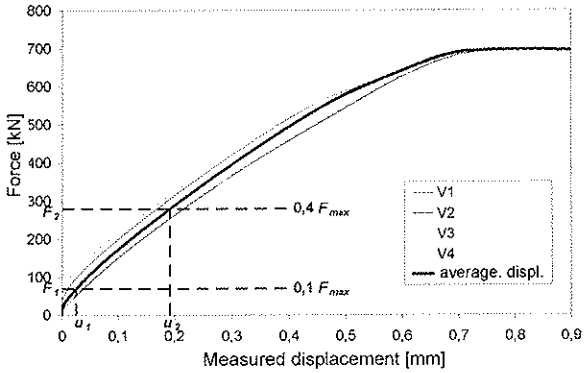

Fig.10: An example of measured displacements for determination of E-modulus in the main load bearing direction of 3 layer X-lam timber plate.

The values of experimentally obtained E-moduli are presented in Table 1. The E-moduli are also shown in Fig.11 as tg α, where α is the slope angle of the elastic portion of the stress-strain curve. E-modulus in load-bearing direction ($E_{p,0}$) was approximately 9 GPa and was about double that in the perpendicular direction ($E_{p,90}$).

Table 1: Experimental values of E-moduli of 3-layer X-lam timber plates in load-bearing direction and in perpendicular direction.

	$E_{p,0}$ [kN/cm²]	Mean value	Standard deviation	C.O.V.
P1v	888.07	897.87	93.43	0.10
P2v	995.81			
P3v	809.72			
	$E_{p,90}$ [kN/cm²]	Mean value	Standard deviation	C.O.V.
P1h	410.51	443.03	105.51	0.24
P2h	357.60			
P3h	560.97			

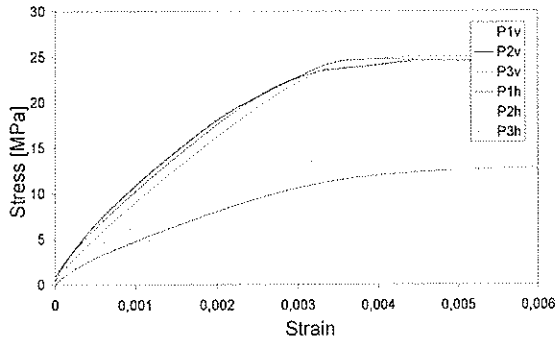

Fig.11: Strain-stress relation at compressive loading in two orthogonal directions.

Table 2 shows relatively good agreement between the calculated and experimental values of E-moduli and. Calculation of effective mechanical properties for solid wood panels with cross layers was

proposed by Blass [8]. The analytical approach determines homogenisation of cross section (as all wood fibres are oriented just in one direction) with composition factors, where stiffness of cross layer is also taken into account. Rough estimation of E-moduli and strengths for solid wood panels with cross layers could also be done by not taking into account the perpendicular layers. This simple estimation is presented in Fig.12 and can significantly underestimate mechanical properties of X-lam timber panel.

Table 2: Calculated [8] and experimentally obtained E-moduli of X-lam timber plates in two orthogonal directions.

GL28h	Compositions factors	Calculated E-modulus	Experimental results
$E_{0,g,mean} = E_0$ [kN/cm²]	k_3	$E_{0,cf}$ [kN/cm²]	$E_{p,0}$ [kN/cm²]
1260	0.65	819	897
$E_{90,g,mean} = E_{90}$ [kN/cm²]	k_4	$E_{90,cf}$ [kN/cm²]	$E_{p,90}$ [kN/cm²]
42	0.383	483	443

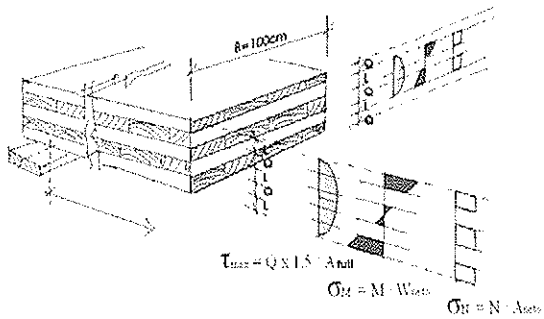

Fig.12: Approximate stress distribution under bending-axial loading of X-lam timber plate.

3.2.2 Shear modulus

Shear modulus was obtained by experimental tests on X-lam wall segments, where three specimens (P1s, P2s and P3s) were loaded by compressive force in diagonal direction through rigid shoes with concrete pads of 150 mm length (Fig.13). Loading rate with increasing displacement of hydraulic actuator was 0.012 mm/s, so that failure occurred within the time interval of 300±120 s.

Vertical displacements were measured by two extensometers (V1 and V2) with the gage length of 375 mm, and horizontal displacements were measured with two LVDT's (I1 and I2) with the gage length of 345 mm.

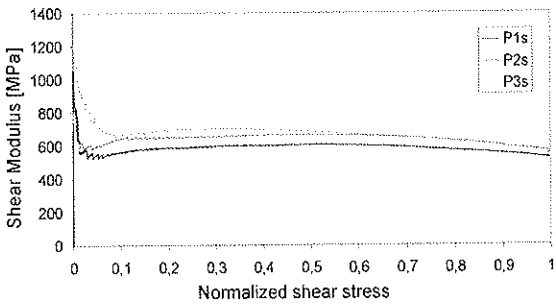

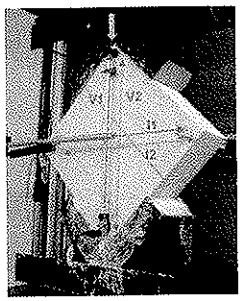

Fig.13: Shear modulus test on X-lam panel.

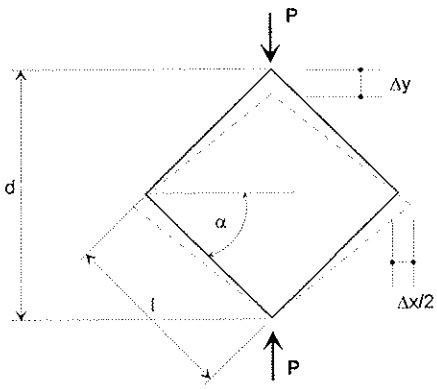

Where:

τ_d shear stress in the specimen,

γ_d shear strain in the specimen,

G_d shear modulus of the specimen,

P acting force on the specimen,

l, t width and thickness of the specimen,

d diagonal length of the specimen and

$\Delta x, \Delta y$ horizontal and vertical displacements, respectively.

Fig.14: Symbols for shear modulus determination.

Based on the measurements obtained from the shear stress, the shear stress, strain and the shear modulus were determined using the following equations (see Fig. 14):

$$\tau_d = \frac{P}{\sqrt{2} \cdot l \cdot t}\ ; \qquad \gamma_d = \frac{\Delta x + \Delta y}{2d}(\tan\alpha + \frac{1}{\tan\alpha})\ ; \qquad G_d = \frac{\tau_d}{\gamma_d} \tag{4}$$

From the diagram in Figure 13 it can be seen that measured deformations at the initial stage of the shear tests do not represent correct value of the shear modulus. At higher load level, the shear stress distribution in the specimen is not infected by local effects and therefore the shear modulus is relatively stable and follows the curve from minimum value of 0.5 GPa up to 0.65 GPa and than again decreases to 0.5 GPa. G-modulus of 0.5 GPa was used in numerical analyses of racking response of X-lam walls.

3.2.3 Moisture content and density

The moisture content (MC) of wood specimens was measured using electric moisture meter. The average MC was 12±2%. Dimensions and mass of each specimen were measured prior to destructive testing. Determined mean density was 418 kg/m^3 with standard deviation of 11 kg/m^3.

3.3 Tension and shear behaviour of anchors

The main purpose of tension and shear tests of anchors was to determine the global response of this constituent part of the shear wall, which significantly influences its racking behaviour.

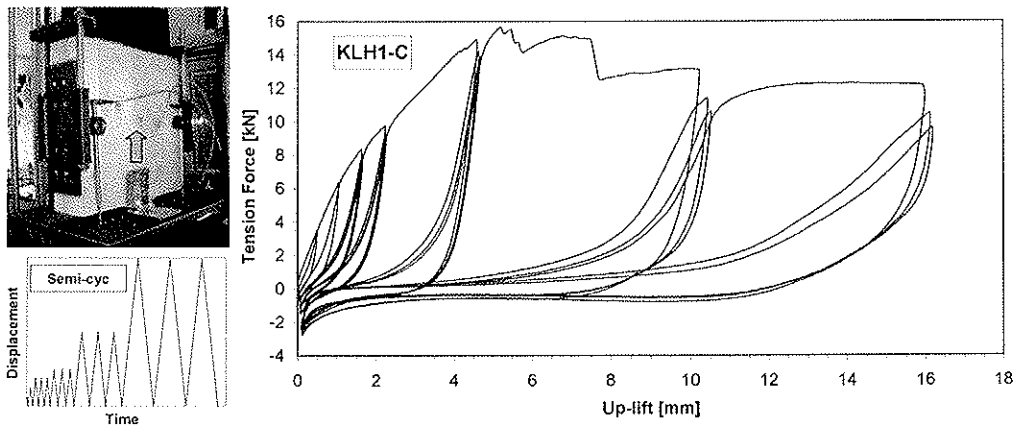

Fig.15: Semi-cyclic up-lift corner connector test.

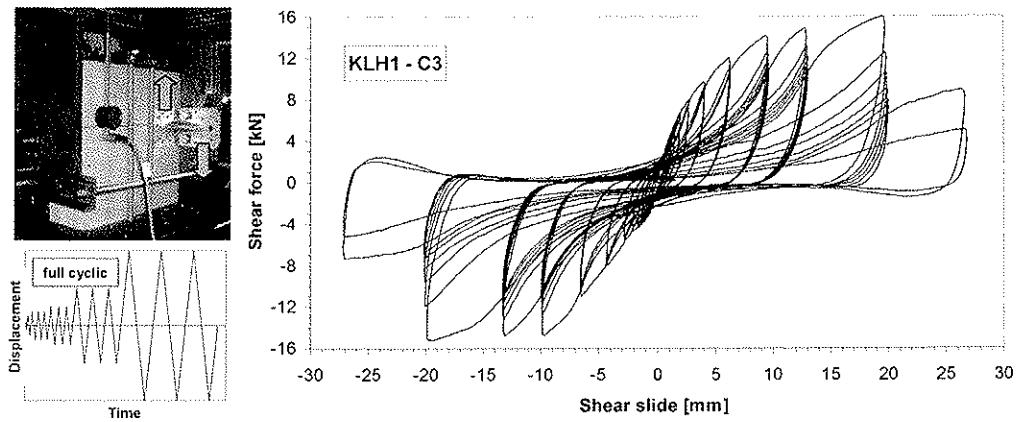

Fig.16: Cyclic slide connector test.

X-lam wall segments were attached to a steel plate using 105 mm BMF corner connectors with ribs. The corner connector was fastened to the X-lam wall segment with ten annularly threaded 4.0/40 mm nails and with two M12 bolts to the steel plate.

Shear wall anchors are subject to a combination of tension and shear forces. Therefore the segments of X-lam wall were tested in two perpendicular directions. In the "up-lift tests" (Fig.15), tension load on anchor was applied, and in the "slide tests" (Fig.16), shear load was applied. Monotonic and cyclic tests were performed according to EN 26891 and EN 12512 standards, respectively. Total of four tests in each direction were carried out, one with monotonic and three with cyclic loading. From cyclic tests the envelopes of the hysteretic responses were obtained and basic mechanical characteristics were defined for use in the numerical model (Fig.17).

4 Numerical analysis

Prediction of racking behaviour of X-lam walls using the commercially available finite-element program SAP2000 is presented in this section. An attempt was made to develop as much as possible exact mathematical model of X-lam wall (Fig.17) taking into account realistic mechanical properties of all constituent elements. Experimental results of racking tests as presented above served for the model verification (Fig.8).

The model is composed of orthotropic membrane elements and longitudinal sprigs which simulate anchors. Three cross-laminated glued layers of KLH walls were taken into account as homogeneous orthotropic material. Material characteristics for the membrane elements of thickness of 9.4 cm have been defined according to the results of tests on wall segments. Contact between wall elements and RC foundation is represented by set of springs which are absolutely stiff in the direction of foundation and allow free movement away from foundation. Friction between foundation and wall element is modeled using bi-linear link elements placed in horizontal direction along the whole length of the lower edge of the panel. The value of friction coefficient between the rough concrete and X-lam wooden surface was estimated at 0.7. Springs are absolutely stiff until the shear flow in the contact zone does not attain the estimated friction force. After this, friction springs have constant load-bearing capacity and resist sliding of the panel in combination with non-linear springs, which represent shear behaviour of the corner connectors as determined from tests (Fig.15 and 16). Experimentally obtained envelopes were incorporated in the model as multi linear springs.

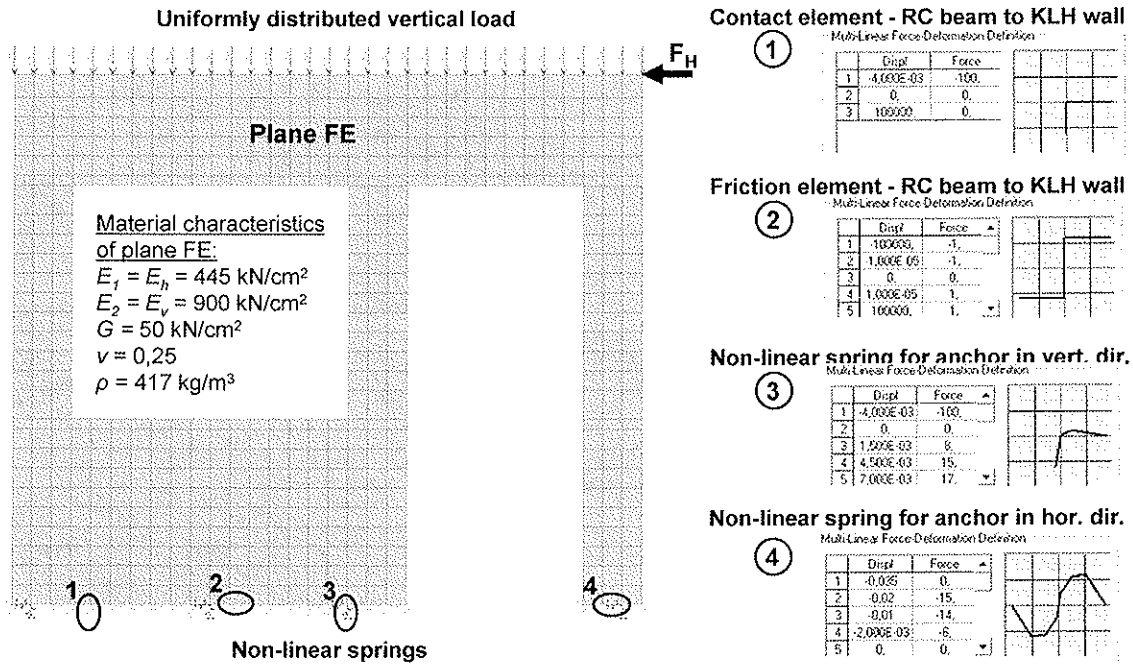

Fig.17: Finite-element model of Wall 13 in SAP2000.

In the numerical model, vertical load of 15 kN/m was imposed on the top of the wall. Horizontal load was applied once in positive and once in negative direction as the response of the wooden panel is not equal in two different directions as a result of asymmetrical placement of the anchors and openings. Non-linear static pushover analysis using SAP 2000 was executed and the obtained results were presented in a form of horizontal force-displacement diagrams (Fig.18 and 19).

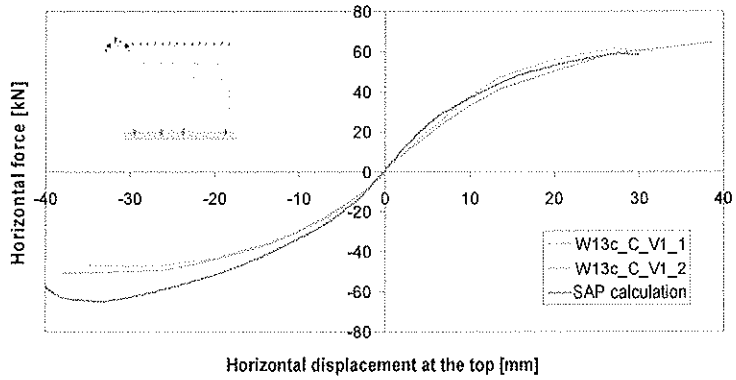

Fig.18: Comparison of experimental and calculated response of fenestrated wall with r=0.41.

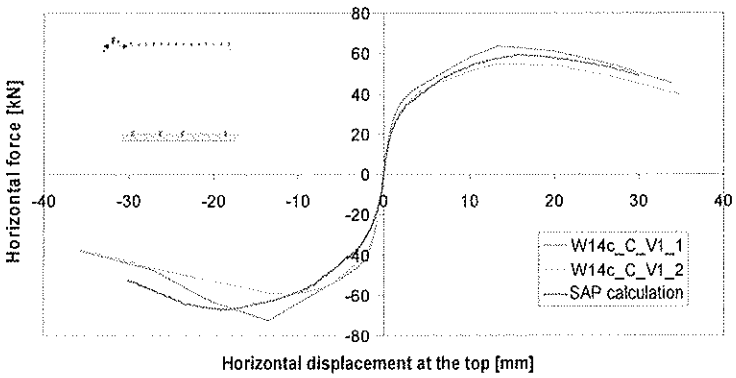

Fig.19: Comparison of experimental and calculated response of non-fenestrated wall with asymmetrical distribution of anchors.

Comparison of the calculated and experimentally obtained envelopes shows reasonably good agreement between the results. In case of Wall 13, the resistance in the negative direction is over predicted because P-Δ effect due to out-of-plane movement of the narrow segment of the wall was not accounted for in the model.

5 Parametric study of influence of openings

The numerical model presented above was used in a parametric study to determine the influence of the size and layout of openings on the load-bearing capacity and stiffness of fenestrated X-lam timber walls.

Total of 36 configurations of fenestrated walls of three different lengths, 240 cm, 320 cm and 400 cm, were modeled and analysed. For each length an additional non-fenestrated wall was modeled to obtain the shear capacity ratios. All fenestrated models had a symmetrical openings, which varied in length and height according to the matrix by one quarter of wall dimension. In Table 3 the matrix of fenestrated models having wall length of 320 cm is presented. The openings in walls of other lengths were configured in a similar fashion.

Numerical analyses were performed as non-linear static pushover analyses. In every model analysis results for each loading step were compiled and presented in a form of response diagrams as relation between horizontal force and displacement (Fig.20). At higher loads, stress distributions around

openings were verified against compression or tension failure of wood, because the model using orthotropic membrane elements is not able to recognize non-linear mechanical properties of timber cross-section. The characteristic strength of homogenised 3-layer X-lam cross section was determined by analytical approach using composition factors [8].

Table 3: Matrix of numerical models with wall length of 320 cm.

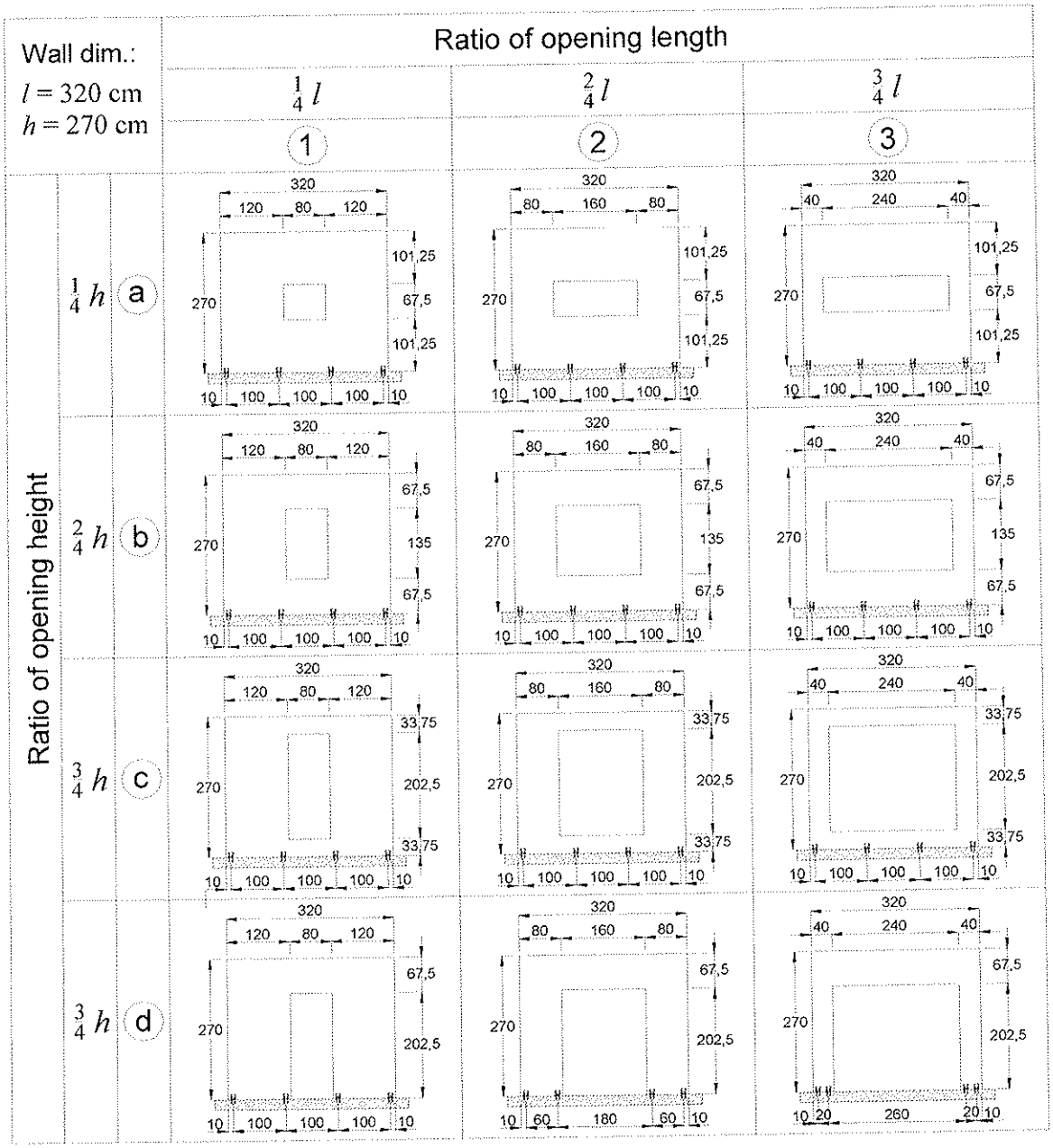

On Figure 20 definition of shear stiffness of calculated racking response is presented. Shear stiffness is defined as a slope of the line which goes through the yielding point determined according to CEN II. In this definition the yield limit state is set as the point of intersection between two lines. The lines are the secant of the skeleton curve defined by points at 10 % and 40% of horizontal load-bearing capacity and tangent on the upper part of the envelope, which is parallel to the secant through the skeleton curve at 40% and 90% of horizontal load-bearing capacity. The shear force values at horizontal displacement of h/200 or 0.5% of story drift were set as horizontal load-bearing capacity of calculated response according to EC 8 recommendation for structures attached to brittle elements.

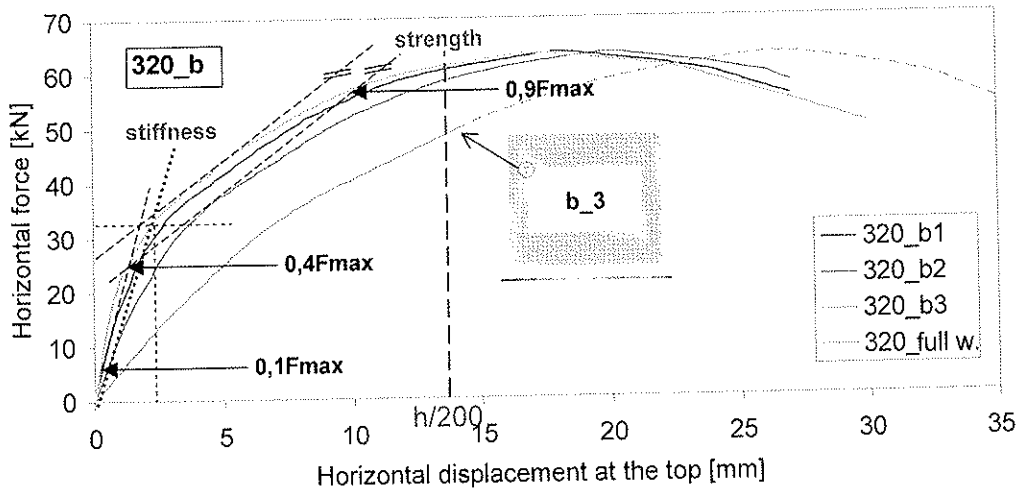

Fig.20: Calculated responses of 3 fenestrated walls and one non-fenestrated with length of 320 cm.

The accuracy of calculated response of fenestrated model with large openings at higher stage of deformation is questionable as failure usually occurs by smashing or tearing wood fibres in the corners around openings. Therefore in calculated racking response shear strength was set at deformation of 0.5% of the story drift, which corresponds to the horizontal displacement of 13.5 mm. As the normal stresses in analysed specimens with the largest opening attain maximum values (due to yielding of anchors) at story drift higher than 0.5%, it can be concluded that the models produce acceptable results up to this deformation level. When the stress level corresponds to wood failure in the cross-laminated panel the rest of calculated racking response is presented by dashed curve (Fig.20).

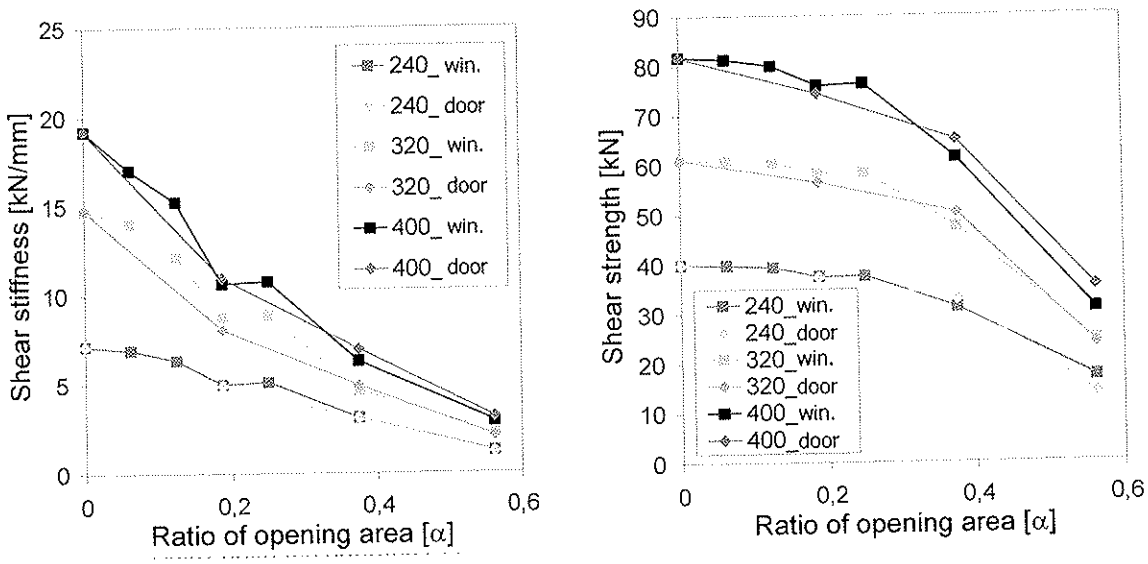

Fig.21: Calculated shear stiffness (a) and shear strength (b) in relation to ratio of opening area for different X-lam walls.

Figure 21 shows the diagrams of relationship between the calculated shear stiffness (Fig.21a) and shear strength (Fig.21b) and ratio of opening area for different X-lam walls (wall length and shape of opening). The parametric study resulted in diagrams (Fig.22a and 22b) which show the relation between panel area ratio and normalized values of shear capacities expressed as ratio of racking load and stiffness of fenestrated X-lam walls against non-fenestrated one. The diagrams in Fig. 22 and Eq. 4 also present simple formulas of regression lines which were fit to the results of the numerical analysis.

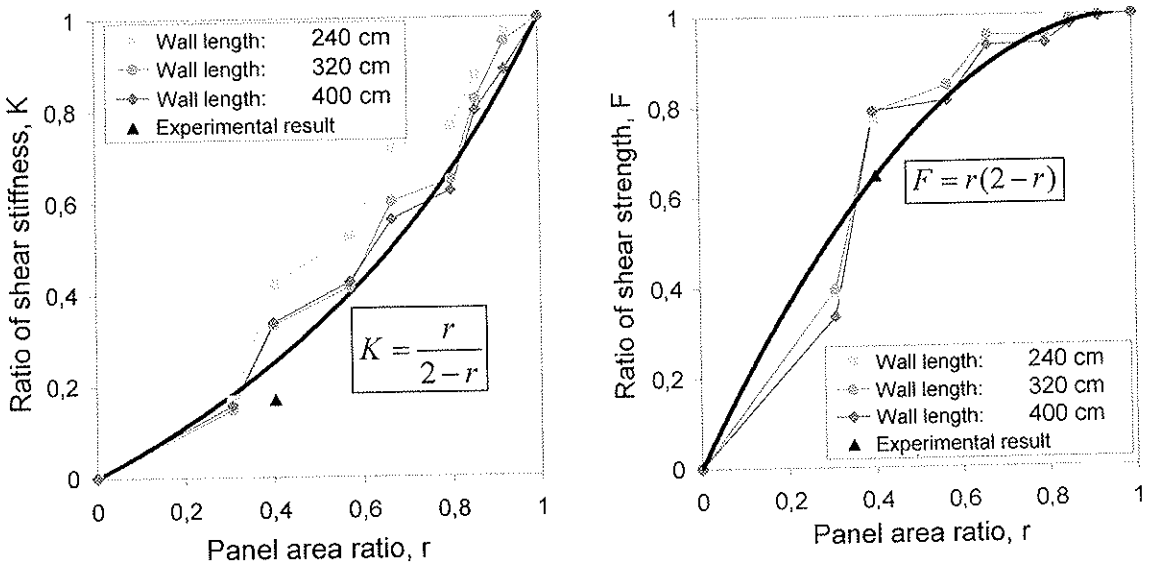

Fig.22: Calculated shear stiffness (a) and shear strength (b) reduction regarding the panel area ratio for X-lam walls.

Comparing the influence of openings on shear capacities of X-lam and light-frame walls similar trends were obtained for reduction of shear stiffness (Fig.23) while for reduction of the shear strength the trend curve with the opposite curvature was established. The experimentally obtained empirical equations (Eq.4) are expressed by panel area ratio and could be used for direct evaluation of reduced shear capacities if shear stiffness and shear strength of non-fenestrated wall are already known.

$$K_{opening} = K_{full} \cdot \frac{r}{2-r} \qquad \text{and} \qquad F_{opening} = F_{full} \cdot r(2-r) \tag{4}$$

If simple formulas are confirmed by further experimental results, they could effectively serve in X-lam timber structure design, where horizontal building resistance has to be analysed.

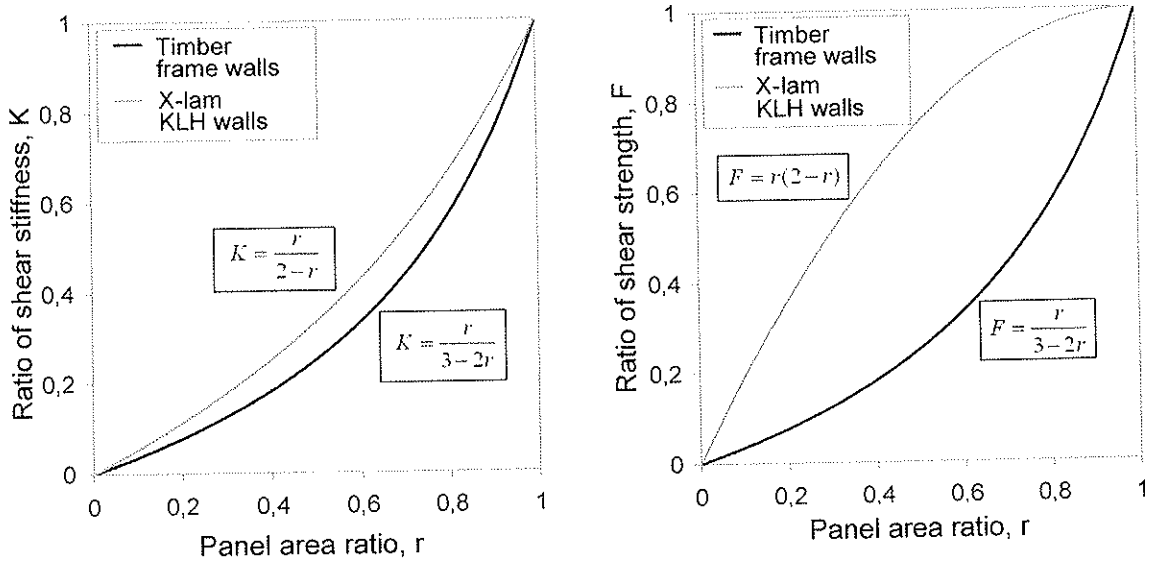

Fig.23: Comparison of shear stiffness (a) and shear strength (b) reduction for light-frame wall and X-lam solid timber walls with respect to the panel area ratio, r.

6 Conclusion

Non-fenestrated cross-laminated wooden walls have relatively high stiffness and load-bearing capacity. Therefore, the critical elements that govern the X-lam timber shear wall response to earthquake excitations are anchors connecting the panels to the building foundation. X-lam panel with large openings has lower shear stiffness, but its load-bearing capacity is not reduced as much, because failures are mostly concentrated in anchoring areas and in the corners around openings with smashing and tearing of wood. To evaluate the trends of shear strength and stiffness reduction for different fenestrations a numerical model was utilised and verified with experimental tests on full-size X-lam walls. To reduce the number of tests a numerical parametric study was performed for 36 configurations of openings in the walls of three different lengths. The study resulted in diagrams that could serve for simple engineering design of X-lam timber walls with openings using a reduction factor based on the ratio of the openings similar to light-frame walls. The parametric study showed that the openings with the area up to 30% of the wall surface do not reduce the load-bearing capacity significantly, while the stiffness is reduced for about 50%.

Additional experimental tests and numerical analyses will enlarge the knowledge related to lateral stiffness and stability of X-lam wooden walls with openings. Additional tests, already started at University in Ljubljana, Faculty of Civil and Geodetic Engineering, will serve the verification of the empirical equations presented herein.

7 References

[1] Dujic, B., Aicher, S. and Zarnic, R., "Testing of Wooden Wall Panels Applying Realistic Boundary Conditions", Proceedings of the 9th World Conference on Timber Engineering WCTE 2006, August 6-10, Portland, Oregon. USA, 2006, 8p.

[2] Dujic, B., "Experimental Supported Modelling of Response of the Timber-Framed Wall Panels to Horizontal Cyclic Load". Ph.D. Thesis (in Slovenian), UL FGG, Ljubljana, Slovenia, 2001, 239p.

[3] Klobcar, S., "Influence of openings on Shear Capacity of Wooden Walls", Diploma Thesis (in Slovenian), UL FGG, Ljubljana, Slovenia, 2001, 95p.

[4] Yasumura, M. and Sugiyama, H., "Shear Properties of Plywood-sheathed Wall Panels with Opening" Trans. of the Architectural Institute of Japan, No. 338, April 1984, pp. 88-98.

[5] Yasumura, M., "Racking Resistance of Wooden Frame Walls with Various Openings" Proceedings CIB-W18, paper 19-15-3, Florence, Italy, 1986, 24p.

[6] Johnson, A. C., Dolan, J. D., "Performance of Long Shear Walls with Openings" International Wood Engineering Conference, New Orleans, Louisiana: 1996, pp. 337-344.

[7] Massivholz GmbH KLH Technical Documentation

[8] Blass, H. J., Fellmoser, P., "Design of solid wood panels with cross layers", Proceedings of the 8th World Conference on Timber Engineering, WCTE 2004, June 14-17, Lahti, Finland, 2004, pp. 543-548.

INTERNATIONAL COUNCIL FOR RESEARCH AND INNOVATION
IN BUILDING AND CONSTRUCTION

WORKING COMMISSION W18 - TIMBER STRUCTURES

BONDED TIMBER DECK PLATES IN FIRE

J König

SP Trätek/Wood Technology
SWEDEN

J Schmid

kppk ziviltechniker gmbh
Vienna

AUSTRIA

MEETING FORTY

BLED

SLOVENIA

AUGUST 2007

Presented by J. König
H. Blass asked whether the results are applicable to beams. J. König replied that the results are not applicable to beams therefore beams are okay.
A. Frangi asked if the possibility of char layer falling off was considered in the study. J. König replied that the assumption is that the char layer remains intact. The possibility of char layer falling off would represent complication as temperature increases as char protection level increases provided the char layer stays intact. Char layer falling would mean a bond line issue.

Bonded timber deck plates in fire

Jürgen König
SP Trätek/Wood Technology, Sweden

Joachim Schmid
kppk ziviltechniker gmbh
Vienna, Austria

Abstract

Laminated deck plates, made of edgewise or flatwise laminations, are increasingly used as structural elements in housing and commercial buildings, both in floors and walls. In structural fire design, EN 1995-1-2 gives a simplified method for the calculation of the mechanical resistance of structural timber members. Apart from charring, the effect of elevated temperature is taken into account by assuming a zero-strength layer below the charring depth of thickness 7 mm, reached after the first 20 minutes of the fire exposure. For rectangular cross-sections this model gives reasonably good agreement with advanced calculations. EN 1995-1-2 also permits the application of this model to timber slabs exposed on one side. This paper gives some results from advanced calculations – using the thermal and thermo-mechanical properties of wood given by EN 1995-1-2 – of the bending resistance of both homogenous and cross-laminated timber slabs exposed to fire. It is shown that the depth of the zero-strength layer should be increased considerably above the value of 7 mm given by EN 1995-1-2 for beams and columns. Also, there is a significant effect of the state of stress of the fire exposed side of the slab, that is when the fire exposed side is in compression, the reduction of bending strength is greater than in the opposite case.

1 Introduction

Laminated deck plates made of edgewise or flatwise laminations are increasingly used as structural elements in housing and commercial buildings, both in floors and walls. The laminations are held together by mechanical fasteners or by bonding; the latter becoming more and more important in practice. In structural fire design, EN 1995-1-2 [1] gives a simplified method for the calculation of the mechanical resistance of structural timber members (reduced cross-section model). Apart from charring that reduces the size of the cross-section of the member, the effect of elevated temperature is taken into account by assuming a zero-strength layer of depth 7 mm immediately below the charring depth. For unprotected timber members, this zero-strength layer is assumed to increase linearly from zero to its maximum value during the first 20 minutes of the fire exposure.

When EN 1995-1-2 was drafted, it was believed that the reduced cross-section method could be applied to edgewise laminated timber slabs exposed to fire on one side, contrary to the alternative method given EN 1995-1-2 that uses modification factors for the reduction of strength parameters to account for the effect of elevated temperature in parts of the residual cross-section of the member (reduced properties model). At that time the use of cross-laminated slabs in housing was in the beginning; it was not intended that the reduced cross-section method could be applied to this new type of construction without further investigation. Meanwhile, cross-laminated timber decks and walls have been used in a large number of wooden buildings. There is a need to know to what extend the

Eurocode model can be assessed to the design of such structural elements.

This paper deals with laminated timber deck plates made of flatwise or edgewise laminated laminations, held together by bonding.

2 Computer simulations

2.1 Thermal analysis

The thermal analysis was performed as a one-dimensional heat transfer analysis, using the ISO 834 standard fire curve for the temperature development in the compartment and the thermal properties of wood given in EN 1995-1-2. The software used was either TCD (with TEMPCALC), and more recently SAFIR 2004. The char-line was defined as the location of the 300°C isotherm. Typical temperatures in the residual cross-section below the char-line are shown in Figure 1. It can be seen, that the shape of the temperature profiles has stabilized after about 20 minutes. At that time an approximately 40 mm deep zone is heated above ambient temperature, whereas, after five minutes of fire exposure, the depth of this zone is only about 20 mm.

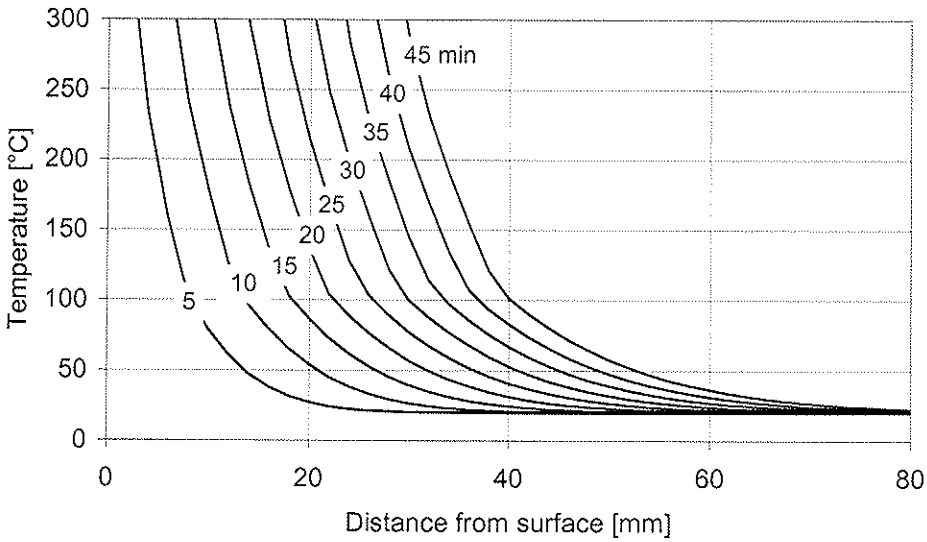

Figure 1 – Temperature profiles in timber plate at various times.

2.2 Structural analysis

For the structural analysis, a computer program CSTFire, written as a Visual Basic macro embedded in Excel, was developed, using the temperature output from the heat transfer calculations and the relative strength and stiffness values given by EN 1995-1-2 [1], i.e. compressive and tensile strengths, f_c and f_t, and moduli of elasticity in compression and tension, E_c and E_t. These values are given as bi-linear functions of temperature from 20 to 300°C with breakpoints at 100°C, also taking into account the effects of transient moisture situations and creep, see Figure 2. The software takes into account the possibility of permitting ductile behaviour of wood under elevated temperature. Contrary to ambient conditions where failure on the tension side of a beam is brittle, in the fire situation tensile failure of the outermost fibres won't cause immediate collapse of the member since a redistribution of internal stresses will take place as long as equilibrium is maintained.

Since the reduction of strength and stiffness properties is different for tension and compression, CSTFire uses an iteration process, increasing the curvature of the member until the maximum moment resistance is reached. The element size used for the structural analysis was chosen as 1 mm × 1 mm.

Since a coarser grid 2 mm × 2 mm was used in the thermal analysis, intermediate temperature values were determined by linear interpolation.

The calculations were conducted assuming material properties that are representative for timber deck plates used in practice, using the stress-strain relationship shown in Figure 3. Since the values of tensile and compressive strength of solid timber given in design or product standards, e.g. EN 338 [2], are values related to the whole cross-section and were determined on the assumption of a linear relationship between stress and strain until failure, the use of these values in a finite element analysis would not be correct [3]. Therefore, compressive strength values were determined using the data from Thunell [4] as shown in [3]. For the timber slabs assumed here the compressive strength was f_c = 30 N/mm^2, while the tensile strength was taken as f_t = 27 N/mm^2, that is the ratio of f_t/f_c is 0,9. The results of simulations of cross-laminated timber slabs were taken from [5]. These calculations were made assuming f_t/f_c = 0,92. It has been shown that the ratio has only a small influence on the results and therefore can be neglected for practical application. For layers with the grain direction perpendicular to the longitudinal direction of the plate, the modulus of elasticity was assumed to be zero, while these layers were assumed to be completely effective with respect to shear stiffness, that is complete composite action of the longitudinal layers was assumed.

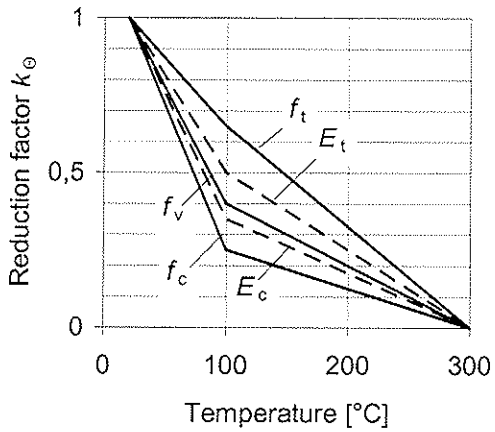

Figure 2 – Reduction factors for strength and stiffness properties according to EN 1995-1-2 [1].

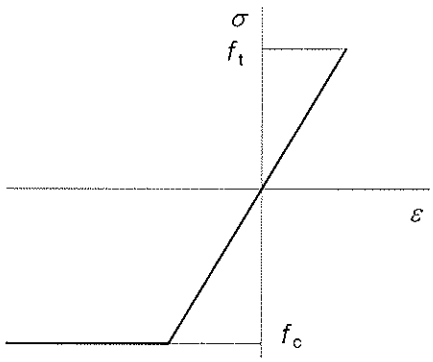

Figure 3 – Stress-strain relationships of wood.

3 RESULTS AND MODELLING

3.1 Homogeneous timber deck plates

In the following, the results of analyses of two homogeneous deck plates are shown. The term "homogeneous" refers to that the plate consists of one single layer in the direction perpendicular to the surfaces of the plate. The calculations were performed for time intervals as indicated by the data points in the graphs.

a) Plate depth 100 mm

The relationship of the relative bending resistance vs. time is shown in Figure 4. The effect of charring alone, without reduction of strength properties of the residual cross-section is dominating. The effect of reduction of strength properties is dependent on the state of stress of the fire exposed side of the plate: When the bending stresses are negative, that is when the fire exposed side is in compression, the bending resistance decreases at a greater rate than in the opposite case. EN 1995-1-2 [1] gives only one relationship, since – apart from the rules given for timber frame members in assemblies with completely insulated voids – no distinction is made with respect to the state of stress of the fire exposed parts of the cross-section. For load ratios between 20 and 40 %, that is the interval of load

levels most relevant in practice, both curves give lower values in relation the results obtained from EN 1995-1-2 using the effective cross-section method (the reduced properties method of EN 1995-1-2 cannot be applied to timber plates).

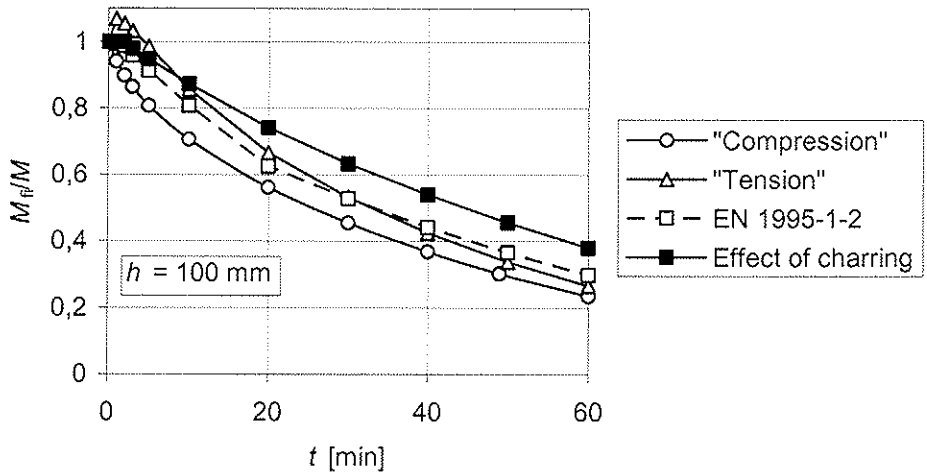

Figure 4 – Relative bending resistance vs. time of homogeneous timber deck plate of 100 mm depth.

The effect of the state of stress can also be seen from Figure 5, showing the modification factors for bending strength vs. time. These relationships could be used to derive expression for the modification factor for fire using the reduced properties method. For assessment of the effective cross-section method, the depths d_0 of the corresponding zero-strength layers were determined, Figure 6. For load ratios below 40 %, both values are above the depth of seven millimetres stipulated by EN 1995-1-2 and vary considerably with time.

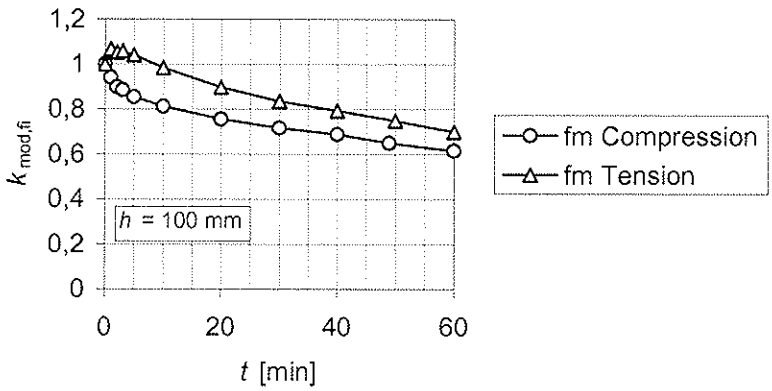

Figure 5 – Modification factor for fire vs. time of homogeneous timber deck plate of 100 mm depth.

EN 1995-1-2 uses the same depth of the zero-strength layer both for strength and stiffness parameters. Since timber plates are also used as load-carrying walls, the evidence of this statement was checked by determining the corresponding modification factors for fire for bending with the fire exposed side in compression (in a fire situation, a timber wall will always deflect away from the fire, giving rise to greater compressive stresses on the fire exposed side, and finally tensile stresses on the unexposed side). The modification factor for fire for modulus of elasticity, $k_{mod,E,fi}$, was determined for the three load ratios 30, 40 and 50 %, however, the influence of the load ratio is small, see Figure 7. The corresponding values of depths of the zero-strength layer for bending strength and bending stiffness differ only slightly, see Figure 8.

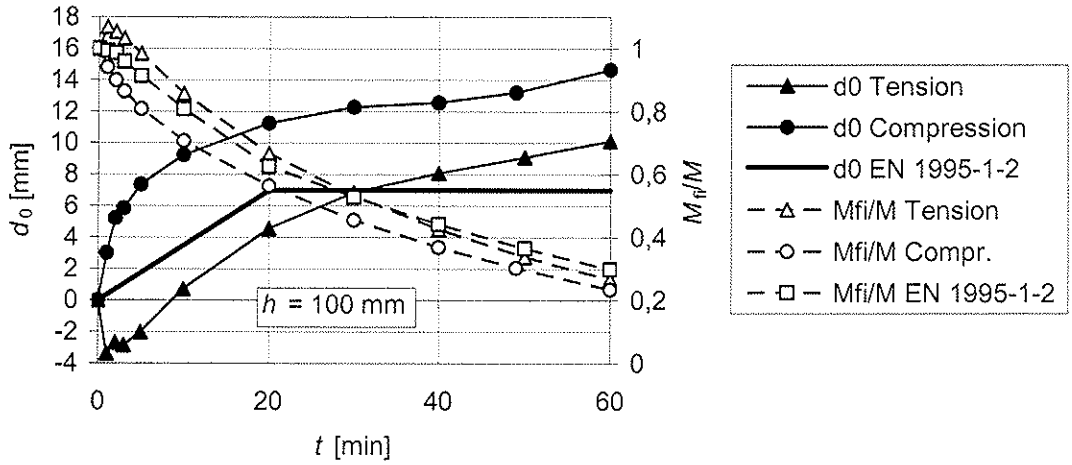

Figure 6 – Zero-strength layer and relative bending resistance vs. time of homogeneous timber deck plate of 100 mm depth.

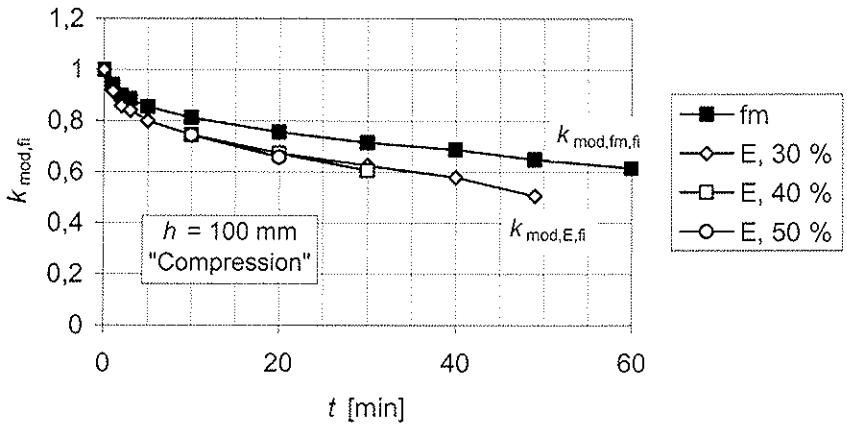

Figure 7 – Modification factor for fire vs. time for bending strength and modulus of elasticity when the fire exposed side is in compression.

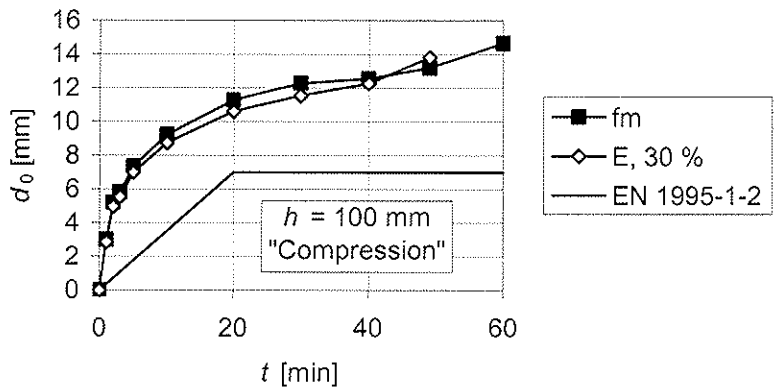

Figure 8 – Comparison of zero-strength layer for bending strength and modulus of elasticity when the fire exposed side is in compression.

b) Plate depth 140 mm.
The results obtained for a 140 mm thick plate are similar as above. Some of the results are shown in Figure 9 to 11. The main difference is that the depth of the zero-strength layer is slightly greater.

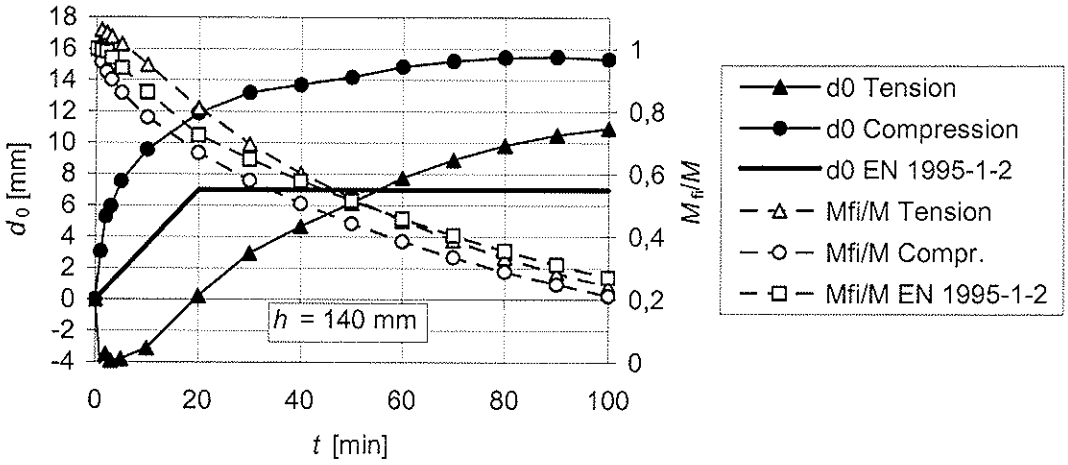

Figure 9 – Zero-strength layer and relative bending resistance vs. time of homogeneous timber deck plate of 140 mm depth.

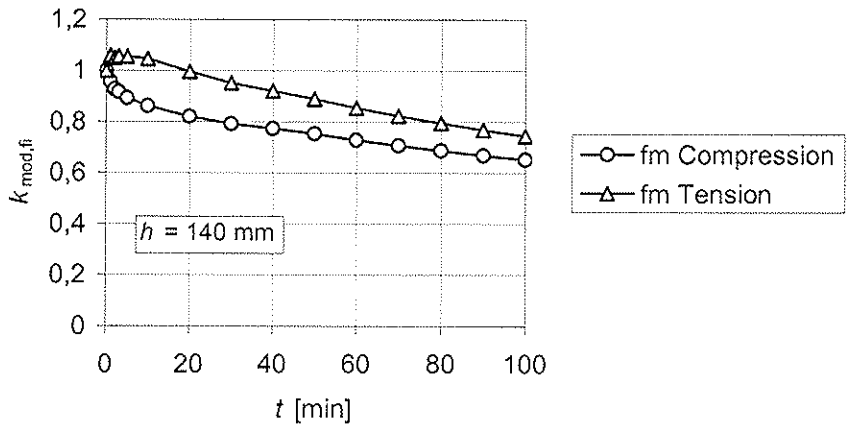

Figure 10 – Modification factor for fire vs. time of homogeneous timber deck plate of 100 mm depth.

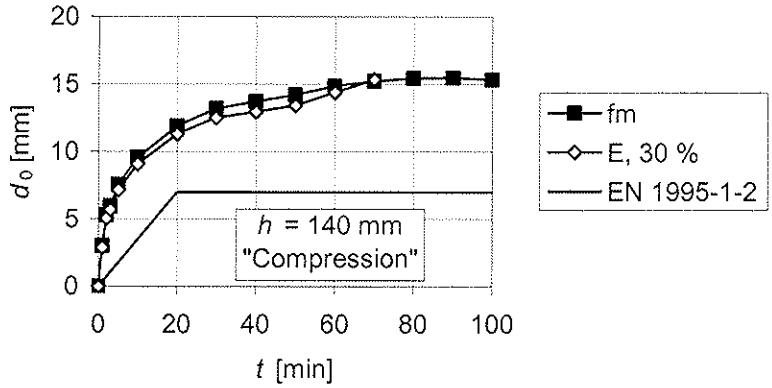

Figure 11 – Comparison of zero-strength layer for bending strength and modulus of elasticity when the fire exposed side is in compression.

3.2 Cross-laminated timber deck plates

In the following the results of some numerical simulations, taken from [5], are shown. The format of the graphs has been modified in order to be comparable with the results shown for homogeneous timber plates. Since the composition of the cross-section of cross-laminated timber plates gives rise to sudden changes of the strength and stiffness properties in the direction perpendicular to the plate, the simulations were performed at intervals of 36 seconds.

a) Depth 100 mm, 5 × 20 mm.
The relationship of the relative bending resistance vs. time is shown in Figure 12. The effect of reduction of strength properties is dependent on the state of stress of the fire exposed side of the plate: When the bending stresses are negative, that is when the fire exposed side is in compression, the bending resistance decreases at a greater rate than in the opposite case, however the relationship for a plate with the fire exposed side in compression is somewhat smoother due to plastic material behaviour on the compression side, see Figure 3. In Figure 12 the times when the first two layers have completely charred are shown as a broken line at 29,2 and a dotted line at 63,6 minutes respectively. We can see that the initial decrease of the bending resistance is slowing down after some time since a greater part of the temperature profile is moving into the statically ineffective second layer, see the temperature profiles shown in Figure 1. After 16,8 minutes, for fire exposed side in tension, failure in the first layer won't cause collapse of the plate since redistribution of internal forces takes place. At this stage layer 3 is almost fully effective since this layer is not significantly affected by elevated temperatures. First after about 14 minutes the temperature in parts of layer 3 are approaching about 100°C, causing accelerated decrease of bending resistance. When the second layer has completely charred at 63,6 minutes bending resistance is close to 20 % of its ambient value.

The modification factors for bending strength vs. time are shown in Figure 13. The relationships exhibit the influence of state of stress on the fire exposed side and the influence of changes of strength and stiffness properties in the layers. The corresponding depths of the zero-strength layer according to the effective cross-section model are shown in Figure 14 and Figure 15. The values vary with time and are, for load ratios between 20 and 40 % greater than the value seven millimetres stipulated by EN 1995-1-2. Consequently, applying EN 1995-1-2 would considerably overpredict the bending resistance of this timber plate. A value of d_0 = 9 mm would give reasonable agreement with the calculated relative bending resistance when the fire exposed side is in tension, while a value of d_0 = 13 mm should be used when the fire exposed side is in compression.

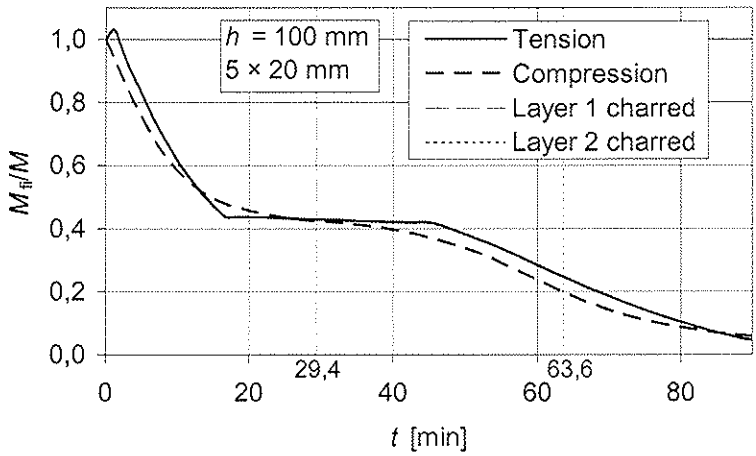

Figure 12 – Relative bending resistance vs. time of a five-layer cross-laminated timber deck plate of 100 mm depth.

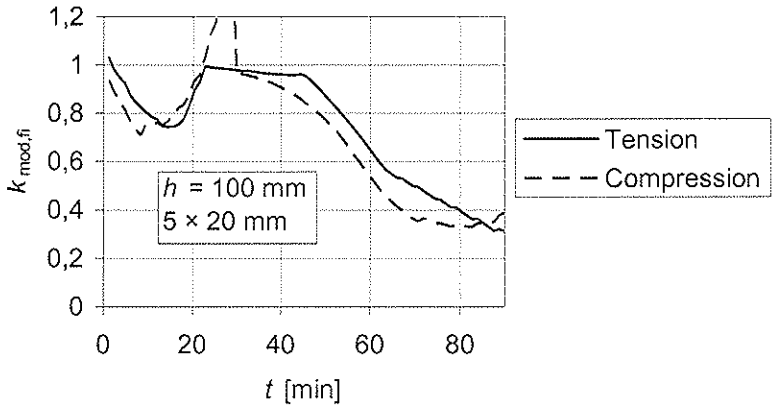

Figure 13 – Modification factor for fire vs. time of a five-layer cross-laminated timber deck plate of 100 mm depth.

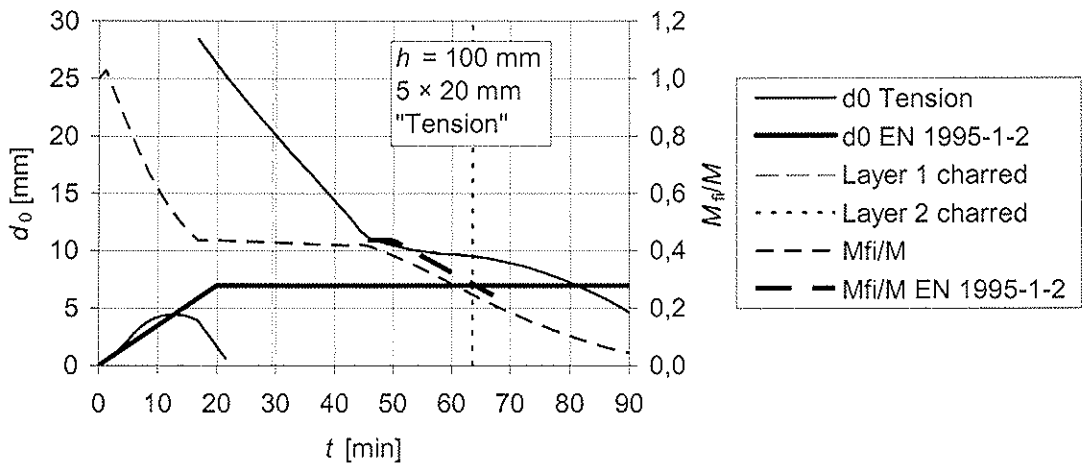

Figure 14 – Zero-strength layer and relative bending resistance vs. time of a five-layer cross-laminated timber deck plate of 100 mm depth with the fire exposed side in tension.

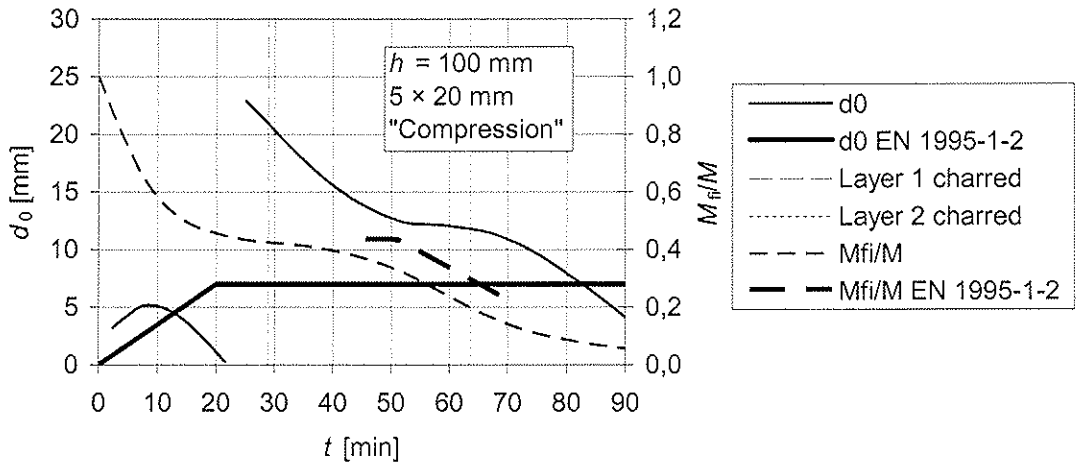

Figure 15 – Zero-strength layer and relative bending resistance vs. time of a five-layer cross-laminated timber deck plate of 100 mm depth with the fire exposed side in compression.

b) Other dimensions.
A number of various cross-laminated timber plates were analysed, however detailed results cannot be shown here. The depths of zero-strength layers which should be applied according to the effective cross-section model were derived aiming at obtaining reasonably well fitted bending resistance for load ratios between 20 and 40 %, see Table 1. For greater load ratios, the values are conservative; these are, however, without relevance for practical application.

Table 1 – Values of d_0 for cross-laminated timber plates in bending. "Tension" and "Compression" refer to the state of stress on the fire exposed side of the plate.

h	h_{lam}	n_{lam}	d_0 "Tension"	d_0 "Compression"
mm	mm	–	mm	mm
60	20	3	6	
96	32	3	7	9
100	20	5	9	13
160	32	5	11,5	15
≥ 140	20	≥ 7	9	12
≥ 224	32	≥ 7	10	13
100	100	1	10	14
200	200	1	9	18

For simplicity, the values of Table 1, except those for plate depths of 200 mm or more, are shown in Figure 16 as functions of the plate depth. The values for tension and compression, respectively, can be represented by linear trendlines. Timber deck plates of depth 200 mm or more are of minor interest, since the relative bending resistance is never below 40 % of its ambient value during the first 90 minutes. Therefore, fire safety is not an issue for these timber deck plates, unless fire resistance of unprotected plates is required for more than 90 minutes.

4 Conclusions and further research needs

For the design of timber beams and columns, EN 1995-1-2 gives two alternative methods. The effective cross-section method introduces a zero strength layer of uniform depth of seven millimetres to take into account the reduction of strength and stiffness properties of the member. The results of

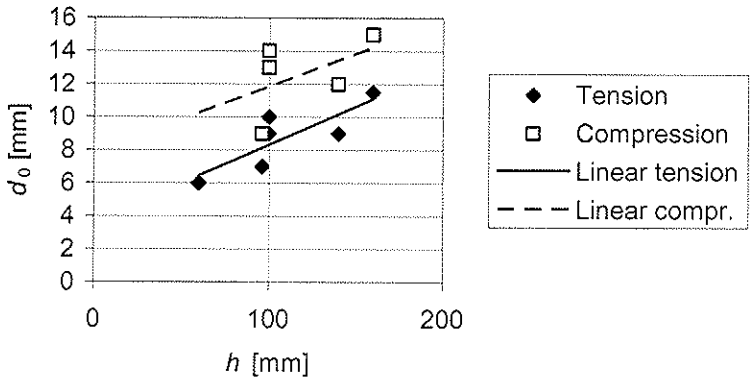

Figure 16 – Zero-strength layer depth vs. plate depth

simulations of fire exposed homogeneous and cross-laminated timber plates show that the application of the effective cross-section method would require zero-strength layer depths that are dependent on plate depth, the composition of layers and the state of stress on the fire exposed side of the plate. A considerable advantage of the method would disappear. After simplification, the zero-strength layer depths can be given as linear functions of the plate depth.

These results are preliminary. More timber plate configurations need to be investigated and it must be checked if these zero-strength layer depths also apply to bending stiffness when these elements are used as wall. Also, the effect of fire protective claddings needs to be investigated. It can be expected that, in some cases, considerably smaller zero-strength depths would apply.

Since the accumulation of moisture has a significant effect on strength and stiffness at elevated temperature, it should also be investigated if there is any effect of the adhesive on the transport of vapour in the plate.

5 Acknowledgement

Most simulations within this project were conducted by the co-author of this paper preparing his master thesis during his visit at Trätek, Stockholm, and at the University of Natural Resources and Applied Life Sciences, Vienna. This investigation was also supported by the Nordic Innovation Centre (NICe) and the Swedish Agency for Innovation Systems (Vinnova).

6 References

[1] EN 1995-1-2:2004 Eurocode 5: Design of timber structures – Part 1-2: General – Structural fire design. European Standard. European Committee for Standardization, Brussels, 2004.

[2] EN 338:2003, Structural timber – Strength classes. European Standard. European Committee for Standardization, Brussels, 2003.

[3] Källsner, B. and König, J., Thermal and mechanical properties of timber and some other materials used in light timber frame construction. Proceedings of CIB W18, Meeting 33, Delft, Lehrstuhl für Ingenieurbau, University Karlsruhe, Karlsruhe, Germany, 2000.

[4] Thunell, B., Hållfasthetsegenskaper hos svenskt furuvirke utan kvistar och defekter. Royal Swedish Institute for Engineering Research, Proceedings No. 161, Stockholm, 1941.

[5] Schmid, J., Simulation of cross laminated timber boards under fire exposure. Master thesis, University of Natural Resources and Applied Life Sciences, Vienna, 2006.

INTERNATIONAL COUNCIL FOR RESEARCH AND INNOVATION
IN BUILDING AND CONSTRUCTION

WORKING COMMISSION W18 - TIMBER STRUCTURES

DESIGN OF TIMBER FRAME FLOOR ASSEMBLIES IN FIRE

A Frangi
C Erchinger

Institute of Structural Engineering, ETH Zurich

SWITZERLAND

MEETING FORTY

BLED

SLOVENIA

AUGUST 2007

Presented by A. Frangi

J. König commented that at the time of drafting of Eurocode 5 narrow cross section was assumed. He discussed the issue of zero strength layer. If one increases the charring model, it would be easier to model the influence of temperature on cross section. He would like to see an expansion of the model to consider 4 sides. A. Frangi agreed that expansion to column where the 4 side issue might be important. He agreed that the zero strength layer not to be fixed but a function of properties.

I. Smith commented that in the structural design side mechanistic calculations are considered too complicated for structural engineers. He wondered whether the same reactions are faced with the fire side. A. Frangi replied one needs only two extra minutes for this type of calculations and it should not be a problem for the design engineers. H. Blass commented the engineers tend to avoid anything new in code until the old version is deemed obsolete.

Design of timber frame floor assemblies in fire

Andrea Frangi & Carsten Erchinger
Institute of Structural Engineering, ETH Zurich, 8093 Zurich, Switzerland

1 Introduction

Timber frame floor assemblies are typical structural elements used in timber engineering. The floor assemblies consist of solid timber beams with claddings of gypsum plasterboards, wood based panels or combinations of these layers. The cavities may be filled with insulation made of rock, glass or wood fibre. The fire behaviour of timber frame floor assemblies is characterised by different charring phases. After the fire exposed claddings fall off, the timber beams are exposed directly to high temperatures leading to an increased charring rate in comparison to timber elements that are initially unprotected from fire exposure. Thus the fire performance of timber frame floor assemblies is influenced by the protection provided by the claddings. Further the size of the timber beams and the protection provided by the cavity insulation play an important role on the fire performance of the floor assemblies [9].

Design models of timber structures in fire usually take into account the loss in cross-section due to charring of wood and the temperature dependent reduction of strength and stiffness of the unburned residual cross-section. For timber frame wall and floor assemblies whose cavities are completely filled with insulation, Annex C of EN 1995-1-2 [2] provides a simplified calculation model based on the reduced properties method. The design model based on fire tests performed on light timber frame assemblies with studs and joists with small cross-sections. For timber frame wall and floor assemblies with void cavities only very little information is available in Annex D of EN 1995-1-2 [2].

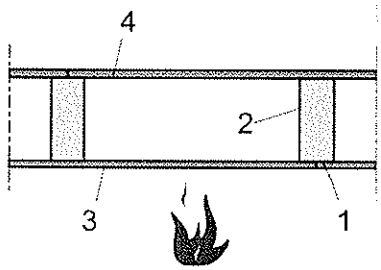

Definition:
1. Narrow side of timber beam exposed to fire
2. Wide side of timber beam facing the cavity
3. Fire protective cladding (lining) on exposed side of timber frame floor assembly
4. Fire protective cladding (lining) on side of timber frame floor assembly not exposed to fire

Figure 1 Timber frame floor assemblies with void cavities

A comprehensive research project on the fire behaviour of timber frame floor assemblies is currently ongoing at the ETH Zurich in cooperation with the Swiss Federal Laboratories for Materials Testing and Research (EMPA). The aim of the research project is the development of a design model for the fire resistance of timber frame floor assemblies with and without cavity insulation, primarily based on the reduced cross-section method. In addition to small-scale fire tests on protective claddings [12], the fire behaviour of timber frame floor assemblies was experimental analysed with a large-scale fire test. All fire tests were based on ISO-fire exposure and performed at the EMPA in Dubendorf.

The paper analyses the fire behaviour of timber frame floor assemblies with void cavities (see figure 1). The results of FE-thermal simulations in combination with results of fire tests permit to develop a simplified charring model to be included in EN 1995-1-2. In the first part of the paper the results of FE-thermal simulations are described. The second part of the paper presents the simplified charring model for timber frame floor assemblies with void cavities.

2 Design models in fire according to EN 1995-1-2

Design models of timber structures in fire given in EN 1995-1-2 take into account the loss in cross-section due to charring of wood and the temperature dependent reduction of strength and stiffness of the unburned residual cross-section. As a basic value, the one-dimensional charring rate β_0 is used as observed for one-dimensional heat transfer under standard fire exposure in a semi-infinite timber slab. At the corners of the cross-section an increased charring occurred. In order to simplify the calculation of cross-sectional properties (area, section modulus and second moment of area) by assuming an equivalent rectangular residual cross-section, notional charring rates β_n are given in EN 1995-1-2 such that they implicitly include the effect of corner roundings and give approximately the same results [10].

Claddings of timber frame floor assemblies usually consist of one or several layers of wood based panels, gypsum plasterboards, or combinations of these layers. Depending on the material, thickness, density and position of the layers the timber beams are not directly exposed to fire during a so called protection phase. EN 1995-1-2 gives rules for the calculation of failure times for fire protective claddings made of wood-based panels or wood panelling as well as for gypsum plasterboards type A or H. For this type of fire protective claddings it can be assumed that the start of charring t_{ch} of the protected timber beams corresponds to the failure time t_f of the fire protective claddings, i.e. $t_f = t_{ch}$. Gypsum plasterboards type F typically remain in place after the protected timber beams start charring, so that $t_f > t_{ch}$. Failure of gypsum plasterboards type F may take place due to thermal degradation of the boards or pull-out/pull-through failure of fasteners. Since no generic data are available for the failure due to thermal degradation, failure times of gypsum plasterboards type F must be determined by testing [10].

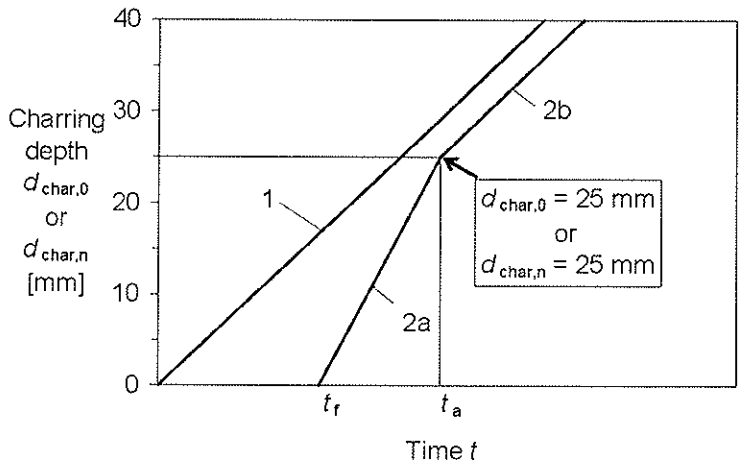

Figure 2 General description of charring phases for one-dimensional charring according to EN 1995-1-2 when failure of the cladding t_f occurs at the time of start of charring t_{ch} (lines 2a and 2b). Line 1 is for initially unprotected timber surfaces.

For protected timber surfaces different charring rates should be therefore applied during different phases of the fire exposure [8]. Figure 2 gives the simplified bi-linear model adopted by EN 1995-1-2 when failure of the cladding t_f occurs at the time of start of charring t_{ch}. This model can be used for protective claddings made of wood-based panels or wood panelling as well as for gypsum plasterboards type A or H. After the claddings fall of, charring is assumed to take place at double rate of initially unprotected surfaces. The protection provided by the char-layer is assumed to be built up until its thickness has reached 25 mm. Then the charring rate decreases to the value for initially unprotected surfaces. For simplicity, the 25 mm criterion is adopted for both the one-dimensional and notional charring depth. For the case $t_f > t_{ch}$ (typically for protective claddings made of gypsum plasterboards type F) the simplified model adopted by EN 1995-1-2 takes into account 3 different charring phases. The first one describes the charring of timber until failure of the protective claddings ($t_{ch} \leq t \leq t_f$) and is characterised by a reduced charring rate. The other following charring phases ($t > t_f$) are the same as described previously.

3 FE-thermal analysis

3.1 Introduction

Timber is a combustible material and thus differs from most other common structural building materials. When sufficient heat is applied to wood, a process of thermal degradation (pyrolysis) takes place producing combustible gases, accompanied by a loss in mass. A charred layer is then formed on the fire-exposed surfaces and the char-layer grows in thickness as the fire progresses, reducing the cross-sectional dimensions of the timber member. Because of its low thermal conductivity, the char-layer protects the remaining unburned residual cross-section against heat.

For the calculation of the temperature development in timber members subjected to ISO-standard fire exposure a FE-thermal analysis was conducted using the package ANSYS Workbench (in combination with ANSYS Release 10.0). The heat transfer to the surface of the member was considered by constant values according to EN 1991-1-2 for the resultant emissivity ε_{res} by radiation and the coefficient of heat transfer α_c by convection. Density, thermal conductivity and specific heat capacity of wood and charcoal vary as a function of the temperature. The change of moisture, i.e. the evaporation of water at a temperature of about 100°C was implemented into the FE-simulation as latent heat. In the FE-simulations, charring of timber (i.e. reduction of cross-section) was taken into account by gradually changing the thermal properties of wood into those of charcoal with increasing temperature.

For the FE-thermal calculation an initial density of 450 kg/m^3 and an initial moisture content of 12% were considered, as these values were determined for timber members used in the fire tests. The temperature dependent relationships for the density and specific heat of wood and charcoal were assumed according to EN 1995-1-2. Cracks in the charcoal increase the heat flux due to radiation and convection. Thus thermal conductivity values of the char-layer used in FE-thermal simulations are often apparent values rather than measured values in order to take into account the increased heat flux due to shrinkage cracks above about 500°C and the degradation of the char-layer at about 1000°C [7]. For the FE-thermal calculation the temperature dependent relationship for the thermal conductivity of wood and charcoal was assumed according to EN 1995-1-2.

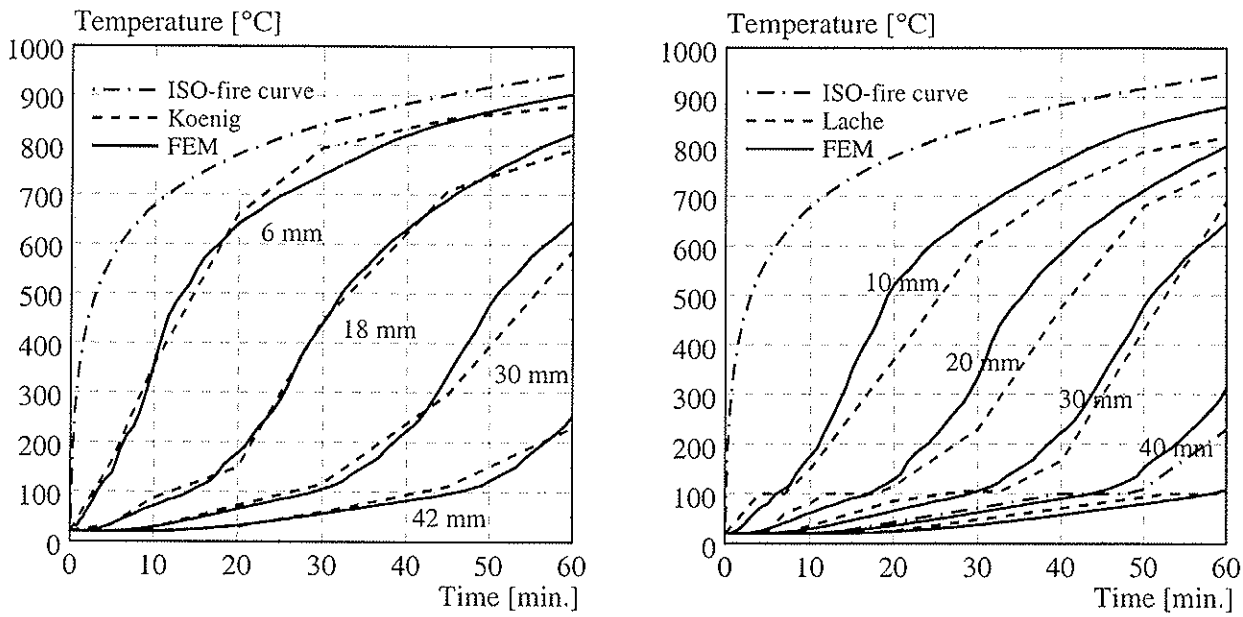

Figure 3 Comparison of FE-simulated temperatures in different timber depths to fire tests conducted by König [8] and Lache [11] under ISO-fire exposure on one side

The FE-model was verified with two independent series of fire tests performed by König [8] and Lache [11] on spruce timber specimens exposed to ISO-fire only on one side. The specimens used by König had a moisture content of about 12%. Temperatures were measured

in a depth of 6, 18, 30 and 42 mm from the surface exposed to fire. The specimens used by Lache had a higher moisture content of about 20%. Temperatures were measured in a depth of 10, 20, 30, 40 and 50 mm. Figure 3 shows the comparison between fire tests and FE-results for the temperatures measured in different timber depths. In figure 3 the mean temperature values of the fire tests are shown. Experimental and numerical results are in good agreement, especially in comparison to the test results of König. Compared to the FE-results conducted with a moisture content of 12%, the test results of Lache show slightly higher temperatures in the range between room temperature and 100°C and a slightly lower temperatures above 100°C. A possible reason may be the higher moisture content under 100°C which leads to a higher thermal conductivity, i.e. the temperatures rise faster until reaching 100°C. More details of the validation of the FE-model can be found in [3].

3.2 Results of the FE-thermal analysis

The fire behaviour of timber frame floor assemblies with void cavities was studied with the FE-thermal analysis for timber beams with following cross-sections: 60x200, 80x200, 100x200, 120x200, 140x200, 160x200, 180x200 and 200x200 mm. In order to simplify the thermal analysis only the fire behaviour of the timber beams subjected to ISO-fire exposure on 3 sides after the fire exposed claddings fall off was analysed. For the FE-simulations it was assumed that $t_f = t_{ch}$. Further in order to reduce the number of FE-calculations the following 3 basic cases for the failure time of the protective claddings were studied:

- the claddings fall off after 15 minutes, i.e. the initially protected timber beams start charring after 15 minutes ISO-fire exposure: $t_f = t_{ch} = 15$ minutes
- the claddings fall off after 30 minutes, i.e. the initially protected timber beams start charring after 30 minutes ISO-fire exposure: $t_f = t_{ch} = 30$ minutes
- the claddings fall off after 45 minutes, i.e. the initially protected timber beams start charring after 45 minutes ISO-fire exposure: $t_f = t_{ch} = 45$ minutes

In the following figures this is represented with start of charring $t_{ch} = 15$ min, $t_{ch} = 30$ min and $t_{ch} = 45$ min, respectively. Figure 4 and 5 show the calculated charring depth $d_{char,1}$ on the wide side and $d_{char,2}$ on the narrow side of the timber beam (see also figure 6 for the position of $d_{char,1}$ and $d_{char,2}$) as a function of the time for different cross-sections and different start of charring t_{ch} studied. The charring depth was calculated as the position of the 300°C isotherm according to EN 1995-1-2. In figures also the calculated charring depth for the unprotected cross-section ($t_{ch} = 0$ min) is represented.

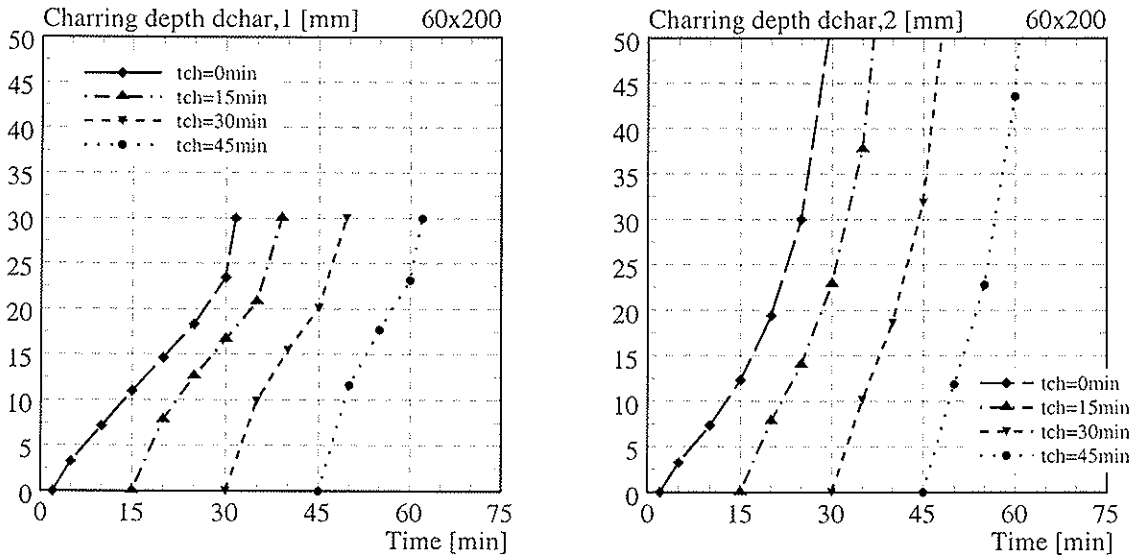

Figure 4 Calculated charring depth $d_{char,1}$ and $d_{char,2}$ as a function of the time for the cross-section 60x200 and different start of charring t_{ch} studied

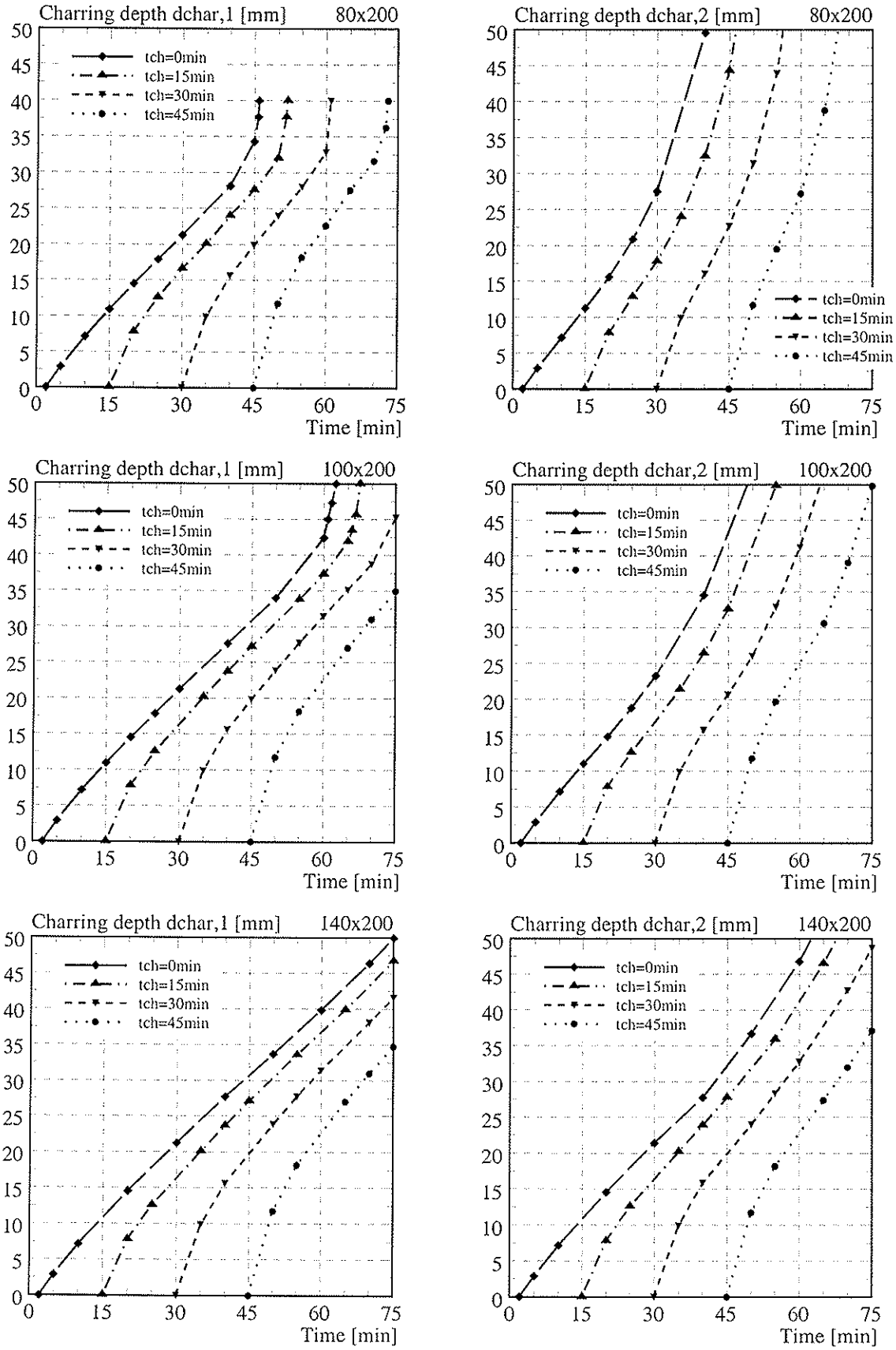

Figure 5 Calculated charring depth $d_{char,1}$ and $d_{char,2}$ as a function of the time for different cross-sections and different start of charring t_{ch} studied

Figure 6 left reports the calculated temperature field of the cross-section 100x200 mm after 30 minutes ISO-fire exposure on 3 sides assuming that the cross-section is initially protected for 30 minutes from fire exposure (t_{ch} = 30 min; t_{tot} = 60 min). Figure 6 right shows the calculated temperature field for the same timber cross-section after 30 minutes ISO-fire exposure on 3 sides assuming that the cross-section is initially unprotected from fire exposure (t_{ch} = 0 min; t_{tot} = 30 min).

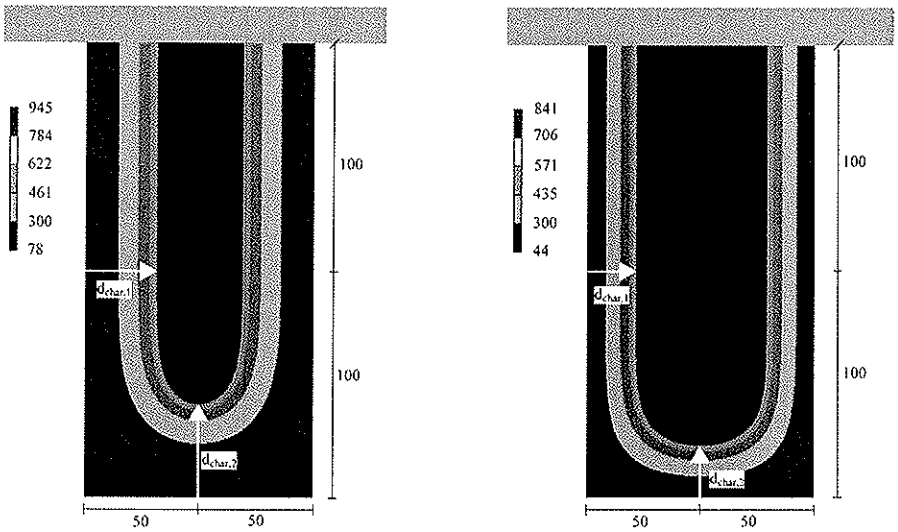

Figure 6 Calculated temperature field of the cross-section 100x200 mm after 30 minutes ISO-fire exposure for the initially protected timber beam (t_{ch} = 30 min, figure left) and the initially unprotected timber beam (t_{ch} = 0 min, figure right)

The FE-thermal analysis (see fig. 4, 5 and 6) clearly shows the increased charring rate after failure of the protective claddings. It can be seen that the charring rate depends also on the failure time of the protective claddings. The more the protective cladding delays the start of charring, the more the charring rate increases after failure of the protective cladding. Further for narrow cross-sections the charring rate on the narrow side is much greater than on the wide side. The reason for the increased charring rate observed on the narrow side is the superposition of the heat flux from 3 sides. The charring rate calculated for the unprotected timber beams on the wide side (with conditions similar to one-dimensional) charring is about 0.7 mm/min and is in good agreement with charring rate measured in fire tests [4]. For initially unprotected timber EN 1995-1-2 assumes a value of 0.65 mm/min for the one-dimensional charring rate.

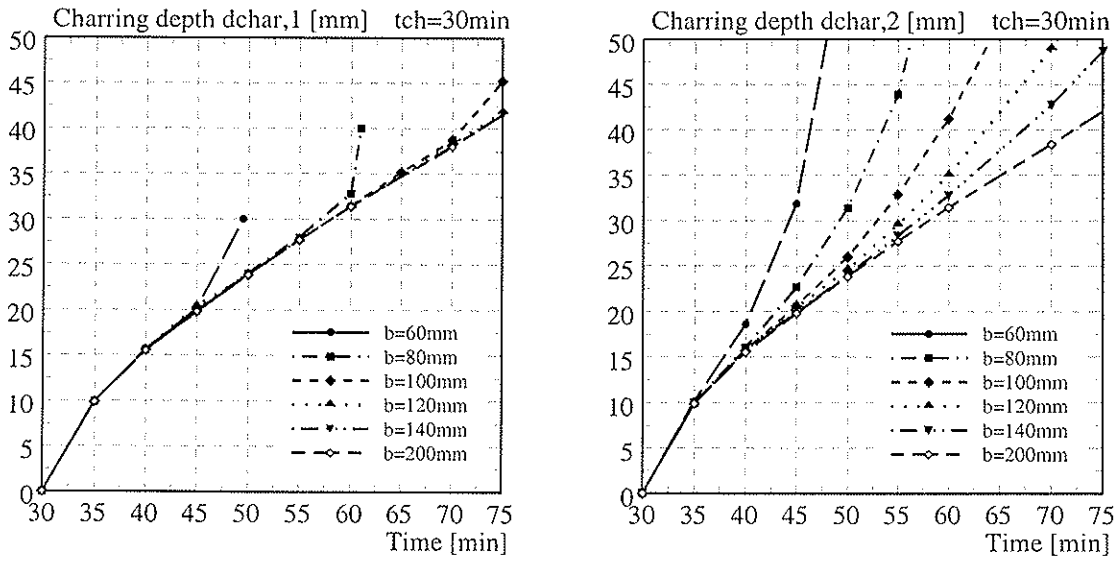

Figure 7 Calculated charring depth $d_{char,1}$ and $d_{char,2}$ as a function of the time for different cross-sections for the case t_{ch} = 30 min

Figure 7 compares the calculated charring depth $d_{char,1}$ and $d_{char,2}$ as a function of the time for different cross-sections for the case t_{ch} = 30 min. Following remarks can be drawn:

- the charring depth $d_{char,1}$ measured on the wide side is independent from the width of the timber beam. Thus the fire conditions on the wide side are similar to one-dimensional charring observed in semi-infinite timber slabs. However, this is only valid if the residual uncharred width of the cross-section is more than about 20mm. Further it can be seen that after the char depth exceeds about 10 mm the charring rate starts reducing to the value of the one-dimensional charring rate for initially unprotected timber.
- the charring depth $d_{char,2}$ measured on the narrow side is strongly influenced by the width of the timber beam. For wide cross-sections the same effect as on the wide side of the timber beams is observed, i.e. after the char depth exceeds about 10 mm the charring rate starts reducing to the value of the one-dimensional charring rate for initially unprotected timber. For the 200 mm wide cross-section no significant difference between charring rate on the wide side and charring rate on the narrow side is observed. On the other hand for narrow cross-sections no significant reduction of the charring rate is observed although the char-layer grows in thickness as the fire progresses. The reason for this effect is that the protection provided by the char-layer is less important than the influence of the heat flux superposition from 3 sides.

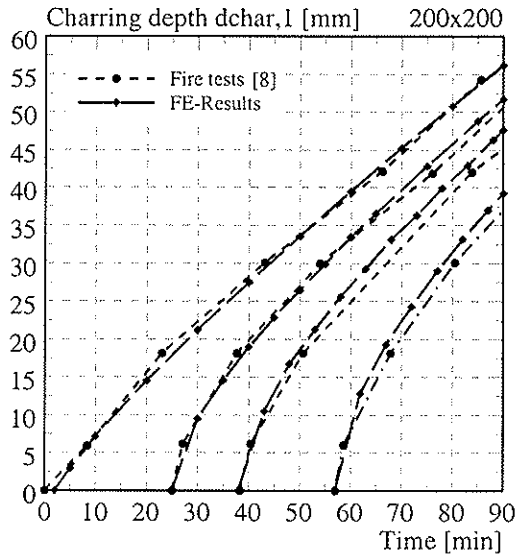

Figure 8 Comparison of the calculated charring depth $d_{char,1}$ with fire tests on protected timber specimens exposed to ISO-fire only on one side

Figure 8 compares the calculated charring depth $d_{char,1}$ on the wide side of the timber beam 200x200 with results of fire tests performed by König [8] on protected timber specimens exposed to ISO-fire only on one side after failure of the claddings (particleboards or gypsum plasterboards). Experimental and numerical results are in fairly good agreement.

3.3 Comparison to EN 1995-1-2

Figure 9 compares the calculated charring depth $d_{char,1}$ and $d_{char,2}$ with the simplified bilinear model adopted by EN 1995-1-2 for initially protected surfaces. For the calculation according to EN 1995-1-2 a value of 0.65mm/min was used for the one-dimensional charring rate β_0 for initially unprotected timber surfaces. As the charring depth $d_{char,1}$ calculated on the wide side is not influenced by the width of the timber beam only the results of cross-section 140x200mm are represented in figure 9 left. Figure 9 right shows the charring depth $d_{char,2}$ calculated on the narrow side of different timber beams for t_{ch} = 30 minutes.

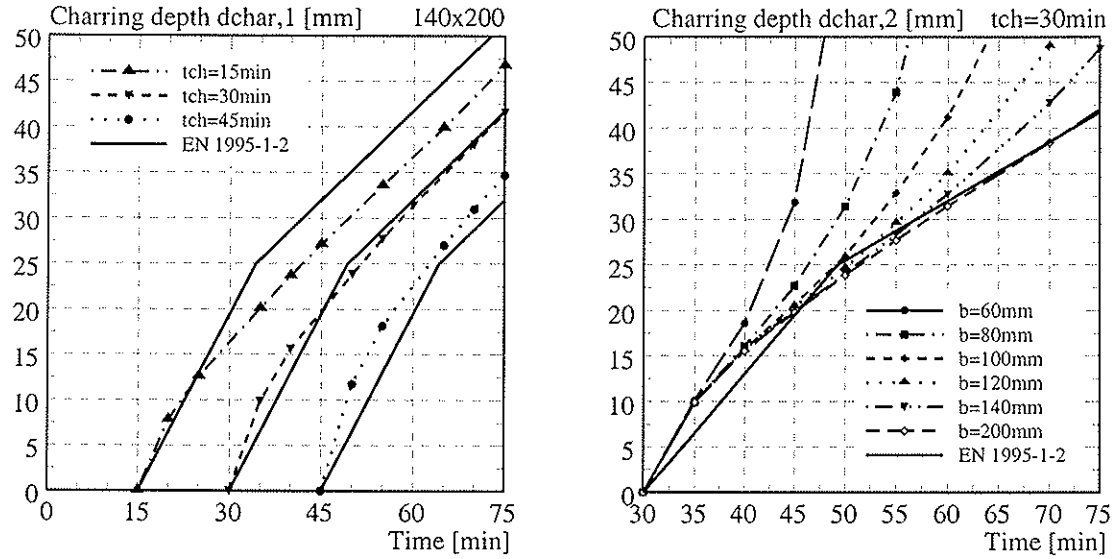

Figure 9 Comparison of the calculated charring depth with the simplified bi-linear model adopted by EN 1995-1-2 for initially protected timber surfaces

From figure 9 following remarks can be drawn:

- charring depth $d_{char,1}$ on the wide side (fig. 9 left): the agreement between calculated charring depth according to the simplified bi-linear model adopted by EN 1995-1-2 and the FE-thermal analysis is fairly good for the case t_{ch} = 30 min. The calculated charring depth is underestimated (unsafe) for the case t_{ch} = 45 min, overestimated (conservative) for the case t_{ch} = 15 min. Further the assumption that the protection provided by the char-layer is built up when its thickness has reached 25 mm is conservative. It can be seen that after the char depth already exceeds about 10 mm the charring rate starts reducing to the value of the one-dimensional charring rate for initially unprotected cross-sections. The thermal analysis shows that the charring rate for protected timber depends on the failure time of the protective claddings. This is confirmed also by the fire tests conducted by König [8]. However the simplified charring model adopted by EN 1995-1-2 is independent from the failure time of the protective claddings leading to conservative or unsafe results.
- charring depth $d_{char,2}$ on the narrow side (fig. 9 right): the charring depth on the narrow side is strongly underestimated by the simplified bi-linear model for most all cross-sections studied. The model leads to safe results only for wide cross-sections. The main reason is that the model based on the one-dimensional charring of timber, thus the influence of the heat flux superposition from 3 sides as the fire progresses is not considered in the model. A slightly better agreement can be achieved if the protective function of the char-layer is neglected, i.e. charring is assumed to take place at double rate without reduction. This assumption has been already used for the charring model adopted in Annex C of EN 1995-1-2 for timber frame assemblies whose cavities are completely filled with insulation. However in order to get a good agreement the charring rate on the narrow side should be expressed as a function of the failure time of the claddings as well as the width of the timber beam.

4 Charring model for timber assemblies with void cavities

Based on the results of the FE-thermal analysis a simplified charring model for timber assemblies with void cavities was developed following the method and terminology given in EN 1995-1-2. The charring model takes into account following two relevant effects as shown in the thermal analysis:

- the influence of high temperatures on the charring rate after failure of the fire protective claddings. The more the protective cladding delays the start of charring, the more the charring rate increases after failure of the protective cladding. The charring rate is therefore a function of the failure time of the protective claddings.

- the influence of the heat flux superposition on the charring rate on the narrow side of the timber beam after failure of the fire protective claddings as the fire progresses. This effect mainly depends on the width of the timber beam and the failure time of the fire protective claddings. On the other hand the charring rate on the wide side of the timber beam can be assumed to be independent from the width of the timber beam.

In order to make the charring model easy to use a bi-linear approach is adopted to describe the post-protection phase, i.e. two charring phases (2b) and (2c) are considered (see figure 10). Based on the results of the thermal analysis the charring phases are defined as following:

- charring phase (2b) describes the increased charring rate after failure of the protective claddings and is assumed to have duration of 5min. During this phase, a char-layer of about 10mm thickness has built-up.
- charring phase (2c) describes the charring of timber after the protective char-layer starts reducing the effect of the temperature.

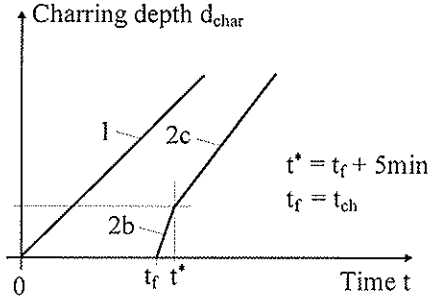

Figure 10 Charring phases for initially protected timber beams exposed to ISO-fire on 3 sides assuming that the failure time t_f of the fire protective cladding occurs at the time of start of charring t_{ch} of the timber beam (line 2). Line 1 is for initially unprotected timber surfaces.

Starting from the one-dimensional charring β_0 assumed as 0.65 mm/min according to EN 1995-1-2 the notional charring rate β_n for the timber beams after failure of the protective claddings (post-protection phase) can be calculated as:

$$\beta_n = k_s \cdot k_p \cdot k_n \cdot \beta_0 \tag{1}$$

The cross-section factor k_s takes into account the influence of the width of the timber beam. The FE-thermal analysis showed that this parameter is only significant for the charring rate on the narrow side of the timber beam. For charring on the wide side fire conditions similar to one-dimensional charring can be assumed, thus the factor k_s can be neglected (k_s = 1.0). Further, it was observed that the charring rate on the narrow side of the timber beam during the charring phase (2b) is more or less independent from the width of the timber beam. Therefore, the factor k_s is only used for the calculation of the charring rate on the narrow side during the charring phase (2c). The results of the FE-thermal analysis also demonstrated that for wide timber beams the heat flux is mainly one-dimensional. For timber beams with a width $b \geq 150$mm the influence of the heat flux superposition can be neglected, thus for $b \geq 150$mm it is assumed that k_s = 1.0. Based on the results of the FE-thermal analysis the cross-section factor k_s can be calculated as:

$$k_s = \left(\frac{150}{b}\right)^{\left(\frac{17}{300}\cdot t_f\right)} \geq 1.0 \qquad \text{for } 0 \leq t_f \leq 15 \text{ min} \tag{2}$$

$$k_s = \left(\frac{150}{b}\right)^{\left(\frac{1}{75}\cdot t_f + 0.65\right)} \geq 1.0 \qquad \text{for } 15 \leq t_f \leq 60 \text{ min} \tag{3}$$

With b: width of timber beam in mm

t_f: failure time of fire protective claddings in minutes

Equations 2 and 3 should only be used for cross-sections with b ≥ 60mm, as no FE-thermal analysis was performed for cross-sections with b < 60mm. Because of the strong influence of the heat flux superposition from 3 sides it is recommended that cross-sections with b < 60mm should not be exposed to fire on 3 sides during the post-protection phase. This can be achieved in two different ways:

- the fire protective claddings are designed in a way so that the timber beams are not directly exposed to fire for the whole required fire duration
- the cavities are filled with insulation material so that after failure of the fire protective claddings charring occurs mainly on the narrow side of the timber beams, while the wide sides are protected by the insulation. This approach has been used for the design model of timber slabs made of hollow core elements presented in [5].

The post-protection factor k_p takes into account the influence of high temperature on the charring rate after failure of the fire protective claddings. Based on the results of the FE-thermal analysis the post-protection factor $k_{p,2b}$ for charring phase (2b) and $k_{p,2c}$ for charring phase (2c) can be calculated as:

$$k_{p,2b} = 1 + \frac{8}{75} \cdot t_f \qquad \text{for } 0 \le t_f \le 15 \text{ min} \qquad (4)$$

$$k_{p,2b} = 1.9 + \frac{7}{150} \cdot t_f \qquad \text{for } 15 \le t_f \le 60 \text{ min} \qquad (5)$$

$$k_{p,2c} = 1 + \frac{2}{225} \cdot t_f \qquad \text{for } 0 \le t_f \le 60 \text{ min} \qquad (6)$$

With t_f: failure time of fire protective claddings in minutes

Figure 11 shows the cross-section factor k_s as a function of the width of the timber beam as well as the post-protection factor $k_{p,2b}$ for charring phase (2b) and $k_{p,2c}$ for charring phase (2c) as a function of the failure time t_f of the protective claddings.

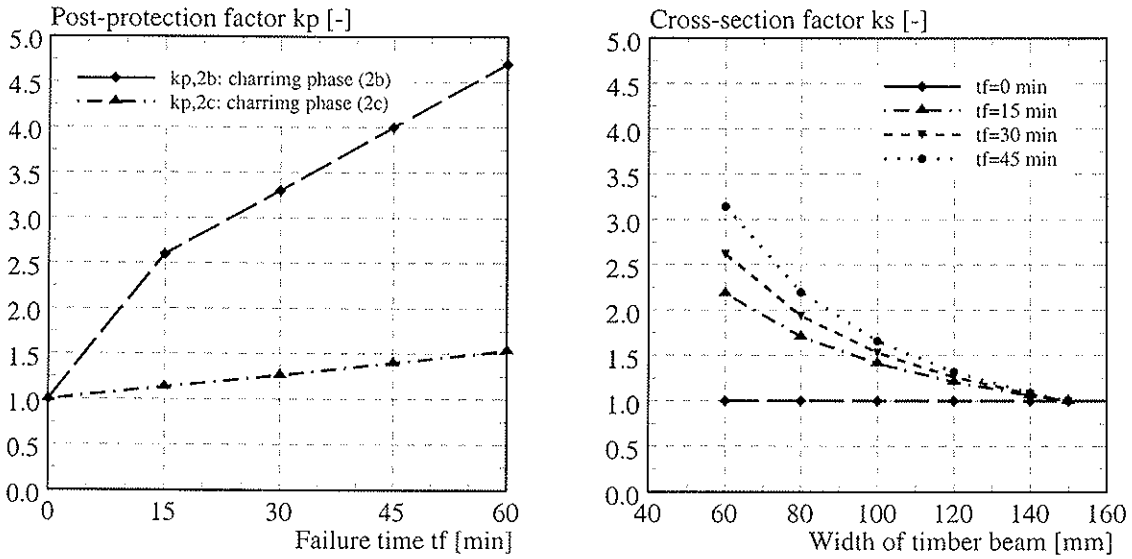

Figure 11 Post-protection factor k_p as a function of the failure time t_f of the fire protective claddings (left) and cross-section factor k_s as a function of the width of the timber beam (right)

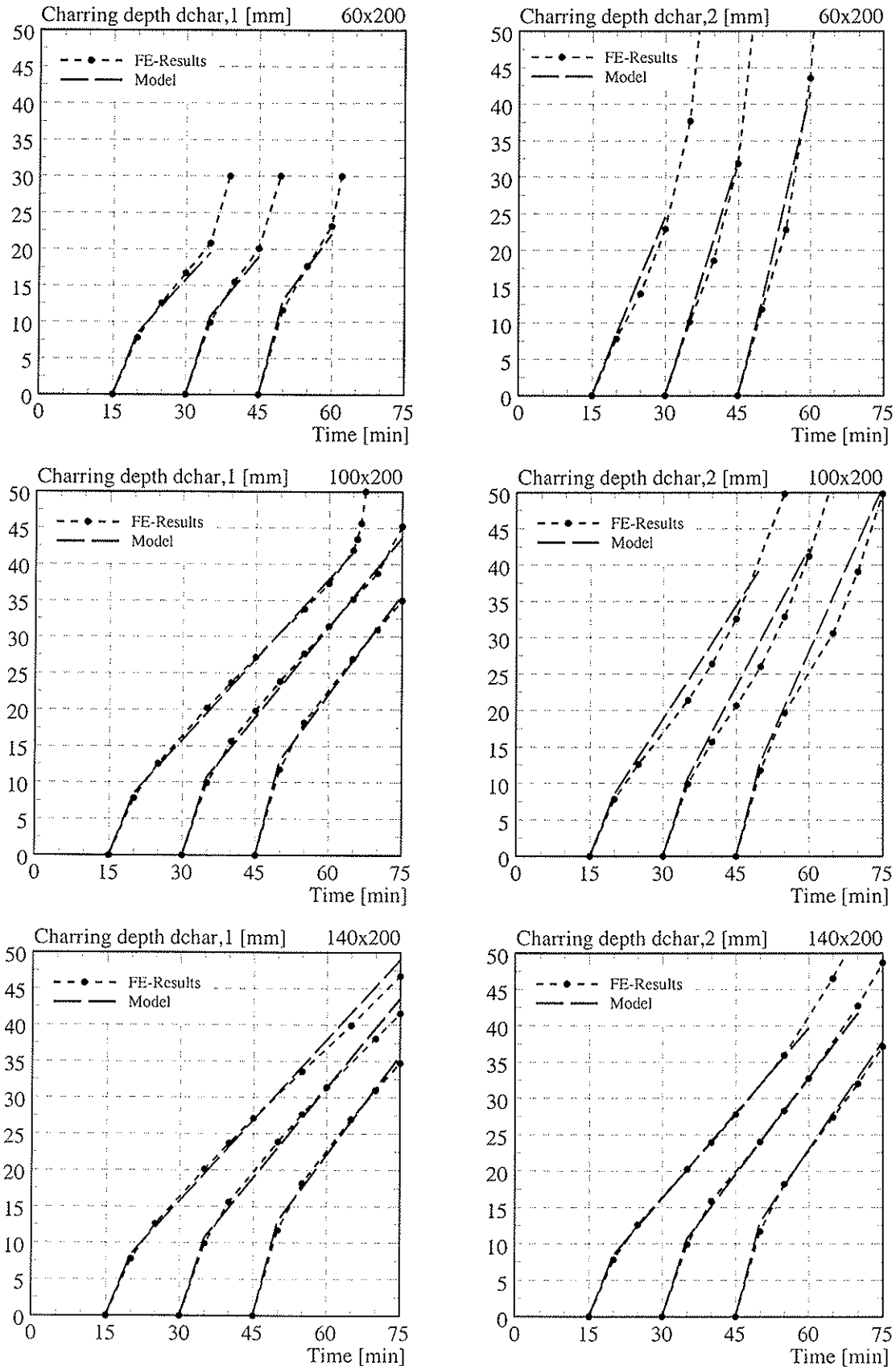

Figure 12 Comparison between charring depths calculated according to the proposed simplified charring model and FE-thermal analysis

Figure 12 compares the calculated charring depth according to the FE-thermal analysis with the results of the proposed charring model. The agreement between charring model and FE-results is good, especially for the charring depth on the wide side. The calculated charring depth on the narrow side is slightly overestimated, i.e. the charring model leads to conservative results. However, because of the strong influence of the heat flux superposition from 3 sides the charring model should only be used for the maximum time of fire exposure as given in table 1 in order to get safe results (see figure 12). The proposed bilinear model can be improved by choosing a non linear model. As the differences between analytical calculation and FE-thermal analysis are small, the proposed bilinear charring model has not been modified making the calculation easier for the design.

Table 1 Maximum period of validity of the charring model as a function of the width b of the timber beam and the time of start of charring t_{ch}

Start of charring	b = 60mm	b = 80mm	b = 100mm	b = 120mm	b = 140mm	b = 160mm	b ≥ 180mm
t_{ch} = 15 min	30min	40min	50min	55min	60min	65min	75min
t_{ch} = 30 min	45min	55min	60min	65min	70min	70min	75min
t_{ch} = 45 min	60min	65min	75min	75min	75min	75min	75min

The factor k_n permits to convert the irregular residual cross-section due to increased charring at the corners (see fig. 6) to an equivalent rectangular residual cross-section, simplifying the calculation of cross-sectional properties. The conversion factor k_n was derived from the FE-results for the different cross-sections and start of charring studied. The analysis shows that the factor k_n is a function of width of timber beam, failure time of protective claddings and cross-sectional property studied (area, section modulus and moment of inertia). For simplicity it can be assumed k_n = 1.25 for the calculation of the charring depth on the narrow side of the beam and k_n = 1.0 for the calculation of the charring depth on the wide side of the beam. This assumption leads to safe results.

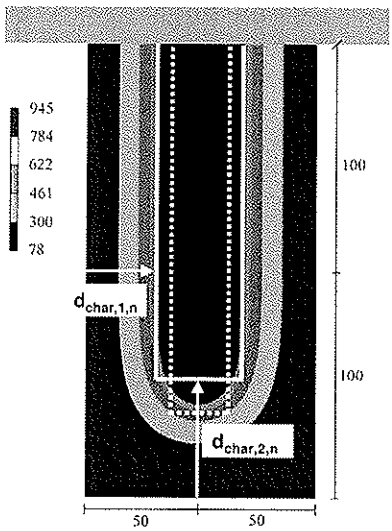

Residual cross-section calculated according to the new charring model (continuous line in figure):
$d_{char,1,n}$ = 31,3 mm
$d_{char,2,n}$ = 52.8 mm
W = 810*103 mm^3
A = 5505 mm^2

Residual cross-section calculated according to the charring model of EN 1995-1-2 (dotted line in figure):
$d_{char,1,n}$ = 36.5 mm
$d_{char,2,n}$ = 36.5 mm
W = 721*103 mm^3
A = 4414 mm^2

Figure 13 Comparison of the residual cross-section calculated according to the new charring model (continuous line) and the charring model adopted by EN 1995-1-2 (dotted line)

Figure 13 compares the residual cross-section calculated according to the new charring model and the charring model adopted by EN 1995-1-2 for the cross-section 100x200 and start of charring t_{ch} =30 min (total time of fire exposure t_{tot} = 60 min). For the calculation according to EN 1995-1-2 the notional charring rate β_n = 0.8mm/min was used. It can be seen that the new charring model permits a more accurate calculation of the residual cross-section in comparison to the charring model of EN 1995-1-2. Because of the strong overestimation of the notional charring depth $d_{char,1,n}$ on the wide side of the beam, the charring model adopted by EN 1995-1-2 leads to conservative results with regard to area A and section modulus W of the residual cross-section (see figure 13).

5 Summary and conclusions

Design models of timber structures in fire usually take into account the loss in cross-section due to charring of wood and the temperature dependent reduction of strength and stiffness of the unburned residual cross-section. The paper presented a simplified charring model for timber frame floor assemblies with void cavities. The charring model was developed following the method and terminology given in EN 1995-1-2 so that it is easy to use and can be included in Annex D of EN 1995-1-2. The simplified model based on extensive FE-simulations and takes into account for the post-protection phase (i.e. after failure of the fire protective claddings) the influence of high temperatures as well as the heat flux superposition on the charring rate of the timber beams. The FE-model for the thermal analysis was verified by fire tests on protected specimens exposed to one-dimensional charring.

The simplified charring model was developed for the case that the failure of the claddings t_f occurs at the same time of start of charring t_{ch} (typically for protective claddings made of wood-based panels or wood panelling as well as for gypsum plasterboards type A or H). For the case $t_f > t_{ch}$ (typically for protective claddings made of gypsum plasterboards type F) the simplified charring model should be modified in order to include charring of the timber beams until failure of the protective claddings. For the calculation of the mechanical resistance of the timber beams of the floor assemblies with void cavities, also the temperature dependent reduction of strength and stiffness of the unburned residual cross-section shall be taken into account, e.g. by modification factors for the material properties or the use of an effective reduced residual cross-section. The modification factors or the zero-strength layer can be calculated combining the results of the thermal analysis with the structural analysis of the timber beams in fire. The results of the structural analysis will be presented in a future publication.

6 References

[1] Buchanan H., *Fire performance of timber construction*, Progress in Structural Engineering and Materials, Vol. 2, 2000.

[2] EN 1995-1-2 (Eurocode 5), *Design of timber structures, Part 1-2 General rules-Structural fire design*, CEN, Brussel, 2004.

[3] Erchinger C., Frangi A., Mischler A., *Thermal investigations on multiple shear steel-to-timber connections*, Proceedings of 9th World Conference on Timber Engineering (WCTE), Portland, 2006.

[4] Frangi A., Fontana M., *Charring rates and temperature profiles of wood sections*, Fire and Materials, Volume 27, Issue 2, 2003, John Wiley & Sons, Ltd.

[5] Frangi A., Fontana M., *A design model for timber slabs made of hollow core elements in fire*, Proceedings of 39th CIB-W18 Meeting, Florence, 2006

[7] Källsner, B., König, J., *Thermal and mechanical properties of timber and some other materials used in light timber frame construction.* Proceedings of 33th CIB-W18 Meeting, Delft, 2000.

[8] König J., Walleij L., *One-dimensional charring of timber exposed to standard and parametric fires in initially protected and non-protected fire situations*, Trätek – Swedish Institute for Wood Technology Research, Report No. I 9908029, Stockholm, 1999.

[9] König J., Walleij L., *Timber frame assemblies exposed to standard and parametric fires, Part 2: a design model for standard fire exposure*, Trätek – Swedish Institute for Wood Technology Research, Report I 0001001, Stockholm, 2000.

[10] König, J., *Structural fire design according to Eurocode 5 - Design rules and their background*, Fire and Materials, Vol. 29, 2005.

[11] Lache M., *Untersuchungen zur Abbrandgeschwindigkeit von Vollholz und zur Feuerwiderstandsdauer biegebeanspruchter Brettschichtholzträger*, PhD thesis, Ludwig-Maximilians-Universität, München, 1992.

[12] Schleifer V., Frangi A., Fontana M., *Experimentelle Untersuchungen zum Brandverhalten von Plattenelementen*, IBK-testing report, Institute of Structural Engineering (IBK), ETH Zurich, 2007.

INTERNATIONAL COUNCIL FOR RESEARCH AND INNOVATION
IN BUILDING AND CONSTRUCTION

WORKING COMMISSION W18 - TIMBER STRUCTURES

ASTM D198 - INTERLABORATORY STUDY FOR MODULUS OF ELASTICITY OF LUMBER IN BENDING

A Salenikovich

Université Laval

CANADA

MEETING FORTY

BLED

SLOVENIA

AUGUST 2007

Presented by A. Salenikovich
E. Gehri commented that this shows limitations of our measurements. Even with simple tests 1st two figures may be correct but other figures are not accurate.
I. Smith wondered whether actual MOE are less variable than measured ones and commented that two sided MOE measurement be done.

ASTM D198 - Interlaboratory Study for Modulus of Elasticity of Lumber in Bending

Alexander Salenikovich
Université Laval, Canada

1 Introduction

The American Society for Testing and Materials (ASTM) standard test method D198 covers a method for determination of the flexural properties of structural beams made of solid or laminated wood or of composite constructions of various sizes and cross-sections. The structural member is supported near its ends and is subjected to a bending moment by applying transverse loads symmetrically between the supports at a prescribed rate until rupture occurs. To determine the modulus of elasticity (MOE), "the deflection of the neutral axis of the beam at the centre of the span is measured with respect to a straight line joining two reference points equidistant from the reactions and on the neutral axis of the beam" [1]. The description of the flexure test method is given in sections 4 to 11 of the standard and additional guidance is given in Appendices X1, X2, and X5 [1].

The standard was originally approved in 1924 and has served as a reference test method in numerous standards used by the wood industry in North America and elsewhere. Despite its wide acceptance and importance to the industry, the standard lacks a formal statement concerning the accuracy of the test method. Although there are requirements for individual measurements, such as specimen dimensions and deflections to be recorded to the nearest three digits, there are uncertainties related to the test apparatus, procedure, data analysis methods, etc., affecting the overall accuracy of test results.

Informally speaking, the *accuracy* of a quantitative test method (measurement process) is the degree of agreement of a set of test results with the actual value of the quantity being measured. In ASTM standards, the accuracy is defined in terms of *precision* and *bias*. The use of these terms is described in ASTM E177 Standard Practice [2]. Precision is defined as "the closeness of agreement between independent test results obtained under stipulated conditions" and is expressed in terms of *repeatability* and *reproducibility*. Repeatability measures the variability between independent test results obtained under *repeatability conditions*; i.e., "with the same method on identical test items in the same laboratory by the same operator using the same equipment within short intervals of time". Reproducibility concerns the variability between single test results obtained in different measurement processes under *reproducibility conditions*; i.e., "with the same method on identical test items in different laboratories with different operators using different equipment". Both terms characterize random errors of the measurement process, which is assumed to be in a state of statistical control, and are expressed as the standard deviation or some multiple of the standard deviation. A separate precision statement is applied to each combination of

sources of variability. Bias is defined as the systematic difference between the expectation of test results and an accepted reference value. When an accepted reference value is not available, the bias cannot be established.

The objective of this interlaboratory study (ILS) was to evaluate the precision of the D198 method of determination of the *apparent MOE* based on measurements of the full-span deflection of the neutral axis of the beam at the centre of the span with the use of a yoke deflectometer. For comparison purposes, the MOE was also determined from the measurements of the load head displacement, similar to the ASTM D4761 [3] edge-wise bending test method under third-point loading.

2 Methodology

2.1 General

The ILS was planned and conducted according to ASTM E691 Standard Practice [4] in a round-robin fashion, so that a set of specimens was shipped from one lab to the next for independent testing. At the end, the specimens were returned to the originating lab for additional testing and comparison with the original data to verify if there was any drift in the MOE values. Sixteen laboratories (ten in the US and six in Canada) from wood products industry, wood research institutions and universities volunteered to participate in the study. The shipping of the specimens was sponsored by the ASTM.

2.2 Specimens

The scope of the study was limited to edgewise and flatwise bending MOE tests of 38x89-mm (2x4-nominal) dimension materials of three product families: machine stress rated (MSR) lumber, laminated veneer lumber (LVL) and laminated strand lumber (LSL). The list of test specimens and loading conditions is shown in Table 1. The beams were cut to the length of 1.75 m. The test spans for wood materials represented 21 and 18 times depth for flatwise and edgewise tests, respectively.

Table 1. Test specimens, configuration, and load levels.

	Material	Number of Specimens	Test Orientation	Width	Depth	Test Span	Upper Load Limit	Rate of Head Motion	Number of Trials per Specimen	Total Number of Trials
				mm	mm	mm	kN	mm/min		
				b	*h*	*L*	P_2	*N*		
A	MSR Lumber	5	Edgewise	38	89	1600	3.7	5.3	4	20
			Flatwise	89	38	800	3.5	3.0	4	20
B	LSL	5	Edgewise	38	89	1600	3.0	5.3	4	20
			Flatwise	89	38	800	2.5	3.0	4	20
C	LVL	5	Edgewise	38	89	1600	5.5	5.3	4	20
			Flatwise	89	38	800	4.7	3.0	4	20
D	Calibration Bar (HSS)	1	Edgewise	25	51	1600	1.3	9.4	4	4
			Flatwise	51	25	800	1.8	4.6	4	4

The wood materials had been equilibrated in normal conditions (20°C and 65% RH) prior to the beginning of the study. To minimize any damage and influence of weather conditions on the moisture content during shipping the specimens were wrapped in plastic and transported in a wooden crate. In each lab, the materials were to be stored in a room

with the normal conditions. The weight of each specimen as received and at test was recorded in a log journal accompanying the shipment. After conditioning for at least 48 hours, the materials were tested if the difference from the original weight did not exceed 2%. A steel calibration bar was included to estimate the bias in the weight measurements between the labs and to trace any possible drift of MOE of wood materials assuming that the weight and stiffness of the bar remain constant.

2.3 Apparatus

Section 7 of the standard [1] gives requirements on the apparatus for the flexure tests. The lateral support was not required because the depth-to-width ratio of the beams was less than three. Figure 1 is a schematic of the test setup. The standard does not specify hardware details but provides photos of an example test setup; therefore, the design of the loading and deflection measuring apparatus remains at the discretion of the user. Each participating lab was requested to provide photographs and to fill a questionnaire describing the load heads, supports and load/deflection measurement apparatus including tolerances and frequency of data sampling.

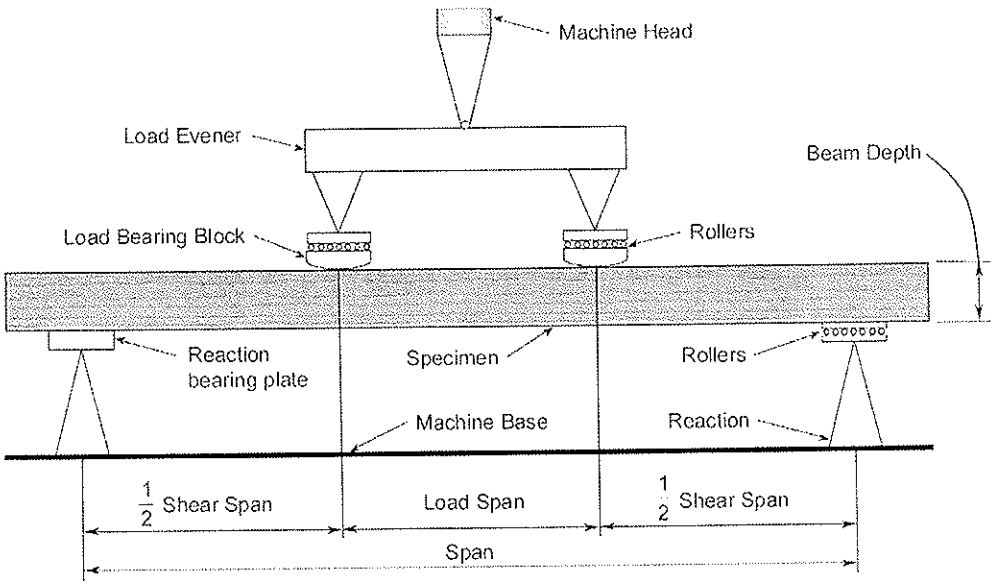

Figure 1. D198 flexure method. Example of two-point loading (from [1]).

To measure the full-span deflection, a yoke deflectometer is mounted on the specimen at the reference points positioned such that a line perpendicular to the neutral axis of the beam at the location of the reference point passes through the centre of the support. In practice, different labs use different hardware for supporting the yoke (pins, nails, screws, etc.). Considering the large number of tests on each specimen in multiple labs, the ILS task group decided that screws installed in predrilled holes would be the least harmful and reusable fastener for the purpose of this study. For the calibration bar, steel pins inserted in predrilled holes were used. The screws and the pins were provided with the specimens.

2.4 Procedure

Beams were loaded in third-point bending to a load level not exceeding the upper limit (P_2) shown in Table 1. For repeatability measurements, each specimen went under four trials flatwise on one specified wide face and four trials edgewise on one specified narrow face. Each trial under repeatability test conditions consisted of one loading cycle. Removal of the specimen from the testing machine and rotation of the ends without changing the face of edge under tension was required between the trials. The speed of loading was setup so that the rate of strain of the outer fibre was 0.001 mm/mm/min (see Table 1). To measure the reproducibility, the specimens were tested in different labs using the same instructions. Test results for each specimen were reported to the ILS coordinator. Each lab had access to its own data only.

Two load-deflection curves were obtained simultaneously in each trial using 1) full-span deflection of the neutral axis of the beam at the centre of the span measured as described above and 2) displacement of the loading head of the testing machine as per Section 8.2 of D4761 [3]. The latter represented the average deflection of the load points with respect to the reaction plates and included extraneous deformation components related to the stiffness and imperfections of the test frame, compression of wood fibres under load heads and at supports, and other uncertainties.

2.5 Calculation

Apparent MOE E_{yoke} and E_{stroke} were calculated from each trial of each wooden specimen using the guidance of D198 Appendix X2.5 [1] and the following formulae:

$$E_{yoke} = \frac{23L^3}{108bh^3}\frac{P}{\Delta} \tag{1}$$

$$E_{stroke} = \frac{5L^3}{27bh^3}\frac{P}{\Delta_a} \tag{2}$$

Stiffness of the calibration bar was calculated using the following formulae:

$$EI_{yoke} = \frac{23L^3}{1296}\frac{P}{\Delta} \tag{3}$$

$$EI_{stroke} = \frac{5L^3}{324}\frac{P}{\Delta_a} \tag{4}$$

where:

b, h and L = width, depth and span of the beam, respectively, as measured at test,

P/Δ = slope of load-deflection curve based on full-span deflection of the beam's neutral axis at the center of span within a load range determined by user,

P/Δ_a = slope of load-deflection curve based on displacement of the loading head of the testing machine in third-point bending within the same load range.

A one-way analysis of variance of the MOE data (within- and between-laboratories) was carried out separately for each material using ASTM E691 [4] as guidance to determine if the collected data are adequately consistent, to act on any data considered inconsistent, and to obtain the precision statistics on which the precision statement can be based. The statistical procedure is outlined in the Appendix.

3 Results and Discussion

3.1 General

In the course of the study, which took 45 weeks, each specimen was tested 68 times edgewise and 68 times flatwise. All specimens survived except one (A4), which was accidentally overloaded in the 15th lab. Figure 2 shows that the mass of the specimens remained steady enough to neglect the moisture content variation (average CV = 0.25%). No trend was detected in the MOE values as the study progressed. The MOE determined at the beginning and at the end of the study in the same lab was reproduced within the repeatability standard deviation of that lab. Therefore, it was concluded that the test samples were homogeneous for the purpose of the interlaboratory comparison.

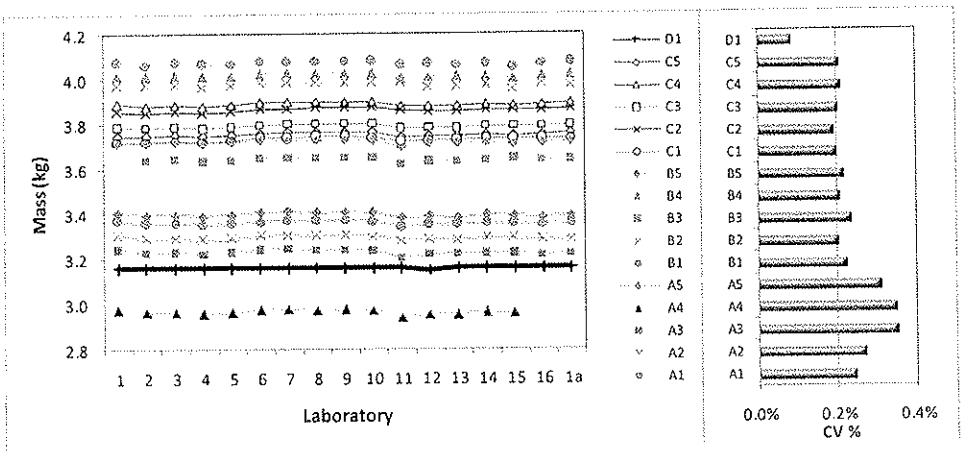

Figure 2. Mass of the specimens: measured values (left) and between-lab variation (right).

3.2 Consistency of E_{yoke}

Figure 3 shows consistency statistics of E_{yoke} calculated for all 16 labs. In this figure, the labs are ranked on the basis of the overall between-lab (h) and within-lab (k) consistency of their test results (see formulae in the Appendix). Critical values of the h and k statistics were calculated at 0.5% significance level according to the E691 [4] recommendations. The information from the labs where the critical values were exceeded was investigated using the photographs and questionnaires. In several instances, mechanical deficiencies of the test setup and/or deflection measurement apparatus were found; e.g., supports or load heads lacked free pivoting movement in one or another direction, yoke was mounted too loose or too tight on the side of the beam, contact between the displacement transducer and the screw was not secured, etc. In some instances, the reasons for inconsistent data could not be established from the available information, but the order of consistency statistics suggested that there could be similar problems in the setup. Based on the established evidence and/or order of consistency statistics, the data sets from the labs with the highest ranking inconsistency were excluded from the data pool one by one, and the analysis was repeated. Once the number of labs considered was reduced to seven, the last six of these seven labs were observed to have similar overall ranking and with no obvious reasons to suspect data to be out of statistical control. Figure 4 shows the h and k graphs for these six labs. The one lab that was in statistical control but that differed from the others was ranked #1 and showed significantly higher consistency (the lowest h and k) than every other lab. Although the reason for this perhaps requires further study, it should be noted that this is the only lab in the project that used the yoke deflectometers on both sides of the beam.

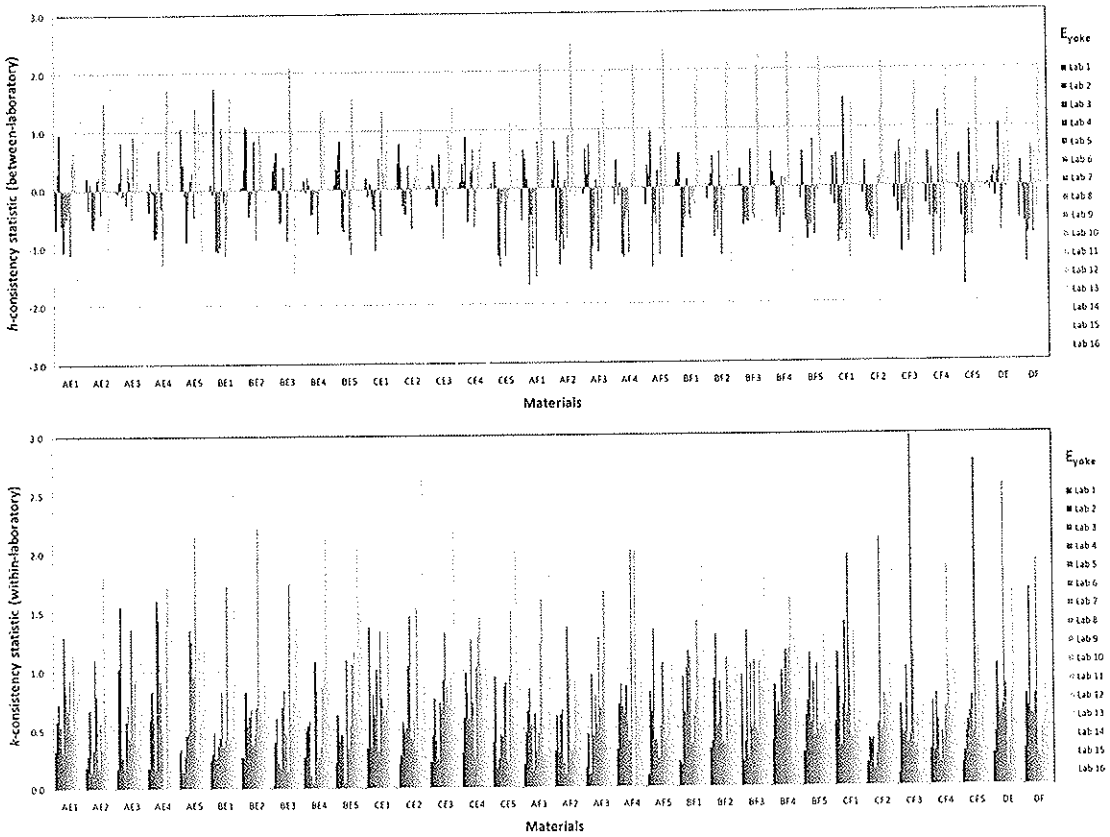

Figure 3. E_{yoke} consistency statistics for 16 labs. Critical values: h = 2.49, k = 1.98.

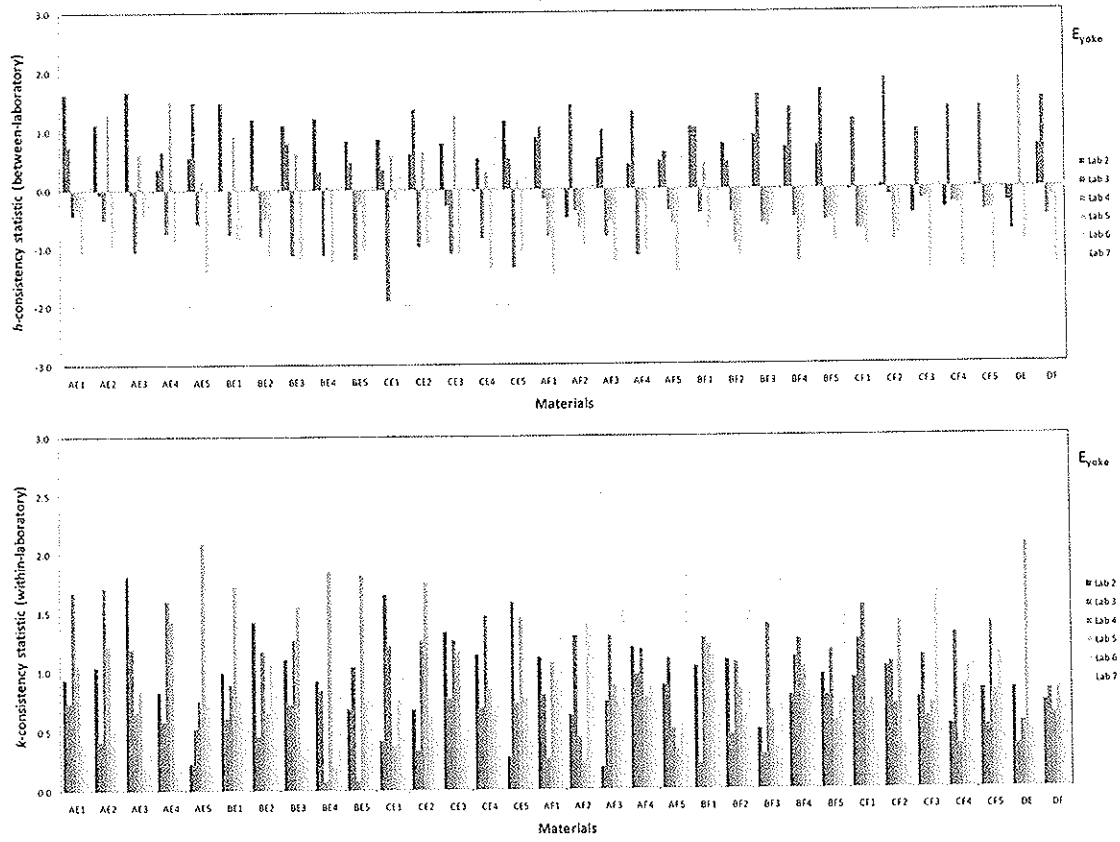

Figure 4. E_{yoke} consistency statistics for 6 labs. Critical values: h = 1.92, k = 1.84.

3.3 Precision Statistics of E_{yoke}

Table 2 presents the average precision statistics (in percent) calculated according to ASTM E177 [2] (see Appendix) using the data from the six labs that produced the most consistent test results using one full-span yoke deflectometer and whose setups seemed to be conforming to the standard. The data from the #1 ranked lab that used two yokes is not included in this calculation because it represents a higher order of precision. The "two" CV limit (2CV%) indicates that approximately 95% of individual test results from labs similar to these six can be expected to differ in absolute value from their average value by less than 1.96 standard deviations (about $2s$). The difference "two" CV limit (d2CV%) indicates that approximately 95% of all pairs of test results from labs similar to these six can be expected to differ in absolute value by less than $1.96 \cdot 2^{1/2} s = 2.77s$ [2].

Table 2. Precision statistics for apparent MOE determined with one full-span yoke.

	Material	Test Orientation	Width/ Depth	Test Span	Average MOE (yoke)	Repeatability Coefficient of Variation	Reproducibility Coefficient of Variation	Repeatability Limits		Reproducibility Limits	
			b/h	L	E_{yoke}	CV_r	CV_R	$2CV_r$	$d2CV_r$	$2CV_R$	$d2CV_R$
			mm	mm	GPa						
A	Lumber	Edgewise	38/89	1600	13.9	1.3%	1.8%	2.5%	3.5%	3.6%	5.1%
		Flatwise	89/38	800	15.0	1.1%	3.5%	2.1%	3.0%	6.8%	9.7%
B	LSL	Edgewise	38/89	1600	10.3	0.8%	1.7%	1.6%	2.2%	3.4%	4.8%
		Flatwise	89/38	800	10.6	1.3%	2.9%	2.5%	3.6%	5.8%	8.2%
C	LVL	Edgewise	38/89	1600	16.2	1.2%	1.9%	2.3%	3.2%	3.8%	5.3%
		Flatwise	89/38	800	19.0	0.9%	3.7%	1.8%	2.6%	7.2%	10.2%
	Average (ABC)	Edgewise				1.1%	1.8%	2.1%	3.0%	3.6%	5.1%
		Flatwise				1.1%	3.4%	2.2%	3.1%	6.6%	9.3%
D	Calibration bar	Edgewise	25/51	1600	16.4*	1.5%	1.6%	2.9%	4.1%	3.2%	4.5%
		Flatwise	51/25	800	5.42*	1.2%	2.4%	2.4%	3.4%	4.6%	6.6%

* EI_{yoke}, kN·mm²

The precision statistics determined in this ILS did not show any trend related to the level of the property measured in the range of MOE between 10 and 19 GPa, regardless of the number of labs included in the analysis. The within-lab repeatability did not depend on the test orientation (edgewise or flatwise). The between-lab reproducibility limits for flatwise tests were between 1.7 and 1.9 times those for edgewise tests. The CV_R values were often twice the CV_r for edgewise tests and up to 4 times the CV_r for flatwise tests.

Among the uncertainties contributing to these patterns were measurements of the test span (L), beam dimensions (b/h), load (P) and deflection (Δ). Within one lab, the L, b and h of each beam were measured once, and the span was not reset between trials and, therefore, the within-lab repeatability was mostly affected by consistency of the P/Δ measurements. The uncertainty due to the span and beam dimensions measurements was revealed in between-lab comparisons only. Since $L_{flat}/L_{edge} = 1/2$, and $h_{flat}/h_{edge} = 38/89 = 0.43$, the percent error components of these measurements increased in the inverse proportion in E_{flat} calculations. However, these uncertainty components did not appear to explain the overall differences in repeatability and reproducibility observed from the ILS. Upon further investigation, it is possible that the major contribution to the uncertainty could be from the differences in the yoke deflectometer installation.

Figure 5 illustrates extraneous deflection components due to eccentric loading or imperfections of the specimens and that the errors can be amplified due to differences in the yoke installation in edgewise and flatwise tests. If the beam rotates an angle φ, then deflections measured at point A, at a distance e from the side face of the beam, are overestimated by the value of δ_o and the measurements at point B on the opposite side of

the beam are underestimated by the value of δ_u. To estimate the values of the extraneous components, Solli [5] assumed that the beam rotates around its geometric centre and then:

$$\delta_o = -\delta_u = (e + 0.5b)\tan\varphi . \tag{5}$$

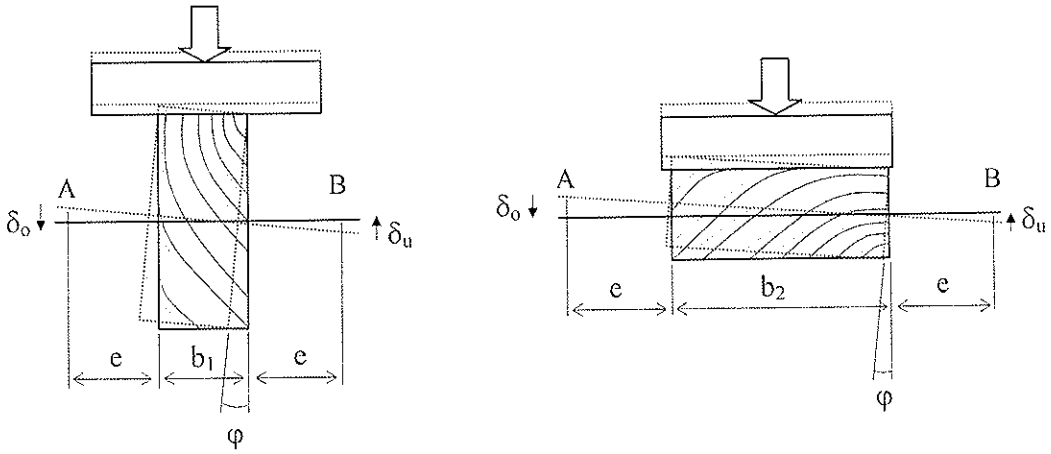

Figure 5. Uncertainty components in deflection measurements.

If the errors are expressed as fractions of the true deflection of the neutral axis (Δ): δ_o/Δ (or δ_u/Δ), then the ratio of the errors between two different setups can be readily estimated, regardless of the rotation angle:

$$\frac{\delta_{o,flat}}{\delta_{o,edge}} = \frac{e + 0.5b_2}{e + 0.5b_1} \tag{6}$$

In this study, the distance e in different labs varied between 10 and 50 mm. Then, the contribution of $\delta_{o,flat}$ to deflection measurement error could vary between 1.9 and 1.4 times $\delta_{o,edge}$, respectively. Similarly, one can estimate the influence of the distance e on the error components: $\delta_{o,e=50mm}$ could be 1.7 to 2.4 times $\delta_{o,e=10mm}$ for flatwise and edgewise tests, respectively. Considering that the data obtained with two yokes was approximately twice as consistent as the other top ranked data, one can assume that the deflection measurement error contributed about 50% of the CV.

The steel calibration bar tests did not produce much greater consistency in the stiffness measurements. A higher CV_r might be due to lower test load levels used for the calibration bar, but given that the consistency statistics of the results from the calibration bar are comparable to the wood samples suggest that the D198 deflection measurements, in general, may require further study. It should be noted that the ILS results were obtained under refined conditions. The specimens used in the study were predominantly straight (the maximum twist and bow measured on the 1.75-m length following the ILS was 1.6 mm). The test instructions were more detailed than the standard (e.g., single cycle loading, use of screws for yoke installation, fixed upper load limit, etc.), and the influence of the span and dimension measurements were not included in the within-lab repeatability calculations. Therefore, one can expect that real test data might show even lower precision than those presented in Table 2.

3.4 Consistency and Precision Statistics of E_{stroke}

Analysis of E_{stroke} data, similar to that described in 3.2 and 3.3, also showed that not all of the participating labs were in statistical control with this test. Although the ranking of the labs was different from that of E_{yoke} measurements, Table 3 is compiled to show a general trend in precision statistics obtained from the data of the same six labs as in Table 2.

Table 3. Precision statistics for apparent MOE determined with the load head stroke.

	Material	Test Orientation	Width/ Depth	Test Span	Average MOE (yoke)	Repeatability Coefficient of Variation	Reproducibility Coefficient of Variation	Repeatability Limits		Reproducibility Limits	
			b/h	L	E_{stroke}	CV_r	CV_R	$2CV_r$	$d2CV_r$	$2CV_R$	$d2CV_R$
			mm	mm	GPa						
A	Lumber	Edgewise	38/89	1600	12.8	0.8%	1.3%	1.7%	2.4%	2.6%	3.6%
		Flatwise	89/38	800	13.7	1.1%	3.5%	2.1%	3.0%	6.8%	9.7%
B	LSL	Edgewise	38/89	1600	9.70	0.5%	2.0%	0.9%	1.3%	3.8%	5.4%
		Flatwise	89/38	800	9.76	0.9%	4.3%	1.8%	2.6%	8.4%	11.9%
C	LVL	Edgewise	38/89	1600	14.7	1.0%	1.5%	1.9%	2.7%	2.9%	4.0%
		Flatwise	89/38	800	16.9	1.2%	3.7%	2.3%	3.3%	7.3%	10.4%
	Average (ABC)	Edgewise				0.8%	1.6%	1.5%	2.1%	3.1%	4.4%
		Flatwise				1.1%	3.8%	2.1%	3.0%	7.5%	10.6%
D	Calibration bar	Edgewise	25/51	1600	15.4*	0.7%	3.9%	1.4%	2.0%	7.7%	10.9%
		Flatwise	51/25	800	4.70*	1.5%	6.1%	2.9%	4.0%	12.0%	16.9%

* EI_{stroke}, kN·mm²

The order of precision statistics of wood materials appears very similar to that in Table 2. Edgewise E_{stroke} measurements seem to be even more precise than those with the yoke. This precision, however, does not grant closeness to the true value or E_{yoke}. Obviously, unadjusted E_{stroke} values were always lower than E_{yoke} (i.e. biased), and the difference between E_{stroke} and E_{yoke} varied greatly between labs, and within-lab differences between the two were also very inconsistent. Table 4 shows the average differences between pairs $E_{yoke,i}$ and $E_{stroke,i}$ calculated for individual series of 20 trials per material and CV% of these differences for each of the same six labs as in Table 3. The CV% varied from 4% to 42% with the global average of 12%. This inconsistency can be partially attributed to the fact that this was not a routine testing procedure for most of the labs. D4761 tests are usually performed using equipment dedicated to the D4761 bending test method, as opposed to being carried out at the same time as the D198 bending test. Therefore, no direct inferences can be made with regard to the accuracy of the D4761 method.

Table 4. Differences between E_{yoke} and E_{stroke} (average and CV%).*

	A-edge		B-edge		C-edge		A-flat		B-flat		C-flat	
Lab	AVG	CV	AVG	CV	AVG	CV	AVG	CV	AVG	CV	AVG	CV
2	7%	14%	4%	12%	7%	8%	6%	13%	8%	42%	8%	11%
3	8%	11%	5%	13%	8%	10%	6%	17%	6%	10%	9%	15%
4	9%	12%	6%	10%	9%	6%	7%	11%	5%	18%	8%	14%
5	10%	11%	9%	4%	10%	9%	7%	17%	7%	15%	8%	13%
6	11%	14%	6%	11%	11%	12%	10%	6%	8%	8%	13%	9%
7	8%	13%	5%	14%	9%	19%	17%	6%	13%	7%	19%	10%

* $(E_{yoke,i} - E_{stroke,i})/(E_{yoke,i})(100\%)$.

4 Conclusions

- Precision statistics presented in Table 2 are based on data from six similar labs that were found to be in statistical control using one full-span yoke deflectometer. The statistics are valid for the conditions stated in the table and can serve as a basis for the precision statement of the D198 flexure test method for apparent MOE.
- The indexes of precision of the tested wood materials did not seem to depend on the MOE value; therefore, the average indexes can be applied. Reproducibility indexes, however, differed considerably between the edgewise and flatwise tests and, therefore, shall be stated separately.
- The different interpretations of the D198 flexure test method for MOE determination observed suggest that the standard is still too vague and could be improved. Inconsistency of test results and lack of statistical control of the measurement process demonstrated by several labs may be attributed to non-conformity to the standard requirements and/or differences in the interpretation of the test method.
- MOE measurements using the load-head movement can be as precise as the measurements with one yoke. However, the trueness of this measurement was found inconsistent.
- It was observed in one lab that using two yokes on both sides of the beam improved the within- and between-lab consistency. This observation should be confirmed through trials in multiple laboratories.

Acknowledgements

Acknowledgement is extended to the ASTM ILS Program for sponsoring the study. Sincere thanks to all participating labs and personnel involved. Special thanks to Conroy Lum and Ned Waltz for all the help during this project!

References

[1] ASTM D198-05a: Standard Test Methods of Static Tests of Lumber in Structural Sizes. ASTM Annual Book of Standards.

[2] ASTM E177-04: Standard Practice for Use of the Terms Precision and Bias in ASTM Test Methods. ASTM Annual Book of Standards.

[3] ASTM D4761-05: Standard Test Methods for Mechanical Properties of Lumber and Wood-Base Structural Material. ASTM Annual Book of Standards.

[4] ASTM E691-99: Standard Practice for Conducting an Interlaboratory Study to Determine the Precision of a Test Method.

[5] Solli, K.H. 1996. Determination of Modulus of Elasticity in Bending According to EN 408. Paper 29-10-2 in: Proceedings of CIB-W18 Meeting 29. Bordeaux, France.

Appendix: Calculation of the statistics

Test results from one laboratory on one material constitute a *cell* (e.g., four replicates of E_{yoke} for material A1 determined in lab #1).

Cell average, $\bar{x}$ (for each cell):

$$\bar{x} = \sum_{1}^{n} \frac{x}{n}$$

where,

x = the individual test results in one cell, and
n = the number of test results in one cell ($n = 4$ in this study).

Cell standard deviation, s (for each cell):

$$s = \sqrt{\sum_{1}^{n} (x - \bar{x})^2/(n-1)}$$

Average of cell averages, $\bar{\bar{x}}$, for each material (e.g., A1):

$$\bar{\bar{x}} = \sum_{1}^{p} \frac{\bar{x}}{p}$$

where,

$\bar{x}$ = the individual cell average, and
p = the number of laboratories considered in the ILS.

Cell deviation, d, for each laboratory, for each material:

$$d = \bar{x} - \bar{\bar{x}}$$

Precision statistics:

Standard deviation of the cell averages, $s_{\bar{x}}$, for each material (e.g., A1):

$$s_{\bar{x}} = \sqrt{\sum_{1}^{p} d^2/(p-1)}$$

Repeatability standard deviation, s_r, for each material (e.g., A1):

$$s_r = \sqrt{\sum_{1}^{p} s^2/p}$$

Reproducibility standard deviation, s_R, for each material (e.g., A1):

$$s_R = \sqrt{(s_{\bar{x}})^2 + (s_r)^2(n-1)/n}$$

Consistency statistics, h and k, for each cell:

$$h = d/s_{\bar{x}}$$

$$k = s/s_r$$

where,

h = the between-laboratory consistency statistic,
k = the within-laboratory consistency statistic.

INTERNATIONAL COUNCIL FOR RESEARCH AND INNOVATION
IN BUILDING AND CONSTRUCTION

WORKING COMMISSION W18 - TIMBER STRUCTURES

NEW TEST CONFIGURATION FOR CLT-WALL-ELEMENTS UNDER SHEAR LOAD

T Bogensperger
T Moosbrugger
G Schickhofer

Institute for Timber Engineering and Wood Technology
Graz University of Technology

AUSTRIA

MEETING FORTY
BLED
SLOVENIA
AUGUST 2007

Presented by T. Bogensperger
H. Blass and T. Bogensperger discussed issues relating the shear strength of glue line versus the shear strength of the material.
R. Zarnic asked about the efficiency of simple model versus the more complicated test method. T. Bogensperger and G. Schickhofer responded the simple one is not wrong with respect to stiffness but there are some issues with respect to strength as shown in the paper; therefore, comparison is not appropriate. R. Zarnic commented that the simple method is cheaper and would like to see some harmonization of available methods. G. Schickhofer agreed that the more complicated method is expensive and maybe the less expensive method that can yield accurate results is also needed.
There were further discussions and clarifications that the shear strength is in the plane parallel to the element. Rolling shear can occur but not the main mode. The shear locking effect was discussed and geometry of the board with respect to the glue area will have an influence.
B.J. Yeh commented that the overhang can increase shear strength significantly. G. Schickhofer replied that the overhang did not affect the shear strength as the failure mode in bending is in the cross ply.

NEW TEST CONFIGURATION FOR CLT-WALL-ELEMENTS UNDER SHEAR LOAD

Th. Bogensperger [1], Th. Moosbrugger [1], G. Schickhofer [1]

[1] Institute for Timber Engineering and Wood Technology, Graz University of Technology, Austria

1 Introduction

Cross laminated timber plates (CLT) are planar timber elements and used e.g. for wall elements with or without openings (Fig. 1) in constructional timber engineering. Whereas the transmission of normal stresses horizontally and vertically causes little demands with the exception of stability under compression, little investigations can be found in load transmission behaviour for shear loads in plane ([Bosl], [Jeitler], [Wallner] and [5. GraHFT'06]). Until now the mechanical behaviour in respect to stiffness and ultimate limit loads of a single CLT element is not known sufficiently. The shear forces between two adjacent timber boards are transmitted by local torsional moments in each glue interface in order to obtain the equilibrium in shear stresses (duality of shear stresses) [Blaß/Görlacher] and induce the so called rolling shear stresses. By contrast a homogeneous CLT-plate, laterally glued together with the adjacent board, which implies full shear force transmission at the lateral sides thereby [Blaß/Görlacher], is able to carry the resulting shear stresses in each single layer.

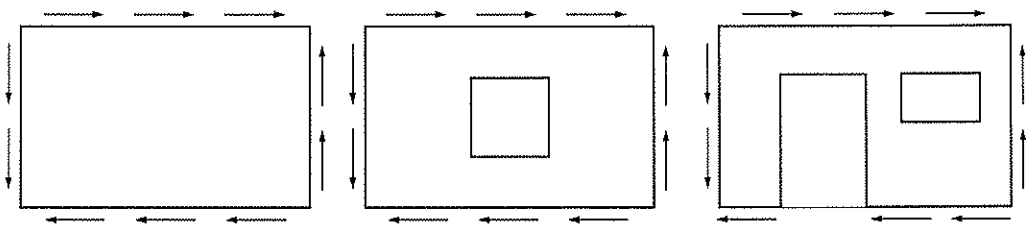

Figure 1: Cross laminated timber plates (CLT) used as wall elements with and without openings

2 Mechanical treatment of CLT-structures under shear loads

2.1 Internal structure of CLT-structures

Cross laminated timber plates can be viewed as a discrete multi-layer grid structure which consists of several layers (usually 3 to 7) of single boards with the special feature that the boards within each layer have parallel orientation but the board orientations of neighbouring layers in thickness direction are always orthogonal to each other. The stacking sequence of the layers in thickness direction is usually symmetric with respect to the plate mid-plane. The individual board layers are connected to

each other by full gluing over the wide faces of crossing neighbouring boards. The narrow faces of the boards of one layer may either be in contact with or without being glued together, or they may be uniformly arranged with a certain small spacing between each other (Fig. 2.a).

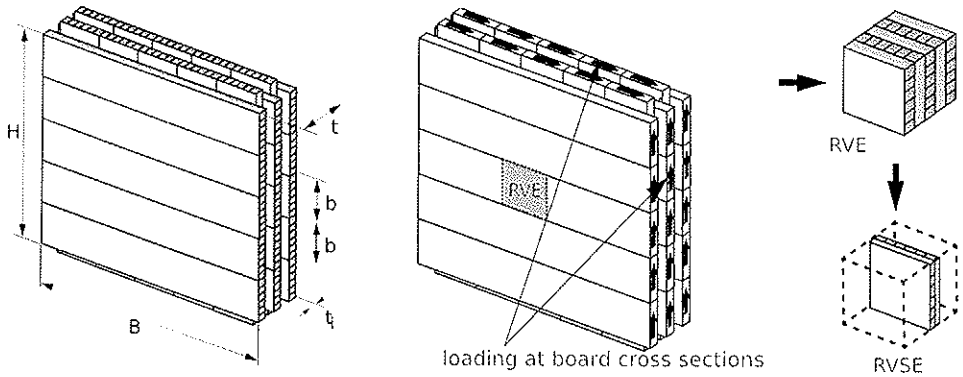

(a) Terminology and definitions for CLT plate elements (b) Specific kind of load introduction (c) RVE, RVSE

Figure 2: Terminology, load introduction and RVE-definition for CLT plate elements

2.2 Efficient mechanical modelling

The regular periodic internal geometric structure of the considered CLT-wall element (Fig. 2.a,b), in combination with the uniformly applied shear loading over the board cross sections hitting the boundaries of the CLT-element, – from the theoretical point of view – results in periodically repeated patterns of stresses and deformations. The smallest unit cell which represents the basic result pattern and which is periodically repeated over the whole volume of the CLT-plate is called the "representative volume element (RVE)". This terminology is well-known and taken over from the field of multi-scale modelling. The representative volume element extends over the whole plate thickness and can be further sub-divided in plate thickness direction leading to the even more fundamental so-called "representative volume sub-element (RVSE)" (Fig. 2.c).

2.3 Decomposition in pure shear and local torsion in the RVSE

For better understanding of the mechanical behaviour, the fundamental representative volume sub-element (RVSE) is shown in Fig. 3.a with the shear forces transmitted at the vertical and horizontal pairs of planes of periodicity (anti-symmetry). It can be clearly recognised that the shear forces between neighbouring RVSE's are transmitted over related (vertical and horizontal) board cross sections only. Therefore the narrow faces of neighbouring boards of each layer remain always stress-free. For enabling better understanding, the complete state of shear loading as shown in Fig. 3.a can be decomposed into two basic mechanisms, i.e. a mechanism of pure shear (Fig. 3.b) and a remaining mechanism of "torsion-like" behaviour (Fig. 3.c).

More details and the mathematical formulation of these both mechanism's can be found in [WCTE'06], where a mechanical based approach of the symmetric and antimetric loading is introduced and superposed as a serial system. Furthermore another mechanism ("finite in-layer board spacing") is considerated in [WCTE'06]. Because of the approximation of the anti-symmetric mechanism, the gained model is fitted to a FE-model by a correction function.

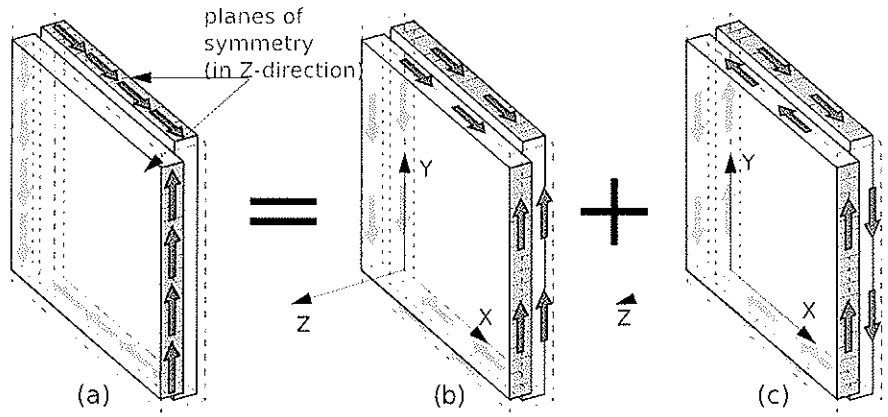

Figure 3: Superposition of load carrying mechanisms, (a) original situation, (b) partial state of pure shear and (c) partial state of torsion-like behaviour.

2.4 Finite element modelling of the RVSE

A finite element analysis is performed at the representative volume subelement (RVSE) under uniform shear loading (Fig. 4) utilising three-dimensional solid modelling. The relevant periodic boundary conditions were imposed by suitable linear constraint equations. $G_{\parallel}$ resp. $G^*_{\parallel}$ characterise the shear modulus of a single board resp. the effective shear stiffness of the entire CLT-structure. F is the shear force, acting at one anti-symmetric cross section, δ represents the tangential displacements of the anti-symmetric cross section resp. the reference-point

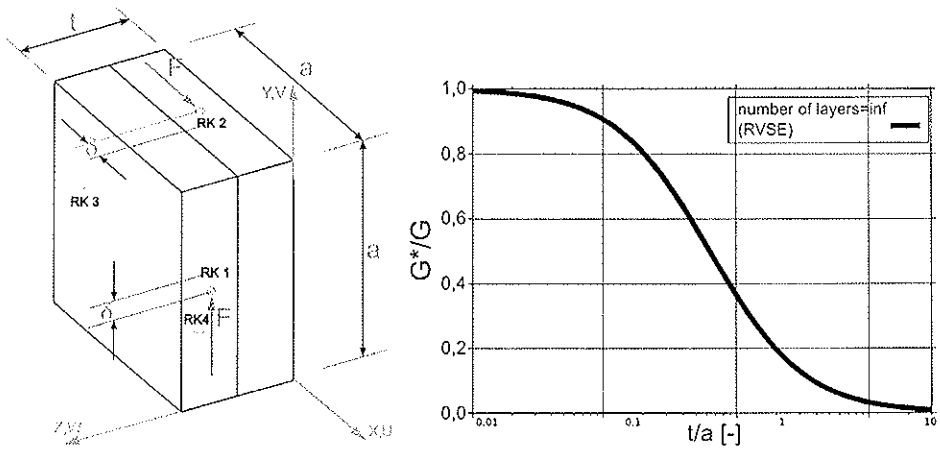

(a) Loads and displacements of the FE-model

(b) Stiffness behaviour of a CLT-wall under shear in dependency on the parameter $\frac{t}{a}$

Figure 4: Finite–Element modelling of the RVE

A complete description of all applied boundary conditions in the FE-model is given in [hbf–report 2007]. The effective shear stiffness of the RVE and in consequence of the entire CLT-structure is determined by use of the equations 1, 2 and 3, where F is the applied load and δ the calculated displacement of the reference-point of the cross section in the FE-model.

$$\gamma^* = \frac{\tau}{G^*_{\parallel}} = \frac{F}{G^*_{\parallel} \cdot a \cdot t} \tag{1}$$

$$\gamma^* = \frac{4 \cdot \delta}{a} \tag{2}$$

$$\frac{G^*_{\parallel}}{G_{\parallel}} = \frac{F}{4 \cdot t \cdot \delta \cdot G_{\parallel}} \tag{3}$$

Because of the applied symmetry conditions (Fig. 3.a) in both middle areas of the boards, a CLT-plate with an infinite number of RVSE-elements ($t \rightarrow \infty$) is modelled, which does not correspond to a real CLT-plate.

2.5 Finite element modelling of the RVE (boundary effects)

The effect of limited number of layers in the CLT-plate and the resulting boundary effects are investigated in a finite element analysis of the representative volume element (RVE). In the following figure (Fig. 5), it can be seen, that both outward zones with a thickness of each $\frac{t}{2}$ (Fig. 5.b) are not regarded in the RVSE-model (Fig. 5.a). Although these additional structure stiffen the RVE-element, a general loss of stiffness is registered, because the shear stiffness of the RVE-element is not related to the sum of thickness of all RVSE-models, but the sum of thickness of all layers, which is $2 \cdot \frac{t}{2}$ thicker than the sum of the thickness of all RVSE-models.

The results of the effective shear stiffness of the 3-layered and 5-layered CLT-plate in comparison to the RVSE-element is illustrated in Fig.5.c.

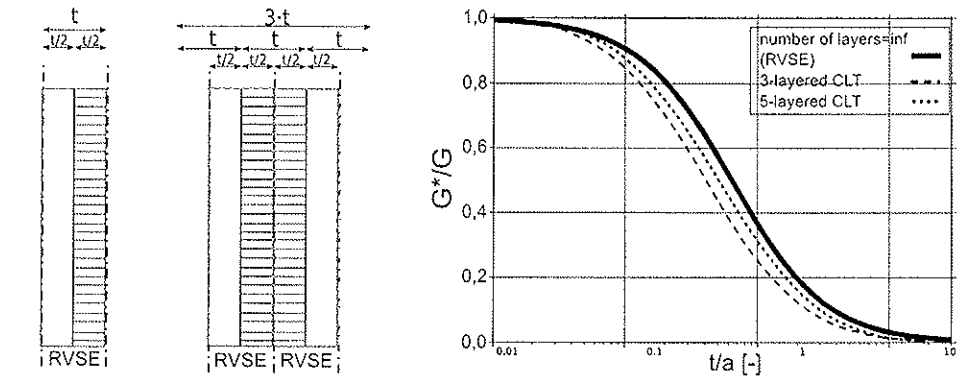

(a) RVSE (b) 3-layered CLT plate (c) 3- and 5-layered CLT plate in comparison with the RVSE-element

Figure 5: Boundary effects of CLT-structures

3 Test configuration, developed by Bosl

Bosl [Bosl] carried out several shear tests on CLT-plates in his PhD work at the Munich Military University in 2002. The test configuration is illustrated in Fig. 6.a. In Fig. 6.b one test field is shown in detail exemplarily. Fig. 5.c demonstrates the appeared main failure mechanisms. In this snapshot it is obviously, that the main problem of this test configuration is pure compression stress introduction in

the test specimen, whereas the introduction of tension stresses fails. This leads to a stress distribution, which deviates from a pure, ideal shear stress distribution and causes failure at those two ends, where the compression forces are introduced.

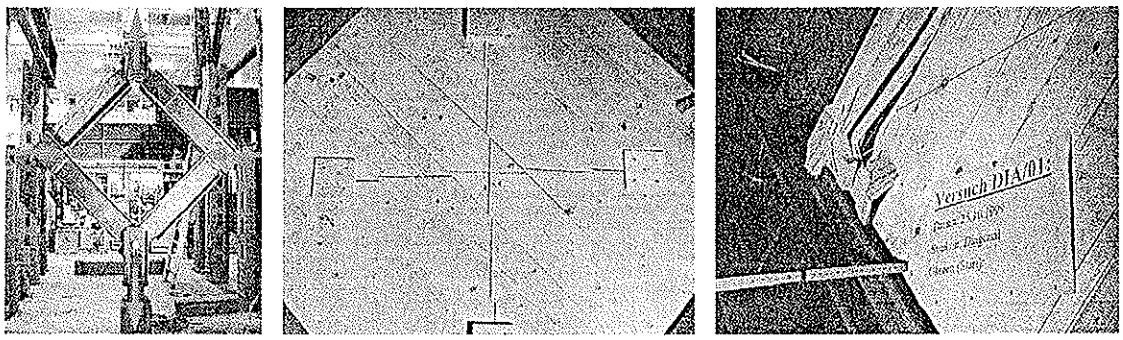

(a) Test configuration acc. to Bosl

(b) Deformations in the test field

(c) Observed failure mechanisms near the introduced compression forces

Figure 6: Test configuration acc. to Bosl, 2002

4 Developed new test configuration

4.1 General considerations on the developed new test configuration

A new test configuration was developed under the following considerations (Fig. 7, 8) at the holz.bau forschungs gmbh, Graz, Austria. Following consideration are made for the investigated 3-layered CLT-plate, but they can be assigned to a 5- or 7-layered CLT-plate as well:

- In order to neglect effects due to the boundary effects, described in 2.5, the thickness are chosen in such a way, which is not typical for a commercial CLT-plate, but gives good accordance with the RVSE-model. The outer layer thickness are built with half of the thickness of the central, middle layer (see Fig. 5.a, 5.b). The boundary effect according to 2.5 is reduced to the missing of one plane of symmetry thereby. It can be shown by a numerical study (FE-analysis), that the difference in the stiffness of a CLT-plate without this plane of symmetry in comparison to a ideal RVSE-like CLT-plate remains small.

- With double thickness of the middle layer the load introduction can be established easier. The middle layer is subjected to double amount of shear forces in relation to each outer layer. Load introcuction should be arranged continuously by glued steel plates in contradiction to [Bosl], where load introduction was achieved only by compression on the test specimen (Fig. 8.a).

- In order to exclude any friction between adjacent narrow faces of each board, an overall spacing between the boards was chosen with 5 [mm]. Beyond that, gaps in this range are not avoidable in CLT-plates due to climate effects like shrinking (Fig. 7.a).

- As described in section 2.2, the shear forces of a pure shear stress field are transmitted only over the cross sections of each board. In contradiction the chosen load introduction the shear loads applies at the narrow faces of the outer boards, which leads to some local stress peaks in the

outer zones of the test specimen. In order to reduce this effect, hard wood is chosen as material for the outer boards (Fig. 7.b).

- Above facts lead to unusual board sizes of 75 [mm] width and 60 [mm] thickness for the middle layer and 75 [mm] width by 30 [mm] thickness for both outer layers. 7 boards and gaps with 5 [mm] lead to an overall size of 560 [mm] by 560 [mm]. The total thickness t is 120 [mm] (Fig. 7.a).

4.2 Test configuration

Basic of the developed test configuration is the 3-point bending-shear test according to [EN 384:2004]. The test configuration consists of a quasi rigid steel frame, pin–connected in all edges (Fig. 8). The steel frame is built up with pairs of steel plates, glued together with the exterior boards at their narrow sides. This assures a continuous load introduction from the steel frame into the test specimen. In a uniform shear stressed test specimen, the loads are transmitted only over the adjacent cross sections, not over the narrow sides of the single board. This fact results in a violation of the pure shear stress field. Numerical studies show, that the resulting deviations of the shear stiffness remain small for the CLT-plate. A almost pure shear stress field can be assumed in the inner part of the CLT-plate and proved with a FE-analysis as well.

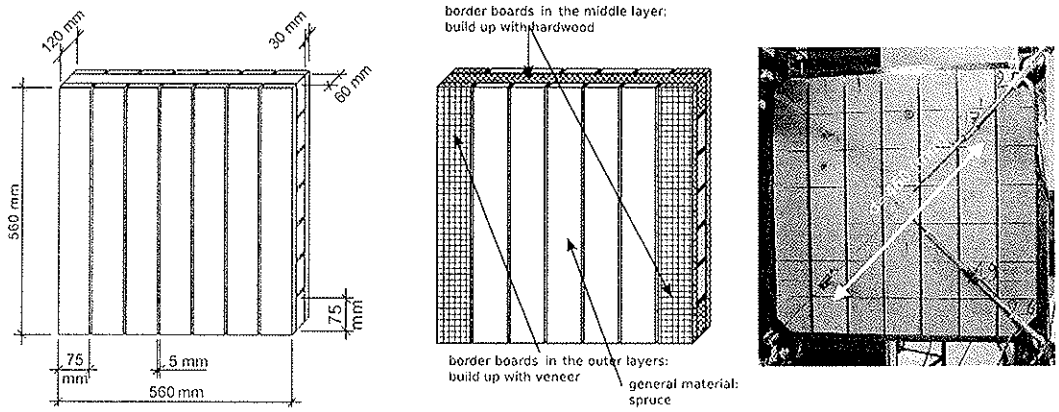

(a) Test configuration for the first experiment (b) Test configuration for the subsequent experiments (c) Measurement of diagonal length alterations

Figure 7: Test specimen for shear tests of CLT-plates

The effective shear stiffness of the test specimen is determined by use of the equations 4. The shear strain $\gamma^* = \frac{\delta}{l} = \frac{\Delta\bar{d}\cdot\sqrt{2}}{l}$ is calculated on basis of the mean value of the length alterations $\Delta\bar{d}$ of both diagonals (Δd_1, Δd_2) of the shear strain field (Fig 8.b). δ is the calculated vertical increase of displacement on basis of $\Delta\bar{d}$. F denotes the observed test load for the shear field, t the overall thickness of the CLT-plate (120 [mm]), L the length of the test specimen (560 [mm]) and l denotes the local length in the measuring field (325 [mm], see Fig. 8.b).

The effective shear stiffness $G^*_{\parallel}$ of the CLT-plate is calculated with Eq. 4.

$$G^*_{\parallel} = \frac{F\cdot\frac{l}{L}}{t\cdot\Delta\bar{d}\cdot\sqrt{2}} = \frac{F\cdot\frac{l}{L}}{t\cdot\frac{1}{2}\left(\Delta d_1+\Delta d_2\right)\cdot\sqrt{2}} \tag{4}$$

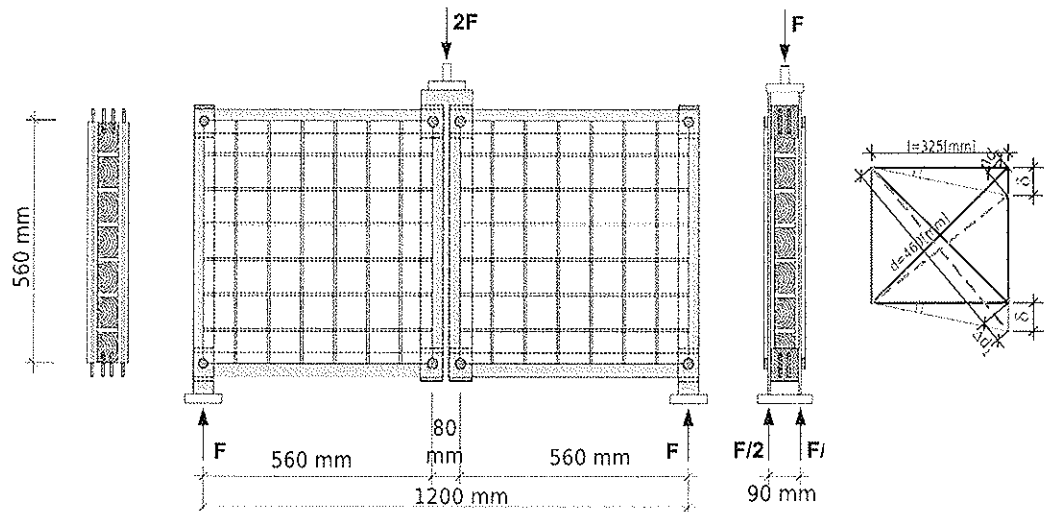

(a) Geometry, dimensions of the test configuration

(b) Kinematic in the measuring field

Figure 8: Developed test configuration

Formular 4 is valid for an ideal elastic behaviour, which can not be found under laboratory conditions overall. The load is introduced according to [ON EN 26891:1991]. Therefore an adequate linearisation has to be performed for all measured kinetic and kinematic input values (F, Δd_1, Δd_2) of equation 4.

5 Conducted tests

5.1 Overview of the tests

Three tests were conducted at the holz.bau forschungs gmbh, Graz, Austria. For symmetry reason, one test always consists of two test specimens (Fig. 9.a).

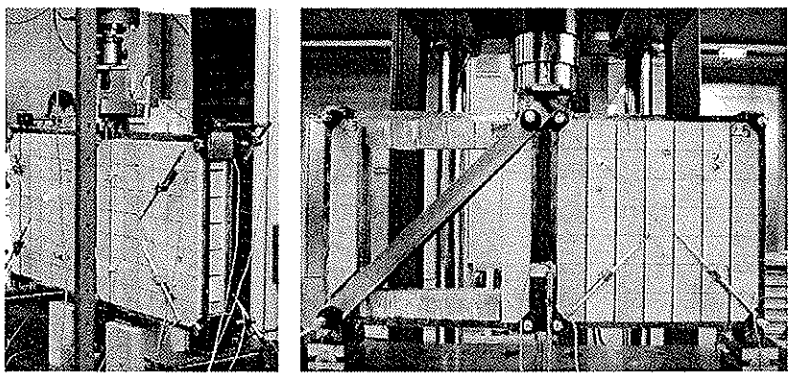

(a) Test configuration in the laboratory

(b) Test III: Test configuration with steel diagonal

Figure 9: Test configuration in the laboratory and Test III

- **Test I:** The test consisted of two test specimens, which were not reinforced by hard wood boards acc. to Fig. 7.b. Local failure due to tension normal to grain near the load introduction was determined, which was the initial point for the introducted outer hard wood boards (Fig. 7.b). Pictures of the test are shown in Fig. 10.a.
- **Test II:** Local failure due to tension normal to grain near the load introduction was prevented, but failure occurred in the load introduction between the outer and middle layer near the load introduction. The inner part of the test specimen remained almost undamaged (Fig 10.b).
- **Test III:** After replacing of the weaker test specimen of Test II by a steel diagonal, the introduced load was increased until failure of the second test specimen (Fig. 9.b).

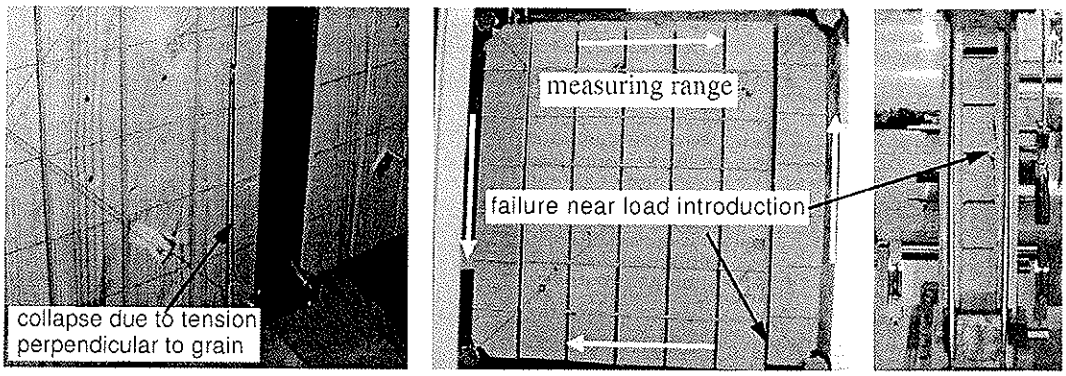

(a) Test I: local collapse due to tension perpendicular to grain

(b) Test II: local collapse near load introduction

Figure 10: Test I+II

5.2 Evaluation of the tests

The results of Test 1, 2 and 3 are presented in Tab. 1. Eq. 4 is applied in the linear range of the test results. Therfore always differences of measured values at a lower force level from values at an upper force level, e.g. $F \doteq F_o - F_u$ and $\Delta\bar{d} \doteq \Delta\bar{d}_o - \Delta\bar{d}_u$ have to be used for evaluation purposes.

6 FE calculation

For verification purpose a FE-analysis (3D-solid) of the test specimen under shear load was carried out. Two cases were regarded: On the one hand an ideal model with load introduction at the outer cross sections (Fig. 11.a) under coexistent anti-symmetric boundary conditions was established. In addition a model of the test specimen, which describes the real boundary conditions and the specific load introduction as realistic as possible, was adopted for comparison (Fig. 11.b). The material parameters were chosen as orthotropic linear elastic constants and can be found in table 2. Influences, caused by poisson's ratio, are neglected. The applied element was the C3D27 element with 27 nods of the FE program ABAQUS. Due to symmetry and anti-symmetry, only $\frac{1}{8}$ of the entire test specimen has to be modelled effectively (Fig. 11). A front view of the deformed modells can be found at Fig. 12.a and Fig. 12.b. A comparison of the shear stiffness of the CLT-structure between both models on basis of

	test specimen	F_{max}		F		Δd	$G^*_{experiment}$
		[N]		[N]		[mm]	[N/mm^2]
Test I	test specimen 1	78100	F_u	39463	Δd_u	0,376	240
			F_o	61453	Δd_o	0,689	
	test specimen 2	78100	F_u	43816	Δd_u	0,438	192
			F_o	60953	Δd_o	0,743	
Test II	test specimen 3	123000	F_u	40187	Δd_u	0,443	221
			F_o	100035	Δd_o	1,370	
	test specimen 4	123000	F_u	40187	Δd_u	0,383	240
			F_o	100035	Δd_o	1,237	
Test III	test specimen 4*	134000	F_u	52310	Δd_u	0,609	253
			F_o	120209	Δd_o	1,527	
		mean value of all shear stiffness					**229**
		standard deviation					**23,7**
		cov [%]					**10,3%**

Table 1: Results of shear tests

the calculated displacements (eq. 3) is arranged in table 3. It can be shown, that the calculated ideal model is 14,6% weaker (Tab. 3) than the real test specimen, when the inner measuring range (Fig. 7.b, 10.b) is regarded. Measuring the global displacements at the outside of the test specimen leads to increased divergence up to 26,4% (Tab. 3), which can be regarded as too high. Our suggestion is, that a calibration factor of 0,90 should be introduced for the actual configuration to correct the calculated shear stiffness on basis of the test results when using displacements of the inner measuring range (e.g. 5*5 measuring range).

	Dimension	**Value**		**Dimension**	**Value**		**Dimension**	**Value**
E_{11}	[N/mm^2]	10000	V_{12}	[-]	0,00	G_{12}	[N/mm^2]	750
E_{22}	[N/mm^2]	400	V_{13}	[-]	0,00	G_{13}	[N/mm^2]	750
E_{33}	[N/mm^2]	400	V_{23}	[-]	0,00	G_{23}	[N/mm^2]	75

Table 2: Orthotropic linear elastic constants in the FE model

Case	F [N]	t [mm]	$G_{\|\|}$ [N/mm^2]	δ [mm]	$\frac{G^*}{G_{\|\|}}$ [-]	G^* [N/mm^2]	Diff. [%]
RVSE	15000	60	750	0,291	0,286	215	
Ideal test specimen	105000	60	750	2,04	0,286	215	
Real test specimen							
3*3 measuring field	30000	60	750	0,520	0,321	241	11,9%
5*5 measuring field	105000	60	750	1,02	0,328	247	14,6%
outside deformations	105000	60	750	1,61	0,362	272	26,4%

Table 3: Comparison of the effective shear stiffness of the ideal model and the test specimen under real conditions

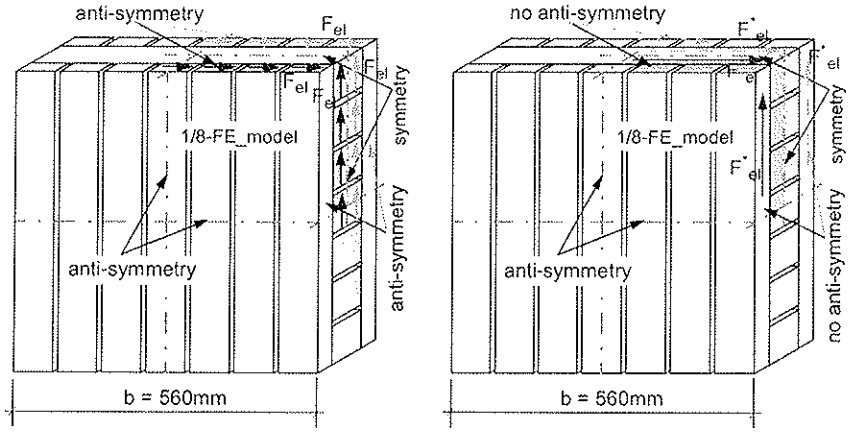

(a) FE-model of an ideal model under constant, pure shear stress

(b) FE-model of the test configuration with real load introduction

Figure 11: FE-model with various load intoduction and various planes of symmetry and antimetry

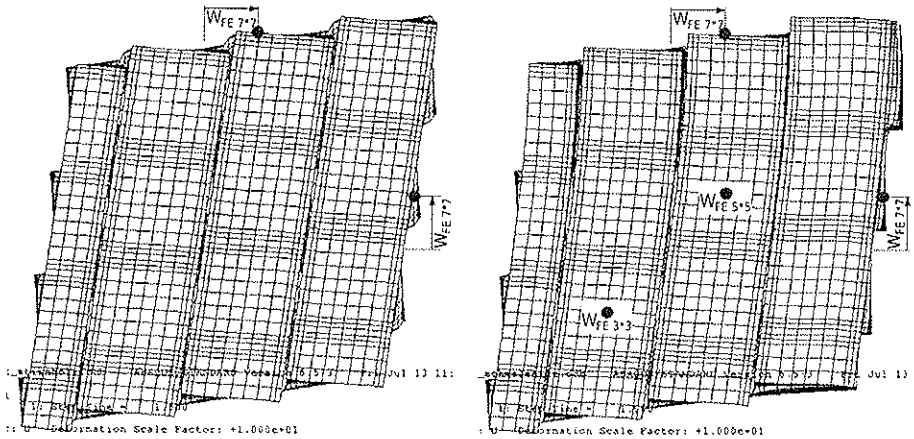

(a) Deformation of an ideal model under constant, pure shear stress

(b) Deformation of the test configuration with real load introduction

Figure 12: Deformations of the ideal model and the test specimen under real conditions

7 Shear Strength

The test configuration can also be used for determination of a technical shear strength. The term "technical" should express, that the observed strength is not a shear strength, because local failures occurred in the near of the load introduction. In respect to strength, two mechanisms have to be verified.

- It has to be verified (mechanism I, see Fig. 3.a), that the shear strength of each layer is sufficient (mechanism of pure shear). Mechanism I is often of greater importance in practical cases. Therefore a reliable estimation of the shear strength for mechanism I should be sought.
- It has further to be verified (mechanism II, see Fig. 3.c), that the local torsional moment can be

carried over the glueing interface.

According to [DIN 1052:2004] a characteristic strength value of 2,50 N/mm^2 (shear strength for glulam with cracks, $k_{cr}=\frac{2}{3}$) can be applied to mechanism I. The coincidentally same strength value should be applied for mechanism II, according to e.g. [Approval Z-9.1-680]. The conducted tests have shown, that an increase of the shear strength values can be applied for CLT elements. A reason for this enforced strength might be found in the strain locking due to the orthogonality of adjacent layers of the structure. The actual strength values according to [DIN 1052:2004], [Approval Z-9.1-680] and possible technical strength values on basis of the conducted test results for a parameter $\frac{t}{a} = 0,80$ are presented in table 4. The 5% quantile values of table 4 are based on an estimated coefficient of variation of COV=10%, because only a few experiments were carried out yet.

		Mechanism I [N/mm^2]	Mechanism II [N/mm^2]
DIN 1052:2004	$f_{v,k,mech\_I}$	2,5	
Approval Z-9.1-680	$f_{v,k,mech\_II}$		2,5
conducted tests	mean value	4,0	5,4
5%-Quantile (COV=10% estimated)		3,3	4,5

Table 4: Actual and possible technical strength values for CLT-structures with a parameter $\frac{t}{a} = 0,80$ under shear in plane

Additional tests with an alternative test configuration [HMS–report], according to the requirements of [CUAP], have shown higher technical strength values for mechanism I. The tests consisted of 5-layered CLT-structures (Fig. 13), where all boards are glued together at their narrow sides only in both vertically oriented layers. Therefore a strength determination for mechanism II is not admissible. The

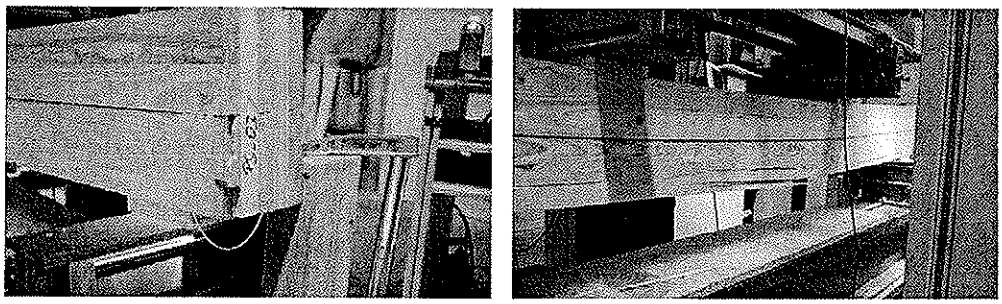

(a) Infrequent shear failure: loss of shear strength in the buttom, external board

(b) Mostly bending failure: loss of bending strength

Figure 13: CLT-tests, carried out at hbf in June 2007, according to [CUAP]

primary failure reason was loss of bending strength in most cases. The dimension of the boards are 25 [mm] thickness and 130 [mm] width, which leads to a parameter of $\frac{t}{a} = 0,192$. The evaluated technical strength values of these tests are summarised in table 5.

An evaluation of the shear strength can not be found in the work of [Bosl]. Based on 4 experiments for the 5-layered orthogonal CLT-structures in [Bosl], a mean technical shear strength of 11,3 N/mm^2 can be gained. A 5% quantile value can be further estimated with 9,78 N/mm^2, if a COV-value of 10% is assumed. With board width of b =150mm and thickness of t =17mm, the parameter $\frac{t}{a}$ can be calculated with 0,1133.

		Mechanism I [N/mm^2]	Mechanism II [N/mm^2]
DIN 1052:2004	$f_{v,k,mech\_I}$	2,5	
[CUAP]/[HMS–report]	mean value	8,9	[–]
	5%-Quantile	7,0	[–]

Table 5: Actual and possible technical strength values for CLT-structures with a parameter $\frac{t}{a} = 0,192$ under bending and shear in plane, according to [HMS–report]

In table F.11 of [DIN 1052:2004] strength values for plywood (density $\varrho = 400$ [kg/m^3], $\frac{t}{a} \rightarrow$ small) can be found on basis of the shear strength configuration in [EN 789:2005], which are once more higher than values of table 4 and 5. Values of table F.11 are valid for the total thickness of a plywood structure. For a 3-layered CLT-structure with equal thickness of all layers a comparable strength value for a softwood-plywood plate, related to the controlling single layer, can be derivated with $f_{v,k} = 3 \cdot 5\,[\mathrm{N/mm^2}] = 15\,[\mathrm{N/mm^2}]$. The values are even higher for 5- and more layered structures. For a n-layered CLT-structure an effective strength value, related to the controlling single layer, can be assumed with $f_{v,k} = 2 \cdot 8\,[\mathrm{N/mm^2}] = 16\,[\mathrm{N/mm^2}]$.

In Fig. 14.a various shear strength values are shown for comparison purpose as a function of the parameter $\frac{t}{a}$, which represents the quantity "strain-locking-effect" of the entire structure due to the orthogonality of adjacent layers. Fig. 14.b shows the respective test configuration, which has to be used for these various shear strength values.

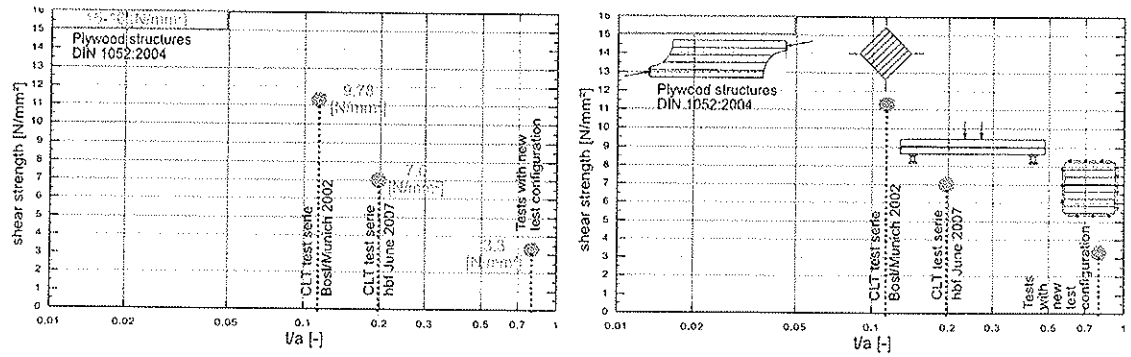

(a) Comparison of various shear strength values, depending on the quantity of the "strain-locking-effect"

(b) Basic test configurations for various shear strength values

Figure 14: Different shear strength values of CLT and plywood structures

8 Summary

Due to discrepancies of stresses and strains between an ideal CLT-structure and the test configuration under shear load near the load introduction a calibration factor $< 1,0$ (in the actual configuration: 0,90) is suggested, which corrects the shear stiffness, evaluated on basis of experimentally measured displacements.

In respect to strength, it is not able to determine a load level, at which the entire structure fails due to one classical failure mode like "shear fracture in a single layer" or "local torsional fracture in the glueing interface". Rather local failures near the load introduction can be observed.

The authors suggest a discusion, which configuration should be the favourate one for determination of a technical strength of a CLT-structure under shear. It is obvious, that the shear strength of such a structure is very high and is is hardly feasible to introduce these loads in the structure in practise. When dealing with CLT-structures with large openings, importance of such a strength rapidly increases, because in such a case the shear strength serves as a basic value for the structure and in a second step suitable reduction factors are needed, which consider special geometric like edges or openings. The developing of such a suitable reduction factor is still an open task.

Generally 3 possibilities for an experimental verification of the shear strength are available:

- Test configuration due to [EN 789:2005] (see Fig. 15.a). The scope of this test configuration lies more in testing of plywood and similar products. When adopting for CLT-structures, dimensions and forces develop very high. Because of fullfilling equilibrium conditions always shear loads and compression loads have to be introducted in the test specimen.
- Test configuration due to [CUAP] (see Fig. 15.b). This test configuration is demanded by the [CUAP] rules and tests were performed at hbf [HMS–report]. The primary failure in these tests was failure due to loss of bending strength. Therefore the suggested shear strength is also a technical shear strength analogous to the suggested test configuration of hbf–Graz (section 7).
- Test configuration of hbf–Graz (see Fig. 15.c), suggested and described in detail in this paper.

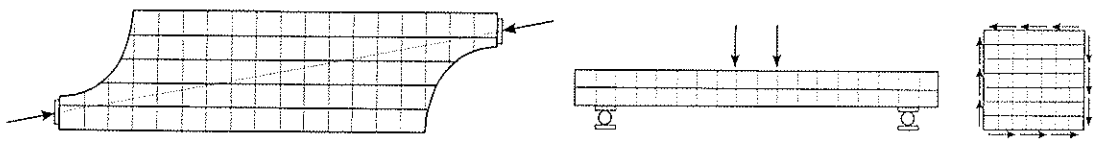

(a) Possible test configuration for CLT, based on [EN 789:2005]

(b) Test configuration according to [CUAP]

(c) Test configuration "hbf–Graz"

Figure 15: Systematic illustration of principle other possible test methods for CLT-structures under shear

Special thanks

The authors thank Mr. Robert August Jöbstl (Institut for Timber and Wood Technology, Graz Universtity of Technology) for strong support on development of the test configuration and Mr. Gianluigi Traetta (holz.bau forschungs gmbh, Graz, Austria) for conducting the experimental tests.

Literatur

[Bosl] Bosl R.: *Zum Nachweis des Trag- und Verformungsverhaltens von Wandscheiben aus Brettsperrholz*,
Institut for structural engineering, Military University Munich, January 2002.

[Jeitler] Jeitler G.: *Versuchstechnische Ermittlung der Verdrehungskenngrößen von orthogonal verklebten Brettlamellen*,
Institute for steel, timber and spatial structure, Graz University of Technology, January 2004.

Literatur

[Wallner] Wallner G.: *Versuchstechnische Ermittlung der Verschiebungskenngrößen von orthogonal verklebten Brettlamellen*,
Institute for steel, timber and spatial structure, Graz University of Technology, January 2004.

[Blaß/Görlacher] Blaß H. J.,Görlacher R.: *Zum Trag- und Verformungsverhalten von Brettsperrholz-Elementen bei Beanspruchung in Plattenebene*, in "Bauen mit Holz" p. 34-41, Bruderverlag Karlsruhe, 11/2002.

[5. GraHFT'06] Moosbrugger Th., Schickhofer G.: *5. GraHFT'06: Brettsperrholz – Ein Blick auf Forschung und Entwicklung*, 2006-09-29.

[WCTE'06] Moosbrugger Th., Guggenberger W., Bogensperger Th.: *Cross Laminated Timber Wall Segments under homogeneous Shear – with and without Openings*,
WCTE, Portland, Oregon, USA, August 6-10, 2006.

[hbf–report 2007] Guggenberger W., Moosbrugger Th., Bogensperger Th.: *P01 shell_structures – "Ebene Tragstrukturen im konstruktiven Holzbau" – "Wandscheiben – Einzelknoten"*,
Evaluation report of the competence centre "holz.bau forschungs gmbh, Graz, Austria", 29th May, 2007.

[EN 384:2004] EN 384:2004: *Structural timber - Determination of characteristic values of mechanical properties and density*, ratified 2003-02-20.

[ON EN 26891:1991] ON EN 26891:1991: *Holzbauwerke – Verbindungen mit mechanischen Verbindungsmitteln – Allgemeine Grundsätze für die Ermittlung der Tragfähigkeit und des Verformungsverhaltens*, (ISO 6891:1983).

[DIN 1052:2004] DIN 1052:2004: *Entwurf, Berechnung und Bemessung von Holzbauwerken*, german code, 2004.

[Approval Z-9.1-680] Zulassung Z-9.1-680: *HMS - Elemente*, german admission, 2007, valid until 2012.

[HMS–report] Prüfbericht P01_IV-3: *Scheibenbiegeversuche an HMS–Elementen*, internal test report, hbf–Graz, 2007.

[CUAP] Common Understanding of Assessment Procedure: *Solid wood slab element to be used as a structural element in buildings*, ETA request No 03.04/06, prepared by "OIB Österreichisches Institut für Bautechnik", Schenkenstraße 4, 1010 Wien, Austria, June 2005.

[EN 789:2005] EN 789-2005: *Determination of mechanical properties of wood-based panels*, ratified 2005-04-01.